The control of nanomorphology in star-shaped mesogens

Dissertation zur Erlangung des naturwissenschaftlichen Doktorgrades der Julius-Maximilians-Universität Würzburg

vorgelegt von

Markus Hügel

aus Aschaffenburg

Würzburg 2018

Eingereicht bei der Fakultät für Chemie und Pharmazie am

. . . . . .

Gutachter der schriftlichen Arbeit

1. Gutachter: . . . . . .

2. Gutachter: . . . . . .

Prüfer des öffentlichen Promotionskolloquiums

1. Prüfer: . . . . . .

2. Prüfer: . . . . . .

3. Prüfer: . . . . . .

Datum des öffentlichen Promotionskolloquiums

. . . . . .

Doktorurkunde ausgehändigt am

. . . . . .

Danksagung

Ein besonderer Dank gilt zunächst meinem Betreuer Prof. Dr. Matthias Lehmann für die Bereitstellung des spannenden Themas und für die intensive Betreuung dieser Arbeit. Seine Hilfe und Unterstützung bei dem Erstellen von Modellen waren ausgesprochen lehrreich. Hierbei danke ich Ihm insbesondere für das Erstellen der Modelle von **S2**$_{C12}$**-F1**$_{C10}$ und **S2**$_{C12}$**-F1**$_{C16}$. Auch für die Möglichkeit, an zahlreichen Tagungen teilzunehmen, bin ich ihm sehr dankbar. Weiterhin möchte ich dem gesamtem Arbeitskreis für fachliche Diskussionen und das stets hervorragende Arbeitsklima danken. Moralische Unterstützung habe ich von meiner Frau Linda und meiner Familie erfahren, wofür ich ihnen herzlichst danke. Darüber hinaus danke ich:

- Dr. Matthias Grüne für die Durchführung von NMR-Messungen und anschließenden Diskussionen
- Dr. Michael Büchner für die Einweisung in die MALDI-Messtechnik sowie Juliane Adelmann und Antje Heckmann für die Durchführung von diversen MS-Analysen
- Prof. Dr. Frank Würthner für die Bereitstellung von Messgeräten für die Absorptions- sowie Fluoreszenzspektroskopie sowie Moritz Dechant, Julian Herbert, Prof. Matthias Lehmann und Nikolai Scheuring für das Durchführen der vergleichenden UV/VIS-Messungen zwischen **S2**$_{C12}$**-F1**$_{C4}$, **S2**$_{C12}$**-F1**$_{C10}$ und **S2**$_{C12}$**-F1**$_{C16}$
- Ana-Maria Krause für die Durchführung der DSC-Messungen
- Prof. Dr. Christoph Lambert für das Ermöglichen von Cyclovoltammetrie-Messungen sowie Julian Schäfer für die Unterstützung bei der Durchführung dieser Experimente
- Prof. Dr. Heiner Detert für das Ermöglichen von Elementaranalysen an der Johannes Gutenberg Universität in Mainz
- Prof. Dr. Nazario Martín der Universität Complutense in Madrid für die Bereitstellung der chiralen Cyclopentenofulleren-Bausteine **76** und **77**
- Dr. Robert Graf für die Festkörper-NMR-Messungen am Max-Planck-Institut für Polymerforschung in Mainz
- Moritz Dechant und Nikolai Scheuring für das „Nachkochen“ der Verbindung **S2**$_{C12}$**-F1**$_{C4}$ für UV/VIS-Messungen einer frischen Probe
- allen Menschen, die sich an der Weiterentwicklung des Softwarepakets LaTeX beteiligen; insbesondere Clemens Niederberger für die Bereitstellung des Pakets „chemnum“, was das Verfassen dieser Arbeit wesentlich erleichtert hat

Veröffentlichungen

Teile dieser Arbeit wurden in folgenden Artikeln veröffentlicht oder sind dementsprechend in Vorbereitung:

- Hügel, M.; Dechant, M.; Scheuring, N.; Ghosh, T.; Lehmann, M. *ACS publications* **2018**, in Vorbereitung
- Lehmann, M.; Maier, P.; Grüne, M.; Hügel, M. *Chemistry - A European Journal* **2017**, *23*, 1060 – 1068
- Lehmann, M.; Hügel, M. *Angewandte Chemie International Edition* **2015**, *54*, 4110 – 4114; Deutsche Version: Lehmann, M.; Hügel, M. *Angewandte Chemie* **2015**, *127*, 4183 – 4187

Die Ergebnisse wurden bei folgendem mündlichen Vortrag vorgestellt:

Hügel, M. „New shape-amphiphiles self-assembling in filled columnar mesophases“, März 2016, BLCS DFKG Konferenz in Edinburgh, Vereinigtes Königreich

Ergebnispräsentationen in Form von Postervorträgen auf Konferenzen fanden wie folgt statt:

- Hügel, M.; Lehmann, M. „Oligo(ethyleneoxy) chains and their impact on the self-assembly of star shaped donor-acceptor mesogens“, April 2017, DFKG BLCS Konferenz in Würzburg, Deutschland
- Hügel, M.; Lehmann, M. „Star-shaped oligophenylenevinylene mesogens with covalently linked Fullerene guests“, September 2015, 13th European Conference on Liquid Crystals in Manchester, Vereinigtes Königreich
- Hügel, M.; Lehmann, M. „Star-shaped oligo-*p*-phenylenevinylene liquid crystals with fullerene guests“, März 2015, 42nd German Liquid Crystal Conference in Stuttgart, Deutschland
- Posterpreis: Hügel, M.; Lehmann, M. „Star-shaped oligo-*p*-phenylenevinylene mesogens with fullerene guests“, März 2014, 41st German Liquid Crystal Conference in Magdeburg, Deutschland
- Hügel, M.; Lehmann, M. „Star-shaped oligo-*p*-phenylenevinylene mesogens with fullerene guests“, September 2013, 7th Workshop on Conjugated Oligomers and Polymers (COPO) in Retzbach, Deutschland
- Hügel, M.; Lehmann, M. „Ordered Donor-Acceptor-Pairs for Organic Photovoltaics“, März 2013, 40th German Liquid Crystal Conference in Paderborn, Deutschland

Contents

Abbreviations

Col	Columnar phase
Col_{borh}	Body-centered orthorhombic columnar phase
Col_h	Hexagonal columnar phase
Cr	Crystal
DBPO	Dibenzoyl peroxide
DCC	*N*,*N*'-Dicyclohexylcarbodiimide
DCM	Dichloromethane
DIBAL	Diisobutylaluminium hydride
DMF	*N*,*N*-Dimethylformamide
DMSO	Dimethyl sulfoxide
DPTS	4-(Dimethylamino)pyridinium 4-toluenesulfonate
ESI	Electrospray ionization
GPC	Gel permeation chromatography
h	Hour(s)
HRMS	High resolution mass spectrometry
I	Isotropic phase
LC	Liquid Crystal
MALDI	Matrix assisted laser desorption ionization
MAXS	Medium-angle x-ray scattering
M_W	Molar mass
MS	Mass spectrometry
NBS	*N*-Bromosuccinimide
NMG	*N*-Methylglycine
NMR	Nuclear magnetic resonance
PPTS	Pyridinium *p*-toluenesulfonate
rt	Room temperature
SAXS	Small-angle X-ray scattering
SmA	Smectic A phase
TCBQ	Tetrachloro-1,4-benzoquinone
THF	Tetrahydrofuran
TLC	Thin layer chromatography
TOF	Time of flight
v/v	Volume ratio
WAXS	Wide-angle X-ray scattering
XRS	X-ray scattering

Abbreviations for NMR-technique:

δ	Chemical shift
J	Coupling constant
$\Delta\nu$	Difference in frequency
C_p	Primary carbon
C_s	Secondary carbon
C_t	Tertiary carbon
C_q	Quaternary carbon
s	Singlet
d	Doublet
t	Triplet
q	Quartet
m	Multiplet
ov	Overlapped
COSY	Correlation Spectroscopy
DEPT	Distortionless Enhancement by Polarization Transfer
HMBC	Heteronuclear Multiple Bond Correlation
HSQC	Heteronuclear Single Quantum Coherence

1 Motivation

Facing worldwide increasing energy consumption, the established industries that are mainly based on fossil fuels will struggle to keep up with the demands within the next decades. Additionally, environmental concerns propose a rather swift transition to alternative energy resources with a stronger focus on sustainability. Therefore, a lot of effort is put into the development of new methods relying on hydropower, wind power and solar energy. Since the power generation by moving water or air is linked with strong geographical constraints, collecting the almost endlessly available light energy will become one of the most important types of power production on the global market. The direct conversion of photon energy to electric energy is currently dominated by inorganic multijunction cells and silicon based photovoltaic cells, the latter reaching efficiencies of 20 to 25% (see figure 1). Due to the high material costs and the toxicity related to the manufacturing process, new cell designs are investigated. Perovskite cells emerged only a few years ago and already show efficiencies around 20%.[1] However, in these types of cells the usage of lead still is vital and therefore their utilization is highly controversial. Purely organic structures as active materials so far show promisingly low production costs, but long-term stability and conversion efficiencies do not meet the desired standards. The tremendous research in this field has not yet brought forth the significant improvement needed in these terms.

For a striking performance, the morphology of the organic material is of utter importance. Inspired by nature, scientists try to imitate the vast processes given e.g. in the photosynthetic apparatus. The complexity of self-assembly mechanisms and nanosegregation of the functional units here are unrivaled. Liquid crystals (LC) bear the unique combination of anisotropic properties and fluidity and therefore are promising candidates in this regard. In LC phases with positional order, there are at least two nanosegregated building blocks. Self-assembly and an optimized filling of free space in these systems in principle allow for the precise control of interesting supramolecular structures. Moreover, stability

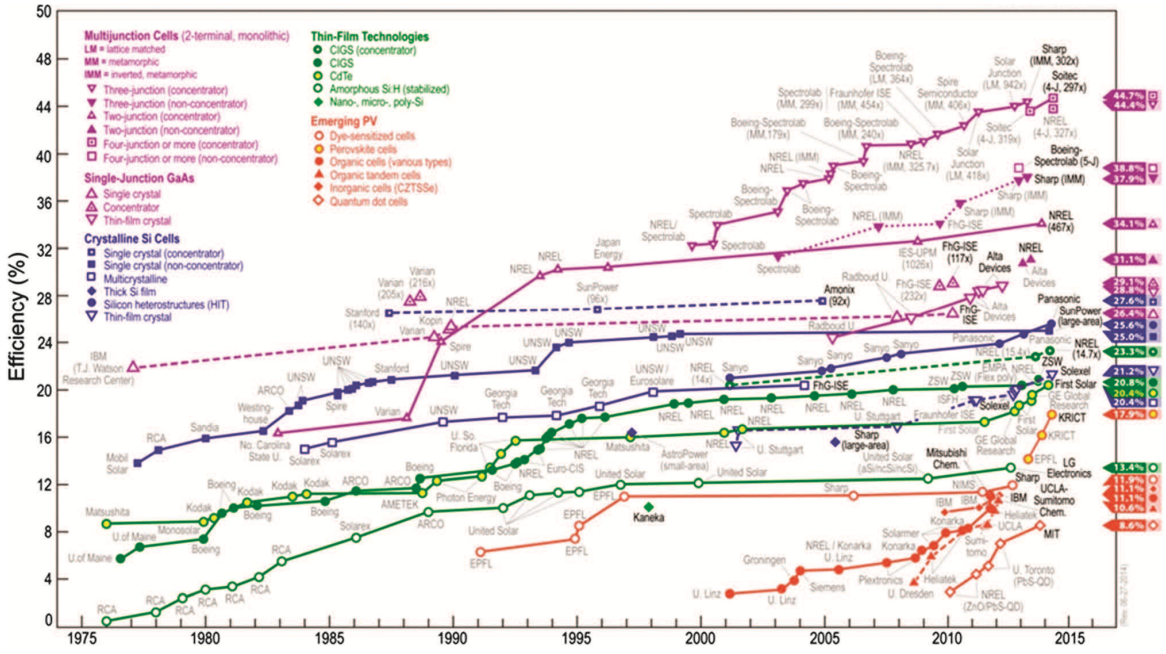

Figure 1: Current certified best power conversion efficiencies for a variety of photovoltaic cell designs. Image reproduced with permission of the rights holder, The Royal Society of Chemistry.

issues of photovoltaic cells can be addressed with the self-healing properties of the fluid LCs. Several liquid crystals have already been reported to show competitive charge transport.[2–4] Despite these encouraging findings, LC materials so far have only been used as mixtures or additives in organic photovoltaic cells.[5] The challenge of producing an efficient cell can be pinned down to following key points:

- Two semiconductors with distinct electron affinity ("donor" and "acceptor"; D and A) need to be separated in the active material to facilitate charge separation of the migrating excitons at the D-A interface.
- To compensate for the small exciton diffusion length and therefore to afford optimal exciton migration to the D-A interface, the bulk phase must possess a defined nanostructure.
- The size of the donor and acceptor phases ideally amount to approximately 10 nm in order to allow the charges to efficiently separate and thus to minimize charge recombination.
- The conducting channels must be aligned in a way that charge carriers efficiently migrate towards the electrodes.

The first two points can be addressed by the double-cable approach, in which the two distinct semiconductors form a superstructure of continuously adjoined channels. The last condition can be met with the potential alignment of liquid crystals via external stimuli. The required homeotropic alignment, in which the conducting channels are oriented perpendicular to the electrodes, is often achieved by slow cooling of the isotropic melt into the LC phase. This time-consuming process involves the potential risk of thermal decomposition. As a consequence, a clearing temperature < 200 °C for the liquid crystal is desired. The porphyrin fullerene dyad shown in figure 2 forms a liquid crystalline phase, in which the porphyrins give columnar arrangement and the fullerenes form three separate, slightly twisted helical channels along the columnar axis. A polymer solar cell with a physical blend of the dyad and PCPDTBT* with 1:1 weight ratio as the active layer shows a power conversion efficiency of 3.36 %, better than that of a typical 1:1 blend of the well-known fullerene derivative phenyl-C_{61}-butyric acid methyl ester (PCBM) and PCPDTBT.[6]

Ohta *et al.* have prepared several phthalocyanine fullerene dyads, in which the carbon allotrope is attached via a long flexible spacer (see figure 3). Here, the fullerenes might be regarded as exo-ligands and form a single helix along the columnar axis. Many of the compounds shown achieve spontaneous alignment of the channels in their columnar phases on glass substrates.[7,8] These results look promising but no data regarding applications in organic photovoltaic or other semiconductor technologies have been published yet. These examples of the double-cable approach all have the disadvantage of relatively small donor and acceptor areas, facilitating the recombination of the separated charges (third condition). A potential solution is to blend the material with additional fullerene derivatives to increase the size of the acceptor phase.[9]

The aim of this work is the synthesis of a liquid crystalline system, in which a donor oligomeric π-system is attached to a core unit and nanosegregated from an acceptor unit, as depicted in figure 4. The latter has a defined distance to the donor owing to the incorporation in a void provided by the

*[poly[2,6-(4,4-bis-(2-ethylhexyl)-4*H*-cyclopenta[2,1- b;3,4-b']-dithiophene)-*alt*-4,7-(2,1,3-benzothia-diazole)]

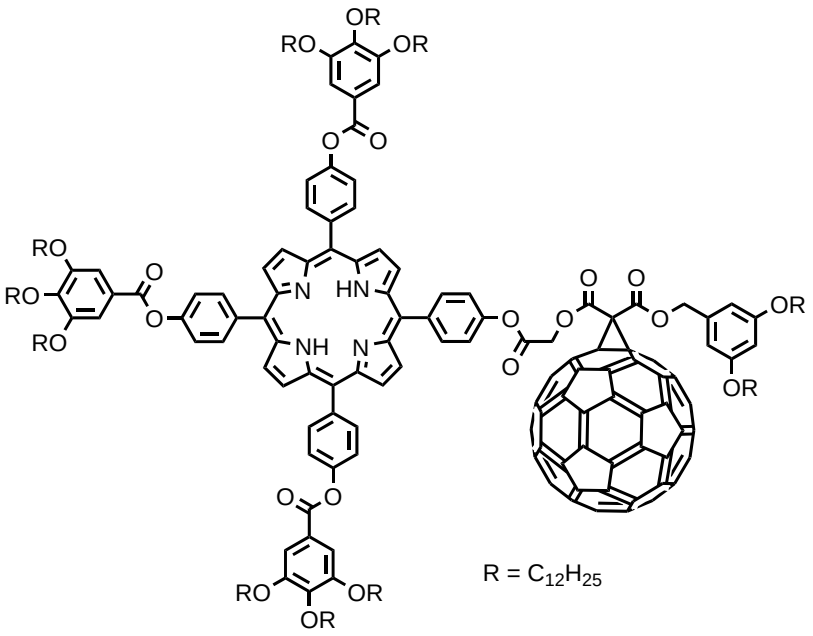

Figure 2: Porphyrin fullerene dyad prepared by Cheng *et al.* utilizing the double-cable approach.

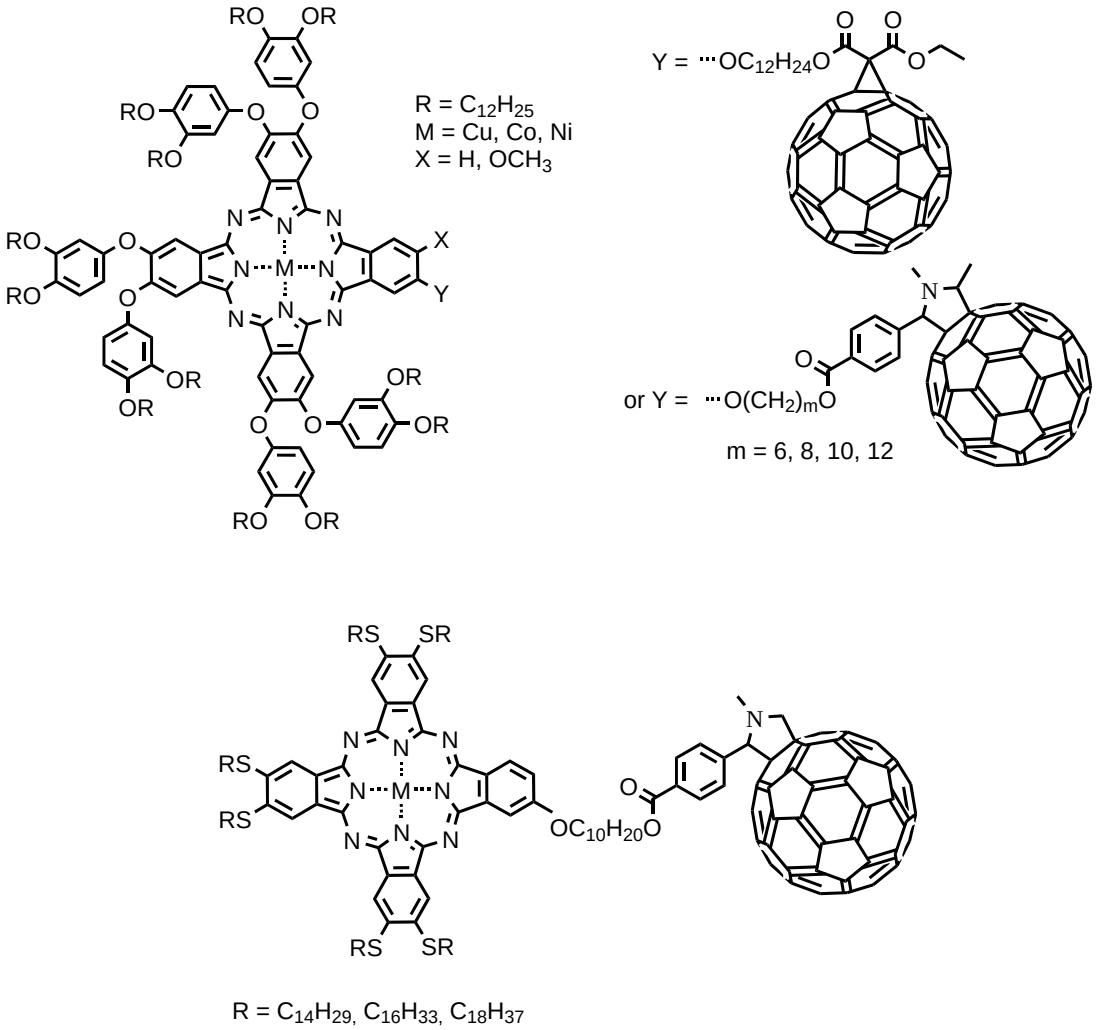

Figure 3: Several dyads examined by the working group of Ohta.

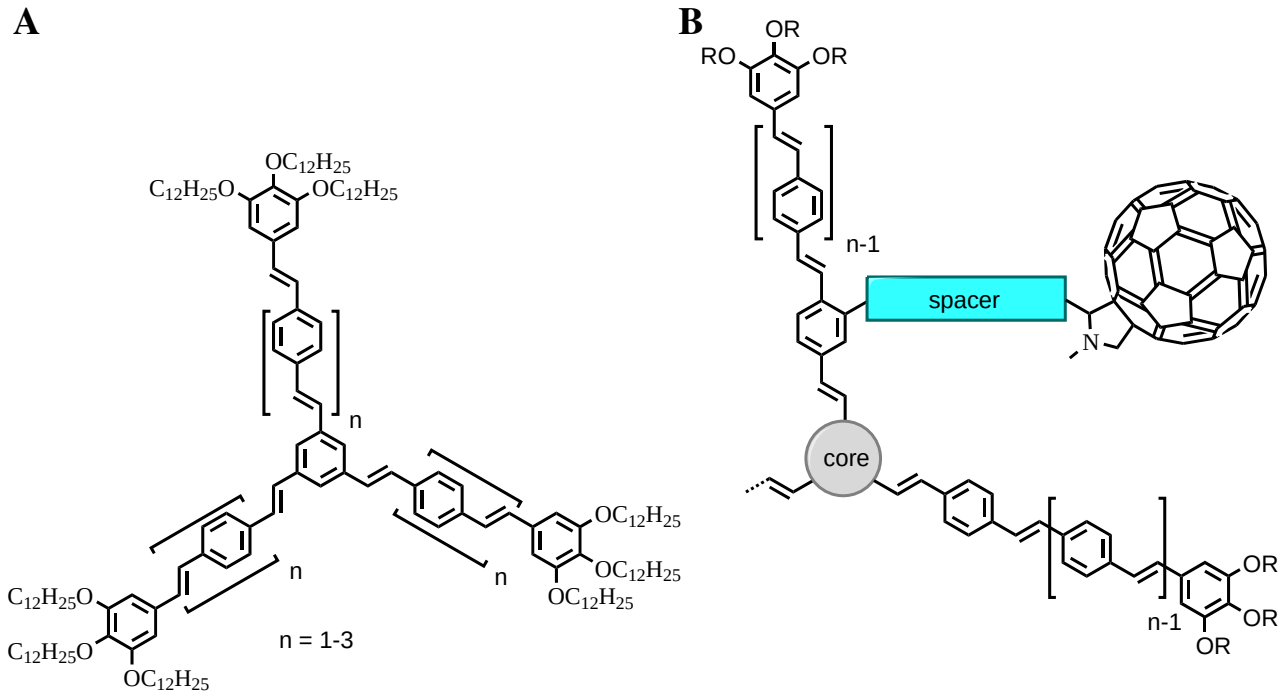

Figure 4: **A**: Star-shaped stilbenoid mesogens forming columnar phases; **B**: Target molecules of this work.

rigid oligomeric scaffold. The resulting nanomorphology shall give separated donor and acceptor assemblies of controlled size with a large interface. As donor material, linear oligomeric stilbene units are promising candidates. Corresponding polymers have already been established in photovoltaic cells.[10] Furthermore, studies revealed that only a few repeating units are necessary to facilitate efficient charge separation.[11] Three-armed stilbene stars with a benzene core (see figure 4A) form liquid crystalline columnar phases over broad ranges of temperature. The packing of these stars in the LC phases is not yet understood. The synthesis of larger derivatives (n > 1) and corresponding structural investigations will clarify the structure-property relationship of these systems. The large intrinsic free space between the arms should qualify these materials for the inclusion of fullerenes as electron conducting material. Oligomeric fullerene-stilbene dyads already have been examined towards their photophysical properties and show long-lived charge separated states for a repeating unit number equal to three or more.[12] Hence, the synthesis of the target compounds shown in figure 4B is desired. The star-shaped molecules consist of a core, to which several linear arms are attached. At one or more arms, an additional flexible spacer will be attached to introduce fullerene building blocks. For a profound understanding of this system, several structural units will be varied:

- The core unit presets the number of arms attached, which has a tremendous impact on the size of the cavities. Additionally, chromophores as core units will shift the hole transport from the stilbene arms to the cores, enhancing charge separation.

- The number of stilbene repeating units also determines the size of the cavities and therefore plays a major role in the potential uptake of the fullerenes in these voids.

- The length of the spacer between the stilbene arms and the fullerenes also sets the distance of the carbon allotropes to the columnar arrangement, influencing the nature of the anticipated fullerene helix.

- The peripheral chains, denoted as R, induce the fluidity of the liquid crystals and determine the nature and clearing temperature of the formed phase. A rather low isotropization temperature is necessary to align the semiconductor channels accordingly. Besides the typical aliphatic chains, also polar oxygen-rich chains will be incorporated. These are known for lowering the clearing temperature and for drastically increasing the dielectric constant for the organic materials, which is predicted to boost the efficiency in photovoltaic cells via a facilitated separation of the bound charge pair.[13]

The shown fulleropyrrolidines have a chiral center and are synthesized as racemic mixtures. An enantiomerically pure target of different structure will also be synthesized in collaboration with the group of Nazario Martín (Universidad Complutense de Madrid) to clarify the role of the chiral fullerene building block on the handedness of the anticipated helix.[14]
A preferably low clearing temperature should be achieved by the molecular design, allowing homeotropic alignment to be obtained by slowly cooling from the isotropic state without the occurrence of thermal decomposition. The thermotropic properties will be examined via polarization microscopy and DSC analysis. Additional structural details of the anticipated assemblies will be studied by X-Ray diffraction, modelling and X-ray simulation. Subsequently, the photophysical properties will be investigated to gain understanding of potential energy and charge transfer properties.

2 Basics

2.1 Liquid crystals

When the "double melting" behavior of cholesteryl benzoate was discovered as early as 1888, it took another few decades for the scientific community to accept the fact, that there is a state of matter, in which the properties of fluidity and anisotropy coexist. In the beginning classified as "liquid crystals" (LC), these phases later turned out to be not crystalline at all. Nevertheless, the term persisted over the time and nowadays is generally accepted. Since these states always lie between the crystalline and the isotropic state, they belong to the group of *meso*phases (from Ancient Greek $\mu\acute{\varepsilon}\sigma\omega\varsigma$, "middle") and the materials capable of forming mesophases are called mesogens. Besides the liquid crystals, other forms of soft matter have shown to be mesophases, e.g. plastic crystals.

The first types of LC phases to be discovered were the ones of rod-like molecules, also called calamitics (see figure 5). In a typical example, a polar and rigid core is combined with a flexible apolar chain. These mesogens tend to align with their long axes parallel to the director *n*, giving the nematic phase (N), in which there is exclusively long-range orientational order. In the case of chiral mesogens or an achiral host doped with a chiral material, an additional helical macrostructure may be formed due to steric repulsions. The director in this chiral nematic phase (N^*) continuously twists along the helical axis. Rods also can form lamellar structures with positional order. The apolar chains and the polar rigid rings then are nanosegregated. In the simplest case, the mesogens are arranged in diffuse layers with their long axes, on average, orthogonal to the layer planes. In this smectic A phase (SmA), the average correlation length along the layer amounts to only a few molecular centers, preventing periodicity between the layers. The diversity of liquid crystalline phases formed by rod-like molecules has been explored with considerable effort. As the arrangements of rods with low viscosity are readily manipulated by electric and magnetic fields, switching technologies such as liquid crystal displays have emerged in everyday life.[15]

In 1977, it was found that not only rod-like but also disc-shaped molecules form liquid crystalline phases.[16,17] The most typical cores used for discotic mesogens are triphenylene, phthalocyanine and hexabenzocoronene derivatives, which are decorated with flexible chains in the periphery (see fig-

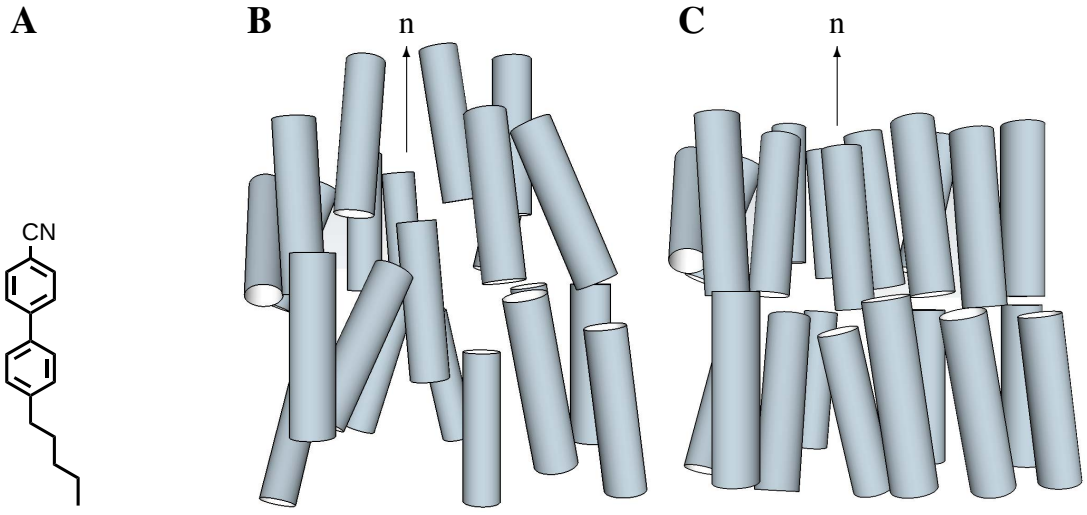

Figure 5: Rod-like liquid crystals. **A:** 5CB, a typical rod-like liquid crystal forming a nematic phase **B**: Schematic illustration of the nematic phase; n: director **C**: Schematic illustration of the smectic A phase; n: director.

ure 6). In the discotic nematic phase (N_D), they align along a director with their short molecular axes and without positional order. However, the most common observed supramolecular structure is the columnar arrangement induced by stacking of the discs, often via $\pi - \pi$ interactions. Additional helical arrangements along the columnar axis are feasible if the discs have lateral bulky groups attached. The columns can pack in different ways to form two-dimensional lattices. The simplest and most observed is the hexagonal arrangement (Col_h), in which every column is equidistantly neighbored by six others. Just as for the smectic A layers, there is no periodicity between the mesogens of different columns and only a short-range positional order within one column. Other arrangements include rectangular and oblique unit cells. Furthermore, the discs can also be tilted with respect to the planes orthogonal to the columnar axis. In some cases even 3D lattices like the body-centered orthorhombic cell are possible (figure 6H,I).[15,18,19] Many discotic mesogens have shown to act as one-dimensional semiconductors along the columnar axis and are considered promising candidates for applications in plastic electronics. However to this day, discotic LCs are not established in commercial technologies such as photovoltaics or thin-film transistors.[20]

Rods and discs belong to the group of conventional liquid crystals, in which the tendency to form mesophases is explained by the shape-anisotropy of the cores. The progress in the development of theoretical concepts for liquid crystallinity led to the understanding that virtually all molecules, regardless of the shape, are capable of forming LC phases with positional order if they possess amphiphilic character. This proposes that every mesogen contains two or more distinct and to a certain degree incompatible segments, including the nature of chemistry (polar $\leftrightarrow$ apolar; hard $\leftrightarrow$ soft), of rigidity (rod, disc or sphere $\leftrightarrow$ flexible chains) and of shape (rod $\leftrightarrow$ sphere $\leftrightarrow$ disc). Figure 7 shows well-known examples of *nonanisometric* mesogens forming columnar LC phases.[21]

Non-conventional mesogens are molecules of non-classical shape. Here, the driving force for the formation of the LC state is the nanosegregation of the incompatible building blocks as well as the filling of space, which is a crucial aspect for the formation of condensed phases in general. The importance of the latter is demonstrated by the binary mixtures of a double-swallow tailed compound (weak donor) and trinitrofluorenone (acceptor), presented by Pelzl *et al.* While the neat donor forms a columnar phase and the acceptor is nonmesogenic, stable nematic, lamellar and cubic phases are formed in the region of well-balanced mixing ratios. The smaller acceptor molecules occupy the free space in the voids of the lamellar arrangements of the donor mesogens. It is noteworthy, that the major role here is played by steric interactions and not donor-acceptor-interactions.[22]

Among the non-conventional liquid crystals are the star-shaped mesogens, in which three or more linear, oligomeric arms with peripheral chains are bound to the same core via covalent or supramolecular interactions to give molecular or supermolecular[23] LCs (see figure 8). Mesogenic stars with just three arms are called Hekate stars and stand out with their large void between the arms. Since a tight packing of the molecules is required, these stars fill those gaps in different ways, strongly depending on the flexibility of the repeating units in the arms.[21,24] Understanding the mechanism of packing and using the voids to incorporate supramolecular guests is part of this work.

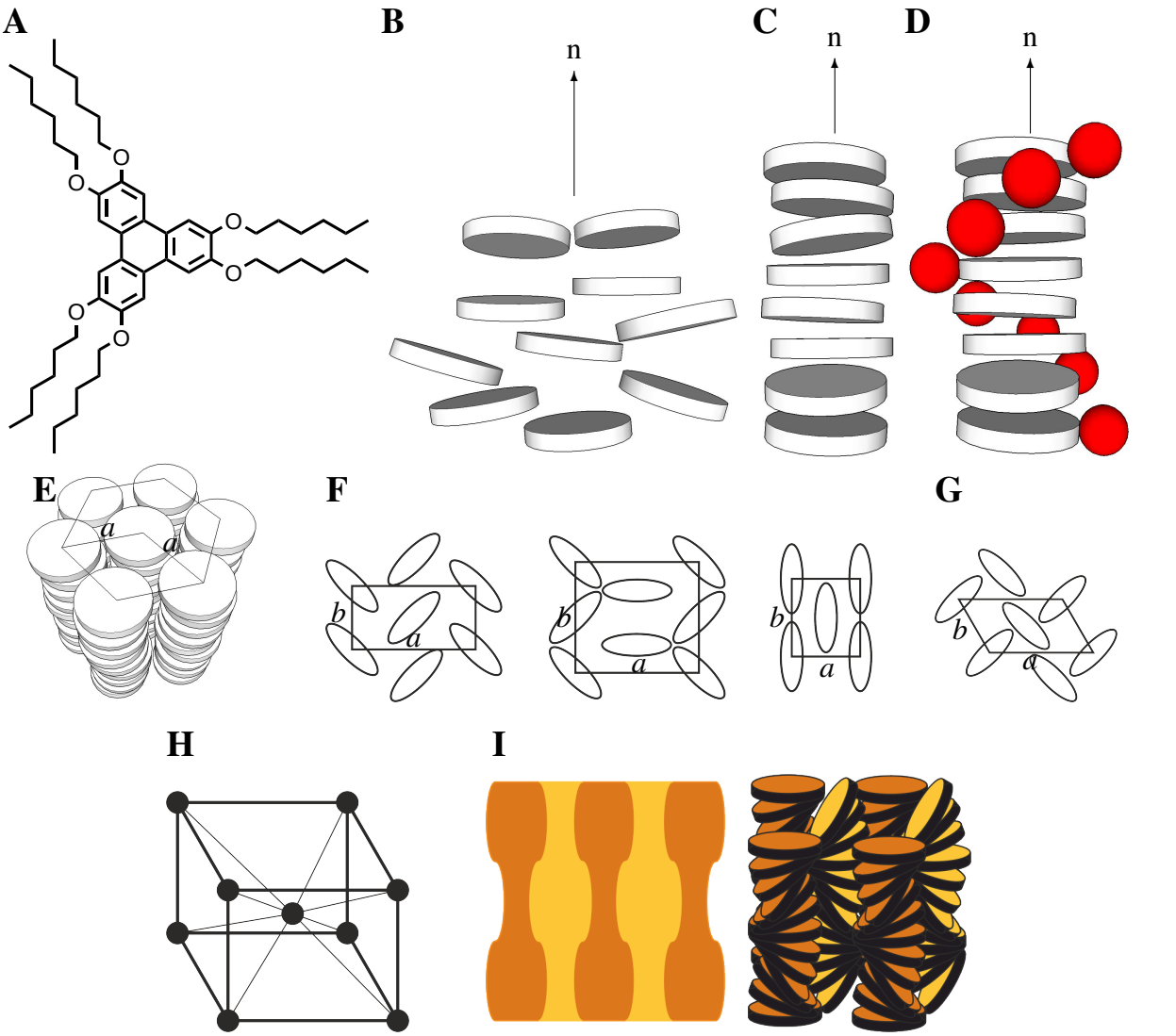

Figure 6: Discotic liquid crystals. **A:** Triphenylene derivatives are one of the most examined discotic mesogens **B**: Arrangement in a nematic phase of discotic mesogens **C**: Schematic illustration of a columnar arrangement; n: director **D**: A helical arrangement along the columnar axis; n: director **E**: Schematic illustration of the hexagonal columnar phase (Col_h); The inserted hexagon pictures the intrinsic symmetry and the parallelogram represents the unit cell; *a*: cell parameter for the hexagonal lattice **F**: Top view of the columnar rectangular (Col_r) arrangements with different space-group symmetries; *a*, *b*: Cell parameters for the rectangular lattice **G**: Top view of the columnar oblique (Col_{ob}) phase; *a*, *b*: Cell parameters for the oblique lattice **H**: Bravais lattice of a body-centered orthorhombic cell **I**: Example for a 3D body-centered orthorhombic LC phase.

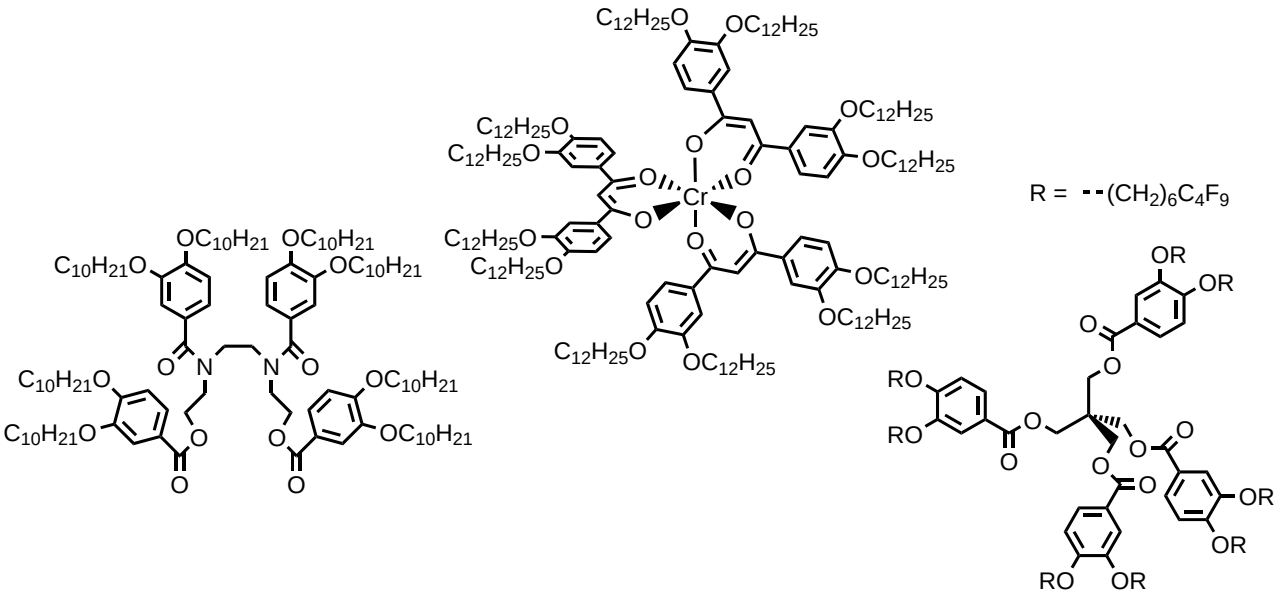

Figure 7: Typical examples of mesogens forming columnar LC phases despite the lack of shape-anisotropy for the cores.

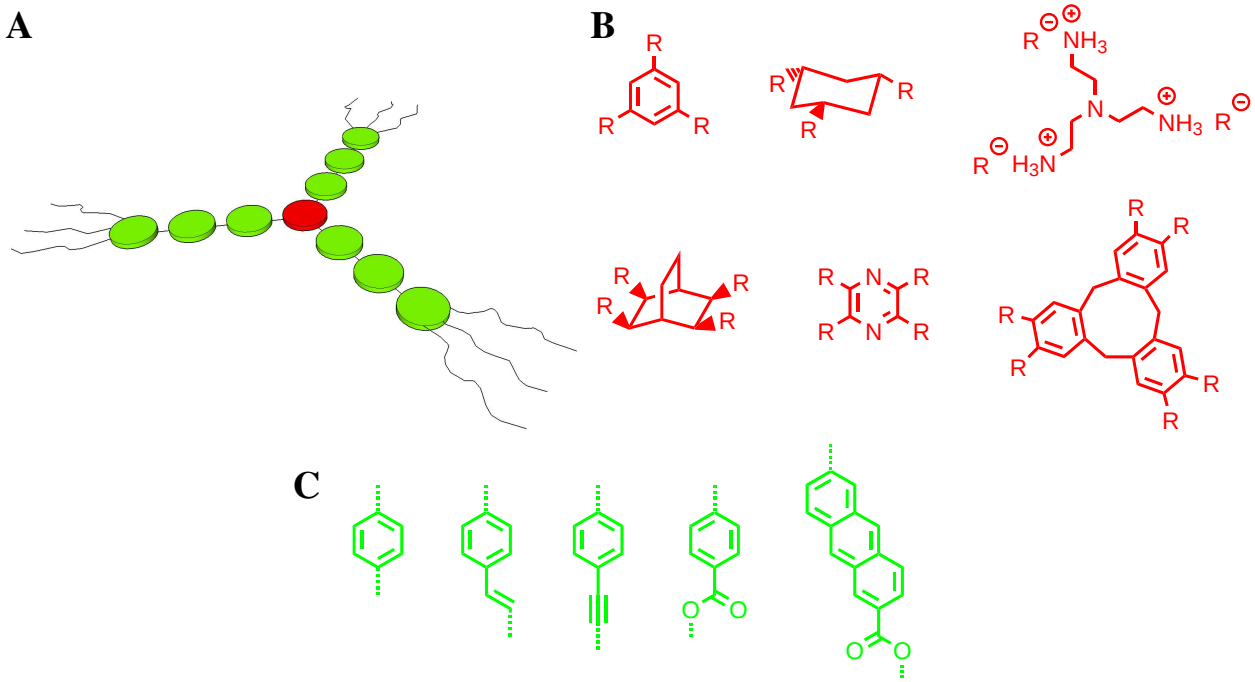

Figure 8: Star-shaped mesogens. **A:** Schematic illustration of a star-shaped mesogen with three arms **B**: Examples for cores in liquid-crystalline stars **C**: Examples for arm repeating units with different rigidity in mesogenic stars.

2.2 Optical microscopy studies

The polarized optical microscopy (POM) technique usually is the first step to quickly gain an overview of the phases formed at different temperatures, since only small amounts of the material are needed and the required devices are rather cheap compared to other methods. The sample, located between two crossed polarizers, is sandwiched between a glass slide and a cover slip. If the examined material is of isotropic nature at the set temperature, the incident beam, linearly polarized from the first filter (polarizer), will pass the sample unaffected. Thus the light rays are blocked at the second filter (analyzer), which is perpendicular to the plane wave, resulting in darkness. If, however, the sample shows anisotropic behavior like most mesophases do, the polarization plane will be rotated and the light will pass the analyzer, resulting in so called textures visible to the human eye (see figure 9). The appearances of these images arise through changes in the orientation of the LC director throughout the sample, caused by defects such as singularities, lines and walls.[15]

For a nematic phase, the most observed textures are the 2-brush and the 4-brush defects (*schlieren* textures, see figure 10). Dark lines, caused by LC directors lying parallel to the polarizers hence not altering the polarization plane, run throughout the sample and converge at a point defect side, giving brushes.[15,18] In the columnar phase, typical patterns are the pseudo focal conic (fan-like) and the mosaic texture, as illustrated in figure 11.[25,26]

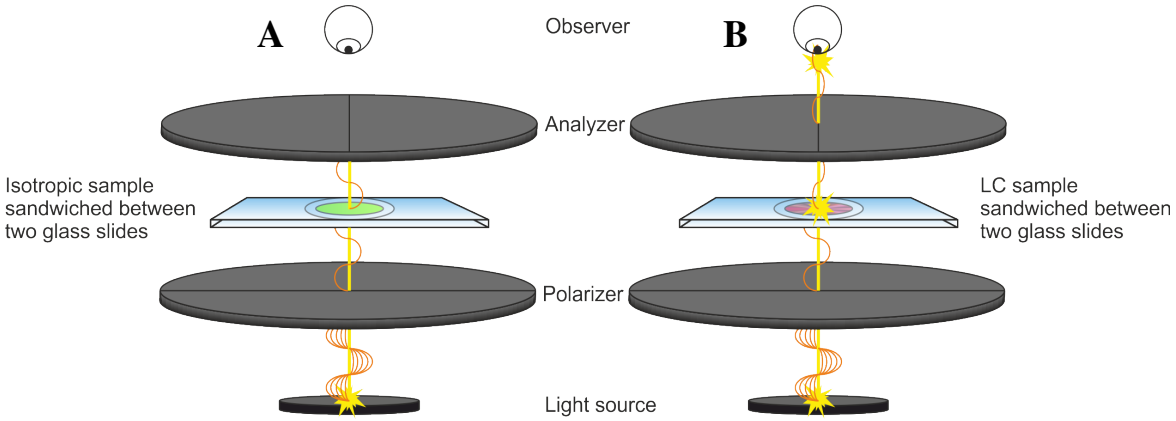

Figure 9: Schematic illustration of POM experiments. **A:** The polarization plane of the incident beam is not altered by the isotropic sample. Therefore, no light is observed **B**: The anisotropic properties of the LC sample rotate the plane of polarization. Hence the analyzer does not block the beam.

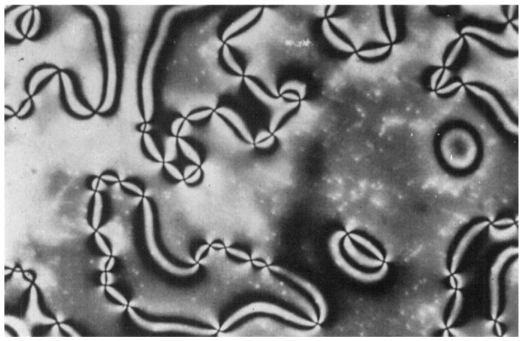

Figure 10: 4-brush defects observed in a nematic liquid crystal. Image reproduced from reference[27] with permission from The Royal Society of Chemistry.

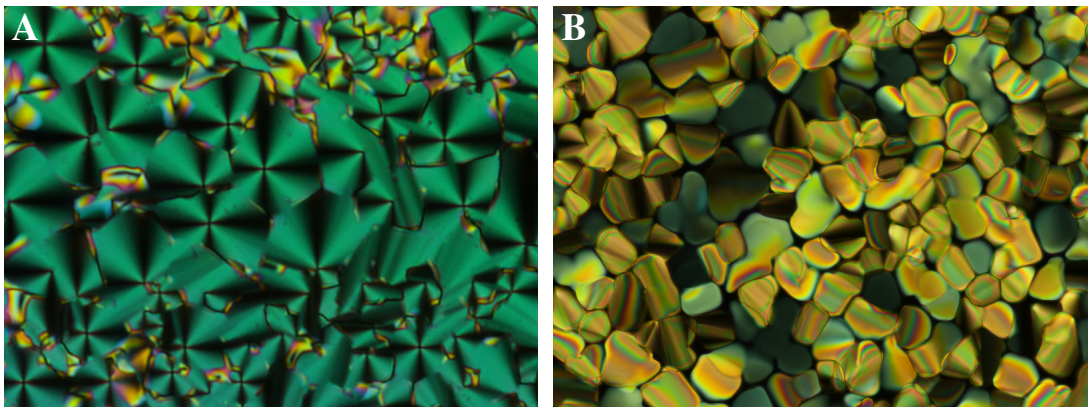

Figure 11: Textures for columnar phases. **A:** Pseudo-focal-conic. **B**: Mosaic-like.

2.3 X-ray scattering investigations

Textures observed with polarized optical microscopy allow to determine the nature of a mesophase. To confirm the proposed structure, additional techniques are required. X-ray scattering (XRS) experiments have several advantages compared to other methods like neutron scattering and electron microscopy, since only rather small quantities of the sample are required and the measurements can be carried out in a large range of temperature.[18] The basis for the XRS technique is the Bragg´s law. It states that constructive interference between the rays reflected by adjacent planes in a crystal will occur, when the path difference $2d \cdot \sin(\theta)$ equals an integral multiple n of the X-ray wavelength λ: $2d \cdot \sin(\theta) = n\lambda$ (see figure 12).[15] Here, θ is the angle of incidence and d is the spacing between crystallographic planes. The direction of propagation of the scattered rays is therefore altered by an angle of 2θ. If the Bragg´s law is not satisfied, the scattering intensity is zero. The position, lineshape and intensity of the Bragg signals give information on properties like the interplanar spacings of the crystal and the correlation volume for the structure.[15]

XRS results with liquid crystals differ significantly from that of actual crystals. Patterns of oriented mesogenic samples usually show weak and diffuse intensities since there is only short-range positional order. In these systems, the correlations between two particles fall off exponentially with distance. The correlation length ξ can be estimated by the Scherrer equation $\xi = K\lambda/(FWHM \cdot \cos(\theta))$, where FWHM is the radian measure of the full width at half maximum of the signal. K is the Scherrer con-

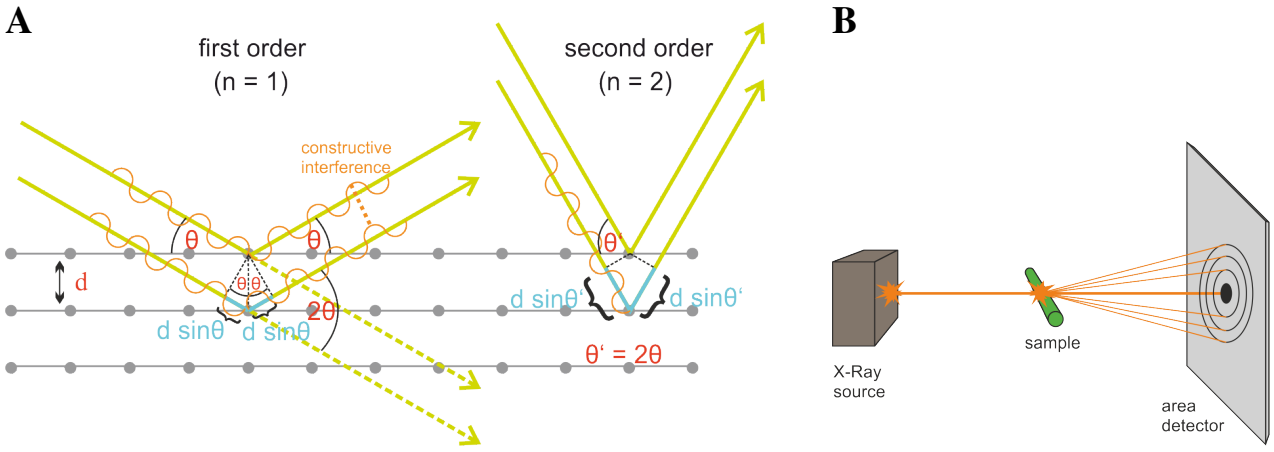

Figure 12: X-ray scattering investigations. **A:** Scattering of X-Rays with an angle of incidence θ from parallel planes of a crystal with a distance of d **B**: Illustration of an experimental XRS setup. For macroscopically unaligned LC samples, diffraction patterns with circular signals are obtained.

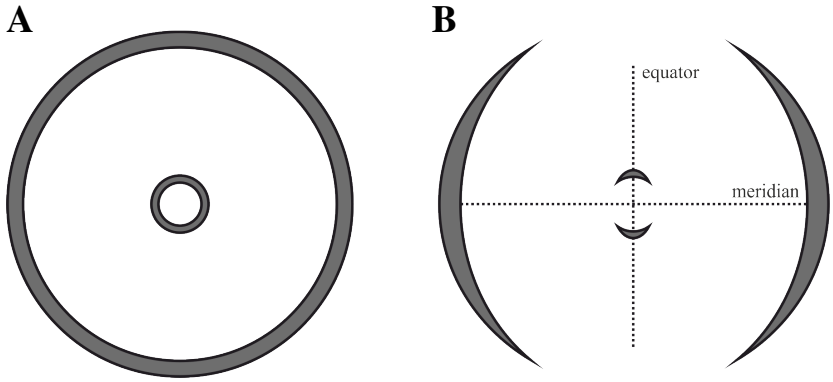

Figure 13: A: Schematic diffraction pattern of an unaligned nematic sample. It only contains ciruclar reflections and cannot be distinguished from an isotropic sample **B**: For an aligned sample, signals with orientation are obtained.

stant and its value depends on many factors like the shape of the crystallites and their size distribution. Its value usually lies close to 1 and for assumed spherical particles can be estimated as 0.9.[15,28,29]
Unaligned samples have multiple domains with random orientation. In that case, the patterns will only give circular rings just as for powder samples of crystals. Figure 13 shows illustrative patterns of an unaligned and aligned nematic sample, respectively. Without macroscopic orientation, the pattern does not differ from an isotropic sample. The sharper reflections in the short-angle region correspond to the average molecular diameter. As the correlation length in these phases is very low, usually only a single reflection is observed along the equator in one direction. The diffuse intensities at the wide-angle region are labeled as halo and mainly origin from chain-chain correlations, which usually have average distances of ~ 4.5 Å, but also from hydrocarbon correlations between aromatics.[15]
For mesogens forming hexagonal columnar phases, a different pattern is obtained, which is highlighted in figure 14. Here, the correlation length is higher between the 2D ordered columns and several reflections appear along the equator.[18] The interplanar spacings of a hexagonal lattice can be calculated via $d_{hk} = \frac{2}{\sqrt{3}a}\sqrt{h^2+k^2+hk}$, where a is the lattice parameter, corresponding to the distance between two columns, and h and k are the Laue indices. These correspond to the Miller indices but also factor in that a reflection can be caused by diffraction of higher order.[30,31] In consequence, the ratio of reciprocal lattice spacings for a hexagonal columnar phase matches the characteristic values of $d_{10} : d_{11} : d_{20} = 1 : \sqrt{3} : 2$. In addition to the diffuse signals in the wide-angle region like for the nematic phase, a second set of sharper reflections arises due to the close packing of the discotic mesogens. Most often caused by $\pi - \pi$ aggregation, these signals correspond to a smaller distance of 3 - 4 Å. It is noteworthy that the signal intensity is strongly dependent on the nature of the core, that is the total electron charge, while the signal sharpness is determined by the correlation length.[18]
Besides $\pi - \pi$ aggregation, other stacking phenomena are known to occur along the columnar axis. Lateral bulky groups may induce helical arrangements to avoid steric repulsions. These structures are identified by a series of X-shaped reflections (see figure 14C). The helical pitch c then can be calculated from the hypothetical meridional distance ($2\theta_c = cos(\frac{\alpha}{2}) \cdot 2\theta_d$) and the Bragg equation ($c = \frac{\lambda/2}{sin(\theta_c/2)}$). The average distance between two molecules along the columnar axis is then c/Z, where Z is the number of molecules per cell unit.
For the analysis of thin films on surfaces, the GISAXS (grazing-incidence small-angle scattering) method has been established.

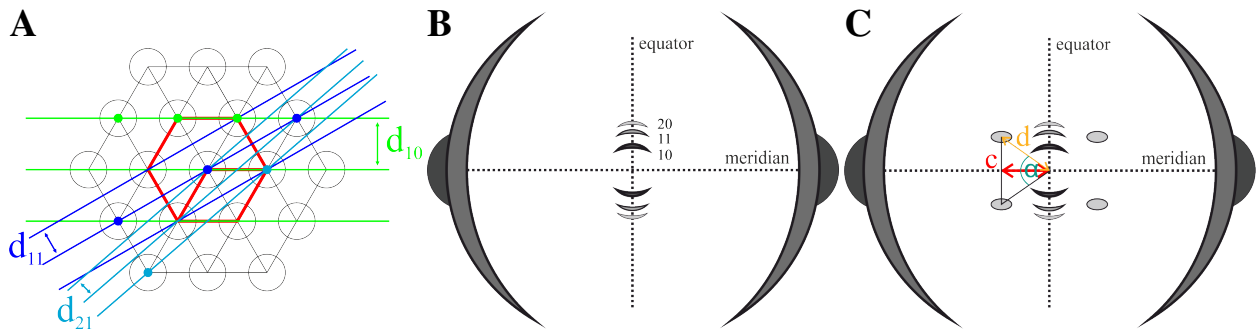

Figure 14: A: Examples of interplanar spacings in a hexagonal cell **B**: For a hexagonal columnar diffraction pattern of an oriented sample, several intensities along the equator with distances according to the hexagonal symmetry are obtained **C**: Additional helical arrangements along the columnar axis cause X-shaped Bragg signal patterns; d: spacing of the additional reflections; c: Hypothetical meridional distance of the reflection corresponding to the helical pitch.

2.4 Differential scanning calorimetry

To determine the temperature range of liquid crystalline phases, the differential scanning calorimetry technique (DSC) is frequently used. By measuring the relative uptake or output of heat from the sample with reference to an empty sample crucible, a thermogram is obtained, which displays the phase transitions as peaks (see figure 15). The underlying peak areas then are the latent heats ΔQ, which typically range from 0 - 10 kJ·mol^{-1}for a LC→LC or a LC→I transition and thus are much smaller than in the case of crystal melting processes. The transition temperatures T_{onset} are calculated by determining the maximum gradient in the heat flow from the peaks (T_{peak}). The thermograms are obtained from both heating and cooling and the process cycles are repeated to ensure reproducibility.[15]

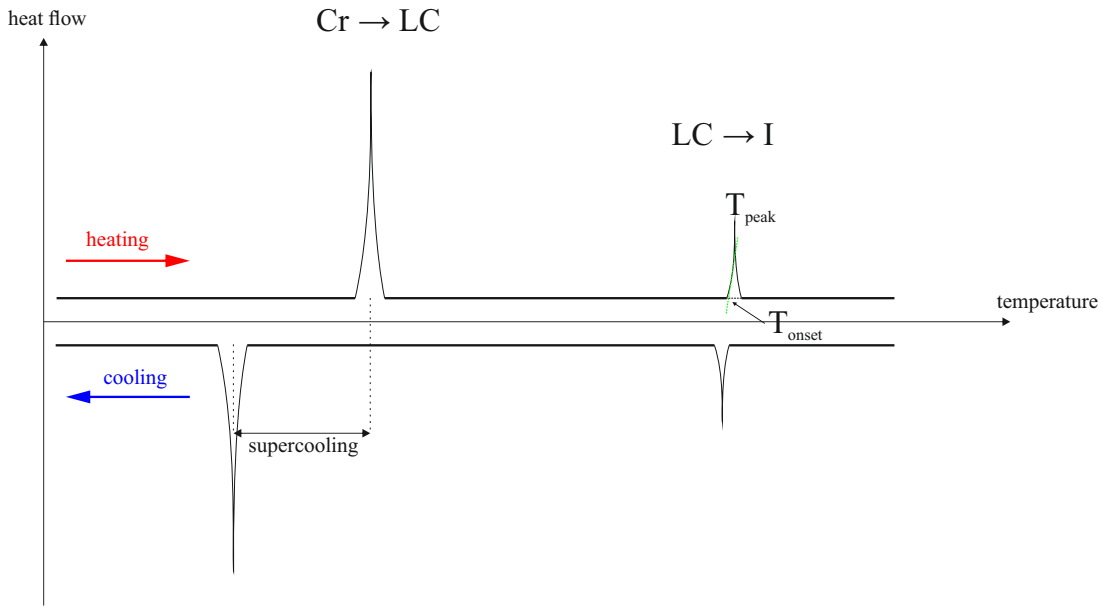

Figure 15: Illustration of a DSC thermogram. Usually, only a single heating-cooling cycle is displayed with the experimental data at the temperature limits capped.

2.5 Alignment of liquid crystals

For the application of liquid crystals in organic electronics, the macroscopic orientation of the LC directors is of utter importance. Figure 16 highlights the homeotropic order, which is achieved when all columns align normal to the given substrate. This arrangement is crucial for photovoltaic cells (here, the electrodes act as the substrates), since charge carrier mobilities along the columnar axis show drastically greater values and exciton diffusion lengths increased values compared to nonaligned samples.[20,32,33] When all columns lie in the plane of the substrates, a planar arrangement is given. This positioning is only of use for devices like thin film transistors if all columns point towards the same direction (unidirectional planar arrangement). However, aligning the mesogens in a columnar mesophase is considerably more challenging than in the case of calamitics for several reasons. In a columnar liquid crystalline phase, the viscosity of the material is notably larger compared to materials in nematic or smectic phases, hindering the spontaneous alignment in electric or magnetic fields. As discotics often possess negative anisotropy of the magnetic susceptibility ($\Delta\chi = \chi_{\parallel} - \chi_{\perp}$), the resulting magnetic field within the plane of the mesogen prevents homeotropic alignment of the columnar axes, when the magnetic field lies orthogonal to the plane of the substrates.[34] In some cases, special design of the mesogens led to a positive dielectric anisotropy, facilitating homeotropic ordering by the application of an electric field.[35–39]

A more versatile method is to slowly withdraw a pin from the material, which has been heated to the isotropic phase and then cooled to the columnar phase. Then, freely suspended strands are obtained.[40] As the columns will rather align with the local flow field, homeotropic ordering is favored. This preference can also be utilized by extruding the sample through a tiny hole, giving fibers with convenient shape for X-ray studies.[41]

However, both techniques cannot be applied to thin films confined between substrates. Spontaneous homeotropic alignment has been achieved by slow cooling of the sandwiched isotropic melt with the substrates acting as nucleation sites. Success depends on many factors like nature of the substrates[42–44], layer thickness[45] and thermal annealing parameters. The induction of homeotropic ordering in columnar LC phases with this approach has been extensively studied[46] for discotic mesogens, such as perylene derivatives,[47–52] phthalocyanines,[42,44,53–59] porphyrins,[60–63] triphenylenes,[45,52,64–70] donor-acceptor mixtures[71–74] and donor-acceptor dyads,[7,8,75,76] while the induction of homeotropic ordering in star-shaped mesogens has been examined only in a few cases[37,77–80]. Other strategies regarding thin films include irradiation[69,81–85] and functionalization of the substrate.[43,68,86–90] The alignment can be verified by either GISAXS studies[91,92] or by optical microscopy with orthoscopic and conoscopic imaging.[93]

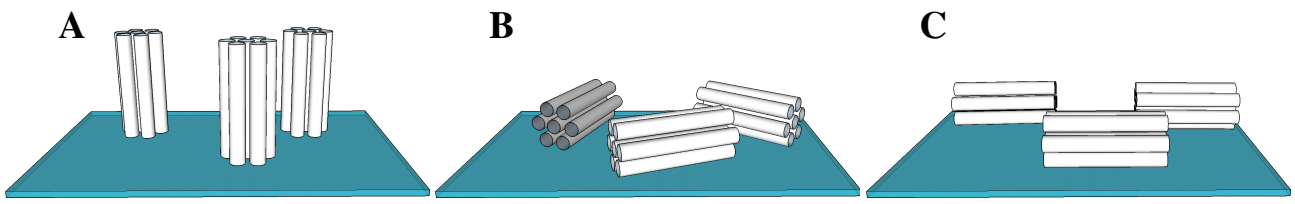

Figure 16: Schematic illustration of different orientations of LC columns in relation to a substrate. **A:** Homeotropic (face-on) alignment; the columns are oriented perpendicular to the substrate **B**: Planar (edge-on) alignment; the columns lie parallel to the substrate with a random distribution of column directors **C**: Uniaxial planar alignment; in addition to the edge-on alignment, the columnar axes point in the same direction.

2.6 Organic photovoltaics and donor-acceptor double cables

Since it became clear that organic materials show great potential for photovoltaic applications when an electron-donor and an electron-acceptor (semiconductors with different electron affinity) are combined in a thin film,[94] much effort has been put into their development and establishment in industry. Although these devices still cannot keep up with the efficiencies of the silicon based counterparts, they are advantageous in terms of production costs and flexibility. Besides, an abundance of design possibilities will boost the improvements of these materials over the next decades.[1] The main difference in the mechanism is that photoabsorption does not directly give charge separation but rather a tightly bound electron-hole pair, the so called exciton, which needs to reach the donor-acceptor interface by diffusion to initiate the ionization. Among the different types of organic photovoltaic cells is the bulk heterojunction cell (BHJ), which aims to maximize the surface between the electron-donor and the electron-acceptor by physical or chemical mixing of the semiconductors (see schematic illustration in figure 17). As the exciton diffusion length usually is limited to ~10 nm before relaxation to the ground state occurs, the separate channel compartments ideally are in the same range of size.[9,95] Besides polymers,[10,96] discotic liquid crystals particularly have been studied for the incorporation into photovoltaic cells as active materials.[97,98] In 1999, Müllen *et al.* demonstrated with a hexabenzocoronene derivative that discotics can act as excellent semiconductors in their liquid-crystalline state.[4] Efforts then were put into the combination of donor and acceptor motifs to facilitate the formation of separate n- and p-type channels. The double-cable approach originating from polymer research was adapted to the low molecular mesogens. Here, the distinct semiconductors form a superstructure of continuously adjoined channels, compensating for small exciton diffusion lengths.[9] However, this design concept raised the issue on how to remain the mesomorphic properties of the discotic mesogens. Bushby *et al.* then showed in their pioneering work that covalently bound fullerenes, which act as acceptor, can be helically arranged in a two-dimensional hexagonal superlattice of a columnar discotic liquid-crystalline donor. The columnar stacking here is obtained by complementary polytopic interactions between the triphenylene motifs of the corresponding dyad shown in figure 18A and a hexaazatriphenylene derivative within a binary mixture. A schematic illustration of the arrangement is displayed in figure 18B.[99] Imahori *et al.* then were able to achieve

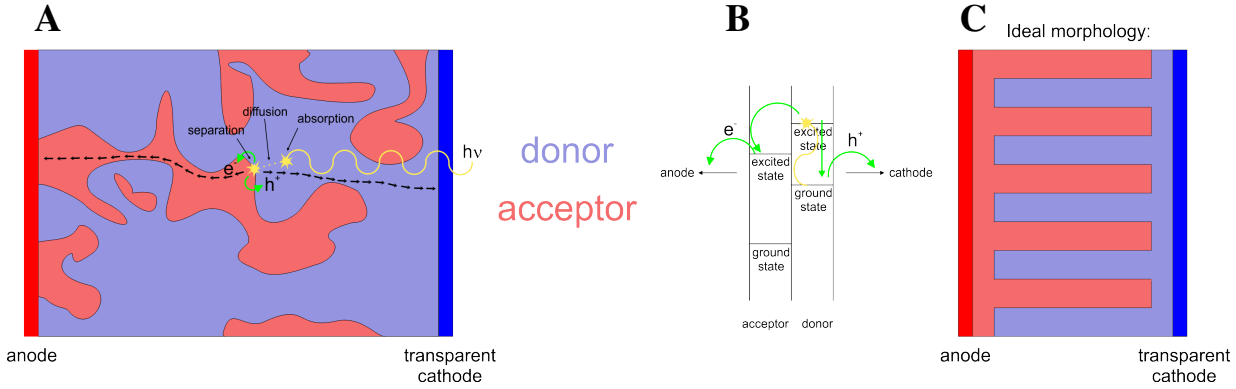

Figure 17: **A**: Schematic illustration of a bulk heterojunction cell (BHJ). A donor molecule absorbs a photon giving an exciton, which migrates to the donor-acceptor interface by diffusion. There, the electron is transferred to the lower lying acceptor LUMO, efficiently separating the charges. The electron and hole are then transported to the corresponding electrodes in the homogeneous channels. **B**: Energy levels at the donor-acceptor interface. **C**: Idealistic morphology for the donor and acceptor compartments in a BHJ cell.

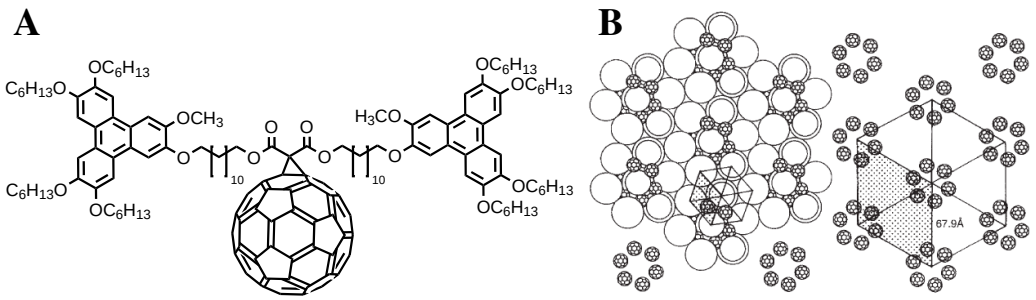

Figure 18: A: Triphenylene-fullerene dyad prepared by Bushby *et al.*. **B**: Proposed structure of the binary mixture between the dyad and a hexabenzocoronene derivative. The hexagonal unit cells of the lattice and superlattice are indicated by shading. Image reproduced with permission of the rights holder, The Royal Society of Chemistry.

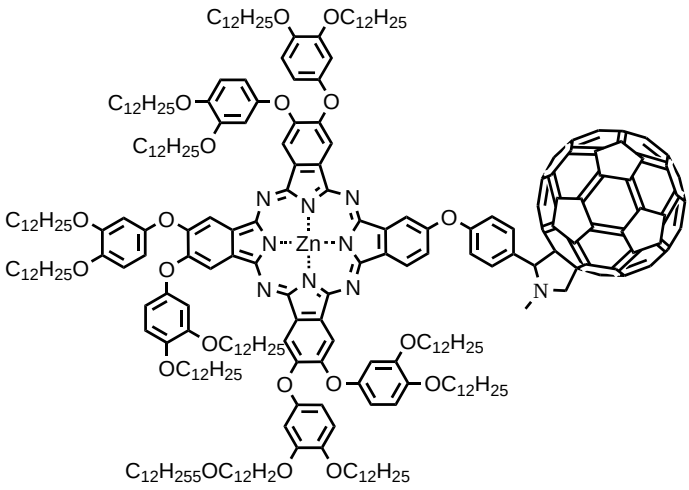

Figure 19: Phthalocyanine-fullerene dyad presented by Imahori *et al.*.

helical columnar ordering of a phthalocyanine-fullerene dyad as a single-component liquid crystal, which is displayed in figure 19. The columnar stacking here is realized by the phthalocyanine cores and the covalently attached fullerene moieties form a helix along the columnar axis. This heterojunction structure showed remarkable charge mobilities for both holes and electrons (TOF $\nu_h = 0.26 cm^2 V^{-1} s^{-1}$, TOF $\nu_e = 0.11 cm^2 V^{-1} s^{-1}$).[2] Geerts *et al.* already showed earlier that phthalocyanine fullerene dyads show LC phase formation behavior. However, the nature of the phase had not been determined.[100]The working group of Cheng presented two porphyrin-fullerene dyads with analogous arrangements. Both materials were blended in a weight ratio of 1 : 1 with the donor polymer SiPCPDTBT* and used as active material layer in BHJ cells. In general the devices showed better open-circuit voltages and short-circuit photocurrents compared to an analogous device consisting of a 1 : 1 blend of the fullerene derivative phenyl-C_{61}-butyric acid methyl ester (PCBM) and PCPDTBT.[6,101]

Ohta *et al.* also designed phthalocyanine-fullerene dyads with various spacers between the two chromophores, giving double-cable-like assemblies.The helical arrangements of the fullerenes are depicted in detail.[7,8] However, no photophysical data regarding potential applications in semiconductor technologies have been published for these materials. In general, mesogens so far only have been reported to be used as additives or in other forms of blends and not as a purely liquid crystalline active material in photovoltaic cells.[6,61,102–106]

*[poly[2,6-(4,4-bis-(2-ethylhexyl)-4*H*-cyclopenta[2,1-b;3,4-b']-dithiophene)-*alt*-4,7-(2,1,3-benzothiadiazole)]

2.7 Stilbenes

In this work, oligo(*p*-phenylene vinylene) motifs (OPV) are used either as donor materials or as π-conjugated bridge between peripheral fullerene acceptor moieties and donor cores. In general, the basic stilbene unit can be classified as *E*- and *Z*-isomers (see scheme 1), whereas the former are more interesting for most applications due to the higher thermal stability and conjugation in oligomers.[107] It is noteworthy that the stilbenes do not show strictly rigid structures in oligomers or polymers (poly(*p*-phenylene vinylene), PPV), since the single bonds between the benzene rings and the double bonds readily rotate at room temperature (see scheme 1).[108] As a consequence of their photophysical properties, stilbenoid materials have been successfully applied as optical brighteners, optical data storage materials and many others.[109] In the field of semiconductors, electron-rich alkoxy-substituted PPVs have been found to show satisfying charge carrier mobilities and were successfully incorporated into photovoltaic solar cells.[10] Effort has also been put into electron-deficient stilbene polymers, which have also shown mobilities as high as 1 $cm^2V^{-1}s^{-1}$.[110] Due to the linear nature of the oligomers, these materials are promising candidates for arm building blocks in star-shaped mesogens.

Many strategies have been developed to synthesize stilbenes.[111] In this work, the Wittig-Horner conditions were chosen since the *E*-selectivity for the formed double bonds is very high (see scheme 2.[112] In the gas phase, the difference in energy for the rate-determining step (formation of the oxaphosphetane) regarding *Z*- and *E*-products amounts to approx. 0.5 kJ/mol.[113] Furthermore, side-product formation like homo-coupling of the corresponding ylides or radical reaction usually is low compared to the Wittig reaction.[79,114] The used phosphonates are available from the corresponding halides via the Michaelis-Arbuzov reaction.[115]

Chemical deactivation of the excited S_1 state plays a major role for stilbenes. Besides the *Z*-*E* isomerization shown in scheme 1, stilbenes undergo photoinduced [2+2] cycloaddition, reducing their long-term stability in organic electronic devices. However, the S_1 state of stilbenes has been demonstrated to be quenched efficiently by intramolecular interactions with acceptor moieties such as fullerenes.[12,109,116] Ideally, this will protect the target materials of this work from chemical degradation when they are irradiated by light.

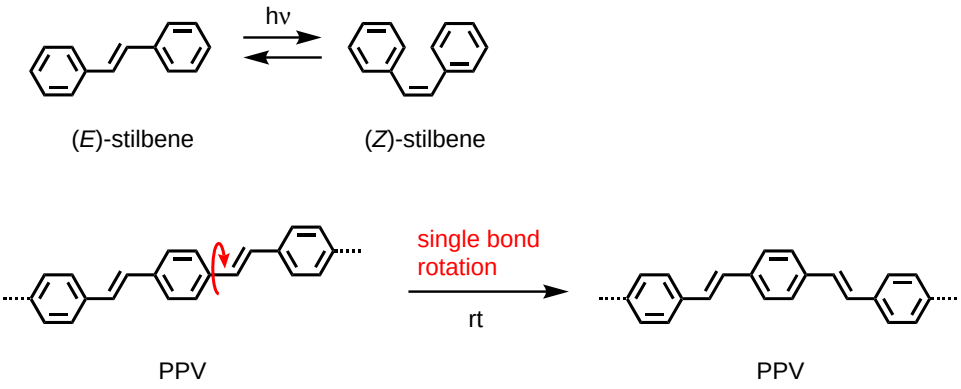

Scheme 1: Illustration of the different stilbenoid structures.

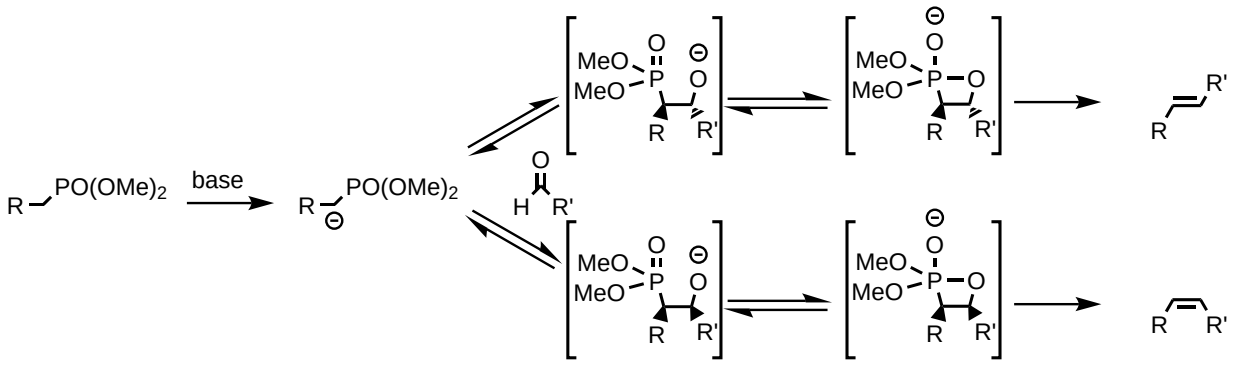

Scheme 2: Mechanism of the Wittig-Horner reaction.

2.8 Fullerenes

Since its discovery in 1985,[117] C_{60}-fullerene has attracted substantial attention in the research fields of organic and materials chemistry. The truncated icosahedral structure (see figure 20) made up only of carbon atoms promises unique properties along with a three-dimensional aromaticity.[118] The high electron affinity and electron mobility led to the establishment of fullerene as standard acceptor material in organic photovoltaics. Cyclic voltammetry measurements show that the carbon allotrope can uptake up to six electrons.[119] When combined with a donor material, the resulting dyad facilitates long-lived photoinduced charge separation due to the small reorganization energy of C_{60}.[120]
The bond lengths between two six-membered rings ((6,6)-bond, 138 pm) are smaller than the ones between a five-membered and a six-membered ring ((5,6)-bond, 145 pm). Consequently, the π-electrons are located in the hexagons. The diameter of the C_{60} molecule amounts to 7.1 Å whereat this value rises to 10.3 Å if the π-electron clouds are factored in.[121]
The slightly electron deficient double bonds are somewhat susceptible to nucleophilic attacks and orbital-driven reactions like cycloadditions. Among the latter, the Prato reaction is a versatile method to incorporate aliphatic or aromatic aldehydes. Here, an *in situ* formed azomethine ylide from the carbonyl and the readily available *N*-methylglycine undergoes a 1,3-dipolar cycloaddition selectively with a (6,6)-double bond of the fullerene.[122] In an excess of aldehyde and *N*-methylglycine, the fullerene easily forms multiple adducts. Even in the case of equimolar amounts, the bisadduct (with

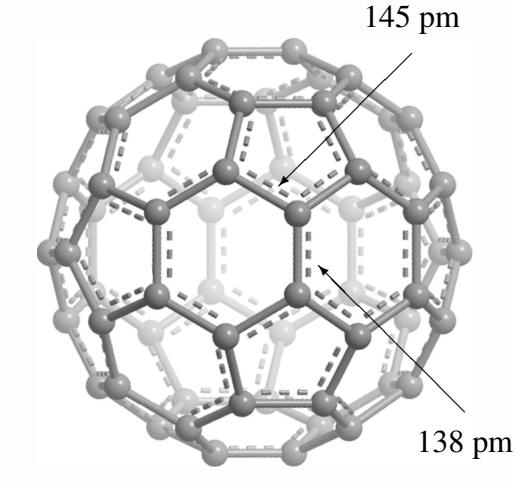

Figure 20: Three-dimensional model of C_{60}.

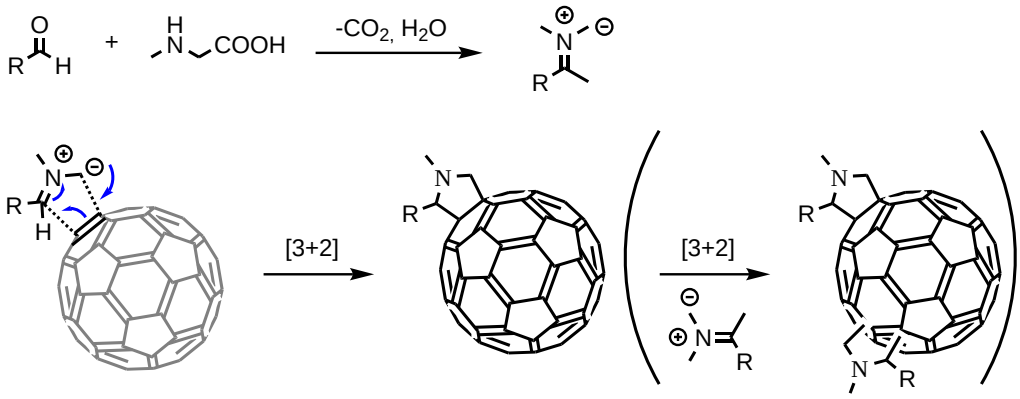

Scheme 3: Mechanism of the Prato reaction. The desired monoadduct may further react with remaining ylides giving bisadducts or even higher adducts with positional isomers.

up to 8 positional isomers) is found, since the reactivity of the remaining double bonds in a monofunctionalized fullerene is barely affected (see scheme 3).[123] However, this drawback effectively is applicable to any reaction involving the functionalization of C_{60}.

The properties of the obtained fulleropyrrolidines resemble those of neat C_{60}. The reduction potentials are slightly shifted to more negative values since the conjugation of the extended π-system is partially lost. In the UV/VIS spectra, strong absorption is observed at approx. 255 and 328 nm for both parental fullerenes and pyrrole derivatives. A small sharp signal at 430 nm and a broader band at approx. 700 nm are also observed.[123]

When fullerene derivatives are covalently linked to stilbenes, a fast singlet energy transfer occurs on photoexcitation, followed by a nearly quantitative intersystem crossing to the fullerene triplet state. A long-lived charge-separated state then is observed for stilbenes with three or more repeating units. This is realized by holes and electrons migrating to other molecules in the solid phase of the material, thus efficiently quenching fluorescence of the stilbenes.[12]

2.9 Porphyrins

Porphyrins play an important role in nature, e.g. transporting oxygen to the cells of our bodies or facilitating photosynthesis in chloroplasts. The strong absorption in the visible spectrum, the high thermal stability and the variety of functionalization possibilities also render these 18 π-electron macrocycles attractive for application in photovoltaics.[124] Due to their planar shape, the porphyrins act as discotic liquid crystals when flexible chains are attached, although LC phase formation behavior can be somewhat complex.[5,59,62,125,126] Here, porphyrin will be used as core building block similar to the discotic LC mesogens introduced by Ohta and Cheng.[6,8]

In this work, the Lindsey method has been chosen to synthesize *meso*-substituted porphyrins as it provides less harsh conditions compared to the conventional Rothemund and Adler-Longo reactions. Aromatic or aliphatic aldehydes undergo condensation with pyrrole via acidic catalysis to give porphyrinogens, which then are converted to the corresponding porphyrins by the use of an oxidant (see scheme 4).[127,128] *Meso*-tetraphenyl derivatives show strong twists of the phenyl rings with respect to the porphyrin ring due to steric repulsions. The corresponding dihedral angles typically range from 30 to 70°.[129]

When porphyrin is covalently linked to fullerene through *p*-phenylene vinylene oligomers, a wirelike

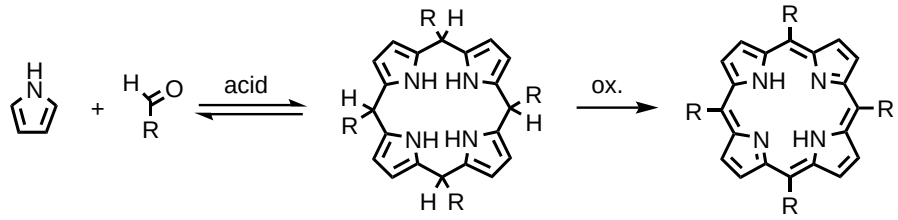

Scheme 4: Mechanism of the Lindsey reaction.

behavior is observed for this kind of triad. Charges then are separated between the fullerene and porphyrin motifs via the stilbene bridge, hampering their recombination.[130,131] Hence, these materials are expected to show longer lifetimes for charge separated states compared to stilbene-fullerene dyads.

3 Plan of synthesis

The retrosynthetic strategy for the C_3-symmetric stars without fullerenes[132,133] and for the C_4-symmetric porphyrin stars without fullerenes[134,135] has already been demonstrated and is illustrated in scheme 5. A porphyrin or benzene core with four or three phosphonate groups respectively reacts with aldehyde bearing arms via Wittig-Horner conditions to give the desired stars.

The retrosynthetic aspects for the Hekate or porphyrin stars with a fullerene attached to each arm are displayed in scheme 6. Since the construction of fulleropyrrolidines as well as stilbenes relies on aldehyde functional groups, the order of synthetic steps has to be planed carefully. In a typical manner, the arms of the star would be fully synthesized and coupled to the core in the final step just as for the stilbene stars in scheme 5. This convergent route, however, implies a Wittig-Horner reaction in the presence of fullerenes, which are known to react with phosphorus ylides.[136,137] Therefore, the star should already be completely build up with functional groups at the arms that can be coupled with spacers bearing the fullerenes. Due to the presence of the fullerenes this linkage should take place under mild conditions. For this purpose, the Steglich esterification shown in scheme 6 seems suitable since it proceeds at room temperature and tolerates many functional groups.[138]

The required carboxylic acid can be attached to the spacer in form of an alkyl ester. Several acidic hydrolysis procedures of fullerene containing esters have been reported with good yields.[139–141] Consequently, linear alkyl chains with terminal aldehyde and alkyl ester functional groups are the starting materials for the fulleropyrrolidines with spacers attached. The hydroxy groups needed in the arms of the stars can be easily incorporated in the form of allyl ethers, which are deprotected under mild conditions with Pd(0) catalysts and either nucleophiles or hydride donors.[142]

In the case of the asymmetric star with a single allyl ether group, an asymmetric core structure is required to facilitate the incorporation of the distinct arms in succession, which is highlighted in scheme 7. As the arm bearing the allyl ether requires additional synthetic effort, it is intended to be attached after the other two arms. Therefore, a V-shaped building block bearing a single phosphonate must be synthesized. This functional group must be protected for the prior attachment of the two arms. However, there is no readily available protecting group for phosphonic acid esters. Nitriles can be converted to these esters in a sequence via reduction followed by bromination of the corre-

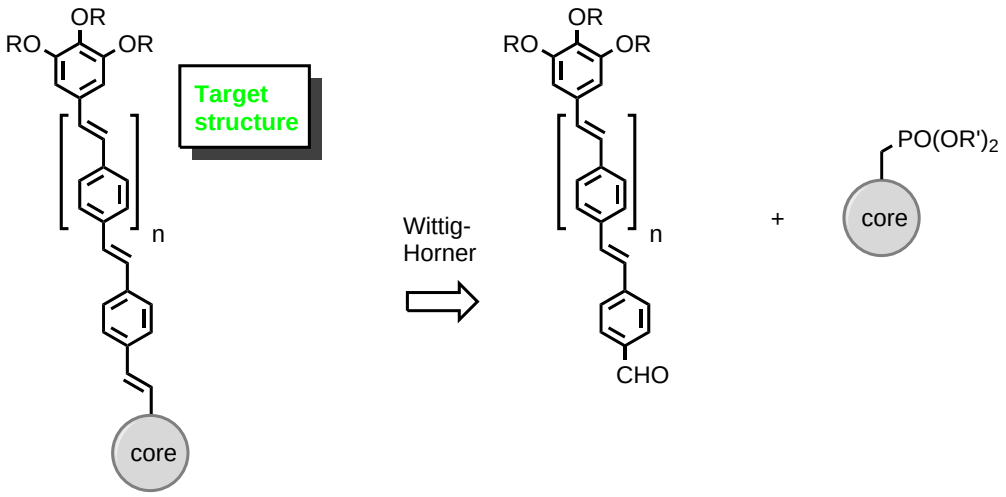

Scheme 5: Retrosynthetic strategy for the desired Hekate or porphyrin stars without fullerenes.

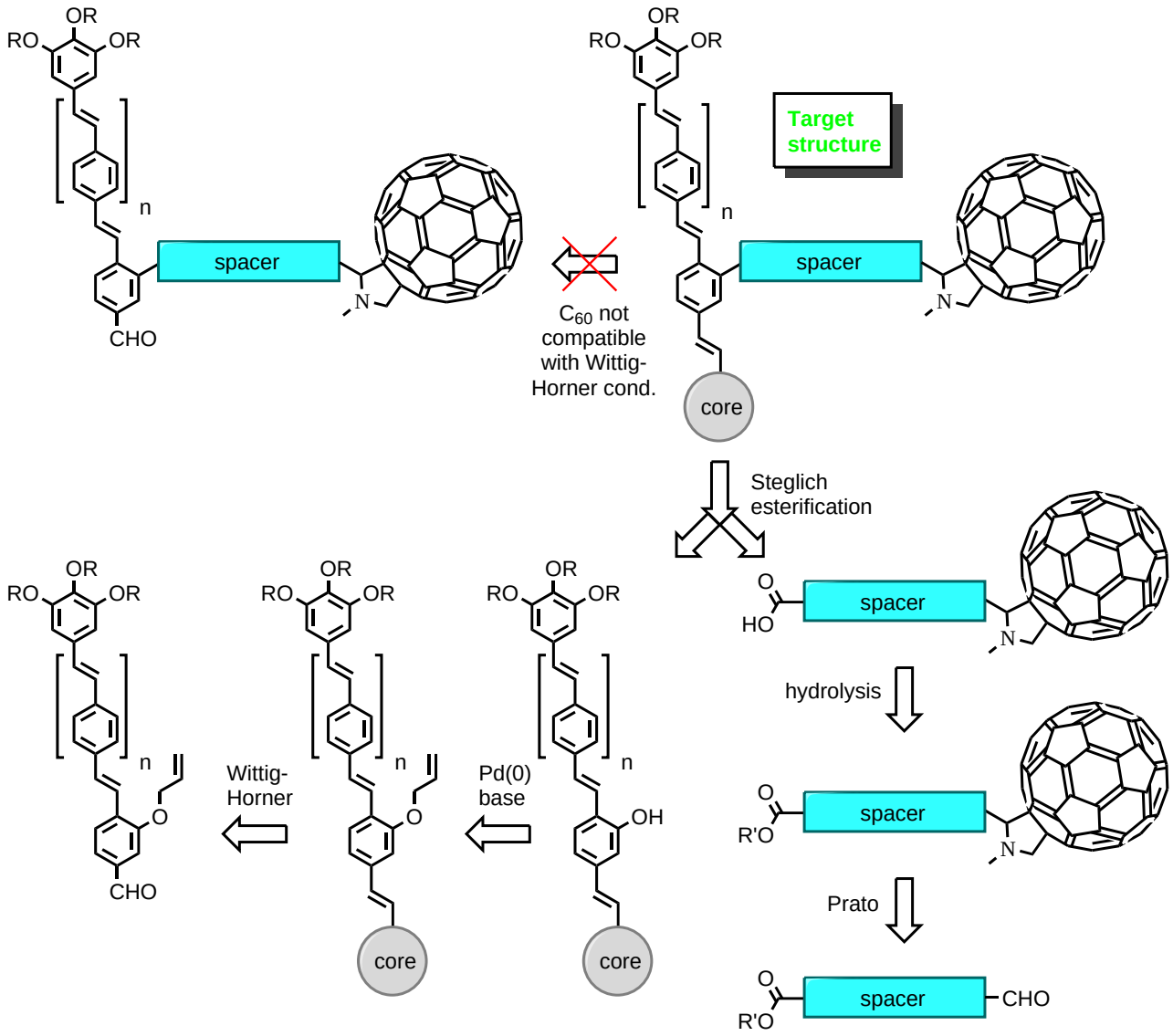

Scheme 6: Retrosynthetic strategy for the desired Hekate or porphyrin stars bearing fullerene units on each arm.

sponding alcohol and subsequent nucleophile attack of the trialkylphosphite.[143] Additionally, they are unaffected by Wittig-Horner conditions. The retrosynthetic steps shown in scheme 7 therefore should represent a convenient route for the asymmetric Hekate stars.

Note that even the stars only bearing a single spacer are disfavored to be functionalized with the Prato reaction as the last step, since the multiadducts of the fullerene motif and the star motifs significantly decrease the yield regarding to the star motif, which has to be synthesized in many steps.

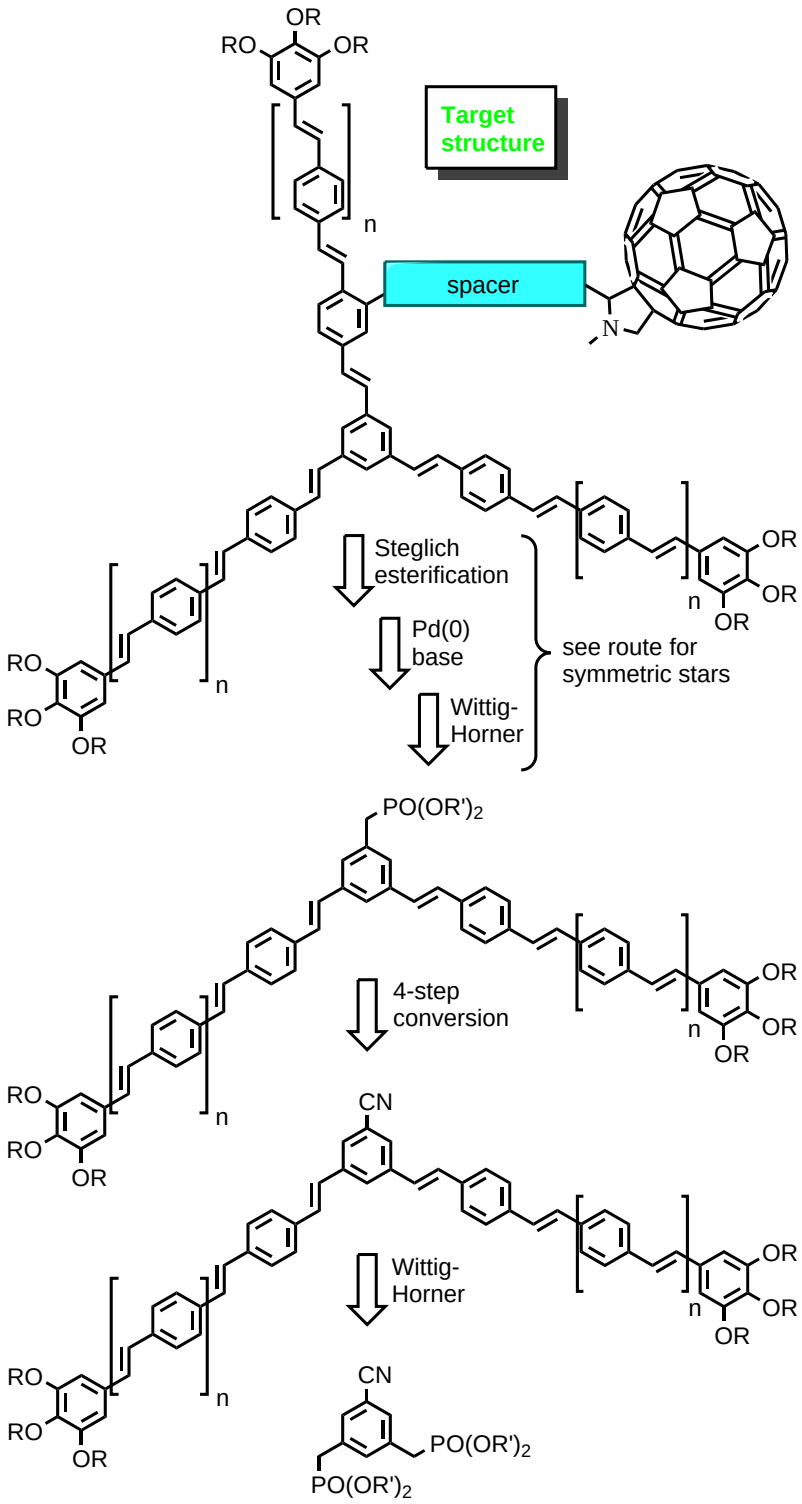

Scheme 7: Retrosynthetic strategy for the asymmetric Hekate stars bearing a single fullerene unit per molecule.

4 Results — Synthesis

4.1 Core building blocks

The C_3-symmetric core for the Hekate stars has been synthesized according to literature and is illustrated in scheme 8. Phosphonate **1**[144] was readily available for the synthesis of the arms that already have a benzene ring with an allyl ether group attached. The trisaldehyde **3**[145] was then synthesized in a new route under Wittig-Horner conditions with a slight excess of (diethoxymethyl)benzaldehyde (**2**). Including the subsequent acidic hydrolysis of the acetal group, the yield amounts to 68%. The core building block with two repeating units (**5**) was obtained via Wittig-Horner reaction of the prolonged core aldehyde **3** and the prolongation unit **4*** with a yield of 52%.

For the synthesis of a core building block suitable for asymmetrical stars, aldehyde **9** has been prepared according to scheme 9. The synthetic strategy is similar to the preparation of the symmetrical core **3** in scheme 8 and the desired aldehyde **9** has been obtained in a good overall yield. 3,5-dimethylbenzonitrile (**6**) has been brominated in benzylic positions according to literature[146] to afford bromide **7**. The following Arbuzov reaction with triethyl phosphite under solvent-free conditions gave phosphonate **8** in a yield of 88%. The desired aldehyde **9** was obtained by Wittig-Horner reaction of the phosphonate **8** and excess of (diethoxymethyl)benzaldehyde, followed by acidic hydrolysis of the acetal group, in a yield of 95%.

Porphyrin stars were synthesized starting from the core **12**, which has been prepared according to literature[147], as illustrated in scheme 10. In the first step, (diethoxymethyl)benzaldehyde (**2**) was reduced to the benzylic alcohol functional group with sodium borohydride.[148] Stirring in concentrated aqueous solution of hydrobromic acid and toluene under reflux afforded the brominated aldehyde **10**[148,149] with a yield of 85%. The porphyrin **11**[147] was synthesized by stirring the aldehyde, pyrrole and catalytic amounts of boron trifluoride diethyl etherate in chloroform with subsequent oxi-

*Compound **4** was synthesized by the intern Moritz Dechant under the supervision of the author of this document.

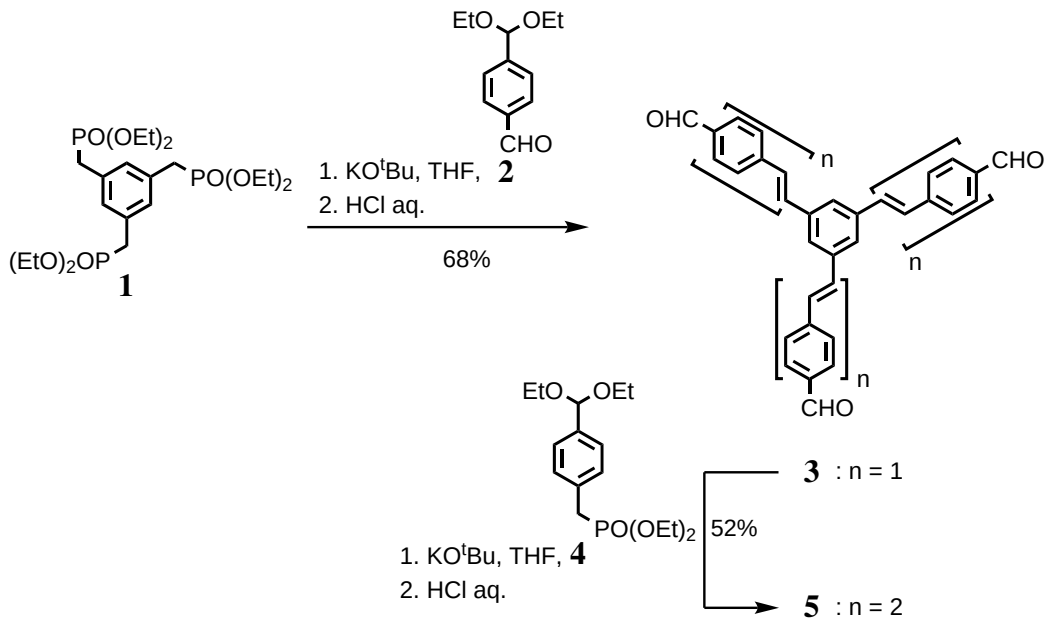

Scheme 8: Synthesis of the desired core building blocks **3** and **5**.

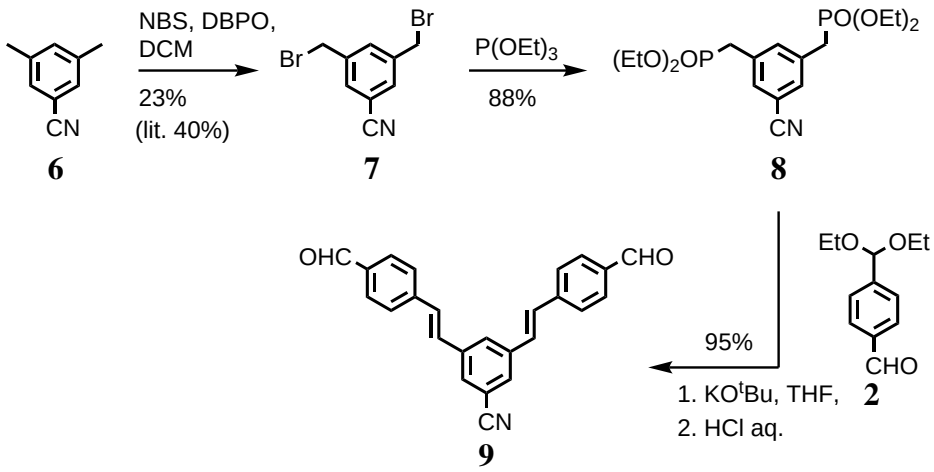

Scheme 9: Synthesis of the desired asymmetrical core building block **9**.

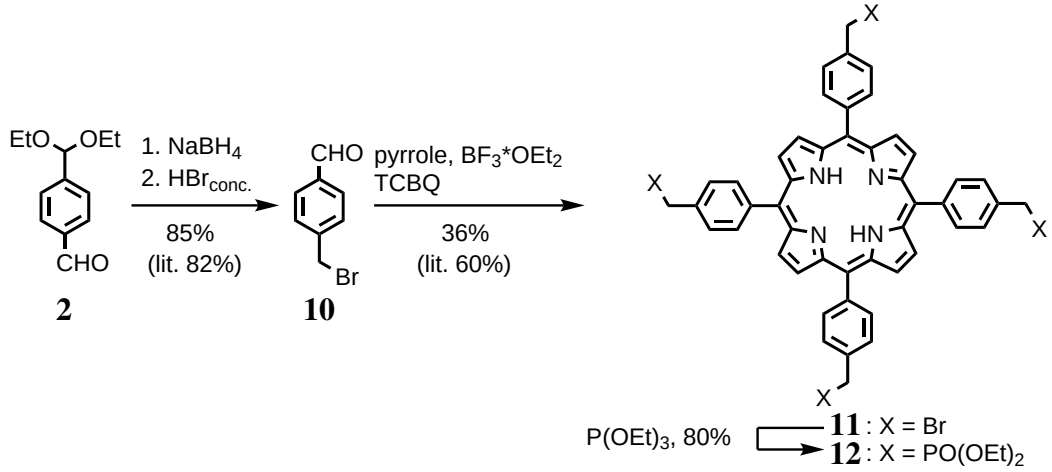

Scheme 10: Synthesis of the desired porpyrin core building block **12**.

dation via tetrachloro-1,4-benzoquinone with a moderate yield of 36%*. The following Arbuzov reaction with triethyl phosphite under solvent-free conditions gave the desired phosphonate **12**[134,135,151] in a yield of 80%.

4.2 Arm prolongation units

The prolongation of stilbenoid arms has been accomplished by incorporation of the reported[133] building block **13**, which has been synthesized according to scheme 11. In contrast to the literature procedure, (diethoxymethyl)benzaldehyde (**2**) was reduced to the benzylic alcohol functional group with sodium borohydride, rather than lithium aluminium hydride. Subsequent acidic hydrolysis deprotected the acetal. In the next step, the alcohol was protected via 3,4-dihydro-2*H*-pyran to obtain the desired aldehyde **13** in an overall yield of 96%.

For the attachment of spacers to stilbenoid arms, reported prolongation building block **18** was synthesized as illustrated in scheme 12. 2-Bromoterephthalic acid (**14**) was modified via aromatic, nucleophilic substitution with potassium hydroxide to obtain 2-hydroxyterephthalic acid (**15**) with a yield of 94%.[152] Esterification of the carboxylic acids was achieved by using methanol as solvent with

*For a high yield it was critical to freshly dry the acid catalyst with calcium hydride.[150]

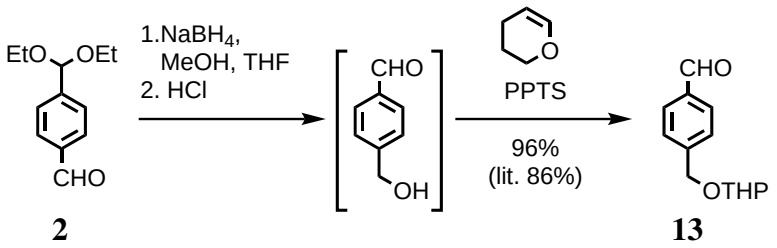

2 **13**

Scheme 11: Synthesis of the desired prolongation building block **13**.

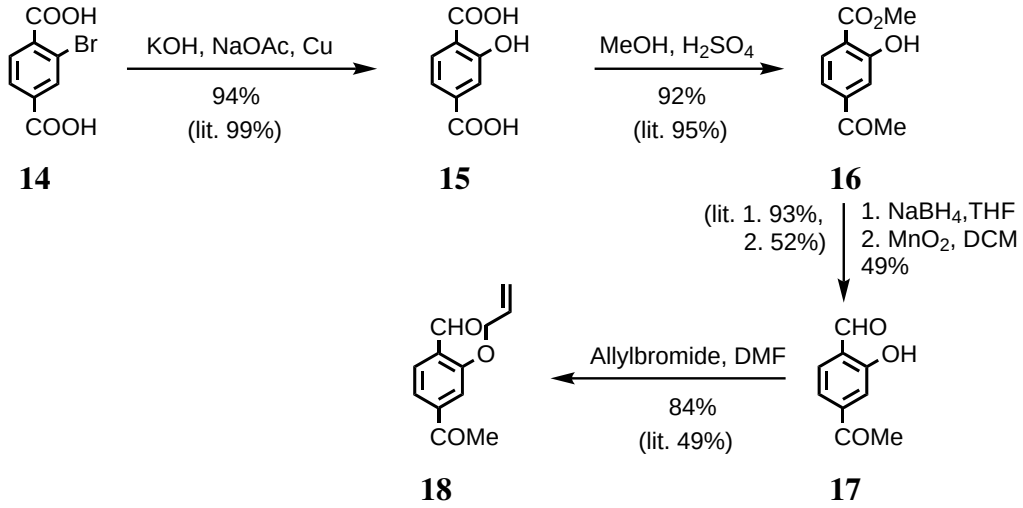

14 **15** **16** **18** **17**

Scheme 12: Synthesis of the desired prolongation building block **18**.

catalytic amounts of sulfuric acid with a yield of 92%.[153] The carbonyl group neighbouring the alcohol functional group of the ester **16** could be selectively reduced with sodium borohydride.[154] Subsequent oxidation of the benzylic alcohol to aldehyde **17** was performed with activated manganese dioxide[155] with a yield of 49% for two steps. The etherification of the phenolic alcohol was achieved according to literature[156]. However, DMF was used as solvent instead of acetone, raising the yield of the desired aldehyde **18** to 84% (lit. yield: 49%).

4.3 Spacers

For the incorporation of fullerenes in the void of star-shaped mesogens, spacers were required to link the fullerenes to one or several stilbenoid arms. Linkers with three different lengths have been succesfully prepared.

The synthetic route for the shortest spacer is illustrated in scheme 13. Starting from γ-butyrolactone (**19**), alcohol **20** was prepared according to literature[157] via transesterification with methanol in the presence of triethylamine. During workup, however, the lactone regenerated in part, as is also reported.[157,158] The molar ratio of desired product and regained starting material varied from batch to batch and could take values of 2 / 1 to 9 / 1. The mixture of **20** and **19** was then oxidized under Swern conditions to yield aldehyde **21**, in which the lactone **19** was still present.[157] The following Prato reaction in refluxing toluene afforded the fullerene bearing ester **22** with a moderate yield of 12%. The deviation from typical yields of prato reactions (>30%) is due to the instability of aldehyde **21** at elevated temperatures under given conditions. NMR data of the raw material **22** indicate

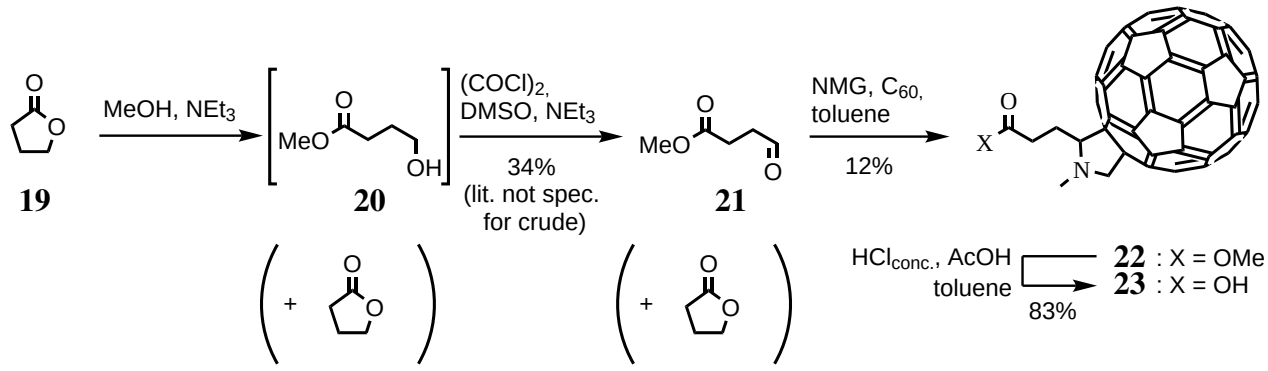

Scheme 13: Synthesis of the desired spacer **23**.

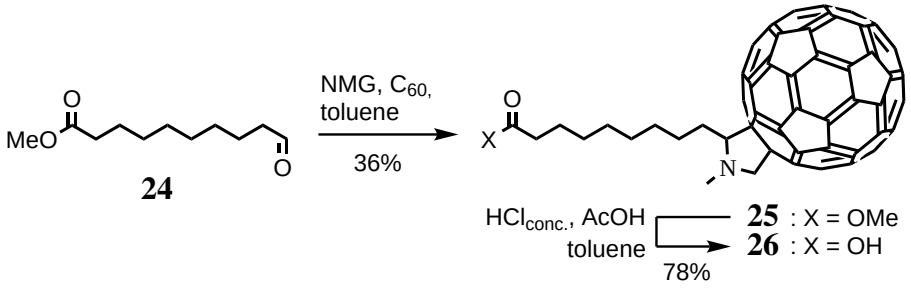

Scheme 14: Synthesis of the desired spacer **26**.

the formation of undefined byproducts, which could be separated via gel permeation chromatography. In the final step, ester **22** is hydrolyzed in acidic media to obtain the desired acid **23** in a yield of 83%. The synthetic route for the spacer with a C_{10}-backbone is illustrated in scheme 14. Aldehyde **24** reacted under Prato conditions to the fullerene bearing ester **25** with a yield of 36%. The formation of undefined byproducts as for the case of the shorter spacer could not be detected. In the second step, hydrolysis of the ester was achieved by acidic media to obtain the desired carboxylic acid **26** with a yield of 78%.

The longest spacer has been synthesized according to scheme 15. Starting from 16-hydroxypalmitic acid (**27**), esterification with methanol in the presence of sulfuric acid was carried out according to literature[159] to afford compound **28** with a yield of 96%. The next step involving the oxidation of the aliphatic alcohol **28** to the aldehyde **29** was first performed with Taber conditions[160] (P_2O_5, DMSO, NEt_3) as reported.[159] However, the starting material could not be completely converted to the aldehyde, even after 24 hours of stirring at room temperature and 2.6 equivalents of P_2O_5. Therefore, a Swern oxidation was carried out with 1.1 equivalents of oxalyl chloride to obtain the desired aldehyde **29** with a yield of 69%. The subsequent Prato reaction gave the fullerene bearing ester **30** with a yield of 42%. Hydrolysis of the ester was achieved by acidic media to obtain the desired carboxylic acid **31** with a yield of 70%.

For a smooth workup of the coupling reaction of the Hekate stars with the fullerene spacer acids, it is important to assure the purity of the linkers. Therefore, the products of the Prato reaction were analyzed regarding the potential presence of unreacted C_{60} or bisadducts of the fulleropyrrolidines. Figure 21 shows the ^{13}C NMR results for the ester compounds **22**, **25** and **30** in the region of aromatic sp^2 carbons. Since the carbon atoms of unreacted C_{60} are chemically equivalent, the presence of small amounts would be accompanied by a strong signal at approx. 143 ppm, which has not been

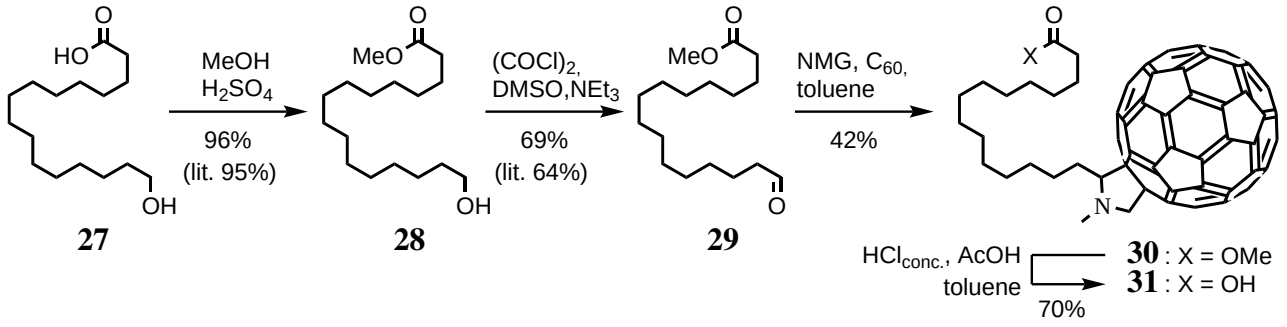

Scheme 15: Synthesis of the desired spacer **31**.

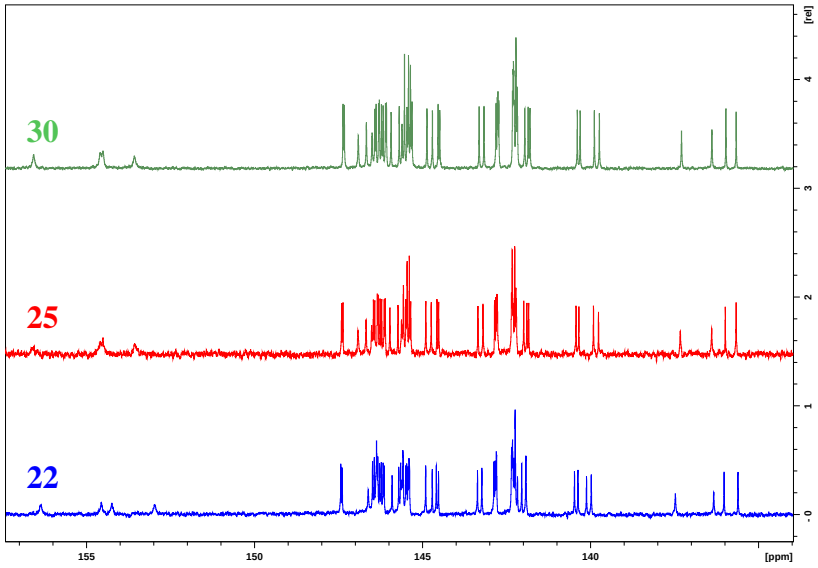

Figure 21: ^{13}C NMR results for the ester compounds **22**, **25** and **30**.

observed.[161] 58 signals for each compound are observed, which is in line with expectations for a monoadduct. For a bisadduct, the number of anticipated signals varies from eight to 30, depending on the symmetry of the eight different isomers.[162] Therefore, the main component of the particular materials are the expected monoadducts.

To further demonstrate the lack of bisadducts and C_{60}, MALDI-MS spectra of the materials were recorded, which are displayed in figure 22A. The given peak labels indicate the found m/z values for the desired products **22** ($C_{67}H_{13}NO_2$), **25** ($C_{73}H_{25}NO_2$) and **30** ($C_{79}H_{37}NO_2$). For the prolonged spacers, only the anticipated signals were found, confirming the lack of C_{60} and the corresponding bisadducts with the respective exact masses of 1146.35 ($C_{84}H_{46}N_2O_4$) and 1314.53 ($C_{96}H_{70}N_2O_4$). For the shortest spacer **22** however, additional intensities are detected. The m/z values 1006.19 and 1149.29 match the exact masses of the hypothetical bisadduct ($C_{74}H_{26}N_2O_4$) and trisadduct ($C_{81}H_{39}N_3O_6$). Additionally, the isotope pattern of the monoadduct does not match the theoretical isotope distribution. The strongest signal located at m/z = 864.13 represents the $[M+1]^{\cdot\cdot}$ fragment, not the expected $[M]^{\cdot\cdot}$. Moreover, the found signal at m/z = 862.11 corresponds to a $[M-1]^{\cdot\cdot}$ fragment, which was not found for the longer spacers. The presence of the bisadduct and especially the trisadduct is highly unlikely, since chromatographic workup easily separates the mono ester / amine from the oligo esters / amines. Rather, the conditions of the mass fragmentation show a stronger im-

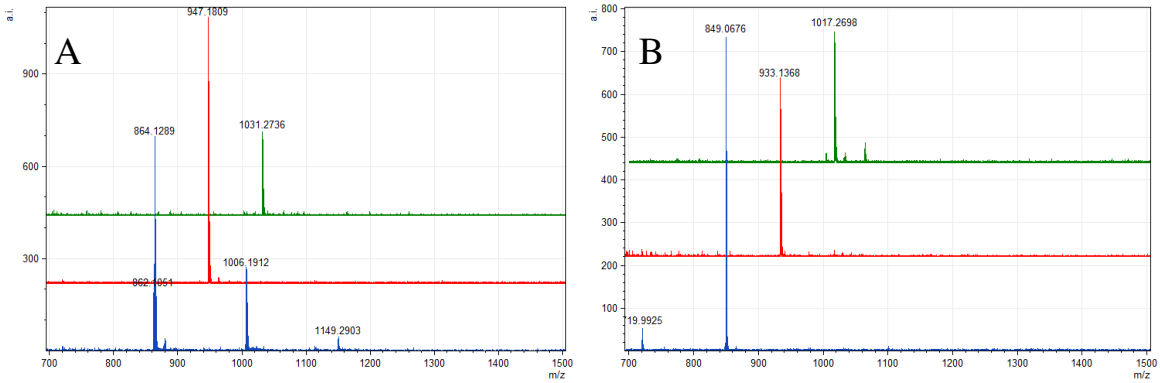

Figure 22: **A**: MALDI-MS spectra for the ester compounds **22** (blue), **25** (red) and **30** (green); **B**: MALDI-MS spectra for the carboxylic acid compounds **23** (blue), **26** (red) and **31** (green).

pact on the short spacer than on the prolonged spacers. Presumably, the small number of chain links between the ester functional group and the pyrrolidine ring facilitates decomposition by intramolecular cyclizations. In addition, MALDI experiments have already been shown to facilitate laser-induced retro-[3+2]-cycloadditions to yield ylides, thus giving the corresponding bisadducts of fulleropyrolidines.[163] To strengthen this point of view, the MALDI-MS spectra of the corresponding carboxylic acid derivatives **23**, **26** and **31** are displayed in figure 22B. The mass spectrum for the shortest spacer **23** reveals that no signals corresponding to bis- or trisadducts are present anymore. Note that no chromatographic workup was part of the synthesis and the yield of the mono acid amounts to admirable 83%. Obviously, the unanticipated signals for the ester **22** shown in figure 22A do not arise from byproducts but from the compound itself. For the acid **23**, a small peak located at 719.99 m/z is detected, which could be attributed to C_{60}, but it is uncertain whether this is caused by mass fragmentation conditions or indeed small portions of C_{60} are present.[164,165] The prolonged linker acids **26** and **31** only show signals affiliated with the desired compounds, apart from a few small peaks for the longest spacer **31**. The respective m/z values do not coincide with bisadducts or C_{60}. Their nature or origin could not be resolved within the scope of this work.

4.4 Arm building blocks with dodecyloxy-chains

The stilbenoid arms bearing dodecyl chains have been prepared starting from the reported[166] compound **36**, which has been synthesized according to scheme 16. Etherification of ethyl gallate (**32**) was carried out in an analogous way to the corresponding etherification of methyl gallate[167] with *n*-dodecylbromide to afford **33** in a yield of 61%. The ester group was reduced with lithium aluminium hydride to obtain the benzylic alcohol **34**[168] with a yield of 97%. The bromide **35** was obtained with the brominating reagent phosphorus tribromide in an analogous way to the corresponding benzylic bromide bearing tetradodecyl chains[169] with a good yield of 93%. In the last step, the Arbuzov reaction with triethyl phosphite under solvent-free conditions gave the desired phosphonate **36**[166] in a yield of 72%.

The corresponding prolonged phosphonate **39**[170] has been synthesized via a new route according to scheme 17. In the initial Wittig-Horner reaction, the phosphonate **36** reacts with the aldehyde **13** to give the stilbene **37** in a yield of 91%. In the next step, the in-situ formation of triphenylphosphine dibromide[171] leads to the direct conversion[172] of the THP protecting group to the bromide **38** in

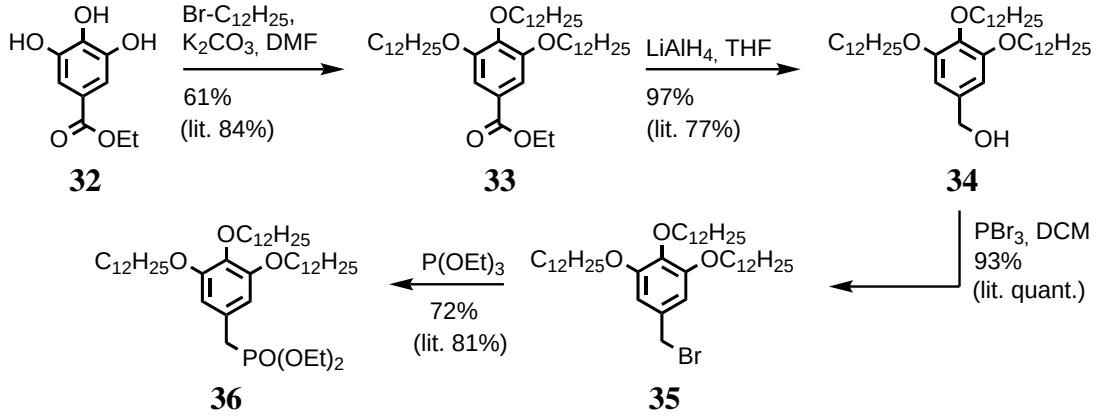

Scheme 16: Synthesis of the arm building block **36**.

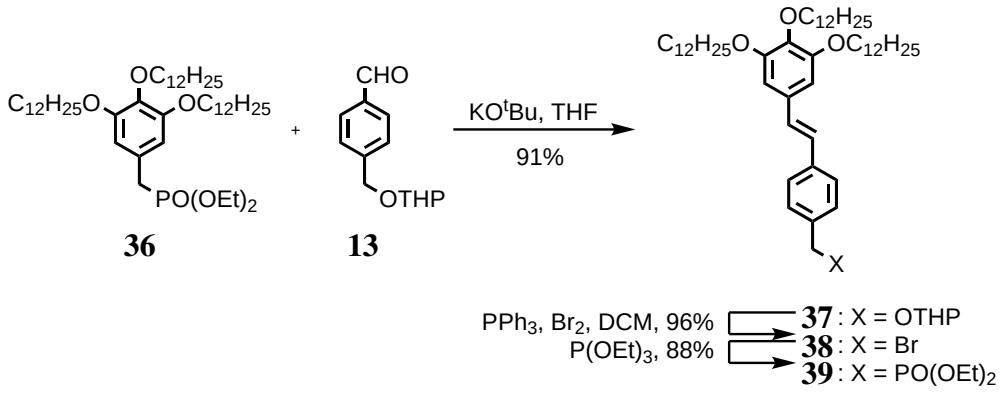

Scheme 17: Synthesis of the arm building block **39**.

a yield of 96%. The subsequent Arbuzov reaction with triethyl phosphite gives the desired phosphonate **39** with a yield of 88%. This route gives the desired phosphonate **39** in a total yield of 51% in 5 steps and therefore is a much better and shorter route compared to the previously reported route with seven steps and a total yield of 29%.[170]

For the preparation of arms bearing a single allyl ether group, the synthetic route shown in scheme 18 has been applied successfully. Starting from either phosphonate **36** or prolonged phosphonate **39**, a Wittig-Horner reaction was carried out with the prolongation unit **18** in THF and with potassium *tert*-butoxide as base. As alkaline hydrolysis of the methyl ester might occur under these conditions, no column chromatography was performed. Instead, lithium aluminium hydride, which reduces both ester and hypothetical acid, was added to give the benzylic alcohols **40** and **42** in a yield of 72 and 75%, respectively, for two steps. Aldehydes **41** and **43** were obtained by oxidation via high excess of activated manganese dioxide with yields of 78 and 91%, respectively. TLC analyses showed that the products slowly decomposed under given reaction conditions. Therefore, highly frequent TLC analyses were required to quench the reactions at the earliest possible time. The products could be subsequently purified from the side product via column chromatography.

For the synthesis of porphyrin based stars, aldehyde arm building block **44**[173] was required and synthesized as illustrated in scheme 19. Reacting phosphonate **39** with (diethoxymethyl)benzaldehyd (**2**) under Wittig-Horner conditions with subsequent acidic hydrolysis of the acetal gave the desired aldehyde **44** in a yield of 91%.

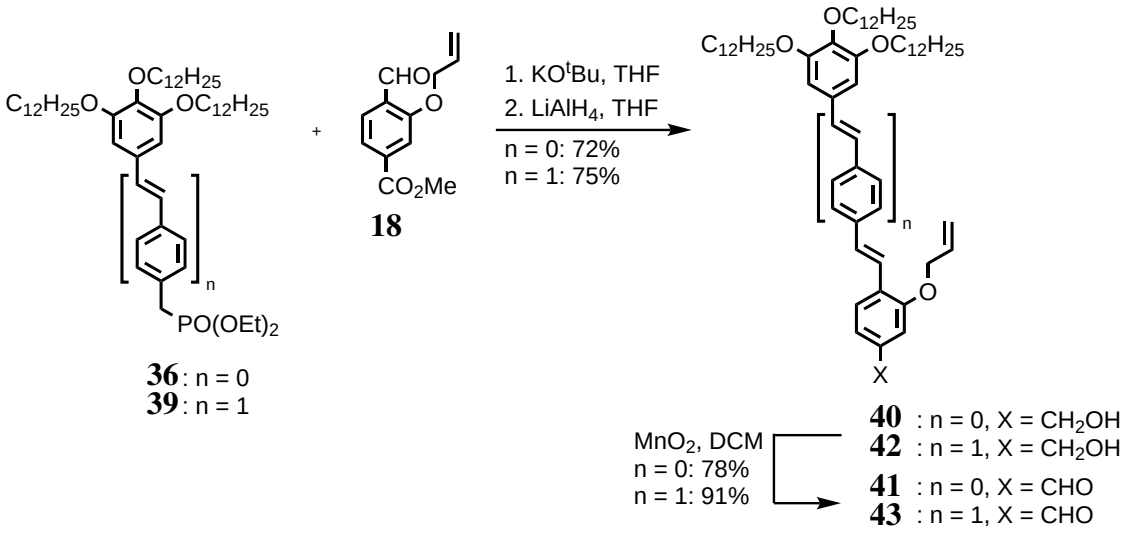

Scheme 18: Synthesis of the arm building blocks **41** and **43**.

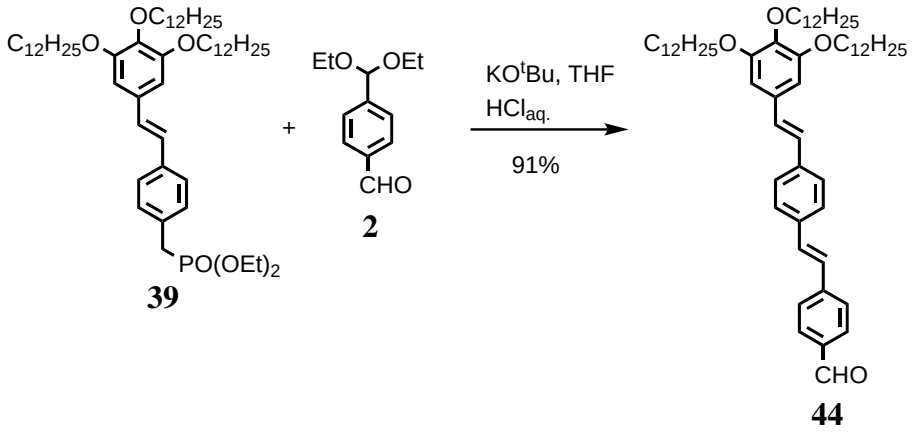

Scheme 19: Synthesis of the arm building block **44**.

4.5 Alternative synthetic strategies for allylether bearing arms

Scheme 20 summarizes the sophisticated synthesis of allylether bearing arms presented in the previous chapters and reveals that it takes a rather large amount of steps to obtain the desired arms. Additionally, the starting material **14** is quite expensive. Therefore, a variety of different synthetic approaches towards hydroxy functionalized arms or cores were elaborated regarding costs of starting materials and number of steps.

In the first strategy (see scheme 21), readily available 3-hydroxybenzaldehyde (**45**) was coupled with the phosphonate **36** via Wittig-Horner conditions. Despite the presence of a hydroxy proton, a satisfying yield of 49% was obtained for equimolar amounts of the starting materials **45** and **36**. Another batch with excess of 2.0 equivalents aldehyde **45** did not raise the yield. In the next step, several attempts have been made to achieve *ortho*-formylation for the phenol **46**. Note the different positioning of the hydroxy group compared to the previously introduced arms. In the first run, typical Reimer-Tiemann[174] conditions were chosen using chloroform and an aqueous solution of potassium hydroxide. With oil bath temperatures up to 75 °C, only weak formation of product was observed by TLC analysis after several hours. Presumably, the highly lipophile starting materials can only be converted slowly in this 2-phase system. To improve the rate of conversion, a modified reaction with tributylamine as phase transfer catalyst[175] and sodium hydroxide as base was carried out. After 5

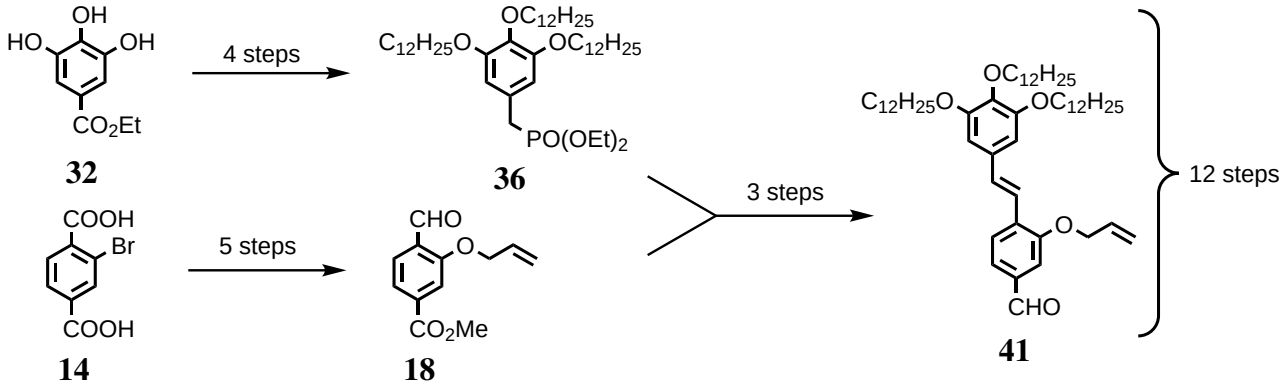

Scheme 20: Summary of the successful synthesis of allylether bearing arms.

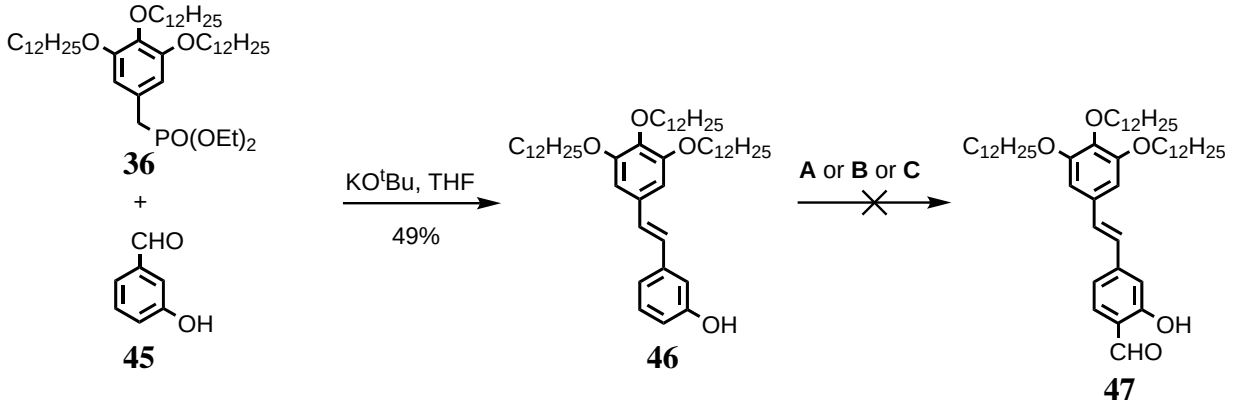

Scheme 21: Attempted synthesis of the arm building block **47** via key compound **45**; **A**: $CHCl_3$, KOH_{aq}; **B**: $CHCl_3$, $NaOH_{aq}$, *n*-Bu_3N; **C**: hexamethylenetetramine, trifluoroacetic acid, 1N HCl.

days of reflux, NMR measurements revealed a ratio of product and starting materials equal to 1 / 45. Note that NMR confirmed the integrity of the stilbene double bond. The Reimer-Tiemann reaction was discarded and the Duff reaction utilizing hexamethylenetetramine and trifluoroacetic acid[176] was employed, which lacks the need of an aqueous phase. According to TLC analysis, the conversion of the starting material at 80 °C was already complete after 20 minutes. When the presumed iminium cation was hydrolyzed, TLC analysis revealed that no product had formed. The low retention factors of the visible spots suggest that cleavage of the dodecyl chains occured. The TLC plate was treated with an acidic 2,4-dinitrophenylhydrazine solution and did not give colored spots, confirming the lack of aldehyde functional groups. In conclusion, the formylation of the phenol **46** did not succeed and **47** could not be synthesized in this way.

Another concept is the hydroxymethylation of phenols with formaldehyde and subsequent formation of the corresponding acetal by the diol, which is shown in scheme 22. The compound **48** is desirable since all functional groups besides the aldehyde are protected. In general, the yield was low due to the carbonyl group and the harsh conditions. Initially, the reaction was carried out in refluxing toluene in the presence of *p*-toluenesulfonic acid as acid catalyst.[177] NMR investigations then revealed that the solvent also underwent reactions giving byproducts that were hard to separate. The usage of 1,4-dioxane as solvent surprisingly hampered the formation of product. Eventually, acetic acid as solvent gave the desired product **48** in a yield of 14%. The conversion was followed by a Wittig-Horner reaction with phosphonate **36** to give stilbene **49** with a moderate yield of 46%. Deprotection of the diol

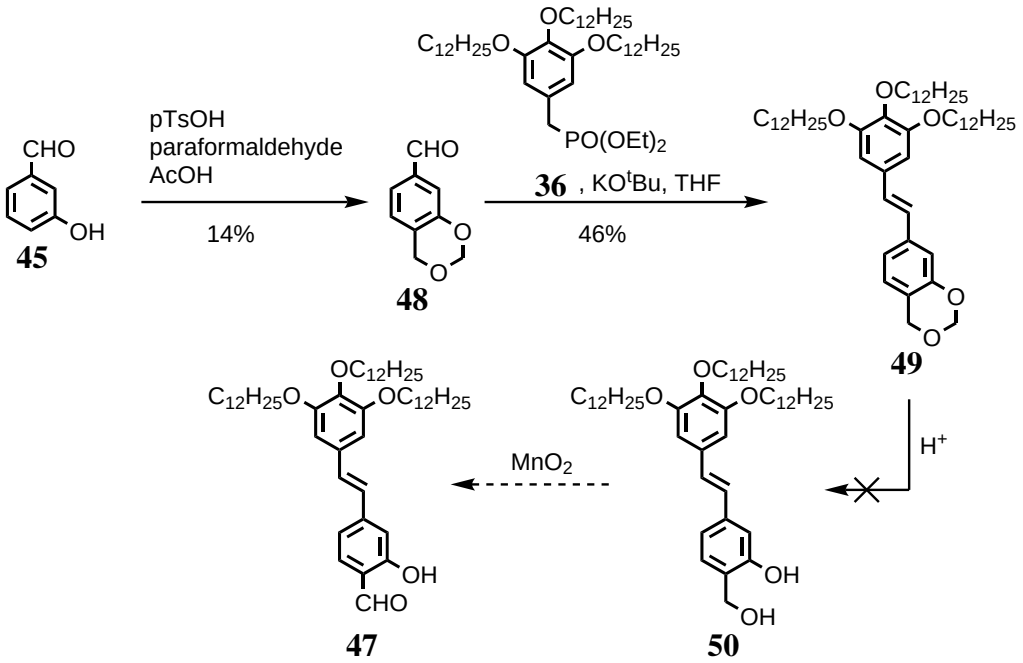

Scheme 22: Attempted synthesis of the arm building block **47** via key compound **48**.

Table 1: Conditions for the attempted deprotection of **49**.

Conditions	Result
BBr_3, DCM, 0 °C[178]	polymerization
1N HCl, 70 °C[179]	no reaction
$HCl_{conc.}$ / H_2O = 1 / 1, reflux[180]	no reaction
EtOH or *n*-PrOH, H_2SO_4 cat.[181]	polymerization

then was attempted with various conditions, which are summarized in table 1. All chemicals used either did not affect the material or initiated polymerization giving undefined products. Therefore, this synthetic strategy was discarded.

Since the hydrolysis of the cyclic acetal **49** with aqueous acid did not proceed, it was presumed that the insolubility of the hydrophobic dodecyl chains prevented the reaction. Therefore, an analogous approach was taken with the core building block **1**, which does not bear aliphatic chains and therefore should be in parts soluble in boiling water. The formation of the triacetal **51** shown in scheme 23 was accomplished by a Wittig-Horner reaction with a yield of 44%. However, the subsequent hydrolysis carried out with refluxing 1M HCl did not show conversion of the acetal either. Similarly to the arm **49**, BBr_3 only gave undefined products. Hence, key compound **48** could not be used as a convenient prolongation building block.

Another readily available and beneficial building block is 2,5-dimethylanisole (**53**), which is reported

Table 2: Conditions for the attempted oxidation of **55**.

Conditions	Result
$K_2S_2O_8$, $CuSO_4$	no reaction
$K_2S_2O_8$, $CuSO_4$, pyridine[182]	no reaction
$K_2S_2O_8$, $CuSO_4$, $AgNO_3$[183]	no reaction

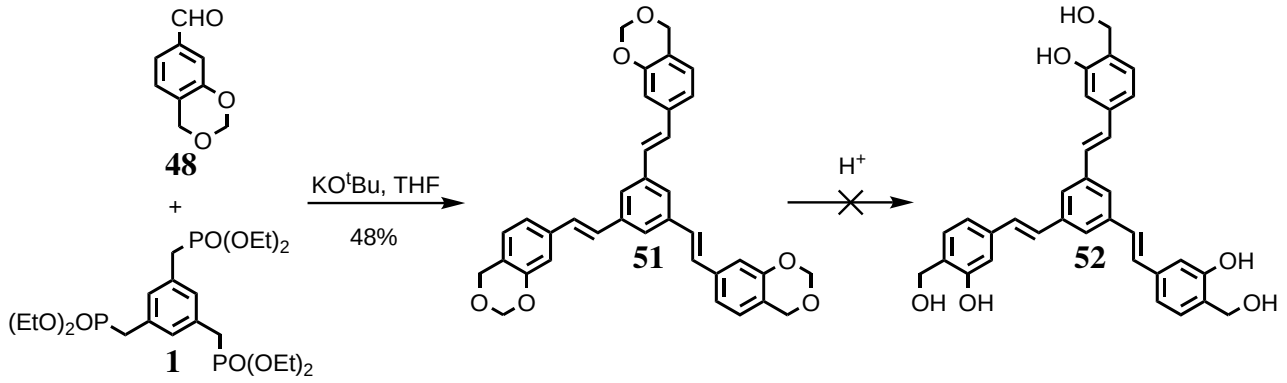

Scheme 23: Attempted synthesis of the core building block **52**.

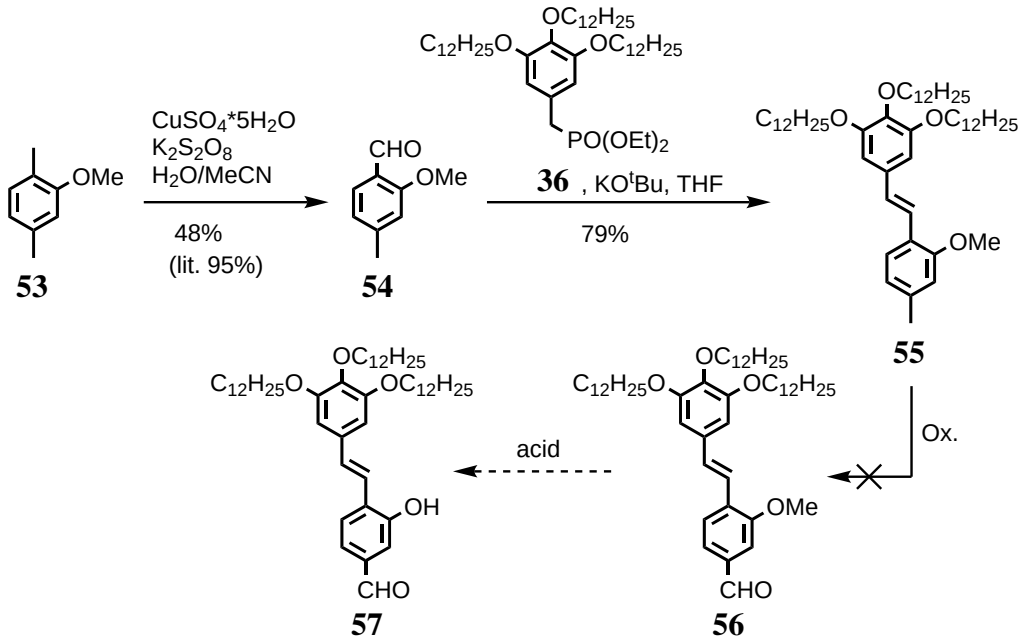

Scheme 24: Attempted synthesis of the arm building block **57**.

to be selectively monooxidized in *ortho*-position via potassium persulfate and Cu^{2+} to give an aldehyde (see scheme 24).[184] When the formylation was carried out with a yield of 48%, small amounts of the regioisomer with the aldehyde in *meta*-position were present and could not be separated via chromatography or distillation. Subsequent Wittig-Horner reaction with phosphonate **36** gave the stilbene **55** in a yield of 79%, along with the corresponding regioisomer. The remaining methyl group then was sought to be oxidized to the corresponding aldehyde with the conditions shown in table 2. In the first run, the same conditions were chosen as for the oxidation of **53**, since the stilbene unit increases the electron density in the methyl group thus facilitating the reaction. However, TLC analysis indicated that no conversion occured. Adding pyridine[182] or silver nitrate[183] did not affect the reaction. Since other typical oxidants only would yield the corresponding carboxylic acid, which would require two additional steps (1. $LiAlH_4$, 2. MnO_2) to give the aldehyde, and the regioisomer could not be separated, this synthetic route did not appear appropriate anymore for the synthesis of **57**.

2,5-dimethylanisole (**53**) can be oxidized at both methyl groups with the strong oxidant permanganate, which yields the corresponding carboxylic diacid.[185] Here, the subsequent reduction with $LiAlH_4$ and oxidation with MnO_2 is viable since the anisole itself is a cheap and readily available starting ma-

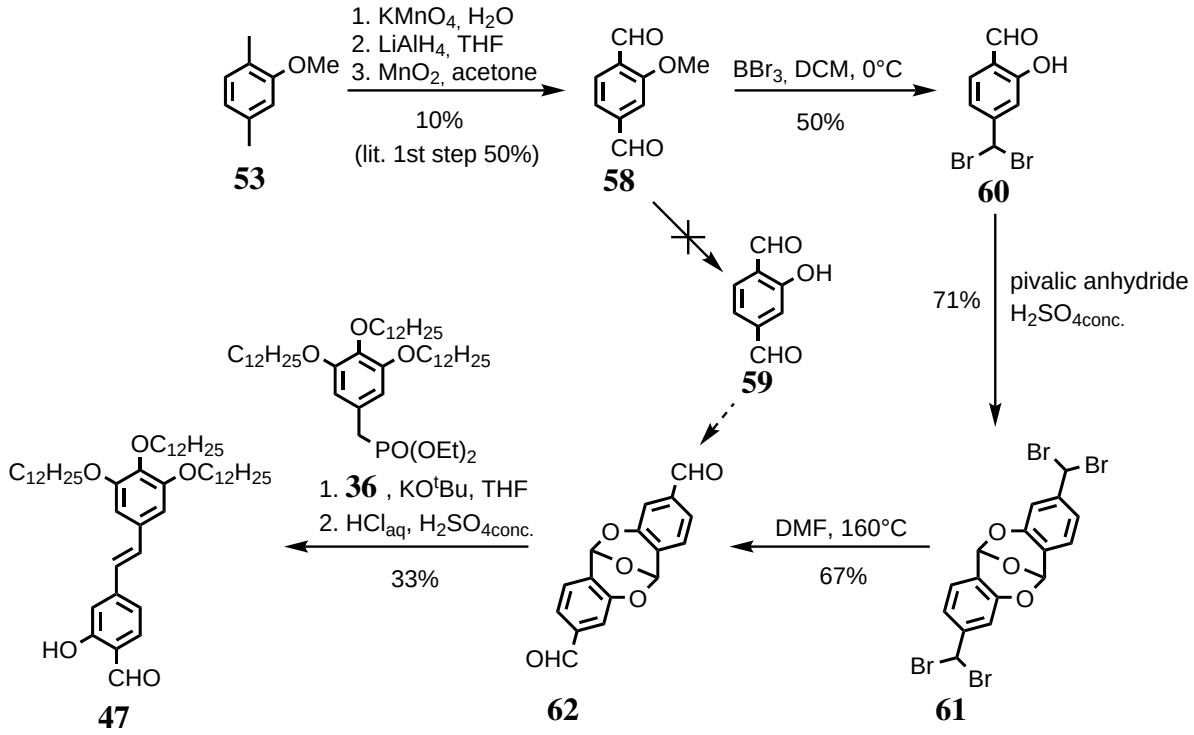

Scheme 25: Synthesis of the arm building block **47** via anhydro-dimers.

terial. Therefore, dialdehyde **58** has been synthesized according to scheme 25. The methoxy group then was cleaved to obtain a salicyl aldehyde derivative, which can be protected in an elegant way: the hydroxy and the aldehyde group can be simultaneously protected by the formation of anhydro-dimers,[186] so only the aldehyde in *meta*-position remains for Wittig-Horner reactions. However, dialdehyde **59** did not form when exposed to boron tribromide. Rather, the aldehyde in *meta*-position was converted to the corresponding dibromide in a yield of 50%, although various ether cleavages tolerating aldehyde groups have been reported with the given conditions.[187–191] Thorough literature research then revealed that formation of dibromide is favored when the aldehyde functional group is located in the *meta*-position of the methoxy group.[192] Nevertheless, the anhydro-dimer was formed with the salicylaldehyde derivative **60** using pivalic anhydride and catalytic amounts of H_2SO_4[193–195] with a yield of 71%. Conversion of the dibromide to the corresponding dialdehyde **62** then was succeeded by simply heating the compound in DMF at 160 °C in a yield of 67%. This reaction relies on the decomposition of DMF at elevated temperatures giving dimethylamin, which forms the corresponding imines. Subsequent hydrolysis then gives the desired dialdehyde.[196] Compound **62** and phosphonate **36** then reacted with Wittig-Horner conditions. The subsequent acidic hydrolysis of the anhydro-dimer was carried out in a mixture of $CHCl_3$ and 1M HCl. At 80 °C, no conversion could be observed by TLC analysis. Therefore, small amounts of H_2SO_4 were added. Several additions of the sulfuric acid were required to advance the progress of the reaction and complete conversion was not succeeded. Eventually, the arm **47** was obtained in a moderate yield of 33%. Due to the additional effort owing to the formation of the dibromide and the problematic hydrolysis of the anhydro-dimer, this synthetic strategy was not further investigated. Hence, the synthesis of the arms shown in the previous chapter is the most promising strategy.

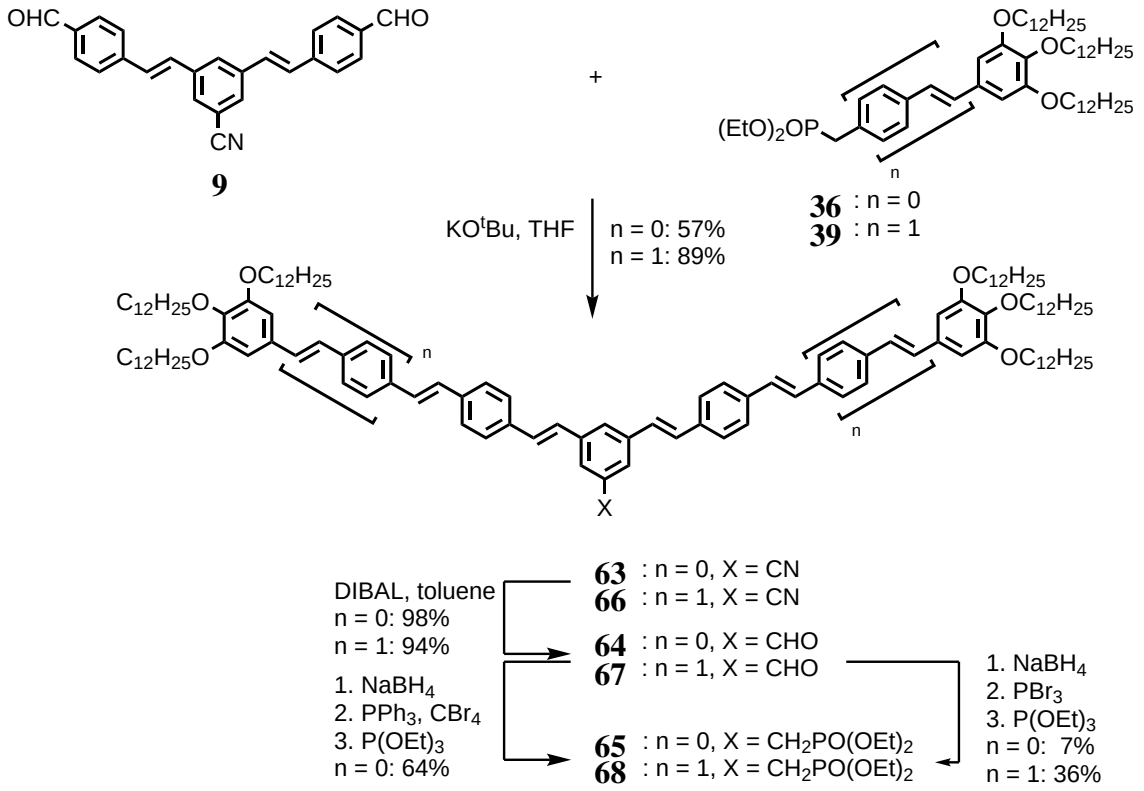

Scheme 26: Synthesis of the V-shaped building blocks **65** and **68**.

4.6 V-shaped building blocks with dodecyloxy-chains

Asymmetrical Hekate stars require the V-shaped building blocks **65** and **68**, which have been succesfully synthesized as illustrated in scheme 26. Core building block **9** has been reacted with either phosphonate **36** or prolonged phosphonate **39** under Wittig-Horner conditions to obtain the compounds **63** and **66** with a yield of 57% and 89%, respectively. The reduction to the aldehydes **64** and **67** was achieved by adding a solution of diisobutylaluminium hydride in toluene at 0 °C with a yield of 98% and 94%, respectively. The formation of the phosphonates **65** and **68** was performed via a three step procedure: Reduction of the aldehyde to the corresponding benzylic alcohol was achieved by sodium borohydride and methanol. The alcohols were converted to the benzylic bromides by the usage of phosphorus tribromide as brominating reagent and led to a significant loss of yield by the formation of undefined side products. Possibly, the stilbene double bond is brominated with subsequent attack of the nucleophile phosphorous center of PBr_3 to get alkylated bromophosphines.[197] Finally, the Arbuzov reaction with triethyl phosphite under solvent-free conditions gave the desired phosphonates with yields for three steps of 7 and 36%, respectively. For the smaller system (n = 0), the three step synthesis has been repeated with milder conditions for the bromination step via Appel reaction, which immensely increased the total yield to 64%.

4.7 Hekate stars with dodecyloxy-chains

The C_3-symmetric Hekate stars $\mathbf{S1}_{C12}$[132,133], $\mathbf{S2}_{C12}$[132] and $\mathbf{S3}_{C12}$ have been succesfully synthesized as illustrated in scheme 27. Core building block **3** has been reacted with either phosphonate **36** or prolonged phosphonate **39** under Wittig-Horner conditions to obtain the stars $\mathbf{S1}_{C12}$ and $\mathbf{S2}_{C12}$ with

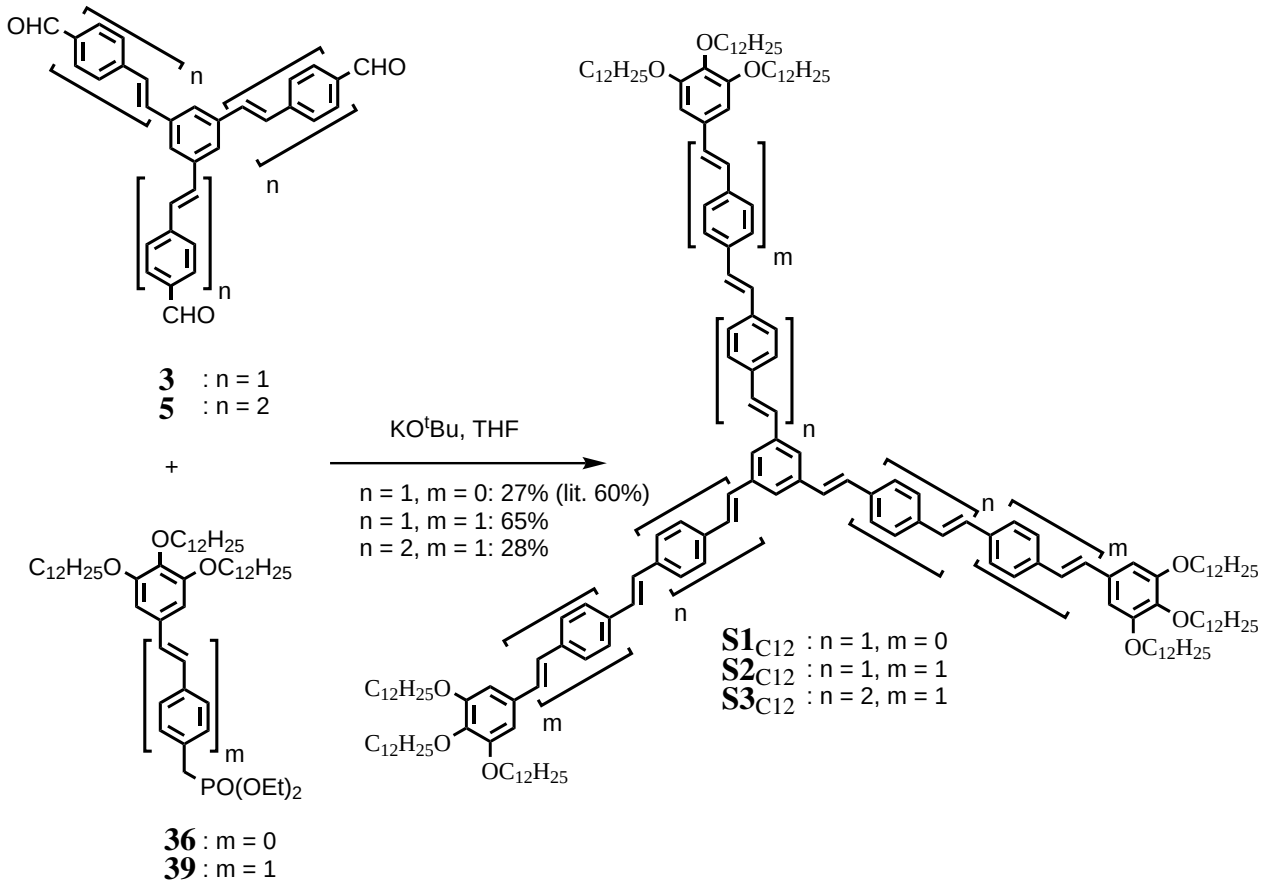

Scheme 27: Synthesis of the stars $\mathbf{S1}_{C12}$, $\mathbf{S2}_{C12}$ and $\mathbf{S3}_{C12}$.

a yield of 27% and 65%, respectively. For the smaller star $\mathbf{S1}_{C12}$, chromatographic workup turned out to be more challenging, giving a reduced yield. The Hekate star $\mathbf{S3}_{C12}$ with three stilbenoid repeating units has been synthesized by a Wittig-Horner reaction of core buiding block **5** and arm phosphonate **39** with a yield of 28%. The decreased yield in comparison to the star $\mathbf{S2}_{C12}$ can be rationalized by the poor solubility of the core building block **5**. Under Wittig-Horner conditions, traces of water might convert the aldehydes to the corresponding carboxylic acids and benzylic alcohols via Cannizzaro reaction. In every case, an excess of phosphonate arm has been used to ensure complete conversion of all three aldehydes.

Figure 23 shows the characteristic NMR signals for the stilbene stars. The protons from the benzene units bearing the chains give singlets at approx. 6.7 ppm. The signals affiliated with the olefinic protons in the stilbene units are located in the range of 6.9 - 7.2 ppm. The protons closest to the core and to the terminal benzene unit show doublets with a strong "leaning" effect, while the inner protons of the stilbene double bonds give pseudo singlets (*). In the range of 7.3 - 7.6 ppm, patterns are observed typical for AA'BB' spin systems. Finally, the protons located at the core of the star mesogen show a singlet at approx. 7.58 ppm.

To link the fullerene bearing spacers with asymmetrical Hekate stars, the phenolic compounds **70** and **72** have been succesfully synthesized as shown in scheme 28. V-shaped building blocks **65** and **68** have been reacted with an excess of aldehyde arms **41** and **43** via Wittig-Horner conditions to form the stilbenoid stars **69** and **71** with yields of 68% and 79%, respectively. The phenolic functions then were deprotected with catalytic amounts of tetrakis(triphenylphosphine)palladium in the presence of

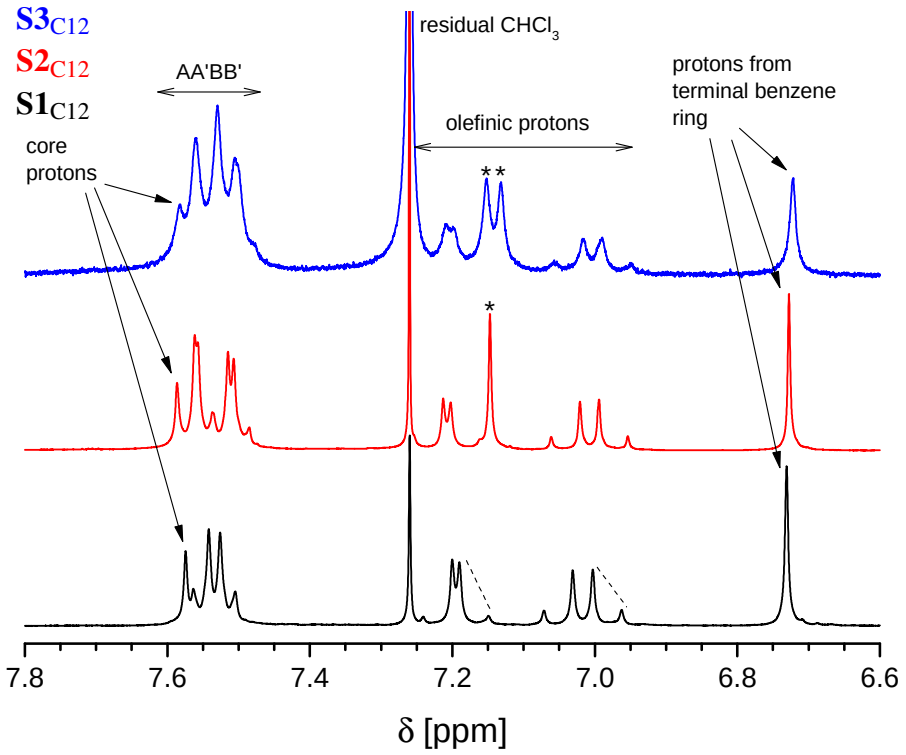

Figure 23: Extract of the NMR data for the Hekate stars **S1**$_{C12}$ (black), **S2**$_{C12}$ (red) and **S3**$_{C12}$ (blue) performed in deuterated chloroform. The dashed lines indicate the "leaning" effect in the signals corresponding to the olefinic protons. The signals marked with * correspond to olefinic protons, which give a pseudo singlet rather than a doublet.

either morpholine or sodium borohydride to give the desired alcohols **70** and **72** in good yields. In the case of the smaller star **70**, the mixture had to be heated to 50 °C to complete the deprotection.

In general, the linkage of the phenolic Hekate stars with spacers bearing fullerenes via Steglich esterification was carried out with an excess of the corresponding acid. In the case of the shortest spacer **23** solubility was very low, with long reaction times as a consequence. Experiments revealed that these stilbene fullerene dyads were decomposing when subjected to gel permeation chromatography. Therefore, tedious separation via liquid chromatography was necessary to obtain the pure target compounds.

The smaller Hekate star bearing a fullerene unit with a short spacer was succesfully synthesized according to scheme 29. Phenolic star **70** was esterified within 7 days with 2.0 equivalents of acid **23** to obtain star **S1**$_{C12}$-**F1**$_{C4}$ with a yield of 15%. This esterification has a substantially lower yield than the Hekate stars with one additional stilbene repeating unit (see scheme 30) owing to a formed byproduct with a similar retention factor compared to the target molecule. As both compounds tail on chromatography, the target compound could only be isolated under high effort and substantial loss of product. The MALDI spectrum of the impurity revealed a strong signal corresponding to the same mass as the target molecule. However, it is uncertain whether this arises from minor amounts of target compound still present in the byproduct or indeed the side product is a conformer of the Hekate star **S1**$_{C12}$-**F1**$_{C4}$.

Figure 24 displays the NMR results for both **S1**$_{C12}$-**F1**$_{C4}$ and its byproduct. The target compound shows two multiplets at 2.97 and 3.33 ppm associated with the ethylene unit from the spacer. The former signal is overlapped by a singlet at 3.01 ppm caused by the NCH_3 group. The signal for the proton located at the stereo center is overlapped by the OCH_2 groups from the dodecyl chains. 2D

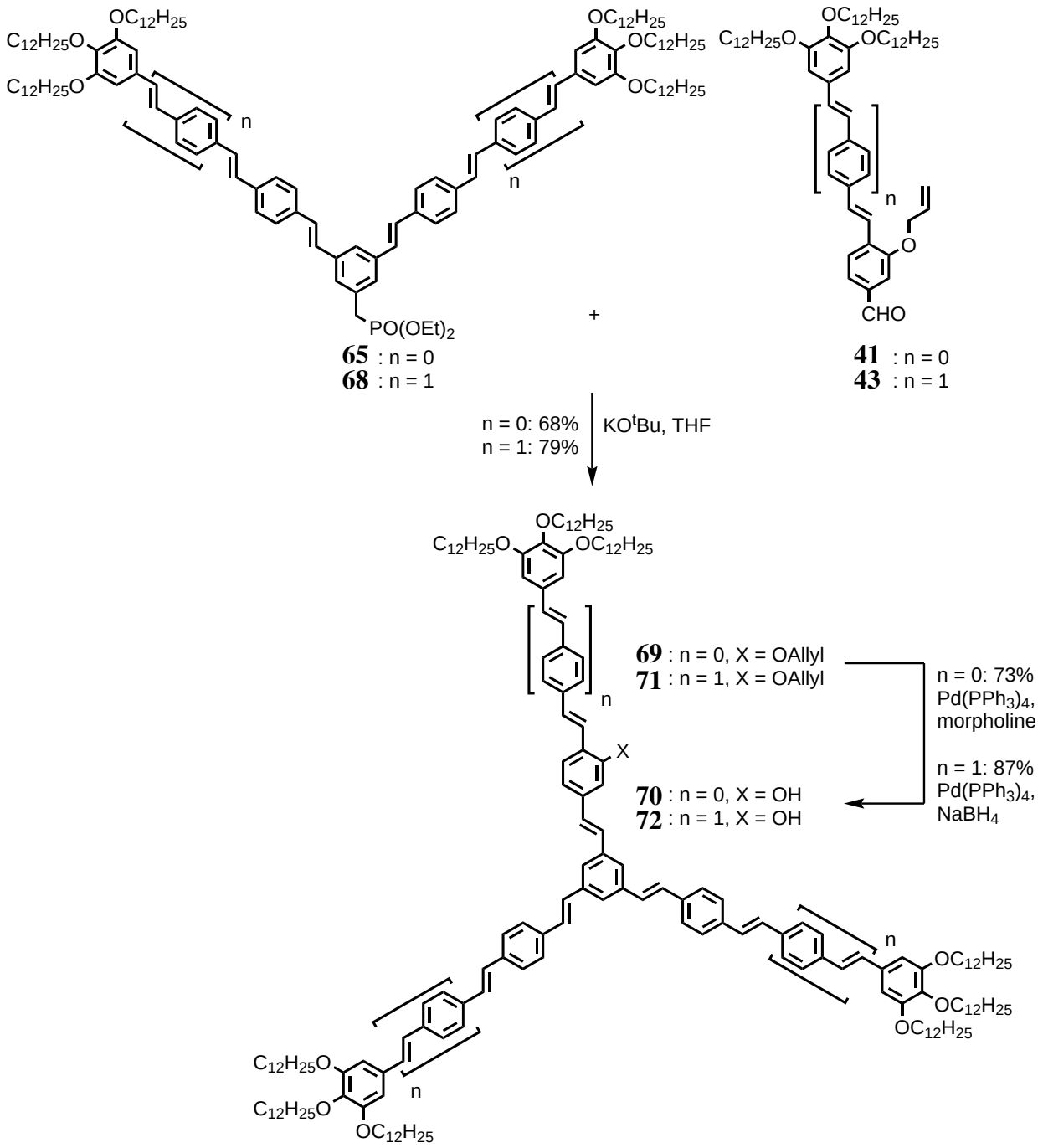

Scheme 28: Synthesis of the stars **70** and **72**.

correlation spectra identify its position at 4.08 ppm. Finally, the diastereotopic NCH_2 protons each give a doublet at 4.17 and 4.83 ppm, respectively. It is noteworthy that all these signals are unusually broad, pointing to a strong aggregation between the fullerenes in solution. The byproduct lacks all of these characteristic[123] patterns. Its brown-colored appearance, however, implies the attachment of a fullerene. For the byproduct, the pyrrolidine ring therefore must have been modified during the course of reaction. The exact nature of the byproduct has not been further investigated.

The Hekate star with an additional stilbenoid repeating unit for each arm was linked to the fullerene bearing spacers with different chain length as illustrated in scheme 30. Steglich esterification was carried out with better yields compared to the synthesis of the smaller star $\mathbf{S1}_{C12}$-$\mathbf{F1}_{C4}$, as all byproducts could easily be separated via column chromatography. The rate of reaction increased with the

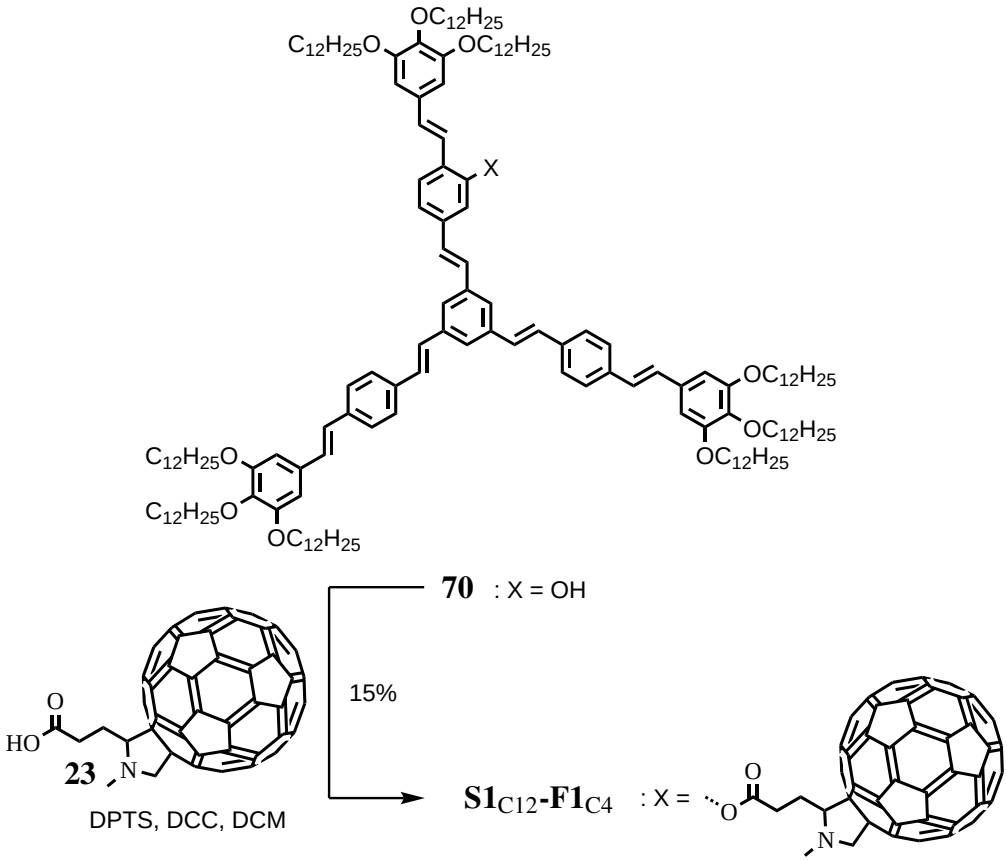

Scheme 29: Synthesis of the stilbene fullerene dyad **S1**$_{C12}$**-F1**$_{C4}$.

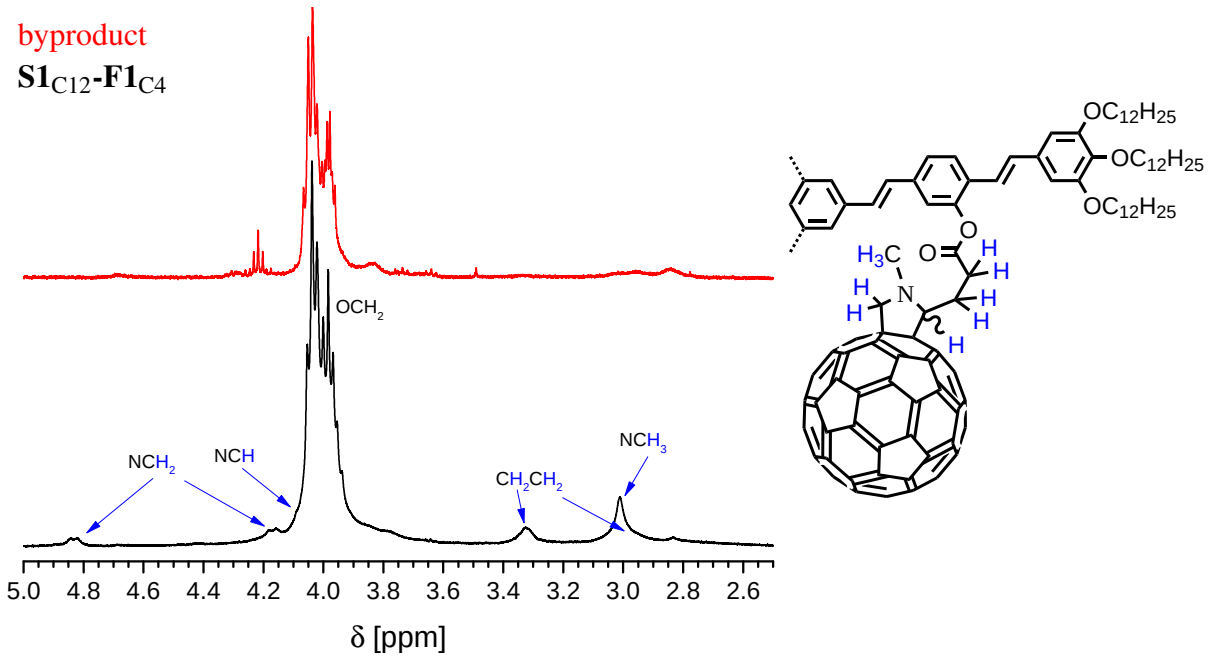

Figure 24: Extract of the NMR data for the Hekate star **S1**$_{C12}$**-F1**$_{C4}$ (black) and its byproduct (red) performed in deuterated chloroform. The signals associated with the fullerene spacer protons are marked with blue arrows.

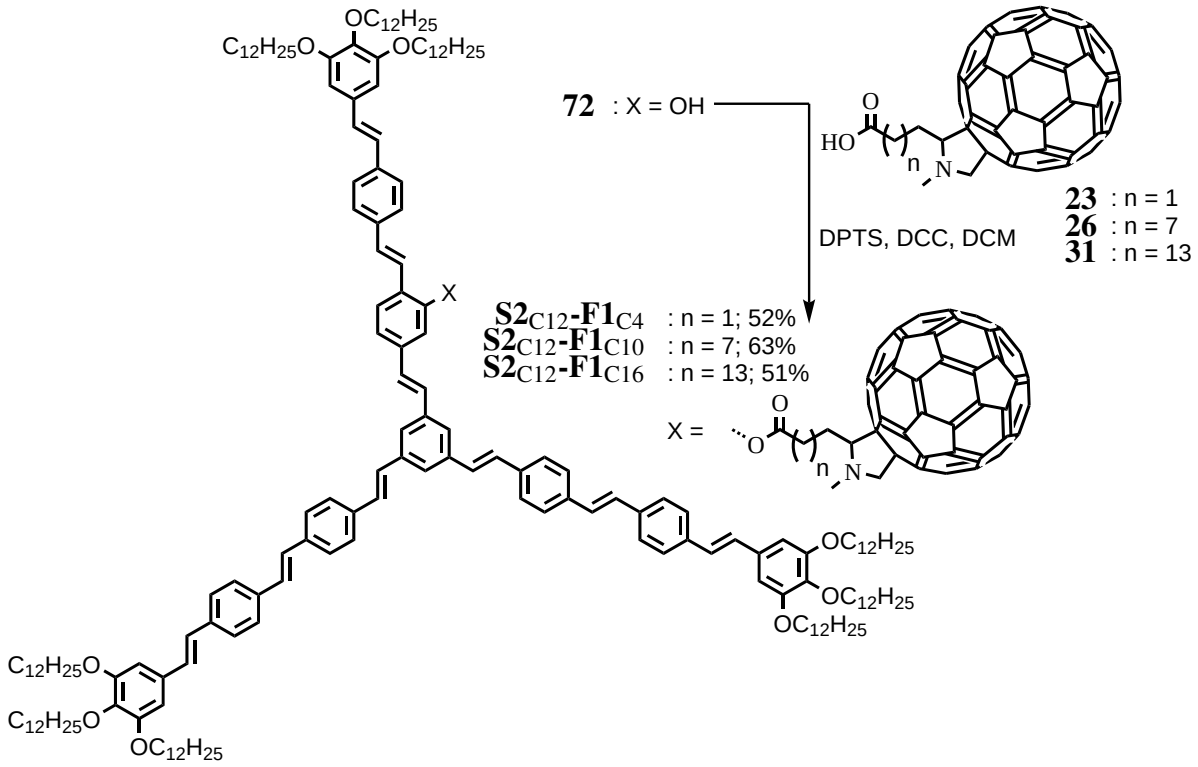

Scheme 30: Synthesis of the stilbene fullerene dyads **S2**$_{C12}$-**F1**$_{C4}$, **S2**$_{C12}$-**F1**$_{C10}$ and **S2**$_{C12}$-**F1**$_{C16}$.

length of the spacers due to the improved solubility of the carboxylic acids. Therefore, the reaction time could be reduced from 8 days (**S2**$_{C12}$-**F1**$_{C4}$) to less than 24 hours (**S2**$_{C12}$-**F1**$_{C16}$).

A C_3-symmetric Hekate star bearing a fullerene unit on each arm has also been synthesized as illustrated in scheme 31. The core building block **1** reacted with three arm building blocks **43** under Wittig-Horner conditions to obtain star **73** with a yield of 77%. Deprotection of the allyl ether was then carried out in the presence of tetrakis(triphenylphosphine)palladium. In the first run (route **A**), sodium borohydride was used as nucleophile to induce the reductive elemination of the π-allyl palladium complex. An NMR spectrum of the isolated product showed that the desired compound contained an impurity. Mass spectra revealed a signal corresponding to the mass of the compound **75** shown in scheme 31. Apparently, to a small percentage the allyl groups were rather hydrogenated than cleaved, giving propyl chains. Cleavage via $Pd(PPh_3)_4/NaBH_4$ is known to proceed very fast[142,198], but in a few cases it has already been reported, that hydrogenation with $NaBH_4$ in the presence of tetrakis(triphenylphosphine)palladium[199,200] or other Pd^0 species[201] can take place. As the target compound and the byproduct could not be separated, the deprotection step was carried out according to route **B** with morpholine as reagent. The pure desired phenol **74** could be obtained in a yield of 79%. The final linkage of the phenol and the fullerene bearing acid **23** via Steglich esterification gave the desired compound **S2**$_{C12}$-**F3**$_{C4}$ with a yield of 26%. Due to the low solubility of the acid **23** and a required threefold esterification, the reaction was stirred for 19 days to complete the conversion.

The identification of the product **S2**$_{C12}$-**F3**$_{C4}$ was hampered by strong aggregation in solution. As can be seen for **S2**$_{C12}$ and **S2**$_{C12}$-**F1**$_{C4}$ in figure 25, the protons located at the 3,4,5-trialkoxy benzene rings (green) face an up-field shift in deuterated chloroform if adjacent to a fulleropyrrolidine unit. Since all signals for these protons in **S2**$_{C12}$-**F3**$_{C4}$ are shifted, it is reasonable to conclude that virtually all chain bearing benzene rings are in the vicinity of a fullerene. Temperature dependent NMR

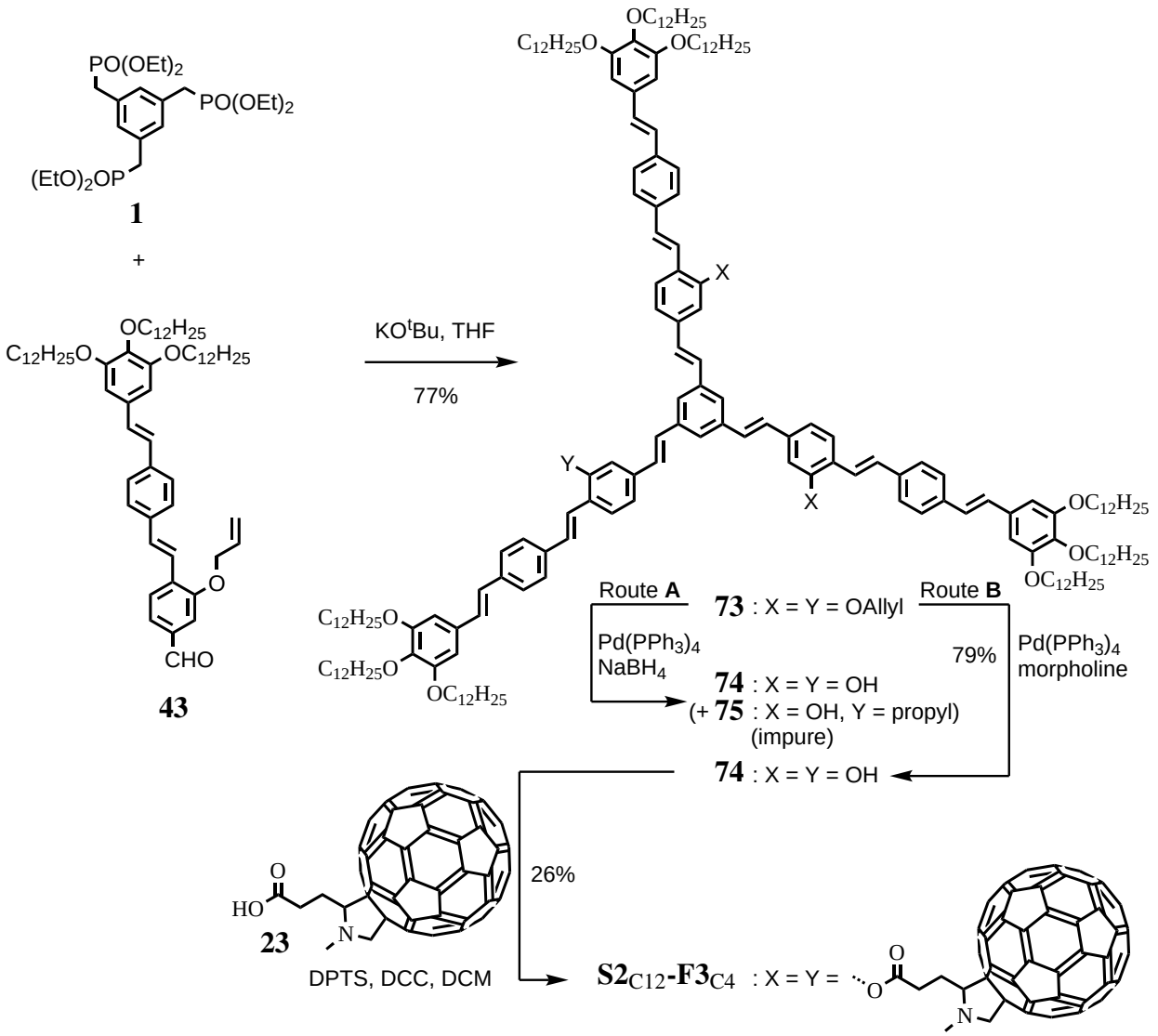

Scheme 31: Synthesis of the stilbene fullerene dyad **S2**$_{C12}$**-F3**$_{C4}$.

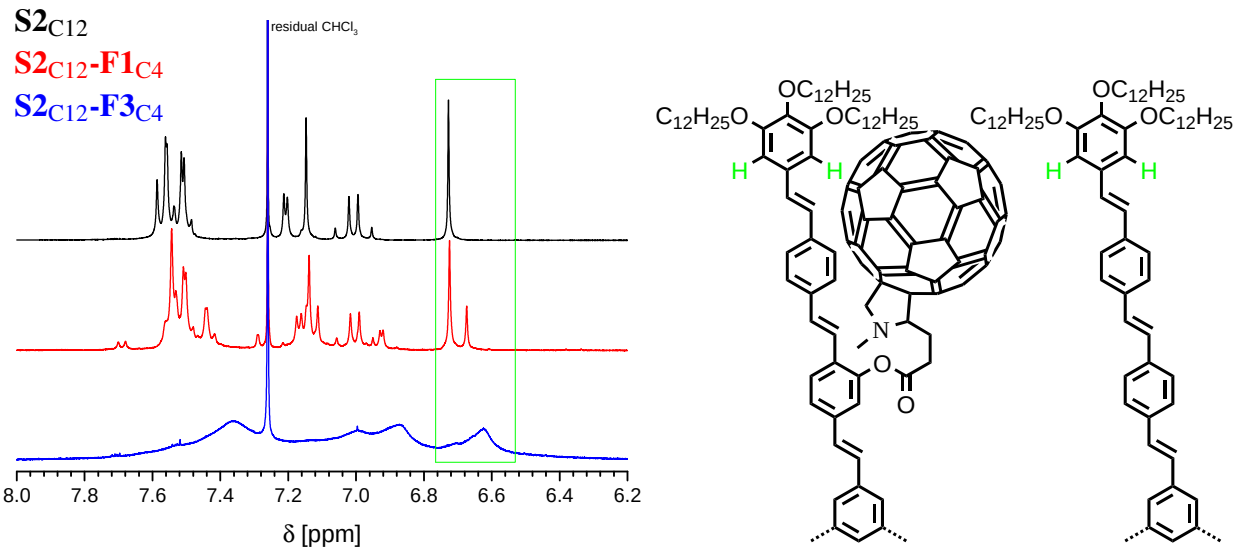

Figure 25: Extracts of the NMR spectra for the compounds **S2**$_{C12}$ (black), **S2**$_{C12}$**-F1**$_{C4}$ (red) and **S2**$_{C12}$**-F3**$_{C4}$ (blue). The signals covered in the green box correspond to the green protons of the chain bearing benzene rings shown in the substructures.

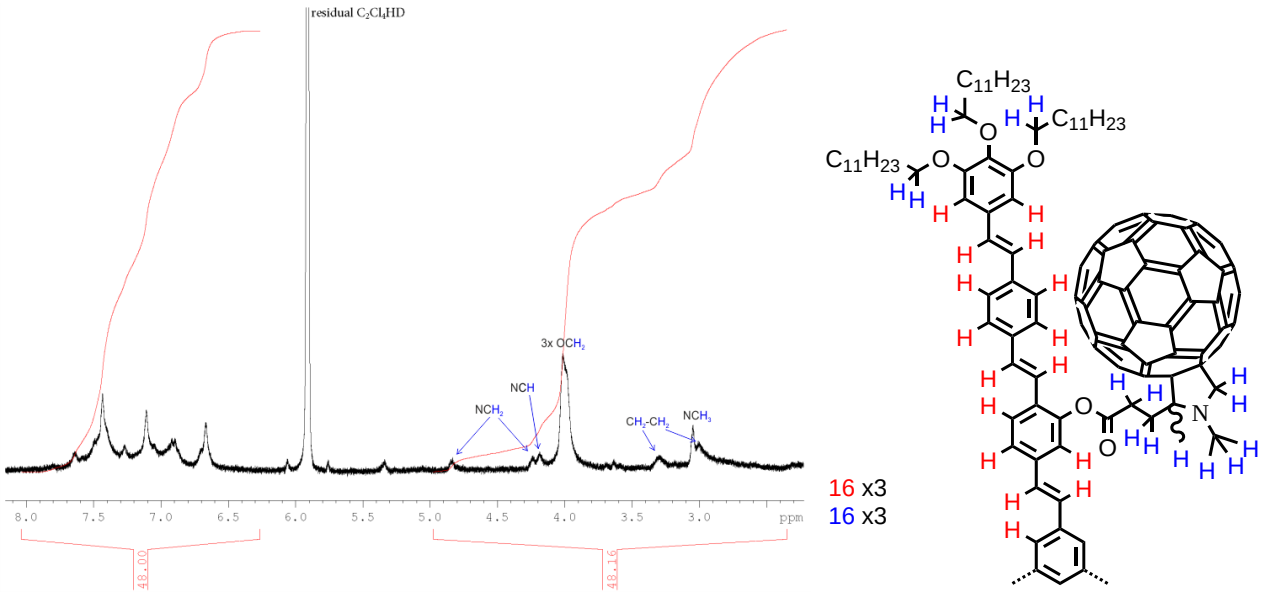

Figure 26: Extract of the NMR spectrum for the compound **S2**$_{C12}$-**F3**$_{C4}$ performed at 120 °C with 1,1,2,2-tetrachloroethane-d2 as solvent. The integrals correspond to the aromatic / olefinic protons (red) and the protons from the -OCH_2- groups and spacer hydrogens (blue).

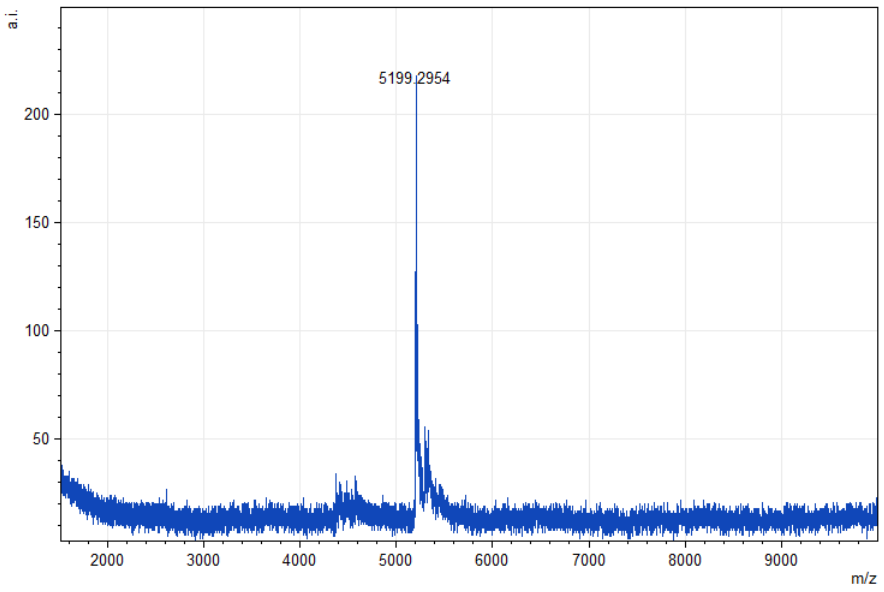

Figure 27: MALDI mass spectrum for the compound **S2**$_{C12}$-**F3**$_{C4}$. M_W = 5199.65 for $C_{384}H_{303}N_3O_{15}$; m/z for $[M+4]^{+\cdot}$ = 5199.32.

experiments in 1,1,2,2-tetrachloroethane-d2 from room temperature to 120 °C have been performed. The results for 120 °C displayed in figure 26 reveal that strong aggregation persists even at this high temperature. Additionally, the material consists of diastereomers owing to the stereo center at the pyrrolidine ring. An individual assignment of all the protons therefore is prevented. Nevertheless, the completeness of the threefold esterification between the phenolic arms and the carboxylic acids bearing the fullerenes can be checked by comparing the integrals between the protons from the -OCH_2- groups and spacer hydrogens (blue) with the aromatic and olefinic protons (red). The expected ratio of 48 : 48 was found, while a missing fullerene spacer would reduce this ratio to 38 : 48. Therefore, it can be concluded that the product bears all three fullerenes. Due to the low concentration achievable for ^{13}C NMR measurements, even long term experiments with a 600 MHz machine could not signif-

icantly improve the signal-to-noise ratio. Consequently, many ternary and quaternary signals of low intensity did not reveal with certainty. Nevertheless, signals typical for the pyrrolidines at 40.2 ppm and 70.3 ppm as well as broadened signals typical for the quaternary fullerene carbons in the region of 139.8 -149.1 show the presence of the fulleropyrrolidine unit in the molecule. Eventually the unambiguous signal in the MALDI mass spectrum for the dyad $\mathbf{S2}_{C12}$-$\mathbf{F3}_{C4}$ confirms the proposed structure (see figure 27).

For the introduction of chiral fullerene building blocks, the esters **76** and **77** were kindly provided by Prof. Dr. Nazario Martín from the University Complutense in Madrid. These precursors were hydrolyzed according to scheme 32. The materials were dissolved in a mixture of CF_3COOH and DCM and stirred for a few hours. Workup consisted of simply distilling the solvent, giving the corresponding acids **78** and **79** in quantitative yields. As these fullerene building blocks do not comprise a flexible spacer, the phenolic alcohol **72** was hydroxyalkylated with ethylene carbonate[202,203] as illustrated in scheme 33. Due to the ring strain in the carbonate, the oxygens next to the CH_2 units act as leaving groups in the presence of nucleophiles. Subsequent decarboxylation affords the aliphatic alcohol **80**. In the first run, the reaction was performed with potassium carbonate as base in refluxing toluene.[204,205] As TLC analysis only revealed conversion to a small percentage after several hours, DMF was used as solvent in the next batch.[206,207] The completeness was verified by TLC analysis after two hours. The improved reaction rate probably is due to the better solubility of the base. The chiral fullerene building block was then linked either as a racemic mixture (**78**) or as the pure enantiomer (**79**) with the alcohol **72** via Steglich esterification to obtain the target compounds $\mathbf{S2}_{C12}$-$\mathbf{F}_{rac.}$ and $\mathbf{S2}_{C12}$-$\mathbf{F}_{enan.}$ with a yield of 61% and 60%, respectively. Solubility of the fullerene bearing carboxylic acids was low and comparable to that of the shortest fulleropyrrolidine spacer (**23**). Therefore, the reaction mixture was stirred for several days to complete the esterification.

The NMR results obtained for the product are displayed in figure 28. In the aromatic shift region, strong aggregation prevents the individual characterization of protons. Nevertheless, the protons located at the chains bearing benzene unit are distinguishable and shifted up-field in an analogous way to the fulleropyrrolidines when adjacent to a fullerene bearing cyclopenteno unit (green box). At higher

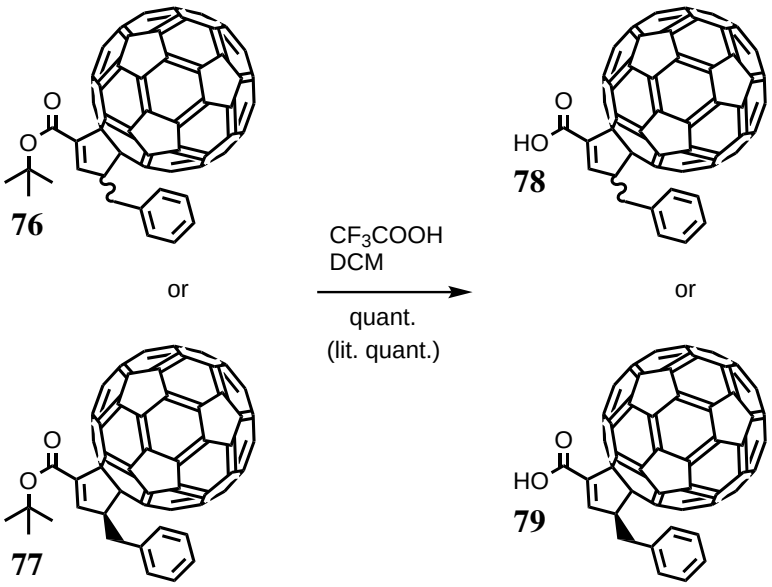

Scheme 32: Synthesis of the chiral fullerene building blocks **78** and **79**.

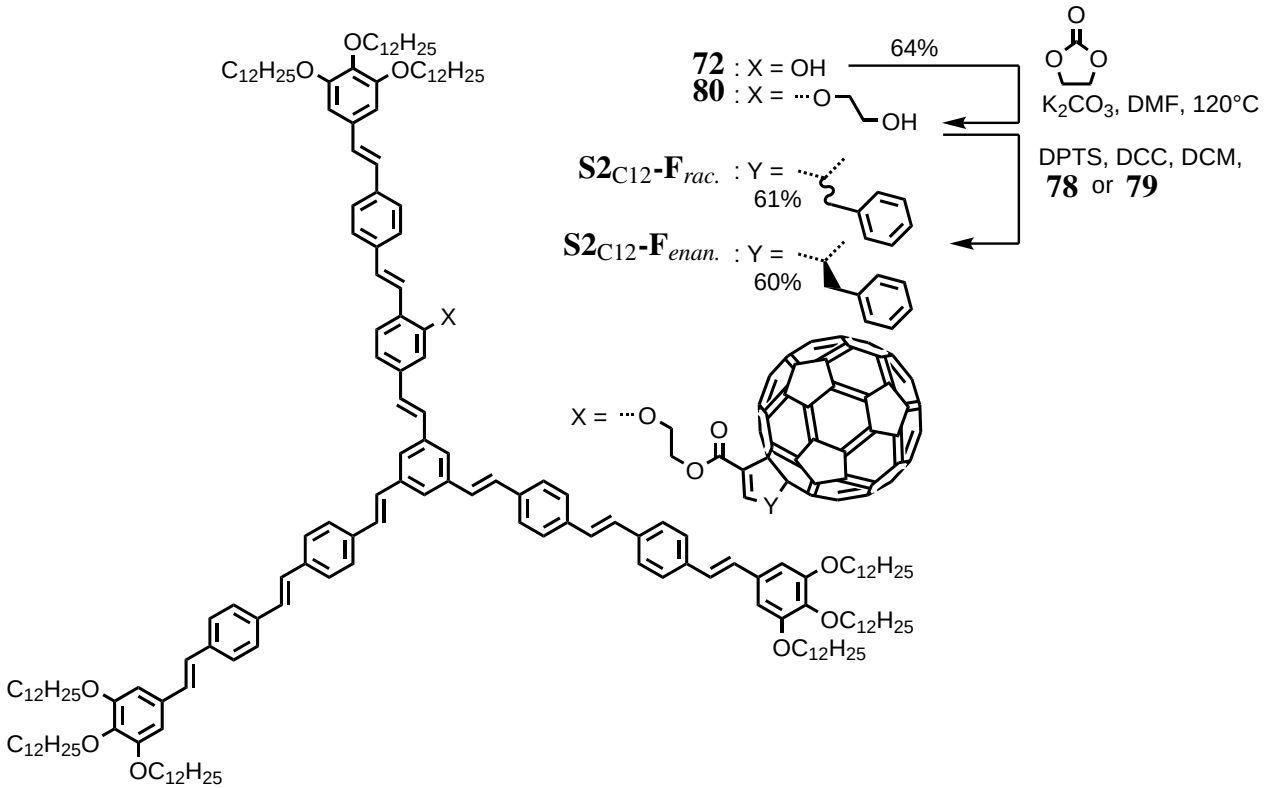

Scheme 33: Synthesis of the stilbene fullerene dyads **S2**$_{C12}$**-F**$_{rac.}$ and **S2**$_{C12}$**-F**$_{enan.}$.

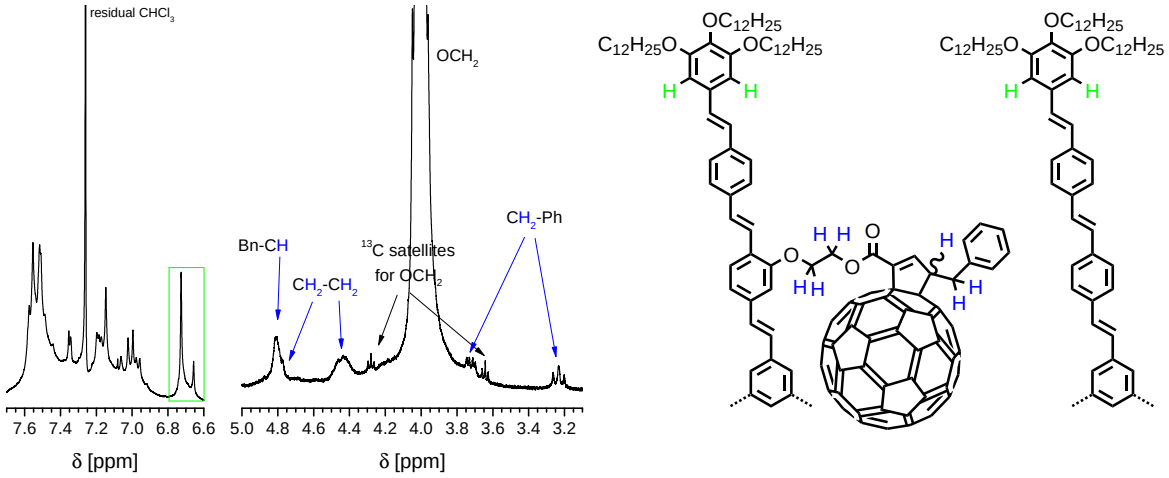

Figure 28: Extracts of the NMR spectra for the compound **S2**$_{C12}$**-F**$_{rac.}$. The signals associated with the non-aromatic and non-olefinic fullerene spacer protons shown in the substructure are marked with blue arrows. The signals covered in the green box correspond to the protons of the dodecyl chains bearing benzene rings.

fields, characteristic signals[14] caused by the cyclopenteno fullerenes are revealed, which were assigned with assistance of 2D NMR experiments. The diastereotopic benzylic protons each show a doublet of doublets at 3.23 and 3.72 ppm, respectively. The proton located at the stereo center shows a broad multiplet at 4.80 ppm. Additionally, the ethylene unit gives two broad signal at 4.43 and 4.79 ppm. The signals for the single olefinic and the five aromatic protons are expected in the low-field region of the other aromatic protons and therefore cannot be located. The proposed monoadduct structures were confirmed by MALDI MS experiments.

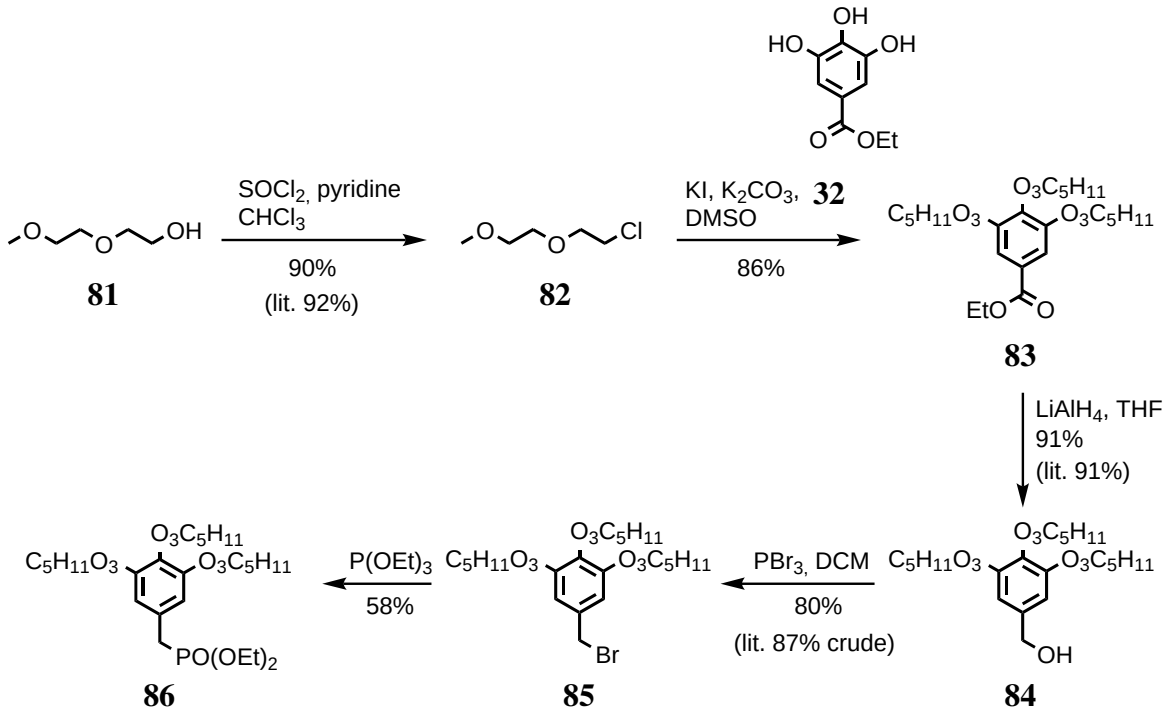

Scheme 34: Synthesis of the arm building block **86**.

4.8 Arm building blocks with short ethyleneoxy-chains

The stilbenoid arms bearing short ethyleneoxy-chains have been prepared starting from phosphonate **86**, which has been synthesized according to scheme 34 and in a similar way to the corresponding phosphonate bearing dodecyl chains (scheme 16, page 38). In the first step, 2-(2-methoxyethoxy)ethanol (**81**) was chlorinated under standard conditions to yield compound **82**[208] with a yield of 90%. Etherification of ethylgallat (**32**) with the chloride gave the ester **83**[209] with a yield of 86%. The reduction of the ester to the benzylic alcohol **84** was achieved by excess of lithium aluminium hydride in THF[209] in a yield of 91%. The bromide **85**[210] was obtained with the brominating reagent phosphorus tribromide in a yield of 80%.* In the last step, the Arbuzov reaction with triethyl phosphite under solvent-free conditions gave the desired phosphonate **86** with a yield of 58%. The corresponding prolonged phosphonate **88** has been synthesized succesfully according to scheme 35. In the initial Wittig-Horner reaction, the phosphonate **86** reacted with the aldehyde **13** to obtain the stilbene **87** as a raw product with a yield of 64%. Without further purification, the THP ether was converted to the corresponding benzylic bromide via the in-situ formation of triphenylphosphine dibromide. The subsequent Arbuzov reaction with triethyl phosphite under solvent-free conditions gave the desired phosphonate **88**, which could be isolated by column chromatography with a yield of 64% for two steps.

For the synthesis of porphyrin based stars, aldehyde arm building block **89** was required and synthesized as illustrated in scheme 36. Reacting phosphonate **88** with (diethoxymethyl)benzaldehyd (**2**) under Wittig-Horner conditions with subsequent acidic hydrolysis of the acetal gave the desired aldehyde **89** in a yield of 83%.

*The synthesis from compound **81** to compound **85** has been executed by the intern Alexander Hermann in April 2015 under the supervision of the author of this document.

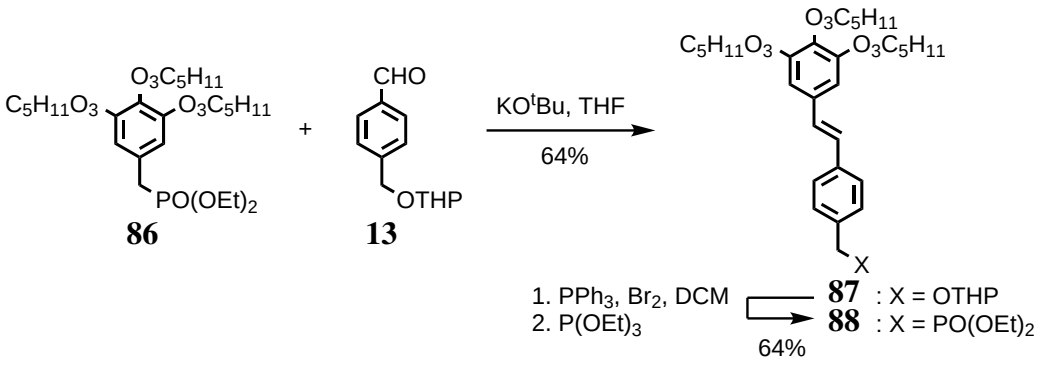

Scheme 35: Synthesis of the arm building block **88**.

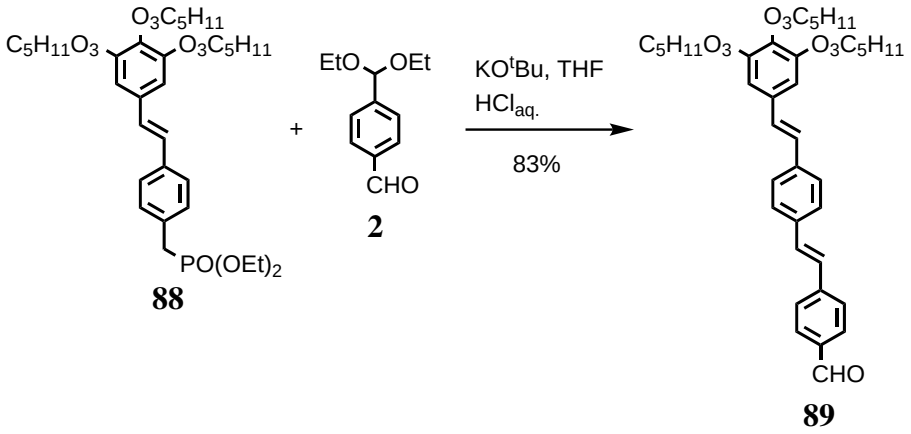

Scheme 36: Synthesis of the arm building block **89**.

4.9 Hekate star with short ethyleneoxy-chains

A C_3-symmetric Hekate star with short ethyleneoxy-chains has been succesfully synthesized as illustrated in scheme 37. The core building block **3** reacted with an excess of the arm buidling block **88** under Wittig-Horner conditions. In contrast to the phosphonate, the target compound slowly precipitated in a petroleum ether solution when stored in the cold. Additional purification via gel permeation chromatography afforded the desired star compound $\mathbf{S2}_{O2}$ in a yield of 39%.

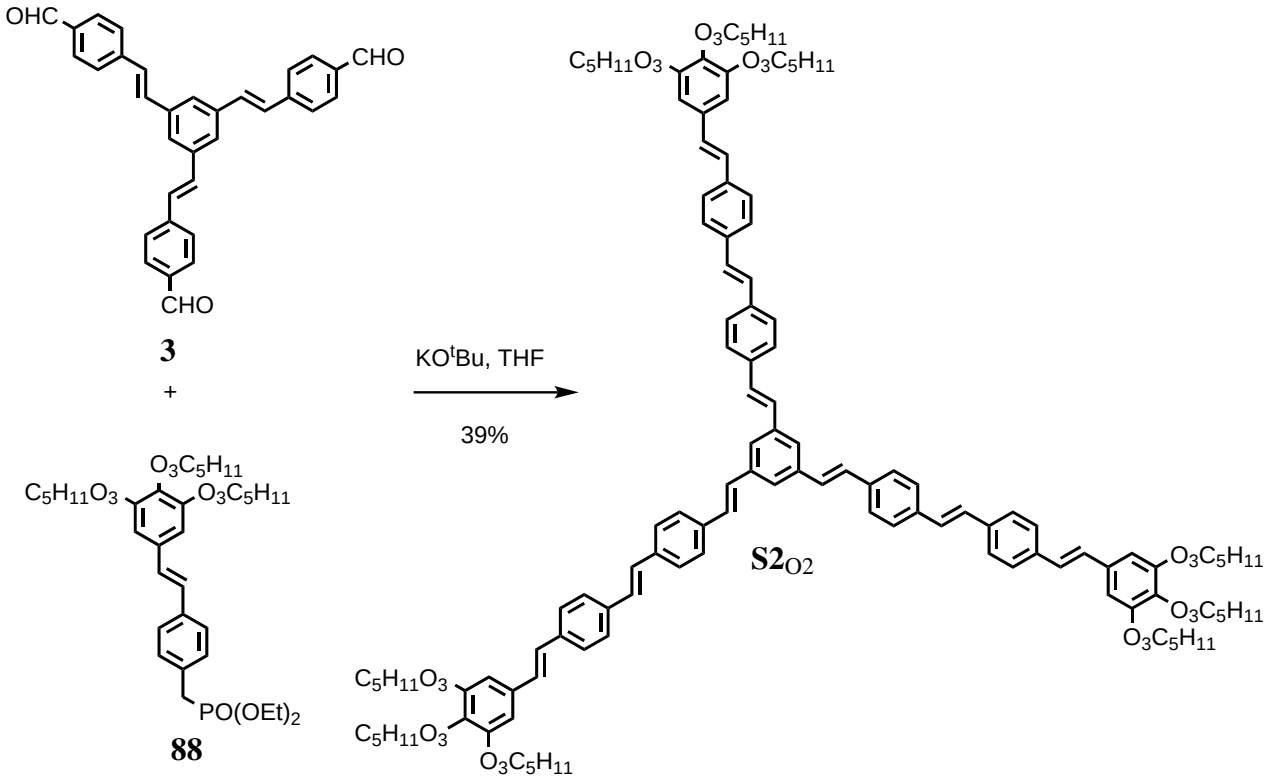

Scheme 37: Synthesis of the Hekate star $\mathbf{S2}_{O2}$.

4.10 Arm building blocks with long ethyleneoxy-chains

The stilbenoid arms bearing long ethyleneoxy-chains have been prepared starting from phosphonate **94**, which has been synthesized according to scheme 38 and in a similar way to the corresponding phosphonate bearing short ethyleneoxy chains (scheme 34, page 54). In the first step, triethylene glycol monoethyl ether (**90**) was tosylated under reported conditions[211] to give compound **91** with a yield of 39%. Etherification of ethyl gallate (**32**) in an analogous way to the corresponding etherification of methyl gallate[211] with the tosylate gave the ester **92** with a yield of 32%.* The reduction of the ester to the benzylic alcohol **93** was achieved by excess of lithium aluminium hydride in THF[211] in an excellent yield of 98%. The phosphonate **94** was obtained by first adding the brominating reagent phosphorus tribromide and then carrying out an Arbuzov reaction with triethyl phosphite under solvent-free conditions with a yield of 69%.

*The synthesis of the compounds **91** and **92** has been executed by the technician Felix Weißenberger in October 2014 under the supervision of the author of this document.

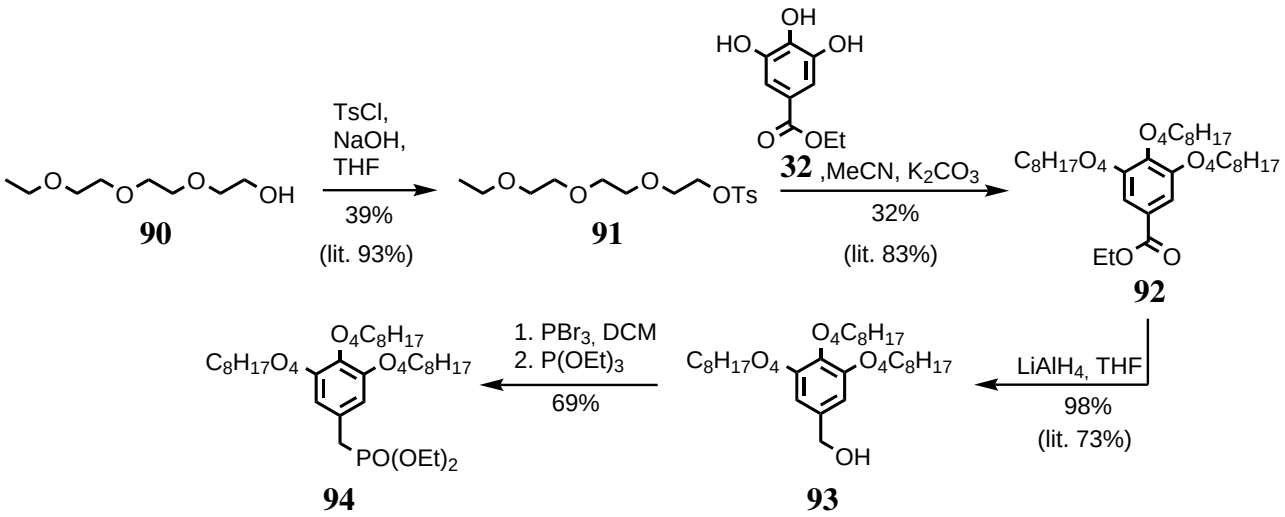

Scheme 38: Synthesis of the arm building block **94**.

The corresponding prolonged phosphonate **96** has been synthesized succesfully according to scheme 39. In the initial Wittig-Horner reaction, the phosphonate **94** reacted with the aldehyde **13** to obtain the stilbene **95** as a raw product with a yield of 81%. Without further purification, the THP ether was converted to the corresponding benzylic bromide via the in-situ formation of triphenylphosphine dibromide. The subsequent Arbuzov reaction with triethyl phosphite under solvent-free conditions gave the desired phosphonate **96**, which could be isolated by column chromatography with a yield of 60% for two steps.

For the preparation of arms bearing a single allyl ether group, the synthetic route shown in scheme 40 has been applied successfully. Starting from phosphonate **96**, a Wittig-Horner reaction was carried out with the prolongation unit **18** in THF and with potassium *tert*-butoxide as base. Lithium aluminium hydride was added to give the corresponding benzylic alcohol. Aldehyde **97** was obtained by oxidation via high excess of activated manganese dioxide with an overall yield of 67%, with minor impurities still present.

For the synthesis of porphyrin based stars, aldehyde arm building block **98** was required and synthesized as illustrated in scheme 41. Reacting phosphonate **96** with (diethoxymethyl)benzaldehyd (**2**) under Wittig-Horner conditions with subsequent acidic hydrolysis of the acetal gave the desired aldehyde **98** in a yield of 81%.

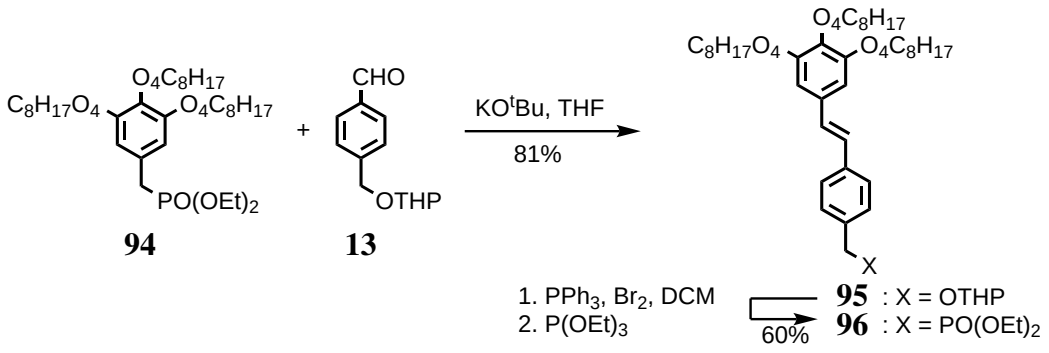

Scheme 39: Synthesis of the arm building block **96**.

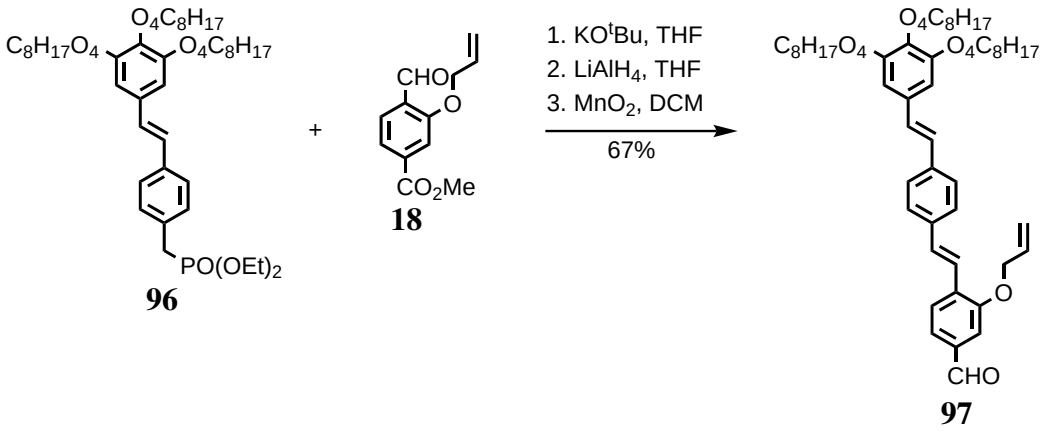

Scheme 40: Synthesis of the arm building block **97**.

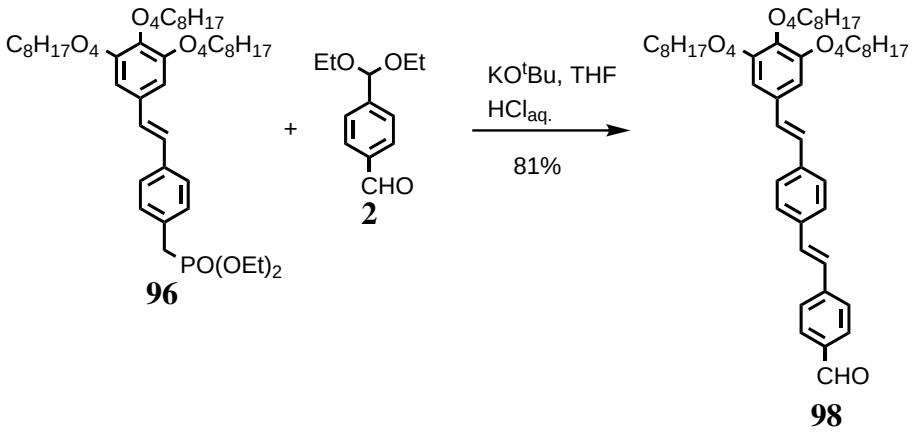

Scheme 41: Synthesis of the arm building block **98**.

4.11 V-shaped building blocks with long ethyleneoxy-chains

V-shaped building block **101** has been succesfully synthesized as illustrated in scheme 42. Core building block **9** has been reacted with prolonged phosphonate **96** under Wittig-Horner conditions to obtain the compound **99** with a yield of 52%. Compared to the alkyl chain derivative **66**, workup of this reaction turned out to be sophisticated. The product is of waxy nature and could not be precipitated from any tested solvent. Additionally, the oligo(ethyleneoxy) chain compounds in general do not show efficient separation on silica gel columns. Hence, a mixture of the excess phosphonate arm and the desired product was obtained after chromatographic workup. The pure target compound finally was isolated via size exclusion chromatography of aliquots of the raw material. The reduction to the aldehyde **100** was achieved by adding a solution of diisobutylaluminium hydride in toluene at 0 °C with a yield of 87%. The formation of the phosphonate **101** was performed via a three step procedure: Reduction of the aldehyde to the corresponding benzylic alcohol was achieved by sodium borohydride and methanol. The alcohol was converted to the benzylic bromide by an Appel reaction with triphenylphosphine and carbon tetrabromide. This step required tedious chromatographic workup since the formed byproduct triphenylphosphine oxide showed a similar retention factor compared to the desired bromide. Nevertheless, side-product formation in this step was low just like for the brominated precursor of the alkyl chain derivative **65**. This confirms the superiority of these reaction conditions compared to the derivatization via PBr_3 (brominated precursor of the alkyl chain derivative **68**) for these structures. Finally, the Arbuzov reaction with triethyl phosphite under solvent-free conditions gave the desired phosphonate with a yields for three steps of 41%.

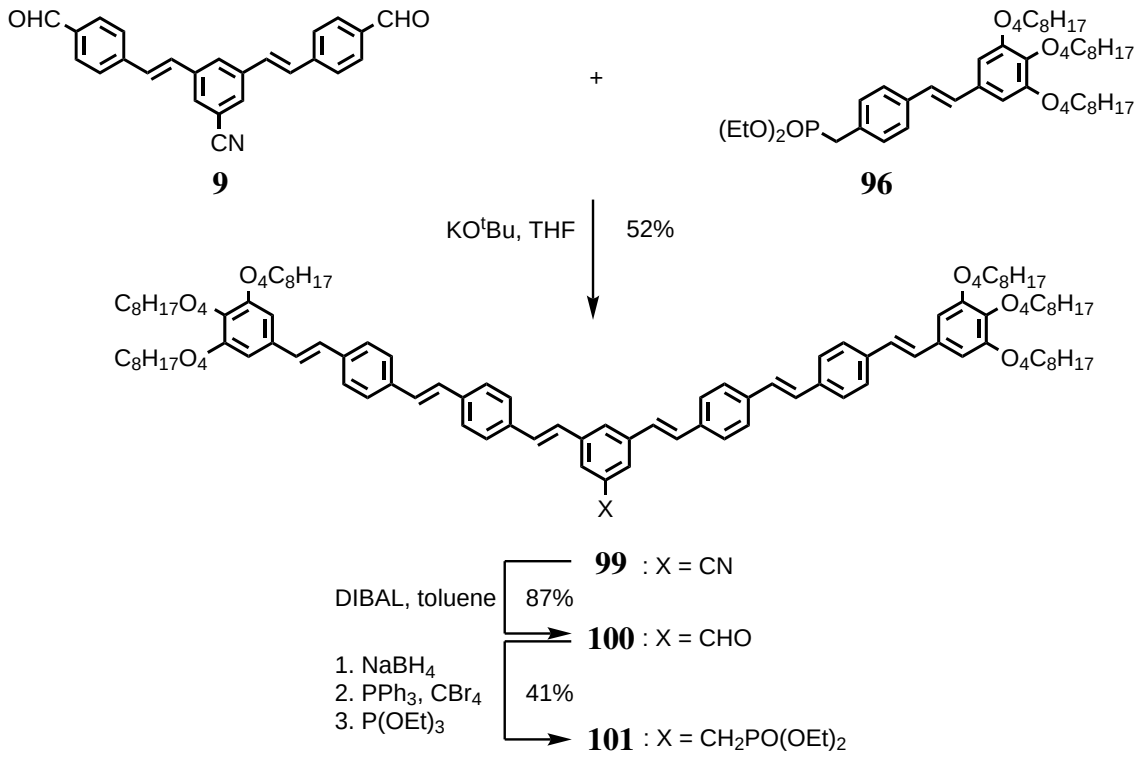

Scheme 42: Synthesis of the V-shaped building block **101**.

4.12 Hekate stars with long ethyleneoxy-chains

A C_3-symmetric Hekate star with long ethyleneoxy-chains has been succesfully synthesized as illustrated in scheme 43. The core building block **3** reacted with an excess of the arm buidling block **96** under Wittig-Horner conditions. In contrast to the phosphonate, the target compound slowly precipitated in a n-hexane solution when stored in the cold. Additional purification via gel permeation chromatography afforded the desired star compound $\mathbf{S2}_{O3}$ in a yield of 62%.

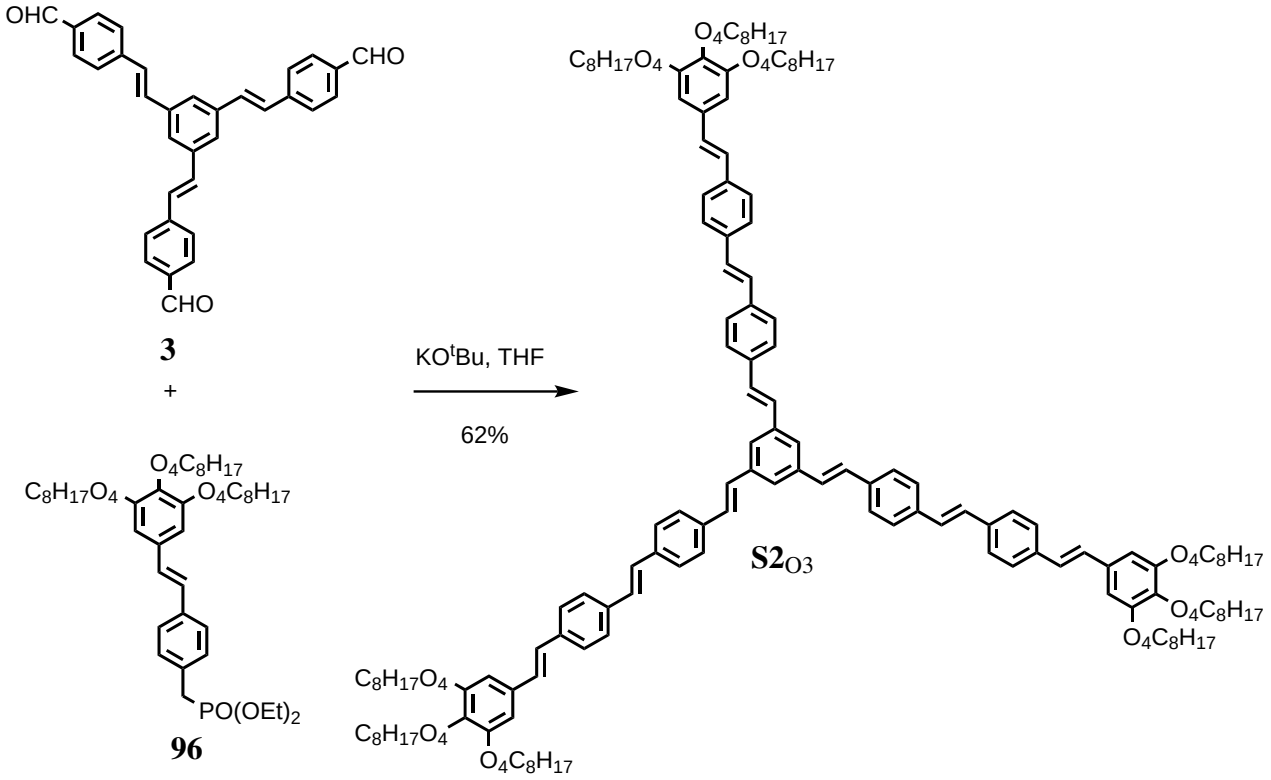

Scheme 43: Synthesis of the Hekate star $\mathbf{S2}_{O2}$.

A fullerene bearing, asymmetrical Hekate star ($\mathbf{S2}_{O3}$-$\mathbf{F1}_{C4}$) has been succesfully synthesized as shown in scheme 44. The V-shaped building block **101** has been reacted with an excess of the aldehyde arm **97** via Wittig-Horner to form the stilbenoid star **102** with a yield of 58%. The phenolic function was deprotected with tetrakis(triphenylphosphine)palladium in the presence of an excess of morpholine to give the alcohol **103** in a yield of 70%. In the last step, the fullerene bearing acid **23** was linked to the phenol **103** via Steglich esterification. Due to the poor solubility of the acid, the reaction time was high and comparable to that of the dodecyl chain derivative $\mathbf{S2}_{C12}$-$\mathbf{F1}_{C4}$. Therefore, the mixture was stirred for 5 days before workup. The product is not soluble in petroleum ether and thus could be purified via precipitation. However, not all impurities could be removed in that manner. Owing to the attached fullerene, the dyad gave cloudy solutions when mixed with methanol. With the aid of a filter funnel with a pore size $\leq$ 1.6 µm, the product could be isolated while all other oligo-(ethyleneoxy) chains bearing side-products remained in the alcoholic phase. This way, the desired fullerene-stilbene dyad $\mathbf{S2}_{O3}$-$\mathbf{F1}_{C4}$ was obtained with a yield of 69%.

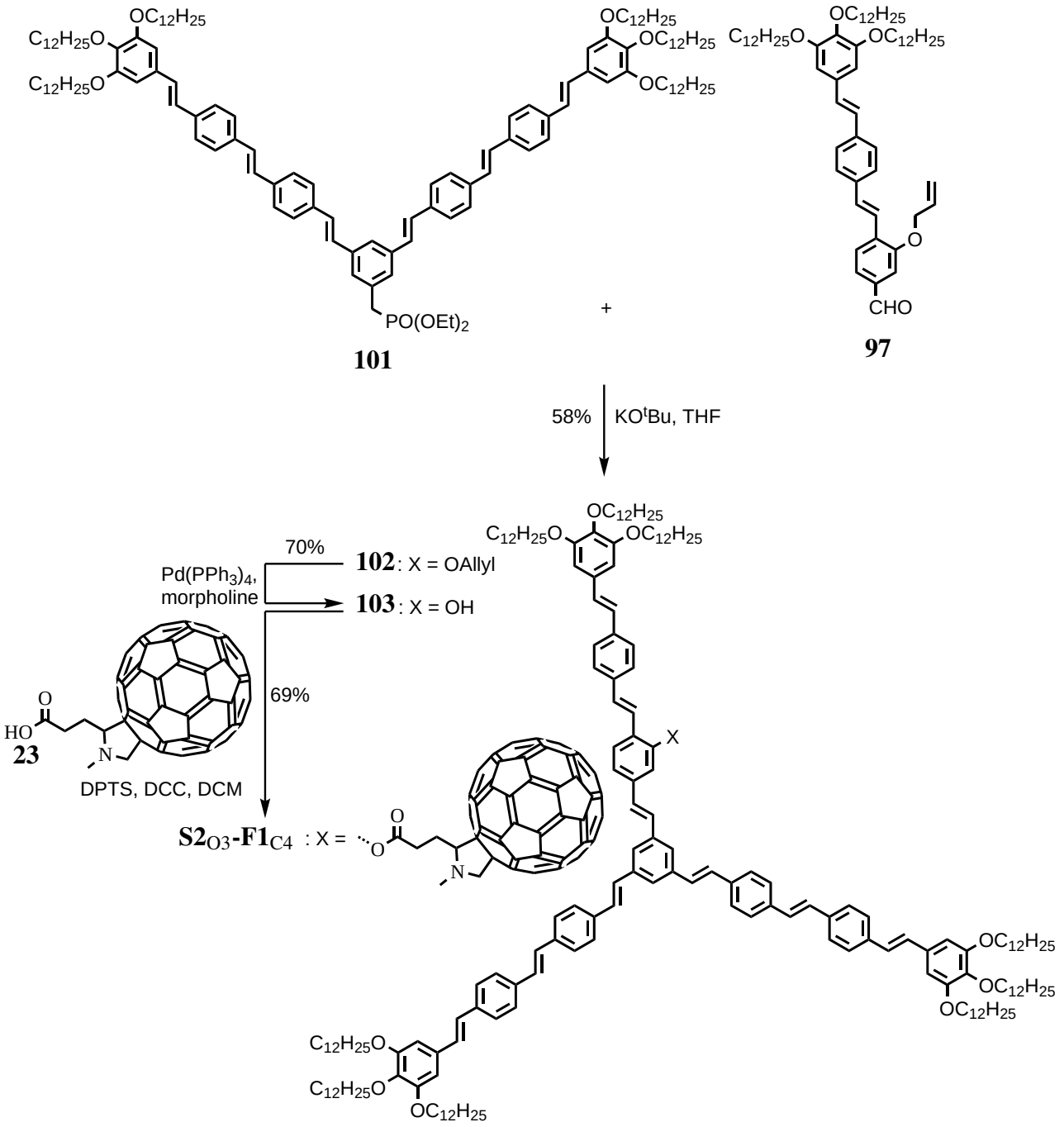

Scheme 44: Synthesis of the star **S2**$_{O3}$-**F1**$_{C4}$.

To certify the identity of the product, the NMR results were compared to that of **S2**$_{C12}$-**F1**$_{C4}$ (see figure 29). The signals affiliated with the protons located at the pyrrolidine ring are much broader than in the case of the dodecyl chain derivative. Additionally, the ethyleneoxy chain protons cause strong signals that in parts cover the much weaker spacer proton signals. Nevertheless, it is evident that the esterification was successful. Figure 30 highlights the aromatic region of the corresponding NMR spectra. Due to the strong aggregation, the individual signals could not be assigned. MALDI MS experiments confirm the proposed structure and lack signals pointing to any multifold attachments of fullerenes.

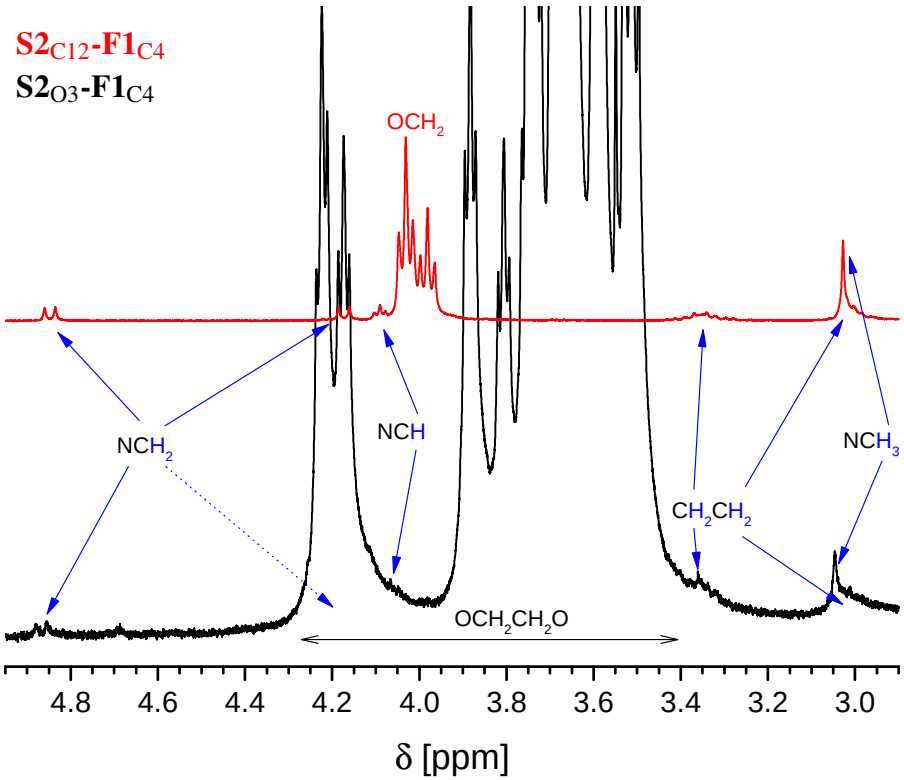

Figure 29: Extract of the NMR data for the Hekate stars **S2**$_{O3}$-**F1**$_{C4}$ (black) and **S2**$_{C12}$-**F1**$_{C4}$ (red) performed in deuterated chloroform. The signals associated with the fullerene spacer protons are marked with blue arrows.

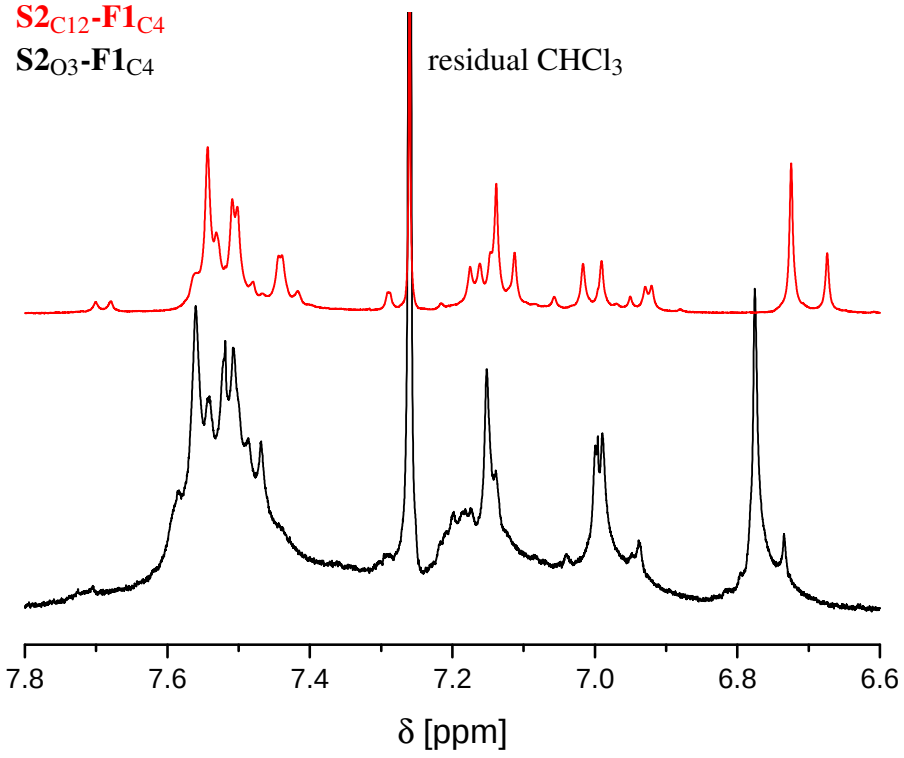

Figure 30: Extract of the NMR data of the aromatic region for the Hekate stars **S2**$_{O3}$-**F1**$_{C4}$ (black) and **S2**$_{C12}$-**F1**$_{C4}$ (red) performed in deuterated chloroform.

4.13 Porphyrin stars

The porphyrin stars **Por**$_{C12}$, **Por**$_{O2}$, and **Por**$_{O3}$ have been succesfully synthesized as illustrated in scheme 45. Core building block **12** has been reacted with an excess of the aldehyde arms **44**, **89** and **98** under Wittig-Horner conditions to give C_4-symmetric stars with yields of 65%, 55% and 35%, respectively. In general, monitoring the reaction progress was hampered since all intermediate and final products showed heavy tailing in TLC. Furthermore, NMR spectra of quenched samples of the reaction mixtures did not show the characteristic doublets of the -CH_2P- groups in the core building block, although they were present as evidenced by mass spectrometry. Therefore, the reaction progress solely was monitored by MALDI mass spectrometry. A high excess of the aldehydes was required to complete the reactions. Purification was then achieved by preparative column and gel permeation chromatography.

Since the porphyrin star **Por**$_{C12}$ bearing dodecyl chains already showed a clearing temperature too high for potential applications (see discussion on page 94), the synthesis of a porphyrin star with these chains and with four fullerenes attached was skipped. Rather, a porphyrin fullerene mesogen with the longer oligo(ethyleneoxy) chains was prepared according to scheme 45 since at that time, the already available results for the comparable Hekate star **S2**$_{O3}$ showed a drop of clearing temperature for the columnar phase by 100 °C compared to the aliphatic derivative **S2**$_{C12}$. In the first step, the Wittig-Horner reaction of the porphyrin core building block **12** with the arm building block **97** was performed and monitored in an analogous way to the preparation of the C_4-symmetric porphyrin stars **Por**$_{C12}$, **Por**$_{O2}$ and **Por**$_{O3}$ with a yield of 52%. Allyl ether deprotection then was carried out in the presence of tetrakis(triphenylphosphine)palladium and morpholine giving a yield of 61%. As the reaction proceeded slowly, the mixture was stirred for 18 days. In the final step, the carboxylic acid **23** bearing the fullerene was attached via Steglich esterification. Due to the low solubility of the fullerene bearing acid **23**, the reaction was stirred for 26 days before workup. 8.0 equivalents of the acid were used to allow for a good yield for the fourfold esterification. As column chromatography did not remove all side products according to TLC, the product was isolated by tedious precipitation procedures with a yield of 68%.

The NMR results in the range of the aromatic protons are displayed in figure 31 for the porphyrin stars **Por**$_{O3}$ (red) and **Por**$_{O3}$**-F4**$_{C4}$ (black). For the stilbene star **Por**$_{O3}$, defined signals are obtained, which allow the individual assignment of all protons with the aid of 2D correlation spectra. Besides the AA'BB' and double bond patterns that resemble the ones of the Hekate stars, additional peaks characteristic for *meso*-substituted porphyrins appear in a more downfield region. The protons located at the porphyrin ring (β-position) show a singlet at 8.94 ppm, owing to the strong deshielding effect of the π-electrons.[212] The protons from the benzene ring located at the *meso*-position of the porphyrin show 2 signals according to a slightly distorted AA'XX' spin system ($\Delta\nu/J \approx 17$). In the case of the porphyrin stilbene fullerene triad **Por**$_{O3}$**-F4**$_{C4}$, strong aggregation is observed and therefore individual proton assignment is hampered. By comparing the results with **Por**$_{O3}$, however, the peaks characteristic for the *meso*-substituted porphyrin can be located. Just as for the Hekate stars with fullerenes, the protons located at the terminal benzene unit bearing the chains face an upfield shift when adjacent to a fullerene (green box). The signals associated with the fulleropyrrolidine are displayed in figure 32. Similar to the Hekate star **S2**$_{O3}$**-F1**$_{C4}$ with an attached fullerene and ethyleneoxy

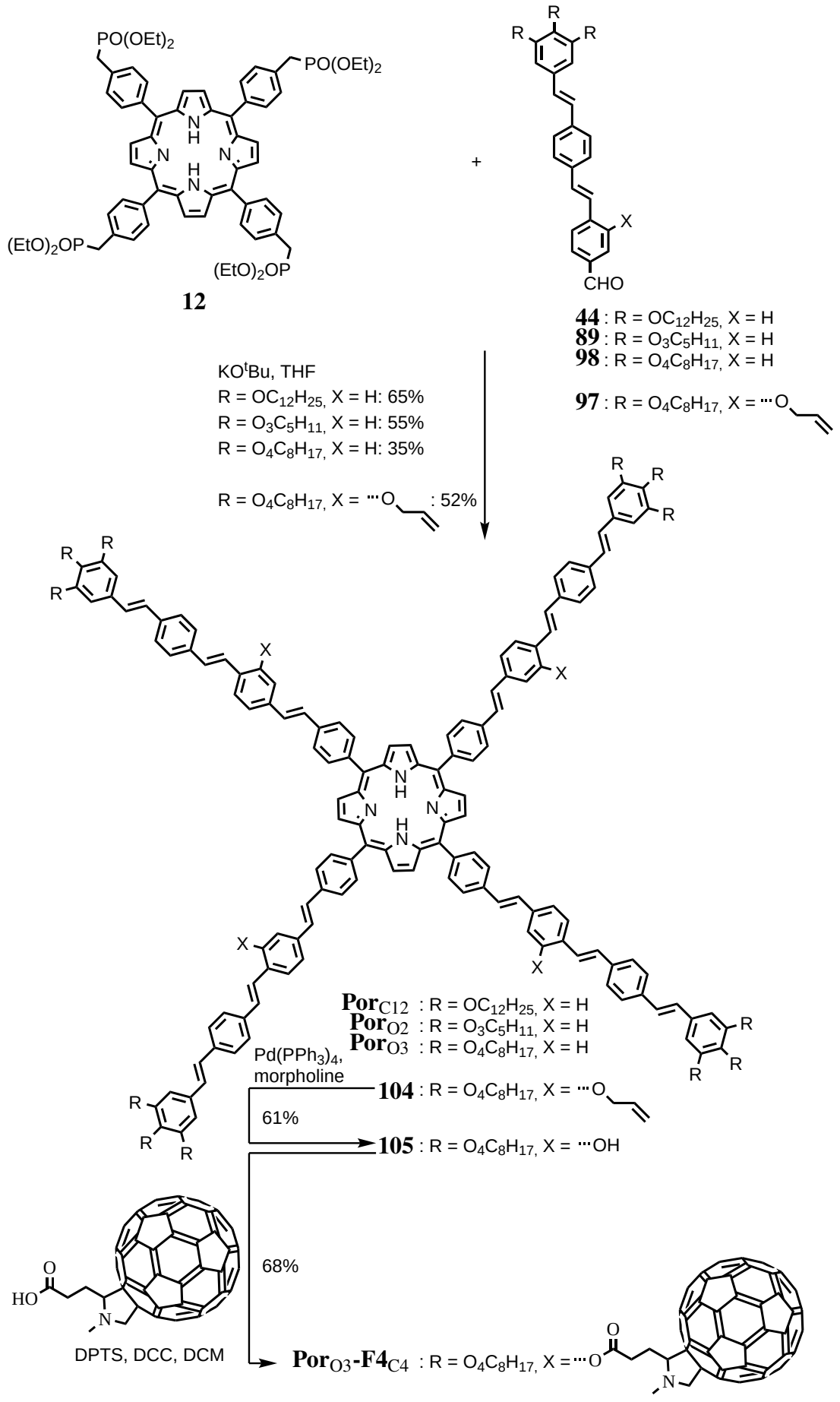

Scheme 45: Synthesis of the porphyrin stars $\mathbf{Por}_{C12}$, $\mathbf{Por}_{O2}$, $\mathbf{Por}_{O3}$ and $\mathbf{Por}_{O3}$-$\mathbf{F4}_{C4}$.

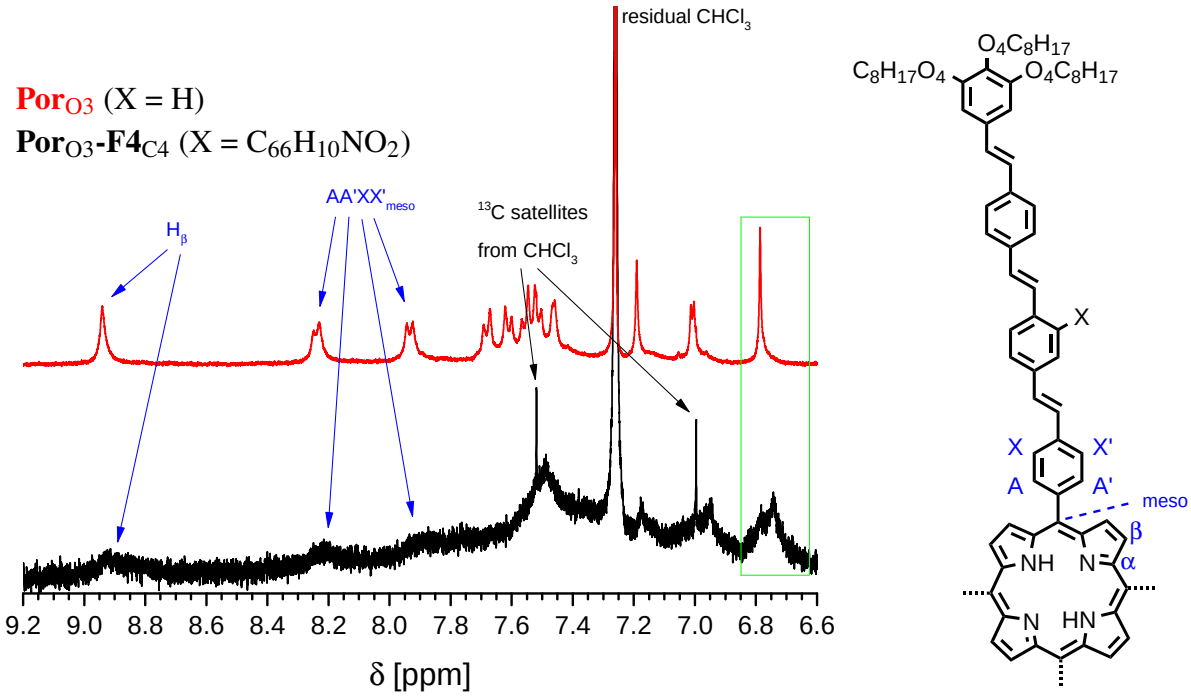

Figure 31: Extract of the NMR data for the porphyrin stars **Por**$_{O3}$**-F4**$_{C4}$ (black) and **Por**$_{O3}$ (red) performed in deuterated chloroform. The signals associated with the porphyrin core unit are marked with blue arrows. The signals covered in the green box correspond to the protons of the ethyleneoxy chains bearing benzene rings.

chains, the corresponding signals are highly broadened. Even though, in the case of **Por**$_{O3}$**-F4**$_{C4}$, a spacer is attached to every arm of the molecule, most signals are barely visible. The ethylene protons and NCH_3 groups, however, do unambiguously give a broad signal as indicated by the blue arrows. To further confirm the molecular structure of the obtained material, MALDI MS measurements were performed. As it turned out, the fragmentation of the triad and the detection of the corresponding ion was difficult to achieve. Under standard conditions, no corresponding signal could be observed. Merely by using high concentrations of the material and unfavorably high laser power, the molecule peak could be detected. As a consequence, a series of other signals was observed, which are depicted in figure 33. The broad peaks could not be attributed to a molecule of defined m/z ratio. However, the relatively sharp signal at m/z = 7368 corresponds to a $[M+Na]^+$ signal. The broad peaks located at approx. 6594 ($[M+Na-774]^+$), 5835 ($[M+Na-1533]^+$) and 5049 ($[M+Na-2319]^+$) m/z could point to retro cycloadditions of the pyrrolidines occuring in the MS experiments. Hypothetical stilbene fragments of the terminal benzene ring of the arm bearing the three oligo(ethyleneoxy) chains have a molecular weight of 633 g / mol and therefore are unlikely related to the discussed intensities.

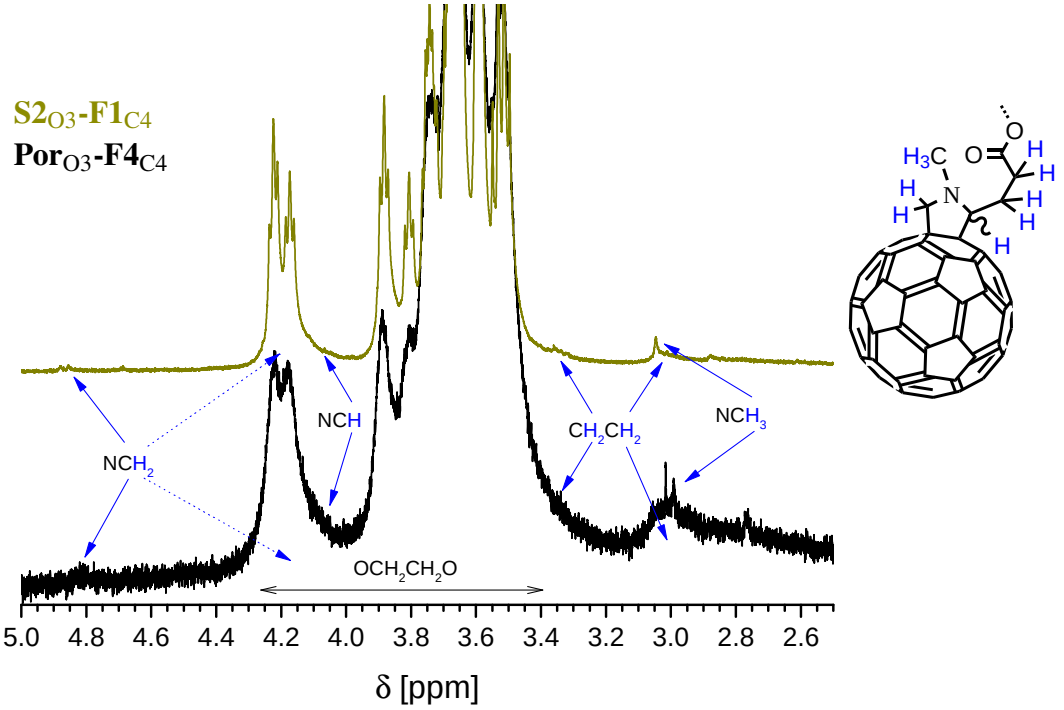

Figure 32: Extract of the NMR data for the porphyrin star **Por**$_{O3}$**-F4**$_{C4}$ (black) and the Hekate star **S2**$_{O3}$**-F1**$_{C4}$ (dark yellow) performed in deuterated chloroform. The signals associated with the fullerene spacer protons are marked with blue arrows.

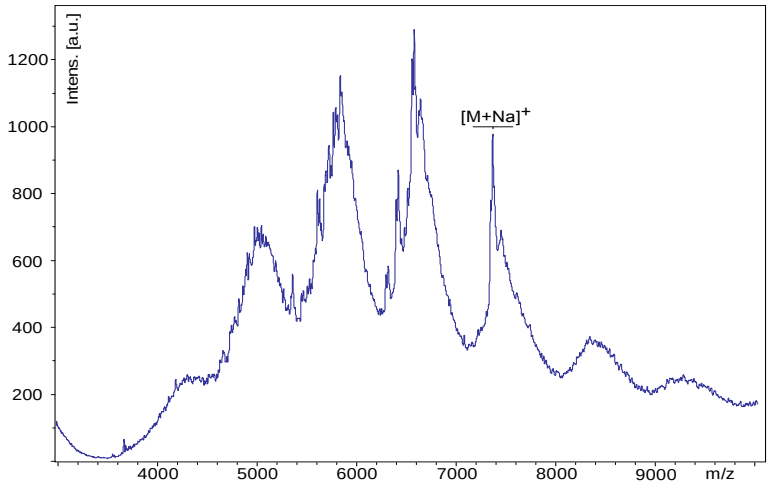

Figure 33: MALDI mass spectrum for compound **S2**$_{O3}$**-F1**$_{C4}$. The sample was directly dissolved in the matrix solution rather than prior dilution. High laser power was necessary to obtain signals. M_W = 7369.13 for $C_{500}H_{330}N_8NaO_{56}$; $[M+5+Na]^+$ = 7368.33.

5 Results — Thermotropic properties

5.1 Parent stars with dodecyl chains

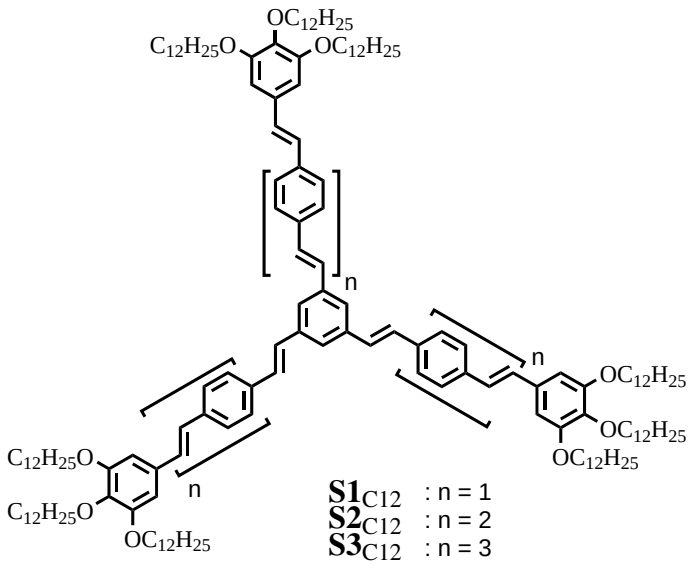

Figure 34: Structures of the examined C_3-symmetric parent stars with dodecyl chains.

The C_3-symmetric Hekate stars **S1**$_{C12}$, **S2**$_{C12}$ and **S3**$_{C12}$ have been examined towards their thermotropic properties via polarization microscope, differential scanning calorimetry, X-ray analysis and modelation. Table 3 summarizes the results. The mosaic textures obtained from POM measurements for all compounds indicate the formation of columnar phases (figure 35). Figure 36 highlights the results obtained by DSC measurements. The transitions obtained from the heating and cooling runs for the compounds **S2**$_{C12}$ and **S3**$_{C12}$ show rather broad signals and low enthalpies. At temperatures close to room temperature, the materials tend to assume a glassy state indicated by second order transitions.

The XRS data for the stilbene stars will be discussed to gain a deeper understanding of the nature of the found phases. Details for the lattice spacings of the compounds at different temperatures can be found in the section 11.1 on page 188. For an oriented fiber of compound **S1**$_{C12}$, the diffraction pattern is displayed in figure 37. It shows that equatorial reflections are obtained with a ratio of reciprocal lattice spacings equal to $1 : \sqrt{3} : 2$, indicating the formation of a hexagonal columnar phase. This characteristic diffraction pattern remains until the material is heated to the isotropic phase. In the wide-angle region a broad halo is observed, which corresponds to the average distance between the isotropically distributed alkyl chains. No sharper reflection along the meridian was found, which

Table 3: Thermotropic properties of the C_3-symmetric parent stars with dodecyl chains.

Compound	Transition temp. onset [°C]	ΔH [kJ·mol^{-1}]
S1$_{C12}$	Col_h 108 [133] (POM: 116.0†) I	4 [133]
S2$_{C12}$	Col_h 205.5 I	2.4
S3$_{C12}$	Col_1 171.7 Col_2 303.5	6.6; 4.4

†: The transition temperature obtained by POM is based on the formation of a texture in the cooling process.

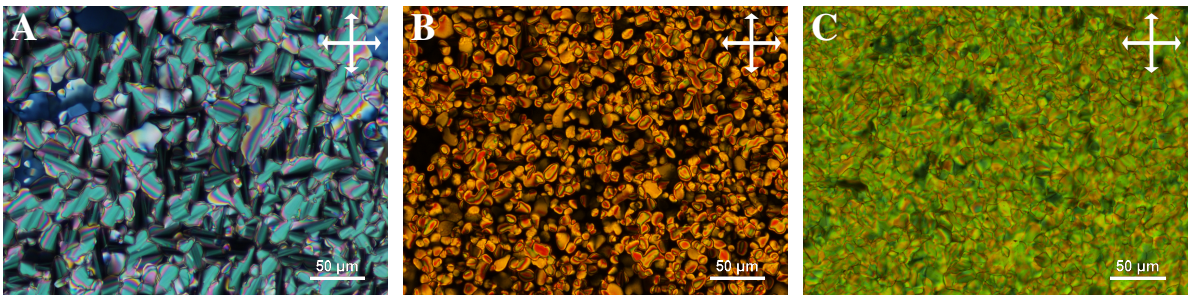

Figure 35: Polarization microscope textures of the compounds **S1**$_{C12}$ (**A**, 114 °C), **S2**$_{C12}$ (**B**, 211 °C, UV filter applied) and **S3**$_{C12}$ (**C**, 265 °C) with crossed polarizers.

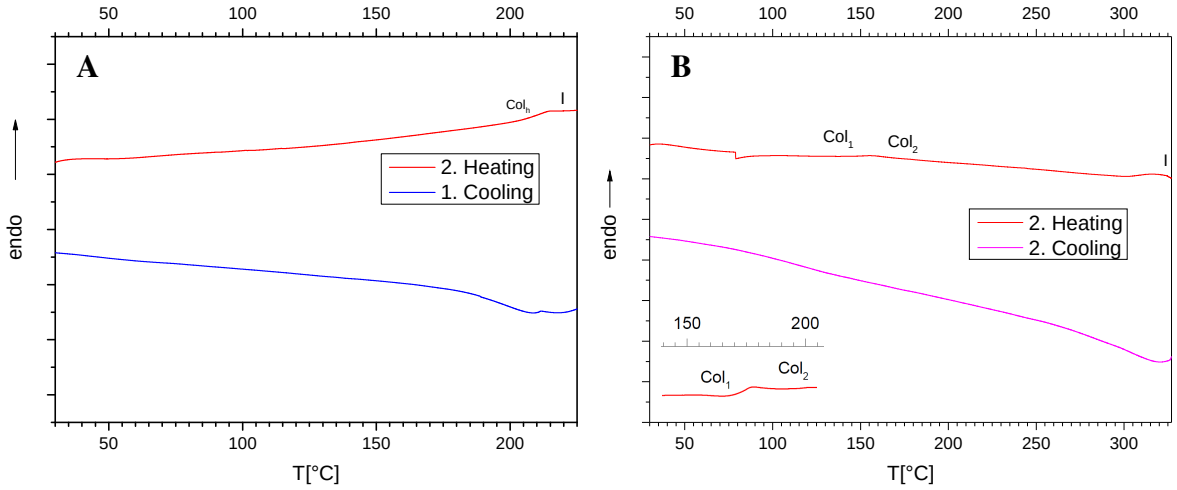

Figure 36: DSC thermograms obtained for **S2**$_{C12}$ (**A**) and **S3**$_{C12}$ (**B**; Inset: Extract of the thermogram obtained for an extruded sample of **S3**$_{C12}$ highlighting the transition between the two LC phases in the heating cycle.

could be assigned to the average π-π distance between the stilbenoid, rigid mesogens. A diffuse set of meridional reflections indicates a periodicity along the columnar axis (figure 37B,D; blue arrows). The broadness of these signals, however, corresponds to a poor correlation of this assembly as small as a a few repeating units. Assuming that these reflections are positioned at the *hk*1 layer line, the *c* parameter for the unit cell is deduced to be 38.0 Å. In the case of a co-facial stacking, a typical π-π distance of 3.4 Å would result in an arrangement of approximately 11 mesogens per unit cell (38.0 Å/3.4 Å), leading to a density value of less than 0.53 g·cm^{-3}. It is clear that a condensed phase like a LC phase must exhibit much larger density values and therefore this arrangement is not plausible. Assuming a density close to 1.0 g·cm^{-3}, the molecules then have an average axial distance of 1.90 Å. As this distance is unfavorably small for π-π interactions,[213] it is reasonable to assume that the arms of the stars avoid each other by translational and rotational displacement. The benzene cores accordingly are dislocated from the columnar axis. Following from these considerations, a unit cell would comprise 20 mesogens. Hence, only a helix is feasible for such a large arrangement and the cell parameter *c* corresponds to the helical pitch. Besides a single helix, a triple helix might also be formed by the three-armed stars. In that case, the reflections would correlate with a third of the helical pitch and would be positioned at the *hk*3 layer line. Note however, that the phenylene vinylene repeating units easily are rotated around the carbon-carbon single bonds. Hence, the stars are not strictly C_3-symmetric and a triple helix cannot be formed. A model has been built based on the concept of a single helix, which is displayed in figure 37E. The cores (magenta) are slightly displaced from the columnar axis and the arms form a single helix (orange). In addition, the stilbenoid scaffolds distort

and consequently their conformations deviate from the ideal planar structure and the C_3 symmetry. The increase of torsional energy is rather low probably due to the flat anharmonic potential curve for rotation of the benzene rings out of the plane of the double bond.[109] This is easily compensated by the decrease of energy via attractive intermolecular non-binding interactions. These features enable the dense packing along the columnar axis. The simulated diffraction pattern obtained from this model is displayed as inset in figure 37B. It matches well with the experimental pattern showing diffuse meridional signals and confirms the model of a single helix.

The star $\mathbf{S2}_{C12}$ with an additional repeating unit also forms a liquid crystalline phase with a clearing temperature, which is 98 °C higher compared to the star $\mathbf{S1}_{C12}$. As for the smaller star $\mathbf{S1}_{C12}$, equatorial reflections are obtained with a ratio of reciprocal lattice spacings equal to $1 : \sqrt{3} : 2$ (see figure 38). The formation of a columnar phase is surprising, as the void between the arms is rather large, exacerbating the filling of space, which is crucial for condensed matter. Also, a broad halo reflection and no sharper signals affiliated with the average π-π distance could be observed at the meridian. The four diffuse signals along the meridian imply the formation of a helix, similar to star $\mathbf{S1}_{C12}$. Hence, these reflections are positioned at the *hk*1 layer line and the unit cell parameter *c* is equivalent to the helical pitch. The correlation of the helical arrangement along the columnar axis determined by the Scherrer formula amounts to 2-3 helical pitches.* The density of this material has been experimentally determined to be 0.98 g·cm^{-3} at 22 °C. Note that this is only the minimum value since the trapping of air in this experiment could not entirely be eliminated.† Consequently, a single unit cell comprises 32 mesogens (ρ = 0.99 g·cm^{-3}) with an average axial distance of 1.36 Å. Compared to the smaller star $\mathbf{S1}_{C12}$ this value is even smaller, indicating that the larger void space has to be compensated by the packing of more molecules per columnar slice.

Modeling of the phase revealed that nanosegregation of the rigid aromatic building blocks and the flexible apolar chains is possible by a helical stacking of the stars with an additional lateral displacement of the molecular centers from the columnar axis, avoiding steric repulsion along the stacking direction (figure 38E,F).‡ Similar to the star $\mathbf{S1}_{C12}$, the stilbenoid scaffolds are conformationally deformed from the ideal planar C_3-symmetric structure, leading to an increase of torsional energy, which is accompanied by a much larger decrease in energy in terms of attractive intermolecular interactions. The simulated X-ray pattern obtained from this model (figure 38B inset) is in accordance with the experimental data.

*For explanation, see page 19.
†For more information, see page 186.
‡The model was obtained by collaboration with Prof. Matthias Lehmann.

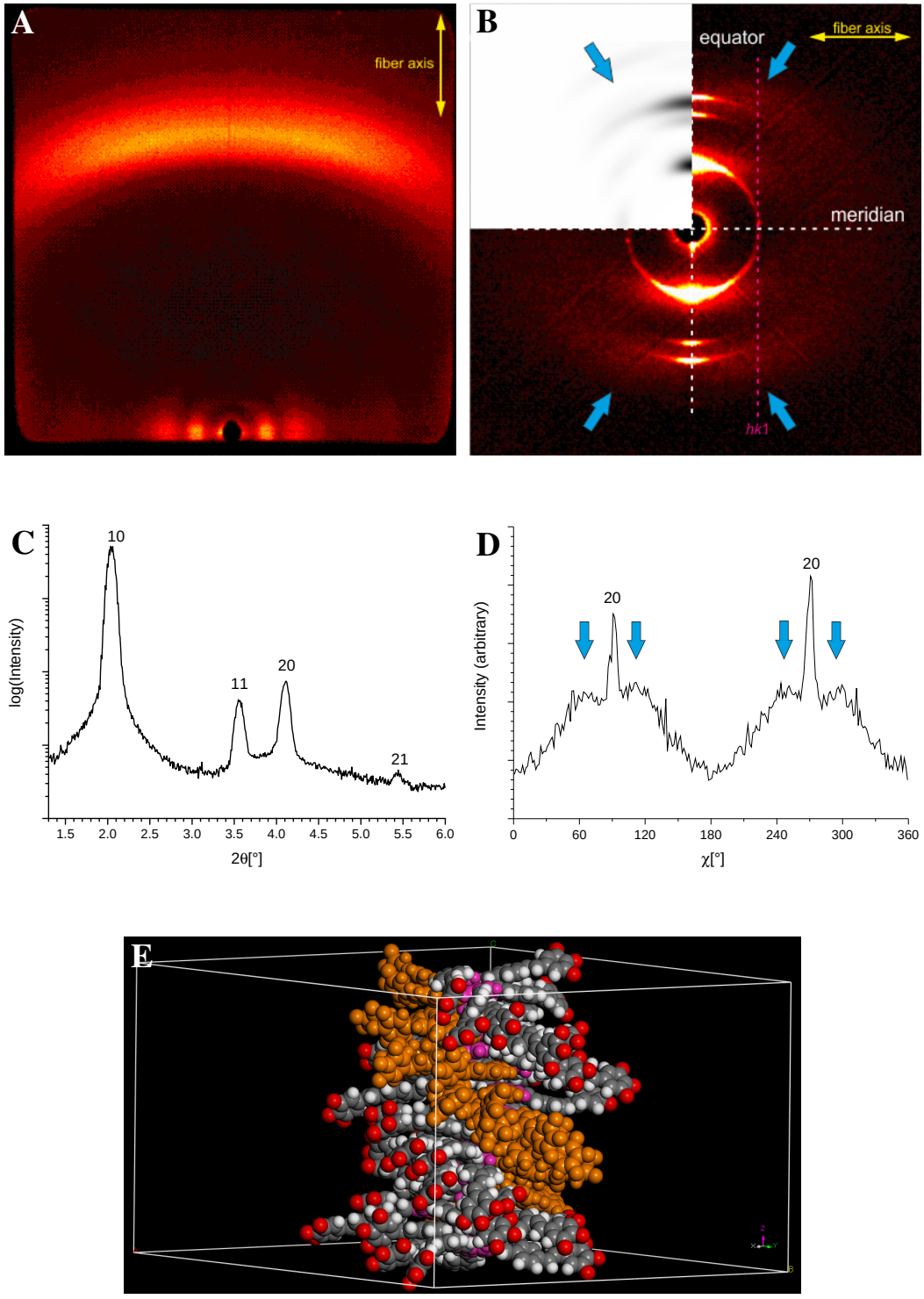

Figure 37: X-ray results obtained for extruded samples of compound $\mathbf{S1}_{C12}$ at 25 °C. **A**: Wide-angle region; **B**: Medium-angle region. The blue arrows indicate the position of the diffuse signals affiliated with the formation of a helix; inset: simulated diffraction pattern obtained from the model; **C**: Integrated intensity along the equator of the diffraction pattern showing the reflections indexed according to the hexagonal symmetry ; **D**: Chi scan between $2\theta = 4.14 - 5.20°$ showing the intensity of the highly diffuse set of four meridional signals. The sharper reflections correspond to the 20 reflections; **E**: Modeling of the columnar phase. The dodecyl chains are omitted for illustrating purposes. The core units (magenta) are slightly dislocated from the columnar axis and the arms form a helix (highlighted for one arm, orange).

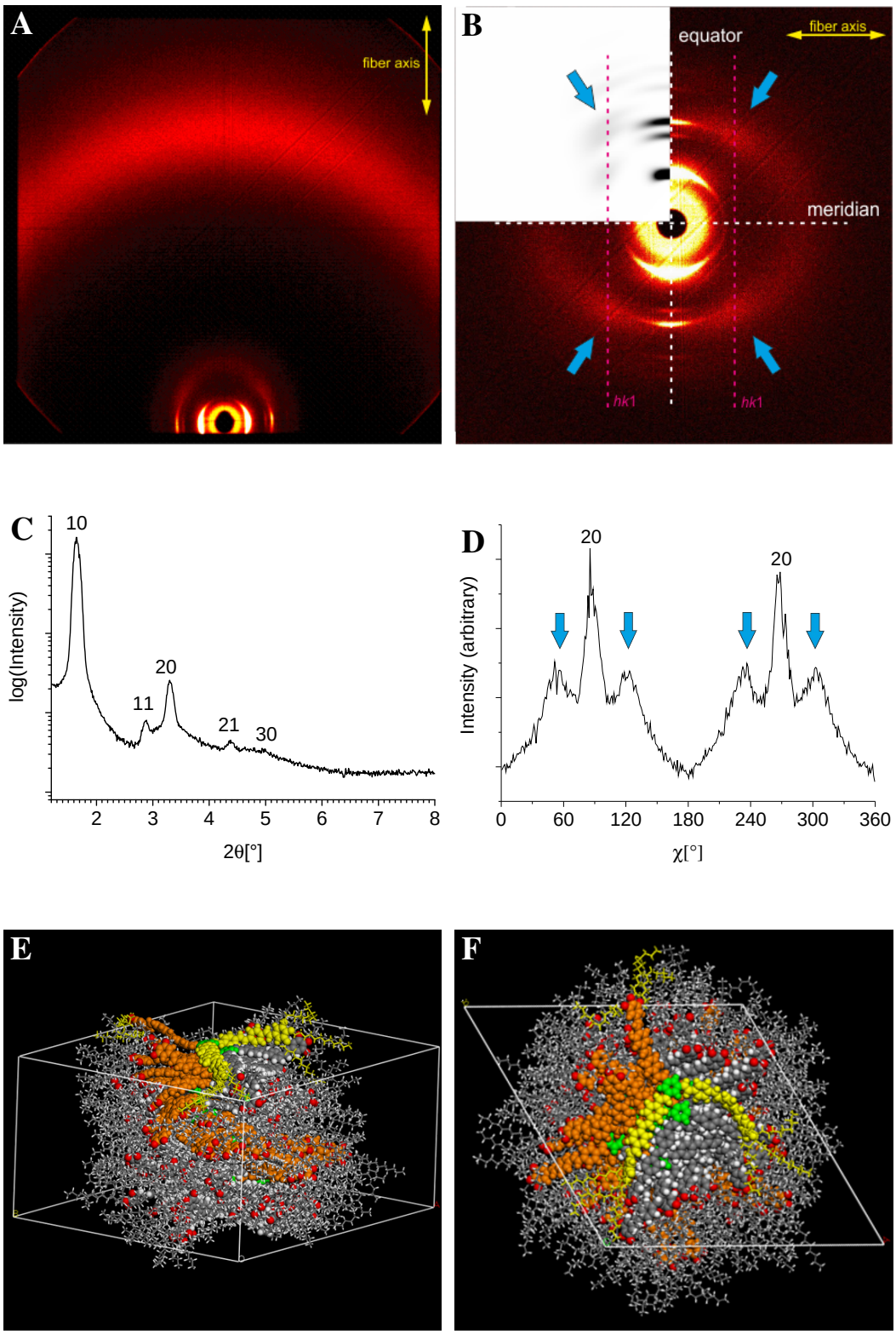

Figure 38: X-ray results obtained for extruded samples of compound **S2**$_{C12}$ at 25 °C. **A**: Wide-angle region; **B**: Medium-angle region. The blue arrows indicate the position of the diffuse signals affiliated with the formation of a helix. The inset represents the simulated X-ray diffraction pattern; **C**: Integrated intensity along the equator of the diffraction pattern showing the reflections indexed according to the hexagonal symmetry ; **D**: Chi scan between 2θ = 3.3 - 4.0° showing the intensity of the highly diffuse set of four meridional signals. The sharper reflections correspond to the 20 reflections; **E**: Modeling of the columnar phase. Helical packing with short correlation length highlighted for one arm (orange). Center of mesogens (green), one complete molecule (additional arms in yellow). Side view; **F**: Top view of the modelation. Image reproduced and adapted from reference [214] with permission of the rights holder, Wiley-VCH.

The Hekate star $\mathbf{S3}_{C12}$ with three repeating units interestingly shows two different columnar phases formed from room temperature to 172 °C (Col_1) and from there to 304 °C (Col_2), respectively. The X-ray results are illustrated in figure 39. Throughout the liquid crystalline state, no signal can be associated with $\pi - \pi$ aggregation in the wide-angle region.

In the Col_1 phase, a set of Bragg reflections along the equator is observed at low angles, which can be indexed according to a hexagonal symmetry (a = 69.4 Å at 25 °C). Several meridional signals are observed at different *hkl* layer lines (see figure 39C). Due to their given distances to the *hk*0 layer line and to each other, these lines can be assigned as *hk*1 and *hk*3. The intensities located at the *hk*3 layer line are not split into an X-shaped set of reflections or the split is so small that it cannot be resolved for the broad signals. The c parameter calculated from this reflection at room temperature amounts to 71.7 Å. Assuming a density of 0.99 g·cm^{-3}, the average axial distance then equals 1.20 Å for 60 molecules per cell. This is smaller than the axial separation found for the stars $\mathbf{S1}_{C12}$ and $\mathbf{S2}_{C12}$ and indicates the packing of even more molecules in the columnar slice. A set of four weak reflections appears at the *hk*1 layer lines, suggesting the formation of a helix with small correlation length. To conclude, the Col_1 phase is a hexagonal columnar helical phase similar to the phases formed by the smaller stars $\mathbf{S1}_{C12}$ and $\mathbf{S2}_{C12}$.

For the Col_2 phase, the equatorial intensities are slightly distorted from the pattern of a hexagonal cell. In fact, the most prominent peak now shows a small shoulder at approx. 2θ = 1.54°, confirming the desymmetrization of the unit cell. An X-shaped pattern is clearly given at the *hk*3 layer line (figure 39D,F; blue arrows). Also, a very weak signal appears at the 002 position (yellow area). The c-parameter calculated from these reflections amounts to 68.5 Å. A set of 4·3 reflections (green area) appears at the *hk*1 layer line whose signals are much more intense compared to the single reflection observed at 136 °C. Hence, a 3D liquid crystalline phase is given. No 001 signal has been observed. Presumably, a body-centered orthorhombic cell is formed with the parameters a_{borh} = 121.5 Å, b_{borh} = 74.2 Å and c_{borh} = 68.5 Å. The theoretical 2θ values match well with the findings of the intensities located at the *hk*1, *hk*2 and *hk*3 layer lines. As there must be a periodicity along the columnar axis for a 3D phase, a helix is also formed in this case. However, the evaluation of the meridional reflections could not reveal the nature of this helix. Since a three-dimensional phase has a higher degree of order compared to a hexagonal columnar helical phase, it is expected to be formed at lower temperatures.[215] Instead, the hexagonal columnar phase is present. This may be explained by the gained free space at high temperatures. The molecules can optimize the packing and are not hindered by sterical effects.

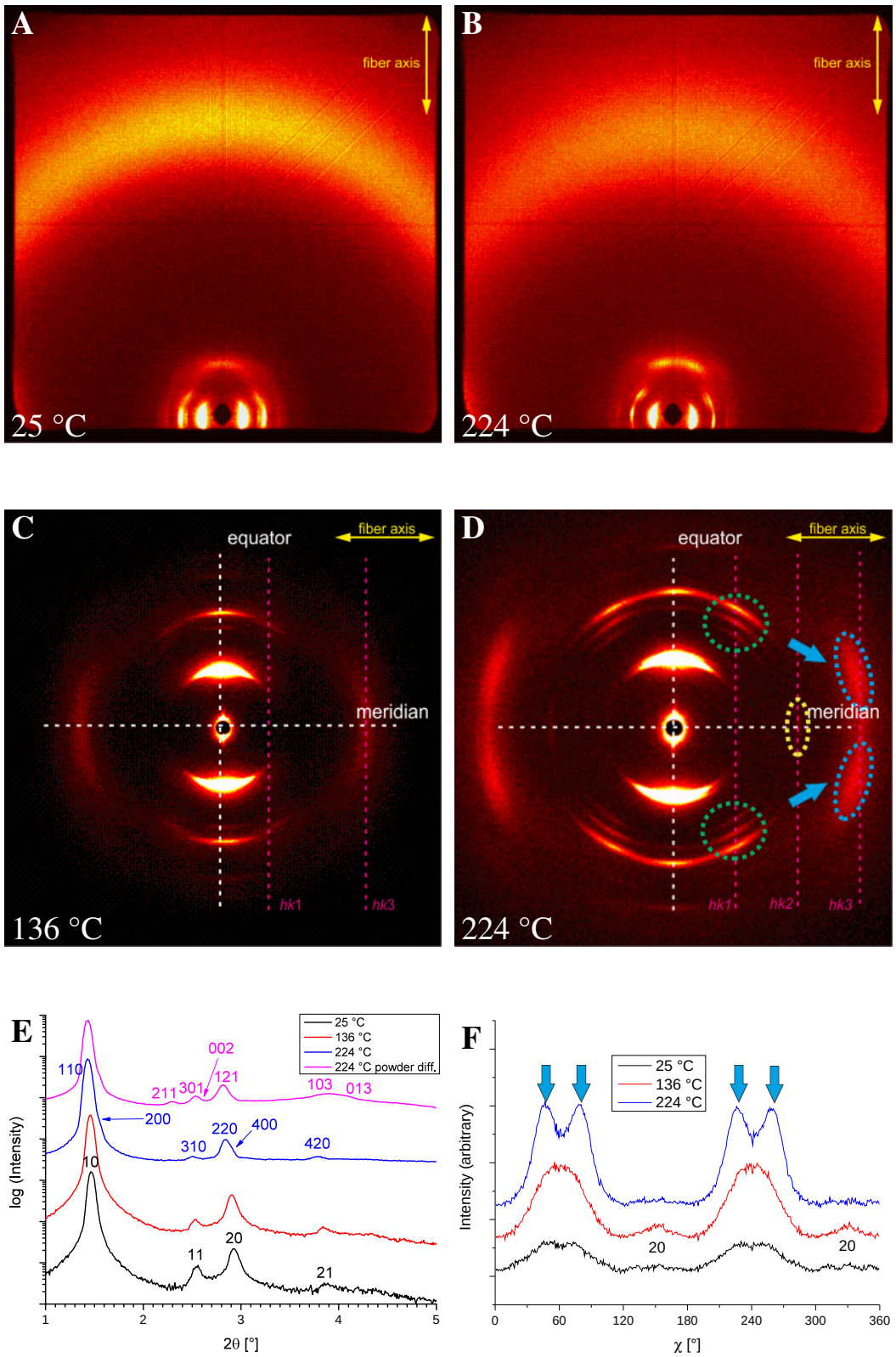

Figure 39: X-ray results obtained for extruded samples of compound $\mathbf{S3}_{C12}$. **A**: Wide-angle region at 25 °C; **B**: Wide-angle region at 224 °C; **C**: Medium-angle region at 136 °C; **D**: Medium-angle region at 224 °C. The blue arrows indicate the position of the diffuse signals affiliated with the formation of a helix; **E**: Integrated intensity along the equator of the diffraction pattern at 25 °C (black, indices according to the hexagonal symmetry), 136 °C (red) and 224 °C (blue, indices according to the body-centered orthorhombic symmetry). The purple line displays the powder diffraction pattern at 224 °C with indices given for the meridional signals; **F**: Chi scan between 2θ = 3.4 – 4.1 showing the intensities of the meridional signals at 25 °C (black, indices according to the hexagonal symmetry), 136 °C (red) and 224 °C (blue).

Table 4: Parameters *a*, *b* and *c* for the unit cells of $\mathbf{S1}_{C12}$, $\mathbf{S2}_{C12}$ and $\mathbf{S3}_{C12}$ at different temperatures. The *c* parameter is calculated based on the meridional signals of the X-Ray measurements.

$\mathbf{S1}_{C12}$

T [°C]	*a* [Å]	*c* (*c*/Z) [Å]
25	49.7	38.0† (1.90)
49	48.5	
93	46.7	
106	46.2	

$\mathbf{S2}_{C12}$

T [°C]	*a* [Å]	*c* (*c*/Z) [Å]
25	61.5	43.6 (1.36)
49	61.7	
93	60.7	
136	60.2	
180	59.5	

$\mathbf{S3}_{C12}$

T [°C]	*a* [Å]	*b* [Å]	*c* (c/Z) [Å]
25	69.4	–	71.7 (1.20)
136	70.0	–	73.5
224	121.5	74.2	68.5

Z: number of molecules per unit cell. The expression c/Z therefore is a measure for the average axial distance between the mesogens. The resulting densities for the materials amount to 1.01 g·cm^{-3} ($\mathbf{S1}_{C12}$), 0.98 g·cm^{-3} ($\mathbf{S2}_{C12}$) and 0.99 g·cm^{-3} ($\mathbf{S3}_{C12}$). †: Due to the low intensity of the meridional signals and their proximity to the 20 reflections (see figure 37), the calculation of the *c* parameter is rather erroneous.

The cell parameters for the compounds $\mathbf{S1}_{C12}$, $\mathbf{S2}_{C12}$ and $\mathbf{S3}_{C12}$ are summarized in table 4. As expected, the *a* parameter at room temperature rises with the number of phenylene vinylene repeating units for the Hekate stars. An ideal rigid molecule of $\mathbf{S1}_{C12}$ possesses a diameter of 58.5 Å, hence the aliphatic chains in parts overlap in a cell with *a* = 49.6 Å. The *a* parameter for the medium-sized star $\mathbf{S2}_{C12}$ at room temperature is increased by 12.1 Å compared to the smallest star $\mathbf{S1}_{C12}$, which roughly matches the expected value of two times the length of a stilbene repeating unit. For $\mathbf{S3}_{C12}$, the *a* parameter only increased by 7.7 Å compared to the star $\mathbf{S2}_{C12}$. Since the number of peripheral chains is not varying for these stars but the free space between the columns grows with increasing diameter of the stilbenoid scaffolds, the chains can fill this additional space, effectively reducing the intercolumnar distance.

With rising temperature, the cell parameter *a* decreases for compounds $\mathbf{S1}_{C12}$ and $\mathbf{S2}_{C12}$. This behavior is common and can be explained by the increasing intracolumnar distance of the mesogens. This additional space is then filled by the chains via conformational changes and interdigitation. As a result, the intercolumnar distance and thus the *a* parameter decreases.[216–218] For $\mathbf{S3}_{C12}$, however, a cell parameter is obtained, which rises with temperature. Only few similar cases have been published so far with no explanation given.[219,220] Due to the strong expansion in the plane perpendicular to the columnar axis, the average axial distance between the mesogens must rise rather slowly with the temperature. The *c* parameter increases from 71.7 Å at room temperature to 73.5 Å at 136 °C, yielding an additional average axial distance of only 2% per mesogen. Further heating to 224 °C reduces the *c* parameter due to the formation of a new LC phase.

5.2 Parent stars with oligoethyleneoxy chains

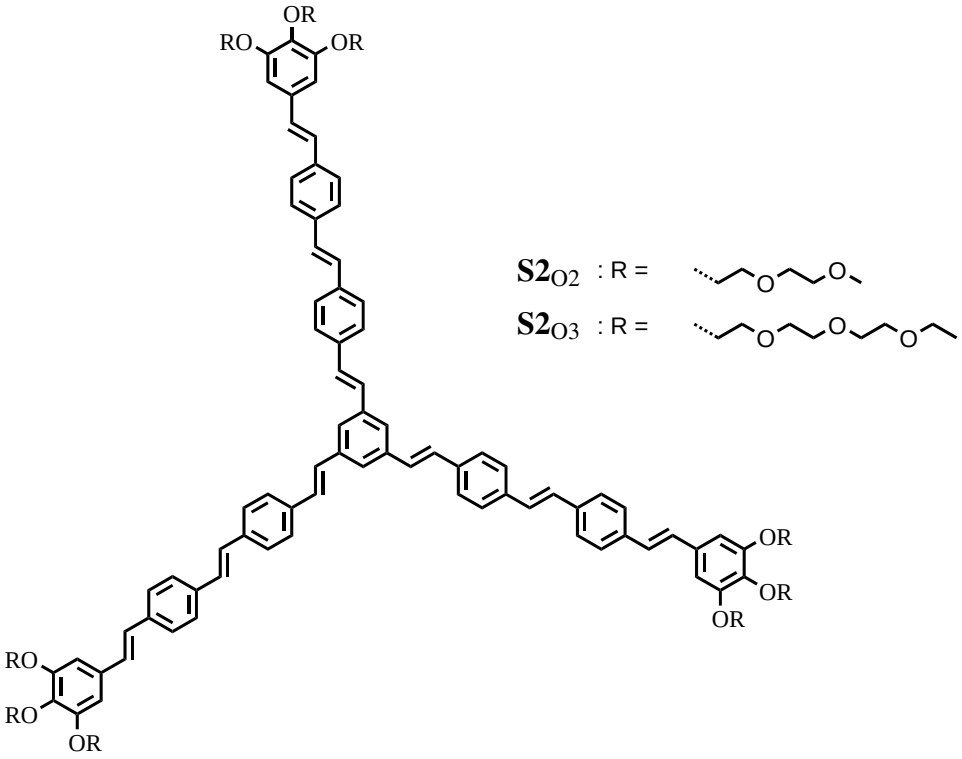

Figure 40: Structures of the examined C_3-symmetric parent stars with oligoethyleneoxy chains.

The thermotropic properties of the stars with oligoethyleneoxy chains are summarized in table 5. The data show dramatic changes compared to the alkyl chain derivatives. DSC measurements displayed in figure 41 reveal second order transitions close to room temperature for both materials, pointing to glassy states. In a range up to 200 °C, no well-defined transitions were obtained for compound **S2**$_{O2}$. The results for optical polarization microscopy are illustrated in figure 42. In the case of **S2**$_{O2}$, uncharacteristic textures are obtained up to approximately 55 °C (figure 42A). Additional heating consumes the texture. However, in a range up to almost 80 °C, applying shearing stress produces textures that disappear within several seconds (figure 42B). Conoscopic images[93] revealed that the disappearance is not a consequence of homeotropic ordering. Therefore, the sample either slowly returns from a pressure-driven LC phase to the isotropic state or an optically extinct cubic phase is recovered by self-healing processes. The material appears as a highly viscous oil and lacks the unambiguous waxy nature of the dodecyl chain derivatives. Slowly cooling a drop of the material did not yield a facet-like appearance, typical for cubic phases.[15,221] For the star with longer chains **S2**$_{O3}$, a peak was obtained at 92 °C. Thus the clearing temperature has significantly dropped compared to the alkyl chain derivative **S2**$_{C12}$ (T_{cl} = 206 °C). POM measurements reveal a mosaic texture, indicating the formation of a columnar arrangement (figure 42C).

The X-ray results for the compounds **S2**$_{O2}$ and **S2**$_{O3}$ are illustrated in figures 43 and 44, respectively. Besides the halo in the wide-angle region, a few highly broadened signals with low intensity can be observed in the low-angle region for **S2**$_{O2}$. Since **S2**$_{O3}$ with longer chains forms a columnar phase, the ratio between core volume and peripheral chain volume for **S2**$_{O2}$ is increased by comparison, pushing the preferred type of formed phase towards cubic or lamellar structures.[21] However, the

Table 5: Thermotropic properties of the C_3-symmetric parent stars with ethyleneoxy chains.

Compound	Transition temp. onset [°C]	ΔH [kJ·mol^{-1}]
S2$_{O2}$	undet.	–
S2$_{O3}$	Col$_h$ 92.4 I	1.1

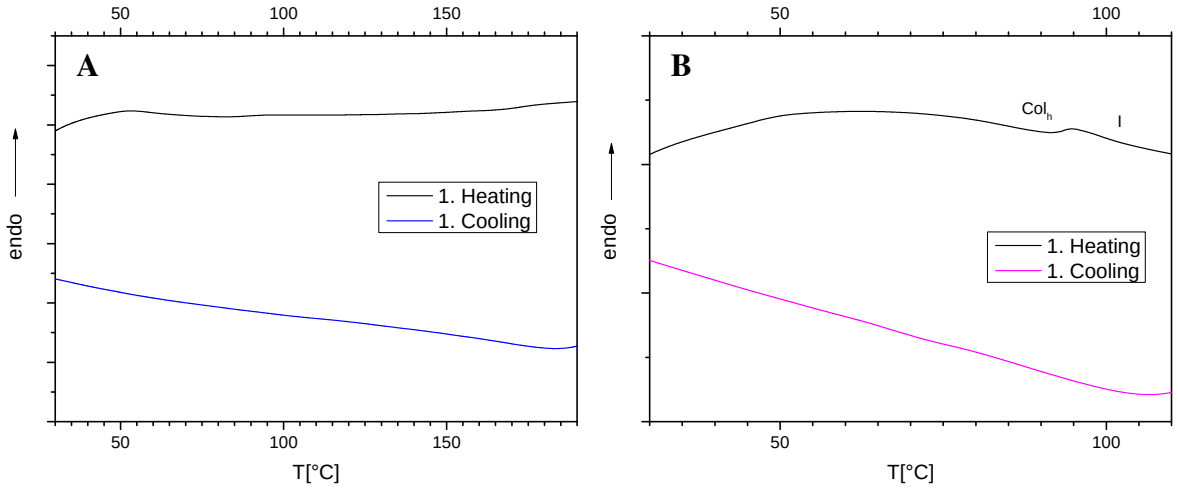

Figure 41: DSC thermograms obtained for stars **S2**$_{O2}$ (**A**) and **S2**$_{O3}$ (**B**).

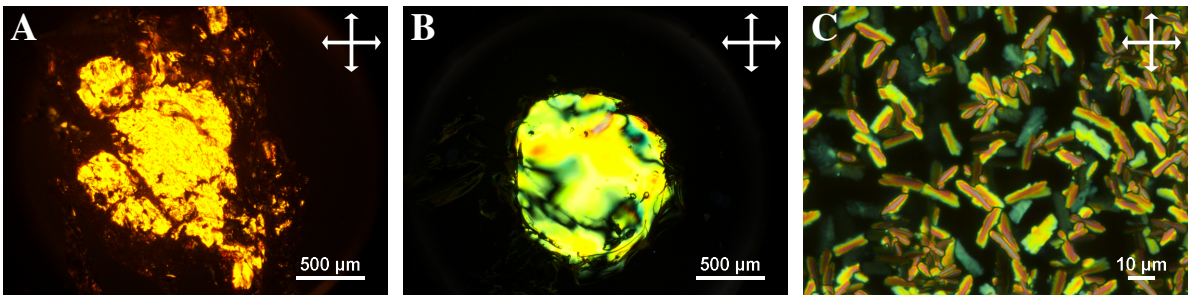

Figure 42: Polarization microscope textures of the compounds **S2**$_{O2}$ (**A**, 50 °C, UV filter applied; **B**, 60 °C, shortly after shearing process) and **S2**$_{O3}$ (**C**, 76 °C) with crossed polarizers.

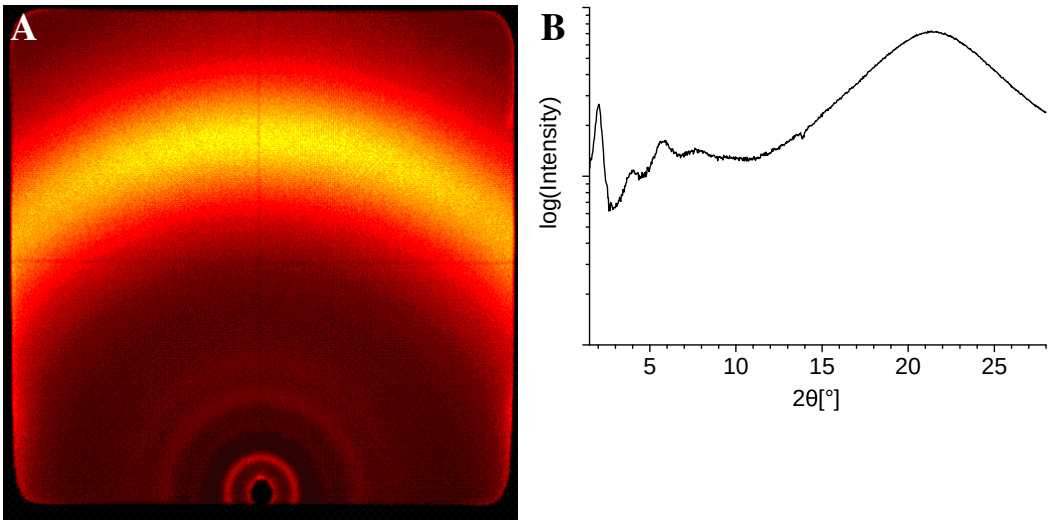

Figure 43: X-ray results obtained for extruded samples of compound **S2**$_{O2}$ at 25 °C. **A**: Wide-angle region; **B**: Integrated intensity of the diffraction pattern.

Table 6: Parameters for the hexagonal unit cell of $\mathbf{S2}_{O3}$ at different temperatures.

T [°C]	*a* [Å]
25	53.5
49	53.4
75	53.2

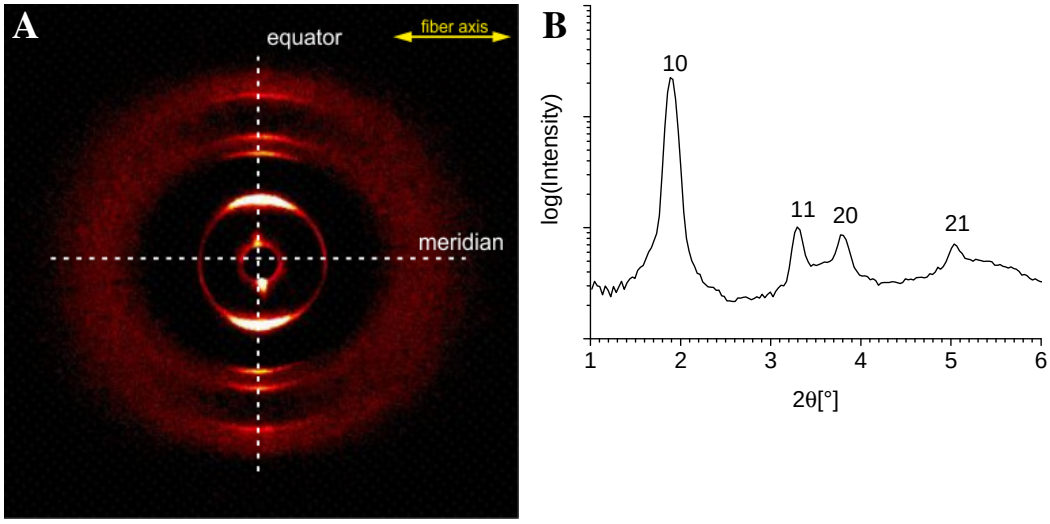

Figure 44: X-ray results obtained for extruded samples of compound $\mathbf{S2}_{O3}$ at 25 °C. **A**: Medium-angle region; **B**: Integrated intensity along the equator of the diffraction pattern showing the reflections indexed according to the hexagonal symmetry.

found reflections do not fit any common pattern. The present structure could not be determined with certainty, but the material behavior resembles those of other stars forming cubic phases.[221] In the case of $\mathbf{S2}_{O3}$, the diffraction patterns reveal an equatorial set of reflections fitting to the hexagonal pattern. Signals with weak intensities along the meridian point to additional assemblies, but could not be resolved due to poor alignment. The cell parameter *a* amounts to 53.5 Å at 25 °C and decreases to 53.2 Å at 75 °C (see table 6). In an arbitrarily chosen unit cell height of 100 Å, 58 molecules are separated by an average axial distance of 1.72 Å per molecule, when a density of 1.00 g·cm^{-3} is assumed. This value is greater compared to that of the dodecyl derivative $\mathbf{S2}_{C12}$ (1.36 Å) and demonstrates the strong influence of the oxygen-rich chains on the stilbene assemblies. The combination of a low clearing temperature and an ordered columnar phase is a promising result for potential application in semiconductor technologies. Slow cooling from the isotropic state to columnar arrangements allows macroscopic alignment, which is crucial for charge transport between electrodes. Due to the low temperatures, no decomposition of the material will occur. Incorporating a fullerene unit into this structure therefore was expected to give an ordered donor-acceptor structure with aligned assemblies.

5.3 Three-armed stars bearing fulleropyrrolidines

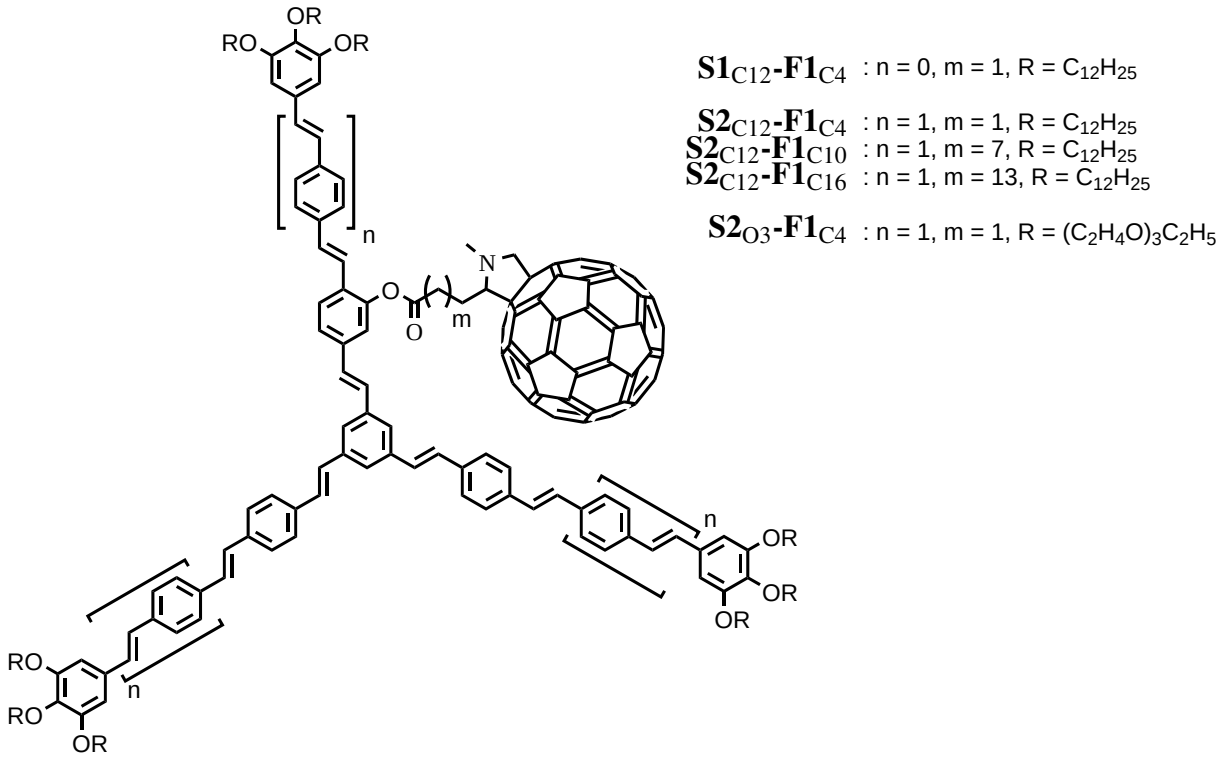

Figure 45: Structures of the examined three-armed stars bearing a single fulleropyrrolidine.

The Hekate stars bearing a single fulleropyrrolidine displayed in figure 45 have been examined towards their thermotropic properties via polarization microscope, differential scanning calorimetry, X-ray analysis and modelation. These mesogens can be considered as shape-amphiphiles meaning that both the rigid star and the spherical fullerenes tend to nanosegregate in their own compartments. Mosaic textures are obtained for all compounds bearing dodecyl chains, indicating the formation

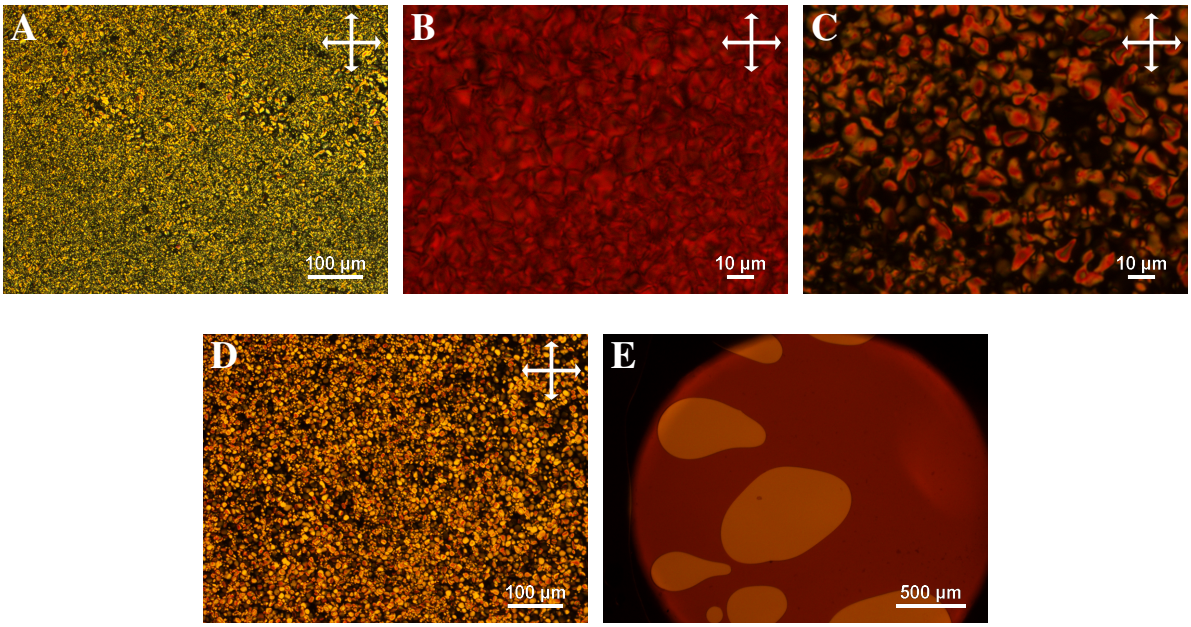

Figure 46: Polarization microscope textures of the compounds **S1**$_{C12}$-**F1**$_{C4}$ (**A**, 57 °C), **S2**$_{C12}$-**F1**$_{C4}$ (**B**, 120 °C, UV filter applied), **S2**$_{C12}$-**F1**$_{C10}$ (**C**, 239 °C) and **S2**$_{C12}$-**F1**$_{C16}$ (**D**, 214 °C, UV filter applied) with crossed polarizers and **S2**$_{O3}$-**F1**$_{C4}$ (**E**, 230 °C) with uncrossed polarizers and applied UV filter.

Table 7: Thermotropic properties of the stilbene stars bearing a single fulleropyrrolidine.

Compound	Transition temp. onset [°C]	ΔH [kJ·mol^{-1}]
S1$_{C12}$**-F1**$_{C4}$	Col 156.0 I†	–†
S2$_{C12}$**-F1**$_{C4}$	Col$_h$ 280.6 I	2.9
S2$_{C12}$**-F1**$_{C10}$	Col$_{borh}$ 239.6 I	8.7
S2$_{C12}$**-F1**$_{C16}$	Col$_{borh}$ 204.7 I	3.7
S2$_{O3}$**-F1**$_{C4}$	amorphous	–

†: No peak could be observed in DSC measurements. The given transition temperature is based on the formation of a texture in the cooling process of POM experiments.

of columnar phases (figure 46A-D). For compound **S2**$_{O3}$**-F1**$_{C4}$ with longer ethyleneoxy chains, no texture is observed with crossed polarizers. At elevated temperatures, strong dewetting effects are observed for this material (figure 46E).

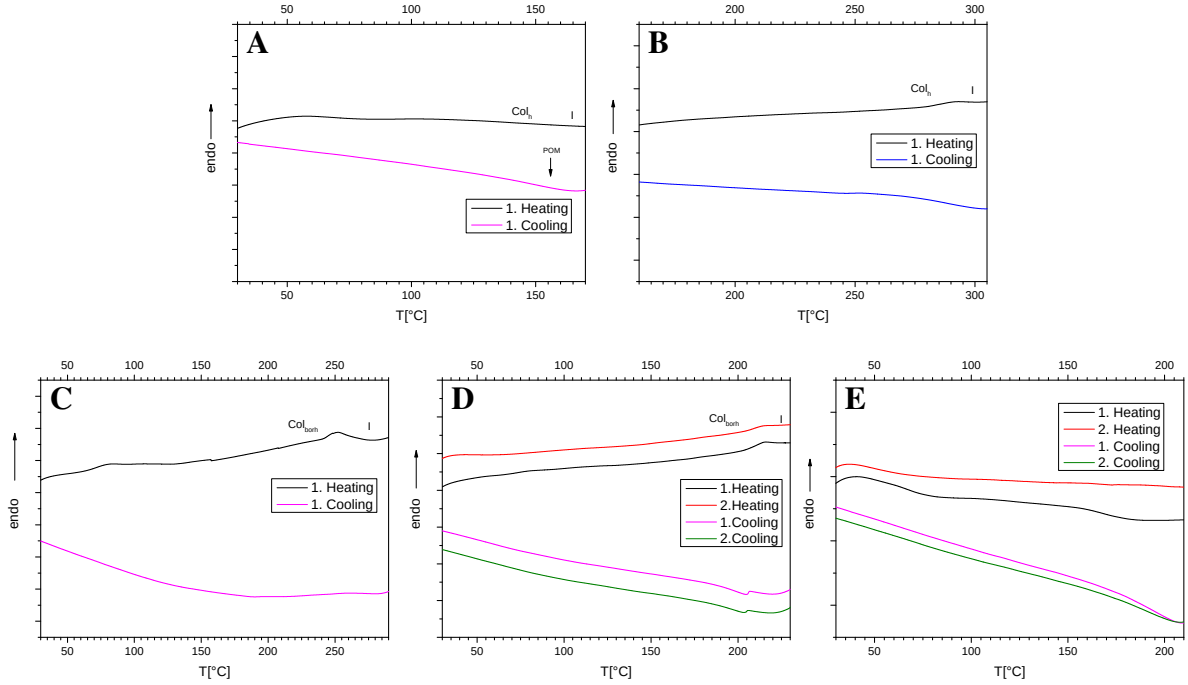

Figure 47: DSC thermograms obtained for stars **S1**$_{C12}$**-F1**$_{C4}$ (**A**), **S2**$_{C12}$**-F1**$_{C4}$ (**B**), **S2**$_{C12}$**-F1**$_{C10}$ (**C**), **S2**$_{C12}$**-F1**$_{C16}$ (**D**) and **S2**$_{O3}$**-F1**$_{C4}$ (**E**). The transition to the isotropic state could not be observed for **S1**$_{C12}$**-F1**$_{C4}$. The arrow indicates the temperature, at which the formation of the mosaic texture was observed in the cooling process of POM experiments.

Table 7 summarizes the results obtained by DSC measurements. The transitions obtained in the thermograms for the dodecyl derivatives are illustrated in figure 47. For the smaller star **S1**$_{C12}$**-F1**$_{C4}$, no peak is obtained for the transition to the isotropic state. However, polarization microscope studies clearly show the formation and vanishing of a texture in the heating cycle. The reformation in the cooling process starts at 156 °C. For the stars with two stilbene repeating units, broad signals are observed in the thermograms, which only occur in the first heating process for the stars with the highest clearing temperature (**S2**$_{C12}$**-F1**$_{C4}$ and **S2**$_{C12}$**-F1**$_{C10}$). This is a sign that these materials in parts decompose when heated to the isotropic phase. The stars with dodecyl chains form columnar

Table 8: Parameters for the unit cells of **S1**$_{C12}$-**F1**$_{C4}$, **S2**$_{C12}$-**F1**$_{C4}$, **S2**$_{C12}$-**F1**$_{C10}$ and **S2**$_{C12}$-**F1**$_{C16}$ at different temperatures. The *c* parameter is calculated based on the meridional signals of the X-Ray measurements. The samples were extruded prior to the X-ray experiments. The given values then were obtained after at least once heating the respective sample close to the isotropization temperature with subsequent slow cooling. †: These values were obtained in the first heating process of the X-ray experiments right after the extrusion procedure.

S1$_{C12}$-**F1**$_{C4}$ (Col_h)

T [°C]	*a* [Å]
25	44.0
49	44.2
136	43.8†

S2$_{C12}$-**F1**$_{C4}$ (Col_h)

T [°C]	*a* [Å]	*c* (*c*/Z) [Å]
25	56.1	102.6 (2.14)
136	56.7	
224	55.9	

S2$_{C12}$-**F1**$_{C10}$ (Col_{borh})

T [°C]	*a* [Å]	*b* [Å]	*c* (2*c*/Z) [Å]
30	97.1	56.4	121.5 (2.13)
128	96.8	55.9	129.4†

S2$_{C12}$-**F1**$_{C16}$ (Col_{borh})

T [°C]	*a* [Å]	*b* [Å]	*c* (2*c*/Z) [Å]
30	96.7	56.1	142.5 (2.16)

Z: number of molecules per unit cell. The expression c/Z (Col_{borh}: 2c/Z) therefore is a measure for the average axial distance between the mesogens. The resulting densities for the materials amount to 1.0 g·cm^{-3}.

liquid crystalline phases over a broad range of temperature and the stability of the phase correlates with the number of stilbenoid repeating units, just as for the parent stars **S1**$_{C12}$ and **S2**$_{C12}$. Furthermore, the clearing temperatures in general are higher compared to the parent stars. This is surprising as dendrimers forming liquid crystalline phases of different nature so far have all shown to lower their clearing temperatures when fullerenes are incorporated.[222,223] With increasing spacer length, the clearing temperature decreases and roughly the same clearing temperature for **S2**$_{C12}$-**F1**$_{C16}$ is obtained compared to the parent star **S2**$_{C12}$. Apparently not only nanosegregation but also other factors play a role for the stability of these mesophases. Only transitions of second order have been observed for the compound **S2**$_{O3}$-**F1**$_{C4}$, indicating the presence of an amorphous material (see figure 47E). Here, the fullerene does not account for a rise in the clearing temperature compared to the parent star **S2**$_{O3}$ (T_{cl} = 92 °C).

To gain a deep understanding of the behavior of these donor-acceptor materials, the X-ray results were studied in detail. The corresponding cell parameters are summarized in table 8.

The star **S2**$_{C12}$-**F1**$_{C4}$ with two repeating units and the shortest fullerene bearing spacer forms a hexagonal columnar phase with a clearing temperature as high as 281 °C. The incorporation of a fullerene here appears to efficiently stabilize the LC phase in comparison to the parent star **S2**$_{C12}$ (T_{cl} = 206 °C). Figure 48 reveals that only a halo corresponding to the interchain distance and no sharper reflection indicating $\pi-\pi$-aggregation is observable. The equatorial Bragg signals correspond to the hexagonal symmetry and can be observed up to *hk* = 40, pointing to a high order of the 2D columnar assembly. The meridional signals indicated by blue arrows in figure 48 point to a helical arrangement along the columnar axis and amount to a periodical arrangement of 34.2 Å, when a single helix is assumed. This scenario is not possible to realize, which will be discussed below. A more convenient assembly is imaginable: Assuming that each fullerene fills one cavity of the corresponding star-shaped meso-

gen, then three molecules can form an aggregate with each molecule rotated by 120° with respect to each other. Consequently, all three cavities are filled for each mesogen (see model in figure 48F). When these trimers then arrange in a helical fashion, a triple helix is formed. In this case, the strongest meridional signals are positioned at the third layer line (*hk*3) and the helical pitch amounts to 102.6 Å. The density of this material has been experimentally determined as $\rho \geq 1.0$ g·cm^{-3}, resulting in an arrangement of either 48 mesogens (16 trimers, triple helix) or 16 mesogens (single helix) per unit cell. The average axial distance between two mesogens either way is then 34.2Å /16 = 2.14 Å. Figure 48E illustrates the idealized arrangement of two neighbored fullerenes (brown) in a helix. In this scenario, the fullerenes are separated by two times the Van der Waals radius of C_{60} and the distance d then equals 10.3 Å.[121] The average distance of the fullerenes from the helical axis then can be calculated via $r = a/(2 \cdot sin(\frac{\alpha}{2}))$, $a = d \cdot sin\beta$ and $\beta = arccos(\frac{h}{d})$. Note that the rotation angle $\alpha = 22.5°$ is obtained from the model, which in turn is based on the experimental XRS data. The main difference for the distinct helices is the height h, which equals to 2.14 Å (average axial distance) in the case of a single helix and to 3·2.14 Å= 6.42 Å for a triple helix. Following from these considerations, the lateral displacement r of the fullerenes from the helical axis would amount to 25.8 Å for the single helix and 20.6 Å for the triple helix. The distances of the fullerene shells, regarding the side facing the linker, to the axes then equal to 20.7 Å and 15.5 Å, respectively. The former by far exceeds the achievable length of the short (straightened) spacer. Only a strong lateral displacement of the whole molecules could realize these distances, resulting in a huge area of unfilled space at the columnar axis. Therefore, the single helix is not feasible and indeed a triple helix is formed, in which the cavities of the arms are filled by the fullerenes. The meridional reflections accordingly correspond to the *hk3* layer, giving a helical pitch of $c = 3 \cdot d_{hk3} = 102.6$ Å.

Even for the shorter distance in a triple helix, the spacer has to be fairly stretched and the mesogen cores have to be dislocated from the helical axis to give a perfect helix regarding the Van der Waals radius of the fullerenes. Moreover, an efficient filling of the cavities between the arms also plays a role in the stability of this phase. It has to be clarified how a deviation of the ideal helical structure affects the filling of space for this system. Based on these considerations, a model of the hexagonal cell for $\mathbf{S2}_{C12}$-$\mathbf{F1}_{C4}$ with a rather short helix radius as initial structure was geometrically optimized, which is depicted in figure 48G.* Details of the generation of such models can be found in chapter 11.2 on page 192. The fullerenes form a triple helix and pack rather close to the columnar axis. Since the average distance between two C_{60} units now is smaller than two times the Van der Waals radius, the fullerenes now face spatial restrictions. This is demonstrated by sporadic displacements of fullerene units from the helical assembly in the model. In contrast, the cavities between the arms now are efficiently filled by the spherical C_{60} units. A simulated X-ray pattern obtained from the model (see figure 48B, inset) is in good accordance with the experimental data. A geometrically optimized model with an enlarged helix radius and straightened spacers as initial structure also yielded attractive non-covalent interactions in total, but the corresponding simulation pattern did not match with the experimental findings.

*The model was obtained by collaboration with Prof. Matthias Lehmann.

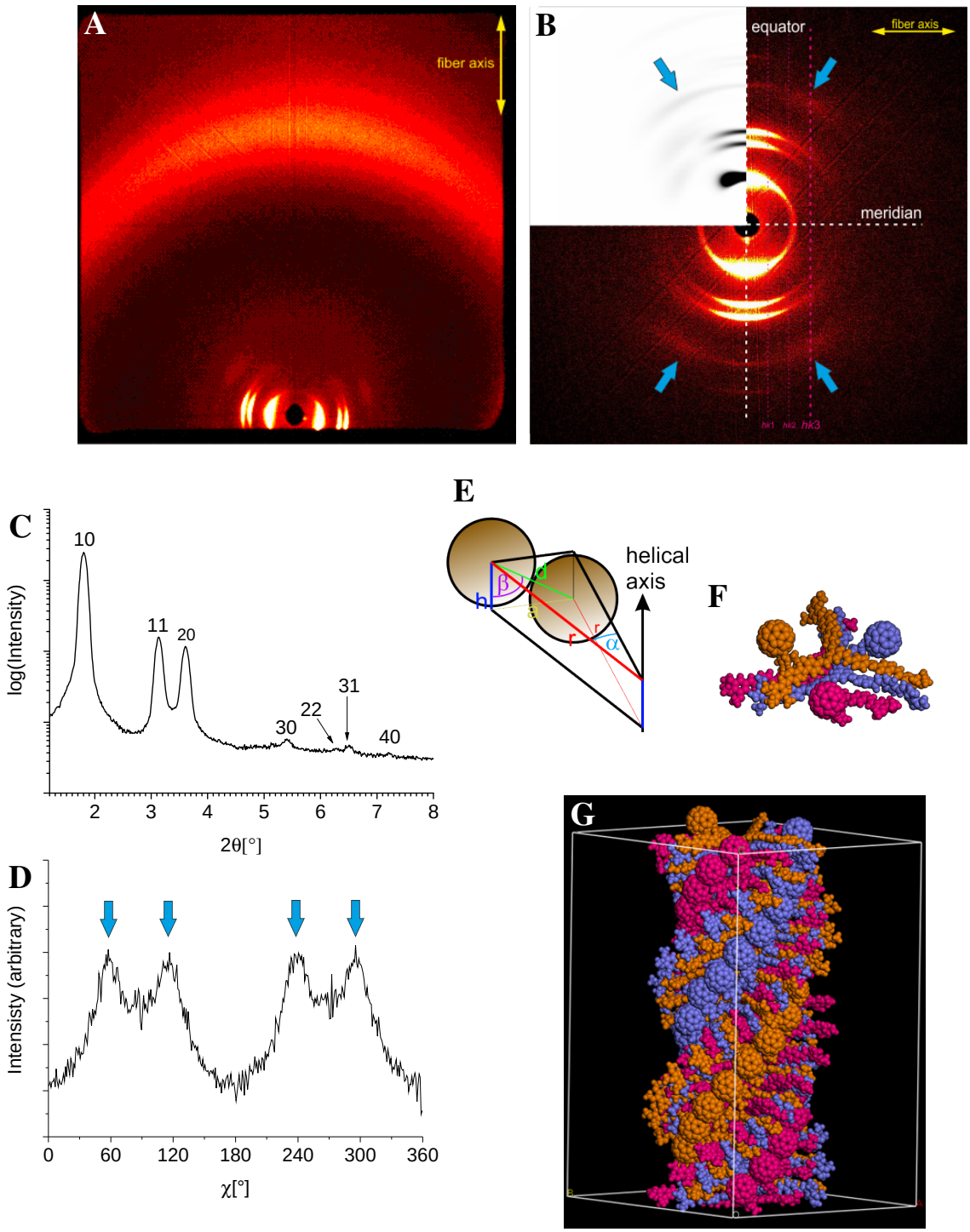

Figure 48: X-ray results obtained for extruded samples of compound **S2**$_{C12}$**-F1**$_{C4}$ at 25 °C. **A**: Wide-angle region; **B**: Medium-angle region. The blue arrows indicate the position of the diffuse signals affiliated with the formation of a helix; inset: simulated diffraction pattern obtained from the model; **C**: Integrated intensity along the equator of the diffraction pattern showing the reflections indexed according to the hexagonal symmetry ; **D**: Chi scan between 2θ = 4.5 - 6.1° showing the intensity of the highly diffuse set of four meridional signals; **E**: Schematic illustration of two neighbored fullerenes in a helix; **F**: Model of the trimer formed; **G**: Model of the trimers stacking in a helical manner. The dodecyloxy chains are omitted for displaying purposes. Image reproduced and adapted from reference [214] with permission of the rights holder, Wiley-VCH.

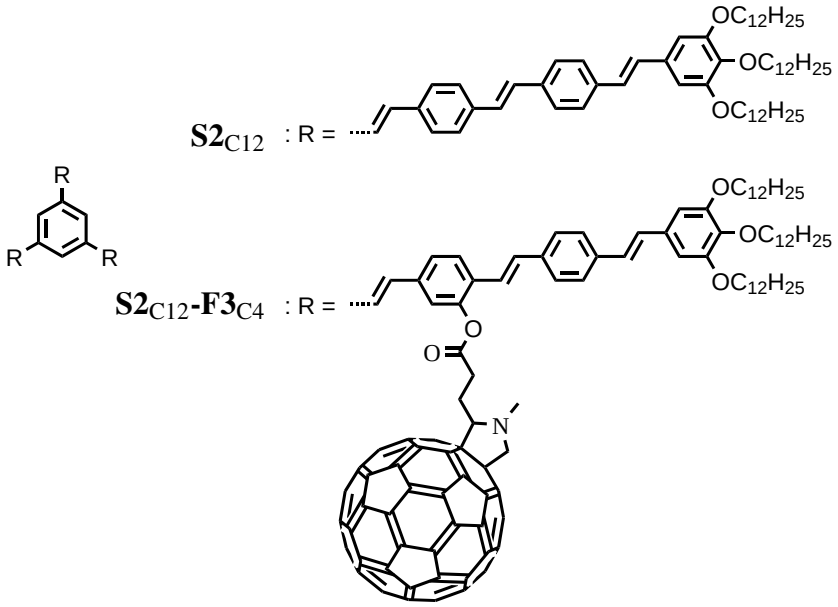

Figure 49: Structures of the materials used for the mixture **Mix_S**.

Further evidence for the formation of the proposed kind of triple helix is provided by the analysis of the compound **S2**$_{C12}$**-F3**$_{C4}$ bearing three fullerene units. When mixed with the star **S2**$_{C12}$ in a ratio of **S2**$_{C12}$**-F3**$_{C4}$ / **S2**$_{C12}$ = 1 / 2, the average number of spacers per trimer is the same as for **S2**$_{C12}$**-F1**$_{C4}$. Since all fullerenes of a trimer are attached to the same molecule, the radius of the helix cannot be enlarged by displacing the core of the corresponding dyad from the columnar axis. Therefore, an assembly comparable to that of **S2**$_{C12}$**-F1**$_{C4}$ is expected. The mosaic texture obtained for this mixture **Mix_S** is illustrated in figure 50 and points to a columnar arrangement. DSC measurements reveal a clearing temperature of 275 °C, being close to the 281 °C of the neat compound **S2**$_{C12}$**-F1**$_{C4}$. It is noteworthy that the clearing temperature of the mix has been determined by the peak of the highly broadened signal in the DSC thermogram. The onset lies at 254 °C. This is a result of the flawed array of the distinct mesogens within a column, leading to inhomogeneity of the material. Figure 51 shows the X-ray results obtained for this blend. Indeed the diffraction pattern strongly correlates with the results of **S2**$_{C12}$**-F1**$_{C4}$ and the cell parameters given in table 9 are almost identical to that of **S2**$_{C12}$**-F1**$_{C4}$. Due to the inherent nature of the mixture **Mix_S**, the ideal stacking order **S2**$_{C12}$ $\rightarrow$ **S2**$_{C12}$**-F3**$_{C4}$ $\rightarrow$ **S2**$_{C12}$ is not perfectly realized and thus the Bragg reflections are less well resolved. The meridional signals are less intense but show the same position as in the case of **S2**$_{C12}$**-F1**$_{C4}$. Thus the analytic results for **Mix_S** and the model obtained for **S2**$_{C12}$**-F1**$_{C4}$ confirm the proposed assembly of **S2**$_{C12}$**-F1**$_{C4}$. Note that the synthetic procedures for the C_3-symmetric **S2**$_{C12}$**-F3**$_{C4}$ are less complex than for the asymmetric star **S2**$_{C12}$**-F1**$_{C4}$. Hence these results show that further research efforts on the synthesis of symmetric mesogens and the analysis of their blends will be promising in the future.

Neat **S2**$_{C12}$**-F3**$_{C4}$ has also been examined and does not form liquid crystal phases. It melts and slowly decomposes at temperatures above 300 °C. Obviously the void between the arms in one molecule is too small to efficiently incorporate three fullerene units. Here, presumably fullerene-fullerene interactions dominate the aggregation behavior.

To examine the influence of the length of the spacers, star **S2**$_{C12}$**-F1**$_{C16}$ with twelve additional methylene units compared to **S2**$_{C12}$**-F1**$_{C4}$ has been analyzed by means of X-ray diffraction. The findings

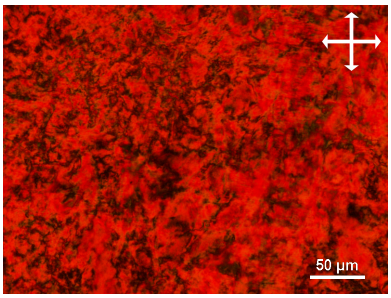

Figure 50: Polarization microscope texture of the 2:1 mixture of **S2**$_{C12}$**-F3**$_{C4}$ and **S2**$_{C12}$ (250 °C) with crossed polarizers and applied UV filter.

Table 9: Cell parameters *a* and *c* for the hexagonal, helical unit cell of a 2:1 mixture of **S2**$_{C12}$**-F3**$_{C4}$ and **S2**$_{C12}$ at different temperatures. The *c* parameter is calculated based on the meridional signals of the X-Ray measurements.

T [°C]	*a* [Å]	*c* [Å]
30	55.7	101.7
150	56.2	–
197	55.7	–

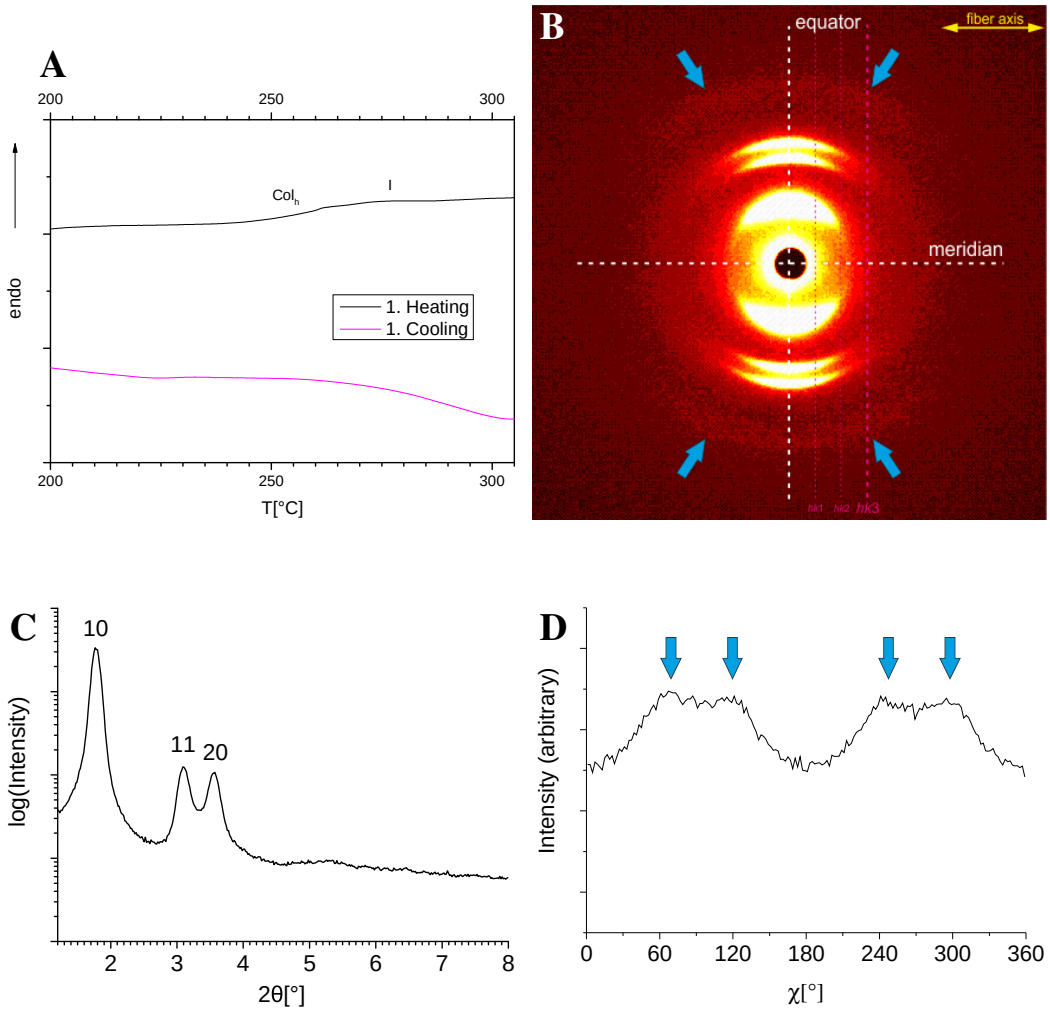

Figure 51: DSC and X-ray results obtained for extruded samples of a 2:1 mixture of the C_3-symmetric stars **S2**$_{C12}$**-F3**$_{C4}$ and **S2**$_{C12}$ (**Mix_S**) at 25 °C. **A**: DSC thermogram; **B**: Medium-angle region. The blue arrows indicate the position of the diffuse signals affiliated with the formation of a helix; **C**: Integrated intensity along the equator of the diffraction pattern showing the reflections indexed according to the hexagonal symmetry ; **D**: Chi scan between 2θ = 4.7 - 5.8° showing the intensity of the highly diffuse set of four meridional signals.

shown in figure 52A reveal that a slightly distinct pattern is obtained compared to the derivative with shortest spacer. The typical X-shaped meridional signals pointing to a helical arrangement are absent or at least very low in intensity. Along the equator a set of reflections appears, which can be indexed according to a hexagonal symmetry with an *a* parameter close to the one for **S2**$_{C12}$-**F1**$_{C4}$. After heating the freshly extruded sample to 128 °C however, the broad 10 signal splits into two reflections that can be distinguished in short-angle X-Ray scattering investigations. Apparently, the additional signal shows a slighty smaller Bragg angle and is not situated on the equator (see figure 52B and D). Interpreting these signals as located on the *hk*3 layer line similar to the star **S2**$_{C12}$-**F1**$_{C4}$ would result in a *c*-parameter amounting to 447 Å, which is unlikely large. The reflections are instead pointing to a body-centered orthorhombic cell, in which the meridional signals correspond to the 011 Bragg reflection, giving the parameters a = 96.7 Å, b = 56.1 Å and c = 142.5 Å at 30 °C. Note that the 2D ordering of the body-centered orthorhombic cell can also be described as hexagonal as long as $a_{borh} = 2a_{hex}sin(60°)$ when $b_{borh} = a_{hex}$, or $b_{borh} = \frac{a_{borh}}{2sin(60°)}$ (see figure 52E). This approximately is given here since $\frac{96.7Å}{2sin(60°)} = 55.8Å$. The diffuse intensity observed between the 310 and 400 signals could not be indexed with certainty, but the 121 signal is expected at roughly the same Bragg angle and the corresponding *hk*1 layers are rather close to the equator. Note that the intensity of the 011 reflection is much higher compared to the meridional reflections affiliated with the formation of a helix in the previous discussed stars. Hence, a highly ordered phase is obtained despite the long flexible spacer. The periodicity of more than 14 nm in the orthorhombic cell again points to a helical arrangement of the mesogens in the LC phase.

In this cell consisting of two columns, rhe number of molecules is 132, when a density of 1.04 g·cm^{-3} is assumed. Therefore, 66 molecules participate in the periodicity along the columnar axis with an average axial distance of 2.16 Å. If a single helix was present, the idealized rotation angle α between two fullerenes, calculated analogous to the previous dyad **S2**$_{C12}$-**F1**$_{C4}$, would only amount to 360°/66 = 5.45°. In a helix with two times the van der Waals radius as distance between the fullerenes, the average distance of the fullerene centers to the helical axis then would be equal to 106 Å, which is insupportable. The ideal triple helix in contrast would imply a more reasonable rotation angle of 16.36° for the trimers, resulting in a theoretical distance for the fullerene centers of 28.1 Å and therefore a distance of 33.3 Å for fullerene shells, regarding the side opposite to the linker. Hence, the ideal fullerene triple helix has a diameter of 66.6 Å. The average distance between two columns is 56.0 Å, suggesting that the fullerenes interfere with their neighboring columns.

Similar to the star **S2**$_{C12}$-**F1**$_{C4}$ with the shortest spacer, other effects might lead to deviations from the ideal diameter of the helix. In the case of **S2**$_{C12}$-**F1**$_{C16}$, it is reasonable to assume that the fullerenes exert strong influence on the aggregation behavior via interactions with the fullerenes of the neighbored columns. For this nanosegregation to happen, the helix diameters are reduced, allowing spherical fullerene units to interact with each other at the interface of the columns. This also reduces the steric repulsions caused by fullerenes reaching too far into the vicinal columns. Based on these considerations, a body-centered orthorhombic cell with two helices has been constructed and geometry optimized.* The small initial helical radius generated sterical stress. Consequently, the helices for **S2**$_{C12}$-**F1**$_{C16}$ are deformed and characterized by sporadic disruptive placements of fullerenes closer

*The corresponding model has been provided by Prof. Matthias Lehmann.

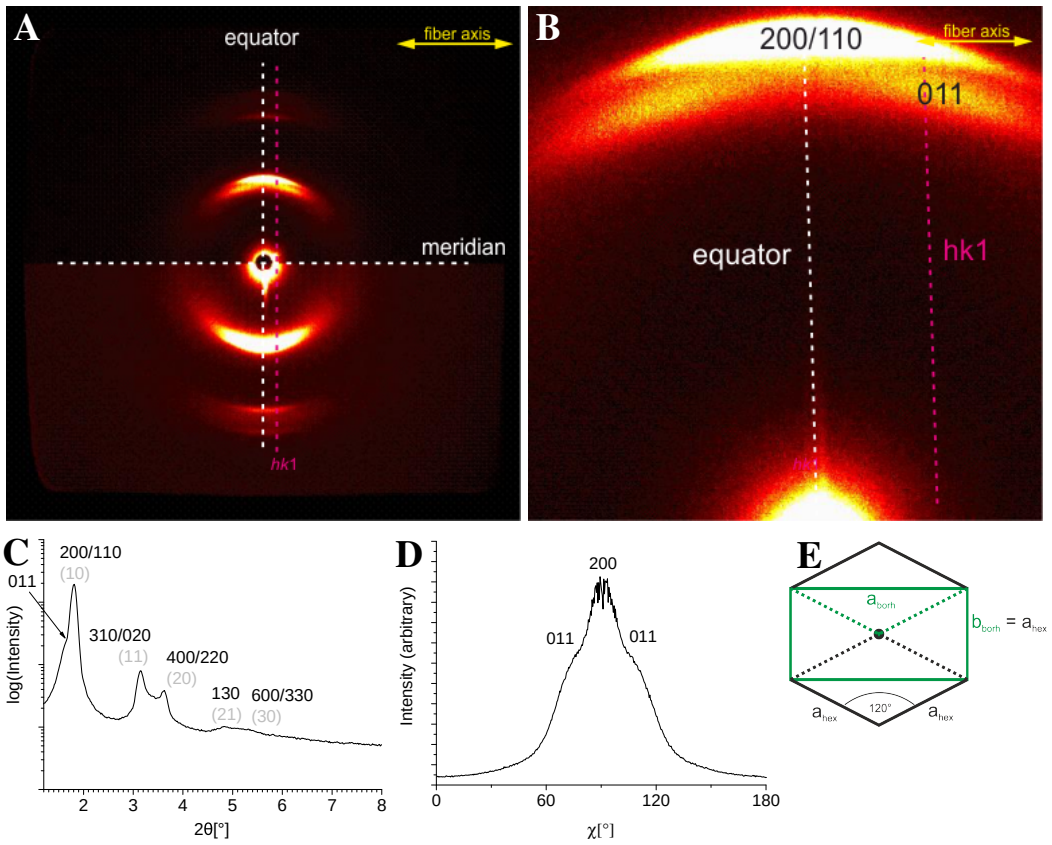

Figure 52: X-ray results obtained for extruded samples of compound **S2**$_{C12}$-**F1**$_{C16}$. **A**: Medium-angle region at 25 °C; **B**: Short-angle region at 30 °C; **C**: Integrated intensity of the diffraction pattern showing the reflections indexed according to the body-centered orthorhombic symmetry (black) and the hexagonal symmetry (grey); **D**: Chi scan between 2θ = 1.6 - 1.8° at 30 °C showing the reflections indexed according to the body-centered orthorhombic symmetry; **E**: Top view of a body-centered orthorhombic cell matching the 2D hexagonal symmetry.

to the helical axis, as can be seen in figure 53A and B. The fullerenes of the different columns show points of intersections at periodic distances. Hence, a three-dimensional network of fullerenes is formed, which explains the rather sharp and strong meridional reflections of the X-ray results. Despite this highly ordered arrangement, the clearing temperature has dropped to 205 °C, being close to the parental mesogen **S2**$_{C12}$ without any fullerene (T_{cl} = 206 °C). In the LC state of **S2**$_{C12}$-**F1**$_{C16}$, the methylene units of the spacers are restricted to certain conformations to facilitate the defined positioning of the fullerenes. In the isotropic state however, the now non-segregated molecules allow any kind of conformation for the linkers. Consequently, the mixing entropy rises with increased spacer length of the stilbene fullerene dyads. When assuming that the three rotamers for each methylene unit are degenerate, the gain in entropy can be roughly estimated by $RTln3$ per methylene unit, which amounts to 33 kJ/mol for twelve methylene units at room temperature for **S2**$_{C12}$-**F1**$_{C16}$.[224,225] The significance of this effect has already been demonstrated by a hexabenzocoronene mesogen, which has oligothiophene units attached via flexible spacers and clears at a temperature of approx. 100 °C. Most hexabenzocoronene based LCs show isotropization temperatures above 300 °C.[35] The low clearing temperature of **S2**$_{C12}$-**F1**$_{C16}$ is interesting in regard to the macroscopic alignment of the material. Furthermore, the distance between the two chromophores of the dyad in the given assembly is ideal for charge separation in a photovoltaic cell.

Star **S2**$_{C12}$-**F1**$_{C10}$ bears a spacer prolonged by six methylene units compared to **S2**$_{C12}$-**F1**$_{C4}$ and shortened by six methylene units compared to **S2**$_{C12}$-**F1**$_{C16}$. X-ray measurements were performed to clar-

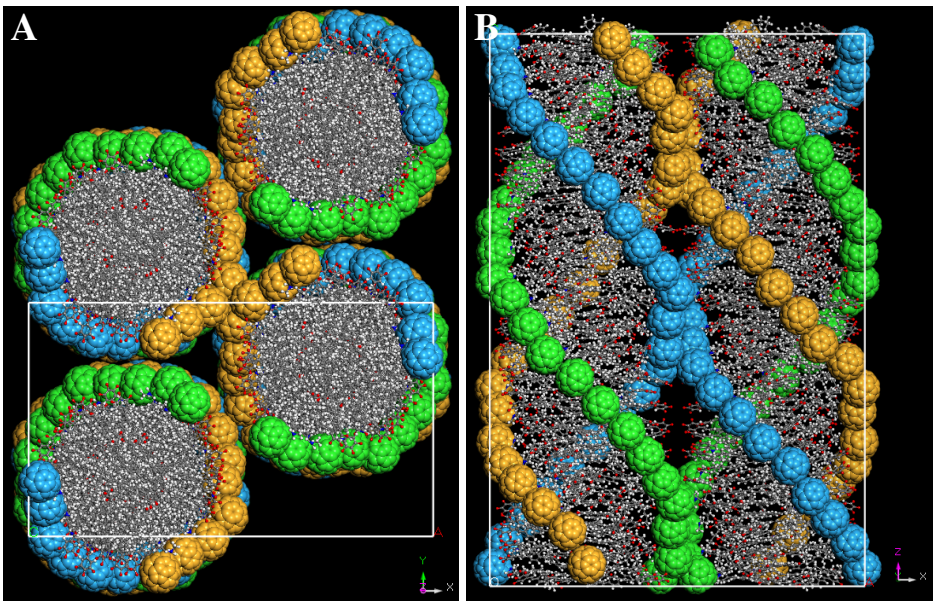

Figure 53: Model obtained for compound **S2**$_{C12}$-**F1**$_{C16}$. **A**: Top view; **B**: Side view. The chains are omitted for illustration purposes.

ify how the middle-sized linker will influence the nature of the formed LC phase. The corresponding results are highlighted in figure 54. At first sight of the medium-angle pattern shown in figure 54A, the obtained diffraction pattern resembles the one of the short spacer derivative **S2**$_{C12}$-**F1**$_{C4}$, as an X-shaped pattern pointing to a triple helix is given. The equatorial Bragg reflections may be indexed according to a hexagonal symmetry and are observable until hk = 31. In general, the signals are broader than compared to **S2**$_{C12}$-**F1**$_{C4}$. However, the short-angle area in figure 54B does show additional intensities located close to the 10 and between the 11 and 20 reflections of the preliminary assigned hexagonal pattern. When the corresponding intensity scan along the equator is plotted , a broad signal located close to the most prominent peak is revealed (see figure 54C). These results indicate that an orthorhombic cell is also formed for the star **S2**$_{C12}$-**F1**$_{C10}$. The meridional intensities located at the $hk3$ layer line simply are more prominent compared to **S2**$_{C12}$-**F1**$_{C16}$ and indicate the presence of a helical structure. The parameters then correspond to a = 97.1 Å, b = 56.4 Å and c = 121.5 Å at 30 °C. The resulting cell volume corresponds to the presence of 114 molecules within the cell, when a density of 1.04 g·cm^{-3} is assumed. Therefore, 114 / 2 = 57 molecules participate in the periodicity along the columnar axis with an average axial distance of 121.5 Å / 57 = 2.13 Å. Analogous to the star **S2**$_{C12}$-**F1**$_{C16}$, parameters for an idealized triple helix can be calculated. The rotation angle for the trimers in that case amounts to 18.95°, resulting in a distance for the fullerene centers of 24.5 Å and therefore a distance of 29.7 Å for the fullerene shells, regarding the side opposite to the linker. The corresponding helical diameter then amounts to 59.4 Å. The intercolumnar distance amounts to 56.5 Å, demonstrating that the fullerenes in this scenario also interfere with the neighboring columns. In this case, the ideal helix diameter and the intercolumnar distance are rather close. Accordingly, the fullerenes form a three-dimensional network analogous to the star **S2**$_{C12}$-**F1**$_{C10}$ and the deformation of the triple helix is small compared to **S2**$_{C12}$-**F1**$_{C10}$. A geometrically optimized model similar to **S2**$_{C12}$-**F1**$_{C16}$ has been obtained, which is highlighted in figure 54A and B.* Here, the rotation angle between the fullerenes is larger compared to **S2**$_{C12}$-**F1**$_{C16}$, reducing the

*The corresponding model has been provided by Prof. Matthias Lehmann.

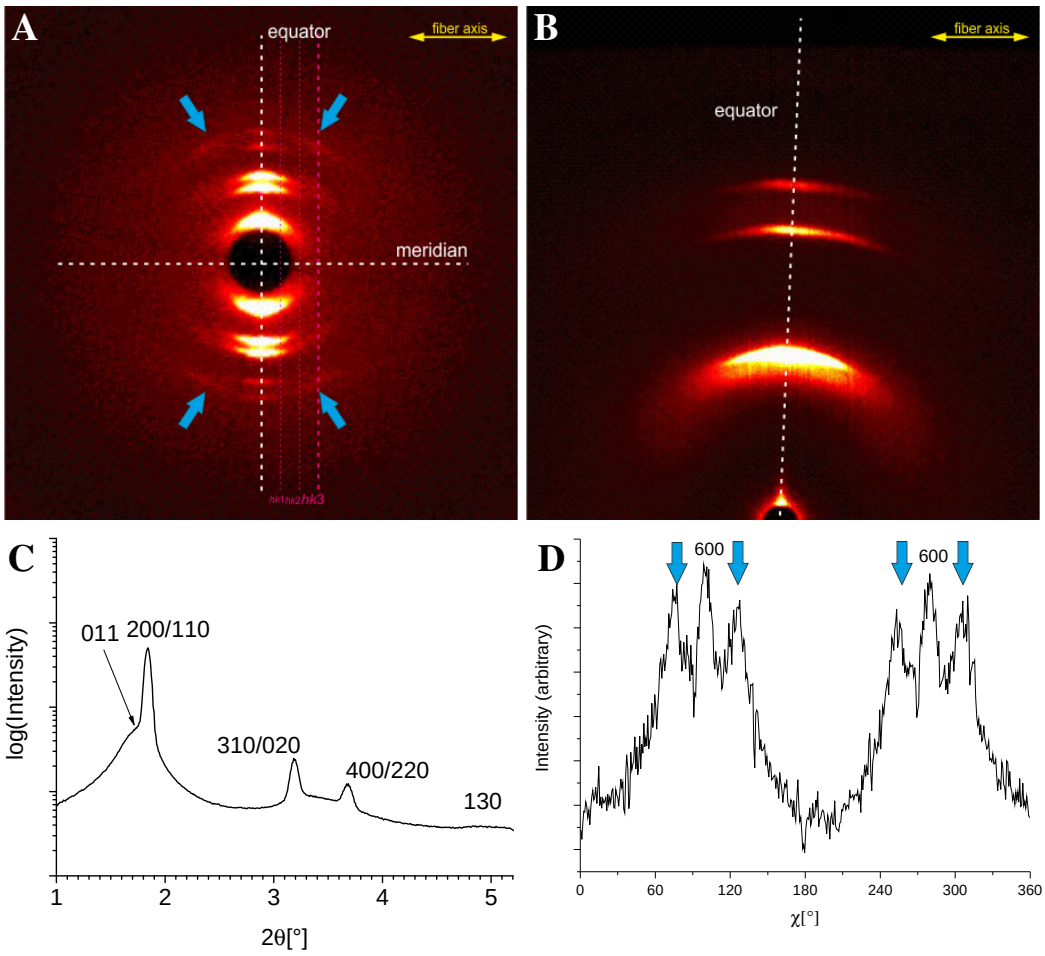

Figure 54: X-ray results obtained for extruded samples of compound **S2**$_{C12}$**-F1**$_{C10}$. **A**: Medium-angle region at 30 °C. The blue arrows indicate the position of the diffuse signals affiliated with the formation of a helix; **B**: Short-angle region at 25 °C; **C**: Integrated intensity along the equator of the diffraction pattern at 25 °C showing the reflections indexed according to the body-centered orthorhombic symmetry; **D**: Chi scan between 2θ = 5.2 - 5.9° at 30 °C showing the intensity of the highly diffuse set of four meridional signals.

steric repulsions and thus the deformation of the helices. With a clearing temperature of 240 °C, the phase stability of this material still is decreased compared to the short spacer derivative **S2**$_{C12}$**-F1**$_{C4}$. Nevertheless, heating **S2**$_{C12}$**-F1**$_{C10}$ to the clearing point for a prolonged time initiates decomposition, impeding the formation of macroscopic alignment. Analogous to the star **S2**$_{C12}$**-F1**$_{C16}$, the drop of the clearing temperature compared to **S2**$_{C12}$**-F1**$_{C4}$ is a consequence of the gained levels of freedom for the six additional methylene units and may be estimated as $6 \cdot RTln3$ = 16.3 kJ/mol at room temperature.

The length of the spacer in stilbene fullerene stars has been demonstrated to be an important factor for the nature of the formed assemblies. To further investigate the design possibilities for these dyads, star **S1**$_{C12}$**-F1**$_{C4}$ with smaller cavities between the arms has been synthesized and analyzed. Due to the lack of one *p*-phenylene vinylene repeating unit per arm, it is of interest how the fullerene guests will adapt to the spatial restriction compared to **S2**$_{C12}$**-F1**$_{C4}$. Figure 56 highlights the X-ray results obtained for **S1**$_{C12}$**-F1**$_{C4}$. In general a poor alignment of the material is observed, impeding the distinction between equatorial and meridional reflections. The most prominent signals can be indexed according to the hexagonal symmetry and are highly broadened. The 10 signal appears to overlay an additional even broader intensity and it cannot be excluded that this reflection is caused by an

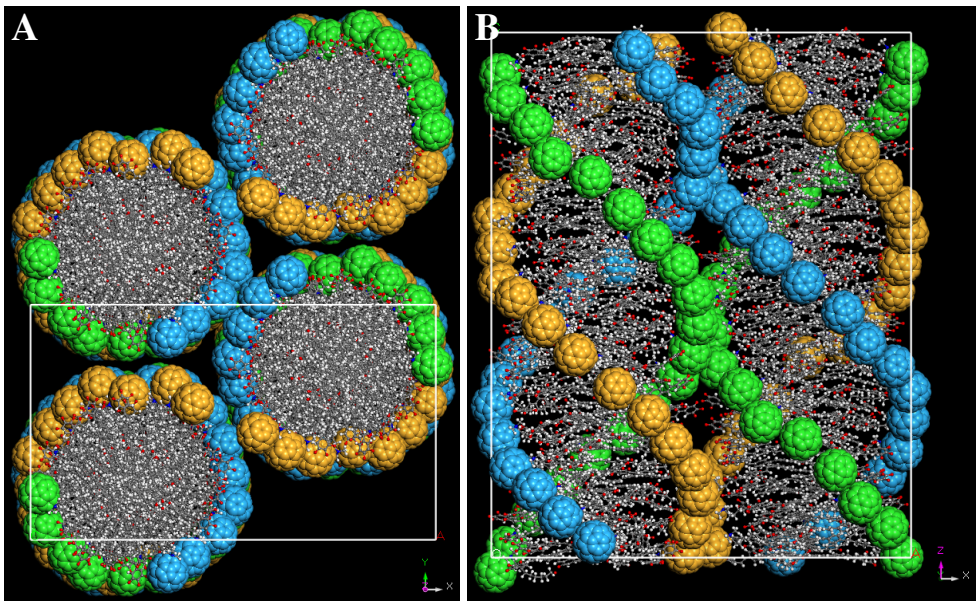

Figure 55: Model obtained for compound **S2**$_{C12}$**-F1**$_{C10}$. **A**: Top view; **B**: Side view. The chains are omitted for illustration purposes.

additional arrangement along the columnar axis. However, the material lacks orientability, rendering this signal so broad that reliable peak values cannot be obtained from curve fitting. Therefore, the exact nature of this phase cannot be determined. Assuming that a 2D hexagonal pattern is given, the *a*-parameter amounts to 44.0 Å at room temperature and therefore is decreased by 5.6 Å compared to the parent star **S1**$_{C12}$. When a density of 0.98 g·cm^{-3} is assumed, the average axial distance between two stilbene-fullerene dyads in **S1**$_{C12}$**-F1**$_{C4}$ amounts to 3.23 Å (31 molecules in an arbitrarily chosen unit cell height of 100 Å), which is much greater compared to the parent star **S1**$_{C12}$ (1.90 Å) and approaches the typical values of $\pi-\pi$-distances. Regardless, no Bragg reflection that would indicate $\pi-\pi$-interactions was found in the wide-angle region of the X-Ray diffraction pattern (figure 56B). The cavities between the arms appear to be too small to efficiently incorporate the fullerene guests, raising the average axial distance between the star molecules. The shortening of the arms therefore displays an unfavorable effect on the nature of the assembly of these systems.

To combine the helical structure of the star **S2**$_{C12}$**-F1**$_{C4}$ with the short spacer and the low clearing temperature of the stilbene star **S2**$_{O3}$, compound **S2**$_{O3}$**-F1**$_{C4}$ has been proposed to lower the clearing temperature. Surprisingly, the material was found to form an amorphous state as discussed on page 80. The X-ray results illustrated in figure 57 only show reflections of highest broadness, which do not fit any common symmetry pattern. The most intense signal corresponds to a spacing of roughly 47 Å. The *a* parameter for the parent star **S2**$_{O3}$ amounts to 53.5 Å, which equals a lattice spacing of 46.3 Å. Hence, the introduction of the fullerene does not lead to a reduction of the average lateral distance between two mesogens in this case. Evidently, the nature of the chains has a tremendous impact on the nanosegregation in this system. Special interactions between fullerenes and ethyleneoxy units are discussed in literature by means of NMR. It was demonstrated, that neat fullerene can interact with polyethyleneoxide via n-π interactions.[226] Imaginably, the chains might in parts be fastened around the spherical fullerenes, preventing the segregation of the arms and the chains.[227] To further investigate this notion, solid-state NMR measurements were performed on **S2**$_{O3}$**-F1**$_{C4}$ in collaboration with Robert Graf at the Max-Planck-Institut für Polymerforschung in Mainz, Germany. The displayed

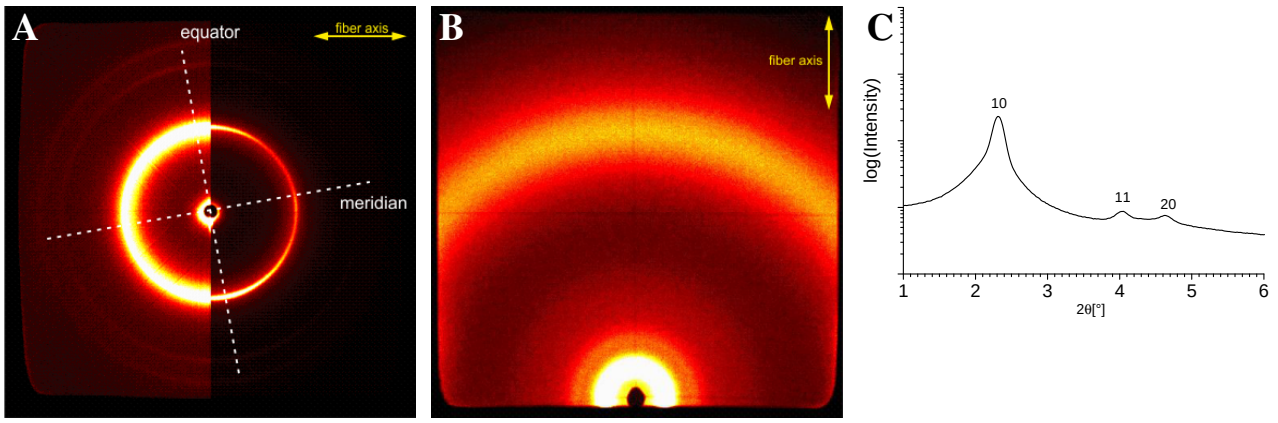

Figure 56: X-ray results obtained for extruded samples of compound **S1**$_{C12}$**-F1**$_{C4}$ at 25 °C. **A**: Wide-angle region; **B**: Medium-angle region; **C**: Integrated intensity indexed according to the hexagonal symmetry. It is not excluded that a 3D phase with higher order is present, in which the signal distances still match the values of a 2D hexagonal pattern but have to be indexed differently.

Lee–Goldburg contour plot[228] in figure 58C points on close proximities of ^{1}H and ^{13}C atoms. In the two-dimensional correlation spectrum, significant interactions between the ethyleneoxy protons, which are located at approx. 3.5 ppm in the ^{1}H NMR spectrum, and the fullerene carbons, present in the range of 135 - 150 ppm, could not be observed. Presumably, these interactions are not responsible for the lack of segregation of the stars and chains.

Another study suggests that ethyleneoxy based chains strongly demand space close to the mesogen core in the molecular plane due to the formation of random coils rather than straight chains.* Hence, the limitation of steric repulsion and therefore an efficient packing is regulated by the pitch angle of the neighbored, stacked mesogens.[229] For the three-armed star **S2**$_{O3}$ without fullerene, a minimal intermolecular chain-chain repulsion along the columnar axis theoretically can be realized with a pitch angle of 60°. **S2**$_{O3}$**-F1**$_{C4}$ bears a fullerene which, in contrast, requires the formation of a trimer to efficiently fill the space, as has been demonstrated for the alkyl chain derivatives. In this assembly the average pitch angle amounts to approx. 120°, giving maximal repulsion between the chains of the superimposed arms. Consequently, an efficient packing and therefore the formation of a LC phase is hindered. Note that conventional discotics with $\pi - \pi$ stacking features were investigated in the cited literature. Further effort is required to confirm the adaptability of this model to the shape-amphiphile **S2**$_{O3}$**-F1**$_{C4}$.

*The author of this document is thankful for helpful discussions with Robert Graf from the Max-Planck-Institut für Polymerforschung in Mainz, Germany

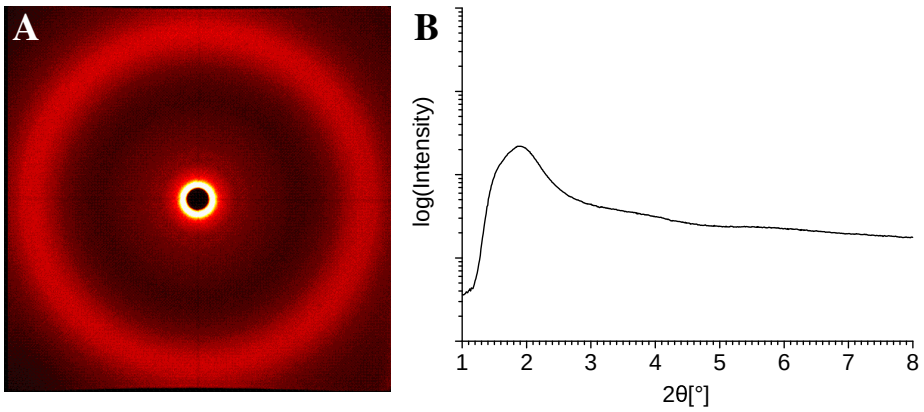

Figure 57: X-ray results obtained for extruded samples of compound **S2**$_{O3}$**-F1**$_{C4}$ at 25 °C. **A**: Wide-angle region. **B**: Integrated intensity.

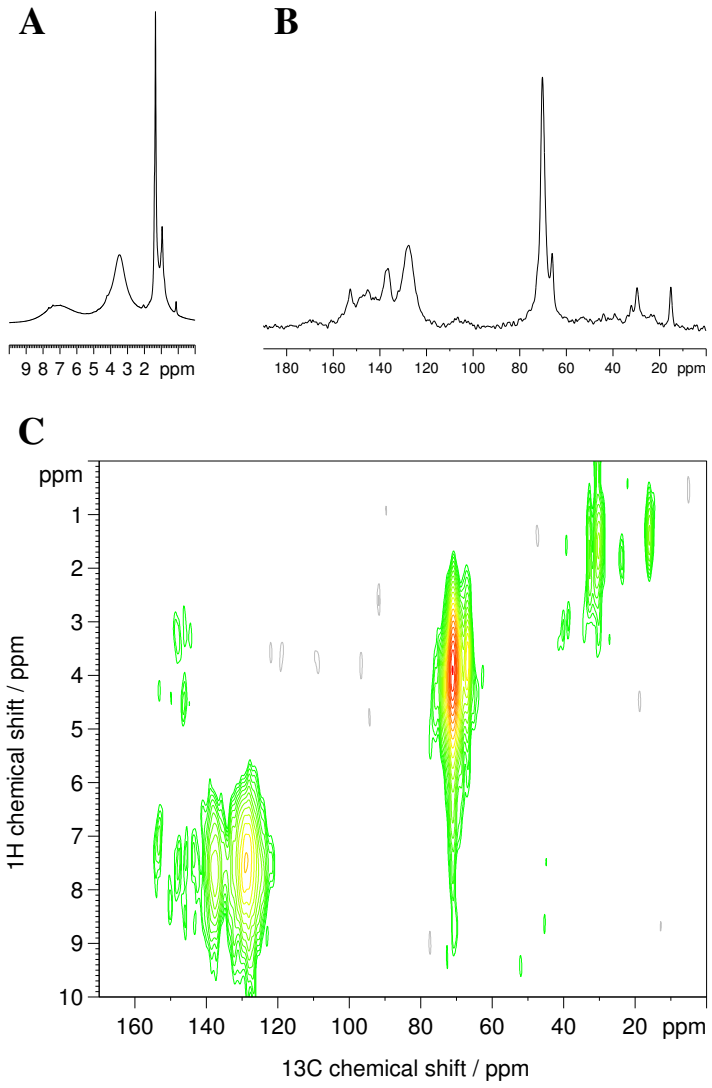

Figure 58: Solid-state NMR measurements for **S2**$_{O3}$**-F1**$_{C4}$. **A**: ^{1}H NMR; 25 kHz MAS, 850 MHz Larmor; **B**: ^{13}C NMR; 18 kHz MAS, 213.8 MHz Larmor, 2 ms Lee–Goldberg CP; **C**: Lee–Goldburg CP contour plot; 850 MHz ^{1}H Larmor, 18 kHz MAS, 2 ms LG–CP, FSLG decoupling during ^{1}H evolution, swf–TPPM decoupling during ^{13}C detection.

5.4 Three-armed stars bearing cyclopenteno fullerenes

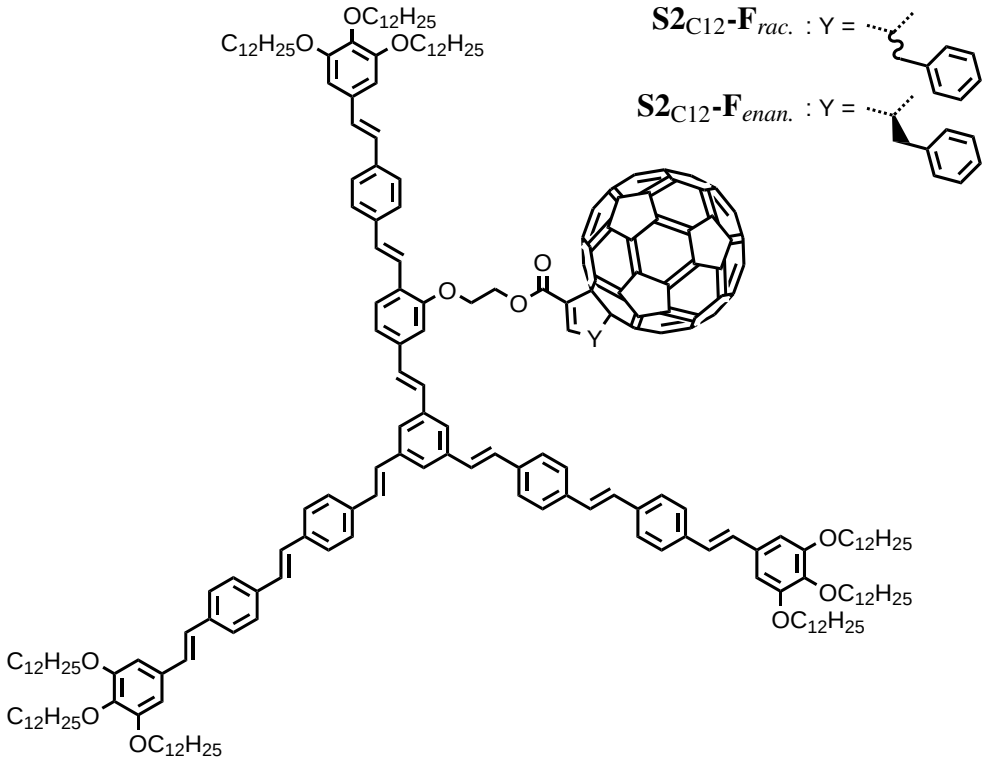

Figure 59: Structures of the examined three-armed stars bearing cyclopentenofullerenes.

The stars **S2**$_{C12}$**-F**$_{rac.}$ and **S2**$_{C12}$**-F**$_{enan.}$ have been examined towards their thermotropic properties via polarization microscope, differential scanning calorimetry and X-ray scattering. **S2**$_{C12}$**-F**$_{enan.}$ is of special interest since the enantiomeric pure fullerene substituent might have a tremendous impact on the handedness of the helical columnar arrangement.[230] The textures obtained for both compounds are illustrated in figure 60 and only show weak birefringence. They disappear at temperatures above 200 °C and only recover in the cooling process when shearing stress is applied. DSC measurements up to 250 °C for compound **S2**$_{C12}$**-F**$_{rac.}$ highlighted in figure 61 do not reveal a defined transition. The X-ray results for **S2**$_{C12}$**-F**$_{rac.}$ are illustrated in figure 62. No predominant orientation is obtained for the extruded sample. Two diffuse signals in the small-angle region are observed, corresponding to spacings of 48.2 Å and 25.1Å. The former is 7.8 Å smaller than the *a* parameter for the stilbene-fullerene dyad **S2**$_{C12}$**-F1**$_{C4}$ at room temperature. For compound **S2**$_{C12}$**-F**$_{enan.}$, the results are similar. Evidently, the bulky phenyl substituents close to the chiral center of the cyclopenteno fullerenes do not allow for a stable helical columnar assembly. The precise structure of the soft phases is unknown, but the experimental results point to an optical isotropic, amorphous and disordered solid phase.

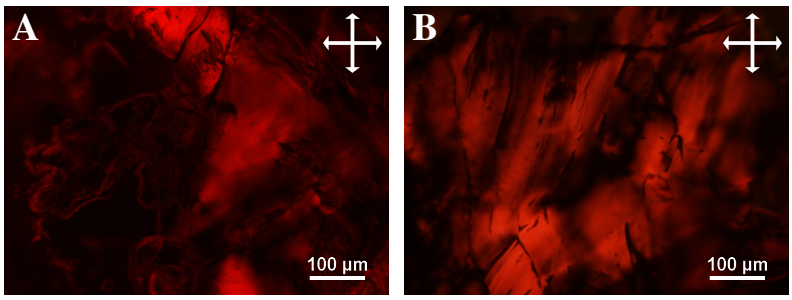

Figure 60: Polarization microscope textures of the compounds **S2**$_{C12}$**-F**$_{rac.}$ (**A**, 69 °C in the cooling stage after shearing procedure) and **S2**$_{C12}$**-F**$_{enan.}$ (**B**, 200 °C in the heating cycle) with crossed polarizers and applied UV filters.

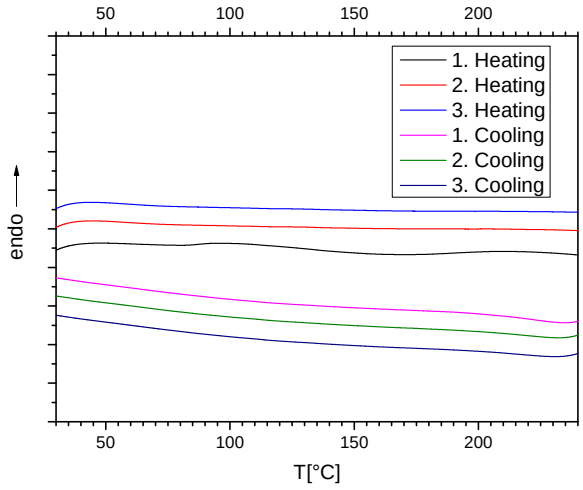

Figure 61: DSC data obtained for the star **S2**$_{C12}$**-F**$_{rac.}$.

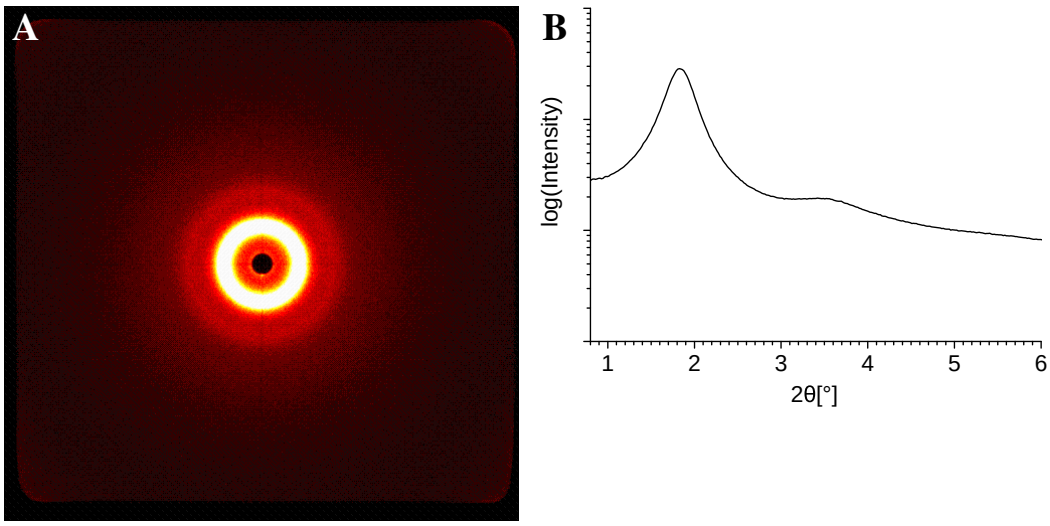

Figure 62: X-ray results obtained at 25 °C for samples of compound **S2**$_{C12}$**-F**$_{rac.}$ extruded at 120 °C. **A**: Medium-angle region; **B**: Integrated intensity of the diffraction pattern. The results are identical to that of **S2**$_{C12}$**-F**$_{enan.}$.

5.5 Porphyrin stilbene stars

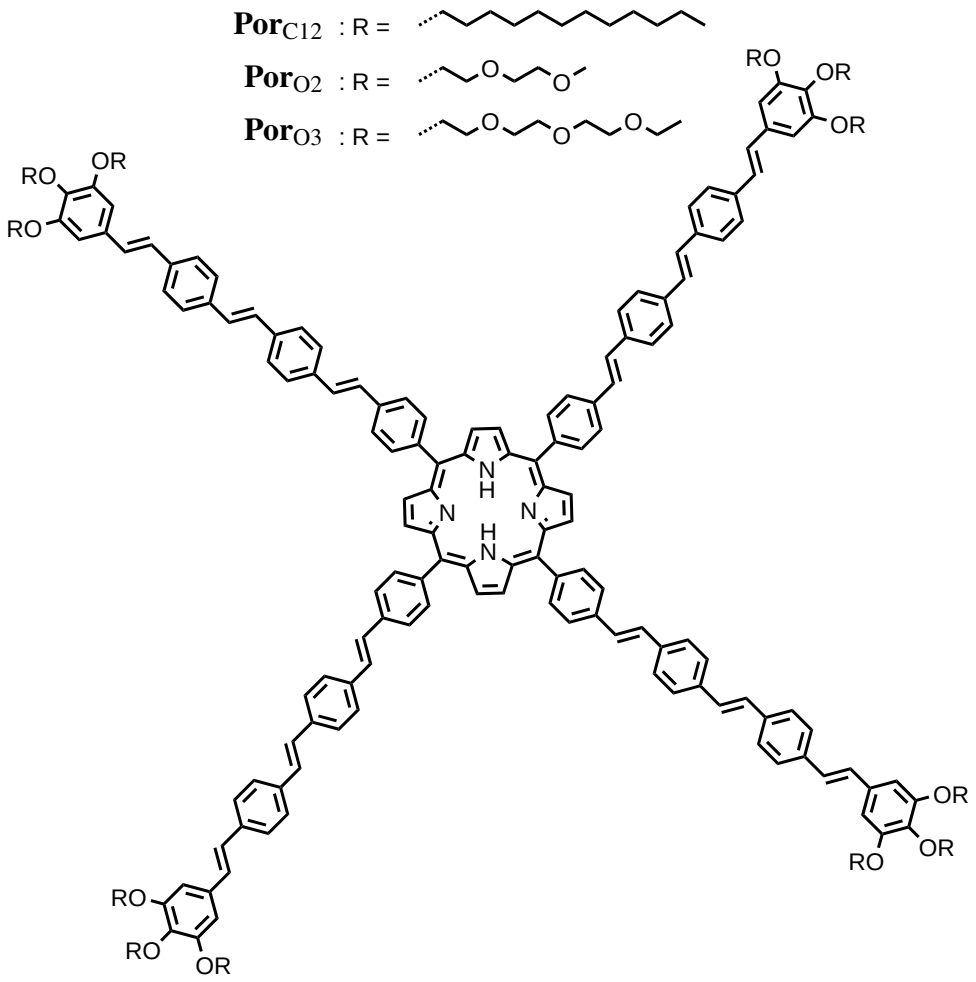

Figure 63: Structures of the examined C_4-symmetric porphyrin stars.

The C_4-symmetric porphyrin stars **Por**$_{C12}$, **Por**$_{O2}$ and **Por**$_{O3}$ have been examined towards their thermotropic properties via polarization microscope, differential scanning calorimetry, X-ray analysis and modelation. Figure 64 illustrates that only the dodecyl chains derivative **Por**$_{C12}$ shows a texture pointing to a columnar arrangement. For both oligo(ethyleneoxy) compounds, no texture under crossed polarizers is found and they show strong dewetting effects just as in the case of the stilbene star **S2**$_{O2}$. DSC results for all porphyrin stars are illustrated in figure 65 and for **Por**$_{C12}$, a clearing temperature as high as 328 °C (ΔH = 2.53 kJ·mol^{-1}) is obtained. Additionally, second order transitions below 100 °C point to a glassy state at low temperatures. A single peak in the second and third cooling process points to the formation of an additional phase. However, POM measurements and X-ray results do not considerably differ at the corresponding temperatures. For the oligo(ethyleneoxy) derivatives **Por**$_{O2}$ and **Por**$_{O3}$, unusually broad signals are obtained in the first heating process of the DSC results. Presumably, these correspond to the liquefaction of a glassy state. In further heating or cooling processes, no transition signals are obtained.

The X-ray results for **Por**$_{C12}$ are displayed in figure 66 and table 10 shows the corresponding cell parameters for the hexagonal columnar phase. Along the equator, a set of signals appears that can be indexed according to a hexagonal symmetry. Besides the d_{10} signal, all reflections are rather weak in-

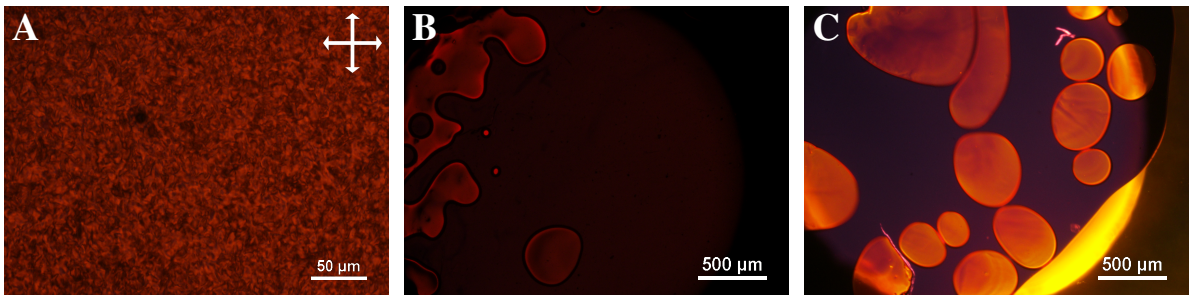

Figure 64: Polarization microscope textures of the compound **Por**$_{C12}$ (**A**, 66 °C) with crossed polarizers and compounds **Por**$_{O2}$ (**B**, 220 °C, UV filter applied) and **Por**$_{O3}$ (**C**, 250 °C, UV filter applied) with uncrossed polarizers.

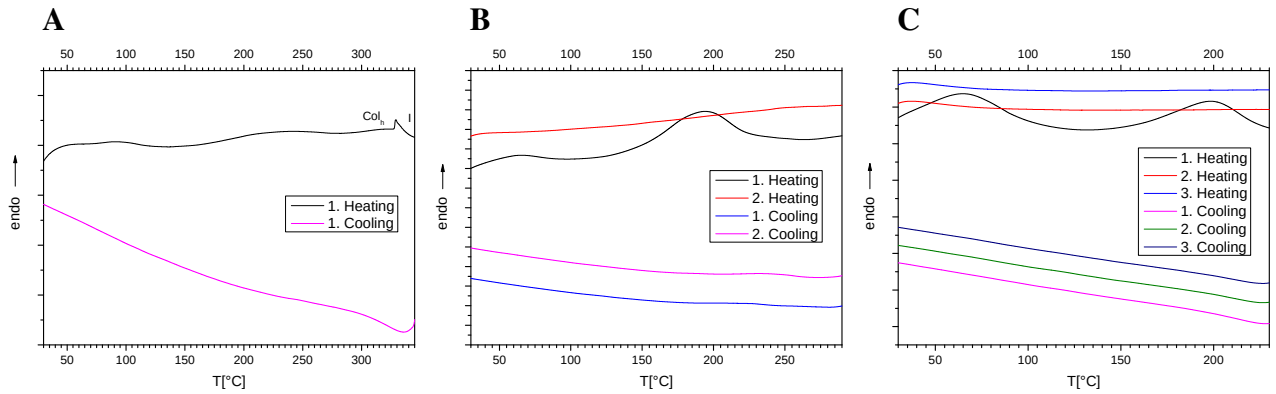

Figure 65: DSC thermograms obtained for **Por**$_{C12}$ (**A**), **Por**$_{O2}$ (**B**) and **Por**$_{O3}$ (**C**).

dicating a low ordered 2D arrangement. In the wide-angle region, a halo corresponding to the average chain-chain distance is observed but no sharper reflection caused by $\pi - \pi$ interactions between the porphyrins or stilbenes reveals. In the meridional region, diffuse Bragg reflections (green area) are observed with an X-shaped set of sharper reflections (blue area, blue arrows), the latter pointing to the formation of a helix. The corresponding correlation length roughly equates to three helical pitches. Assuming that these reflections are positioned at the *hk*1 layer line, the *c* parameter for the hexagonal helical arrangement is deduced to be 29.2 Å. For a density close to 1.0 g·cm^{-3}, the molecules have an average axial distance of 1.95 Å. Consequently, the mesogens do not stack by $\pi - \pi$ aggregation but rather in an analogous fashion to the Hekate stars **S1**$_{C12}$ and **S2**$_{C12}$. The arms of the porphyrin stars avoid each other by rotation out of the idealistic planar structure and rather interdigitate to give a closely packed material. The porphyrin cores are dislocated from the columnar axis and arrange as a single helix. Geometry optimization of these considerations led to the model displayed in figure 66E. The lateral displacement of the porphyrin cores is found to be tremendous. A simulated fiber X-ray diffraction pattern obtained from this model is displayed as inset in figure 66B and coincides strongly with the experimental results.

The parameter *a* continuously rises with higher temperatures, just like for the Hekate star **S3**$_{C12}$. Presumably, the interactions between two stacked mesogens caused by either the two porphyrin groups or by a single porphyrin group and a stilbene group are so strong that the distance along the columnar axis barely increases with rising temperature. Therefore, the intrinsic cell volume expansion caused by a higher temperature must be realized with an increase in the plane perpendicular to the columnar axis. This can be either accomplished by further stretching of the flexible chains or by further lateral displacement of the molecular centers from the columnar axis.

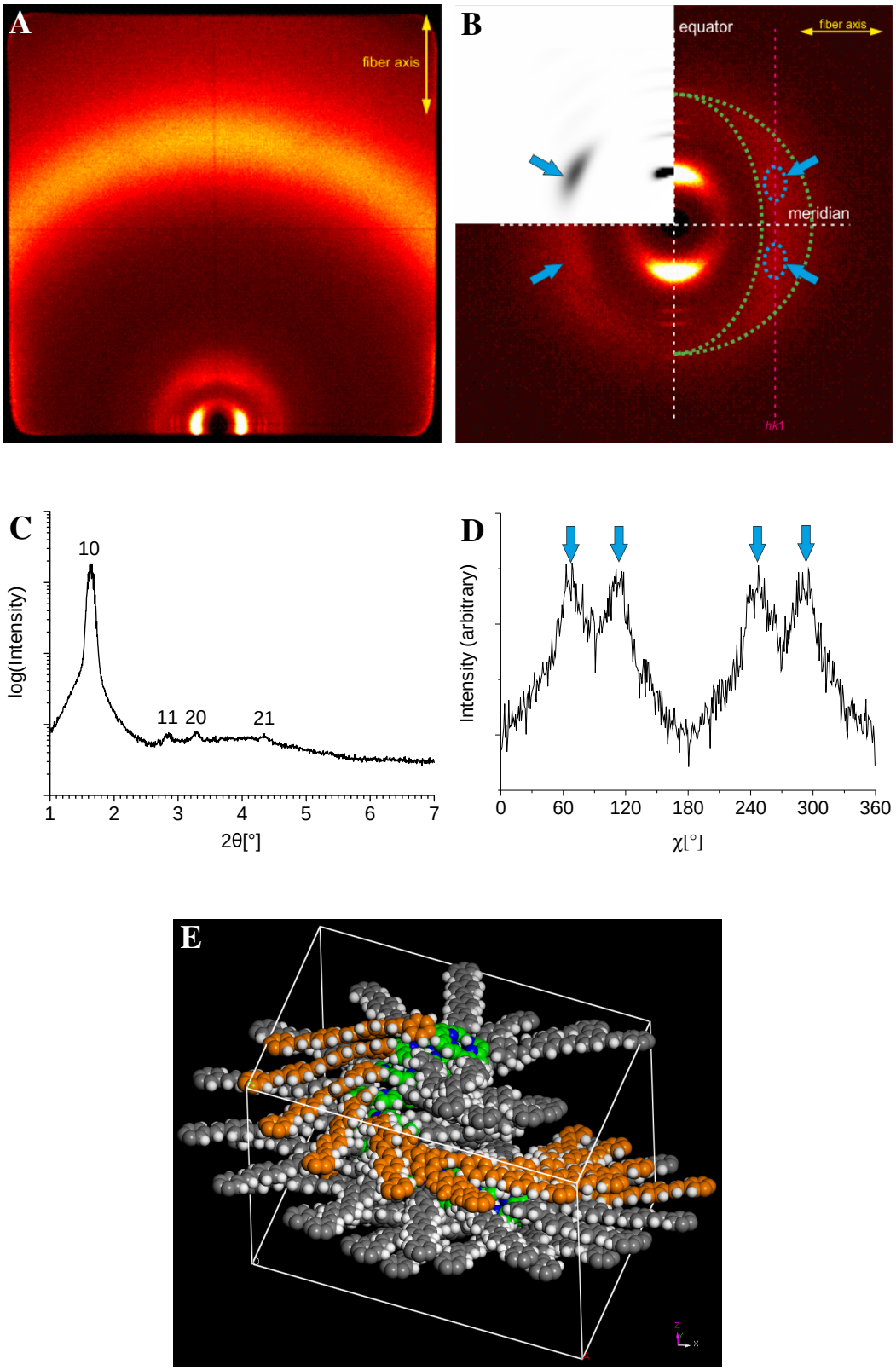

Figure 66: X-ray results obtained for extruded samples of compound $\mathbf{Por}_{C12}$ at 25 °C. **A**: Wide-angle region; **B**: Medium-angle region. The blue arrows point to the position of the diffuse signals indicating the formation of a helix; inset: simulated diffraction pattern obtained from the model; the green marked area arises from additional arrangements along the columnar axis, which could not be assigned due to the broadness of the signal **C**: Integrated intensity along the equator of the diffraction pattern showing the reflections indexed according to the hexagonal symmetry; **D**: Chi scan between $2\theta = 3.33 - 3.80°$ highlighting the intensity of the highly diffuse set of four meridional signals. **E**: Model of the laterally displaced porphyrins.

Table 10: Cell parameters *a* and *c* for the hexagonal, helical unit cells of $\mathbf{Por}_{C12}$ at different temperatures. The *c* parameter is calculated based on the meridional signals of the X-Ray measurements.

T [°C]	*a* [Å]	*c* (*c*/Z) [Å]
25	62.3	29.2 (1.95)
93	63.1	–
136	63.8	–
224	63.9	–

Figure 67 shows the X-ray results for the porphyrin stars with oligo(ethyleneoxy) chains $\mathbf{Por}_{O2}$ and $\mathbf{Por}_{O3}$. Despite the high clearing temperature of the dodecyl derivative $\mathbf{Por}_{C12}$, these molecules do not show ordered arrangements. Only highly broadened signals are observed (see figure 67). The results for $\mathbf{Por}_{O2}$ show that initially a set of reflections can be indexed according to a lamellar structure, corresponding to a spacing of 46.4 Å for the 10 reflection. Additionally, a meridional signal is observed, giving a spacing of 19.2 Å. Upon heating, however, these signals disappear and do not reestablish when cooled to room temperature (see figure 67B). Presumably, the order was introduced by the shearing stress caused by extrusion of the sample and is not a stable arrangement. $\mathbf{Por}_{O3}$ does not show any order, not even by extrusion. Apparently the oxygen-rich chains have a tremendous impact on the nanosegregation of these materials. In a few other cases in the literature, no mesogenic behavior was found for porphyrins bearing oligo(ethyleneoxy) chains. The authors either do not explain the lack of mesogenic behavior or argue that the rotated phenyl rings in *meso*-position hinder the stacking of the porphyrin rings.[59,62,231] Since the alkyl derivative $\mathbf{Por}_{C12}$ does form a columnar phase, this argument can not be valid for $\mathbf{Por}_{O2}$ or $\mathbf{Por}_{O3}$. Cook *et al.* found that certain phthalocyanine derivatives gain mesogenic properties, when ether linkages located close to the flat core are replaced by methylene units. They suspect that these ether units cause local interactions, which interfere with the ordered molecular packing of the macrocycles.[232] The oxygens of the oligo(ethyleneoxy) chains in the porphyrin stars therefore might prevent a columnar assembly. However, no experimental data were published to substantiate the speculations of the authors. Moreover, stars with an analogous structure in relation to the discussed porphyrins but with a phthalocyanine core as replacement do form columnar phases with oligo(ethyleneoxy) chains.[233] The origin of the absence of LC phase formation is not known for the presented porphyrin stars.

Since no other literature was found to explain the surprising behavior of the these materials, a more general approach was applied to evaluate the phase stability of the stars. Positionally ordered LC phases are based on a positive Gibbs free energy of mixing for the incompatible building blocks: $\Delta G_{mix} = \Delta H_{mix} - T\Delta S_{mix} > 0$. The mixing enthalpy ΔH_{mix} is related to the difference in cohesive energy density *ced* of the corresponding building blocks A and B: $\Delta H_{mix} \sim (ced_A - ced_B)$. The *ced* values depend on the molecular volume V_{mol} and can be calculated from tabulated Hildebrand solubility parameters δ via $\delta = \sqrt{ced}$. Therefore, $\Delta\delta = \delta_A - \delta_B$ is a measure for the incompatibility of two different segments. The Flory-Huggins interaction parameter χ, which primarily describes the solubility of flexible polymers, considers the influence of the respective block volumes and the mixing enthalpy. When applied to LC systems, it may be denoted as: $\chi_{core-chain} = V_{mol}(\delta_{core} - \delta_{chain})^2(RT)^{-1}$ with $V_{mol}(RT)^{-1}$ also representing the contribution of entropy. Here, the solubility parameters for the covalently linked but segregated regions are estimated from segmental group contributions ac-

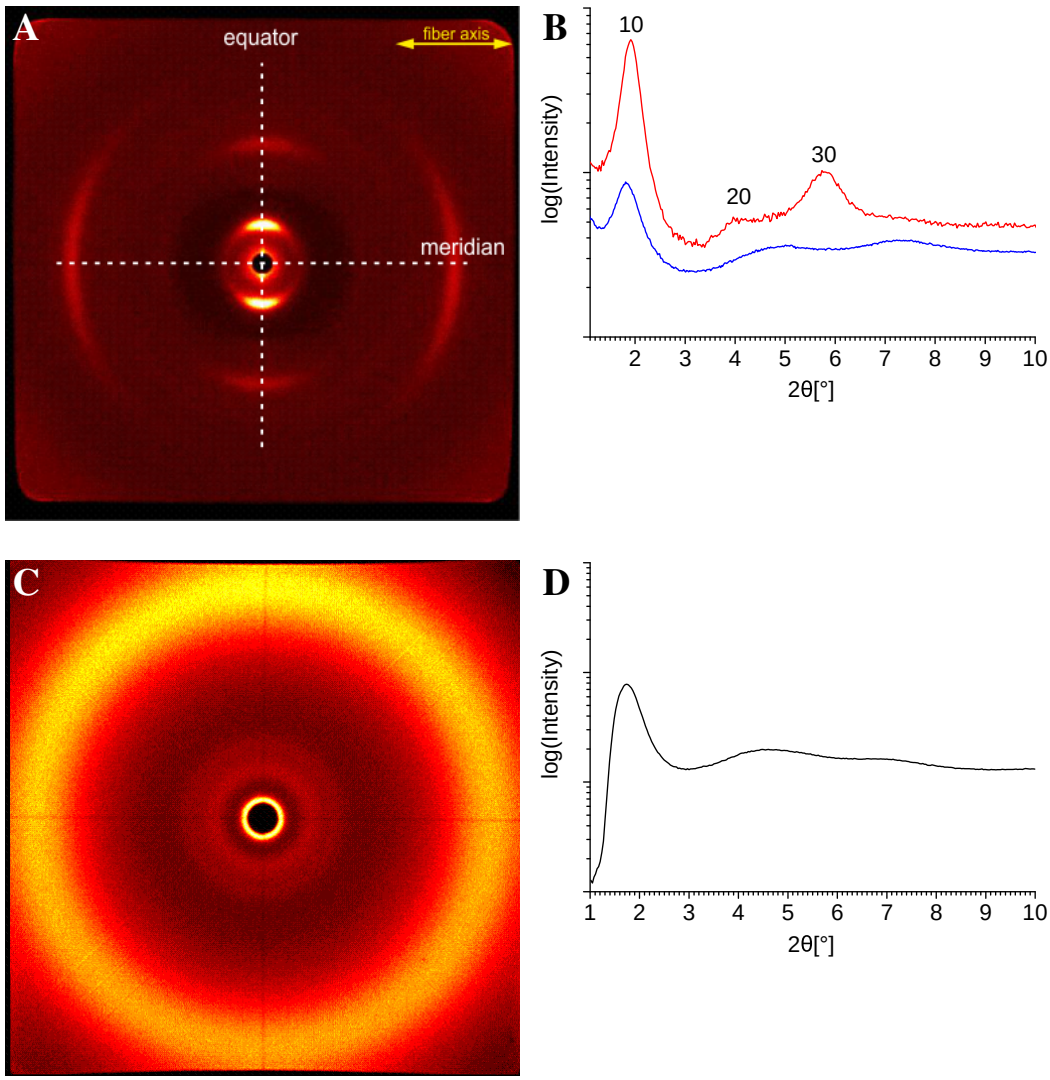

Figure 67: X-ray results obtained for extruded samples of compounds $\mathbf{Por}_{O2}$ (A, B) and $\mathbf{Por}_{O3}$ (C, D) at 25 °C. **A**: Medium-angle region diffraction pattern for a non-annealed sample of $\mathbf{Por}_{O2}$; **B**: Integrated intensity along the equator for the sample prior to (red) and after (blue) annealing; reflections indexed according to a lamellar symmetry **C**: Wide-angle region for $\mathbf{Por}_{O3}$. **D**: Integrated intensity.

cording to $\delta = \sqrt{\frac{-\sum U}{\sum V}}$ via tabulated values for small molecular fragments. A sufficiently high value for χ is required to facilitate the nanosegregation in LC systems. Additionally, the order-disorder transition temperature depends on the volume fractions f of the incompatible building blocks. The mean field diagram of f against χ displayed in figure 68 shows that phases formed by imbalanced volume fractions of the building blocks such as hexagonal columnar phases also need slightly higher χ-parameters in order to be generated.[21,234]

The Flory-Huggins parameters and volume fractions for the cores/arms and chains of the porphyrin stars have been calculated by tabulated values from literature[235] and are displayed in figure 68. It has to be stressed that the calculation of the parameters for the structural complex porphyrin unit is based on improper molecular fragments and therefore does not give appropriate absolute values. Nevertheless, a comparison of the values obtained for the porphyrin stars with chains of different nature gives information about the tendency to segregate. Figure 68 illustrates that the fractional volume of the core is smallest for the dodecyl derivative $\mathbf{Por}_{C12}$. The increased values for both ethyleneoxy derivatives $\mathbf{Por}_{O2}$ and $\mathbf{Por}_{O3}$ can be regarded as disadvantageous for the general formation of colum-

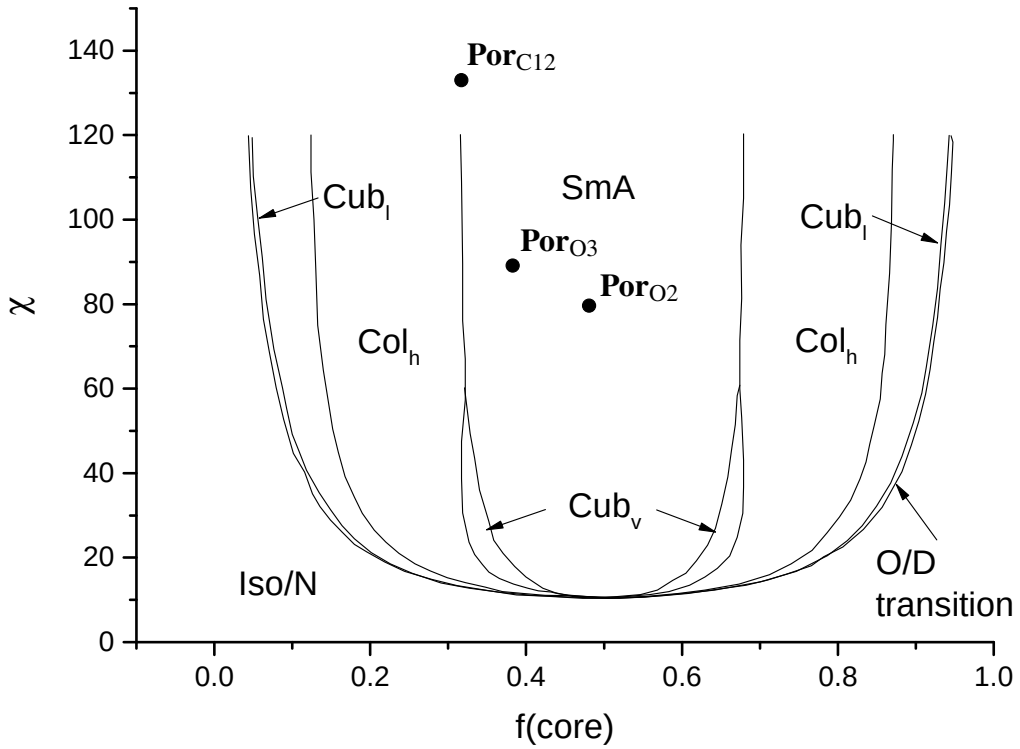

Figure 68: Mean field diagram of volume fractions f against Flory-Huggins parameter χ and corresponding values for the porphyrin stars. Note that the calculation of the parameters for the structural complex porphyrin unit is based on improper molecular fragments and therefore does not give appropriate absolute values. Reprinted and adapted with permission from Matsen, M.; Bates, F. S. *Macromolecules* **1996**, *29*, 1091 – 1098. Copyright 1996 American Chemical Society.

nar phases. Additionally, the Flory-Huggins parameter χ is also greatest for **Por**$_{C12}$. Apparently, the oxygen atoms reduce the cohesive energy density difference and thus the tendency to nanosegregate for **Por**$_{O2}$ and **Por**$_{O3}$. Both effects combined certainly have a great impact on the clearing temperature of the porphyrin stars. However, it remains uncertain whether additional phenomena are responsible for the inhibition of the formation of columnar arrangements.

To take an influence on the aggregation behavior of the porphyrins **Por**$_{O2}$ and **Por**$_{O3}$, NaOTf salt was added in a molar ratio of 1/1. These ions have already shown to push other mesogens towards the formation of columnar phases, when oligoether chains were attached.[236–238] The resulting materials were examined via polarization microscopy; however, no texture was obtained with crossed polarizers and thus the formation of LC phases were obviously not induced in the present case.

5.6 Mixtures of Fullerene bearing porphyrins

Similar to the mixture **Mix_S** of the corresponding Hekate stars presented on page 83, a blend of porphyrin stars and porphyrin-stilbene-fullerene triads was anticipated to form LC phases with interesting assemblies. The main difference here is the attachment of four arms to the mesogen core, reducing the available space for the fullerenes within the molecular plane. To gain information on how well these spherical units would fit between the narrowed voids, a model of the hypothetical 1 : 2 mixture of **Por**$_{C12}$ and the corresponding star with four attached fullerenes was build and geometry optimized. Figure 69 shows that in this system of 9 molecules with arbitrarily chosen parameters, the fullerenes align unrestrictedly in the voids to form a quadruple helix. Here, a density of close to

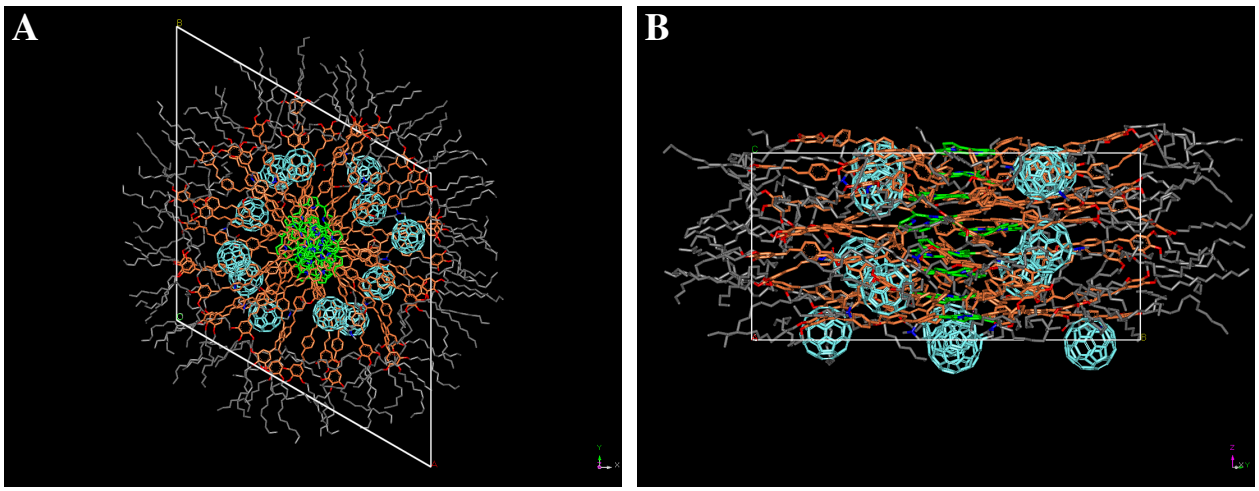

Figure 69: Modelling of a 2:1 mixture of $\mathbf{Por}_{C12}$ and the corresponding hypothetical derivative with four fullerene units ($\mathbf{Por}_{C12}$-$\mathbf{F4}_{C4}$). Hydrogen atoms omitted for clarity. Green: porphyrins; orange: stilbenes; pale blue: fullerenes. Parameters: a = 60.0 Å; c = 25.0 Å; 9 molecules; ρ = 0.994 g·cm^{-3}; **A**: Top view; **B**: Side view.

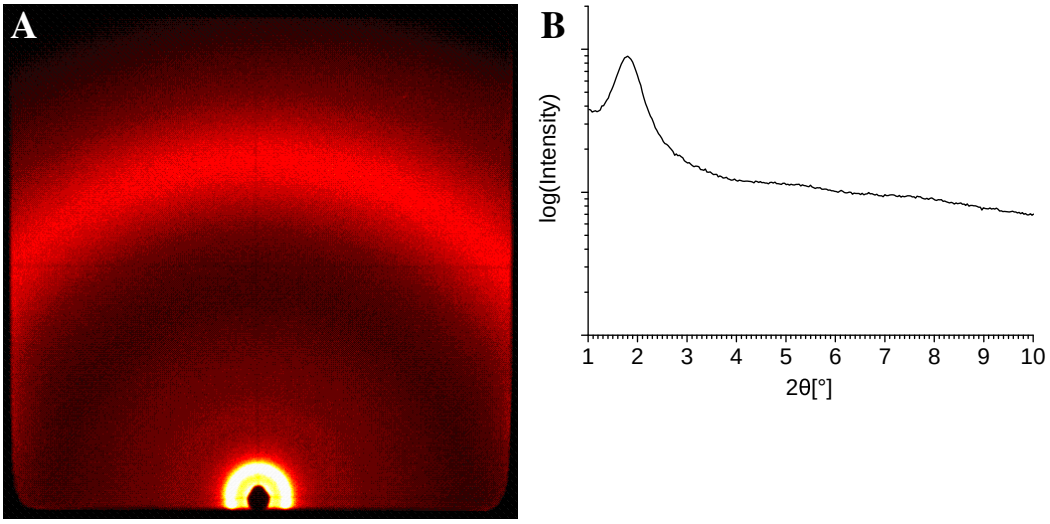

Figure 70: X-ray results obtained for extruded samples of the mixture **Mix_P** at 25 °C. **A**: Wide-angle region. **B**: Integrated intensity.

1.0 g·cm^{-3} is realized with large and negative non-covalent bonding energies (van der Waals: -1752.8 kcal/mol; electrostatic: -478.0 kcal/mol). These results boosted the aim to synthesize both porphyrin stars. The porphyrin star $\mathbf{Por}_{C12}$ then however showed a clearing temperature of above 300 °C. The synthesis and examination of a corresponding star with fullerene units was omitted since materials with low clearing temperatures for macroscopic alignment are desired.

Instead, $\mathbf{Por}_{O3}$-$\mathbf{F4}_{C4}$ was synthesized and mixed with non-liquid crystalline $\mathbf{Por}_{O3}$ in a ratio of 2 : 1 in order to obtain liquid crystalline systems (mixture **Mix_P**). The X-Ray results for this blend are illustrated in figure 70. The material does not show orientational or positional order, just like neat $\mathbf{Por}_{O3}$. No wide-angle reflection corresponding to $\pi - \pi$ interactions was observed. These results point to the presence of an amorphous solid. Similar to the findings for the compound $\mathbf{S2}_{O3}$-$\mathbf{F1}_{C4}$ discussed on page 90, the superimposing of the arms in a trimer of mesogens might give strong sterical repulsions caused by the ethyleneoxy chains. Moreover, the reduced difference in cohesive energy density for the porphyrin stars $\mathbf{Por}_{O2}$ and $\mathbf{Por}_{O3}$ compared to the alkyl derivative $\mathbf{Por}_{C12}$ discussed on page 99 also applies to this binary mixture. Apparently the nature of the oligo(ethyleneoxy) chains

influences the LC properties tremendously. Eventually, the formation of mesophases in the series of fullerene containing star-shaped mesogens with benzene and porphyrin cores was not predictable.

6 Results — Spectroscopic studies in solution

6.1 NMR studies of stilbene-fullerene dyads

The NMR spectra of the stilbene-fullerene dyads **S2**$_{C12}$-**F1**$_{C4}$, **S2**$_{C12}$-**F1**$_{C10}$ and **S2**$_{C12}$-**F1**$_{C16}$ have been analyzed in more detail, since significant changes were observed as a function of the spacer lengths. Figure 71 illustrates that many protons face an up-field shift in these materials compared to the stilbene star **S2**$_{C12}$. Obviously this must be an effect of the spatial proximity between the peripheral hydrogen atoms of the arm and the fulleropyrrolidine unit. The shielding or deshielding caused by fullerenes is hard to predict due to the complex spherical structure. When a magnetic field is directed perpendicular to the plane of the particular ring, diatropic ring currents are present in the hexagons, while the pentagons show slightly paratropic currents.[118] Consequently, protons are shielded when located above the six-membered rings and deshielded when above five-membered rings.[239–241] Exohedral adducts like fulleropyrrolidines differ in their π-system compared to neat C_{60}, decreasing the paratropicity of the next-nearest five-membered rings and increasing the diatropicity of the remaining aromatic hexagons. Apart from this finding, most studies focus on the change of endohedral shielding for trapped helium in fullerene cages.[242]

The stilbene-fullerene dyads presented in this work show shielding effects for the stilbene protons. The protons located at the terminal benzene ring bearing the dodecyl chains (green) split into two signals for the dyads. However, only in the case of the shortest spacer, there is a significant impact (0.05 ppm). As this molecule possesses drastically reduced degrees of freedom compared to the longer

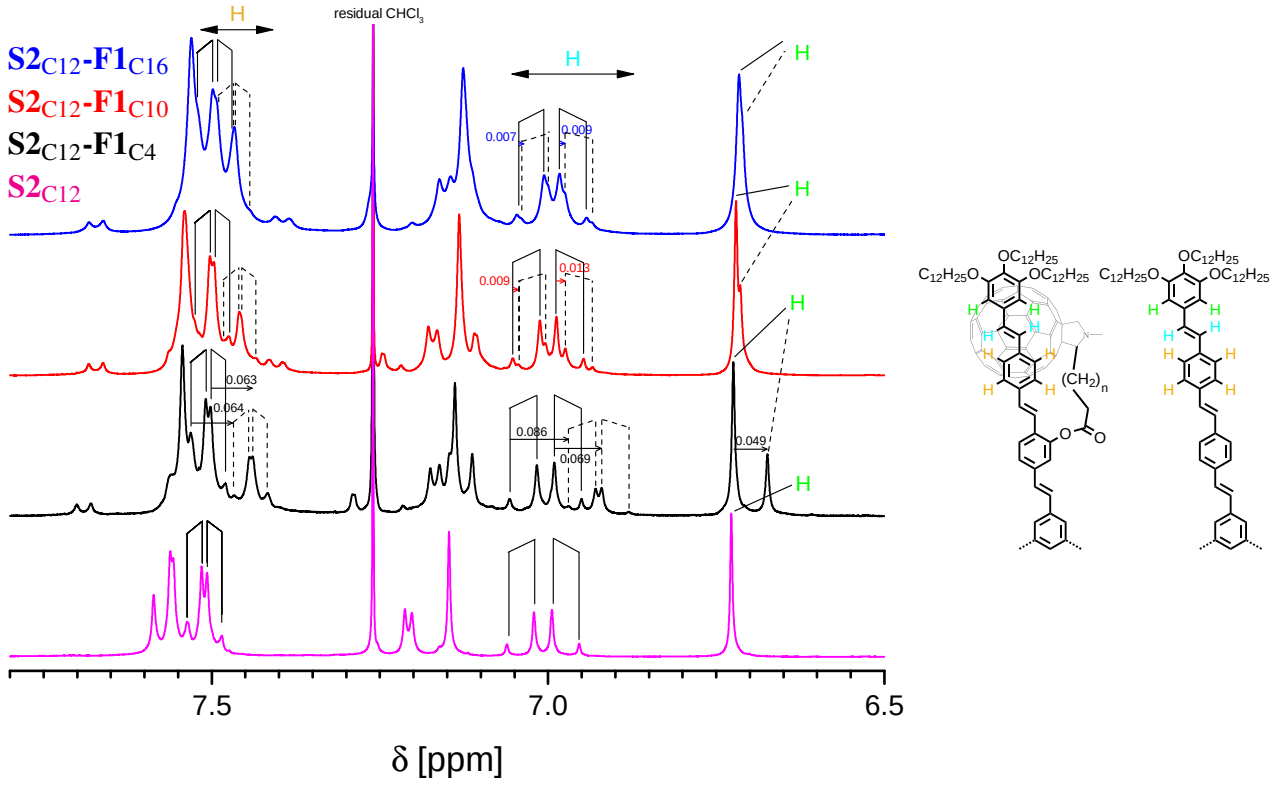

Figure 71: Magnetic shielding of aromatic protons for the Hekate stars **S2**$_{C12}$-**F1**$_{C4}$ (black), **S2**$_{C12}$-**F1**$_{C10}$ (red) and **S2**$_{C12}$-**F1**$_{C16}$ (blue) observed in deuterated chloroform. NMR results of **S2**$_{C12}$ (magenta) displayed for comparison. The solid lines indicate the positions of the protons located at the arms not affected by the presence of fullerenes while the dashed lines represent the protons that face magnetic shielding. The corresponding shifts are given by the displayed numbers in ppm and are pictured by the arrows.

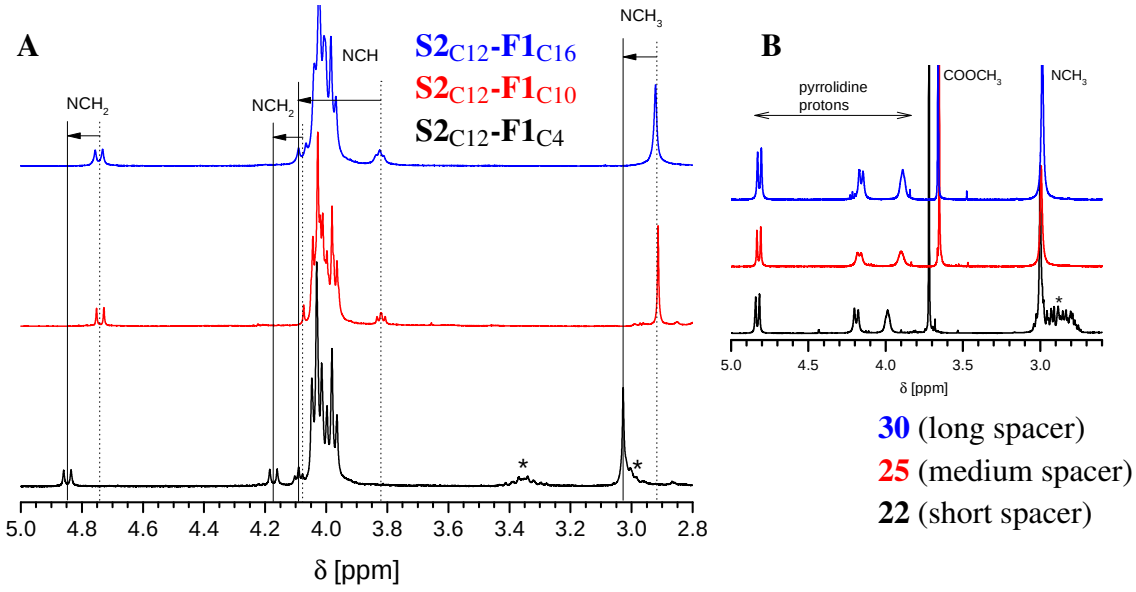

Figure 72: A: Magnetic deshielding observed for the pyrrolidine protons from the Hekate star **S2**$_{C12}$-**F1**$_{C4}$ (black) in relation to **S2**$_{C12}$-**F1**$_{C10}$ (red) and **S2**$_{C12}$-**F1**$_{C16}$ (blue). The lines (**S2**$_{C12}$-**F1**$_{C4}$: solid; **S2**$_{C12}$-**F1**$_{C10}$ and **S2**$_{C12}$-**F1**$_{C16}$: dotted) indicate the positions of the fulleropyrrolidine protons and the arrows show the corresponding shift for these protons between the mesogens with different spacer lengths. **B**: Extract of the NMR data for the methyl ester spacers **22**, **25** and **30**. *: These signals correspond to the ethylene unit in the shortest spacer. Due to the vicinity of these protons to the nitrogen atom, they show higher ppm values compared to the longer spacers. Therefore, analogous signals for the prolonged linkers face an up-field shift and are not observable in the given frequency range.

spacers, it is plausible to assume that the fullerene sphere only shows limited mobility and therefore interacts with the outer part of the oligo(*p*-phenylenevinylene) arms. For increased lengths of the linkers, the interaction between the chromophores is not strong enough to overcome the disadvantageous entropy. For the most-outer double bond protons (cyan), an even stronger impact is observed. Interestingly, the shifts for both protons are comparable in magnitude, suggesting that the fullerene sits on top of the corresponding π-system or that a fast dynamic process takes place, in which both protons face a comparable shielding in average. The AA'BB' protons next to the outer-most double bond (golden) also face an up-field shift. It is strongest for the shortest spacer, but even in the case of prolonged linkers, a significant impact is observed. However, these protons are rather close to the attached oxygen and therefore electronic effects cannot be excluded. This structural influence has been determined as small for the allyl ether derivative **71**, but at the given proximity is not comparable to an ester anymore.

Figure 72A shows the NMR data in the range of the pyrrolidine protons obtained for **S2**$_{C12}$-**F1**$_{C4}$, **S2**$_{C12}$-**F1**$_{C10}$ and **S2**$_{C12}$-**F1**$_{C16}$. Interestingly, all pyrrolidine proton signals for the shortest spacer are shifted down-field compared to the stars **S2**$_{C12}$-**F1**$_{C10}$ and **S2**$_{C12}$-**F1**$_{C16}$. Note that this effect is also observed for the methyl ester spacers **22**, **25** and **30**, but only the methyl ester protons and the proton located at the stereo center of the pyrrolidine ring are affected with a much smaller impact compared to the stilbene fullerene dyads (figure 72B). Therefore, the magnetic anisotropy of the conjugated arms in the vicinity of the pyrrolidine ring plays the major role in the deshielding of the stilbene-fullerene dyads.

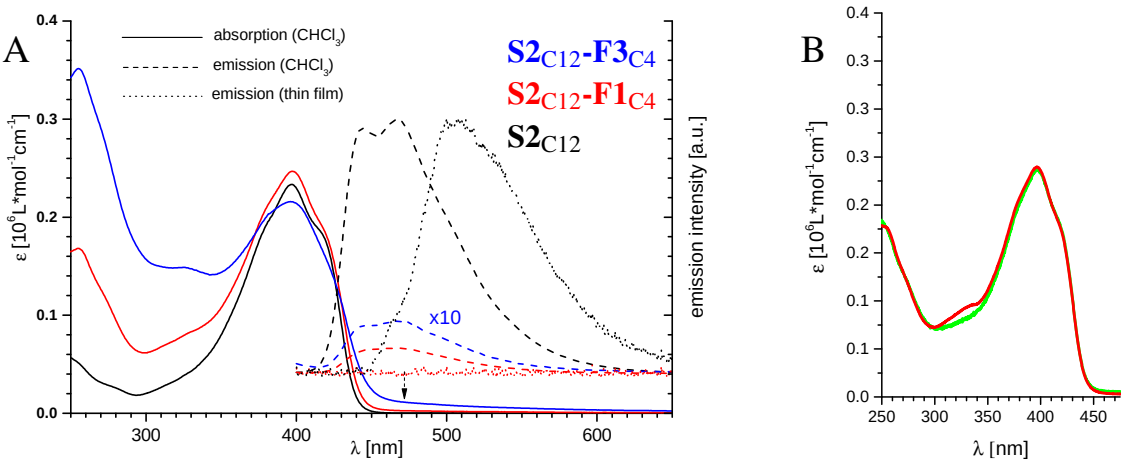

Figure 73: **A**: Photophysical measurements for the Hekate stars **S2**$_{C12}$ (black), **S2**$_{C12}$**-F1**$_{C4}$ (red) and **S2**$_{C12}$**-F3**$_{C4}$ (blue). Absorption spectra are represented by the solid lines and were performed in $CHCl_3$ solutions. The arrow at approx. 470 nm indicates the shoulder for **S2**$_{C12}$**-F1**$_{C4}$ and **S2**$_{C12}$**-F3**$_{C4}$. Emission spectra in solution are displayed as dashed lines and the values for **S2**$_{C12}$**-F3**$_{C4}$ are magnified by a factor of 10 for illustration purposes. Finally, the dotted lines show the emission spectra for the corresponding thin films of **S2**$_{C12}$ and **S2**$_{C12}$**-F1**$_{C4}$. All emission spectra are raised from the ground level for illustration purposes. Image reproduced and adapted from reference [214] with permission of the rights holder, Wiley-VCH; **B**: Comparison of UV/VIS absorption spectra for an aged sample (red) and a freshly synthesized sample (green) of **S2**$_{C12}$**-F1**$_{C4}$.

6.2 Photophysical measurements

Absorption and emission spectra have been performed for the Hekate stars **S2**$_{C12}$, **S2**$_{C12}$**-F1**$_{C4}$ and **S2**$_{C12}$**-F3**$_{C4}$ (see figure 73A). All stilbenes show an absorption maximum in chloroform at 400 nm. Compounds **S2**$_{C12}$**-F1**$_{C4}$ and **S2**$_{C12}$**-F3**$_{C4}$ also show maxima at 255 nm and 327 nm, typical for fulleropyrrolidines,[123] and a shoulder at 470 nm. These maxima are increasing linearly with the number of fullerenes attached to the star-shaped molecules. The emissions spectra shown in figure 73A reveal that **S2**$_{C12}$ shows a strong maximum at 468 nm in chloroform. Substantial quenching is observed when one fullerene is attached (**S2**$_{C12}$**-F1**$_{C4}$), demonstrating an efficient energy and charge-transfer between the donor stilbene and the acceptor fullerene. These processes are more effective for compound **S2**$_{C12}$**-F3**$_{C4}$ with its additional fullerenes since here all stilbenes have a fullerene in their vicinity. Finally, the emission spectrum of a thin film of **S2**$_{C12}$**-F1**$_{C4}$ with undefined thickness exposes a quantitative quench of the excitation, caused by the formation of the tightly packed triple helix. In this aggregate, the stilbenes are always surrounded by the fullerenes.

To investigate the influence of the spacer length of the stilbene-fullerene dyads **S2**$_{C12}$**-F1**$_{C4}$, **S2**$_{C12}$**-F1**$_{C4}$ and **S2**$_{C12}$**-F1**$_{C4}$, corresponding absorption and fluorescence studies in solution were performed (see figure 74).* All fluorescence spectra were recorded under the same conditions (excitation, emission slits, excitation wave length) and concentration corrected to ensure the comparability of the emission intensities. The absorption spectra are almost identical with no visible influence of the spacer length, which defines the maximum distance between the stilbenoid donor scaffold and the fullerene acceptor. In contrast, the fluorescence spectra show increased emission quenching with decreasing spacer lengths. At first glance, this can be explained by the distance dependence of the nonradiative energy transfer mechanisms (Dexter or Förster).[243] However, it is known that the 1,3,5-substitution pattern of the mesogen core hampers the conjugation between the three distinct arms. Therefore,

*The corresponding experiments were thankfully performed by Moritz Dechant, Julian Herbert, Prof. Matthias Lehmann and Nikolai Scheuring

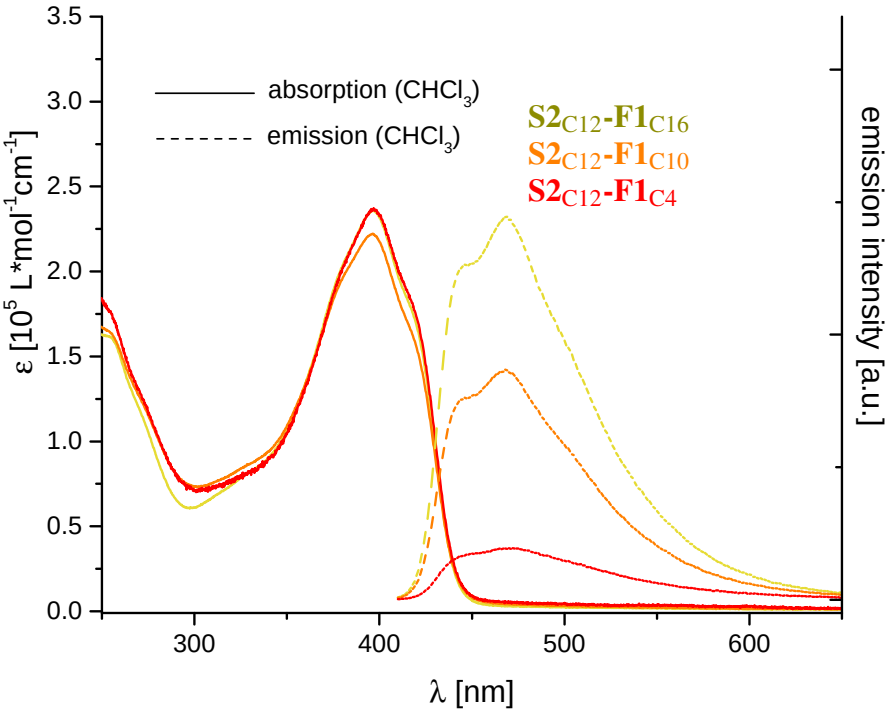

Figure 74: Photophysical measurements for the Hekate stars **S2**$_{C12}$**-F1**$_{C4}$ (red), **S2**$_{C12}$**-F1**$_{C10}$ (orange) and **S2**$_{C12}$**-F1**$_{C16}$ (golden). Absorption spectra are represented by the solid lines and were performed in $CHCl_3$ solutions. Emission spectra in solution are displayed as dashed lines and are raised from the ground level for illustration purposes.

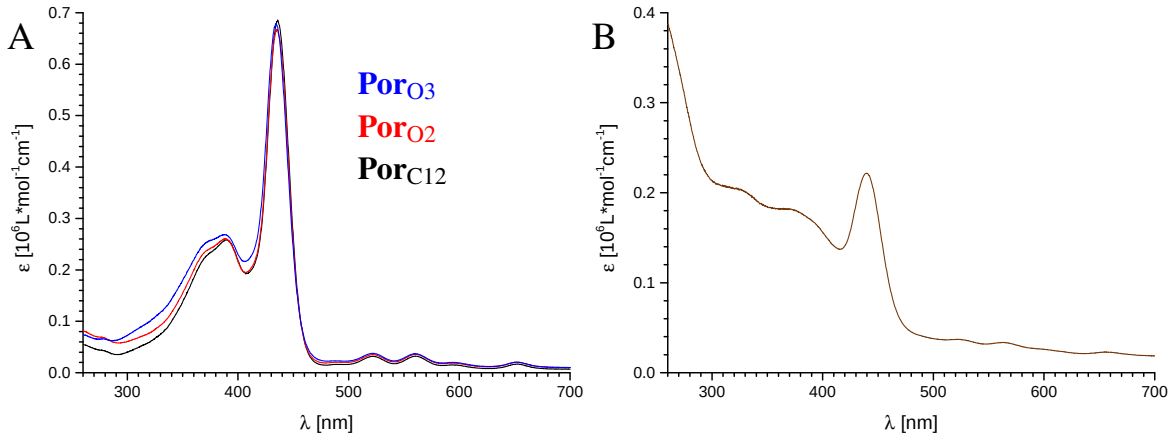

Figure 75: **A**: Absorption spectra for the porphyrin stars **Por**$_{C12}$ (black), **Por**$_{O2}$ (red) and **Por**$_{O3}$ (blue) in $CHCl_3$ solutions; B: Absorption spectra for the porphyrin-fullerene-stilbene dryad **Por**$_{O3}$**-F4**$_{C4}$

these can be regarded as independent chromophores.[24] NMR studies in the same solvent revealed that the fullerene attached to the shortest spacer (**S2**$_{C12}$**-F1**$_{C4}$) in time average is positioned around the peripheral units of the linked arm and not close to the center of the star mesogen. Hence, the excitation of the unsubstituted arms in the case of non-interconjugated arms would not be quenched by the fullerene acceptor and a rather strong emission would be expected for **S2**$_{C12}$**-F1**$_{C4}$. As the opposite is given, a transfer between the stilbenoid arms is reasonable.

In general, the discussed dyads are subjected to decomposition in the long term. This is demonstrated by the peak of **S2**$_{C12}$**-F1**$_{C4}$ located at 327 nm in the absorption spectrum in figure 73A, which in fact can be associated with the presence of a by-product in the measured sample. Figure 73B shows the

absorption spectra for an aged and a freshly synthesized sample* of **S2**$_{C12}$-**F1**$_{C4}$ and clearly demonstrates the lack of the maximum for the fresh sample. Numerous articles have reported solar cells with mixtures of poly (*p*-phenylene vinylene) and fullerene derivatives. In the sense of chemical decomposition, no stability issues have been reported for such systems.[10,244,245] However, one study suggests that C_{60} as well as functionalized fullerenes undergo photoinduced [2+2] cycloadditions with stilbene double bonds when irradiated with a sodium lamp.[246] Since these experiments were conducted for intermolecular reactions, it is reasonable to assume that this kind of cyclization will take place easily in an intramolecular case, when the corresponding spatial conditions are met. For **S2**$_{C12}$-**F1**$_{C4}$ and **S2**$_{C12}$-**F3**$_{C4}$, the small length of the spacer does not allow the fullerenes and the conjugated arms to be separated over a long distance. Hence, [2+2] cycloadditions may be responsible for the decomposition of the dyad **S2**$_{C12}$-**F1**$_{C4}$. Additionally, intermolecular reactions are facilitated in neat material.
For the porphyrin stars **Por**$_{C12}$, **Por**$_{O2}$ and **Por**$_{O3}$, the absorption spectra in chloroform solutions are displayed in figure 75A. At 436 nm, a strong Soret band is observed accompanied by a set of four weak Q bands at 523, 560, 596, and 653 nm, typical for free base porphyrins.[247] Transitions affiliated with the stilbene units are observed at 390 nm. Similar results have been obtained for porphyrin stilbene compounds with additional lateral alkoxy chains.[134,135]
The absorption spectrum for the porphyrin-fullerene-stilbene triad **Por**$_{O3}$-**F4**$_{C4}$ is illustrated in figure 75B. Here, the influence of the four attached fullerene units is visible in the high frequency range of the spectrum, similar to the star **S2**$_{C12}$-**F3**$_{C4}$. Note that the sample did not completely dissolve when performing the absorption tests, contrary to freshly prepared material. Accordingly, the value of the molar extinction coefficient for the Soret band located at 436 nm is lower than anticipated. Presumably, this substance also is affected by intramolecular and intermolecular reactions. Apparently, the decomposition leads to products which lack solubility in all tested solvents.

6.3 Cyclovoltametric measurements

Compound **S2**$_{O3}$-**F1**$_{C4}$ has been examined towards its electrochemical behavior to gain an understanding of the redox processes in these stilbene-fullerene dyad structures. The corresponding cyclic voltammograms are highlighted in figure 76. The scan in figure 76A reveals that a single oxidation process with the maximum located at 1.68 V can be observed in the given scan range, which corresponds to the removal of an electron from the *p*-phenylene vinylene moiety HOMO. The subsequent reduction scan from 2.0 V to 0.0 V lacks the corresponding reduction peak of the oxidized conjugated moiety, speaking for a highly irreversible process of oxidation. The scan towards negative voltage values displayed in figure 76B reveal three reduction peaks with their maxima located at -0.68 V, -1.15 V and -1.66 V. Note that for fulleropyrrolidines, so far only 5 out of 6 possible peaks have been observed in the possible energy range as the potentials are shifted towards negative values compared to neat C_{60}.[248] The shape of the line representing the subsequent reoxidation reveal that the intensities of the oxidation processes are strongly degraded compared to the reduction peaks. Hence, the major part of redox chemistry for **S2**$_{O3}$-**F1**$_{C4}$ is irreversible. Merely the uptake and subsequent release of the first electron appear reversible at first glance. For confirmation, a multi thin layer experiment has been performed, which is composed of a high repetition of redox cycles for the material being confined

*The fresh sample was thankfully synthesized by Moritz Dechant and Nikolai Scheuring.

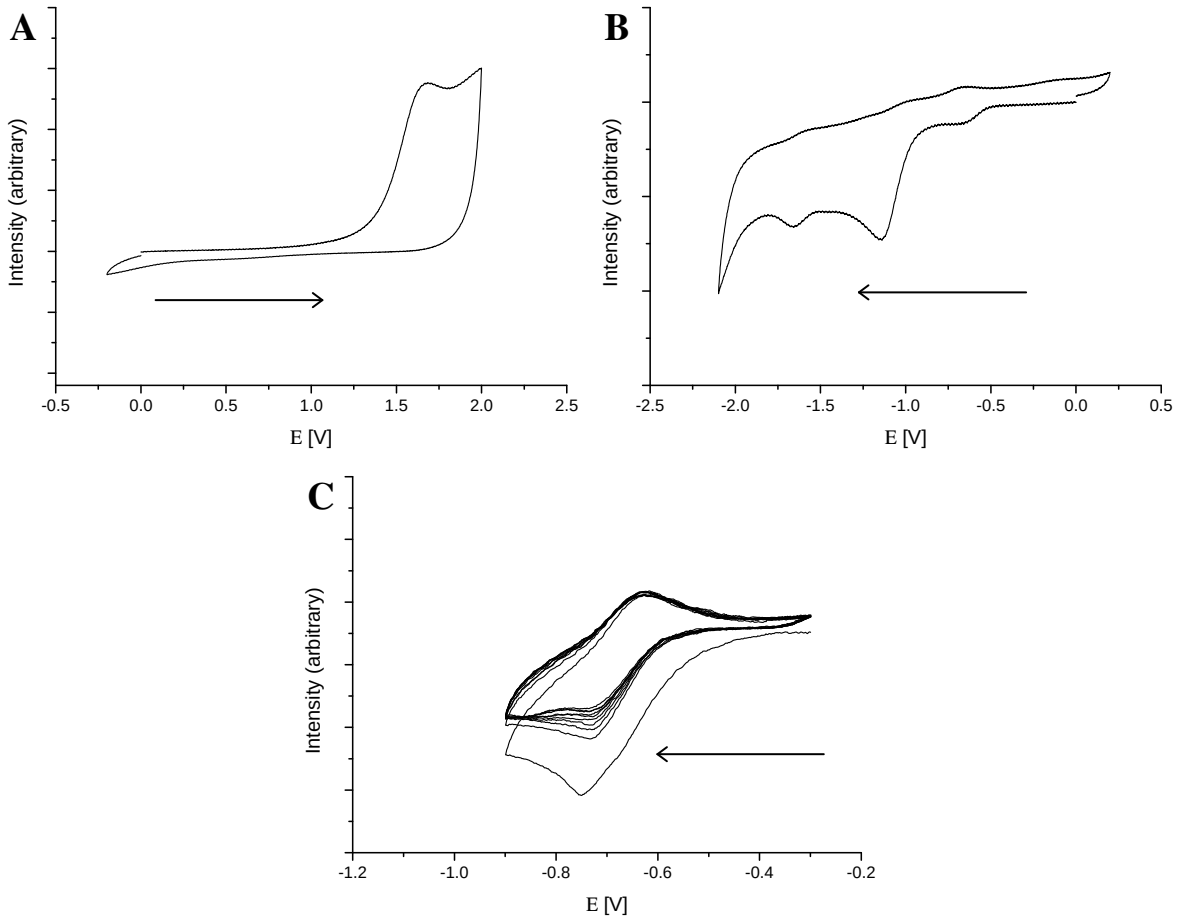

Figure 76: Cyclic voltammograms obtained for $\mathbf{S2}_{O3}$-$\mathbf{F1}_{C4}$. **A**: Oxidation processes scanned at 1000 mV s^{-1} **B**: Reduction processes scanned at 1000 mV s^{-1} **C**: Multi thin layer experiment for the first reduction process scanned at 50 mV s^{-1}. The direction of scan is indicated by the arrows.

within the thin layer of a corresponding cell. Hence, the measured current is not limited by diffusion and represents the behavior of the entire amount of the present material.[249] Figure 76C illustrates that the intensities of the signals slightly decline with each redox cycle. Therefore, the process is accompanied by slow decomposition of the compound. To conclude, all electrochemical processes occur in an irreversible manner, suggesting that further structural modifications are necessary to make this material suitable for applications in organic electronics.

7 Summary

The aim of this work was the establishment of a defined morphology for star-shaped liquid crystals, in which the nanostructures involve the separation of donor and acceptor moieties. At first, it was essential to understand the packing of the target stilbene stars with the intrinsic void between their oligomeric arms. Then, fullerene guests incorporated into this free space should clarify, how the spherical building blocks arrange in the presence of the star scaffolds. The obtained dyads or triads (porphyrin core) ideally would show a high order within the LC phase and a low clearing temperature to facilitate alignment processes. The structures of the target compounds are summarized in figure 77. Several features of these nonconventional mesogens have been varied, such as the nature of the core, the number of repeating units of the stilbenoid arms, the nature of the peripheral chains, which are responsible for the facilitation of the liquid-crystalline state, and the incorporation of various fullerene guests via a flexible spacer.

The syntheses were performed based on the formation of stilbenoid double bonds via Wittig-Horner reaction, which is known for its high *E*-selectivity. Hence, the prepared oligo(phenylenevinylene) arms have been coupled with the corresponding cores to obtain three- or four-armed stars. For the introduction of fullerenes, arms functionalized with an allyl ether group were used. After the formation of the star scaffold, this group was deprotected and coupled via Steglich esterification with various carboxylic acids. These consist of linear aliphatics with terminal acid groups and fulleropyrrolidine units on the opposite side, which were introduced by Prato reactions. In the case of the shown cyclopenteno fullerenes, the corresponding precursors did not bear an aliphatic chain. The hydroxy group of the arm here had to be hydroxyethylated prior to the esterification. The synthesis of the non-C_3-symmetric stars (arm X $\neq$ arm Y) was highly demanding since the utilized asymmetric core had to be functionalized successively. When the non-functionalized stilbenoid arms were attached, the cyano protecting group of the core was converted to a phosphonate group to allow the subsequent attachment of the allyl ether functionalized arm. Eventually, all stilbenoid stars, dyads and triads were synthesized successfully.

The thermotropic properties of the target compounds are summarized in table 11 and have been investigated by means of polarized optical microscopy studies, X-ray investigations, modelling and simulation of fiber X-ray studies. For the stilbenoid stars with dodecyl chains (**Sn**$_{C12}$), it is evident that columnar phases are formed regardless of the size of the void between the arms. The phase stability rises with increasing arm lengths. A dense packing here is realized by translational and rotational displacement of the helically assembled mesogens from the center of the column and by torsional deformation of the star morphology (see figure 78A).

When fullerenes are attached to these mesogens, they fill the space in the voids and therefore mitigate the deformation and displacement processes of the stilbenoid scaffolds. By forming a triple helix as depicted in figure 78B, the fullerenes are nanosegregated alongside the columns and cause an increase in the phase stability. For other shape-amphiphiles presented in literature such as fullerenes coupled with discotic mesogens, analogous segregations rather led to a decrease in the stability, emphasizing the distinctiveness of the presented assembly. The nature of the helical arrangement is confirmed by the almost identical results for the 2 : 1 mixture of **S2**$_{C12}$ and **S2**$_{C12}$**-F3**$_{C4}$ (**Mix_S**) compared with **S2**$_{C12}$**-F1**$_{C4}$. The cyclopenteno fullerene derivatives **S2**$_{C12}$**-F**$_{rac.}$ and **S2**$_{C12}$**-F**$_{enan.}$ surprisingly

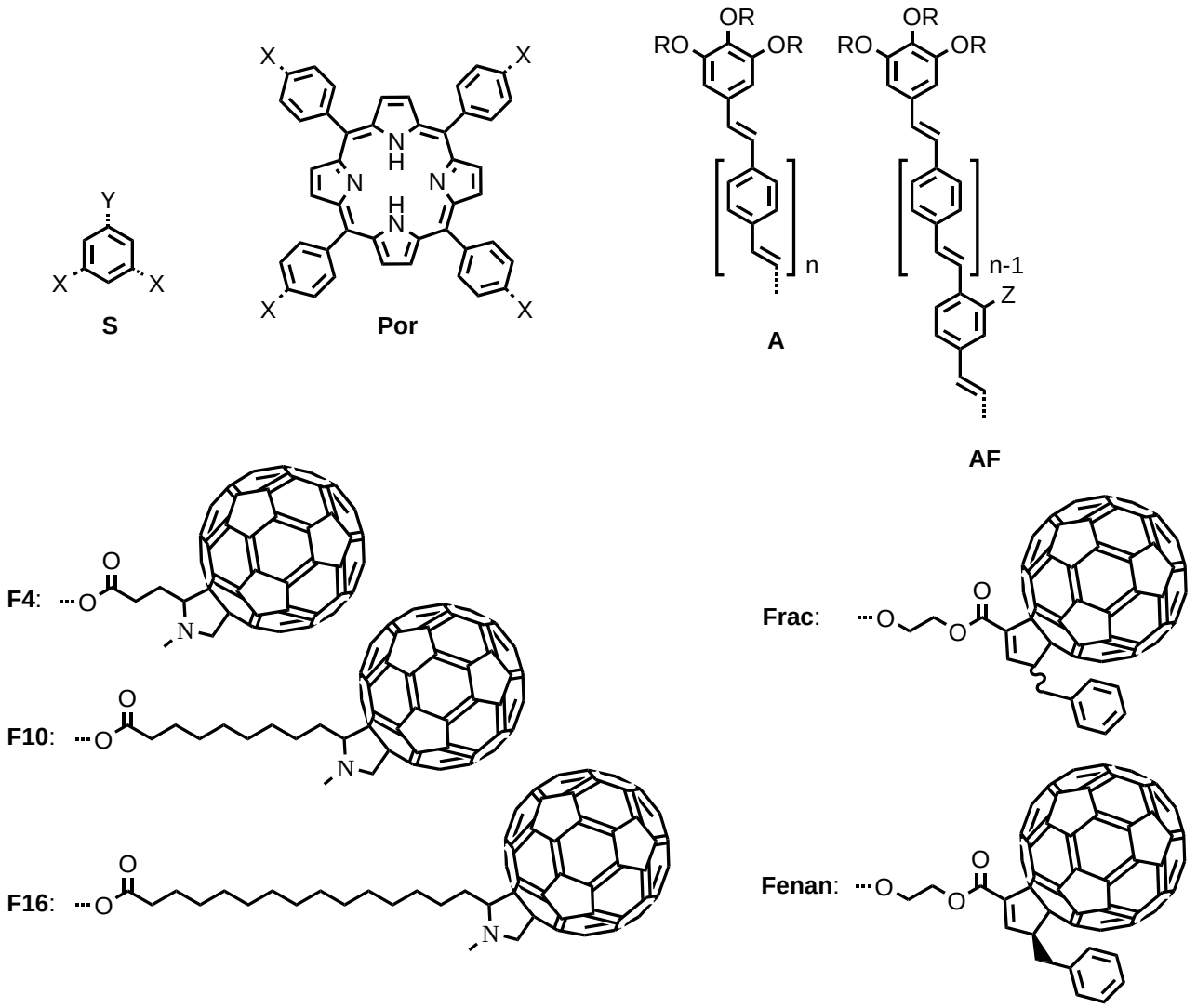

Compound	Core	Arm X	Arm Y	n	Z	R
S1$_{C12}$	S	A	A	1	–	$C_{12}H_{25}$
S2$_{C12}$	S	A	A	2	–	$C_{12}H_{25}$
S3$_{C12}$	S	A	A	3	–	$C_{12}H_{25}$
S2$_{O2}$	S	A	A	2	–	$(C_2H_4O)_2CH_3$
S2$_{O3}$	S	A	A	2	–	$(C_2H_4O)_3C_2H_5$
S1$_{C12}$**-F1**$_{C4}$	S	A	AF	1	F4	$C_{12}H_{25}$
S2$_{C12}$**-F1**$_{C4}$	S	A	AF	2	F4	$C_{12}H_{25}$
S2$_{C12}$**-F3**$_{C4}$	S	AF	AF	2	F4	$C_{12}H_{25}$
S2$_{C12}$**-F1**$_{C10}$	S	A	AF	2	F10	$C_{12}H_{25}$
S2$_{C12}$**-F1**$_{C16}$	S	A	AF	2	F16	$C_{12}H_{25}$
S2$_{O3}$**-F1**$_{C4}$	S	A	AF	2	F4	$(C_2H_4O)_2C_2H_5$
S2$_{C12}$**-F**$_{rac.}$	S	A	AF	2	Frac	$C_{12}H_{25}$
S2$_{C12}$**-F**$_{enan.}$	S	A	AF	2	Fenan	$C_{12}H_{25}$
Por$_{C12}$	Por	A	–	2	–	$C_{12}H_{25}$
Por$_{O2}$	Por	A	–	2	–	$(C_2H_4O)_2CH_3$
Por$_{O3}$	Por	A	–	2	–	$(C_2H_4O)_3C_2H_5$
Por$_{O3}$**-F4**$_{C4}$	Por	AF	–	2	F4	$(C_2H_4O)_3C_2H_5$

Figure 77: Overview of the star compounds presented in this work.

revealed an amorphous state at room temperature. The attached benzyl groups presumably demand too much space to allow the fullerenes to nanosegregate.

The assemblies of the fulleropyrrolidine stilbene dyads (**S2**$_{C12}$-**F1**$_{Cm}$) are strongly influenced by the length m of the linker between the star scaffold and the fullerene. Elongation allows for the spherical building blocks to intersect with the triple helices of the fullerenes of the neighboring columns. Hence, a three-dimensional LC network of fullerenes is obtained, giving body-centered orthorhombic cells (see figure 78C+D). In this supramolecular structure, a high order is combined with the nanosegregation of the donor and acceptor moieties. Furthermore, the additional methylene units in the spacer entropically decrease the high LC phase stability and thus the clearing temperature.

Since thin-film alignment processes for organic electronics applications usually favor even lower isotropization temperatures (< 200 °C), further adaptions were made by altering the nature of the peripheral chains. For the stilbenoid compound **S2**$_{O3}$, the incorporation of oligo(ethyleneoxy) chains resulted in an extraordinary decrease of the clearing temperature whilst maintaining the hexagonal columnar LC phase. These oxygen-rich chains are known for such effects and furthermore are proposed to facilitate charge separation by large dielectric permittivity. In contrast, the triple helical assembly for the fullerene derivative **S2**$_{O3}$-**F1**$_{C4}$ surprisingly was lost. Rather, an amorphous state is obtained for reasons which could not be identified.

Similar effects had been observed for the corresponding porphyrin stars with four arms. Here, the dodecyl chain derivative **Por**$_{C12}$ forms a hexagonal columnar phase, which clears at 328 °C. The corresponding model of this phase is displayed in figure 78E. When the oligo(ethyleneoxy) chains are introduced, the LC phase formation behavior is lost and also cannot be induced by mixing the stilbenoid porphyrin stars with fullerene bearing porphyrins analogous to the mixture **Mix_S**. Hence, the clearing temperature of the discussed LC dyads and triads could not be decreased below 200 °C, which is critical to obtain aligned thin films and therefore to fabricate organic electronic devices.

Optical properties of these systems were investigated by NMR studies and UV-Vis absorption as well as emission spectroscopy. While the absorption spectra for the stilbene fullerene dyads in chloroform are almost identical and simply are composed of the superposition of the signals for the different chromophores, the intensities of the corresponding signals in the emission studies in solution strongly vary with the length of the respective attached spacers. For the shortest spacer derivative **S2**$_{C12}$-**F1**$_{C4}$, the fluorescence quenching is most efficient and at first glance naturally explained by the distance dependence of the nonradiative transfer mechanisms. However, NMR studies revealed that the fullerene in time average is positioned only at the arm to which it is attached. Hence, it is feasible that energy transfers between the different stilbenoid arms of one mesogen occur to obtain the absolute low emission values in this special case. Fluorescence was totally diminished in thin-film experiments of these dyads no matter the length of the spacer, demonstrating efficient charge transfer. In the LC state, the fullerenes are always in the vicinity of stilbenoid chromophores owing to the nanostructure.

To conclude, promising supramolecular structures have been obtained, which involve the nanosegregation of the donor and acceptor motifs. The separation of these scaffolds is controlled by the flexible spacer and the void between the rigid arms. In the LC state, the assemblies allow for an efficient charge transfer between these scaffolds, paving the way for new photovoltaic LC based materials.

Table 11: Summary of the thermotropic properties of the presented stars.

Compound	Transition temp. onset [°C]	ΔH [kJ·mol^{-1}]
S1$_{C12}$	Col$_h$ 108 I[133]	4[133]
S2$_{C12}$	Col$_h$ 205.5 I	2.4
S3$_{C12}$	Col$_1$ 171.7 Col$_2$ 303.5	6.6; 4.4
S2$_{O2}$	undet. (lamellar)	–
S2$_{O3}$	Col$_h$ 92.4 I	1.1
S1$_{C12}$**-F1**$_{C4}$	Col 156.0† I	–
S2$_{C12}$**-F1**$_{C4}$	Col$_h$ 280.6 I	2.9
S2$_{C12}$**-F1**$_{C10}$	Col$_{borh}$ 239.6 I	8.7
S2$_{C12}$**-F1**$_{C16}$	Col$_{borh}$ 204.7 I	3.7
Mix_S (**S2**$_{C12}$:**S2**$_{C12}$**-F3**$_{C4}$ = 2:1)	Col$_h$ 275‡ I	–
S2$_{O3}$**-F1**$_{C4}$	amorph.	–
S2$_{C12}$**-F**$_{\textit{rac.}}$	amorph.	–
S2$_{C12}$**-F**$_{\textit{enan.}}$	amorph.	–
Por$_{C12}$	Col$_h$ 327.7 I	2.5
Por$_{O2}$	amorph.	–
Por$_{O3}$	amorph.	–
Mix_P (**Por**$_{O3}$:**Por**$_{O3}$**-F4**$_{C4}$ = 2:1)	amorph.	–

†: No peak could be observed in DSC measurements. The given transition temperature is based on the formation of a texture in the cooling process of POM experiments. ‡: The clearing temperature of the mix has been determined by the peak of the highly broadened signal in the DSC thermogram. The onset lies at 254 °C.

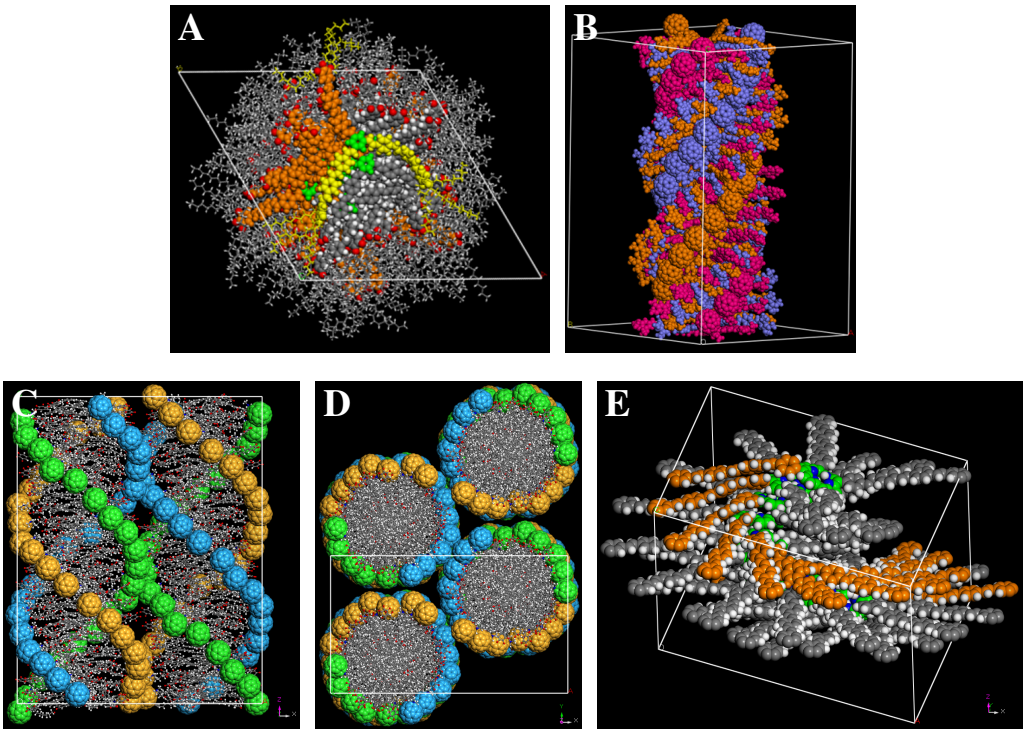

Figure 78: Examples of the models obtained for the star-shaped mesogens. **A**: Single helical arrangement for **S2**$_{C12}$; **B**: Triple helical arrangement for **S2**$_{C12}$**-F1**$_{C4}$; **C**: Side view of the 3D fullerene network for **S2**$_{C12}$**-F1**$_{C10}$; **D**: Top view; **E**: Single helical arrangement for **Por**$_{C12}$ with laterally displaced porphyrin cores.

8 Outlook

As has been summarized in the previous section, interesting helical structures have been obtained that show clearing temperatures too high for alignment procedures. Varying the number of stilbene repeating units, the spacer length or the nature of the peripheral chains so far did not give the ideal combination of an ordered structure and a low clearing temperature. New structural motifs therefore need to be established:

- Bigger macrocyclic π-systems such as phthalocyanines and hexabenzocoronenes as cores should show stronger segregation capabilities, which would allow the usage of the oligoether chains. A hexa-*peri*-hexabenzocoronene derivative with oligoether chains has already been reported to form a columnar phase with a clearing temperature of 150 °C.[250]
- Introducing both dodecyl and oligoether chains in a single molecule is reported to strengthen the tendency to form columnar arrangements since alternative assemblies such as cubic phases or amorphous materials would increase unfavorable interactions.[251]
- Even longer spacers with additional methylene units might further decrease the clearing temperature of the stilbene-fullerene dyads via entropic effects.

Besides these approaches, effort has been put into the replacement of fullerene as the standard electron acceptor.[119] A flat electron-deficient π-system would spawn new design possibilities for star-shaped donor acceptor materials. Yamaguchi *et al.* have synthesized a planarized triphenylborane derivative, which is depicted in figure 79A. This material shows ambipolar charge carrier transport properties and forms a columnar phase at room temperature.[252] Another exceptional example is the nonmesomorphic tris-(triazolyl)triazine motiv shown in figure 79B. Here, the star-shaped acceptor faciliates hydrogen bonding with benzoic acids. The latter can be coupled with donors such as triphenylenes to obtain supermolecular donor-acceptor complexes, which form columnar LC phases.[253] So far, combining a high order with low clearing temperature for dyads with segregtated chromophores remains a sophisticated task.

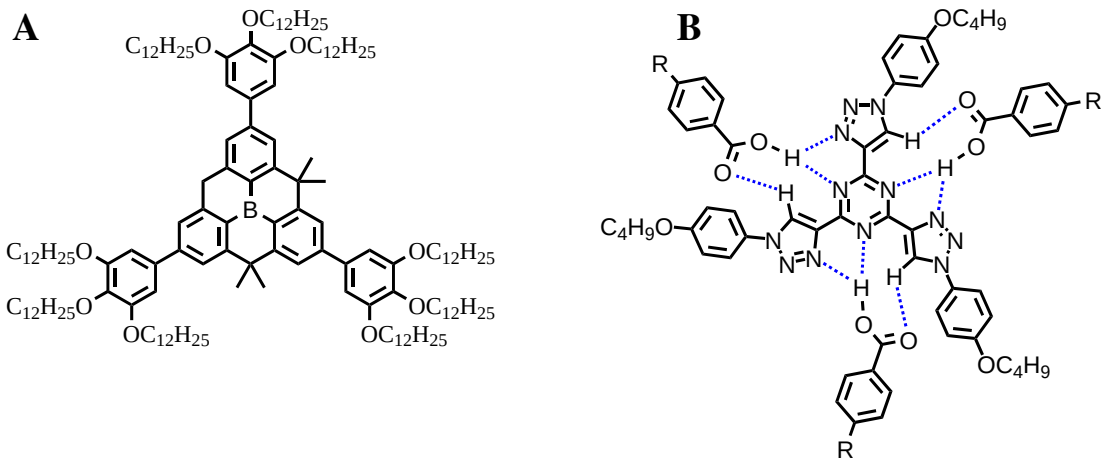

Figure 79: Promising replacements for fullerene as acceptor. **A**: Planarized triphenylborane mesogen introduced by Yamaguchi *et al.*; **B**: Tris-(triazolyl)triazine motif for hydrogen bonded donor-acceptor dyads presented by Sierra *et al.*

9 Zusammenfassung

Das Ziel dieser Arbeit war die Etablierung einer definierten Morphologie für sternförmige Flüssigkristalle, in der die Nanostrukturen die Separation von Donor- und Akzeptor-Bausteinen beinhalten. Zunächst war es wesentlich, die Packung der zum Ziel gesetzten Stilbensterne mit den intrinsischen Hohlräumen zwischen ihren oligomeren Armen zu verstehen. Dann sollten in diese freien Räume eingebrachte Fullerengäste aufklären, wie sich die sphärischen Bausteine in Anwesenheit der Sterngerüste anordnen. Die erhaltenen Dyaden und Triaden (Porphyrinkern) weisen dann idealerweise eine hohe Ordnung innerhalb des flüssigkristallinen Zustands auf und besitzen eine niedrige Klärtemperatur, um Ausrichtungsprozesse zu ermöglichen. Die Strukturen der Zielverbindungen sind in Abbildung 80 zusammengefasst. Mehrere Bestandteile dieser nicht-konventionellen Mesogene wurden variiert, wie zum Beispiel die Art des Kerns, die Anzahl an Wiederholungseinheiten der stilbenoiden Arme, die Art der peripheren Ketten, die die Ausbildung der flüssigkristallinen Phase ermöglichen, und die Einbindung von diversen Fullerengästen mittels eines flexiblen Abstandshalters.
Die Synthesen wurden auf Basis der Herstellung von stilbenoiden Doppelbindungen via Wittig-Horner-Reaktion durchgeführt. Diese ist für ihre hohe *E*-Selektivität bekannt. So konnten die hergestellten Oligo(phenylenvinylen)-Arme mit den entsprechenden Kernen verknüpft werden, um drei- bzw. vierarmige Sterne zu erhalten. Zur Einführung von Fullerenen wurden mit einer Allylethergruppe ausgestattete Arme genutzt. Nach Darstellung des Sterngerüsts konnte diese Gruppe entschützt und via Steglich-Veresterung mit diversen Carbonsäuren verknüpft werden. Diese bestehen aus linearen Aliphaten mit endständigen Säuregruppen und Fulleropyrrolidin-Einheiten auf der gegenüberliegenden Seite. Letztere wurden mittels Prato-Reaktion herbeigeführt. Bei den gezeigten Cyclopenten-Fullerenen lagen bei den entsprechenden Vorstufen keine aliphatischen Ketten vor. Daher wurden in diesem Fall die Hydroxygruppen der Arme vor dem Veresterungsschritt hydroxyethyliert. Die Synthese der nicht-C_3-symmetrischen Sterne (Arm X $\neq$ Arm Y) stellte eine große Herausforderung dar, da die verwendeten asymmetrischen Kerne nacheinanderfolgend funktionalisiert werden mussten. Als die nichtfunktionalisierten stilbenoiden Arme angebracht wurden, wurde die Cyano-Schutzgruppe des Kerns zu einer Phosphonatgruppe umgewandelt, um die folgende Anbringung des mit einer Allylethergruppe ausgestatteten Arms zu ermöglichen. Letzen Endes konnten alle stilbenoiden Sterne, Dyaden und Triaden erfolgreich synthetisiert werden.
Die thermotropen Eigenschaften der Zielverbindungen sind in Tabelle 12 zusammengefasst und wurden mittels Polarisationsmikroskopie, Röntgenuntersuchungen, Modellierung sowie Simulation von Röntgenfaserstudien untersucht. Für die stilbenoiden Sterne mit Dodecylketten ($\mathbf{Sn}_{C12}$) ist ersichtlich, dass unabhängig von der Größe der Hohlräume zwischen den Armen kolumnare Phasen gebildet werden. Die Phasenstabilität nimmt mit wachsender Armlänge zu. Eine dichte Packung wird hier durch translationale und rotationale Verrückung der helikal angeordneten Mesogene von dem Zentrum der Kolumne sowie torsionale Deformation der Sternmorphologie erreicht (siehe Abbildung 81A).
Wenn Fullerene an den Mesogenen angebracht sind, füllen diese den Hohlraum und reduzieren daher die Deformations- und Verrückungsprozesse der stilbenoiden Gerüste. Durch die Bildung einer Tripelhelix, wie sie in Abbildung 81B dargestellt ist, sind die Fullerene entlang der Kolumnen nanosegregiert und die Phasenstabilität ist erhöht. Für andere in der Literatur vorgestellte Form-Amphiphile wie etwa mit Fullerenen verknüpfte Diskoten führen analoge Segregationen eher zu einer Abschwächung

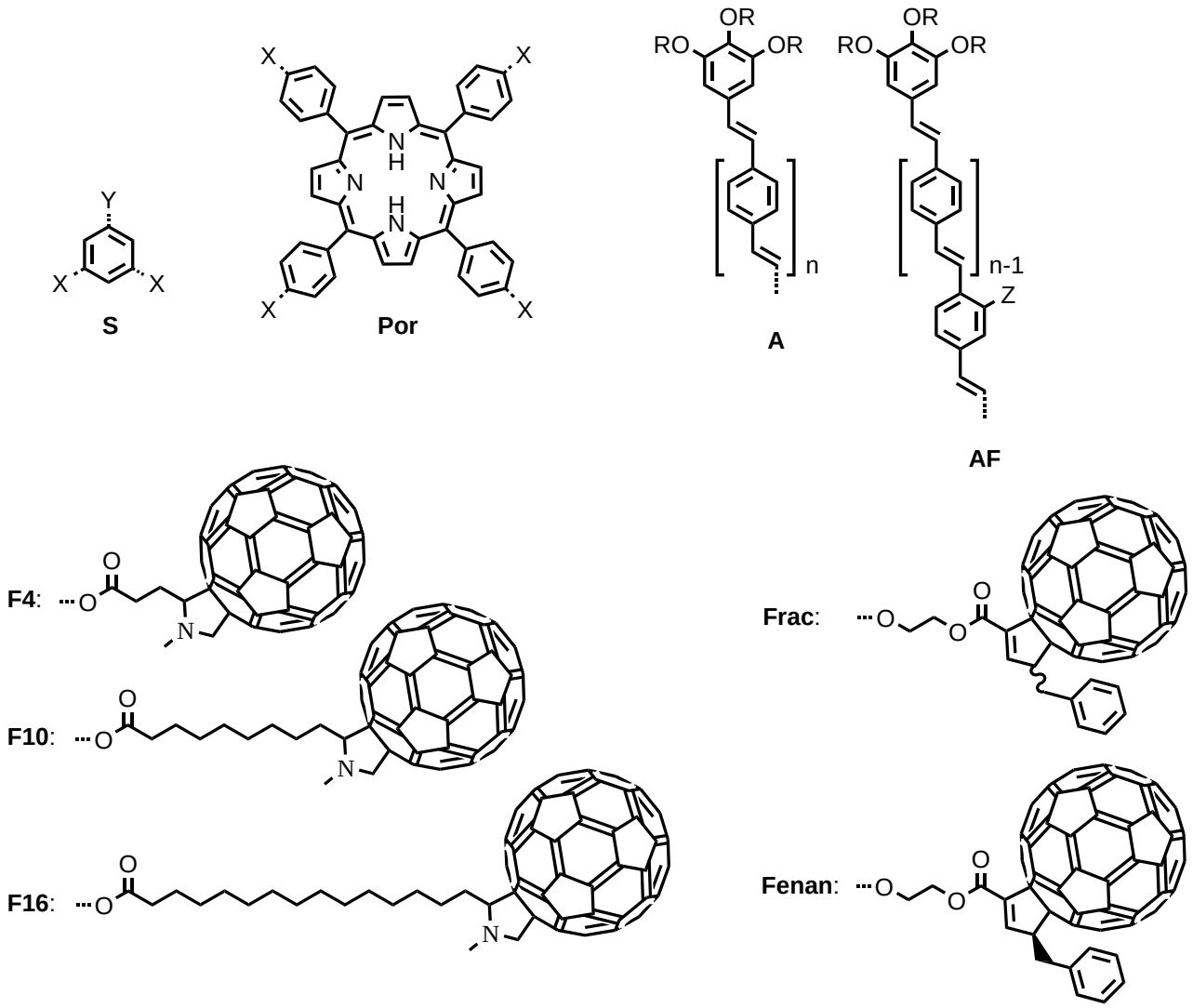

Verbindung	Kern	Arm X	Arm Y	n	Z	R
S1$_{C12}$	S	A	A	1	–	$C_{12}H_{25}$
S2$_{C12}$	S	A	A	2	–	$C_{12}H_{25}$
S3$_{C12}$	S	A	A	3	–	$C_{12}H_{25}$
S2$_{O2}$	S	A	A	2	–	$(C_2H_4O)_2CH_3$
S2$_{O3}$	S	A	A	2	–	$(C_2H_4O)_3C_2H_5$
S1$_{C12}$**-F1**$_{C4}$	S	A	AF	1	F4	$C_{12}H_{25}$
S2$_{C12}$**-F1**$_{C4}$	S	A	AF	2	F4	$C_{12}H_{25}$
S2$_{C12}$**-F3**$_{C4}$	S	AF	AF	2	F4	$C_{12}H_{25}$
S2$_{C12}$**-F1**$_{C10}$	S	A	AF	2	F10	$C_{12}H_{25}$
S2$_{C12}$**-F1**$_{C16}$	S	A	AF	2	F16	$C_{12}H_{25}$
S2$_{O3}$**-F1**$_{C4}$	S	A	AF	2	F4	$(C_2H_4O)_2C_2H_5$
S2$_{C12}$**-F**$_{rac.}$	S	A	AF	2	Frac	$C_{12}H_{25}$
S2$_{C12}$**-F**$_{enan.}$	S	A	AF	2	Fenan	$C_{12}H_{25}$
Por$_{C12}$	Por	A	–	2	–	$C_{12}H_{25}$
Por$_{O2}$	Por	A	–	2	–	$(C_2H_4O)_2CH_3$
Por$_{O3}$	Por	A	–	2	–	$(C_2H_4O)_3C_2H_5$
Por$_{O3}$**-F4**$_{C4}$	Por	AF	–	2	F4	$(C_2H_4O)_3C_2H_5$

Abbildung 80: Übersicht der in diesem Werk vorgestellten Sternverbindungen.

der Phasenstabilität, was die Besonderheit der hier vorgestellten Anordnung betont. Die Art der helikalen Ordnung wird durch die nahezu identischen Ergebnisse für die 2 : 1 Mischung von **S2**$_{C12}$ und **S2**$_{C12}$**-F3**$_{C4}$ (**Mix_S**) verglichen mit **S2**$_{C12}$**-F1**$_{C4}$ bestätigt. Die Cyclopenten-Fullerenderivate **S2**$_{C12}$**-F**$_{rac.}$ und **S2**$_{C12}$**-F**$_{enan.}$ zeigen bei Raumtemperatur überraschenderweise ein amorphes Verhalten. Die hier angebrachten Benzylgruppen nehmen vermutlich zu viel Platz ein, um den Fullerenen Nanosegregation zu gewähren.

Die Anordnungen der Fulleropyrrolidin-Stilben-Dyaden (**S2**$_{C12}$-**F1**$_{Cm}$) werden stark durch die Länge m der Abstandshalter zwischen dem Sterngerüst und den Fullerenen beeinflusst. Eine Verlängerung ermöglicht den sphärischen Bausteinen mit den Tripelhelices der Fullerene der benachbarten Kolumnen zusammenzulaufen. Somit wird ein dreidimensionales LC-Netzwerk von Fullerenen erhalten, was die Bildung von raumzentrierten orthorhombischen Zellen bedingt (siehe Abbildung 81C+D). In dieser supramolekularen Struktur wird eine hohe Ordnung mit der Nanosegregation der Donor- und Akzeptor-Einheiten kombiniert. Weiterhin sorgen die zusätzlichen Methyleneinheiten im Abstandshalter für eine entropische Abnahme der hohen LC-Phasenstabilität und somit der Klärtemperatur.

Da Ausrichtungsprozesse von Dünnfilmen im Anwendungsbereich organische Elektronik üblicherweise noch niedrigere Klärtemperaturen bevorzugen (< 200 °C), wurden noch weitere Anpassungen vorgenommen, indem die Art der peripheren Ketten geändert wurde. Für die stilbenoide Verbindung **S2**$_{O3}$ führte der Einbau von Oligo(ethylenoxy)-Ketten zu einer außergewöhnlichen Abschwächung der Klärtemperatur, während die hexagonal kolumnare Phase erhalten blieb. Diese sauerstoffreichen Ketten sind für solche Effekte bekannt und sollen weiterhin die Ladungsseparation durch eine große Dielektrizitätskonstante begünstigen. Im Gegensatz dazu ist überraschenderweise die tripelhelikale Anordnung für die entsprechende Fulleren-Verbindung **S2**$_{O3}$**-F1**$_{C4}$ verloren gegangen. Es wurde vielmehr ein amorpher Zustand erhalten, dessen Bildungsgründe nicht identifiziert werden konnten.

Ähnliche Effekte wurden für die entsprechenden Porphyrinsterne mit vier Armen beobachtet. Das Dodecyl-Derivat **Por**$_{C12}$ bildet eine hexagonal kolumnare Phase aus, die bei 328 °C klärt. Das entsprechende Modell dieser Phase ist in Abbildung 81E dargestellt. Wenn stattdessen Oligo(ethylenoxy)-Ketten verwendet werden, geht das LC-Phasenbildungsverhalten verloren und kann auch nicht durch das Mischen von stilbenoiden Porphyrinen mit fullerenhaltigen Porphyrinen analog der Mischung **Mix_S** erreicht werden. Letztendlich konnte für die diskutierten flüssigkristallinen Dyaden und Triaden die Klärtemperatur nicht auf unter 200 °C erniedrigt werden, was für das Erhalten von orientierten Dünnfilmen und somit für die Herstellung von organischen Elektronikbauteilen kritisch ist.

Optische Eigenschaften dieser Syteme wurden mittels NMR-Studien und UV-Vis- sowie Emissionsspektroskopie untersucht. Während die Absorptionsspektren für die Stilben-Fulleren-Dyaden in Chloroform nahezu identisch sind und letztlich nur aus einer Überlagerung der Signale der einzelnen Chromophore bestehen, variieren die Intensitäten der entsprechenden Signale in den Emissionsmessungen in Lösung stark mit der Länge der jeweiligen angegliederten Abstandshalter. Für das Derivat **S2**$_{C12}$**-F1**$_{C4}$ mit kürzestem Abstandshalter ist die Fluoreszenzlöschung am effizientesten, was zunächst leicht mit der Abstandsabhängigkeit der strahlungsfreien Übertragungsmechanismen erklärt werden kann. NMR-Messungen zufolge befindet sich das Fulleren jedoch im zeitlichen Schnitt nur an dem Arm, an den es gebunden ist. Folglich ist es für diesen speziellen Fall denkbar, dass die absolut niedrigen Emissionswerte durch Energietransfers zwischen den unterschiedlichen stilbenoiden Armen eines Meso-

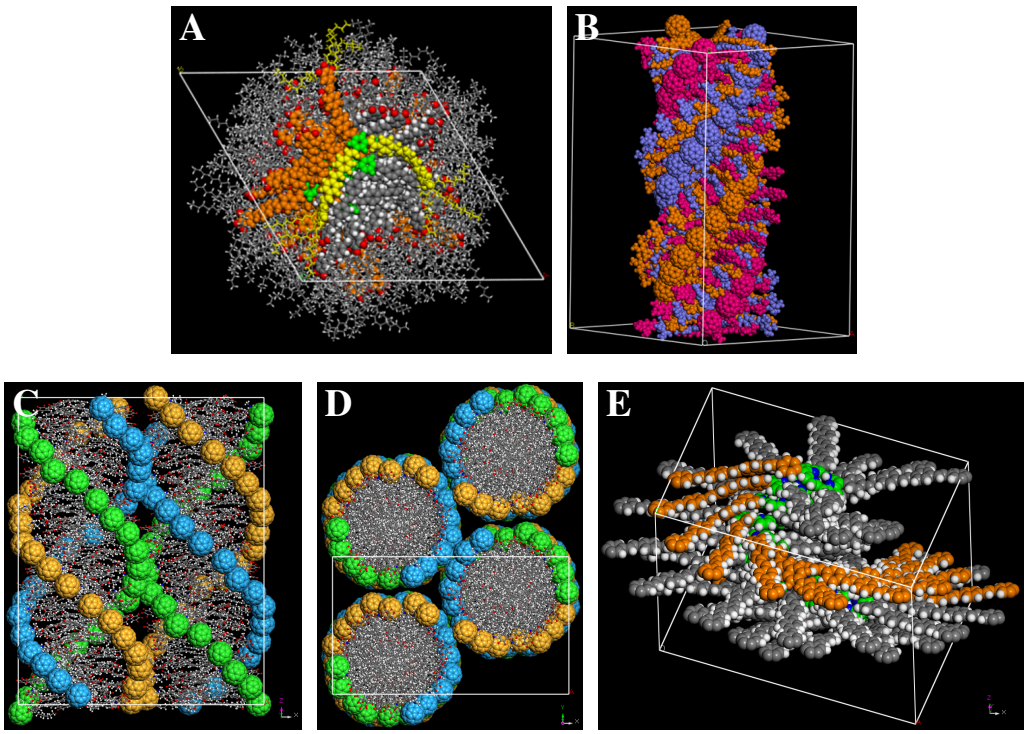

Abbildung 81: Beispiele der erhaltenen Modelle für die sternförmigen Mesogene. **A**: Einfach helikale Anordnung für **S2**$_{C12}$; **B**: Tripel helikale Anordnung für **S2**$_{C12}$-**F1**$_{C4}$; **C**: Seitenansicht der dreidimensionalen Fulleren-Netzwerke für **S2**$_{C12}$-**F1**$_{C10}$; **D**: Draufsicht; **E**: Einfach helikale Anordnung für **Por**$_{C12}$ mit seitlich versetzten Porphyrinkernen.

Tabelle 12: Zusammenfassung der thermotropen Eigenschaften der vorgestellten Sterne.

Verbindung	Übergangstemp. Eintritt [°C]	ΔH [kJ·mol^{-1}]
S1$_{C12}$	Col$_h$ 108 I[133]	4[133]
S2$_{C12}$	Col$_h$ 205.5 I	2.4
S3$_{C12}$	Col$_1$ 171.7 Col$_2$ 303.5	6.6; 4.4
S2$_{O2}$	unbest. (lamellar)	–
S2$_{O3}$	Col$_h$ 92.4 I	1.1
S1$_{C12}$-**F1**$_{C4}$	Col 156.0† I	–
S2$_{C12}$-**F1**$_{C4}$	Col$_h$ 280.6 I	2.9
S2$_{C12}$-**F1**$_{C10}$	Col$_{borh}$ 239.6 I	8.7
S2$_{C12}$-**F1**$_{C16}$	Col$_{borh}$ 204.7 I	3.7
Mix_S (**S2**$_{C12}$:**S2**$_{C12}$-**F3**$_{C4}$ = 2:1)	Col$_h$ 275‡ I	–
S2$_{O3}$-**F1**$_{C4}$	amorph	–
S2$_{C12}$-**F**$_{rac.}$	amorph	–
S2$_{C12}$-**F**$_{enan.}$	amorph	–
Por$_{C12}$	Col$_h$ 327.7 I	2.5
Por$_{O2}$	amorph	–
Por$_{O3}$	amorph	–
Mix_P (**Por**$_{O3}$:**Por**$_{O3}$-**F4**$_{C4}$ = 2:1)	amorph	–

†: In DSC-Messungen wurde kein Signal erhalten. Die angegebene Übergangstemperatur basiert auf der Texturbildung im Kühlprozess von POM-Experimenten. ‡: Die angegebene Klärtemperatur der Mischung wurde anhand des Maximums des stark verbreiterten Signals des DSC-Theromgramms ermittelt. Der Übergangseintritt liegt bei 254 °C.

gens zustande kommen. Die Fluoreszenz wurde in Dünnfilmexperimenten dieser Dyaden unabhängig von der Länge der Abstandshalter vollständig gelöscht. Im flüssigkristallinen Zustand befinden sich die Fullerene Dank der Nanostruktur immer in der Nähe von stilbenoiden Chromophoren.
Zusammengefasst wurden vielversprechende supramolekulare Strukturen erhalten, welche die Nanosegregation der Donor- und Akzeptor-Einheiten beinhalten. Die Separation dieser Bausteine wird durch die flexiblen Abstandshalter und durch die Hohlräume der rigiden Arme kontrolliert. Im flüssigkristallinen Zustand ermöglichen die Anordnungen einen effizienten Ladungstransfer zwischen diesen Blöcken, was den Weg für neue flüssigkristallbasierte Photovoltaik-Materialien ebnet.

10 Experimental

10.1 Materials

Following fine chemicals have been purchased (suppliers given in parentheses):

- 3,5-dimethylbenzonitrile* (Activate Scientific)
- methyl-10-oxodecanoate (TCI Europe)
- 16-hydroxyhexadecanoic acid (Alfa Aesar)
- fullerene C_{60} (IoLiTec Ionic Liquids Technologies GmbH or Solenne B.V.)
- (diethoxymethyl)benzaldehyde (Acros Organics)

Triethylene glycol monoethyl ether, technical grade was purified via following procedure: 100 g crude material was mixed with 300 ml toluene and washed with 15 ml distilled water three times. The organic solution was dried over Na_2SO_4 and evaporated under reduced pressure to yield 40.5 g of the desired compound, free of diethylene glycol according to NMR measurements.
$P(OEt)_3$ and pyrrole were freshly distilled under reduced pressure and all other commercial materials employed were used as received. Solvents were distilled and dried by standard procedures.[254] The solvents used for photophysical measurements had spectroscopy grade purity.

10.2 Equipment

- Thin layer chromatography analysis was performed with Merck silica gel (aluminum plates) coated with fluorescent indicator F254.
- Preparative recycling gel permeation chromatography was performed with the liquid chromatograph *LC-20A* (Shimadzu). The column set (PSS *SDV* 50 Å, $20 \cdot 600$ *mm*; PSS *SDV* 500 Å, $20 \cdot 600$ *mm*) was eluted with HPLC-grade $CHCl_3$ at a flow rate of 4.0 $mL \cdot min^{-1}$, if not stated otherwise.
- If not stated otherwise, NMR spectra were recorded on a Bruker-Daltonics *Avance-400* spectrometer operating at 400 MHz (^{1}H) or 100 MHz (^{13}C). Other measurements were carried out on a Bruker-Daltonics *AC-250* spectrometer operating at 250 MHz (^{1}H) or on a Bruker-Daltonics *Ascend-600* operating at 600 MHz (^{1}H) or 151 MHz (^{13}C). The residual protic solvent was used as the internal standard.[255] The assignment of the signals is backed by multiplicity selective experiments (DEPT) and by two-dimensional correlation spectra (COSY, HSQC, HMBC). Many double bond protons and other structures show AB patterns with second order effects. For the sake of simplicity, these are denoted as doublets.
- MALDI mass spectra were recorded on a Bruker-Daltonics *autflex II* and high resolution mass spectrometry was performed with a Bruker-Daltonics *ultrafleXtreme*. DCTB, which is widely

*3,5-Dimethylbenzonitrile is a strong skin irritant and should be handled with utmost care.

used for derivatives of fullerenes and other compounds, was used as matrix.[256,257] High resolution ESI measurements were performed with a Bruker-Daltonics *micrOTOF focus* and EI spectra were obtained with a Finnigan *MAT90*.

- Differential scanning calorimetry results were obtained by a TA Instruments *Q1000*. The interpretation was achieved with the corresponding software *Universal Analysis 2000*.

- Prior to elemental analysis, the materials were freeze dried via following procedure: The sample was dissolved in 1-2 ml of benzene and cooled with liquid nitrogen for 5 minutes. Then high vacuum was applied and the cooling bath was removed. After several hours, the neat sample was collected as low-density flakes.

- Elemental analysis experiments were performed either at the Institute of Inorganic Chemistry, University of Würzburg or at the Institute of Organic Chemistry, University of Mainz. Note that many fullerene containing compounds show values too low for the content of carbon. This is due to incomplete combustion, as has been demonstrated in several cases already.[258–261] To enhance the conversion, rather large amounts of V_2O_5 have been added. Consequently, trapped air and moisture then led to increased values for hydrogen and nitrogen in some cases. Similar effects have been observed for porphyrin based materials.[135,262,263]

- The studies of optical textures were realized with a Nikon Eclipse *LV100Pol* optical polarizing microscope equipped with a Linkam *LTS420* heating stage and a Linkam *T95-HS* system controller. Thin film fluorescence spectra were recorded on a StellarNet BLACK-Comet *CXR-100* spectrophotometer equipped with a Nikon Intensilight *C-HGFI* illuminator.

- UV-Vis absorption studies in solution were performed with a PerkinElmer *Lambda 35* or with a Jasco *V-770*. Emission studies in solution were realized with a PTI *QM-4/2003*.

- The temperature dependent SAXS, MAXS and WAXS X-ray investigations were performed on a Bruker Nanostar (Detector Vantec2000, Microfocus copper anode X-ray tube Incoatec). The samples were prepared by fiber extrusion using a custom made mini-extruder (see figure 82). The fiber axis then corresponds to the meridian of the diffraction pattern. The measurements were carried out in Mark capillaries (Hilgenberg) positioned perpendicular to the incident X-ray beam.

- The electrochemical measurements were performed with a Gamry Instruments *Reference 600* Potentiostat/Galvanostat/ZRA (v. 6.2.2, Warminster, PA, USA). The cyclic voltammograms were measured under an argon atmosphere in DCM with 0.2M tetrabutylammonium hexafluorophosphate as conducting salt. A conventional set-up was used consisting of a platinum disc working electrode (diam. = 1 mm), a Ag/AgCl *LEAK FREE* reference electrode (Warner Instruments, Hamden, CT, USA) and a platinum wire counter electrode. The measurement cell was dried in an oven and flushed with argon before use. Chemical and electrochemical reversibility of the redox processes were checked by measurements at different scan rates (from 50 to 5000 $mV\,s^{-1}$).

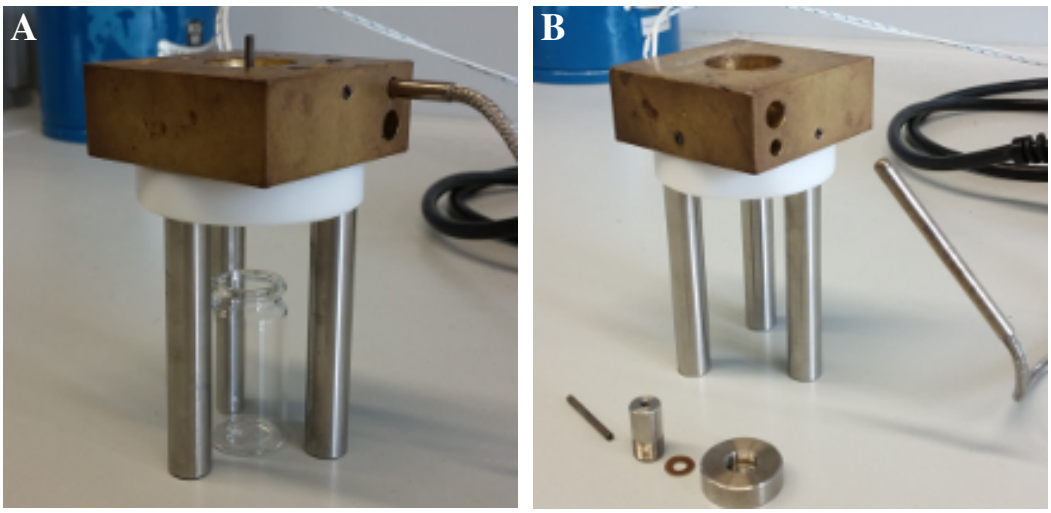

Figure 82: **A**: Functional mini-extruder; **B**: Single components for the extruder.

10.3 Synthesis of the core building blocks

Compound 5

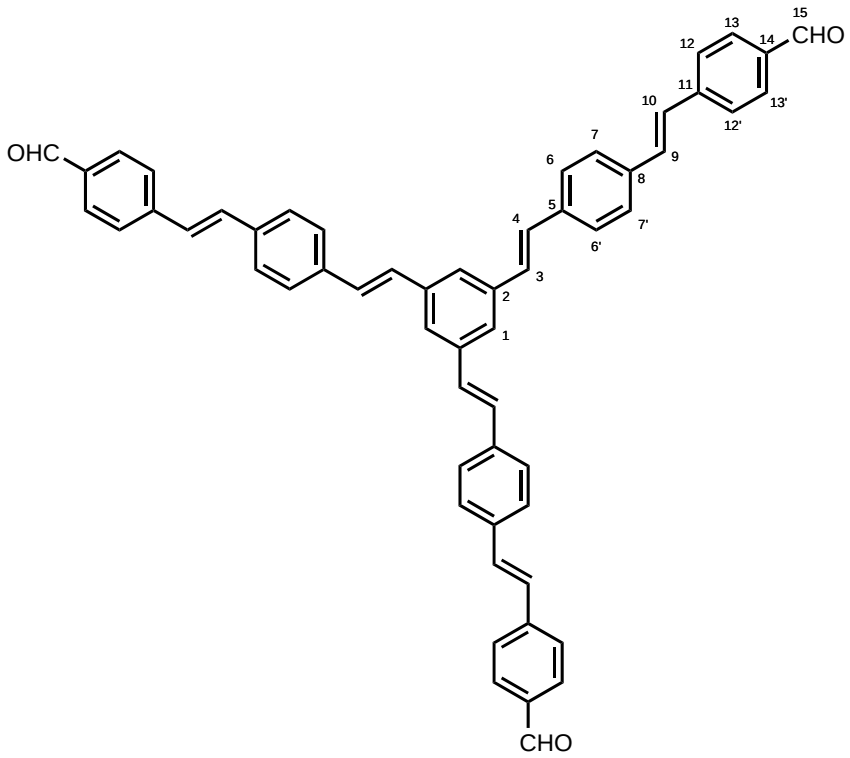

60.0 mg (535 µmol) potassium *tert*-butoxide was added in portions to a stirred solution of 50.0 mg (107 µmol) 1,3,5-tris(*p*-formylstyryl)benzene (**3**) and 138 mg (418 µmol) prolongation unit diethyl [4-(diethoxymethyl)benzyl]phosphonate (**4**) in 2 mL dry THF under nitrogen atmosphere. Stirring at room temperature was continued overnight. The reaction was then quenched with 2N HCl and extracted with chloroform eight times. The organic solution was dried over Na_2SO_4 and evaporated under reduced pressure. The residue was dissolved in 20 ml of chloroform and poured into 60 ml methanol. The precipitate was collected and dried in vacuo to yield 43.3 mg (55.9 µmol, 52%) of a yellow solid. ^{1}H NMR (DMSO-d_6): δ = 7.34 - 7.55 (m, 12 H; H-3 + H-4 + H-9 + H-10), 7.70 + 7.73 (AA'BB', ^3J = 8.66 Hz, 12 H; H-6 + H-6' + H-7 + H-7'), 7.81 (s, 3 H; H-1), 7.84 + 7.92 (AA'BB',

^3J = 8.16 Hz, 12 H; H-12 + H-12' + H-13 + H-13'), 10.0 (s, 3 H; H-15); MALDI-MS: m/z (%) calcd.: 774.31 ([M]$^{+\cdot}$,100), found: 774.38 ([M]$^{+\cdot}$,100).

Compound 8

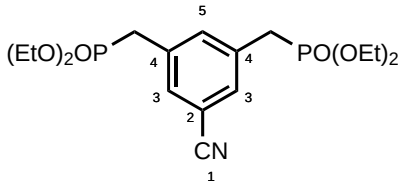

A mixture of 6.27 g (21.7 mmol) 3,5-bis(bromomethyl)benzonitrile (**7**) and 9.7 mL (9.40 g, 56.6 mmol) $P(OEt)_3$ was stirred at 140 °C for 2 hours. The residue was crystallized at 4 °C from cyclohexane with small amounts of ethyl acetate to give 7.12 g (19.1 mmol, 88%) of a colorless solid. ^{1}H NMR ($CDCl_3$): δ = 1.27 (t, ^3J = 7.06 Hz, 12 H; CH_2–CH_3), 3.14 (d, $^3J_{HP}$ = 22.01 Hz, 4 H; CH_2P), 4.05 (m, 8 H; CH_2–CH_3), 7.49 (m, 3 H; ArH); ^{13}C NMR ($CDCl_3$): δ = 16.5 (C_p; CH_3), 33.5 (C_s; d, $^1J_{CP}$ = 138.79 Hz; CH_2P), 62.5 (C_s; d, $^2J_{CP}$ = 7.08 Hz; CH_2–CH_3), 113.0 (C_q; t, $^4J_{CP}$ = 3.06 Hz; C-2), 118.4 (C_q; C-1), 131.8 (C_t; $^3J_{CP}$ = 4.99 Hz; C-3), 134.0 (C_q; m; C-4), 135.8 (C_t; t, $^3J_{CP}$ = 6.51 Hz; C-5); EI-MS, m/z (%): 403 (31, [M]$^{+\cdot}$), 267 (61), 149 (100).

Compound 9

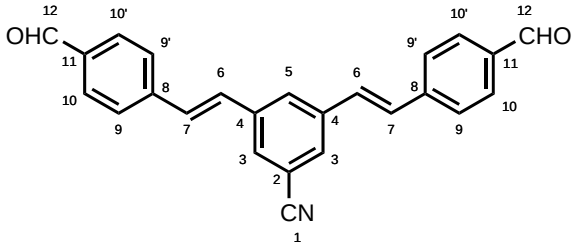

1.13 g (10.1 mmol) potassium *tert*-butoxide was added in portions to a stirred solution of 1.02 g (2.53 mmol) **8** and 1.36 g (6.53 mmol) 4-(diethoxymethyl)benzaldehyde in 3 mL dry DMF under nitrogen atmosphere. Stirring at room temperature was continued for 3.5 hours. The reaction was then quenched with 2N HCl and extracted with a mixture of ethyl acetate and THF. The organic solution was dried over Na_2SO_4 and evaporated under reduced pressure. The residue was washed with DCM, the filtrate was evaporated and again washed with DCM. The combined precipitates were dried in vacuo to yield 687 mg (1.89 mmol, 75%) of a yellow solid. ^{1}H NMR ($CDCl_3$): δ = 7.25 (s, 4 H; H-6 + H-7), 7.70 (AA'BB', 4 H; H-9 + H-9'), 7.75 (d, ^4J = 1.66 Hz, 2 H; H-3), 7.87 (t, ^4J = 1.66 Hz, 1 H; H-5), 7.92 (AA'BB', 4 H; H-10 + H-10'), 10.03 (s, 2 H; H-12); ^{13}C NMR ($CDCl_3$): δ = 114.0 (C_q; C-2), 118.5 (C_q; C-1), 127.5 (C_t; C-9 + C-9'), 129.2 (C_t; C-5), 129.4 + 130.6 (C_t; C-6 + C-7), 129.5 (C_t; C-3), 130.5 (C_t; C-10 + C-10'), 136.2 (C_q; C-11), 138.6 (C_q; C-4), 142.3 (C_q; C-8), 191.6 (C_t; C-12); EI-MS, m/z (%): 363 (100, [M]$^{+\cdot}$), 334 (19), 228 (18).

10.4 Synthesis of the spacers

Compound 22

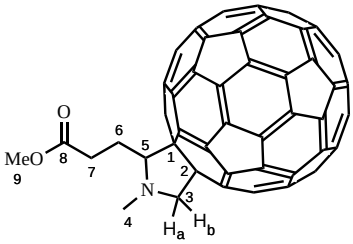

A mixture[157] of γ-butyrolactone and methyl 4-oxo-butanoate (3.0 mmol) was added to a solution of 2.88 g (4.0 mmol) C_{60} and 713 mg (8.0 mmol) N-methylglycine in 800 ml dry toluene under nitrogen atmosphere. After 72 hours of refluxing, the solvent was removed under reduced pressure. The residue was purified by column chromatography on silica gel with toluene as eluent to first afford unreacted C_{60}. Further elution with toluene / ethyl acetate (10 / 1) gave 824 mg of a brown solid. The residue was subjected to preparative recycling GPC to give 310 mg (359 μmol, 12%) of a brown solid. ^{1}H NMR ($CDCl_3$): δ = 2.73 - 3.06 (m, 4 H; H-6 + H-7), 3.00 (s, 3 H; H-4), 3.72 (s, 3 H; H-9), 3.99 (m, 1 H; H-5), 4.19 (d, ^2J = 9.82 Hz, 1 H; H-3a), 4.83 (d, ^3J = 9.82 Hz, 1 H; H-3b); ^{13}C NMR ($CDCl_3$): δ = 25.8 + 31.4 (C_s; C-6 + C-7), 40.1 (C_p; C-4), 52.0 (C_p; C-9), 70.2(8) (C_s; C-3), 70.3(1) (C_q; C-2), 76.1 (C_q; C-1), 77.3 (C_t; C-5), 135.6 + 136.0 + 136.3 + 137.5 + 140.0 + 140.1 + 140.4 + 140.5 + 141.9 + 142.0 + 142.1(7) + 142.2(4) + 142.2(8) + 142.3(2) + 142.3(3) + 142.4 + 142.6 + 142.8 + 142.9 + 143.2 + 143.4 + 144.5 + 144.6 + 144.7 + 144.9 + 145.3(8) + 145.4(0) + 145.4(2) + 145.4(6) + 145.4(9) + 145.5(8) + 145.6(1) + 145.6(4) + 145.7 + 145.9 + 146.1 + 146.1(7) + 146.2(2) + 146.2(7) + 146.3(3) + 146.3(6) + 146.4(3) + 146.5 + 146.6 + 147.3(9) + 147.4(3) + 153.0 + 154.2 + 154.6 (C_q; C_{58}), 173.8 (C_q; C-8); MALDI-MS: m/z (%) calcd.: 863.09 (100,$[M]^{-\cdot}$), found: 863.09 (100, $[M]^{-\cdot}$).

Compound 23

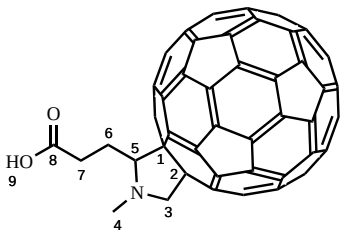

A mixture of 338 mg (391 μmol) **22**, 150 ml toluene, 250 ml acetic acid and 120 ml HCl conc. was stirred at 110 °C overnight. The solvent was removed under reduced pressure and the residue was washed with water, acetone and DCM, respectively, to yield 277 mg (326 μmol, 83%) of a brown solid. Due to poor solubility in all tested organic solvents, no information could be obtained by NMR investigations. MALDI-MS: m/z (%) calcd.: 849.08 (100, $[M]^{-\cdot}$), found: 849.07 (100, $[M]^{-\cdot}$); ESI-HRMS: m/z calcd. for $C_{66}H_{12}NO_2^+$ ($[M+H]^+$): 850.0863, found: 850.0848; Elemental analysis (%) for $C_{66}H_{11}NO_2$ calcd.: C 93.28, H 1.30, N 1.65, found: C 90.09, H 1.31, N 1.64. For the discussion of elemental analysis results regarding fullerene containing materials, see page 119.

Compound 25

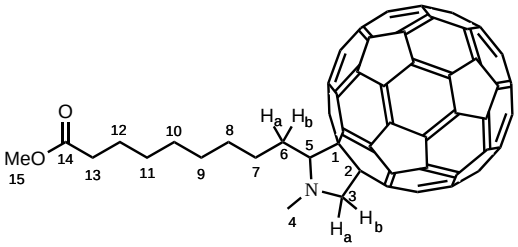

0.28 ml (272 mg, 1.36 mmol) methyl 10-oxodecanoate (**24**) was added to a solution of 1.00 g (1.39 mmol) C_{60} and 248 mg (2.78 mmol) N-methylglycine in 700 ml dry toluene under nitrogen atmosphere. After refluxing overnight, the solvent was removed under reduced pressure. The residue was purified by column chromatography on silica gel with toluene as eluent to first afford unreacted C_{60}. Further elution with toluene / ethyl acetate (9 / 1) gave 816 mg of a brown solid. The residue was subjected to preparative recycling GPC to give 461 mg (486 µmol, 36%) of a brown solid. ^{1}H NMR ($CDCl_3$): δ = 1.30 (m, 6 H; H-9 + H-10 + H-11), 1.46 (m, 2 H; H-8), 1.60 (m, 2 H; H-12), 1.90 (m, 2 H; H-7), 2.29 (t, ^3J = 7.52 Hz, 2 H; H-13), 2.37 (m, 1 H; H-6a), 2.52 (m, 1 H; H-6b), 2.99 (s, 3 H; H-4), 3.65 (s, 3 H; H-15), 3.90 (m, 1 H; H-5), 4.17 (d, ^2J = 9.74 Hz, 1 H; H-3a), 4.82 (d, ^2J = 9.74 Hz, 1 H; H-3b); ^{13}C NMR ($CDCl_3$): δ = 25.1 (C_s; C-12), 27.6 (C_s; C-7), 29.2 + 29.3 + 29.4 (C_s; C-9 + C-10 + C-11), 30.3 (C_s; C-8), 31.2 (C_s; C-6), 34.2 (C_s; C-13), 40.2 (C_p; C-4), 51.6 (C_p; C-15), 70.2 (C_q; C-2), 70.5 (C_s; C-3), 76.4 (C_q; C-1), 78.3 (C_t; C-5), 135.7 + 136.0 + 136.4 + 137.3 + 139.8 + 139.9 + 140.3 + 140.4 + 141.8 + 141.9 + 142.0 + 142.2 + 142.2(5) + 142.2(9) + 142.3(3) + 142.4 + 142.7(6) + 142.7(9) + 142.8(1) + 142.9 + 143.2 + 143.3 + 144.5 + 144.6 + 144.7 + 144.9 + 145.3 + 145.4 + 145.4(5) + 145.4(9) + 145.5(7) + 145.6(2) + 145.7 + 146.0 + 146.1(1) + 146.1(4) + 146.2 + 146.2(6) + 146.3(2) + 146.3(4) + 146.4 + 146.4(6) + 146.5(1) + 146.7 + 146.9 + 147.3(6) + 147.4(0) + 153.6 + 154.5 + 154.6 + 156.6 (C_q; C_{58}), 174.4 (C_q; C-14); MALDI-MS: m/z (%) calcd.: 947.19 (100,$[M]^{-\cdot}$), found: 947.18 (100, $[M]^{-\cdot}$).

Compound 26

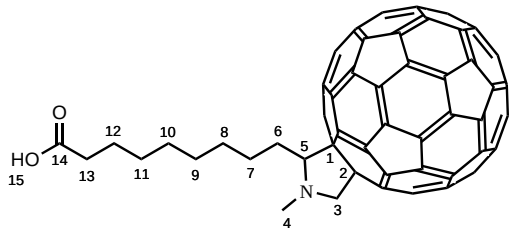

A mixture of 415 mg (438 µmol) **25**, 75 ml toluene, 90 ml acetic acid and 60 ml HCl conc. was stirred at 110 °C overnight. At room temperature, the organic phase was washed with water five times, dried over Na_2SO_4 and evaporated under reduced pressure. The residue was dissolved in 50 ml DCM and poured into 150 ml methanol. The precipitate was collected with a filter funnel (P4) to yield 320 mg (343 µmol, 78%) of a brown solid. ^{1}H NMR ($CDCl_3$): δ = 1.33 (m, 6 H; H-9 + H-10 + H-11), 1.47 (m, 2 H; H-8), 1.62 (m, 2 H; H-12), 1.89 (m, 2 H; H-7), 2.34 (t, ^3J = 7.44 Hz, 2 H; H-13), 2.37 (m, 1 H; H-6a), 2.52 (m, 1 H; H-6b), 3.00 (s, 3 H; H-4), 3.92 (t, ^3J = 5.44 Hz, 1 H; H-5), 4.19 (d, ^2J = 9.84 Hz, 1 H; H-3a), 4.83 (d, ^2J = 9.72 Hz, 1 H; H-3b); MALDI-MS: m/z (%) calcd.: 933.17 (100,

[M]$^{\cdot-}$), found: 933.15 (100, [M]$^{\cdot-}$); ESI-HRMS: m/z calcd. for $C_{72}H_{24}NO_2^+$ ([M+H]$^+$): 934.1802, found: 934.1829; Elemental analysis (%) for $C_{72}H_{23}NO_2$ calcd.: C 92.59, H 2.48, N 1.50, found: C 91.52, H 3.22, N 1.33. For the discussion of elemental analysis results regarding fullerene containing materials, see page 119.

Methyl 16-oxohexadecanoate (29)

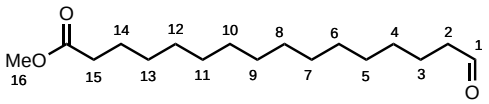

0.50 ml (551 mg, 7.05 mmol) DMSO was added in drops to a solution of 0.19 ml (283 mg, 2.23 mmol) oxalyl chloride in 5 ml DCM at -78 °C. After stirring for 5 minutes, 568 mg (1.98 mmol) methyl 16-hydroxyhexadecanoate (**28**) in 5 ml DCM was added drop by drop. Stirring was continued for 2.5 hours at -78 °C before 2.0 ml (1.46 g, 14.4 mmol) triethylamine was added. The cooling bath was removed and at room temperature, 10 ml deionized water was added and stirring was continued for further 10 minutes. The mixture was extracted with DCM and the organic solvent was washed with 1N HCl and sodium bicarbonate solution, respectively. The solution was dried over Na_2SO_4 and evaporated under reduced pressure. Further purification by silica gel column chromatography with DCM as eluent yielded 388 mg (1.36 mmol, 69%) of a colorless solid. The analytical data is in accordance with the literature.[159] ^{1}H NMR ($CDCl_3$): δ = 1.19 - 1.37 (m, 20 H; H-4 + H-5 + H-6 + H-7 + H-8 + H-9 + H-10 + H-11 + H-12 + H-13), 1.57 - 1.67 (m, 4 H; H-3 + H-14), 2.30 (t, ^3J = 7.55 Hz, 2 H; H-15), 2.42 (td, ^3J = 7.35 Hz, ^3J = 1.88 Hz, 2 H; H-2), 3.66 (s, 3 H; H-16), 9.76 (t, ^3J = 1.88 Hz, 1 H; H-1);

Compound 30

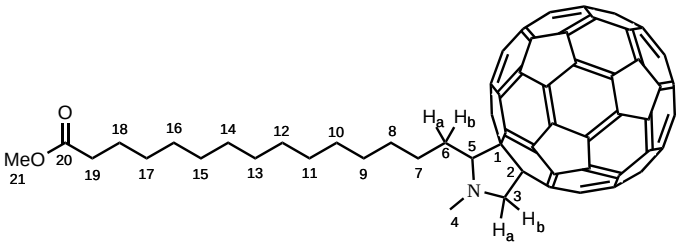

294 mg (1.03 mmol) methyl 16-oxohexadecanoate (**29**) was added to a solution of 905 mg (1.26 mmol) C_{60} and 222 mg (2.49 mmol) N-methylglycine in 900 ml dry toluene under nitrogen atmosphere. After refluxing for 3 days, the solution was concentrated to 100 ml under reduced pressure. The mixture was purified by column chromatography on silica gel with toluene as eluent to first afford unreacted C_{60}. Further elution with toluene / ethyl acetate (9 / 1) gave 789 mg of a brown solid. The residue was subjected to preparative recycling GPC to give 450 mg (436 µmol, 42%) of a brown solid. ^{1}H NMR ($CDCl_3$): δ = 1.23 (m, 18 H; H-9 + H-10 + H-11 + H-12 + H-13 + H-14 + H-15 + H-16 + H-17), 1.46 (m, 2 H; H-8), 1.60 (m, 2 H; H-18), 1.90 (m, 2 H; H-7), 2.29 (t, ^3J = 7.55 Hz, 2 H; H-19), 2.36 (m, 1 H; H-6a), 2.52 (m, 1 H; H-6b), 2.99 (s, 3 H; H-4), 3.65 (s, 3 H; H-21), 3.90 (m, 1 H; H-5), 4.16 (d, ^2J = 9.74 Hz, 1 H; H-3a), 4.81 (d, ^2J = 9.74 Hz, 1 H; H-3b), ^{13}C NMR ($CDCl_3$): δ = 25.1 (C_s; C-18), 27.6 (C_s; C-7), 29.3 + 29.4 + 29.5(6) + 29.6(1) + 29.7 + 29.7(5) + 29.7(9) + 29.8(2) (C_s; C-9 + C-10 + C-11 + C-12 + C-13 + C-14 + C-15 + C-16 + C-17), 30.4 (C_s; C-8), 31.2 (C_s; C-6),

34.3 (C_s; C-19), 40.2 (C_p; C-4), 51.6 (C_p; C-21), 70.2 (C_q; C-2), 70.5 (C_s; C-3), 76.4 (C_q; C-1), 78.3 (C_t; C-5), 135.7 + 136.0 + 136.4 + 137.3 + 139.7 + 139.9 + 140.3 + 140.4 + 141.8 + 141.9 + 142.0 + 142.1(7) + 142.1(8) + 142.2(2) + 142.2(7) + 142.2(8) + 142.2(9) + 142.3(0) + 142.3(2) + 142.7 + 142.7(5) + 142.7(7) + 142.7(7) + 142.8(1) + 143.2 + 143.3 144.4(8) + 144.5(3) + 144.7 + 144.9 + 145.3 + 145.3(5) + 145.4(1) + 145.4(6) + 145.5(3) + 145.6 + 145.7 + 146.0 + 146.0(7) + 146.1(0) + 146.1(7) + 146.2(2) + 146.2(8) + 146.3(0) + 146.3(8) + 146.4(2) + 146.5 + 146.7 + 146.9 + 147.3 + 147.4 + 153.6 + 154.5 + 154.6 + 156.6 (C_q; C_{58}), 174.5 (C_q; C-20); MALDI-MS: m/z (%) calcd.: 1031.28 ($[M]^{-\cdot}$,100), found: 1031.28 ($[M]^{-\cdot}$,100).

Compound 31

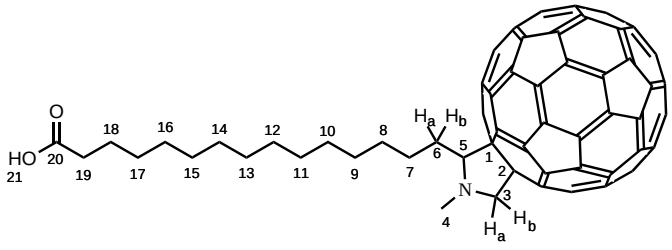

A mixture of 434 mg (420 µmol) **30**, 75 ml toluene, 90 ml acetic acid and 60 ml HCl conc. was stirred at 110 °C for 2 days. At room temperature, the organic phase was washed with water until pH-neutral, dried over Na_2SO_4 and evaporated under reduced pressure. The residue was recrystallized from $CHCl_3$ at -30 °C to yield 299 mg (294 µmol, 70%) of a brown solid. ^{1}H NMR ($CDCl_3$): δ = 1.23 (m, 18 H; H-9 + H-10 + H-11 + H-12 + H-13 + H-14 + H-15 + H-16 + H-17), 1.46 (m, 2 H; H-8), 1.63 (m, 2 H; H-18), 1.90 (m, 2 H; H-7), 2.34 (t, ^3J = 7.44 Hz, 2 H; H-19), 2.38 (m, 1 H; H-6a), 2.53 (m, 1 H; H-6b), 3.01 (s, 3 H; H-4), 3.96 (m, 1 H; H-5), 4.20 (d, ^2J = 9.84 Hz, 1 H; H-3a), 4.85 (d, ^2J = 9.84 Hz, 1 H; H-3b), 12.28 (m, 1 H; H-21); ^{13}C NMR ($CDCl_3$): δ = 24.9 (C_s; C-18), 27.6 (C_s; C-7), 29.2 + 29.3 + 29.5 + 29.5(7) + 29.6(3) + 29.7 (C_s; C-9 + C-10 + C-11 + C-12 + C-13 + C-14 + C-15 + C-16 + C-17), 30.3 (C_s; C-8), 31.1 (C_s; C-6), 34.2 (C_s; C-19), 40.0 (C_p; C-4), 70.3 (C_q; C-2 + C-3), 76.4 (C_q; C-1), 78.2 (C_t; C-5), 136.0 + 136.4 + 137.4 + 139.8 + 139.9 + 140.3 + 140.4 + 141.8 + 141.9 + 142.0 + 142.1(6) + 142.2(2) + 142.2(3) + 142.2(5) + 142.3(1) + 142.3(2) + 142.3(4) + 142.7(6) + 142.7(8) + 142.8(0) + 142.8(4) + 143.2 + 143.3 + 144.5 + 144.6 + 144.7 + 144.9 + 145.3 + 145.4 + 145.4(5) + 145.4(9) + 145.5(6) + 145.6(2) + 145.7 + 145.9 + 146.0(9) + 146.1(3) + 146.2 + 146.2(5) + 146.3(1) + 146.3(3) + 146.4 + 146.5 + 146.7 + 147.3(5) + 147.3(9) + 153.4 + 154.5 + 154.6 + 156.5 (C_q; C_{58}), 179.0 (C_q; C-20); MALDI-MS: m/z (%) calcd.: 1017.27 ($[M]^{-\cdot}$,100), found: 1017.27 ($[M]^{-\cdot}$,100); ESI-HRMS: m/z calcd. for $C_{78}H_{36}NO_2^+$ ($[M+H]^+$): 1018.2741, found: 1018.2741; Elemental analysis (%) for $C_{78}H_{35}NO_2$ calcd.: C 92.02, H 3.47, N 1.38, found: C 93.94, H 4.04, N 1.28. The surprisingly high carbon content is in stark contrast to the discussions shown on page 119 and raises the question, whether the reformation of C_{60} might play a role in this phenomenon. However, ^{13}C NMR measurements clearly demonstrate the lack of C_{60}, which would cause a strong signal located at approx. 143 ppm. Due to lack of material, the elemental analysis could not be repeated.

10.5 Synthesis of the arm building blocks with dodecyloxy-chains

Compound 37

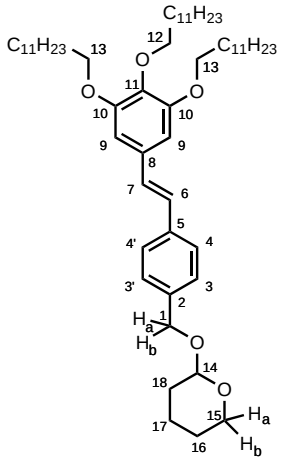

At 0 °C, 708 mg (6.31 mmol) potassium *tert*-butoxide was added in portions to a stirred solution of 2.37 g (3.03 mmol) phosphonate **36** and 800 mg (3.63 mmol) (±)-4-(3,4,5,6-tetrahydro-2*H*-pyran-2-yloxymethyl)benzaldehyde (**13**) in 10 mL dry THF under nitrogen atmosphere. After stirring overnight, the mixture was poured into water and was acidified with 2N HCl. The mixture was extracted with DCM and the organic phase was dried over Na_2SO_4 and $NaHCO_3$. The solution was evaporated under reduced pressure and the crude product was dissolved in ethyl acetate, poured into methanol and stored at -35 °C overnight. The precipitate was washed with cold methanol and dried to yield 2.33 g (2.75 mmol, 91%) of a colorless solid. ^{1}H NMR ($CDCl_3$): δ = 0.89 (t, ^3J = 6.76 Hz, 9 H; CH_3), 1.20 - 1.90 (m, 66 H; H-16 + H-17 + H-18 + $C_{10}H_{20}$), 3.56 + 3.94 (m, 2 H; H-15a + H-15b), 3.97 (t, ^3J = 6.58 Hz, 2 H; H-12), 4.03 (t, ^3J = 6.52 Hz, 4 H; H-13), 4.51 (d, ^2J = 12.16 Hz, 1 H; H-1a), 4.72 (t, ^3J = 3.52 Hz, 1 H; H-14), 4.79 (d, ^2J = 12.16 Hz, 1 H; H-1b), 6.71 (s, 2 H; H-9), 6.96 + 7.01 (d, ^3J = 16.31 Hz, 2 H; H-6 + H-7), 7.35 (AA' of AA'BB', ^3J = 8.24 Hz, 2 H; H-3 + H-3'), 7.47 (BB' of AA'BB', ^3J = 8.28 Hz, 2 H; H-4 + H-4'); ^{13}C NMR ($CDCl_3$): δ = 14.3 (C_p; CH_3), 19.5 + 25.6 + 30.8 (C_s; C-16 + C-17 + C-18), 22.8 - 32.1 (C_s; $C_{10}H_{20}$), 62.3 (C_s; C-15), 68.8 (C_s; C-1), 69.4 (C_s; C-13), 73.7 (C_s; C-12), 97.9 (C_t; C-14), 105.4 (C_t; C-9), 126.5 (C_t; C-4 + C-4'), 127.6 + 129.0 (C_t; C-6 + C-7), 128.4 (C_t; C-3 + C-3'), 132.7 (C_q; C-8), 136.9 (C_q; C-5), 137.7 (C_q; C-2), 138.6 (C_q; C-11), 153.5 (C_q; C-10); MALDI-MS: m/z (%) calcd.: 846.71 ($[M]^{+\cdot}$,100), found: 846.63 ($[M]^{+\cdot}$,100).

Compound 38

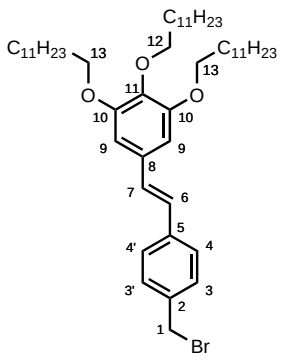

28 ml of a freshly prepared solution[171] of PPh_3Br_2 (3.63 mmol) in DCM was added drop by drop to a mixture of 2.33 g (2.75 mmol) **37** and 10 ml DCM under nitrogen atmosphere. A saturated solution of $NaHCO_3$ was poured into the solution. The mixture was extracted with DCM and the organic phase was washed with water. The aqueous phase was again extracted with DCM and the combined organic solvents were dried over Na_2SO_4. The solvent was evaporated under reduced pressure and the crude product was chromatographed on silica gel with cyclohexane / ethyl acetate (10 / 1) as eluent to yield 2.17 g (2.63 mmol, 96%) of a colorless solid. Analytical data in accordance with literature.[264] ^{1}H NMR ($CDCl_3$): δ = 0.88 (t, ^3J = 6.98 Hz, 9 H; CH_3), 1.20 - 1.90 (m, 60 H; $C_{10}H_{20}$), 3.97 (t, ^3J = 6.62 Hz, 2 H; H-12), 4.02 (t, ^3J = 6.50 Hz, 4 H; H-13), 4.52 (s, 2 H; H-1), 6.71 (s, 2 H; H-9), 6.94 + 7.02 (d, ^3J = 16.22 Hz, 2 H; H-6 + H-7), 7.37 (AA' of AA'BB', ^3J = 8.32 Hz, 2 H; H-3 + H-3'), 7.46 (BB' of AA'BB', ^3J = 8.24 Hz, 2 H; H-4 + H-4').

Compound 39

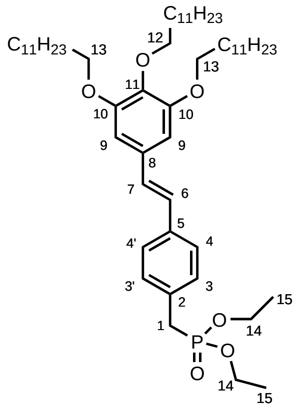

0.63 ml (610 mg, 3.67 mmol) $P(OEt)_3$ was added to 2.17 g (2.63 mmol) **38** and the mixture was stirred in a round-bottom flask equipped with a condenser at 140 °C for 3 hours under nitrogen atmosphere. The distillate was discarded and excess $P(OEt)_3$ was removed via distillation in vacuo. The crude product was subjected to column chromatography (cyclohexane / ethyl acetate = 3 / 1) to yield 2.04 g (2.31 mmol, 88%) of a colorless solid. ^{1}H NMR ($CDCl_3$): δ = 0.88 (t, ^3J = 6.84 Hz, 9 H; CH_3), 1.20 - 1.90 (m, 66 H; $C_{10}H_{20}$ + H-15), 3.15 (d, $^2J_{HP}$ = 21.69 Hz, 2 H; H-1), 3.96 (t, ^3J = 6.60 Hz, 2 H; H-12), 4.02 (t, ^3J = 6.38 Hz, 4 H; H-13), 4.03 (m, 4 H; H-14), 6.70 (s, 2 H; H-9), 6.93 + 6.99 (d, ^3J = 16.29 Hz, 2 H; H-6 + H-7), 7.28 (m, ^3J = 8.40 Hz, $^4J_{HP}$ = 2.48 Hz, 2 H; H-3 + H-3'), 7.44 (AA' of AA'BB', ^3J = 7.80 Hz, 2 H; H-4 + H-4'); MALDI-MS: m/z (%) calcd.: 882.69 ($[M]^{+\cdot}$,100), found: 882.73 ($[M]^{+\cdot}$,100).

Compound 40

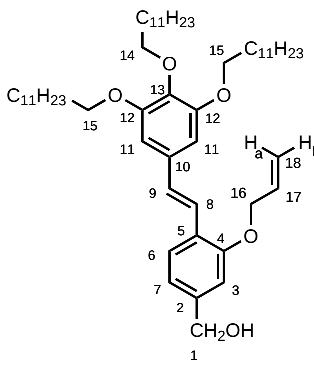

363 mg (3.24 mmol) potassium *tert*-butoxide was added in portions to a stirred solution of 1.80 g (2.30 mmol) phosphonate **36** and 623 mg (2.83 mmol) methyl 3-(allyloxy)-4-formylbenzoate in 10 mL dry THF under nitrogen atmosphere. After stirring overnight, the reaction was quenched with 1M HCl and extracted with DCM. The organic solvent was dried over Na_2SO_4 and evaporated under reduced pressure to afford 2.15 g of a solid.

After dissolving the residue in 20 ml dry THF, 90.0 mg (2.37 mmol) $LiAlH_4$ was added carefully and the mixture was refluxed for 3 hours. At 0 °C, the reaction was quenched cautiously with water and 2M HCl, respectively. The mixture was extracted with DCM and the organic solvent was dried over Na_2SO_4 and evaporated under reduced pressure to afford 1.90 g of a solid. The crude product was chromatographed on silica gel with cyclohexane / ethyl acetate (6 / 1) as eluent to yield 1.36 g (1.66 mmol, 72%) of a colorless solid. ^{1}H NMR ($CDCl_3$): δ = 0.88 (t, ^3J = 6.88 Hz, 9 H; CH_3), 1.20 - 1.90 (m, 60 H; CH_2), 3.97 (t, ^3J = 6.65 Hz, 2 H; H-14), 4.02 (t, ^3J = 6.51 Hz, 4 H; H-15), 4.64 (dt, ^3J = 5.04 Hz, ^4J = 1.65 Hz, 2 H; H-16), 4.68 (s, 2 H; H-1), 5.31 (m, 1 H; H-18b), 5.47 (m, 1 H; H-18a), 6.11 (m, 1 H; H-17), 6.72 (s, 2 H; H-11), 6.94 (m, 2 H; H-3 + H-7), 7.02 (d, ^3J = 16.42 Hz, 1 H; H-9), 7.35 (d, ^3J = 16.42 Hz, 1 H; H-8), 7.55 (d, ^3J = 8.06 Hz, 1 H; H-6); ^{13}C NMR ($CDCl_3$): δ = 14.3 (C_p; CH_3), 22.8 - 32.1 (C_s; CH_2), 65.5 (C_s; C-1), 69.3(7) + 69.4(1) (C_s; C-15 + C-16), 73.7 (C_s; C-14), 105.5 (C_t; C-11), 111.3 (C_t; C-3), 117.3 (C_s; C-18), 119.6 (C_t; C-7), 122.5 (C_t; C-8), 126.5 (C_q; C-5), 126.7 (C_t; C-6), 129.5 (C_t; C-9), 133.3 (C_q; C-10), 133.5 (C_t; C-17), 138.4 (C_q; C-13), 141.5 (C_q; C-2), 153.4 (C_q; C-12), 156.2 (C_q; C-4); MALDI-MS: m/z (%) calcd.: 818.68 ($[M]^{+\cdot}$,100), found: 818.66 ($[M]^{+\cdot}$,100).

Compound 41

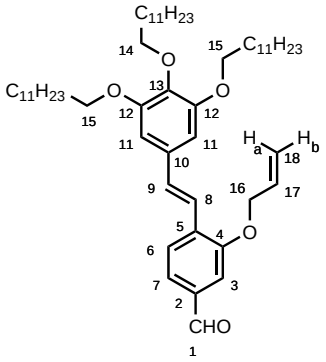

1.32 g (1.61 mmol) **40** and 7.00 g (80.5 mmol) activated MnO_2 were mixed with 50 ml DCM and stirred for 30 minutes at room temperature. The solution was filtered through a celite pad and evaporated under reduced pressure. The crude product was chromatographed on silica gel with light petroleum ether / ethyl acetate (15 / 1) as eluent to yield 1.03 g (1.26 mmol, 78%) of a colorless solid. ^{1}H NMR ($CDCl_3$): δ = 0.88 (t, ^3J = 6.88 Hz, 9 H; CH_3), 1.20 - 1.90 (m, 60 H; CH_2), 3.98 (t, ^3J = 6.62 Hz, 2 H; H-14), 4.03 (t, ^3J = 6.48 Hz, 4 H; H-15), 4.70 (dt, ^3J = 4.96 Hz, ^4J = 1.54 Hz, 2 H; H-16), 5.34 (m, 1 H; H-18b), 5.49 (m, 1 H; H-18a), 6.12 (m, 1 H; H-17), 6.75 (s, 2 H; H-11), 7.17 (d, ^3J = 16.38 Hz, 1 H; H-9), 7.38(6) (d, ^3J = 16.38 Hz, 1 H; H-8), 7.39(1) (d, ^4J = 1.40 Hz, 1 H; H-3), 7.46 (dd, ^3J = 7.94 Hz, ^4J = 1.42 Hz, 1 H; H-7), 7.72 (d, ^3J = 7.92 Hz, 1 H; H-6), ^{13}C NMR ($CDCl_3$): δ = 14.3 (C_p; CH_3), 22.8 - 32.1 (C_s; CH_2), 69.4 (C_s; C-15 + C-16), 73.7 (C_s; C-14), 105.9 (C_t; C-11), 111.2 (C_t; C-3), 117.8 (C_s; C-18), 121.6 (C_t; C-8), 124.5 (C_t; C-7), 126.6 (C_t; C-6), 132.6 (C_q; C-10),

132.9(0) + 132.9(2) (C_t; C-9 + C-17), 133.6 (C_q; C-5), 136.3 (C_q; C-2), 139.1 (C_q; C-13), 153.5 (C_q; C-12), 156.2 (C_q; C-4), 191.6 (C_t; C-1); MALDI-MS: m/z (%) calcd.: 816.66 ($[M]^{+\cdot}$,100), found: 816.69 ($[M]^{+\cdot}$,100).

Compound 44

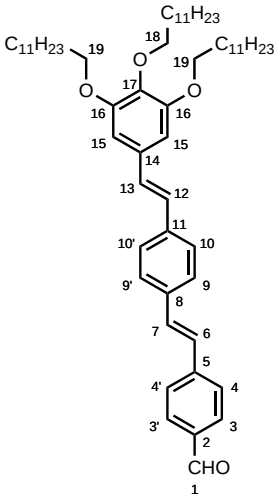

At 0 °C, 505 mg (4.50 mmol) potassium *tert*-butoxide was added in portions to a stirred solution of 2.04 g (2.31 mmol) **39** and 0.6 ml (628 mg, 3.02 mmol) 4-(diethoxymethyl)benzaldehyde (**2**) in 20 mL dry THF under nitrogen atmosphere. After removing the ice bath and stirring overnight, the reaction was quenched with 1M HCl and extracted with DCM. The organic solvent was dried over Na_2SO_4 and evaporated under reduced pressure. The crude product was subjected to silica gel chromatography with DCM as eluent to yield 1.81 g (2.10 mmol, 91%) of a yellow solid. Analytical data in accordance with literature.[173] ^{1}H NMR ($CDCl_3$): δ = 0.88 (t, ^3J = 6.90 Hz, 9 H; CH_3), 1.20 - 1.90 (m, 60 H; CH_2), 3.97 (t, ^3J = 6.56 Hz, 2 H; H-18), 4.03 (t, ^3J = 6.52 Hz, 4 H; H-19), 6.72 (s, 2 H; H-15), 6.97 (d, ^3J = 16.16 Hz, 1 H; H-12), 7.06 (d, ^3J = 16.24 Hz, 1 H; H-13), 7.16 (d, ^3J = 16.24 Hz, 1 H; H-6), 7.27 (d, ^3J = 16.28 Hz, 1 H; H-7), 7.51 (AA' of AA'BB', ^3J = 8.80 Hz, 2 H; H-10 + H-10'), 7.54 (BB' of AA'BB', ^3J = 8.64 Hz, 2 H; H-9 + H-9'), 7.66 (AA' of AA'BB', ^3J = 8.32 Hz, 2 H; H-4 + H-4'), 7.88 (BB' of AA'BB', ^3J = 8.36 Hz, 2 H; H-3 + H-3'), 10.00 (s, 1 H; H-1).

Compound 42

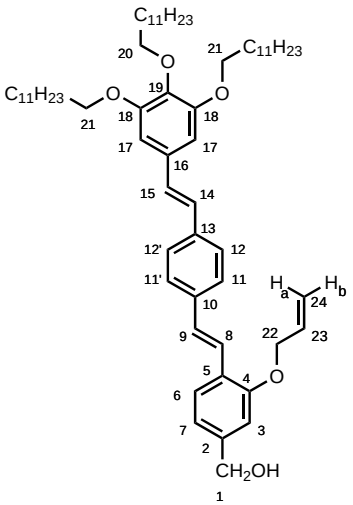

445 mg (3.97 mmol) potassium *tert*-butoxide was added in portions to a stirred solution of 2.50 g (2.83 mmol) **39** and 686 mg (3.12 mmol) methyl 3-(allyloxy)-4-formylbenzoate in 20 mL dry THF under nitrogen atmosphere. Stirring at room temperature was continued for 40 minutes. The reaction was then quenched with 2M HCl and extracted with $CHCl_3$. The organic solvent was dried over Na_2SO_4 and evaporated under reduced pressure to afford 2.77 g of a yellow solid.

After dissolving the residue in 30 ml dry THF, 154 mg (4.06 mmol) $LiAlH_4$ was added carefully and the mixture was refluxed for 4 hours. At 0 °C, the reaction was quenched cautiously with water and 2M HCl, respectively. The mixture was extracted with $CHCl_3$ and the organic solvent was dried over Na_2SO_4 and evaporated under reduced pressure to afford 2.57 g of a yellow solid. The crude product was chromatographed on silica gel with cyclohexane / ethyl acetate (7 / 1) as eluent to yield 1.95 g (2.12 mmol, 75%) of a yellow solid. ^{1}H NMR ($CDCl_3$): δ = 0.89 (t, ^3J = 6.84 Hz, 9 H; CH_3), 1.20-1.60 (m, 54 H ; $(CH_2)_9$–CH_3), 1.70-1.90 (m, 6 H ; OCH_2CH_2), 3.98 (t, ^3J = 6.64 Hz, 2 H; H-20), 4.03 (t, ^3J = 6.56 Hz, 4 H; H-21), 4.64 (dt,^3J = 5.16 Hz, ^4J = 1.56 Hz, 2 H; H-22), 4.69 (m, 2 H; H-1), 5.33 (m, 1 H; H-24b), 5.48 (m, 1 H; H-24a), 6.13 (m, 1 H; H-23), 6.72 (s, 2 H; H-17), 6.93-6.97 (m, 2 H; H-3 + H-7), 6.96 (d, ^3J = 16.21 Hz, 1 H; H-14), 7.02 (d, ^3J = 16.21 Hz, 1 H; H-15), 7.13 (d, ^3J = 16.53 Hz, 1 H; H-9), 7.47 (AA' of AA'BB', ^3J = 8.56 Hz, 2 H; H-12 + H-12'), 7.51(2) (d, ^3J = 16.53 Hz, 1 H; H-8), 7.51(3) (BB' of AA'BB', ^3J = 8.56 Hz, 2 H; H-11 + H-11'), 7.59 (d, ^3J = 7.64 Hz, 1 H; H-6); ^{13}C NMR ($CDCl_3$): δ = 14.3 (C_p; CH_3), 22.9 (C_s; CH_2), 26.3 (C_s; CH_2), 29.4-30.0 (C_s; CH_2), 30.5 (C_s; CH_2), 32.1 (C_s; CH_2), 65.4 (C_s; C-1), 69.3(6) + 69.4(3) (C_s; C-21 + C-22), 73.7 (C_s; C-20), 105.4 (C_t; C-17), 111.2 (C_t; C-3), 117.6 (C_s; C-24), 119.6 (C_t; C-7), 123.2 (C_t; C-8), 126.3 (C_q; C-5), 126.7 (C_t; C-6), 126.8 (C_t; C-12 + C-12'), 127.0 (C_t; C-11 + C-11'), 127.5 (C_t; C-14), 128.8(0) + 128.8(4) (C_t; C-9 + C-15), 132.7 (C_q; C-16), 133.5 (C_t; C-23), 136.7 (C_q; C-13), 137.3 (C_q; C-10), 138.5 (C_q; C-19), 141.7 (C_q; C-2), 153.5 (C_q; C-18), 156.3 (C_q; C-4); MALDI-MS: m/z (%) calcd.: 920.73 ($[M]^{+\cdot}$,100), found: 920.71 ($[M]^{+\cdot}$,100).

Compound 43

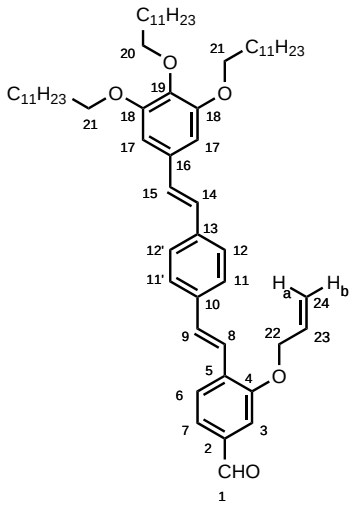

1.93 g (2.09 mmol) **42** and 9.09 g (105 mmol) activated manganese dioxide were mixed with 80 ml DCM and stirred for 15 minutes at room temperature. The solution was filtered through a celite pad and evaporated under reduced pressure. The crude product was crystallized from cold methanol to yield 1.75 g (1.90 mmol, 91%) of a yellow solid. ^{1}H NMR ($CDCl_3$): δ = 0.89 (t, ^3J = 6.86 Hz, 9 H;

CH_3), 1.20-1.60 (m, 54 H ; $(CH_2)_9$–CH_3), 1.70-1.90 (m, 6 H ; OCH_2CH_2), 3.98 (t, ^3J = 6.62 Hz, 2 H; H-20), 4.03 (t, ^3J = 6.50 Hz, 4 H; H-21), 4.71 (dt,^3J = 5.12 Hz, ^4J = 1.52 Hz, 2 H; H-22), 5.36 (m, 1 H; H-24b), 5.50 (m, 1 H; H-24a), 6.14 (m, 1 H; H-23), 6.72 (s, 2 H; H-17), 6.97 (d, ^3J = 16.19 Hz, 1 H; H-14), 7.05 (d, ^3J = 16.19 Hz, 1 H; H-15), 7.28 (d, ^3J = 16.53 Hz, 1 H; H-9), 7.40 (d, ^4J = 1.39 Hz, 1 H; H-3), 7.47 (dd, ^3J = 7.89 Hz, ^4J = 1.39 Hz, 1 H; H-7), 7.50 (AA' of AA'BB', ^3J = 8.42 Hz, 2 H; H-12 + H-12'), 7.54(7) (BB' of AA'BB', ^3J = 8.42 Hz, 2 H; H-11 + H-11'), 7.54(9) (d, ^3J = 16.53 Hz, 1 H; H-9), 7.77 (d, ^3J = 7.89 Hz, 1 H; H-6), 9.95 (s, 1 H; H-1); ^{13}C NMR ($CDCl_3$): δ = 14.3 (C_p; CH_3), 22.9 (C_s; CH_2), 26.3 (C_s; CH_2), 29.4-30.0 (C_s; CH_2), 30.5 (C_s; CH_2), 32.1 (C_s; CH_2), 69.4 + 69.5 (C_s; C-21 + C-22), 73.7 (C_s; C-20), 105.5 (C_t; C-17), 111.1 (C_t; C-3), 118.1 (C_s; C-24), 122.2 (C_t; C-8), 124.5 (C_t; C-7), 126.7 (C_t; C-6), 126.9 (C_t; C-12 + C-12'), 127.3 (C_t; C-14), 127.4 (C_t; C-11 + C-11'), 129.4 (C_t; C-15), 132.2 (C_t; C-9), 132.6 (C_q; C-16), 132.9 (C_t; C-23), 133.4 (C_q; C-5), 136.4 + 136.5 (C_q; C-2 + C-10), 137.6 (C_q; C-13), 138.7 (C_q; C-19), 153.5 (C_q; C-18), 156.3 (C_q; C-4), 191.7 (C_q; C-1); MALDI-MS: m/z (%) calcd.: 918.71 ($[M]^{+\cdot}$,100), found: 918.73 ($[M]^{+\cdot}$,100).

10.6 Synthesis of the V-shaped building blocks with dodecyloxy-chains

Compound 63

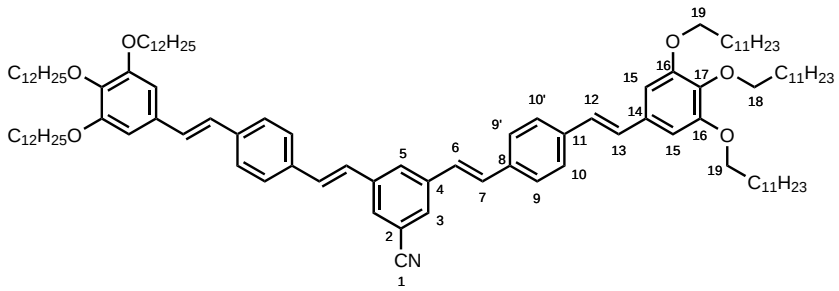

548 mg (4.88 mmol) potassium *tert*-butoxide was added in portions to a stirred solution of 428 mg (1.18 mmol) dialdehyde **9** and 2.02 g (2.59 mmol) phosphonate **36** in 15 mL dry THF under nitrogen atmosphere. The reaction mixture was stirred for 2 hours. Then the reaction was quenched with 2N HCl and the solution was extracted with DCM. The organic solvent was dried over Na_2SO_4 and evaporated under reduced pressure. Subsequently the crude product was purified by column chromatography on silica gel with cyclohexane / DCM (1 / 2) as eluent to yield 1.09 g (674 µmol, 57%) of a yellow solid. ^{1}H NMR ($CDCl_3$): δ = 0.88 (t, ^3J = 6.88 Hz, 18 H; CH_3), 1.20-1.60 (m, 108 H ; $(CH_2)_9$–CH_3), 1.70-1.90 (m, 12 H ; OCH_2CH_2), 3.98 (t, ^3J = 6.58 Hz, 4 H; H-18), 4.03 (t, ^3J = 6.51 Hz, 8 H; H-19), 6.73 (s, 4 H; H-15), 6.98 (d, ^3J = 16.16 Hz, 2 H; H-12), 7.06 (d, ^3J = 16.16 Hz, 2 H; H-13), 7.09 (d, ^3J = 16.29 Hz, 2 H; H-6), 7.20 (d, ^3J = 16.29 Hz, 2 H; H-7), 7.53 (s, 8 H; H-9 + H-9' + H-10 + H-10'), 7.66 (d, ^4J = 1.54 Hz, 2 H; H-3), 7.81 (t, ^4J = 1.54 Hz, 1 H; H-5); ^{13}C NMR ($CDCl_3$): δ = 14.3 (C_p; CH_3), 22.9 (C_s; CH_2), 26.3 (C_s; CH_2), 29.4-30.0 (C_s; CH_2), 30.5 (C_s; CH_2), 32.1 (C_s; CH_2), 69.4 (C_s; C-19), 73.7 (C_s; C-18), 105.5 (C_t; C-15), 113.6 (C_q; C-2), 118.9 (C_q; C-1), 126.0 (C_t; C-6), 127.0 + 127.3(C_t; C-9 + C-9' + C-10 + C-10'), 127.2 (C_t; C-12), 128.5 (C_t; C-3 + C-5), 129.6 (C_t; C-13), 131.2 (C_t; C-7), 132.5 (C_q; C-14), 135.6 (C_q; C-8), 137.9 (C_q; C-11), 138.8 (C_q; C-17), 139.2 (C_q; C-4), 153.5 (C_q; C-16); MALDI-MS: m/z (%) calcd.: 1617.33 ($[M+1]^{+\cdot}$,100), found: 1617.35 ($[M+1]^{+\cdot}$,100).

Compound 64

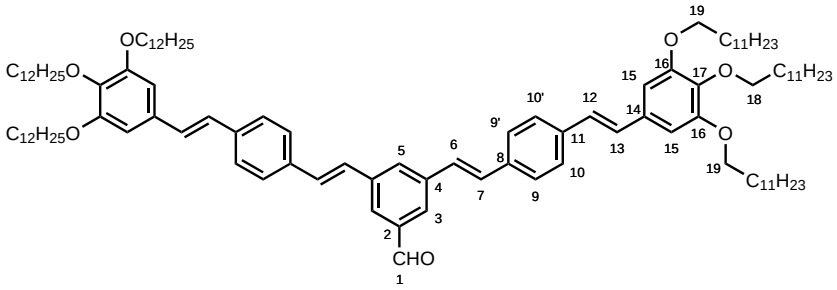

1.0 ml (1.00 mmol) of a 1M DIBAL solution (toluene) was added drop by drop to a stirred solution of 1.01 g (624 µmol) **63** in dry and degassed toluene at 0 °C under nitrogen atmosphere. The solution was then allowed to warm to room temperature and stirred overnight. 4.0 ml methanol was added in drops and the mixture was poured into 1M HCl. The solution was extracted with DCM, the organic solvent dried over Na_2SO_4 and evaporated under reduced pressure to yield 994 mg (613 µmol, 98%) of a yellow solid. ^{1}H NMR ($CDCl_3$): δ = 0.89 (t, ^3J = 6.86 Hz, 18 H; CH_3), 1.20-1.60 (m, 108 H ; $(CH_2)_9$–CH_3), 1.70-1.90 (m, 12 H ; OCH_2CH_2), 3.98 (t, ^3J = 6.58 Hz, 4 H; H-18), 4.04 (t, ^3J = 6.50 Hz, 8 H; H-19), 6.73 (s, 4 H; H-15), 6.98 (d, ^3J = 16.19 Hz, 2 H; H-12), 7.06 (d, ^3J = 16.19 Hz, 2 H; H-13), 7.18 (d, ^3J = 16.29 Hz, 2 H; H-6), 7.26 (d, ^3J = 16.29 Hz, 2 H; H-7), 7.52 (AA' of AA'BB', ^3J = 8.80 Hz, 4 H; H-10 + H-10'), 7.55 (BB' of AA'BB', ^3J = 8.80 Hz, 4 H; H-9 + H-9'), 7.86 (t, ^4J = 1.52 Hz, 1 H; H-5), 7.92 (d, ^4J = 1.52 Hz, 2 H; H-3), 10.09 (s, 1 H; H-1); ^{13}C NMR ($CDCl_3$): δ = 14.3 (C_p; CH_3), 22.9 (C_s; CH_2), 26.3 (C_s; CH_2), 29.4-30.0 (C_s; CH_2), 30.5 (C_s; CH_2), 32.1 (C_s; CH_2), 69.4 (C_s; C-19), 73.7 (C_s; C-18), 105.5 (C_t; C-15), 126.4 (C_t; C-3), 126.9(0) (C_t; C-6), 126.9(4) (C_t; C-10 + C-10'), 127.2 (C_t; C-9 + C-9' + C-12), 129.4 (C_t; C-13), 130.3 (C_t; C-5), 130.5 (C_t; C-7), 132.6 (C_q; C-14), 136.0 (C_q; C-8), 137.4 (C_q; C-2), 137.6 (C_q; C-11), 138.7 (C_q; C-17), 139.0 (C_q; C-4), 153.5 (C_q; C-16), 192.4 (C_t; C-1); MALDI-MS: m/z (%) calcd.: 1620.33 ($[M+1]^{+\cdot}$,100), found: 1620.38 ($[M+1]^{+\cdot}$,100).

Compound 65

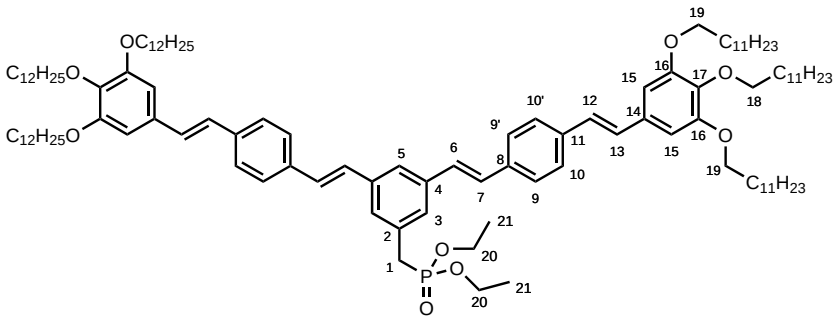

840 mg (518 µmol) **65** and 64.6 mg (1.71 mmol) $NaBH_4$ were refluxed in 30 ml THF and 0.1 ml H_2O overnight. At room temperature, the mixture was poured into 1M HCl, extracted with DCM, dried over Na_2SO_4 and evaporated under reduced pressure to yield 834 mg of a yellow solid.

The residue was dissolved in a solution of 10 ml DCM and 162 mg (618 µmol) PPh_3. At 0 °C under nitrogen atmosphere, a solution of 205 mg (618 µmol) CBr_4 in 1.0 ml DCM was added drop by drop. The solution was then allowed to warm to room temperature and stirred overnight.The solvent was evaporated under reduced pressure and the crude product subsequently was purified by column

chromatography on silica gel. Elution with cyclohexane / DCM (2 / 1) gave excess reagents and further elution with DCM as eluent yielded 690 mg of a yellow solid. The solid was dissolved in few $CHCl_3$ and precipitated from cold methanol to yield 673 mg of a yellow solid.
0.2 ml (194 mg, 1.17 mmol) $P(OEt)_3$ was added and the mixture was stirred at 130 °C for 30 minutes. At room temperature, the mixture was dissolved in few $CHCl_3$ and precipitated from cold methanol. The crude product was chromatographed on silica gel with DCM as eluent to yield 581 mg (333µmol, 64%) of a yellow solid. ^{1}H NMR ($CDCl_3$): δ = 0.88 (t, ^3J = 6.86 Hz, 18 H; CH_3), 1.20-1.60 (m, 108 H ; (CH_2)$_9$–CH_3), 1.70-1.90 (m, 12 H ; OCH_2CH_2), 3.21 (d, $^2J_{HP}$ = 21.56 Hz, 2 H; H-1 3.98 (t, ^3J = 6.58 Hz, 4 H; H-18), 4.03 (t, ^3J = 6.50 Hz, 8 H; H-19), 4.00-4.12 (m, ov, 4 H; H-20), 6.73 (s, 4 H; H-15), 6.98 (d, ^3J = 16.16 Hz, 2 H; H-12), 7.05 (d, ^3J = 16.16 Hz, 2 H; H-13), 7.12 (d, ^3J = 16.28 Hz, 2 H; H-6, 7.17 (d, ^3J = 16.28 Hz, 2 H; H-7, 7.37 (m, 2 H; H-3), 7.51 (AA'BB', 8 H; H-9 + H-9' + H-10 + H-10'), 7.55 (m, 1 H; H-5); ^{13}C NMR ($CDCl_3$): δ = 14.3 (C_p; O(CH$_2$)$_{11}$CH_3), 16.6 (C_p, $^3J_{CP}$ = 5.96 Hz; C-21), 22.9 (C_s; CH_2), 26.3 (C_s; CH_2), 29.4-30.0 (C_s; CH_2), 30.5 (C_s; CH_2), 32.1 (C_s; CH_2), 33.9 (C_s, $^1J_{CP}$ = 137.9 Hz; C-1), 62.4 (C_s, $^2J_{CP}$ = 6.74 Hz; C-20), 69.3 (C_s; C-19), 73.7 (C_s; C-18), 105.3 (C_t; C-15), 123.5 (C_t; C-5), 126.9 + 127.0 (C_t; C-9 + C-9' + C-10 + C-10'), 127.2 (C_t; C-3), 127.4 (C_t; C-12), 128.1 (C_t; C-6), 129.0 + 129.1 (C_t; C-7 + C-13), 132.5(7) (C_q, $^2J_{CP}$ = 9.20 Hz; C-2), 132.6(3) (C_q; C-14), 136.5 (C_q; C-8), 137.1 (C_q; C-11), 138.1 (C_q, $^4J_{CP}$ = 2.90 Hz; C-4), 138.5 (C_q; C-17), 153.5 (C_q; C-16); MALDI-MS: m/z (%) calcd.: 1742.38 ([M+1]$^{+\cdot}$,100), found: 1742.44 ([M+1]$^{+\cdot}$,100).

Compound 66

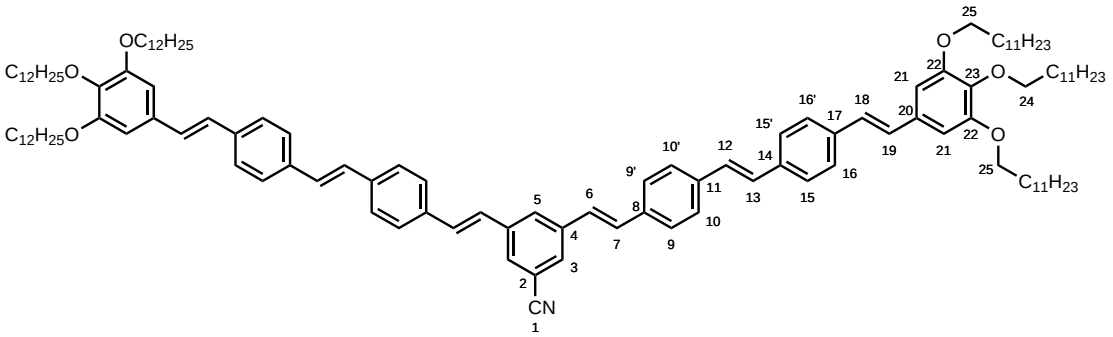

594 mg (5.29 mmol) potassium *tert*-butoxide was added in portions to a stirred solution of 583 mg (1.60 mmol) dialdehyde **9** and 2.95 g (3.34 mmol) phosphonate **39** in 20 mL dry THF under nitrogen atmosphere. Stirring at room temperature was continued for 1.5 hours. The reaction was then quenched with 2N HCl. The precipitate formed was collected, dissolved in few $CHCl_3$ and crystallized from cold methanol. The purification process was repeated and the residue dried in vacuo to yield 2.60 g (1.43 mmol, 89%) of a yellow solid. ^{1}H NMR ($CDCl_3$): δ = 0.89 (t, ^3J = 6.98 Hz, 18 H; CH_3), 1.20-1.60 (m, 108 H ; (CH_2)$_9$–CH_3), 1.70-1.90 (m, 12 H ; OCH_2CH_2), 3.98 (t, ^3J = 6.56 Hz, 4 H; H-24), 4.03 (t, ^3J = 6.48 Hz, 8 H; H-25), 6.73 (s, 4 H; H-21), 6.97 (d, ^3J = 16.20 Hz, 2 H; H-18), 7.04 (d, ^3J = 16.20 Hz, 2 H; H-19), 7.09 (d, ^3J = 16.26 Hz, 2 H; H-6), 7.12 + 7.16 (d, ^3J = 16.60 Hz, 4 H; H-12 + H-13), 7.20 (d, ^3J = 16.26 Hz, 2 H; H-7), 7.46-7.60 (AA'BB', 16 H; H-9 + H-9' + H-10 + H-10' + H-15 + H-15' + H-16 + H-16'), 7.66 (m, 2 H; H-3), 7.80 (m, 1 H; H-5), ^{13}C NMR ($CDCl_3$): δ = 14.3 (C_p; CH_3), 22.9 (C_s; CH_2), 26.3 (C_s; CH_2), 29.4-30.0 (C_s; CH_2), 30.5 (C_s; CH_2), 32.1 (C_s; CH_2), 69.4 (C_s; C-25), 73.7 (C_s; C-24), 105.5 (C_t; C-21), 113.6 (C_q; C-2), 118.9 (C_q; C-1), 126.1

(C_t; C-6), 126.8-127.4 (C_t; C-9 + C-9' + C-10 + C-10' + C-15 + C-15' + C-16 + C-16' + C-18), 128.0 + 129.0 (C_t; C-12 + C-13), 128.5 (C_t; C-3 + C-5), 129.2 (C_t; C-19), 131.2 (C_t; C-7), 132.6 (C_q; C-20), 135.8 + 136.5 + 137.2 + 137.8 (C_q; C-8 + C-11 + C-14 + C-17), 138.7 (C_q; C-23), 139.2 (C_q; C-4), 153.5 (C_q; C-22); MALDI-MS: m/z (%) calcd.: 1821.42 ($[M+1]^{+\cdot}$,100), found: 1821.42 ($[M+1]^{+\cdot}$,100).

Compound 67

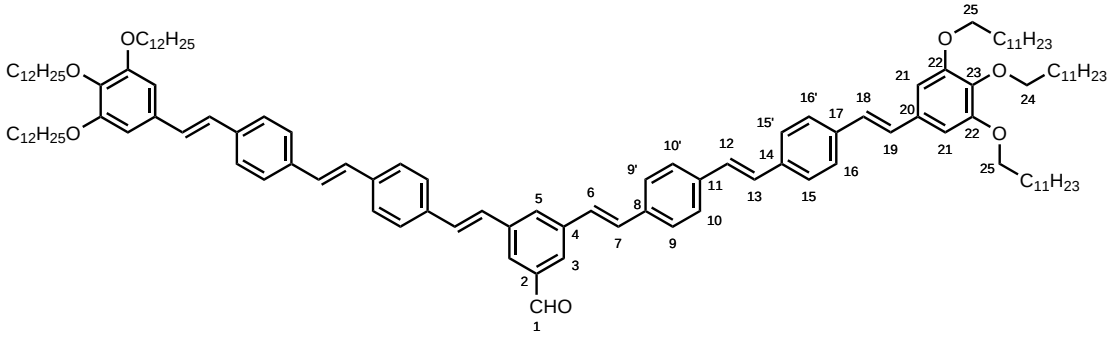

2.2 ml (2.20 mmol) of a 1M DIBAL solution (toluene) was added drop by drop to a stirred solution of 2.60 g (1.43 mmol) **66** in 2 ml dry and degassed toluene at 0 °C under nitrogen atmosphere. The solution was then allowed to warm to room temperature and stirred overnight. 8.0 ml methanol was added in drops and the mixture was poured into 2M HCl. The solution was extracted with $CHCl_3$, the organic solvent dried over Na_2SO_4 and evaporated under reduced pressure. The residue was recrystallized from $CHCl_3$ / methanol (1 / 2) to yield 2.46 g (1.35 mmol, 94%) of a yellow solid, which was used in the next step of synthesis without further purification. ^{1}H NMR ($CDCl_3$): δ = 0.89 (t, ^3J = 6.88 Hz, 18 H; CH_3), 1.20-1.60 (m, 108 H ; $(CH_2)_9$–CH_3), 1.70-1.90 (m, 12 H ; OCH_2CH_2), 3.98 (t, ^3J = 6.56 Hz, 4 H; H-24), 4.03 (t, ^3J = 6.56 Hz, 8 H; H-25), 6.73 (s, 4 H; H-21), 6.97 (d, ^3J = 16.20 Hz, 2 H; H-18), 7.04 (d, ^3J = 16.20 Hz, 2 H; H-19), 7.15 (s, 4 H; H-12 + H-13), 7.20 (d, ^3J = 16.10 Hz, 2 H; H-6), 7.27 (d, ^3J = 16.10 Hz, 2 H; H-7), 7.50 (AA' of AA'BB', ^3J = 8.86 Hz, 4 H; H-16 + H-16'), 7.53 (BB' of AA'BB', ^3J = 8.86 Hz, 4 H; H-15 + H-15'), 7.56 (AA'BB', 8 H; H-9 + H-9' + H-10 + H-10'), 7.88 (m, 1 H; H-5), 7.93 (d, ^4J = 1.48 Hz, 2 H; H-3), 10.10 (s, 1 H; H-1); ^{13}C NMR ($CDCl_3$): δ = 14.3 (C_p; CH_3), 22.9 (C_s; CH_2), 26.3 (C_s; CH_2), 29.4-30.0 (C_s; CH_2), 30.5 (C_s; CH_2), 32.1 (C_s; CH_2), 69.4 (C_s; C-25), 73.7 (C_s; C-24), 105.5 (C_t; C-21), 126.4 (C_t; C-3), 126.9 + 127.0(6) + 127.0(9) + 127.3 (C_t; C-9 + C-9' + C-10 + C-10' + C-15 + C-15' + C-16 + C-16'), 127.0(3) (C_t; C-6), 127.4 (C_t; C-19), 128.1 (C_t; C-12), 128.8 (C_t; C-13), 129.1 (C_t; C-18), 130.4 (C_t; C-5), 130.5 (C_t; C-7), 132.7 (C_q; C-20), 136.2 (C_q; C-8), 136.6 (C_q; C-17), 137.1 (C_q; C-14), 137.4(5) (C_q; C-2), 137.5(4) (C_q; C-11), 138.7 (C_q; C-23), 139.0 (C_q; C-4), 153.5 (C_q; C-22), 192.4 (C_t; C-1); MALDI-MS: m/z (%) calcd.: 1824.42 ($[M+1]^{+\cdot}$,100), found: 1821.45 ($[M+1]^{+\cdot}$,100).

Compound 68

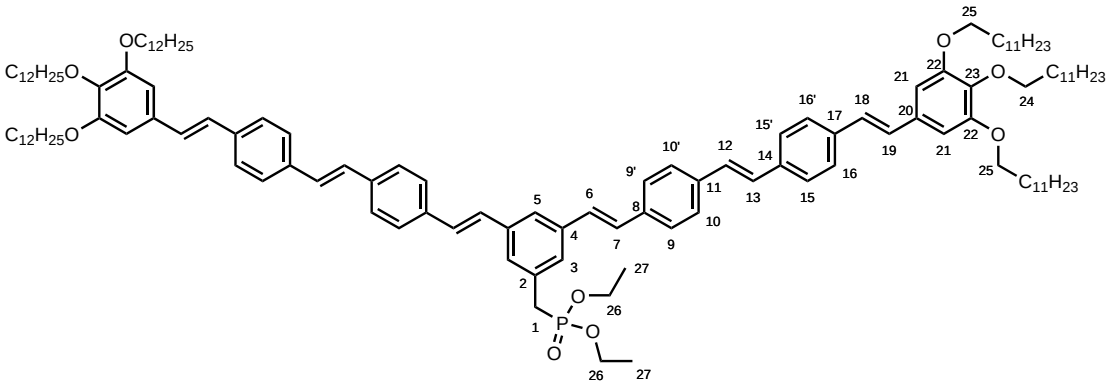

2.46 g (1.35 mmol) **67** and 51.1 mg (1.35 mmol) $NaBH_4$ were refluxed in 50 ml THF overnight. At room temperature, the mixture was poured into 0.5M HCl, extracted with $CHCl_3$, dried over Na_2SO_4 and evaporated under reduced pressure to yield 2.31 g of a yellow solid.

The residue was dissolved in 50 ml DCM and 0.1 ml (288 mg, 1.06 mmol) PBr_3 was added drop by drop at 0 °C. After stirring for 1.5 hours at room temperature, the mixture was treated with water and extracted with $CHCl_3$. The organic solvent was washed with water, dried over Na_2SO_4 and removed under reduced pressure. The residue was passed over a short silica gel column with $CHCl_3$ as eluent to yield 1.59 g of a yellow solid.

0.23 ml (223 mg, 1.34 mmol) $P(OEt)_3$ was added and the mixture was stirred at 140 °C for 3 hours. The crude product was chromatographed on silica gel with DCM as eluent to yield 780 mg (401 µmol, 30%) of a yellow solid. ^{1}H NMR ($CDCl_3$): δ = 0.88 (t, ^3J = 6.88 Hz, 18 H; CH_3), 1.20 - 1.60 (m, 114 H; (CH_2)$_9$–CH_3 + H-27), 1-70 - 1.90 (m, 12 H; OCH_2CH_2), 3.21 (d, $^2J_{HP}$ = 21.29 Hz, 2 H; H-1), 3.98 (t, ^3J = 6.58 Hz, 4 H; H-24), 4.03 (t, ^3J = 6.58 Hz, 8 H; H-25), 4.05 (m, 4 H; H-26), 6.73 (s, 4 H; H-21), 6.97 (d, ^3J = 16.12 Hz, 2 H; H-18), 7.04 (d, ^3J = 16.16 Hz, 2 H; H-19), 7.13 (d, ^3J = 16.20 Hz, 2 H; H-6), 7.14 (s, 4 H; H-12 + H-13), 7.18 (d, ^3J = 16.28 Hz, 2 H; H-7), 7.39 (m, 2 H; H-3), 7.49 (AA' of AA'BB', ^3J = 8.87 Hz, 4 H; H-16 + H-16'), 7.52 (BB' of AA'BB', ^3J = 8.73 Hz, 4 H; H-15 + H-15'), 7.54 (s, 8 H; H-9 + H-9' + H-10 + H-10'), 7.56 (m, 1 H; H-5); ^{13}C NMR ($CDCl_3$): δ = 14.3 (C_p; CH_3), 16.6 (C_p; d, $^3J_{CP}$ = 5.97 Hz, C-27), 22.9 (C_s; CH_2), 26.3 (C_s; CH_2), 29.4 - 30.0 (C_s; CH_2), 30.5 (C_s; CH_2), 32.0(9) (C_s; CH_2), 32.1(1) (C_s; CH_2), 33.9 (C_s; d, $^1J_{CP}$ = 137.8 Hz, C-1), 62.4 (C_s; d, $^2J_{CP}$ = 6.94 Hz, C-26), 69.4 (C_s; C-25), 73.7 (C_s; C-24), 105.4 (C_t; C-21), 123.5 (C_t; C-5), 126.9 + 127.0(2) + 127.0(4) + 127.1 (C_t; C-9 + C-9' + C-10 + C-10' + C-15 + C-15' + C-16 + C-16'), 127.3 (C_t; C-3), 127.4 (C_t; C-18), 128.2 + 128.3 + 128.5 (C_t; C-6 + C-12 + C-13), 129.0 (C_t; C-7 + C-19), 132.6 (C_q; d, $^2J_{CP}$ = 8.86 Hz, C-2), 132.7 (C_q; C-20), 136.6(5) + 136.7(1) + 137.0 + 137.1 (C_q; C-8 + C-11 + C-14 + C-17), 138.2 (C_q; d, $^4J_{CP}$ = 2.50 Hz, C-4), 138.6 (C_q; C-23), 153.5 (C_q; C-22); MALDI-MS: m/z (%) calcd.: 1946.47 ([M+1]$^{+\cdot}$,100), found: 1946.46 ([M+1]$^{+\cdot}$,100).

10.7 Synthesis of the Hekate stars with dodecyloxy-chains

Compound $S1_{C12}$

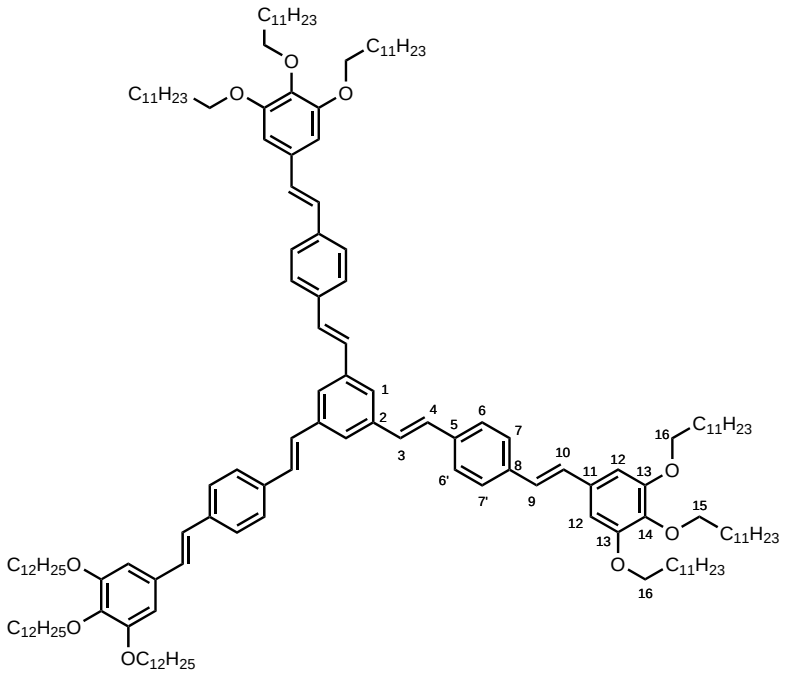

65.3 mg (582 µmol) potassium *tert*-butoxide was added in portions to a stirred solution of 41.3 mg (88.1 µmol) core building block **3** and 227 mg (291 µmol) phosphonate **36** in 5 mL dry THF under nitrogen atmosphere. After stirring overnight, the reaction was quenched with 1N HCl and the mixture was extracted with DCM. The organic solvent was dried over Na_2SO_4 and evaporated under reduced pressure. The residue was subjected to silica gel chromatography with DCM / cyclohexane (5 / 1) as eluent. The crude product was dissolved in few DCM and precipitated from methanol to yield 56.8 mg (24.2 µmol, 27%) of a yellow solid. Analytical data in accordance with literature.[133] ^{1}H NMR ($CDCl_3$): δ = 0.89 (t, ^3J = 6.84 Hz, 27 H; CH_3), 1.18 - 1.56 (m, 162 H; $(CH_2)_9$–CH_3), 1.70 - 1.90 (m, 18 H; OCH_2CH_2), 3.99 (t, ^3J = 7.62 Hz, 6 H; H-15), 4.04 (t, ^3J = 6.48 Hz, 12 H; H-16), 6.73 (s, 6 H; H-12), 6.99 (d, ^3J = 16.09 Hz, 3 H; H-9), 7.06 (d, ^3J = 16.09 Hz, 3 H; H-10), 7.17 (d, ^3J = 16.37 Hz, 3 H; H-3), 7.22 (d, ^3J = 16.37 Hz, 3 H; H-4), 7.52 (AA' of AA'BB', ^3J = 8.60 Hz, 6 H; H-6 + H-6'), 7.56 (BB' of AA'BB', ^3J = 8.60 Hz, 6 H; H-7 + H-7'), 7.58 (s, 3 H; H-1); ^{13}C NMR ($CDCl_3$): δ = 14.3 (C_p; CH_3), 22.9 (C_s; CH_2), 26.3 (C_s; CH_2), 29.5 - 30.0 (C_s; CH_2), 30.5 (C_s; CH_2), 32.1 (C_s; CH_2), 69.3 (C_s; C-16), 73.7 (C_s; C-15), 105.3 (C_t; C-12), 124.1 (C_t; C-1), 126.9 (C_t; C-6 + C-6'), 127.1 (C_t; C-7 + C-7'), 127.4 (C_t; C-9), 128.3 (C_t; C-3), 129.0(8) + 129.0(9) (C_t; C-4 + C-10), 132.6 (C_q; C-11), 136.5 (C_q; C-5), 137.1 (C_q; C-8), 138.3 (C_q; C-2), 138.5 (C_q; C-13), 153.5 (C_q; C-14).

Compound 69

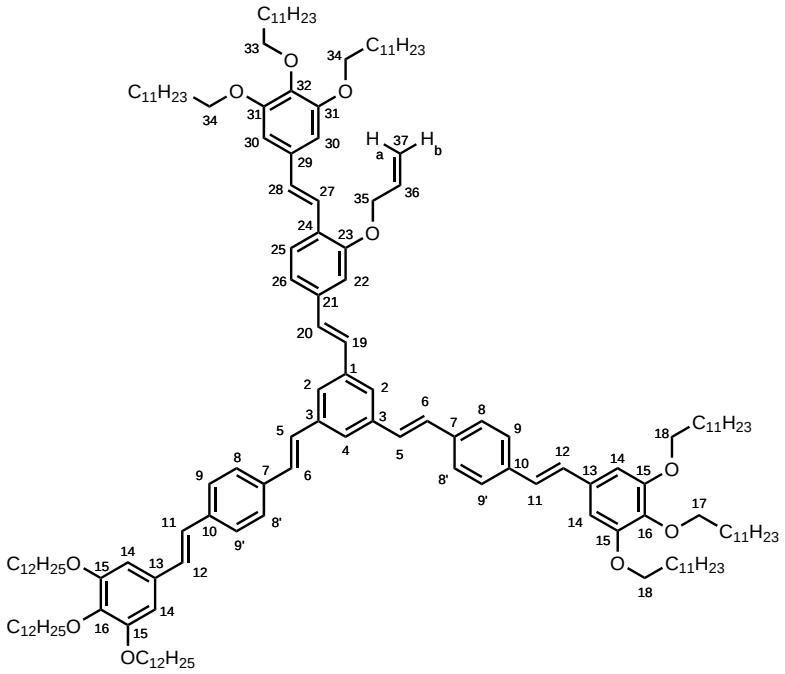

49.5 mg (441 µmol) potassium *tert*-butoxide was added in portions to a stirred solution of 513 mg (294 µmol) V-shaped building block **65** and 267 mg (327 µmol) arm building block **41** in 10 mL dry THF under nitrogen atmosphere. After stirring overnight, the reaction was quenched with 1N HCl and extracted with DCM. The organic solvent was dried over Na_2SO_4 and evaporated under reduced pressure. The residue was passed over a short silica gel column with DCM / cyclohexane (5 / 3) as eluent and the crude product was recrystallized from a mixture of 15 ml DCM and 7 ml ethanol at 4°C to to yield 478 mg (199 µmol, 68%) of a yellow solid. ^{1}H NMR ($CDCl_3$): δ = 0.88 (t, ^3J = 6.95 Hz, 27 H; CH_3), 1.20-1.60 (m, 162 H ; $(CH_2)_9$–CH_3), 1.70-1.90 (m, 18 H ; OCH_2CH_2), 3.98 (t, ^3J = 6.54 Hz, 6 H; H-17 + H-33), 4.04 (t, ^3J = 6.54 Hz, 12 H; H-18 + H-34), 4.72 (dt, ^3J = 4.98 Hz, ^4J= 1.51 Hz, 2 H; H-35), 5.36 (m, 1 H; H-37b), 5.53 (m, 1 H; H-37a), 6.17 (m, 1 H; H-36), 6.73 (s, 4 H; H-14), 6.75 (s, 2 H; H-30), 6.99 (d, ^3J = 16.27 Hz, 2 H; H-11), 7.06 (d, ^3J = 16.27 Hz, 2 H; H-12), 7.07 (d, ^3J = 16.21 Hz, 1 H; H-28), 7.08 (ov, 1 H; H-22), 7.14 (d, ^3J = 16.19 Hz, 1 H; H-19), 7.17 (d, ^3J = 16.27 Hz, 2 H; H-5), 7.18 (ov, 1 H; H-26), 7.20 (d, ^3J = 16.19 Hz, 1 H; H-20), 7.22 (d, ^3J = 16.27 Hz, 2 H; H-6), 7.39 (d, ^3J = 16.21 Hz, 1 H; H-27), 7.52 (AA' of AA'BB', ^3J = 8.76 Hz, 4 H; H-8 + H-8'), 7.56 (BB' of AA'BB', ^3J = 8.76 Hz, 4 H; H-9 + H-9'), 7.58 (s, 3 H; H-2 + H-4), 7.60 (d, ^3J = 8.28 Hz, 1 H; H-25); ^{13}C NMR ($CDCl_3$): δ = 14.3 (C_p; CH_3), 22.9 (C_s; CH_2), 26.3 (C_s; CH_2), 29.4-30.0 (C_s; CH_2), 30.5 (C_s; CH_2), 32.1 (C_s; CH_2), 69.3 (C_s; C-18 + C-34), 69.5 (C_s; C-35), 73.7 (C_s; C-17 + C-33), 105.3 (C_t; C-14), 105.4 (C_t; C-30), 110.7 (C_t; C-22), 117.4 (C_s; C-37), 119.9 (C_t; C-26), 122.3 (C_t; C-27), 124.0 (C_t; C-2), 124.2 (C_t; C-4), 126.7 (C_t; C-25), 126.8 (C_q; C-24), 126.9 (C_t; C-8 + C-8'), 127.1 (C_t; C-9 + C-9'), 127.3 (C_t; C-11), 128.2 (C_t; C-5), 128.4 (C_t; C-19), 129.0(6) + 129.1(0) (C_t; C-6 + C-12), 129.3 (C_t; C-20), 129.5 (C_t; C-28), 132.6 (C_q; C-13), 133.3 (C_q; C-29), 133.5 (C_t; C-36), 136.5 (C_q; C-7), 137.1 (C_q; C-10), 137.6 (C_q; C-21), 138.2 + 138.3 + 138.4 + 138.5 (C_q; C-1 + C-3 + C-16 + C-32), 153.4 (C_q; C-31), 153.5 (C_q; C-15), 156.2 (C_q; C-23); MALDI-MS: m/z (%) calcd.: 2405.00 ($[M+1]^{+\cdot}$,100), found: 2405.09 ($[M+1]^{+\cdot}$,100).

Compound 70

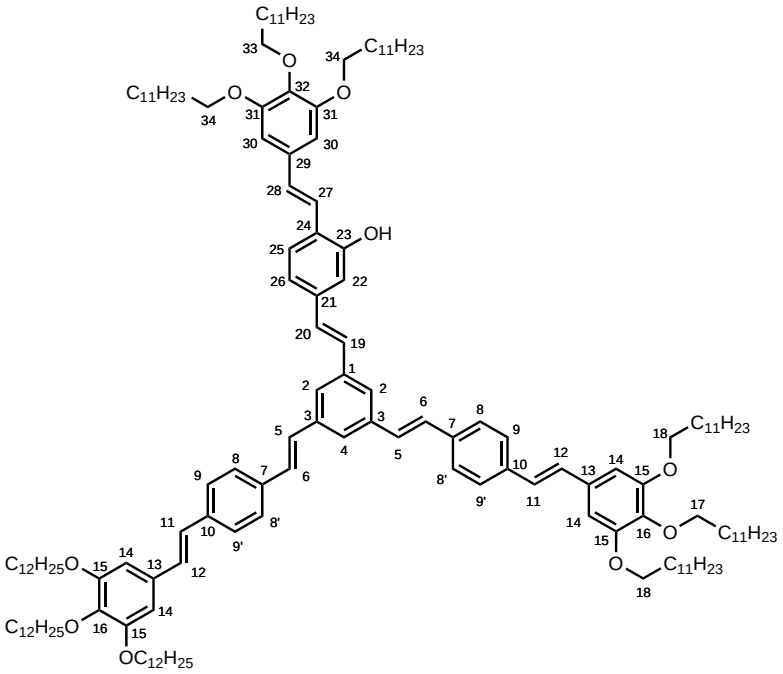

200 mg (83.1 µmol) **69** and 17.1 mg (14.8 µmol) $Pd(PPh_3)_4$ were stirred at room temperature in 5 ml degassed THF under nitrogen atmosphere. 0.25 ml (250 mg, 2.87 mmol) morpholine was then added drop by drop and the reaction was stirred for 7 hours at 50 °C. The reaction was quenched with 1N HCl and extracted with DCM. The organic solvent was dried over Na_2SO_4 and evaporated under reduced pressure. The crude product was chromatographed on silica gel with DCM as eluent to yield 144 mg (60.9 µmol, 73%) of a yellow solid. ^{1}H NMR ($CDCl_3$): δ = 0.89 (t, ^3J = 6.85 Hz, 27 H; CH_3), 1.20-1.60 (m, 162 H ; $(CH_2)_9$–CH_3), 1.70-1.90 (m, 18 H ; OCH_2CH_2), 3.98 (t, ^3J = 6.56 Hz, 6 H; H-17 + H-33), 4.03 (t, ^3J = 6.46 Hz, 12 H; H-18 + H-34), 5.18 (s, 1 H; OH), 6.73 (s, 4 H; H-14), 6.74 (s, 2 H; H-30), 6.98 (d, ^3J = 16.22 Hz, 2 H; H-11), 7.00 (ov, 1 H; H-22), 7.05 (d, ^3J = 16.22 Hz, 2 H; H-12), 7.06 (d, ^3J = 16.32 Hz, 1 H; H-28), 7.12 (s, 2 H; H-19 + H-20), 7.15 (d, ^3J = 8.40 Hz, 1 H; H-26), 7.16 (d, ^3J = 16.38 Hz, 2 H; H-5), 7.21 (d, ^3J = 16.38 Hz, 2 H; H-6), 7.23 (d, ^3J = 16.32 Hz, 1 H; H-27), 7.44-7.55 (m, 11 H; H-2 + H-8 + H-8' + H-9 + H-9' + H-25), 7.56 (m, 1 H; H-4); ^{13}C NMR ($CDCl_3$): δ = 14.3 (C_p; CH_3), 22.9 (C_s; CH_2), 26.3 (C_s; CH_2), 29.4-30.0 (C_s; CH_2), 30.5 (C_s; CH_2), 32.1 (C_s; CH_2), 69.3 (C_s; C-18), 73.7 (C_s; C-33), 73.8 (C_s; C-17), 105.2(8) (C_t; C-14), 105.3(3) (C_t; C-30), 113.7 (C_t; C-22), 120.0 (C_t; C-26), 122.0 (C_t; C-27), 124.0 (C_t; C-4), 124.1 (C_t; C-2), 124.7 (C_q; C-24), 126.9 (C_t; C-8 + C-8'), 127.1 (C_t; C-9 + C-9'), 127.3 (C_t; C-25), 127.4 (C_t; C-11), 128.2 (C_t; C-5), 128.5 + 128.8 (C_t; C-19 + C-20), 129.0 (C_t; C-6 + C-12), 130.1 (C_t; C-28), 132.7 (C_q; C-13), 133.1 (C_q; C-29), 136.5 (C_q; C-7), 137.1 (C_q; C-10), 137.7 (C_q; C-21), 138.1(6) + 138.2(0) + 138.4 (C_q; C-1 + C-3 + C-16 + C-32), 153.4(2) (C_q; C-31), 153.4(4) (C_q; C-15), 153.5 (C_q; C-23); MALDI-MS: m/z (%) calcd.: 2364.97 ($[M+1]^{+\cdot}$,100), found: 2364.99 ($[M+1]^{+\cdot}$,95); ESI-HRMS: m/z calcd. for $C_{162}H_{258}O_{10}Na^+$ ($[M+Na]^+$): 2386.9572, found: 2386.9497.

Compound $S1_{C12}$-$F1_{C4}$

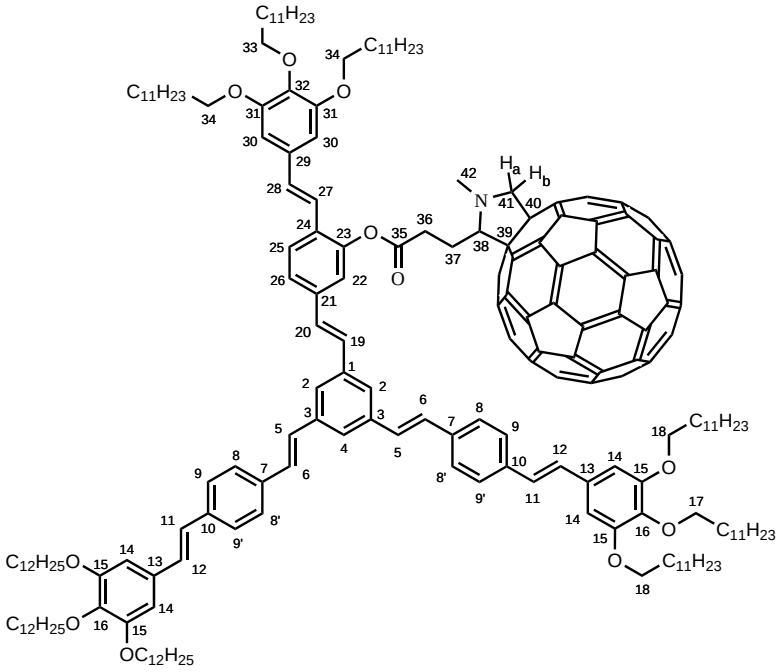

80.2 mg (33.9 µmol) **70**, 57.6 mg (67.8 µmol) carboxylic acid **23**, 26.8 mg (91.0 µmol) DPTS and 79.5 mg (385 µmol) DCC were stirred in 9 ml dry DCM at room temperature under nitrogen atmosphere for 6 days. The solution was concentrated in vacuo and subjected to silica gel chromatography with $CHCl_3$ / cyclohexane (1 / 1 → pure $CHCl_3$) as eluent. The crude product was dissolved in few $CHCl_3$ and precipitated from methanol twice to yield 16.2 mg (5.07 µmol, 15%) of a brown solid. ^{1}H NMR ($CDCl_3$): δ = 0.88 (t, ^3J = 6.82 Hz, 27 H; CH_3), 1.20 - 1.60 (m, 162 H; $(CH_2)_9$–CH_3), 1.70 - 1.90 (m, 18 H; OCH_2CH_2), 2.84 + 3.33 (m, 4 H; H-36 + H-37), 3.02 (s, 3 H; H-42), 3.91 - 4.17 (m, 18 H; H-17 + H-18 + H-33 + H-34), 4.09 (m, 1 H; H-38), 4.17 (m, 1 H; H-41a), 4.84 (m, 1 H; H-41b), 6.70 + 6.73 (s, 6 H; H-14 + H-30), 6.93 - 7.08 (m, 6 H; H-11 + H-12 + H-27 + H-28), 7.14 (d, ^3J = 16.19 Hz, 2 H; H-5), 7.15 (m, 2 H; H-19 + H-20), 7.20 (d, ^3J = 16.19 Hz, 2 H; H-6), 7.24 (m, 1 H; H-22), 7.42 (m, 1 H; H-26), 7.46 - 7.58 (m, 11 H; H-2 + H-4 + H-8 + H-8' + H-9 + H-9'), 7.63 (d, ^3J = 8.56 Hz, 1 H; H-25); ^{13}C NMR ($CDCl_3$): δ = 14.3 (C_p; CH_3), 22.9 (C_s; CH_2), 25.6 + 31.3 (C_s; C-37 + C-38), 26.3 (C_s; CH_2), 26.4 (C_s; CH_2), 29.5 - 30.5 (C_s; CH_2), 32.1 (C_s; CH_2), 40.2 (C_p; C-42), 69.3 + 69.5 (C_s; C-18 + C-34), 70.1(8) (C_q; C-40), 70.2(3) (C_s; C-41), 73.7 (C_s; C-17 + C-33), 76.0 (C_q; C-39), 76.9 (C_t; C-38), 105.3 + 105.8 (C_t; C-14 + C-30), 120.5 (C_t; C-22), 121.1 (C_t; C-27), 124.2 (C_t; C-2 + C-4), 124.9 (C_t; C-26), 126.9 + 127.1 (C_t; C-8 + C-8' + C-9 + C-9'), 127.3 (C_t; C-25), 127.4 (C_t; C-11), 128.1 + 129.4 (C_t; C-19 + C-20), 128.2 (C_t; C-5), 129.1 (C_t; C-6 + C-12), 129.6 (C_q; C-24), 131.8 (C_t; C-28), 132.6* (C_q; C-13), 135.6 (C_q; C_{58}), 136.0 (C_q; C_{58}), 136.4 (C_q; C-7 + C_{58}), 137.1 (C_q; C-10), 137.5 (C_q; C_{58}), 137.8 + 138.3 + 138.5 (C_q; C-1 + C-3 + C-16 + C-21), 139.9 + 140.3 + 140.5 + 140.6 + 141.9 + 142.0 + 142.1(9) + 142.2(2) + 142.2(7) + 142.3(1) + 142.8 + 142.9 + 143.2 + 143.3 + 144.4(7) + 144.5(3) + 144.6 + 144.9 + 145.3(6) + 145.4(2) + 145.5 + 145.6 + 145.7 + 145.9 + 146.1 + 146.1(5) + 146.2(1) + 146.2(6) + 146.3(0) + 146.4 + 146.5 + 147.3(7) + 147.4(3) (C_q; C_{58}), 148.5 (C_q; C-23), 152.8 (C_q; C_{58}), 153.4(6) (C_q;

*A signal corresponding to the atom C-29 could not be located with certainty.

C-15), 153.4(9) (C_q; C-31), 153.7* (C_q; C_{58}), 156.3 (C_q; C_{58}), 171.9 (C_q; C-35); MALDI-MS: m/z (%) calcd.: 3197.04 ([M+2]$^{+\cdot}$,100), found: 3197.05 ([M+2]$^{+\cdot}$,100); MALDI-HRMS: m/z calcd. for $C_{228}H_{266}NO_{11}^+$ ([M-H]$^+$): 3194.0280, found: 3194.0269; Elemental analysis (%) for $C_{228}H_{267}NO_{11}$ calcd.: C 85.64, H 8.42, N 0.44, found: C 82.88, H 8.54, N 0.38. For the discussion of elemental analysis results regarding fullerene containing materials, see page 119.

Compound S2$_{C12}$

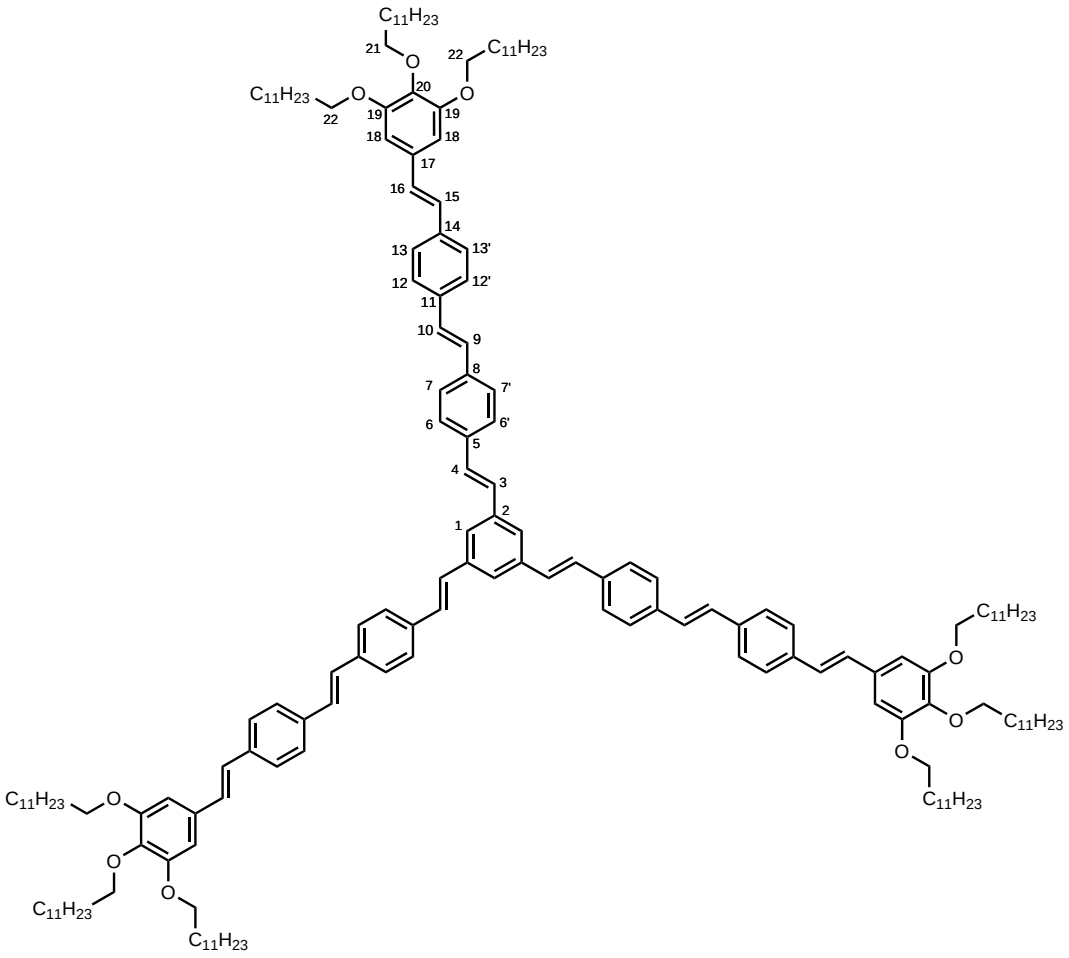

80.3 mg (716 µmol) potassium *tert*-butoxide was added in portions to a stirred solution of 50.0 mg (107 µmol) core building block **3** and 284 mg (322 µmol) phosphonate **39** in 2 mL dry THF under nitrogen atmosphere. After stirring overnight, the reaction was quenched with 1N HCl and the mixture was extracted with DCM. The organic solvent was dried over Na_2SO_4 and evaporated under reduced pressure. The residue was subjected to silica gel chromatography with DCM / cyclohexane (5 / 1) as eluent. The residue was crystallized from cold methanol and passed over a short silica gel column with cyclohexane / ethyl acetate (7 / 1) as eluent to yield 186 mg (70.0 µmol, 65%) of a yellow solid. Analytical data in accordance with literature.[132] ^{1}H NMR ($CDCl_3$): δ = 0.89 (t, ^3J = 6.86 Hz, 27 H; CH_3), 1.18 - 1.56 (m, 162 H; (CH_2)$_9$–CH_3), 1.70 - 1.90 (m, 18 H; OCH_2CH_2), 3.98 (t, ^3J = 6.58 Hz, 6 H; H-21), 4.03 (t, ^3J = 6.52 Hz, 12 H; H-22), 6.73 (s, 6 H; H-18), 6.97 (d, ^3J = 16.12 Hz, 3 H; H-15), 7.04 (d, ^3J = 16.20 Hz, 3 H; H-16), 7.15 (s, 6 H; H-9 + H-10), 7.18 (d, ^3J = 16.20 Hz, 3 H; H-3), 7.23 (d, ^3J = 16.48 Hz, 3 H; H-4), 7.48 - 7.54 (m, 12 H; H-12 + H-12' + H-13 + H-13'), 7.54 - 7.59 (m, 12 H; H-6 + H-6' + H-7 + H-7'), 7.59 (s, 3 H; H-1); ^{13}C NMR ($CDCl_3$): δ = 14.3 (C_p;

*One additional signal with an expected value of approx. 150 ppm (C_{60}) could not be detected with certainty.

CH_3), 22.9 (C_s; CH_2), 26.3 (C_s; CH_2), 29.5 - 30.0 (C_s; CH_2), 30.5 (C_s; CH_2), 32.1 (C_s; CH_2), 69.3 (C_s; C-22), 73.7 (C_s; C-21), 105.3 (C_t; C-18), 124.1 (C_t; C-1), 126.9 + 127.0 + 127.1 (C_t; C-6 + C-6' + C-7 + C-7' + C-12 + C-12' + C-13 + C-13'), 127.3 (C_t; C-15), 128.1 + 128.3 + 128.4 (C_t; C-3 + C-9 + C-10), 128.9 + 129.0 (C_t; C-4 + C-16), 132.6 (C_q; C-17), 136.6 + 136.7 + 137.0 (C_q; C-5 + C-8 + C-11 + C-14), 138.2 (C_q; C-2), 138.5 (C_q; C-20), 153.4 (C_q; C-19); MALDI-MS: m/z (%) calcd.: 2656.1 ([M+2]$^{+\cdot}$,100), found: 2656.2 ([M+2]$^{+\cdot}$,100); Elemental analysis (%) for $C_{186}H_{276}O_9$ calcd.: C 84.11, H 10.47, found: C 83.91, H 10.91.

Compound 71

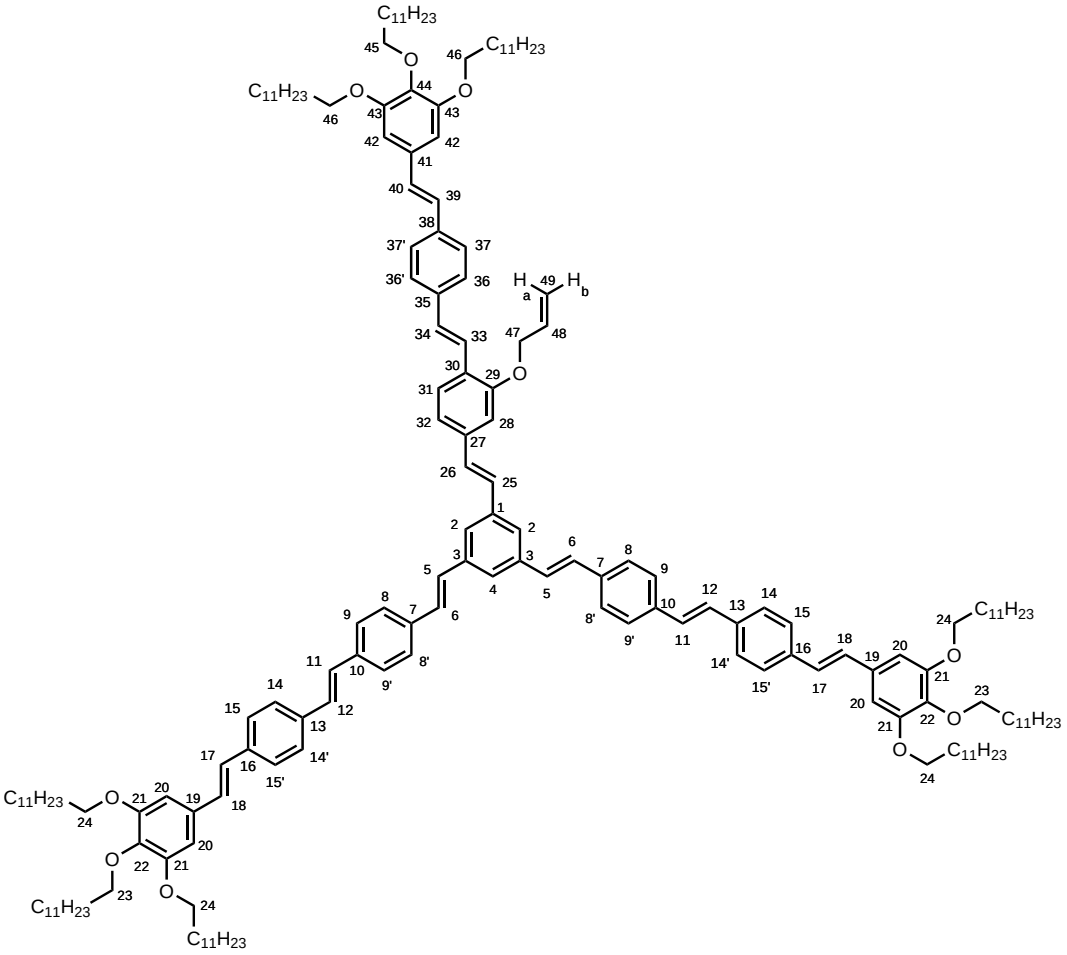

98.7 mg (880 µmol) potassium *tert*-butoxide was added in portions to a stirred solution of 780 mg (401 µmol) V-shaped building block **68** and 411 mg (447 µmol) arm building block **43** in 20 mL dry THF under nitrogen atmosphere. After stirring overnight, the reaction was quenched with 1N HCl and the precipitate was collected, washed with cold methanol and passed over a short silica gel column with DCM / cyclohexane (1 / 1) as eluent to yield 854 mg (315 µmol, 79%) of a yellow solid. ^{1}H NMR ($CDCl_3$): δ = 0.89 (t, ^3J = 6.88 Hz, 27 H; CH_3), 1.20 - 1.90 (m, 180 H; CH_2), 3.98 (t, ^3J = 6.88 Hz, 6 H; H-23 + H-45), 4.03 (t, ^3J = 6.58 Hz, 12 H; H-24 + H-46), 4.73 (dt, ^3J = 5.14 Hz, ^4J = 1.45 Hz, 2 H; H-47), 5.38 (m, 1 H; H-49b), 5.54 (m, 1 H; H-49a), 6.19 (m, 1 H; H-48), 6.73 (s, 6 H; H-20 + H-42), 6.97 (d, ^3J = 16.16 Hz, 3 H; H-17 + H-39), 7.03(4) (d, ^3J = 16.16 Hz, 1 H; H-40), 7.03(9) (d, ^3J = 16.16 Hz, 2 H; H-18), 7.09 (m, 1 H; H-28), 7.12 - 7.26 (m, 12 H; H-5 + H-6 + H-11 + H-12 + H-25 + H-26 + H-32 + H-34), 7.46 - 7.60 (m, 24 H; H-2 + H-4 + H-8 + H-8' + H-9 + H-9' + H-14 + H-14' + H-15 + H-15' + H-33 + H-36 + H-36' + H-37 + H-37'), 7.64 (d, ^3J =

8.32 Hz, 1 H; H-31); ^{13}C NMR ($CDCl_3$): δ = 14.3 (C_p; CH_3), 22.8 - 32.1 (C_s; CH_2), 69.4 (C_s; C-24 + C-46), 69.5 (C_s; C-47), 73.7 (C_s; C-23 + C-45), 105.4 (C_t; C-20 + C-42), 110.6 (C_t; C-28), 117.7 (C_s; C-49), 119.9 (C_t; C-32), 123.1 (C_t; C-33), 124.1 (C_t; C-2 + C-4), 126.7 (C_q; C-30), 126.8 + 126.9 + 127.0 + 127.0(6) + 127.1(2) + 127.4 + 127.5 (C_t; C-8 + C-8' + C-9 + C-9' + C-14 + C-14' + C-15 + C-15' + C-17 + C-31 + C-36 + C-36' + C-37 + C-37' + C-39), 128.2 + 128.4 + 128.5 + 128.78 + 129.1 (C_t; C-5 + C-6 + C-11 + C-12 + C-18 + C-25 + C-26 + C-34 + C-40), 132.6(7) (C_q; C-19), 132.7(4) (C_q; C-41), 133.5 (C_t; C-48), 136.6 + 136.7 + 136.8 + 137.0(5) + 137.1(0) + 137.4 + 138.2 + 138.3 (C_q; C-1 + C-3 + C-7 + C-10 + C-13 + C-16 + C-35 + C-38), 137.8 (C_q; C-27), 138.5(5) (C_q; C-44), 138.6(1) (C_q; C-22), 153.5 (C_q; C-21 + C-43), 156.4 (C_q; C-29); MALDI-MS: m/z (%) calcd.: 2712.15 ($[M+2]^{+\cdot}$,100), found: 2712.17 ($[M+2]^{+\cdot}$,100).

Compound 72

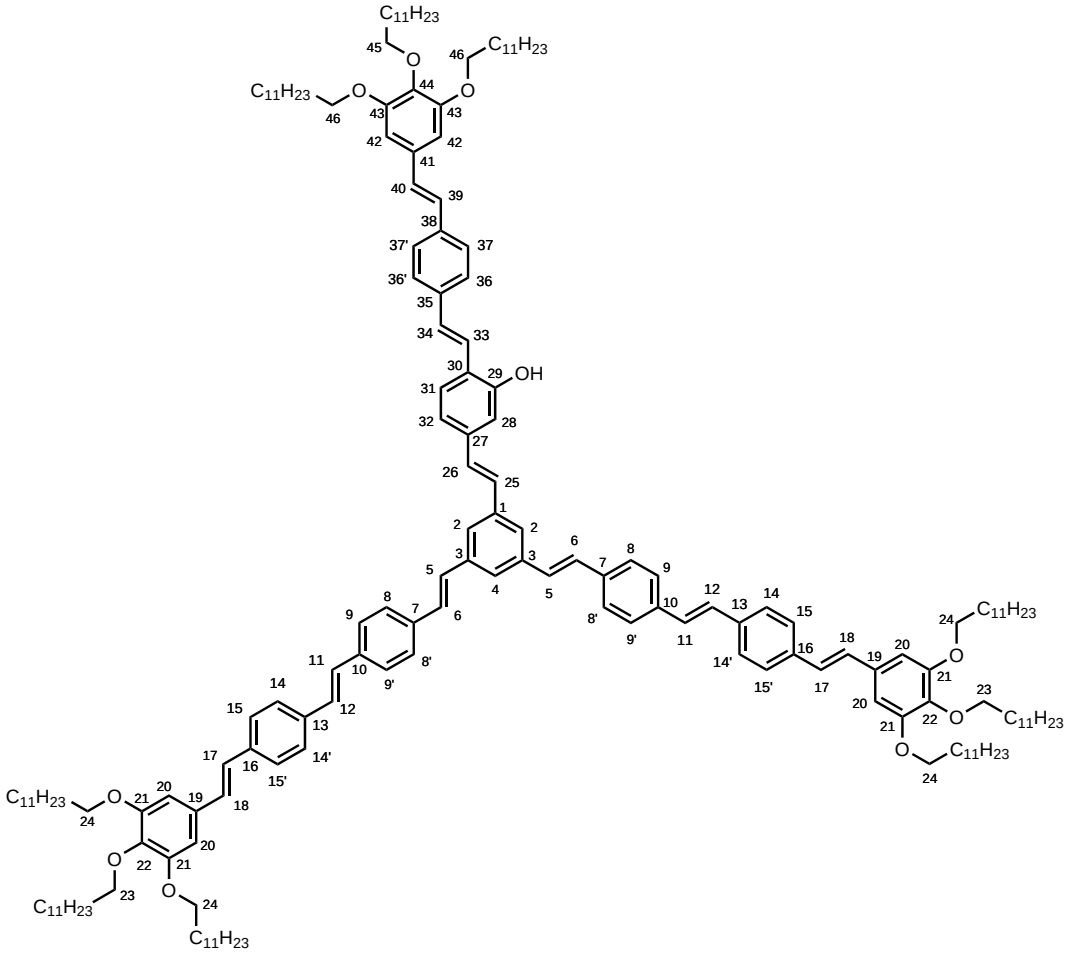

670 mg (247 µmol) **71**, 56.2 mg (1.49 mmol) $NaBH_4$ and 29.2 mg (25.3 µmol) $Pd(PPh_3)_4$ were stirred at room temperature in 30 ml degassed THF under nitrogen atmosphere for 72 hours. The reaction was quenched with 2N HCl and extracted with DCM. The organic solvent was dried over Na_2SO_4 and evaporated under reduced pressure. The residue was passed over a short silica gel column with DCM as eluent and crystallized from cold methanol to yield 578 mg (216 µmol, 87%) of a yellow solid. ^{1}H NMR ($CDCl_3$): δ = 0.89 (t, ^3J = 6.88 Hz, 27 H; CH_3), 1.20 - 1.90 (m, 180 H; CH_2), 3.98 (t, ^3J = 6.58 Hz, 6 H; H-23 + H-45), 4.03 (t, ^3J = 6.28 Hz, 12 H; H-24 + H-26), 6.72 (s, 6 H; H-20 + H-42), 6.92 - 7.08 (m, 7 H; H-17 + H-18 + H-28 + H-39 + H-40), 7.08 - 7.25 (m, 12 H; H-5 + H-6 + H-11 + H-12 + H-25 + H-26 + H-32 + H-34), 7.41 (d, ^3J = 16.25 Hz, 1 H; H-33), 7.45 - 7.59 (m, 25

H; H-2 + H-4 + H-8 + H-8' + H-9 + H-9' + H-14 + H-14' + H-15 + H-15' + H-31 + H-36 + H-36' + H-37 + H-37'), ^{13}C NMR ($CDCl_3$): δ = 14.3 (C_p; CH_3), 22.8 - 32.1 (C_s; CH_2), 69.4 (C_s; C-24 + C-46), 73.8 (C_s; C-23 + C-45), 105.4 (C_t; C-20 + C-42), 113.8 (C_t; C-28), 120.0 (C_t; C-32), 122.9 (C_t; C-33), 124.2 (C_t; C-2 + C-4), 124.6 (C_q; C-30), 126.8 + 126.9 + 127.0 + 127.1 + 127.2 + 127.4 + 127.5 (C_t; C-8 + C-8' + C-9 + C-9' + C-14 + C-14' + C-15 + C-15' + C-17 + C-31 + C-36 + C-36' + C-37 + C-37' + C-39), 128.1 + 128.3 + 128.4 + 128.6 + 128.8 + 129.0 + 129.2 (C_t; C-5 + C-6 + C-11 + C-12 + C-18 + C-25 + C-26 + C-34 + C-40), 132.8 (C_q; C-19 + C-41), 136.6 + 136.7 + 136.8 + 136.9(7) + 137.0(1) + 137.2 + 138.1(4) + 138.1(7) (C_q; C-1 + C-3 + C-7 + C-10 + C-13 + C-16 + C-35 + C-38), 137.9 (C_q; C-27), 138.4 (C_q; C-22), 138.5 (C_q; C-44), 153.4 (C_q; C-21 + C-43), 153.7 (C_q; C-29); MALDI-MS: m/z (%) calcd.: 2672.12 ([M+2]$^{+\cdot}$,100), found: 2672.11 ([M+2]$^{+\cdot}$,100); Elemental analysis (%) for $C_{186}H_{276}O_{10}$ calcd.: C 83.60, H 10.41, found: C 83.51, H 10.45.

Compound S2$_{C12}$-F1$_{C4}$

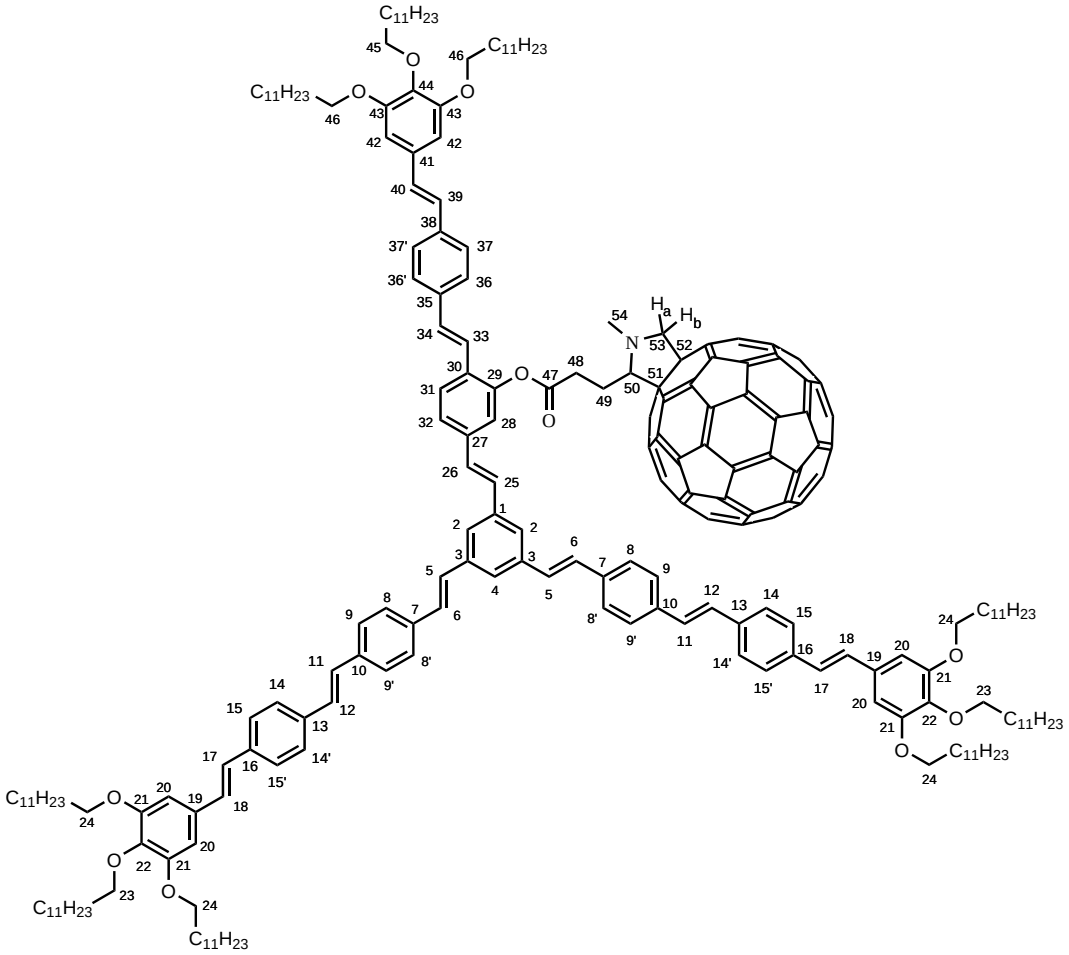

100 mg (37.4 µmol) **72**, 72.7 mg (85.5 µmol) carboxylic acid **23**, 37.5 mg (127 µmol) DPTS and 91.6 mg (444 µmol) DCC were stirred in 10 ml dry DCM at room temperature under nitrogen atmosphere for 8 days. The solution was concentrated in vacuo and subjected to silica gel chromatography with cyclohexane / DCM (4 / 1) as eluent. Excess reagents were removed by crystallizing the crude product from methanol twice to yield 68.7 mg (19.6 µmol, 52%) of a brown solid. ^{1}H NMR ($CDCl_3$): δ = 0.89 (t, ^3J = 6.80 Hz, 27 H; CH_3), 1.20 - 1.90 (m, 180 H; CH_2), 2.95 + 3.35 (m, 4 H; H-48 + H-49), 3.03 (s, 3 H; H-54), 3.98 (t, ^3J = 6.58 Hz, 6 H; H-23 + H-45), 4.03 (t, ^3J = 6.38 Hz, 12 H; H-24 + H-26), 4.09 (t, ^3J = 5.28 Hz, 1 H; H-50), 4.17 (d, ^2J = 9.80 Hz, 1 H; H-53a), 4.85 (d, ^2J = 9.80 Hz,

1 H; H-53b), 6.67 + 6.72 (s, 6 H; H-20 + H-42), 6.88 - 7.24 (m, 18 H; H-5 + H-6 + H-11 + H-12 + H-17 + H-18 + H-25 + H-26 + H-33 + H-34 + H-39 + H-40), 7.29 (m, 1 H; H-28), 7.36 - 7.59 (m, 24 H; H-2 + H-4 + H-8 + H-8' + H-9 + H-9' + H-14 + H-14' + H-15 + H-15' + H-32 + H-36 + H-36' + H-37 + H-37'), 7.69 (d, ^{3}J = 6.80 Hz, 1 H; H-31); ^{13}C NMR ($CDCl_3$): δ = 14.3 (C_p; CH_3), 22.8 - 32.1 (C_s; CH_2), 25.5 + 31.3 (C_s; C-48 + C-49), 40.2 (C_p; C-54), 69.4 (C_s; C-24 + C-46), 70.2 (C_q; C-52), 70.3 (C_s; C-53), 73.7 (C_s; C-23 + C-45), 76.0 (C_q; C-51), 77.0 (C_t; C-50), 105.3(5) + 105.4(2) (C_t; C-20 + C-42), 120.5 (C_t; C-28), 121.4 (C_t; C-33), 124.3 (C_t; C-2 + C-4), 124.9 (C_t; C-32), 126.9 + 127.1 + 127.2 + 127.4 (C_t; C-8 + C-8' + C-9 + C-9' + C-14 + C-14' + C-15 + C-15' + C-17 + C-31 + C-36 + C-36' + C-37 + C-37' + C-39), 128.2 + 128.3 + 128.5 + 129.1 + 129.3(6) + 130.7 (C_t; C-5 + C-6 + C-11 + C-12 + C-18 + C-25 + C-26 + C-34 + C-40), 129.3(9) (C_q; C-30), 132.6 (C_q; C-41), 132.7 (C_q; C-19), 135.6 + 136.2 + 136.4(2) + 137.4 + 137.6 + 140.0 + 140.2 + 140.4 + 140.5 + 141.9 + 142.1 + 142.3 + 142.4 + 142.8 + 142.9 + 143.2 + 143.4 + 144.5 + 144.6 + 144.7 + 144.9 + 145.4 + 145.5 + 145.6(7) + 145.7(1) + 145.9 + 146.1(7) + 146.2(4) + 146.3 + 146.3(9) + 146.4(4) + 146.5 + 146.6 + 147.4 + 147.5 + 152.9 + 154.2 + 154.5 + 156.4 (C_q; C_{58}), 136.3(5) + 136.6 + 136.7 + 137.0 + 137.1 + 137.4 + 137.8 + 138.0 + 138.3 (C_q; C-1 + C-3 + C-7 + C-10 + C-13 + C-16 + C-27 + C-35 + C-38), 138.5(6) (C_q; C-44), 138.5(9) (C_q; C-22), 148.6 (C_q; C-29), 153.5 (C_q; C-21 + C-43), 171.8 (C_q; C-47); MALDI-MS: m/z (%) calcd.: 3503.18 ($[M+2]^{+\cdot}$,100), found: 3503.09 ($[M+2]^{+\cdot}$,100); MALDI-HRMS: m/z calcd. for $C_{252}H_{285}NO_{11}^{+\cdot}$ ($[M]^{+\cdot}$): 3501.1767, found: 3501.1949; Elemental analysis (%) for $C_{252}H_{285}NO_{11}$ calcd.: C 86.38, H 8.20, N 0.40, found: C 85.91, H 8.65, N 0.66. For the discussion of elemental analysis results regarding fullerene containing materials, see page 119.

Compound $S2_{C12}$-$F1_{C10}$

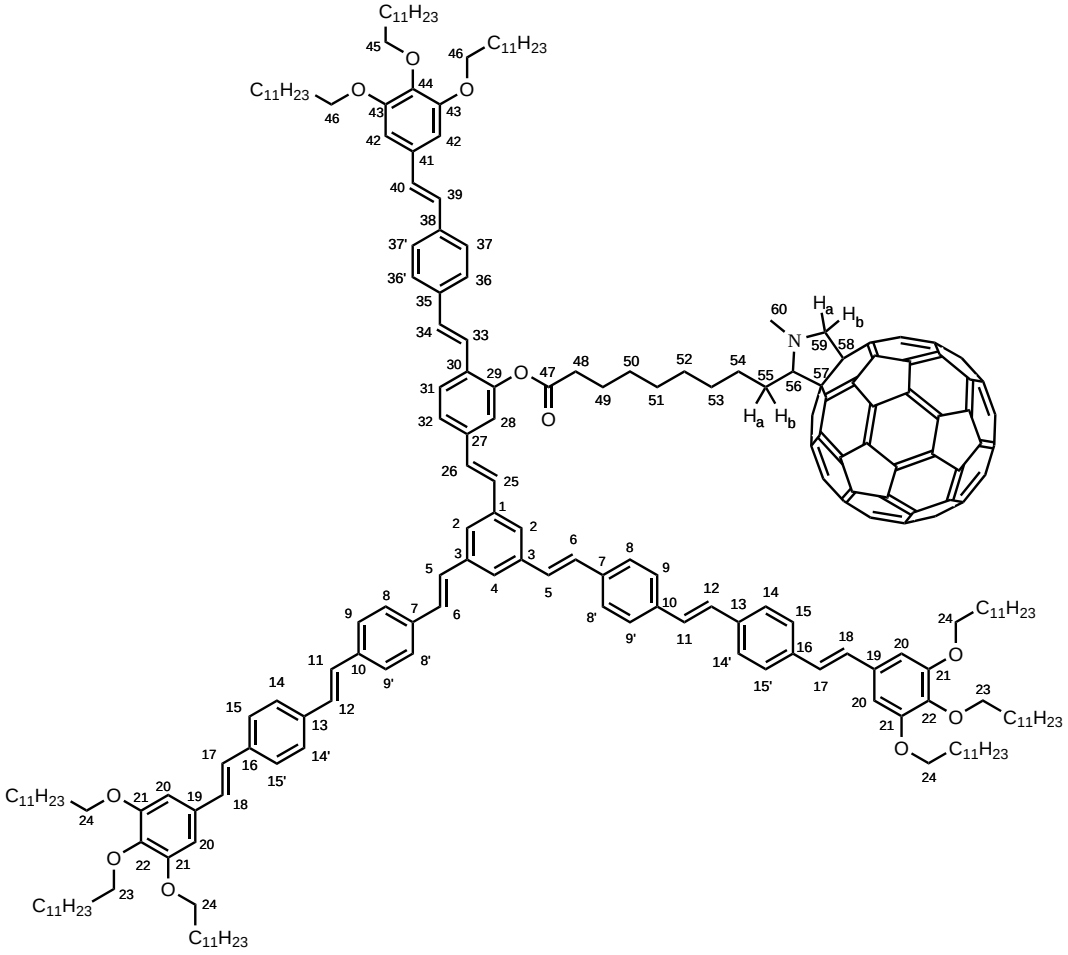

81.8 mg (30.6 µmol) **72**, 37.2 mg (39.8 µmol) carboxylic acid **26**, 23.4 mg (79.5 µmol) DPTS and 32.8 mg (159 µmol) DCC were stirred in 10 ml dry DCM at room temperature under nitrogen atmosphere for 8 days. The solution was concentrated in vacuo and subjected to silica gel chromatography with cyclohexane / DCM (1 / 1) as eluent. Further elution with $CHCl_3$ gave the crude product, which was dissolved in few DCM and precipitated from methanol to yield 69.3 mg (19.3 µmol, 63%) of a brown solid. ^{1}H NMR ($CDCl_3$): δ = 0.89 (t, ^3J = 6.80 Hz, 27 H; CH_3), 1.20 - 1.90 (m, 192 H; CH_2H-49 + H-50 + H-51 + H-52 + H-53 + H-54), 2.33 (m, 1 H; H-55a), 2.48 (m, 1 H; H-55b), 2.67 (t, ^3J = 7.38 Hz, 2 H; H-48), 2.91 (s, 3 H; H-60), 3.82 (t, ^3J = 5.28 Hz, 1 H; H-56), 3.92 - 4-06 (m, 18 H; H-23 + H-24 + H-45 + H-46), 4.06 (d, ^2J = 9.64 Hz, 1 H; H-59a), 4.74 (d, ^2J = 9.64 Hz, 1 H; H-59b), 6.71 + 6.72 (s, 6 H; H-20 + H-42), 6.95 (d, ^3J = 16.18 Hz, 1 H; H-39), 6.97 (d, ^3J = 16.09 Hz, 2 H; H-17), 7.02 (d, ^3J = 16.18 Hz, 1 H; H-40), 7.03 (d, ^3J = 16.09 Hz, 2 H; H-18), 7.06 - 7.23 (m, 12 H; H-5 + H-6 + H-11 + H-12 + H-25 + H-26 + H-33 + H-34), 7.25 (d, ^4J = 1.36 Hz, 1 H; H-28), 7.40 (d, ^3J = 8.42 Hz, 1 H; H-32), 7.36 - 7.59 (m, 23 H; H-2 + H-4 + H-8 + H-8' + H-9 + H-9' + H-14 + H-14' + H-15 + H-15' + H-36 + H-36' + H-37 + H-37'), 7.67 (d, ^3J = 8.42 Hz, 1 H; H-31); ^{13}C NMR ($CDCl_3$): δ = 14.3 (C_p; CH_3), 22.8 - 32.1 (C_s; CH_2), 25.3 (C_s; C-49), 27.4 (C_s; C-54), 29.3 (C_s; C-50 + C-51 + C-52), 30.2 (C_s; C-53), 31.1 (C_s; C-55), 34.6 (C_s; C-48), 40.1 (C_p; C-60), 69.3 (C_s; C-24 + C-46), 70.2 (C_q; C-58), 70.5 (C_s; C-59), 73.7 (C_s; C-23 + C-45), 76.4 (C_q; C-57), 78.2 (C_t; C-56), 105.3 + 105.4 (C_t; C-20 + C-42), 120.8 (C_t; C-28), 121.4 (C_t; C-33), 124.2 (C_t; C-2 + C-4), 124.6 (C_t; C-32), 126.7 (C_t; C-31), 126.9 + 127.0 + 127.2 + 127.3 + 127.4

(C_t; C-8 + C-8' + C-9 + C-9' + C-14 + C-14' + C-15 + C-15' + C-17 + C-36 + C-36' + C-37 + C-37' + C-39), 128.2 + 128.3 + 128.4 + 129.0 + 129.1 + 129.3 + 130.4 (C_t; C-5 + C-6 + C-11 + C-12 + C-18 + C-25 + C-26 + C-34 + C-40), 129.4 (C_q; C-30), 132.6 (C_q; C-41), 132.7 (C_q; C-19), 135.6 + 136.0 + 136.5 + 137.2(7) + 139.7 + 139.8 + 140.3 + 140.4 + 141.7(8) + 141.8(3) + 141.9 + 142.1(7) + 142.2(0) + 142.2(6) + 142.2(8) + 142.3(1) + 142.7 + 142.8 + 143.1 + 143.3 + 144.4(6) + 144.5(2) + 144.7 + 144.9 + 145.3(0) + 145.3(3) + 145.3(9) + 145.4(3) + 145.4(7) + 145.4(9) + 145.6 + 145.7 + 145.9 + 146.0(5) + 146.0(7) + 146.1(5) + 146.2(0) + 146.3 + 146.3(7) + 146.3(9) + 146.5 + 146.6 + 146.9 + 147.3 + 147.4 + 153.6 + 154.5 + 154.6 + 156.6 (C_q; C_{58}), 136.4 + 136.6 + 136.7 + 136.9(9) + 137.0(4) + 137.3(0) + 137.9 + 138.2 (C_q; C-1 + C-3 + C-7 + C-10 + C-13 + C-16 + C-27 + C-35 + C-38), 138.5 (C_q; C-22), 138.6 (C_q; C-44), 148.7 (C_q; C-29), 153.4(5) (C_q; C-21), 153.4(7) (C_q; C-43), 172.2 (C_q; C-47); MALDI-MS: m/z (%) calcd.: 3587.28 ($[M+2]^{+\cdot}$,100), found: 3587.24 ($[M+2]^{+\cdot}$,99); MALDI-HRMS: m/z calcd. for $C_{258}H_{297}NO_{11}^{+\cdot}$ ($[M]^{+\cdot}$): 3585.2706, found: 3585.2572; Elemental analysis (%) for $C_{258}H_{297}NO_{11}$ calcd.: C 86.36, H 8.34, N 0.39, found: C 85.30, H 8.44, N 0.35. For the discussion of elemental analysis results regarding fullerene containing materials, see page 119.

Compound $S2_{C12}$-$F1_{C16}$

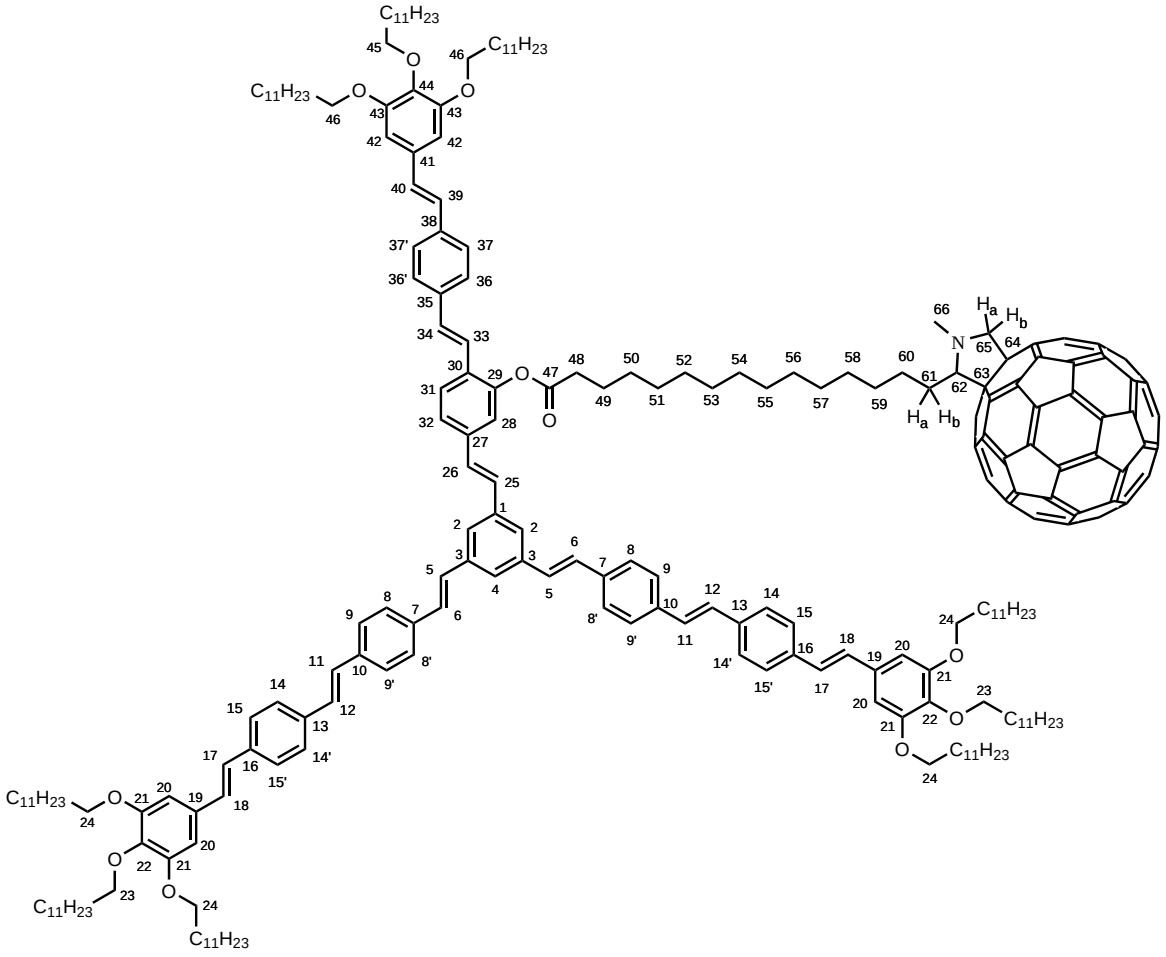

46.0 mg (45.2 µmol) carboxylic acid **31** was mixed with 10 ml of dry DCM under nitrogen atmosphere and stirred overnight. 84.0 mg (31.4 µmol) **72**, 26.6 mg (90.4 µmol) DPTS and 37.3 mg (181 µmol) DCC were added and the solution was stirred overnight. The solution was subjected to silica gel chromatography with cyclohexane / DCM (3 / 1) as eluent. Further elution with cyclohexane / DCM

(1 / 1) and neat DCM gave the crude product. The residue was precipitated from methanol twice to yield 59.2 mg (16.1 μmol, 51%) of a brown solid. ^{1}H NMR ($CDCl_3$): δ = 0.90 (t, ^{3}J = 6.80 Hz, 27 H; CH_3), 1.20 - 1.90 (m, 204 H; $(CH_2)_{10}$–CH_3 + H-49 + H-50 + H-51 + H-52 + H-53 + H-54 + H-55 + H-56 + H-57 + H-58 + H-59 + H-60), 2.33 (m, 1 H; H-61a), 2.48 (m, 1 H; H-61b), 2.69 (t, ^{3}J = 7.20 Hz, 2 H; H-48), 2.92 (s, 3 H; H-66), 3.83 (t, ^{3}J = 5.10 Hz, 1 H; H-62), 3.99 (t, ^{3}J = 6.92 Hz, 6 H; H-23 + H-45), 4.02 (t, ^{3}J = 6.44 Hz, 12 H; H-24 + H-46), 4.08 (d, ^{2}J = 10.02 Hz, 1 H; H-64a), 4.74 (d, ^{2}J = 10.02 Hz, 1 H; H-64b), 6.72 (s, 6 H; H-20 + H-42), 6.95(5) (d, ^{3}J = 16.43 Hz, 1 H; H-39), 6.96(3) (d, ^{3}J = 16.23 Hz, 2 H; H-17), 7.02 (d, ^{3}J = 16.43 Hz, 1 H; H-40), 7.03 (d, ^{3}J = 16.23 Hz, 2 H; H-18), 7.06 - 7.23 (m, 12 H; H-5 + H-6 + H-11 + H-12 + H-25 + H-26 + H-33 + H-34), 7.27 (m, 1 H; H-28), 7.40 (d, ^{3}J = 8.46 Hz, 1 H; H-32), 7.42 - 7.58 (m, 23 H; H-2 + H-4 + H-8 + H-8' + H-9 + H-9' + H-14 + H-14' + H-15 + H-15' + H-36 + H-36' + H-37 + H-37'), 7.67 (d, ^{3}J = 8.46 Hz, 1 H; H-31), ^{13}C NMR ($CDCl_3$): δ = 14.3 (C_p; CH_3), 22.9 - 32.1 (C_s; CH_2C-50 + C-51 + C-52 + C-53 + C-54 + C-55 + C-56 + C-57 + C-58), 25.4 (C_s; C-49), 27.4 (C_s; C-60), 30.3 (C_s; C-59), 31.1 (C_s; C-61), 34.7 (C_s; C-48), 40.1 (C_p; C-66), 69.3 (C_s; C-24 + C-46), 70.2 (C_q; C-64), 70.5 (C_s; C-65), 73.7 (C_s; C-23 + C-45), 76.4 (C_q; C-63), 78.3 (C_t; C-62), 105.3 (C_t; C-20 + C-42), 120.8 (C_t; C-28), 121.4 (C_t; C-33), 124.2 (C_t; C-2 + C-4), 124.6 (C_t; C-32), 126.6 (C_t; C-31), 126.9 + 127.0 + 127.1 + 127.3 + 127.4 (C_t; C-8 + C-8' + C-9 + C-9' + C-14 + C-14' + C-15 + C-15' + C-17 + C-36 + C-36' + C-37 + C-37' + C-39), 128.1 + 128.3 + 128.4 + 129.0 + 129.1 + 129.2 + 130.4 (C_t; C-5 + C-6 + C-11 + C-12 + C-18 + C-25 + C-26 + C-34 + C-40), 129.3 (C_q; C-30), 132.5(9) (C_q; C-41), 132.6(3) (C_q; C-19), 135.6 + 136.0 + 136.5 + 137.2(7) + 139.7 + 139.8 + 140.3 + 140.4 + 141.7(7) + 141.8(2) + 141.9 + 142.2 + 142.3 + 142.7(0) + 142.7(2) + 142.7(5) + 142.7(9) + 143.1 + 143.3 + 144.4(5) + 144.5(0) + 144.7 + 144.8 + 145.2(8) + 145.3(3) + 145.3(9) + 145.4(3) + 145.5 + 145.6 + 145.7 + 145.9 + 146.0 + 146.0(7) + 146.1(4) + 146.2 + 146.3 + 146.3(6) + 146.4(0) + 146.5 + 146.7 + 146.9 + 147.3(0) + 147.3(4) + 153.6 + 154.5 + 154.6 + 156.6 (C_q; C_{58}), 136.4 + 136.6 + 136.7 + 136.9(7) + 137.0(0) + 137.2(5) + 137.9 + 138.2 (C_q; C-1 + C-3 + C-7 + C-10 + C-13 + C-16 + C-27 + C-35 + C-38), 138.4(7) (C_q; C-22), 138.5(3) (C_q; C-44), 148.7 (C_q; C-29), 153.4 (C_q; C-21 + C-43), 172.3 (C_q; C-47); MALDI-MS: m/z (%) calcd.: 3671.37 ($[M+2]^{-\cdot}$,100), found: 3671.91 ($[M+2]^{-\cdot}$,86); MALDI-HRMS: m/z calcd. for $C_{264}H_{309}NO_{11}^{+\cdot}$ ($[M]^{+\cdot}$): 3669.3645, found: 3669.3617; Elemental analysis (%) for $C_{264}H_{309}NO_{11}$ calcd.: C 86.34, H 8.48, N 0.38, found: C 85.51, H 8.62, N 0.30. For the discussion of elemental analysis results regarding fullerene containing materials, see page 119.

Compound 73

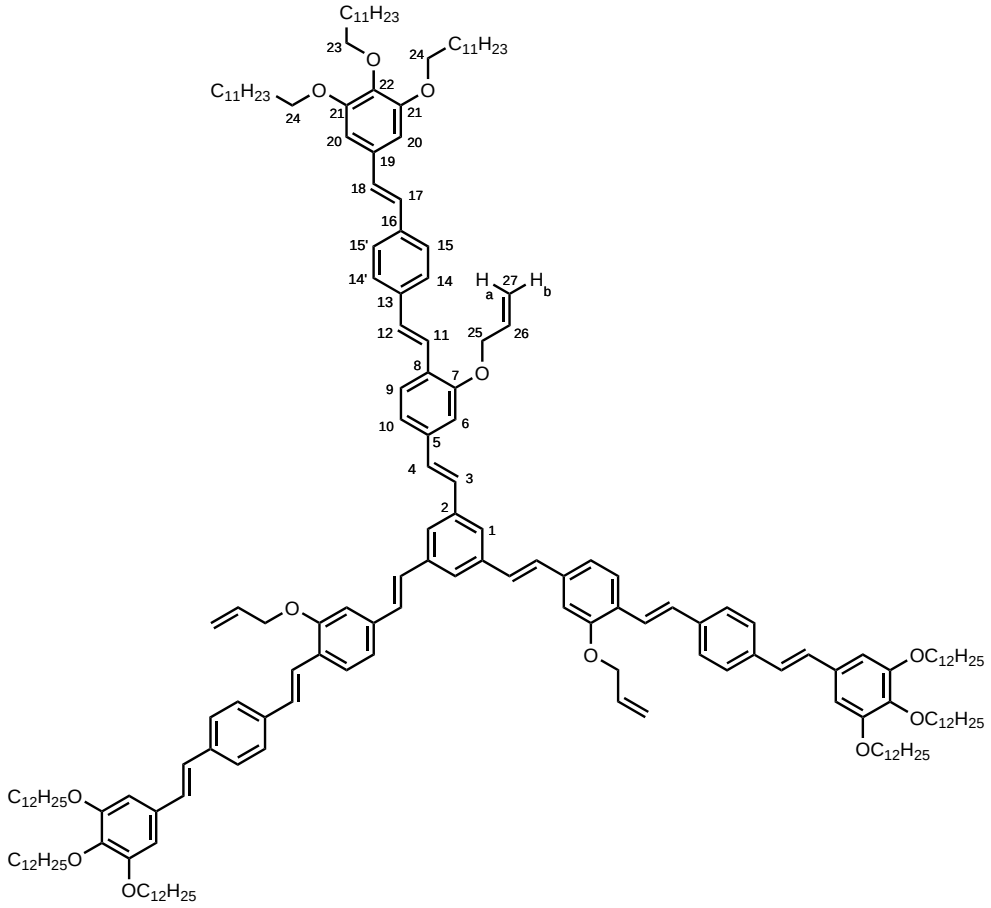

137 mg (1.22 mmol) potassium *tert*-butoxide was added in portions to a stirred solution of 129 mg (244 µmol) core building block **1** and 740 mg (805 µmol) arm building block **42** in 20 mL dry THF under nitrogen atmosphere. After stirring for 72 hours, the reaction was quenched with 1N HCl and the solution was then extracted with $CHCl_3$. The organic solvent was dried over Na_2SO_4 and evaporated under reduced pressure. The crude product was chromatographed on silica gel with cyclohexane / DCM (1 / 1) as eluent to yield 528 mg (187 µmol, 77%) of a yellow solid. ^{1}H NMR ($CDCl_3$): δ = 0.89 (t, ^3J = 6.88 Hz, 27 H; CH_3), 1.20 - 1.90 (m, 180 H; CH_2), 3.98 (t, ^3J = 6.64 Hz, 6 H; H-23), 4.04 (t, ^3J = 6.50 Hz, 12 H; H-24), 4.70 (dt, ^3J = 5.08 Hz, ^4J = 1.46 Hz, 6 H; H-25), 5.38 (m, 3 H; H-27b), 5.54 (m, 3 H; H-27a), 6.19 (m, 3 H; H-26), 6.73 (s, 6 H; H-20), 6.97 (d, ^3J = 16.17 Hz, 3 H; H-17), 7.03 (d, ^3J = 16.17 Hz, 3 H; H-18), 7.09 (m, 3 H; H-6), 7.12 - 7.24 (m, 12 H; H-3 + H-4 + H-10 + H-12), 7.49 (AA' of AA'BB', ^3J = 8.44 Hz, 6 H; H-15 + H-15'), 7.54 (BB' of AA'BB', ^3J = 8.44 Hz, 6 H; H-14 + H-14'), 7.55 (d, ^3J = 16.39 Hz, 3 H; H-11), 7.59 (s, 3 H; H-1), 7.64 (d, ^3J = 8.28 Hz, 3 H; H-9); ^{13}C NMR ($CDCl_3$): δ = 14.3 (C_p; CH_3), 22.8 - 32.1 (C_s; CH_2), 69.4 (C_s; C-24), 69.5 (C_s; C-25), 73.7 (C_s; C-23), 105.4 (C_t; C-20), 110.6 (C_t; C-6), 117.7 (C_s; C-27), 119.9 (C_t; C-10), 123.1 (C_t; C-11), 124.2 (C_t; C-1), 126.7(8) (C_t; C-9), 126.8(1) (C_q; C-8), 126.8(4) (C_t; C-15 + C-15'), 127.1 (C_t; C-14 + C-14'), 127.5 (C_t; C-17), 128.5 (C_t; C-3), 128.8(6) + 128.8(9) (C_t; C-12 + C-18), 129.4 (C_t; C-4), 132.7 (C_q; C-19), 133.5 (C_t; C-26), 136.8 + 137.3 + 137.8 + 138.2 (C_q; C-2 + C-5 + C-13 + C-16), 138.6 (C_q; C-22), 153.5 (C_q; C-21), 156.5 (C_q; C-7); MALDI-MS: m/z (%) calcd.: 2824.20 ($[M+2]^{+\cdot}$,100), found: 2824.20 ($[M+2]^{+\cdot}$,100).

Compound 74

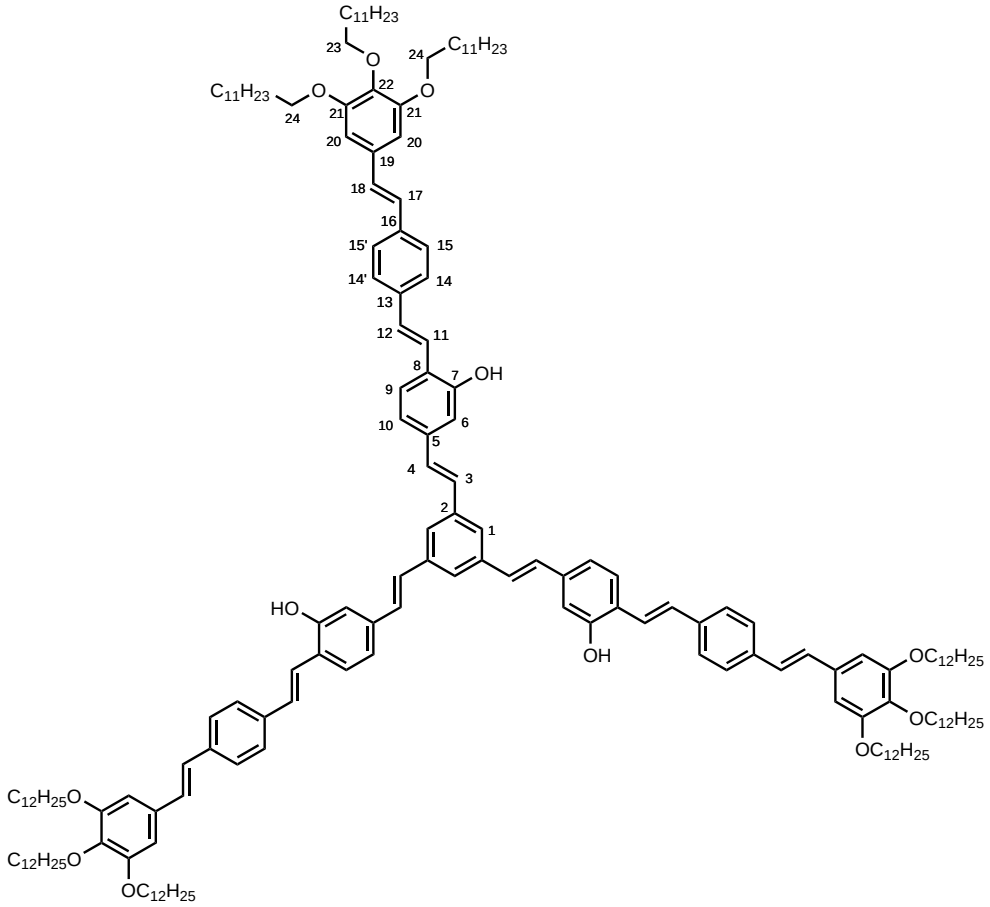

516 mg (183 µmol) **73** and 31.7 mg (27.4 µmol) $Pd(PPh_3)_4$ were stirred at room temperature in 10 ml degassed THF under nitrogen atmosphere. 0.2 ml (200 mg, 2.30 mmol) morpholine was then added drop by drop and the mixture was stirred for 72 hours. The reaction was quenched with 1N HCl and extracted with $CHCl_3$. The organic solvent was dried over Na_2SO_4 and evaporated under reduced pressure. The crude product was chromatographed on silica gel with $CHCl_3$ as eluent to yield 393 mg (145 µmol, 79%) of a yellow solid. ^{1}H NMR ($CDCl_3$): δ = 0.88 (t, ^3J = 6.88 Hz, 27 H; CH_3), 1.20 - 1.90 (m, 180 H; CH_2), 3.98 (t, ^3J = 6.64 Hz, 6 H; H-23), 4.04 (t, ^3J = 6.50 Hz, 12 H; H-24), 5.11 (s, 3 H; OH), 6.73 (s, 6 H; H-20), 6.97 (d, ^3J = 16.32 Hz, 3 H; H-17), 7.01 (m, 1 H; H-6), 7.04 (d, ^3J = 16.32 Hz, 3 H; H-18), 7.13 (m, 6 H; H-3 + H-4), 7.16(9) (d, ^3J = 8.20 Hz, 3 H; H-10), 7.17(1) (d, ^3J = 16.30 Hz, 3 H; H-12), 7.40 (d, ^3J = 16.30 Hz, 3 H; H-11), 7.49 + 7.53 (AA' of AA'BB', ^3J = 7.88 Hz, 3 H; H-14 + H-14' + H-15 + H-15'), 7.55 (s, 3 H; H-1), 7.57 (d, ^3J = 8.20 Hz, 3 H; H-9); ^{13}C NMR ($CDCl_3$): δ = 14.3 (C_p; CH_3), 22.8 - 32.1 (C_s; CH_2), 69.4 (C_s; C-24), 73.9 (C_s; C-23), 105.3 (C_t; C-20), 114.0 (C_t; C-6), 120.4 (C_t; C-10), 122.8 (C_t; C-11), 124.2 (C_t; C-1), 124.7 (C_q; C-8), 126.8 + 127.0 (C_t; C-14 + C-14' + C-15 + C-15' + C-9), 127.6 + 128.5 + 128.6 + 129.0 (C_t; C-3 + C-4 + C-12 + C-17 + C-18), 133.0 (C_q; C-19), 136.6 + 137.1 + 137.8 + 137.9 (C_q; C-2 + C-5 + C-13 + C-16), 138.1 (C_q; C-22), 153.4 (C_q; C-21), 153.7 (C_q; C-7); MALDI-MS: m/z (%) calcd.: 2704.11 ($[M+2]^{+\cdot}$,100), found: 2704.08 ($[M+2]^{+\cdot}$,100); Elemental analysis (%) for $C_{186}H_{276}O_{12}$ calcd.: C 82.61, H 10.29, found: C 82.68, H 10.42.

Compound $S2_{C12}$-$F3_{C4}$

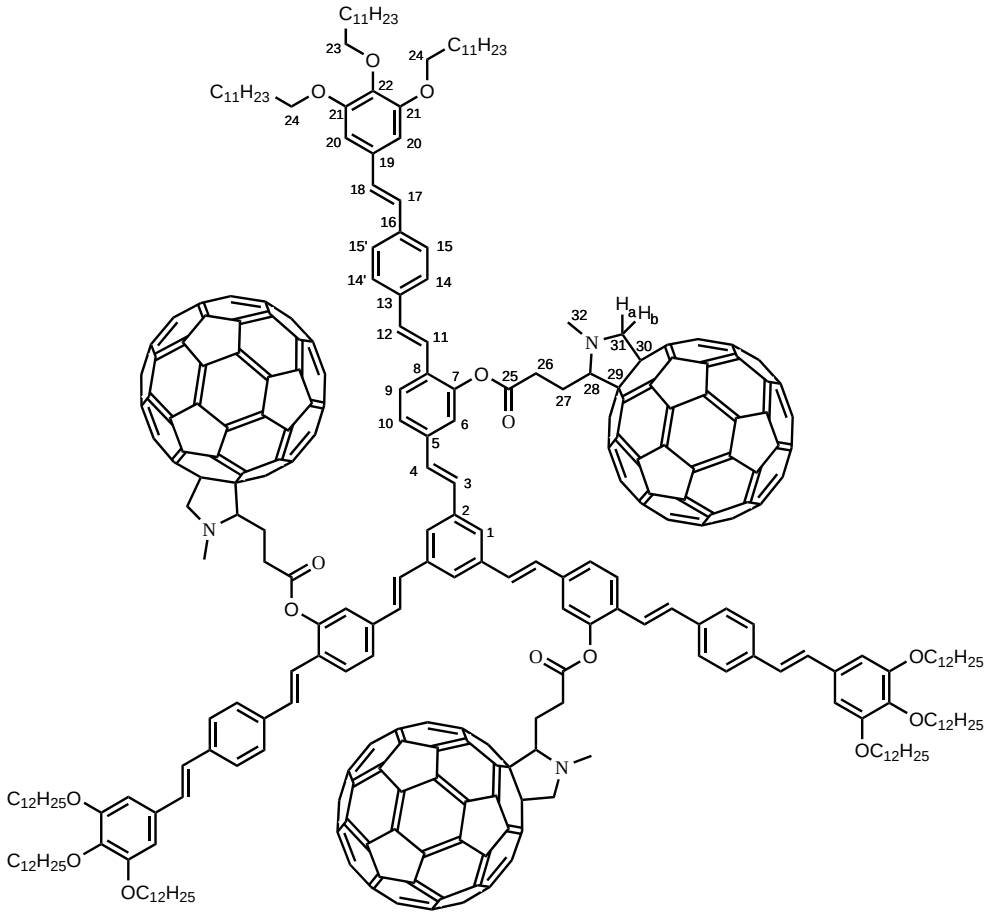

34.3 mg (12.7 µmol) **74**, 43.1 mg (50.7 µmol) carboxylic acid**23**, 29.9 mg (102 µmol) DPTS and 41.9 mg (203 µmol) DCC were stirred in 6 ml dry DCM at room temperature under nitrogen atmosphere for 19 days. The solution was concentrated in vacuo and subjected to silica gel chromatography with DCM as eluent. Excess reagents were removed by crystallizing the crude product from methanol twice to yield 16.9 mg (3.25 µmol, 26%) of a brown solid. ^{1}H NMR ($CDCl_3$): δ = 0.89 (m, 27 H; CH_3), 1.20 - 1.90 (m, 180 H; CH_2), 2.78 + 3.26 (m, 12 H; H-26 + H-27), 2.92 (s, 9 H; H-32), 3.73 - 4.27 (m, 24 H; H-23 + H-24 + H-28 + H-31a), 4.74 (m, 3 H; H-31b), 6.45 - 6.76 (m, 6 H; H-20), 6.76 - 7.80 (m, 42 H; H-1 + H-3 + H-4 + H-6 + H-9 + H-10 + H-11 + H-12 + H-14 + H-14' + H-15 + H-15' + H-17 + H-18). For discussion of NMR results, see page 49. MALDI-MS: m/z (%) calcd.: 5199.3 ([M+4]$^{\cdot-}$, 100), found: 5199.2 ([M+4]$^{\cdot-}$, 100); Elemental analysis (%) for $C_{384}H_{303}N_3O_{15}$ calcd.: C 88.70, H 5.87, N 0.81, found: C 87.21, H 6.73, N 0.92. For the discussion of elemental analysis results regarding fullerene containing materials, see page 119.

Compound S3$_{C12}$

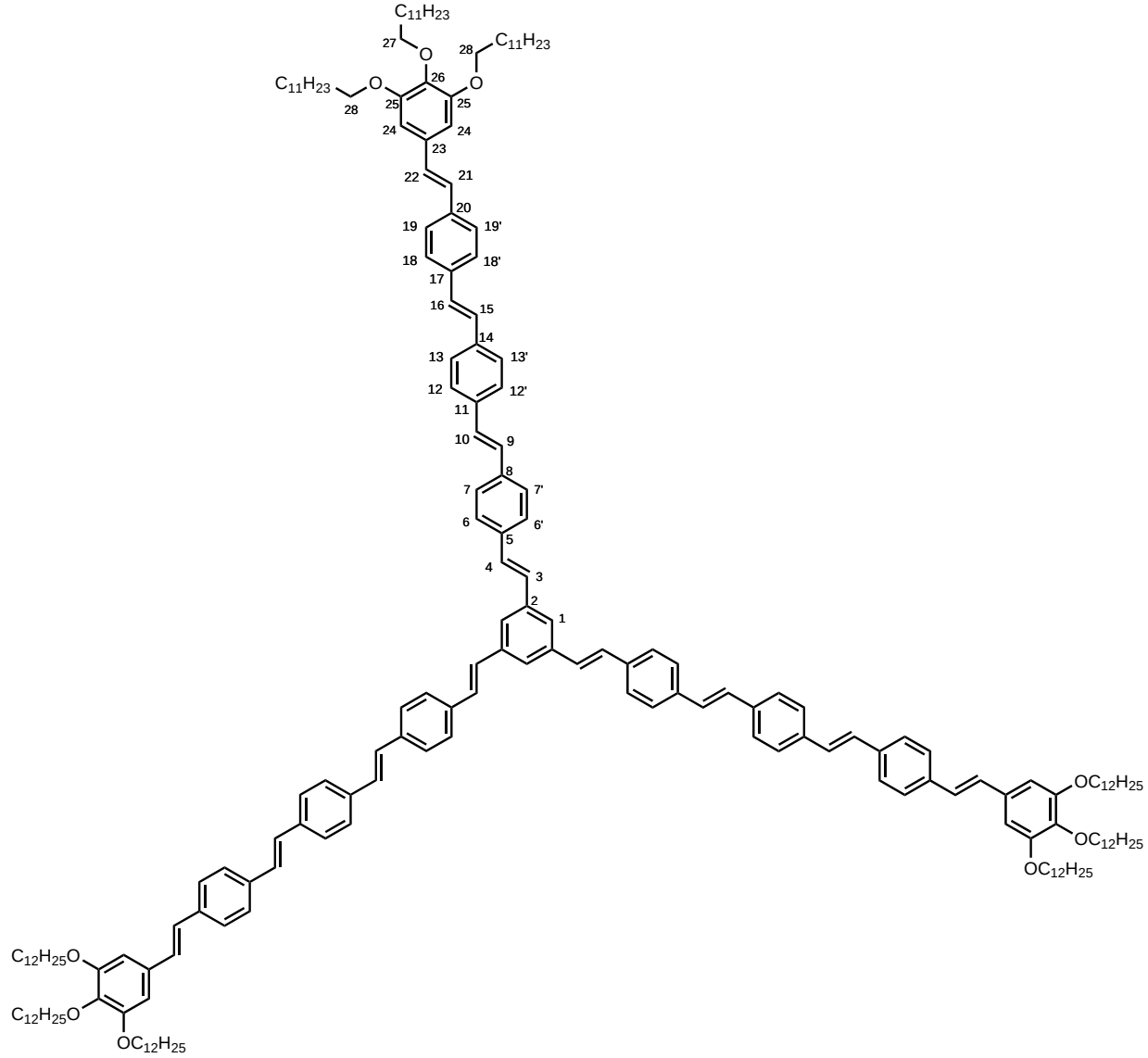

32.5 mg (290 µmol) potassium *tert*-butoxide was added in portions to a stirred solution of 37.4 mg (48.3 µmol) core building block **5** and 166 mg (188 µmol) arm building block **106** in 2 mL dry THF under nitrogen atmosphere. After stirring overnight, the reaction was quenched with 2N HCl and the precipitate was collected and washed with cold methanol. The solid was dissolved in few chloroform and poured into methanol. The precipitate was subjected to silica gel chromatography with DCM as eluent to yield 39.5 mg (13.3 µmol, 28%) of a yellow solid. ^{1}H NMR ($CDCl_3$): δ = 0.88 (t, ^3J = 6.62 Hz, 27 H; CH_3), 1.18 - 1.56 (m, 162 H; (CH_2)$_9$–CH_3), 1.70 - 1.90 (m, 18 H; OCH_2CH_2), 3.97 (t, ^3J = 6.42 Hz, 6 H; H-27), 4.03 (t, ^3J = 6.70 Hz, 12 H; H-28), 6.72 (s, 6 H; H-24), 6.97 (d, ^3J = 16.09 Hz, 3 H; H-21), 7.04 (d, ^3J = 16.09 Hz, 3 H; H-22), 7.08 - 7.16 (m, 12 H; H-9 + H-10 + H-15 + H-16), 7.17 - 7.25 (m, 6 H; H-3 + H-4), 7.45 - 7.60 (m, 39 H; H-1 + H-6 + H-6' + H-7 + H-7' + H-12 + H-12' + H-13 + H-13' + H-18 + H-18' + H-19 + H-19'); ^{13}C NMR ($CDCl_3$): δ = 14.3 (C_p; CH_3), 22.9 (C_s; CH_2), 26.4 (C_s; CH_2), 29.5 - 30.0 (C_s; CH_2), 30.7 (C_s; CH_2), 32.1 (C_s; CH_2), 69.2 (C_s; C-28), 73.6 (C_s; C-27), 105.3 (C_t; C-24), 124.1 (C_t; C-1), 126.5 - 127.6 (C_t; C-6 + C-6' + C-7 + C-7' + C-12 + C-12' + C-13 + C-13' + C-18 + C-18' + C-19 + C-19' + C-21), 127.9 - 128.3 (C_t; C-3 + C-9 + C-10 + C-15 + C-16), 129.1 (C_t; C-4 + C-22), 132.6 (C_q; C-23), 135.9 - 137.0 (C_q; C-5 + C-8

+ C-11 + C-14 + C-17 + C-20), 137.9 (C_q; C-2), 138.5 (C_q; C-25), 153.5 (C_q; C-26); MALDI-MS: m/z (%) calcd.: 2962.26 ($[M+2]^{+\cdot}$,100), found: 2962.26 ($[M+2]^{+\cdot}$,100); Elemental analysis (%) for $C_{210}H_{294}O_9$ calcd.: C 85.14, H 10.00, found: C 84.83, H 10.44.

10.8 Synthesis of the Hekate stars with cyclopenteno-functionalized fullerenes

Compound 80

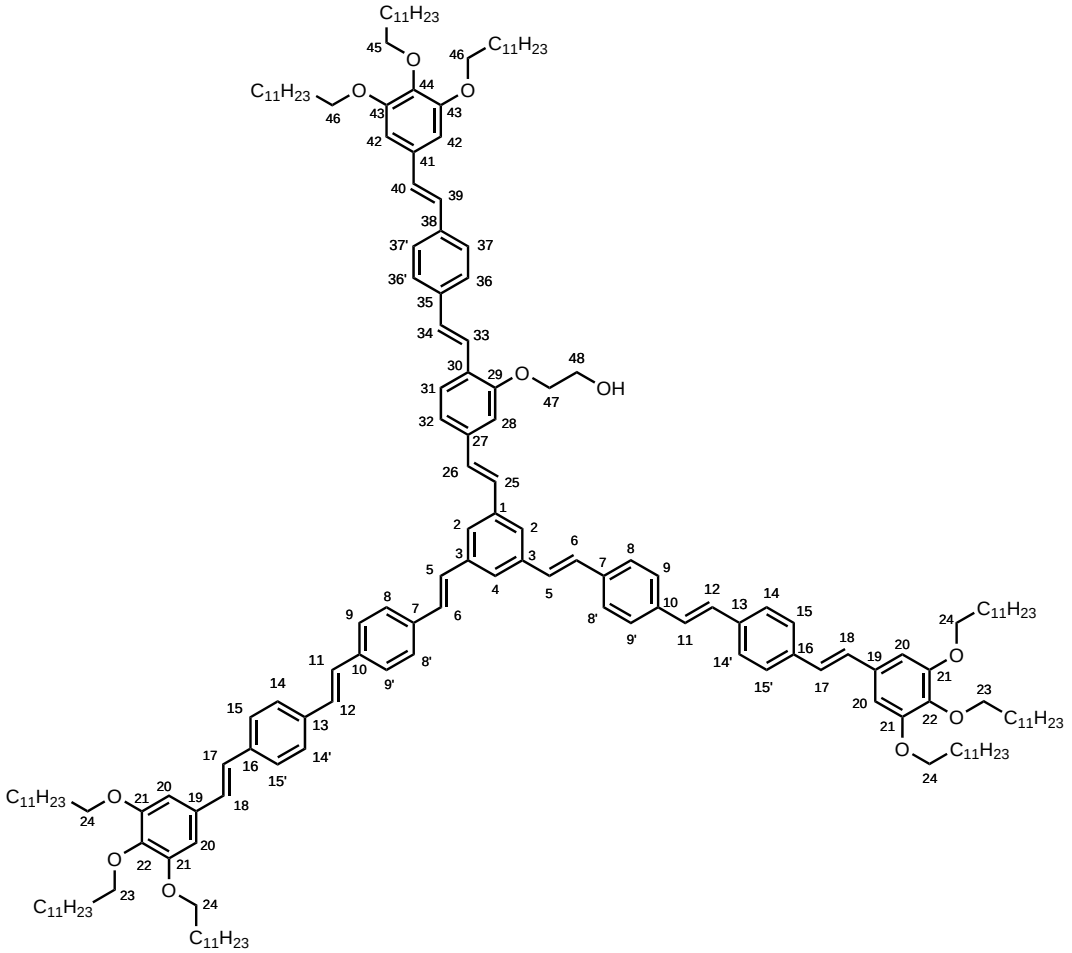

44.3 mg (16.6 µmol) phenol **72**, 4.4 mg (50.0 µmol) ethylene carbonate and 6.9 mg (49.9 µmol) K_2CO_3 were stirred at 120 °C in 5 ml DMF under nitrogen atmosphere for 2 hours. At room temperature, 75 ml H_2O was added. The mixture was acidified with a few drops of 1N HCl and stored at 4 °C. The collected precipitate was subjected to silica gel chromatography with $CHCl_3$ as eluent. Further elution with $CHCl_3$ / ethanol (20 / 1) gave the crude product, which was dissolved in few $CHCl_3$ and precipitated from methanol to yield 28.7 mg (10.6 µmol, 64%) of a yellow solid. ^{1}H NMR ($CDCl_3$): δ = 0.88 (t, ^3J = 6.90 Hz, 27 H; CH_3), 1.20 - 1.90 (m, 180 H; CH_2), 3.98 (t, ^3J = 6.58 Hz, 6 H; H-23 + H-45), 4.03 (t, ^3J = 6.40 Hz, 12 H; H-24 + H-46), 4.11 + 4.28 (m, 4 H; H-47 + H-48), 6.73 (s, 6 H; H-20 + H-42), 6.98 (d, ^3J = 16.29 Hz, 3 H; H-17 + H-39), 7.04 (d, ^3J = 16.29 Hz, 3 H; H-18 + H-40), 7.08 - 7.26 (m, 12 H; H-5 + H-6 + H-11 + H-12 + H-25 + H-26 + H-28 + H-32 + H-34), 7.45 - 7.57 (m, 21 H; H-8 + H-8' + H-9 + H-9' + H-14 + H-14' + H-15 + H-15' + H-33 + H-36 + H-36' + H-37 + H-37'), 7.59 (s, 3 H; H-2 + H-4), 7.65 (d, ^3J = 7.92 Hz, 1 H; H-31); ^{13}C NMR ($CDCl_3$): δ = 14.3 (C_p; CH_3), 22.9 - 32.1 (C_s; CH_2), 61.8 + 70.1 (C_s; C-47 + C-48), 69.3 (C_s; C-24 + C-46), 73.7 (C_s; C-23 + C-45), 105.2 (C_t; C-20 + C-42), 110.5 (C_t; C-28), 120.2 (C_t; C-32), 122.7 (C_t; C-33), 124.1

+ 124.3 (C_t; C-2 + C-4), 126.5 (C_q; C-30), 126.9 + 127.0 + 127.0(7) + 127.1(0) + 127.3 + 127.4 (C_t; C-8 + C-8' + C-9 + C-9' + C-14 + C-14' + C-15 + C-15' + C-17 + C-31 + C-36 + C-36' + C-37 + C-37' + C-39), 128.1 + 128.2 + 128.4 + 128.9 + 129.0 (C_t; C-5 + C-6 + C-11 + C-12 + C-18 + C-25 + C-26 + C-34 + C-40), 132.6(2) (C_q; C-41), 132.6(5) (C_q; C-19), 136.5 + 136.6 + 136.8 + 136.9 + 137.1 + 138.1 (C_q; C-1 + C-3 + C-7 + C-10 + C-13 + C-16 + C-35 + C-38), 137.9 (C_q; C-27), 138.3(7) (C_q; C-44), 138.4(0) (C_q; C-22), 153.4 (C_q; C-21 + C-43), 156.3 (C_q; C-29); MALDI-MS: m/z (%) calcd.: 2716.13 ($[M+2]^{+\cdot}$,100), found: 2716.14 ($[M+2]^{+\cdot}$,100).

Compound $S2_{C12}$-F*rac.*

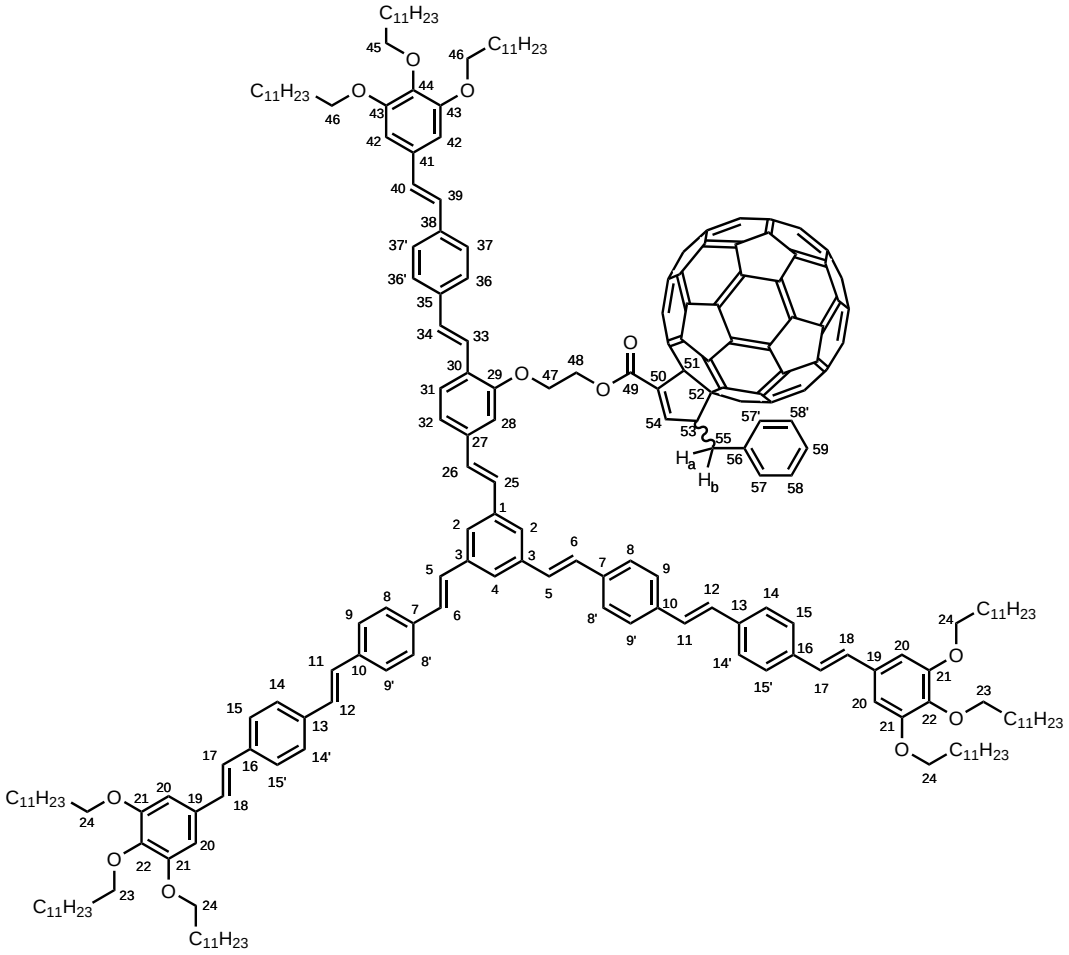

43.5 mg (16.0 µmol) **80**, 28.6 mg (32.0 µmol) carboxylic acid **78**, 12.7 mg (43.1 µmol) DPTS and 37.6 mg (182 µmol) DCC were stirred in 10 ml dry DCM at room temperature under nitrogen atmosphere for 5 days. The solution was subjected to silica gel chromatography with $CHCl_3$ / cyclohexane (3 / 1) as eluent. Excess reagents were removed by crystallizing the crude product from methanol twice. Further purification was achieved by slowly crystallizing the material from the mixture $CHCl_3$ / methanol (2 / 1) at -30 °C twice to yield 34.8 mg (9.69 µmol, 61%) of a brown solid. ^{1}H NMR ($CDCl_3$): δ = 0.89 (t, ^3J = 6.48 Hz, 27 H; CH_3), 1.20 - 1.90 (m, 180 H; CH_2), 3.23 (m, 1 H; H-55a), 3.72 (dd, ^2J = 13.52 Hz, ^3J = 5.72 Hz, 1 H; H-55b), 3.83 - 4.10 (m, 18 H; H-23 + H-24 + H-45 + H-46), 4.43 + 4.79 (m, 4 H; H-47 + H-48), 4.80 (m, 1 H; H-53), 6.66 + 6.73 (s, 6 H; H-20 + H-42), 6.83 - 7.70 (m, 50 H; H-2 + H-4 + H-5 + H-6 + H-8 + H-8' + H-9 + H-9' + H-11 + H-12 + H-14 + H-14' + H-15 + H-15' + H-17 + H-18 + H-25 + H-26 + H-28 + H-31 + H-32 + H-33 + H-34 + H-36 + H-36' + H-37 + H-37' + H-39 + H-40 + H-54 + H-57 + H-57' + H-58 + H-58' + H-59);

^{13}C NMR* ($CDCl_3$): δ = 14.3 (C_p; CH_3), 22.8 - 32.1 (C_s; CH_2), 25.5 + 31.3 (C_s; C-47 + C-48), 41.7 (C_s; C-55), 59.3 (C_t; C-53), 64.0 + 66.8 (C_s; C-47 + C-48), 69.3 (C_s; C-24 + C-26), 73.7 (C_s; C-23 + C-25), 74.1 (C_q; C-51 + 52), 105.2(6) + 105.3 (C_t; C-20 + C-42), 110.6 (C_t; C-28), 120.5 (C_t; C-33), 123.1 (C_t; C-28), 124.2 (C_t; C-2 + C-4), 126.4 (C_q; C-30), 126.9 + 127.0 + 127.1 + 127.4 (C_t; C-8 + C-8' + C-9 + C-9' + C-14 + C-14' + C-15 + C-15' + C-17 + C-31 + C-36 + C-36' + C-37 + C-37' + C-39), 128.1 + 128.3 + 128.5 + 129.0 + 129.4 (C_t; C-5 + C-6 + C-11 + C-12 + C-18 + C-25 + C-26 + C-34 + C-40), 129.3 (C_t), 132.6 (C_q; C-41), 135.9 + 136.1 + 136.5(3) + 139.2(6) + 139.3(4) + 139.6 + 140.2 + 141.5 - 146.5 + 147.3 + 147.4 + 148.1 + 150.6 + 150.8 + 152.6 + 156.7 (C_q; C_{58}), 136.5(7) + 136.6(3) + 136.8 + 137.0(0) + 137.0(4) +138.0 + 139.1(9) + 138.2(3) (C_q; C-1 + C-3 + C-7 + C-10 + C-13 + C-16 + C-27 + C-35 + C-38), 138.4 + 138.5 (C_q; C-22 + C-44), 138.6 (C_t), 149.0 (C_t), 152.3 (C_q), 153.3(9) + 153.4(4) (C_q; C-21 + C-43), 156.8 (C_q; C-29), 163.9 (C_q; C-49); MALDI-MS: m/z (%) calcd.: 3592.20 ([M+2]$^{+\cdot}$,100), found: 3592.30 ([M+2]$^{+\cdot}$,100); MALDI-HRMS: m/z calcd. for $C_{259}H_{288}O_{12}^{+\cdot}$ ([M]$^{+\cdot}$): 3590.1920, found: 3590.1825; For discussion of NMR results, see page 52.

Compound S2$_{C12}$-F*$_{enan.}$*

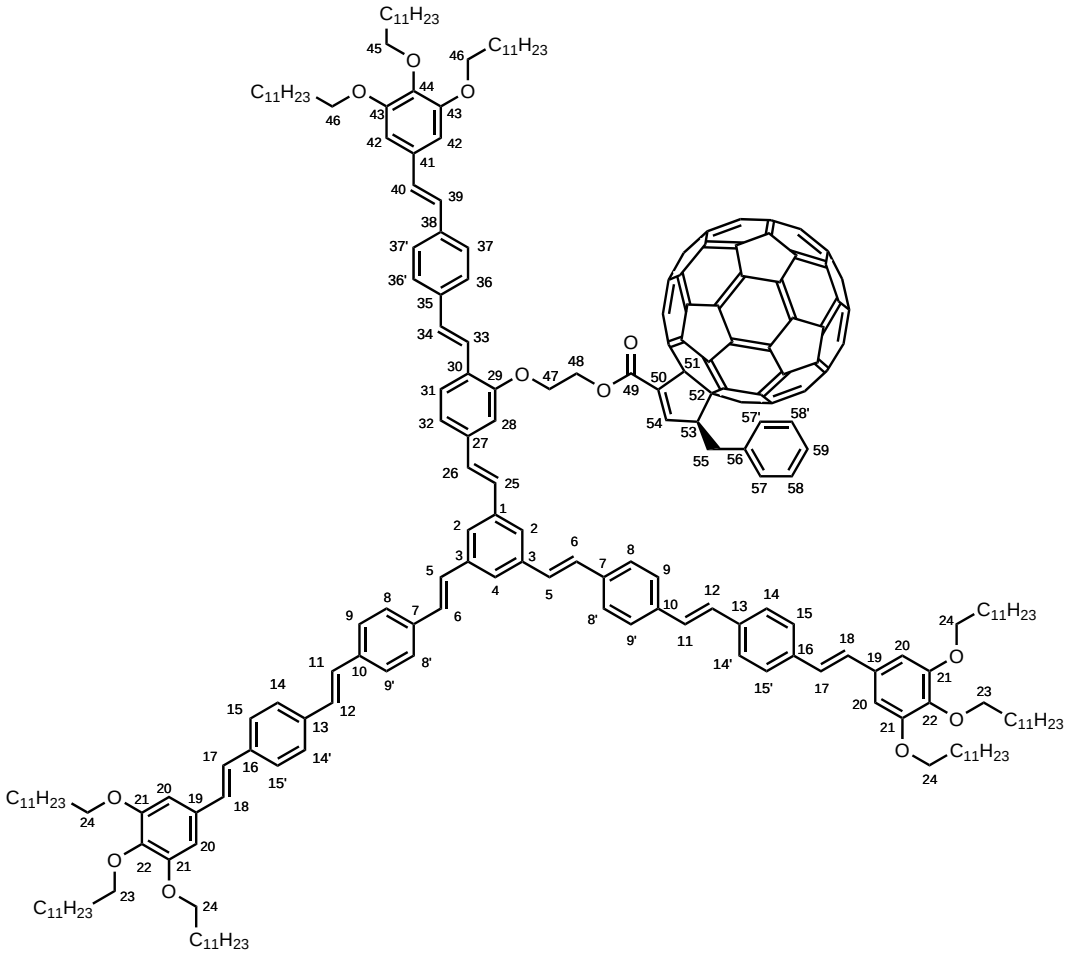

Compound **S2**$_{C12}$**-F***$_{enan.}$* was synthesized in an analogous way to the racemic material **S2**$_{C12}$**-F***$_{rac.}$* with 40.6 mg (14.9 µmol) **80**, 26.7 mg (29.8 µmol) carboxylic acid **79**, 11.8 mg (40.1 µmol) DPTS and 35.0 mg (170 µmol) DCC to yield 32.3 mg (8.99 µmol, 60%) of a brown solid. NMR data and mass spectra identical to that of the racemic compound **S2**$_{C12}$**-F***$_{rac.}$*.

*Due to the low absolute amount obtained for this material, not all signals could be detected or assigned to the corresponding nucleus with certainty.

10.9 Synthesis of the arm building blocks with short ethyleneoxy-chains

Compound 86

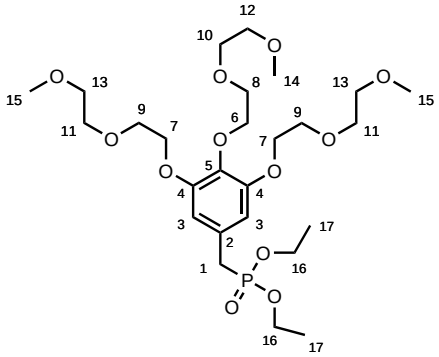

33.2 g (63.2 mmol) bromide **85** and 13.0 ml (12.6 g, 75.8 mmol) $P(OEt)_3$ were stirred at 125 °C in a round-bottom flask equipped with a condenser under nitrogen atmosphere for 2 hours. The distillate was discarded and excess $P(OEt)_3$ was removed via distillation in vacuo. The crude product was subjected to column chromatography (acetone / cyclohexane = 1 / 1, further elution with acetone / cyclohexane / methanol = 2 / 2 / 1) to yield 21.4 g(36.7 mmol. 58%) of a colorless oil. ^{1}H NMR ($CDCl_3$): δ = 1.24 (t, ^3J = 7.05 Hz, 6 H; H-17), 3.03 (d, $^2J_{HP}$ = 21.49 Hz, 2 H; H-1), 3.38 (m, 9 H; H-14 + H-15), 3.55 (m, 6 H; H-12 + H-13), 3.71 (m, 6 H; H-10 + H-11), 3.79 (t, ^3J = 5.13 Hz, 2 H; H-8), 3.84 (t, ^3J = 5.00 Hz, 4 H; H-9), 4.00 (m, 4 H; H-16), 4.13 (m, 6 H; H-6 + H-7), 6.52 (d, $^4J_{HP}$ = 2.48 Hz, 2 H; H-3); ^{13}C NMR ($CDCl_3$): δ = 16.3 (C_p; d, $^3J_{CP}$ = 5.78 Hz, C-17), 33.6 (C_s; d, $^1J_{CP}$ = 138.52 Hz, C-1), 58.9(0) (C_p; C-14), 58.9(3) (C_p; C-15), 62.0 (C_s; d, $^2J_{CP}$ = 6.74 Hz, C-16), 68.7 (C_s; C-7), 69.6 (C_s; C-9), 70.3 + 70.4 (C_s; C-8 + C-12), 70.6 (C_s; C-11), 71.8(6) (C_s; C-13), 71.9(3) (C_s; C-10), 72.3 (C_s; C-6), 109.1 (C_t; d, $^3J_{CP}$ = 6.75 Hz, C-3), 126.8 (C_q; d, $^2J_{CP}$ = 9.06 Hz, C-2), 137.1 (C_q; d, $^5J_{CP}$ = 4.04 Hz, C-5), 152.4 (C_q; d, $^4J_{CP}$ = 3.09 Hz, C-4); MALDI-MS: m/z (%) calcd.: 582.28 ($[M]^{+\cdot}$,100), found: 582.28 ($[M]^{+\cdot}$,100).

Compound 87

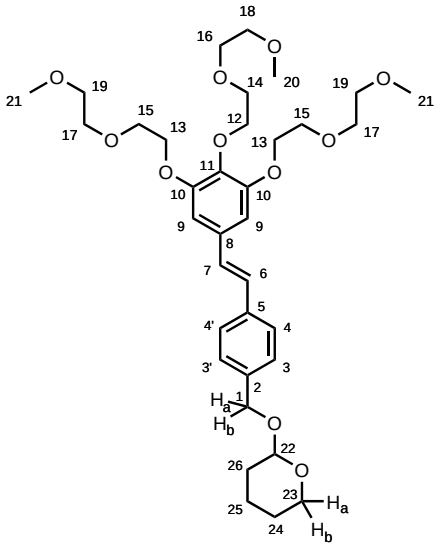

At 0 °C, 7.50 g (66.8 mmol) potassium *tert*-butoxide was added in portions to a stirred solution of 21.4 g (36.7 mmol) **86** and 11.5 g (52.2 mmol) (±)-4-(3,4,5,6-tetrahydro-2*H*-pyran-2-

yloxymethyl)benzaldehyde (**13**) in 100 mL dry THF under nitrogen atmosphere. After stirring overnight, the mixture was poured into an ice-cold aqueous HCl and extracted with ethyl acetate four times. THe organic phase was dried over Na_2SO_4 and evaporated under reduced pressure. The crude product was subjected to column chromatography (pure ethyl acetate, followed by ethyl acetate / acetone = 10 / 1) to afford 15.3 g (23.6 mmol, 64%) of a reddish oil. The product was used in the next step without further purification procedures. ^{1}H NMR ($CDCl_3$): δ = 1.50 - 1.95 (m, 6 H; H-24 + H-25 + H-26), 3.38(5) (s, 3 H; H-20), 3.39(0) (s, 6 H; H-21), 3.54 (m, 1 H; H-23a), 3.58 (m, 6 H; H-18 + H-19), 3.73 (m, 6 H; H-16 + H-17), 3.81 (t, ^3J = 5.10 Hz, 2 H; H-14), 3.88 (t, ^3J = 5.10 Hz, 4 H; H-15), 3.93 (m, 1 H; H-23b), 4.18 (t, ^3J = 5.14 Hz, 2 H; H-12), 4.22 (t, ^3J = 5.10 Hz, 4 H; H-13), 4.51 (d, ^2J = 12.19 Hz, 1 H; H-1a), 4.72 (t, ^3J = 3.53 Hz, 1 H; H-22), 4.79 (d, ^3J = 12.19 Hz, 1 H; H-1b), 6.76 (s, 2 H; H-9 + H-9'), 6.96 (s, 2 H; H-6 + H-7), 7.35 (AA' of AA'BB', ^3J = 8.33 Hz, 2 H; H-3 + H-3'), 7.47 (BB' of AA'BB', ^3J = 8.33 Hz, 2 H; H-4 + H-4');

Compound 88

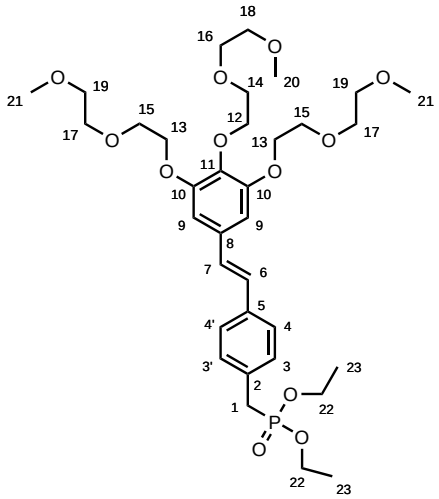

150 ml of a freshly prepared solution[171] of PPh_3Br_2 (31.2 mmol) in DCM was added drop by drop to a mixture of 14.5 g (22.3 mmol) **87** and 50 ml DCM at 0 °C under nitrogen atmosphere. After stirring overnight, a saturated solution of $NaHCO_3$ was poured into the solution. The mixture was extracted with DCM and the organic phase was washed with water. The aqueous phase was again extracted with DCM and the combined organic solvents were dried over Na_2SO_4. The solvent was evaporated under reduced pressure and the crude product was passed over a short silica gel column with ethyl acetate as eluent to give 24.5 g of a dark oil.

4.2 ml (4.07 g, 24.5 mmol) $P(OEt)_3$ was added and the mixture was stirred in a round-bottom flask equipped with a condenser at 140 °C for one hour under nitrogen atmosphere. The distillate was discarded and excess $P(OEt)_3$ was removed via distillation in vacuo. The crude product was subjected to column chromatography (pure ethyl acetate, followed by ethyl acetate / acetone = 6 / 1) to yield 9.70 g (14.2 mmol, 64%) of a yellow oil. ^{1}H NMR ($CDCl_3$): δ = 1.21 (dt, $^4J_{HP}$ = 0.54 Hz, ^3J = 10.6 Hz, 6 H; H-23), 3.12 (d, $^2J_{HP}$ = 21.69 Hz, 2 H; H-1), 3.35 (m, 9 H; H-20 + H-21), 3.53 (m, 6 H; H-18 + H-19), 3.70 (m, 6 H; H-16 + H-17), 3.78 (t, ^3J = 5.10 Hz, 2 H; H-14), 3.84 (t, ^3J = 5.04 Hz, 4 H; H-15), 3.98 (m, 4 H; H-22), 4.15 (t, ^3J = 5.10 Hz, 2 H; H-12), 4.19 (t, ^3J = 5.04 Hz, 4 H; H-13), 6.72 (s, 2 H; H-9), 6.89 (d, ^3J = 16.92 Hz, 1 H; H-7), 6.94 (d, ^3J = 16.92 Hz, 1 H; H-6), 7.25 (m,

$^4J_{HP}$ = 2.18 Hz, ^3J = 8.13 Hz, 2 H; H-3 + H-3'), 7.40 (AA' of AA'BB', ^3J = 8.13 Hz, 2 H; H-4 + H-4'); ^{13}C NMR ($CDCl_3$): δ = 16.4 (C_p; d, $^3J_{CP}$ = 5.97 Hz, C-23), 33.6 (C_s; d, $^1J_{CP}$ = 137.95 Hz, C-1), 59.0(4) (C_p; C-20), 59.0(8) (C_p; C-21), 62.2 (C_s; d, $^2J_{CP}$ = 6.74 Hz, C-22), 68.9 (C_s; C-13), 69.8 (C_s; C-15), 70.4 + 70.6 (C_s; C-14 + C-18), 70.7 (C_s; C-17), 72.0(0) (C_s; C-19), 72.0(5) (C_s; C-16), 72.5 (C_s; C-12), 106.2 (C_t; C-9), 126.6 (C_t; d, $^4J_{CP}$ = 3.28 Hz, C-4 + C-4'), 127.7 (C_t; d, $^7J_{CP}$ = 2.12 Hz, C-7), 128.3 (C_t; d, $^6J_{CP}$ = 1.73 Hz, C-6), 130.1 (C_t; d, $^3J_{CP}$ = 6.74 Hz, C-3 + C-3'), 130.9 (C_q; d, $^2J_{CP}$ = 9.63 Hz, C-2), 132.9 (C_q; C-8), 135.9 (C_q; d, $^5J_{CP}$ = 4.05 Hz, C-5), 138.3 (C_q; C-11), 152.8 (C_q; C-10); MALDI-MS: m/z (%) calcd.: 684.33 ([M]$^{+\cdot}$,100), found: 684.33 ([M]$^{+\cdot}$,100).

Compound 89

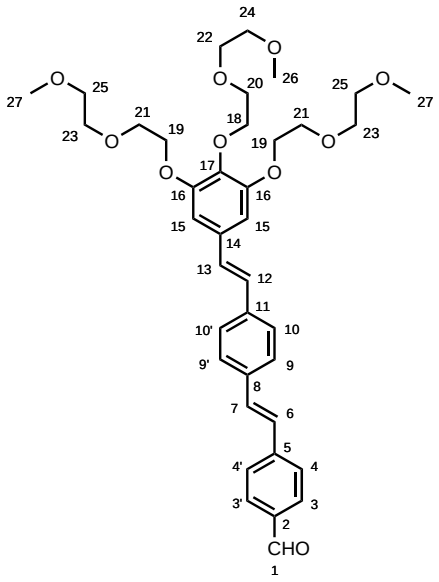

212 mg (1.89 mmol) potassium *tert*-butoxide was added in portions to a stirred solution of 781 mg (1.14 mmol) **88** and 0.25 ml (262 mg, 1.26 mmol) 4-(diethoxymethyl)benzaldehyde (**2**) in 10 ml dry THF under nitrogen atmosphere at room temperature. After stirring overnight, the solution was quenched with 1N HCl and extracted four times with $CHCl_3$. The organic phase was dried over Na_2SO_4 and evaporated under reduced pressure. The crude product was subjected to column chromatography ($CHCl_3$ / acetone = 8 / 1 $\rightarrow$ 1 / 1) to afford 647 mg of a yellowish oil. The material was dissolved in DCM, washed with aqueous sodium carbonate solution* and dried over Na_2SO_4. Evaporation of the solvent under reduced pressure gave 613 mg (922 µmol, 81%) of a yellow oil. ^{1}H NMR ($CDCl_3$): δ = 3.37(3) (s, 3 H; H-26), 3.37(9) (s, 6 H; H-27), 3.57 (m, 6 H; H-24 + H-25), 3.72 (m, 6 H; H-22 + H-23), 3.81 (t, ^3J = 5.10 Hz, 2 H; H-20), 3.87 (t, ^3J = 5.07 Hz, 4 H; H-21), 4.18 (t, ^3J = 5.14 Hz, 2 H; H-18), 4.22 (t, ^3J = 5.10 Hz, 4 H; H-19), 6.76 (s, 2 H; H-15), 6.95 (d, ^3J = 16.25 Hz, 1 H; H-12), 7.01 (d, ^3J = 16.25 Hz, 1 H; H-13), 7.13 (d, ^3J = 16.35 Hz, 1 H; H-6), 7.23 (d, ^3J = 16.35 Hz, 1 H; H-7), 7.48 (AA' of AA'BB', ^3J = 8.60 Hz, 2 H; H-10 + H-10'), 7.52 (BB' of AA'BB', ^3J = 8.60 Hz, 2 H; H-9 + H-9'), 7.63 (AA' of AA'BB', ^3J = 8.23 Hz, 2 H; H-4 + H-4'), 7.85 (BB' of AA'BB', ^3J = 8.23 Hz, 2 H; H-3 + H-3'), 9.97 (s, 1 H; H-1), ^{13}C NMR ($CDCl_3$): δ = 59.1(0) (C_p; C-26), 59.1(4) (C_p; C-27), 68.9 (C_s; C-19), 69.8 (C_s; C-21), 70.5 + 70.6 (C_s; C-20 + C-24), 70.8 (C_s; C-23), 72.0(5) (C_s; C-25), 72.1(0) (C_s; C-22), 72.5 (C_s; C-18), 106.3 (C_t; C-15), 126.8(9) (C_t;

*NMR data indicated the presence of 4-formylbenzoic acid.

C-10 + C-10'), 126.9(2) (C_t; C-4 + C-4'), 127.1 (C_t; C-6), 127.4 (C_t; C-9 + C-9'), 127.5 (C_t; C-12), 129.0 (C_t; C-13), 130.3 (C_t; C-3 + C-3'), 131.8 (C_t; C-7), 132.8 (C_q; C-14), 135.3 (C_q; C-2), 135.8 (C_q; C-8), 137.5 (C_q; C-11), 138.6 (C_q; C-17), 143.5 (C_q; C-5), 152.8 (C_q; C-16), 191.7 (C_t; C-1); MALDI-MS: m/z (%) calcd.: 664.32 ($[M]^{+\cdot}$,100), found: 664.33 ($[M]^{+\cdot}$,100).

10.10 Synthesis of the Hekate star with short ethyleneoxy-chains

Compound $S2_{O2}$

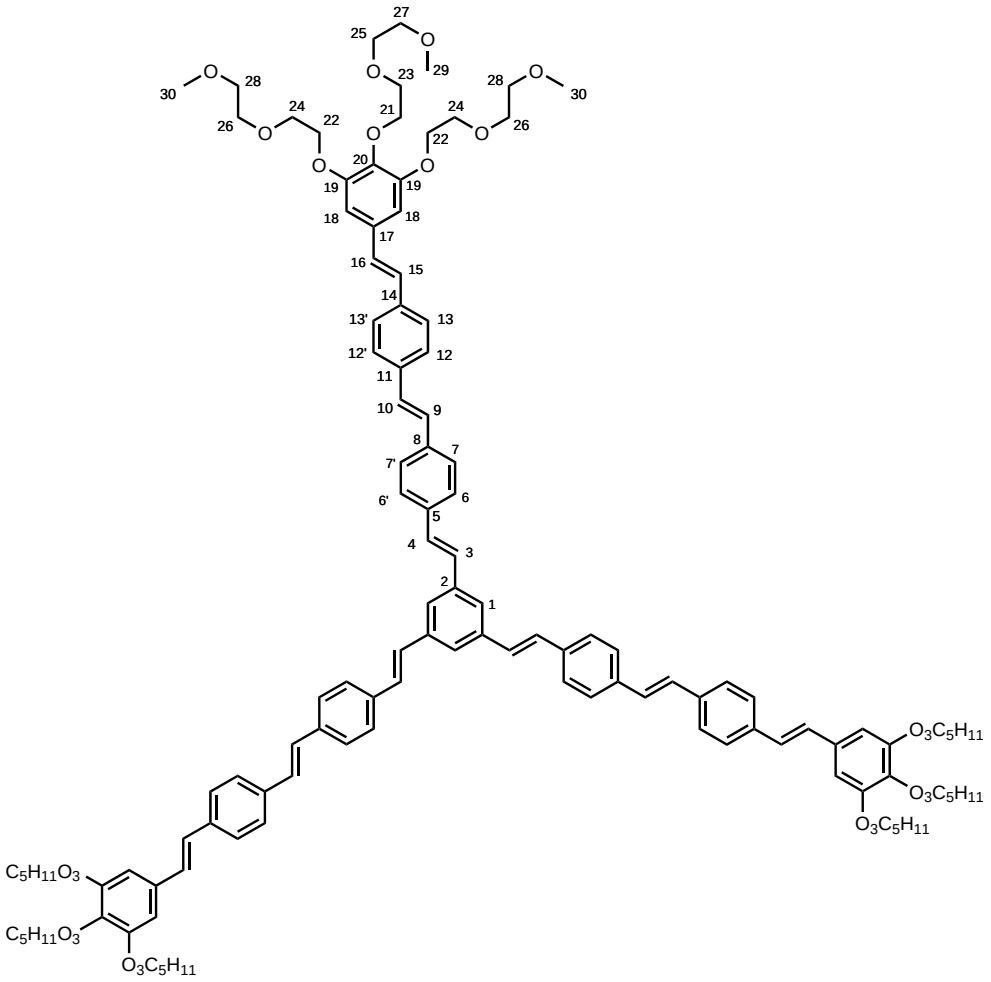

An ultrasonic bath was applied for 5 minutes to a solution of 66.9 mg (143 µmol) core building block **3** and 368 mg (537 µmol) arm building block **107** in 30 mL dry THF under nitrogen atmosphere. 97.5 mg (869 µmol) potassium *tert*-butoxide was added in portions and the solution was stirred at room temperature for 3 days. The mixture was poured into 1N HCl and extracted with chloroform. The organic solvent was dried over Na_2SO_4 and evaporated under reduced pressure. The residue was dissolved in few chloroform, injected into petroleum ether and stored at -35 °C for several days. The precipitate was collected via a filter funnel and subjected to preparative recycling GPC to give 116 mg (56.3 mg, 39%) of a yellow solid. ^{1}H NMR ($CDCl_3$): δ = 3.39 (s, 9 H; H-29), 3.40 (s, 18 H; H-30), 3.58 (m, 18 H; H-27 + H-28), 3.74 (m, 18 H; H-25 + H-26), 3.82 (t, ^3J = 5.20 Hz, 6 H; H-23), 3.89 (t, ^3J = 5.08 Hz, 12 H; H-24), 4.19 (t, ^3J = 5.14 Hz, 6 H; H-21), 4.24 (t, ^3J = 5.17 Hz, 12 H; H-22), 6.78 (s, 6 H; H-18), 6.97 (d, ^3J = 16.16 Hz, 3 H; H-15), 7.02 (d, ^3J = 16.16 Hz, 3 H; H-16), 7.15 (s, 6 H; H-9 + H-10), 7.18 + 7.23 (d, ^3J = 16.42 Hz, 6 H; H-3 + H-4), 7.49 (AA' of AA'BB', ^3J = 8.70 Hz, 6 H; H-13 + H-13'), 7.53 (BB' of AA'BB', ^3J = 8.70 Hz, 6 H; H-12 + H-12'), 7.53 - 7.60 (m, 15 H;

H-1 + H-6 + H-6' + H-7 + H-7'); ^{13}C NMR ($CDCl_3$): δ = 59.1(5) (C_p; C-29), 59.1(9) (C_p; C-30), 69.0 (C_s; C-22), 69.9 (C_s; C-24), 70.5 + 70.7 (C_s; C-23 + C-27), 70.9 (C_s; C-26), 72.1 (C_s; C-28), 72.2 (C_s; C-25), 72.6 (C_s; C-21), 106.3 (C_t; C-18), 124.1 (C_t; C-1), 126.9 + 127.0 + 127.1 (C_t; C-6 + C-6' + C-7 + C-7' + C-12 + C-12' + C-13 + C-13'), 127.8 (C_t; C-15), 128.2 + 128.9 (C_t; C-3 + C-4), 128.3(0) + 128.3(3) (C_t; C-9 + C-10), 128.5 (C_t; C-16), 133.0 (C_q; C-17), 136.6(5) + 136.6(9) + 136.7 + 136.9 (C_q; C-5 + C-8 + C-11 + C-14), 138.1 (C_q; C-2), 138.5 (C_q; C-20), 152.9 (C_q; C-19); MALDI-MS: m/z (%) calcd.: 2060.04 ($[M+1]^{+\cdot}$,100), found: 2060.06 ($[M+1]^{+\cdot}$,100); ESI-HRMS: m/z calcd. for $C_{123}H_{150}O_{27}Na^+$ ($[M+Na]^+$): 2082.0257, found: 2082.0187; Elemental analysis (%) for $C_{123}H_{150}O_{27}$ calcd.: C 71.70, H 7.34, found: C 70.58, H 7.42.

10.11 Synthesis of the arm building blocks with long ethyleneoxy-chains

Compound 94

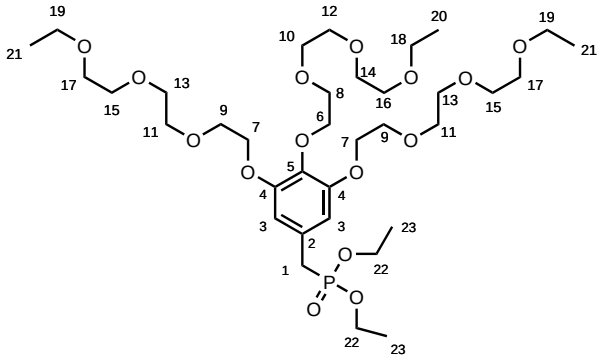

At 0 °C, 2.62 ml (7.55 g, 27.9 mmol) PBr_3 in 20 ml DCM was added in drops to a solution of 35.5 g (55.8 mmol) alcohol **108** in 250 ml DCM and was stirred overnight at room temperature. The mixture was poured into distilled water and extracted with DCM four times. The organic phase was dried over Na_2SO_4 and evaporated under reduced pressure to obtain 37.7 g of a viscous liquid.

14.1 ml (13.7 g, 82.5 mmol) $P(OEt)_3$ was added and the mixture was stirred at 135 °C in a round-bottom flask equipped with a condenser under nitrogen atmosphere for 4 hours. The distillate was discarded and excess $P(OEt)_3$ was removed via distillation en vacuo. The crude product was subjected to column chromatography (ethyl acetate / ethanol = 4 / 1 $\rightarrow$ 3 / 2) to yield 29.0 g (38.3 mmol. 69%) of a colorless oil. ^{1}H NMR ($CDCl_3$): δ = 1.19 (t, ^3J = 7.02 Hz, 9 H; H-20 + H-21), 1.23 (t, ^3J = 7.06 Hz, 6 H; H-23), 3.02 (d, $^2J_{HP}$ = 21.48 Hz, 2 H; H-1), 3.50 (q, ^3J = 7.00 Hz, 6 H; H-18 + H-19), 3.57 (m, 6 H; H-16 + H-17), 3.64 (m, 12 H; H-12 + H-13 + H-14 + H-15), 3.70 (m, 6 H; H-10 + H-11), 3.76 (t, ^3J = 5.17 Hz, 2 H; H-8), 3.82 (t, ^3J = 5.14 Hz, 4 H; H-9), 3.99 (m, 4 H; H-22), 4.11 (m, 6 H; H-6 + H-7), 6.51 (d, $^4J_{HP}$ = 2.56 Hz, 2 H; H-3); ^{13}C NMR ($CDCl_3$): δ = 15.3 (C_p; C-20 + C-21), 16.6 (C_p; d, $^3J_{CP}$ = 5.94 Hz, C-23), 33.9 (C_s; d, $^1J_{CP}$ = 138.7 Hz, C-1), 62.2 (C_s; d, $^2J_{CP}$ = 6.78 Hz, C-22), 66.7 (C_s; C-18 + C-19), 68.9 (C_s; C-7), 69.8 (C_s; C-9), 69.9 (C_s; C-16 + C-17), 70.6 + 70.7(6) + 70.7(9) + 70.9 (C_s; C-8 + C-10 + C-11 + C-12 + C-13 + C-14 + C-15), 72.4 (C_s; C-6), 109.4 (C_t; d, $^3J_{CP}$ = 6.68 Hz, C-3), 127.0 (C_q; d, $^2J_{CP}$ = 8.92 Hz, C-2), 137.4 (C_q; d, $^5J_{CP}$ = 4.04 Hz, C-5), 152.6 (C_q; d, $^4J_{CP}$ = 3.19 Hz, C-4); MALDI-MS: m/z (%) calcd.: 756.41 ($[M]^{+\cdot}$,100), found: 756.32 ($[M]^{+\cdot}$,100).

Compound 95

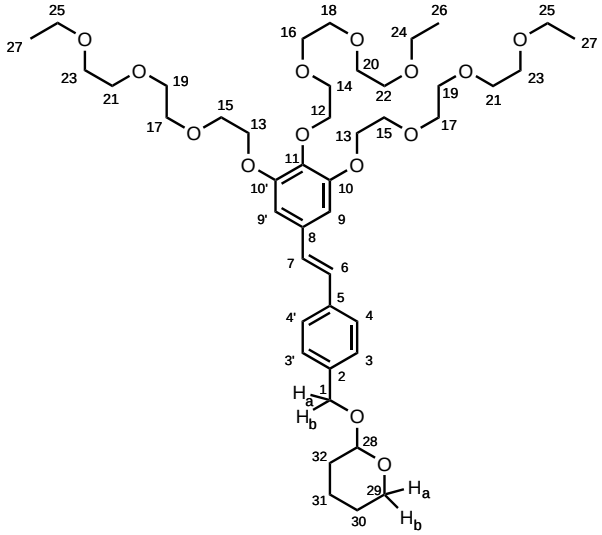

5.08 g (45.3 mmol) potassium *tert*-butoxide was added in portions to a stirred solution of 13.2 g (17.4 mmol) **94** and 4.98 g (22.6 mmol) (±)-4-(3,4,5,6-tetrahydro-2*H*-pyran-2-yloxymethyl)-benzaldehyde (**13**) in 100 mL dry THF under nitrogen atmosphere and cooled with a water bath. After stirring overnight, the mixture was poured into 150 ml 2N HCl and extracted with ethyl acetate four times. The organic phase was dried over Na_2SO_4 and evaporated under reduced pressure. The crude product was subjected to column chromatography (ethyl acetate / ethanol = 5 / 1) to afford 11.6 g (14.1 mmol, 81%) of a reddish oil. The product was used in the next step without further purification procedures. ^{1}H NMR ($CDCl_3$): δ = 1.20(0) (t, ^3J = 7.00 Hz, 6 H; H-27), 1.20(2) (t, ^3J = 7.03 Hz, 3 H; H-26), 1.70 (m, 6 H; H-30 + H-31 + H-32), 3.51(4) (q, ^3J = 7.00 Hz, 4 H; H-25), 3.51(8) (q, ^3J = 7.03 Hz, 2 H; H-24), 3.56 (m, 6 H; H-22 + H-23), 3.59 (m, 1 H; H-29a), 3.67 (m, 12 H; H-18 + H-19 + H-20 + H-21), 3.74 (m, 6 H; H-16 + H-17), 3.80 (t, ^3J = 5.14 Hz, 2 H; H-14), 3.87 (t, ^3J = 5.14 Hz, 4 H; H-15), 3.93 (m, 1 H; H-29b), 4.16 (t, ^3J = 5.14 Hz, 2 H; H-12), 4.21 (t, ^3J = 5.10 Hz, 4 H; H-13), 4.50 (d, ^2J = 12.22 Hz, 1 H; H-1a), 4.72 (t, ^3J = 3.46 Hz, 1 H; H-28), 4.79 (d, ^2J = 12.22 Hz, 1 H; H-1b), 6.75 (s, 2 H; H-9), 6.96 (s, 2 H; H-6 + H-7), 7.35 (AA' of AA'BB', ^3J = 8.26 Hz, 2 H; H-3 + H-3'), 7.47 (BB' of AA'BB', ^3J = 8.26 Hz, 2 H; H-4 + H-4').

Compound 96

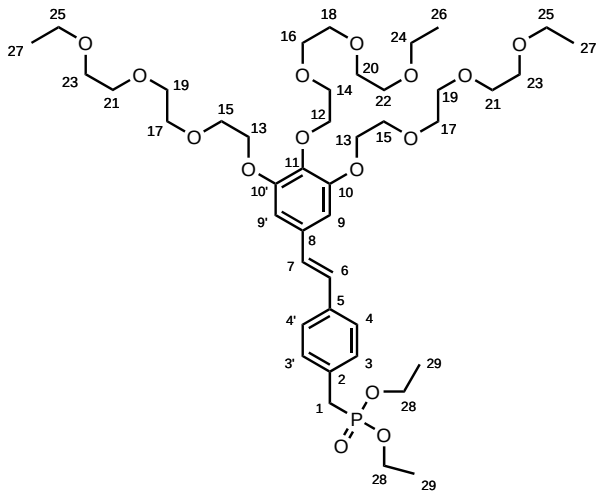

A freshly prepared solution[171] of PPh_3Br_2 (18.5 mmol) in 100 ml DCM was added drop by drop to a mixture of 11.9 g (14.5 mmol) **95** and 30 ml DCM under nitrogen atmosphere. After stirring overnight, a saturated solution of $NaHCO_3$ was poured into the solution. The mixture was extracted with DCM and the organic phase was washed with water. The aqueous phase was again extracted with DCM and the combined organic solvents were dried over Na_2SO_4. The solvent was evaporated under reduced pressure and the crude product was subjected to column chromatography (DCM / acetone = 9 / 1 → 1 / 1) to give 14.4 g of a reddish oil.

2.5 ml (2.42 g, 14.6 mmol) $P(OEt)_3$ was added and the mixture was stirred in a round-bottom flask equipped with a condenser at 135 °C for two hours under nitrogen atmosphere. The distillate was discarded and excess $P(OEt)_3$ was removed via distillation in vacuo. The crude product was subjected to column chromatography (DCM / acetone = 9 / 1 → 1 / 2) to yield 7.48 g (8.71 mmol, 60%) of an amber-colored oil. ^{1}H NMR ($CDCl_3$): δ = 1.16(0) (t, ^3J = 7.02 Hz, 6 H; H-27), 1.16(3) (t, ^3J = 7.02 Hz, 3 H; H-26), 1.21 (t, ^3J = 17.08 Hz, 6 H; H-29), 3.12 (d, $^2J_{HP}$ = 21.77 Hz, 2 H; H-1), 3.47(6) (q, ^3J = 7.02 Hz, 4 H; H-25), 3.48(0) (q, ^3J = 7.02 Hz, 2 H; H-24), 3.57 (m, 6 H; H-22 + H-23), 3.64 (m, 12 H; H-18 + H-19 + H-20 + H-21), 3.70 (m, 6 H; H-16 + H-17), 3.76 (t, ^3J = 5.14 Hz, 2 H; H-14), 3.84 (t, ^3J = 5.10 Hz, 4 H; H-15), 3.99 (m, 4 H; H-28), 4.13 (t, ^3J = 5.10 Hz, 2 H; H-12), 4.17 (t, ^3J = 5.10 Hz, 4 H; H-13), 6.71 (s, 2 H; H-9), 6.89 + 6.94 (d, ^3J = 16.54 Hz, 1 H; H-6 + H-7), 7.25 (AA' of AA'BB', $^4J_{HP}$ = 2.38 Hz, ^3J = 7.76 Hz, 2 H; H-3 + H-3'), 7.40 (BB' of AA'BB', ^3J = 7.76 Hz, 2 H; H-4 + H-4'); ^{13}C NMR ($CDCl_3$): δ = 15.2 (C_p; C-26 + C-27), 16.4 (C_p; d, $^3J_{CP}$ = 5.97 Hz, C-29), 33.6 (C_s; d, $^1J_{CP}$ = 137.9 Hz, C-1), 62.2 (C_s; d, $^2J_{CP}$ = 6.74 Hz, C-28), 66.6 (C_s; C-24 + C-25), 68.9 (C_s; C-13), 69.7(6) (C_s; C-15), 69.8(2) (C_s; C-22 + C-23), 70.5(1) + 70.5(3) + 70.6(8) + 70.6(9) + 70.7 + 70.8 (C_s; C-14 + C-16 + C-17 + C-18 + C-19 + C-20 + C-21), 72.4 (C_s; C-12), 106.3 (C_t; C-9), 126.6 (C_t; d, $^4J_{CP}$ = 3.28 Hz, C-4 + C-4'), 127.7 (C_t; d, $^7J_{CP}$ = 2.12 Hz, C-6), 128.3 (C_t; d, $^6J_{CP}$ = 1.54 Hz, C-7), 130.1 (C_t; d, $^3J_{CP}$ = 6.74 Hz, C-3 + C-3'), 130.9 (C_q; d, $^2J_{CP}$ = 9.63 Hz, C-2), 132.9 (C_q; C-8), 135.9 (C_q; d, $^5J_{CP}$ = 4.05 Hz, C-5), 138.4 (C_q; C-11); MALDI-MS: m/z (%) calcd.: 881.44 ([M+Na]$^+$,100), found: 881.38 ([M+Na]$^+$,100).

Compound 98

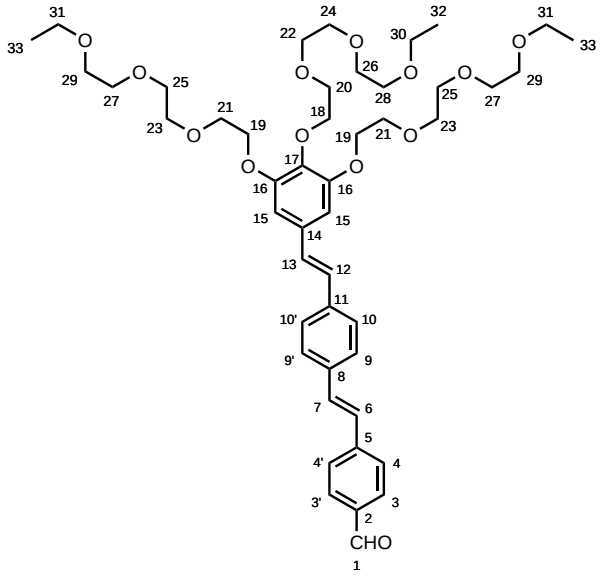

371 mg (3.32 mmol) potassium *tert*-butoxide was added in portions to a stirred solution of 1.71 g

(1.99 mmol) **96** and 0.44 mL (461 mg, 2.21 mmol) 4-(Diethoxymethyl)benzaldehyde in 20 mL dry THF under nitrogen atmosphere. After stirring overnight, the mixture was treated with 1N HCl and extracted with chloroform. The organic phase was washed with sodium carbonate solution* and 1N HCl, dried over Na_2SO_4 and evaporated under reduced pressure. The crude product was subjected to column chromatography ($CHCl_3$ / ethanol = 15 / 1 → 7 / 1) to afford 1.36 g (1.62 mmol, 81%) of a yellow oil. ^{1}H NMR ($CDCl_3$): δ = 1.20(1) (t, ^3J = 7.02 Hz, 6 H; H-33), 1.20(4) (t, ^3J = 6.98 Hz, 3 H; H-32), 3.51(7) (q, ^3J = 6.99 Hz, 4 H; H-31), 3.52(0) (q, ^3J = 6.98 Hz, 2 H; H-30), 3.56 - 3.77 (m, 24 H; H-22 + H-23 + H-24 + H-25 + H-26 + H-27 + H-28 + H-29), 3.80 (t, ^3J = 5.14 Hz, 2 H; H-20), 3.88 (t, ^3J = 5.10 Hz, 4 H; H-21), 4.17 (t, ^3J = 5.14 Hz, 2 H; H-18), 4.22 (t, ^3J = 5.12 Hz, 4 H; H-19), 6.77 (s, 2 H; H-15), 6.97 (d, ^3J = 16.20 Hz, 1 H; H-12), 7.03 (d, ^3J = 16.20 Hz, 1 H; H-13), 7.15 (d, ^3J = 16.33 Hz, 1 H; H-6), 7.26 (d, ^3J = 16.33 Hz, 1 H; H-7), 7.51 (AA' of AA'BB', ^3J = 8.62 Hz, 2 H; H-10 + H-10'), 7.54 (BB' of AA'BB', ^3J = 8.62 Hz, 2 H; H-9 + H-9'), 7.66 (AA' of AA'BB', ^3J = 8.34 Hz, 2 H; H-4 + H-4'), 7.87 (BB' of AA'BB', ^3J = 8.34 Hz, 2 H; H-3 + H-3'), 10.00 (s, 1 H; H-1); ^{13}C NMR ($CDCl_3$): δ = 15.3 (C_p; C-32 + C-33), 66.7 (C_s; C-30 + C-31), 69.0 (C_s; C-19), 69.8(7) + 69.9(2) + 69.9(3) + 70.6(3) + 70.6(4) + 70.7(8) + 70.7(9) + 70.8 + 70.9 (C_s; C-20 + C-21 + C-22 + C-23 + C-24 + C-25 + C-26 + C-27 + C-28 + C-29), 72.5 (C_s; C-18), 106.5 (C_t; C-15), 126.9(4) (C_t; C-10 + C-10'), 126.9(7) (C_t; C-4 + C-4'), 127.2 (C_t; C-6), 127.4 (C_t; C-9 + C-9'), 127.6 (C_t; C-12), 129.0 (C_t; C-13), 130.4 (C_t; C-3 + C-3'), 131.8 (C_t; C-7), 132.8 (C_q; C-14), 135.4 (C_q; C-2), 135.9 (C_q; C-8), 137.6 (C_q; C-11), 138.7 (C_q; C-17), 143.5 (C_q; C-5), 152.9 (C_q; C-16), 191.7 (C_t; C-1); MALDI-MS: m/z (%) calcd.: 839.45 ($[M]^{+\cdot}$,100), found: 838.43 ($[M]^{+\cdot}$,100).

Compound 97

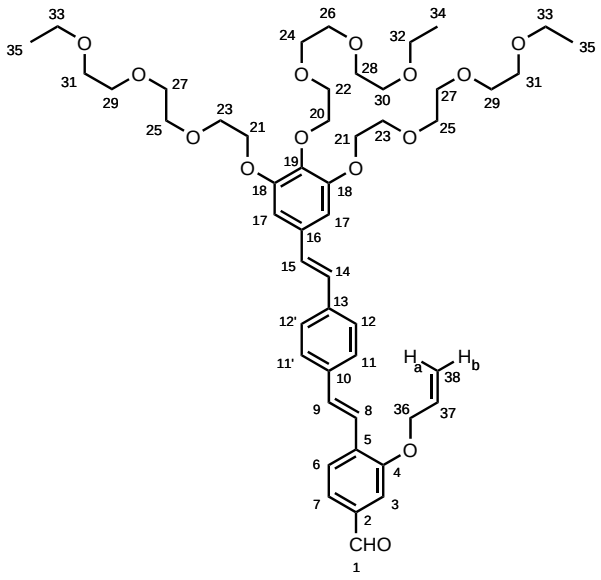

522 mg (4.65 mmol) potassium *tert*-butoxide was added in portions to a stirred solution of 2.22 g (2.58 mmol) **96** and 682 mg (3.10 mmol) methyl 3-(allyloxy)-4-formylbenzoate (**18**) in 20 mL dry THF under nitrogen atmosphere at 0 °C. After 5 minutes, the cooling bath was removed and stirring at room temperature was continued for 3 days. The reaction was then quenched with 1N HCl and extracted with $CHCl_3$. The organic solvent was dried over Na_2SO_4 and evaporated under reduced pressure. The residue was passed over a short silica gel column ($CHCl_3$ / ethanol = 20 / 1 → 4 / 1) to

*NMR data indicated the presence of 4-formylbenzoic acid.

afford 2.47 g of a yellow oil.

After dissolving the residue in 40 ml dry THF, 125 mg (3.29 mmol) $LiAlH_4$ was added carefully and the mixture was refluxed for 2 hours. At 0 °C, the reaction was quenched cautiously with water and 1N HCl, respectively. The mixture was extracted with $CHCl_3$ and the organic solvent was dried over Na_2SO_4 and evaporated under reduced pressure to afford 2.29 g of a highly viscous oil.

The intermediate product, dissolved in 50 ml of dry DCM under nitrogen atmosphere, was mixed with 1.81 g (4.27 mmol) Dess–Martin periodinane and stirring at room temperature was continued for 7 days. The crude product was subjected to column chromatography ($CHCl_3$ / ethanol = 40 / 1 $\rightarrow$ 4 / 1) to afford 1.54 g (1.72 mmol, 67%) of a yellow oil. The product was used in the next step without further purification procedures. ^{1}H NMR ($CDCl_3$): δ = 1.20(2) (t, ^3J = 7.06 Hz, 6 H; H-35), 1.20(5) (t, ^3J = 7.06 Hz, 3 H; H-34), 3.51(8) (q, ^3J = 7.03 Hz, 4 H; H-33), 3.52(0) (q, ^3J = 7.02 Hz, 2 H; H-32), 3.56 - 3.77 (m, 24 H; H-24 + H-25 + H-26 + H-27 + H-28 + H-29 + H-30 + H-31), 3.80 (t, ^3J = 5.10 Hz, 2 H; H-22), 3.88 (t, ^3J = 5.10 Hz, 4 H; H-23), 4.17 (t, ^3J = 5.18 Hz, 2 H; H-20), 4.22 (t, ^3J = 5.10 Hz, 4 H; H-21), 4.71 (dt, ^3J = 5.10 Hz, ^4J = 1.55 Hz, 2 H; H-36), 5.36 (m, 1 H; H-38b), 5.49 (m, 1 H; H-38a), 6.13 (m, 1 H; H-37), 6.77 (s, 2 H; H-17), 6.97 (d, ^3J = 16.28 Hz, 1 H; H-14), 7.02 (d, ^3J = 16.28 Hz, 1 H; H-15), 7.28 (d, ^3J = 16.53 Hz, 1 H; H-9), 7.40 (d, ^4J = 1.48 Hz, 1 H; H-3), 7.47 (dd, ^3J = 7.64 Hz, ^4J = 1.20 Hz, 1 H; H-7), 7.50 (AA' of AA'BB', ^3J = 8.48 Hz, 2 H; H-12 + H-12'), 7.55(0) (BB' of AA'BB', ^3J = 8.48 Hz, 2 H; H-11 + H-11'), 7.55(2) (d, ^3J = 16.53 Hz, 1 H; H-8), 7.77 (d, ^3J = 7.92 Hz, 1 H; H-6), MALDI-MS: m/z (%) calcd.: 894.48 ([M]$^{+\cdot}$,100), found: 894.49 ([M]$^{+\cdot}$,100).

10.12 Synthesis of the V-shaped building blocks with long ethyleneoxy-chains

Compound 99

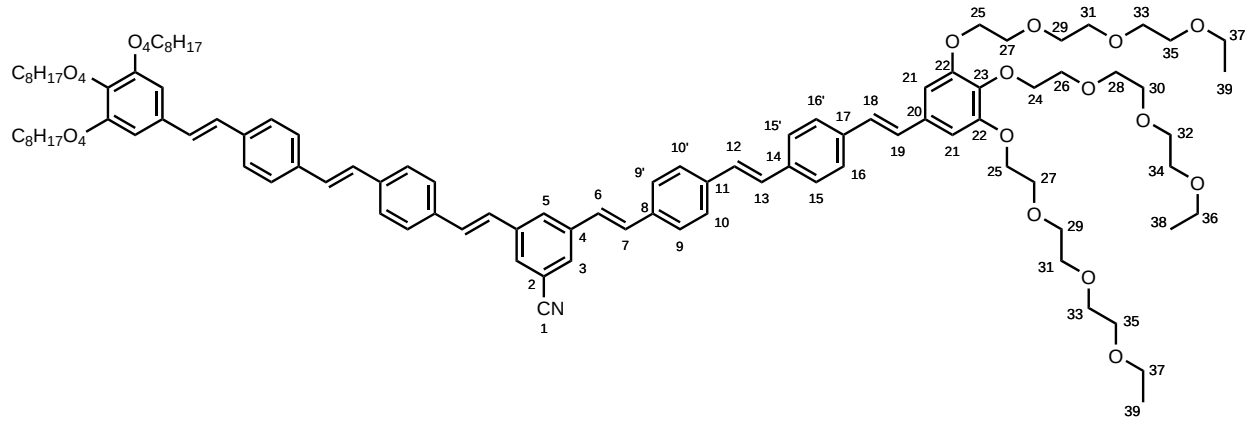

578 mg (5.15 mmol) potassium *tert*-butoxide was added in portions to a stirred solution of 519 mg (1.43 mmol) dialdehyde **9** and 2.72 g (3.17 mmol) phosphonate **96** in 20 mL dry THF under nitrogen atmosphere. After stirring overnight, the reaction was quenched with 1N HCl and extracted with $CHCl_3$ four times. The organic solvent was dried over Na_2SO_4 and evaporated under reduced pressure. The residue was passed over a short silica gel column with $CHCl_3$ / ethanol (10 / 1) as eluent and the crude product obtained was subjected to preparative recycling GPC (flow rate: 6.0 $mL \cdot min^{-1}$) to give 1.32 g (744 µmol, 52%) of a waxy yellow solid. ^{1}H NMR ($CDCl_3$): δ = 1.19(8) (t, ^3J = 7.02 Hz, 12 H; H-39), 1.20(0) (t, ^3J = 7.02 Hz, 6 H; H-38), 3.51(4) (q, ^3J = 7.03 Hz, 8 H; H-37),

3.51(6) (q, ^3J = 7.03 Hz, 4 H; H-36), 3.56 - 3.77 (m, 48 H; H-28 + H-29 + H-30 + H-31 + H-32 + H-33 + H-34 + H-35), 3.80 (t, ^3J = 5.14 Hz, 4 H; H-26), 3.87 (t, ^3J = 5.14 Hz, 8 H; H-27), 4.17 (t, ^3J = 5.22 Hz, 4 H; H-24), 4.21 (t, ^3J = 5.10 Hz, 8 H; H-25), 6.76 (s, 4 H; H-21), 6.95 (d, ^3J = 16.15 Hz, 2 H; H-18), 7.00 (d, ^3J = 16.15 Hz, 2 H; H-19), 7.07 (d, ^3J = 16.25 Hz, 2 H; H-6), 7.11 + 7.15 (d, ^3J = 16.17 Hz, 4 H; H-12 + H-13), 7.18 (d, ^3J = 16.25 Hz, 2 H; H-7), 7.48 (AA' of AA'BB', ^3J = 8.80 Hz, 4 H; H-16 + H-16'), 7.51 (BB' of AA'BB', ^3J = 8.80 Hz, 4 H; H-15 + H-15'), 7.53 (s, 8 H; H-9 + H-9' + H-10 + H-10'), 7.63 (d, ^4J = 1.28 Hz, 2 H; H-3), 7.78 (m, 1 H; H-5); ^{13}C NMR ($CDCl_3$): δ = 15.3 (C_p; C-38 + C-39), 66.7 (C_s; C-36 + C-37), 69.0 (C_s; C-25), 69.8(6) + 69.9(2) + 70.6(2) + 70.6(4) + 70.7(7) + 70.7(8) + 70.8(1) + 70.9 (C_s; C-26 + C-27 + C-28 + C-29 + C-30 + C-31 + C-32 + C-33 + C-34 + C-35), 72.5 (C_s; C-24), 106.4 (C_t; C-21), 113.4 (C_q; C-2), 118.9 (C_q; C-1), 126.0 (C_t; C-6), 126.9 (C_t; C-16 + C-16'), 127.0(3) + 127.0(5) + 127.3 (C_t; C-9 + C-9' + C-10 + C-10' + C-15 + C-15'), 127.7 (C_t; C-18), 127.9 + 128.8 (C_t; C-12 + C-13), 128.4 (C_t; C-3), 128.5 (C_t; C-5), 128.6 (C_t; C-19), 131.1 (C_t; C-7), 133.0 (C_q; C-20), 135.7 + 137.7 (C_q; C-8 + C-11), 136.5 + 136.9 (C_q; C-14 + C-17), 138.6 (C_q; C-23), 139.1 (C_q; C-4), 152.9 (C_q; C-22); MALDI-MS: m/z (%) calcd.: 1772.96 ($[M+1]^{+\cdot}$,100), found: 1772.96 ($[M+1]^{+\cdot}$,100).

Compound 100

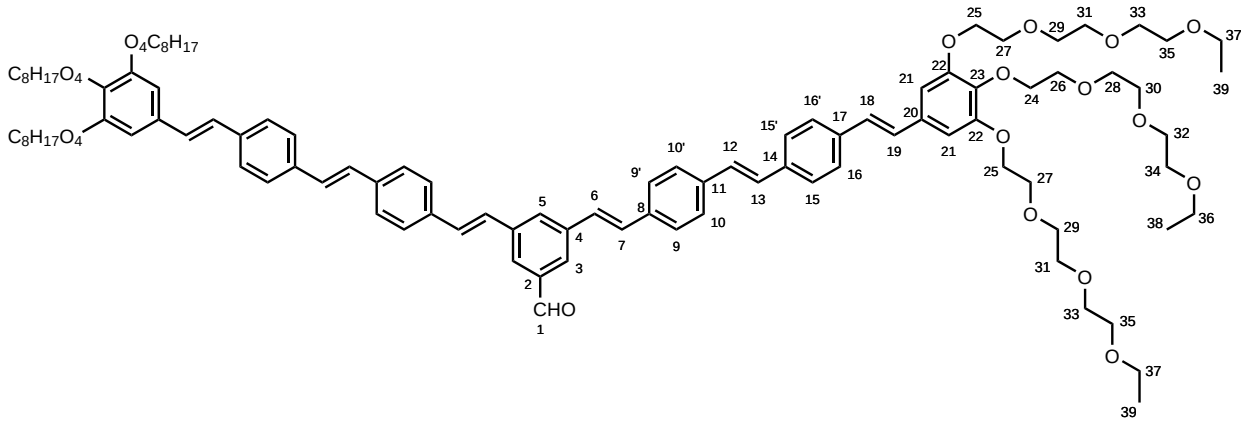

0.6 ml (600 µmol) of a 1M DIBAL solution (toluene) was added drop by drop to a stirred solution of 698 mg (393 µmol) **99** in 3 ml dry toluene at 0 °C under nitrogen atmosphere. The solution was then allowed to warm to room temperature and stirred overnight. 3.0 ml methanol was added in drops and the mixture was poured into 1M HCl. The solution was extracted with $CHCl_3$, the organic solvent dried with Na_2SO_4 and evaporated under reduced pressure to yield 609 mg (343 µmol, 87%) of a yellow waxy solid. ^{1}H NMR ($CDCl_3$): δ = 1.19(8) (t, ^3J = 7.02 Hz, 12 H; H-39), 1.20(0) (t, ^3J = 7.04 Hz, 6 H; H-38), 3.51(4) (q, ^3J = 7.00 Hz, 8 H; H-37), 3.51(7) (q, ^3J = 7.02 Hz, 4 H; H-36), 3.56 - 3.77 (m, 48 H; H-28 + H-29 + H-30 + H-31 + H-32 + H-33 + H-34 + H-35), 3.80 (t, ^3J = 5.06 Hz, 4 H; H-26), 3.87 (t, ^3J = 5.02 Hz, 8 H; H-27), 4.17 (t, ^3J = 5.04 Hz, 4 H; H-24), 4.21 (t, ^3J = 5.02 Hz, 8 H; H-25), 6.76 (s, 4 H; H-21), 6.95 (d, ^3J = 16.29 Hz, 2 H; H-18), 7.00 (d, ^3J = 16.29 Hz, 2 H; H-19), 7.13 (s, 4 H; H-12 + H-13), 7.16 (d, ^3J = 16.45 Hz, 2 H; H-6), 7.24 (d, ^3J = 16.45 Hz, 2 H; H-7), 7.48 (AA' of AA'BB', ^3J = 8.76 Hz, 4 H; H-16 + H-16'), 7.51 (BB' of AA'BB', ^3J = 8.76 Hz, 4 H; H-15 + H-15'), 7.54 (s, 8 H; H-9 + H-9' + H-10 + H-10'), 7.84 (s, 1 H; H-5), 7.90 (s, 2 H; H-3), 10.07 (s, 1 H; H-1); ^{13}C NMR ($CDCl_3$): δ = 15.3 (C_p; C-38 + C-39), 66.7 (C_s; C-36 + C-37), 69.0 (C_s; C-25), 69.8(7) + 69.9(2) + 70.6(2) + 70.6(4) + 70.7(8) + 70.7(9) + 70.8(1) + 70.9 (C_s; C-26 + C-27 +

C-28 + C-29 + C-30 + C-31 + C-32 + C-33 + C-34 + C-35), 72.5 (C_s; C-24), 106.4 (C_t; C-21), 126.4 (C_t; C-3), 126.8(9) + 126.9(2) + 127.0(2) + 127.0(4) + 127.2 (C_t; C-6 + C-9 + C-9' + C-10 + C-10' + C-15 + C-15' + C-16 + C-16'), 127.8 + 128.0 + 128.5 + 128.6 (C_t; C-12 + C-13 + C-18 + C-19), 130.4 (C_t; C-5 + C-7), 133.0 (C_q; C-20), 136.1 (C_q; C-8), 136.6 (C_q; C-17), 136.8 (C_q; C-14), 137.3 (C_q; C-2), 137.4 (C_q; C-11), 138.6 (C_q; C-23), 138.8 (C_q; C-4), 152.9 (C_q; C-22), 192.4 (C_t; C-1); MALDI-MS: m/z (%) calcd.: 1775.96 ($[M+1]^{+\cdot}$,100), found: 1775.96 ($[M+1]^{+\cdot}$,100).

Compound 101

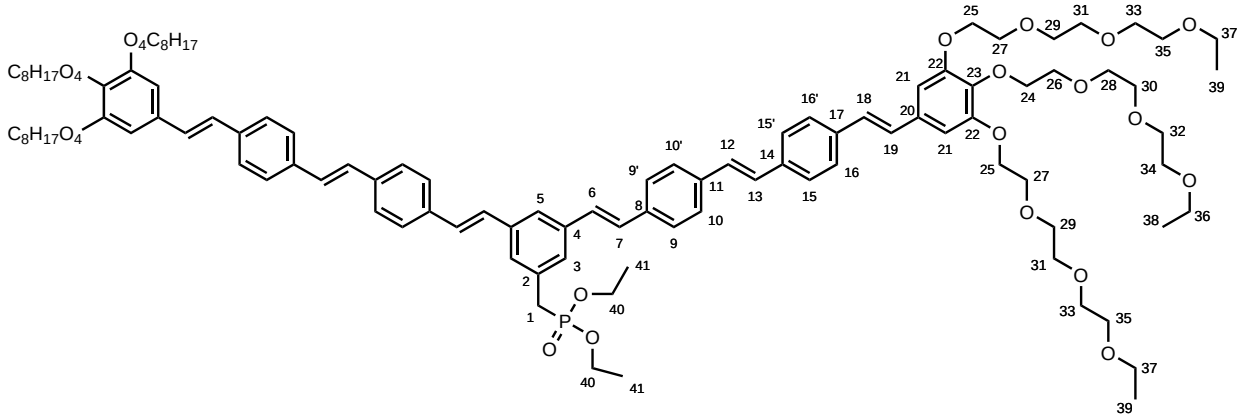

592 mg (333 µmol) **100** in 15 ml THF and 1 ml H_2O was mixed with 19.1 mg (505 µmol) $NaBH_4$ at 0 °C. Afer refluxing for 5 hours, the mixture was poured into 1N HCl, extracted with $CHCl_3$, dried over Na_2SO_4 and evaporated under reduced pressure to yield 535 mg of a yellow, waxy solid.
The residue was mixed with 15 ml of dry DCM and 338 mg (1.29 mmol) PPh_3 under nitrogen atmosphere . At 0 °C, 458 mg (1.38 mmol) CBr_4 dissolved in 3 ml DCM was added in drops. The cooling bath was removed and stirring was continued for 3 days. The solution was injected onto a silica gel column ($CHCl_3$ / ethanol = 10 / 1) to yield a yellow solid.
0.2 ml (194 mg, 1.17 mmol) $P(OEt)_3$ was added and the mixture was stirred at 140 °C for 3 hours. The crude product was subjected to column chromatography ($CHCl_3$ / ethanol = 20 / 1 → 1 / 1). Further purification was achieved by preparative recycling GPC to give 261 mg (137 µmol, 41%) of a yellow, waxy solid. ^{1}H NMR ($CDCl_3$): δ = 1.20(6) (t, ^3J = 7.08 Hz, 12 H; H-39), 1.20(7) (t, ^3J = 7.04 Hz, 6 H; H-38), 1.28 (t, ^3J = 7.06 Hz, 6 H; H-41), 3.21 (d, ^2J = 21.56 Hz, 2 H; H-1), 3.52(2) (q, ^3J = 7.01 Hz, 8 H; H-37), 3.52(3) (q, ^3J = 7.03 Hz, 4 H; H-36), 3.56 - 3.77 (m, 48 H; H-28 + H-29 + H-30 + H-31 + H-32 + H-33 + H-34 + H-35), 3.81 (t, ^3J = 5.18 Hz, 4 H; H-26), 3.88 (t, ^3J = 5.10 Hz, 8 H; H-27), 4.07 (m, 4 H; H-40), 4.17 (t, ^3J = 5.10 Hz, 4 H; H-24), 4.22 (t, ^3J = 5.20 Hz, 8 H; H-25), 6.77 (s, 4 H; H-21), 6.97 (d, ^3J = 16.08 Hz, 2 H; H-18), 7.02 (d, ^3J = 16.08 Hz, 2 H; H-19), 7.13 (d, ^3J = 16.26 Hz, 2 H; H-6), 7.14 (s, 4 H; H-12 + H-13), 7.18 (d, ^3J = 16.26 Hz, 2 H; H-7), 7.38 (m, 2 H; H-3), 7.49 (AA' of AA'BB', ^3J = 9.00 Hz, 4 H; H-16 + H-16'), 7.53 (BB' of AA'BB', ^3J = 9.00 Hz, 4 H; H-15 + H-15'), 7.54 (s, 8 H; H-9 + H-9' + H-10 + H-10'), 7.56 (m, 1 H; H-5); ^{13}C NMR ($CDCl_3$): δ = 15.3 (C_p; C-38 + C-39), 16.5 (C_p; d, $^3J_{CP}$ = 6.16 Hz, C-41), 33.8 (C_s; d, $^1J_{CP}$ = 139.30 Hz, C-1), 62.3 (C_s; d, $^2J_{CP}$ = 6.74 Hz, C-40), 66.7 (C_s; C-36 + C-37), 69.0 (C_s; C-25), 69.8(4) + 69.8(9) + 70.5(9) + 70.6(2) + 70.7(5) + 70.7(6) + 70.7(8) + 70.9 (C_s; C-26 + C-27 + C-28 + C-29 + C-30 + C-31 + C-32 + C-33 + C-34 + C-35), 72.5 (C_s; C-24), 105.4 (C_t; C-21), 123.5 (C_t; C-5), 126.9 + 126.9(5) + 127.0(0) (C_t; C-9 + C-9' + C-10 + C-10' + C-15 + C-15' + C-16 + C-16'),

127.3 (C_t; d, $^3J_{CP}$ = 6.58 Hz, C-3), 127.8 (C_t; C-18), 128.1 + 128.3 + 128.5 (C_t; C-6 + C-12 + C-13 + C-19), 128.9 (C_t; C-7), 132.5 (C_q; d, $^2J_{CP}$ = 8.85 Hz, C-2), 133.0 (C_q; C-20), 136.6 (C_q; C-17), 136.6(7) + 136.7(1) + 136.9 (C_q; C-8 + C-11 + C-14), 138.0 (C_q; d, $^4J_{CP}$ = 2.89 Hz, C-4), 138.5 (C_q; C-23), 152.9 (C_q; C-22); MALDI-MS: m/z (%) calcd.: 1898.01 ([M+1]$^{+\cdot}$,100), found: 1898.02 ([M+1]$^{+\cdot}$,100).

10.13 Synthesis of the Hekate stars with long ethyleneoxy-chains

Compound $S2_{O3}$

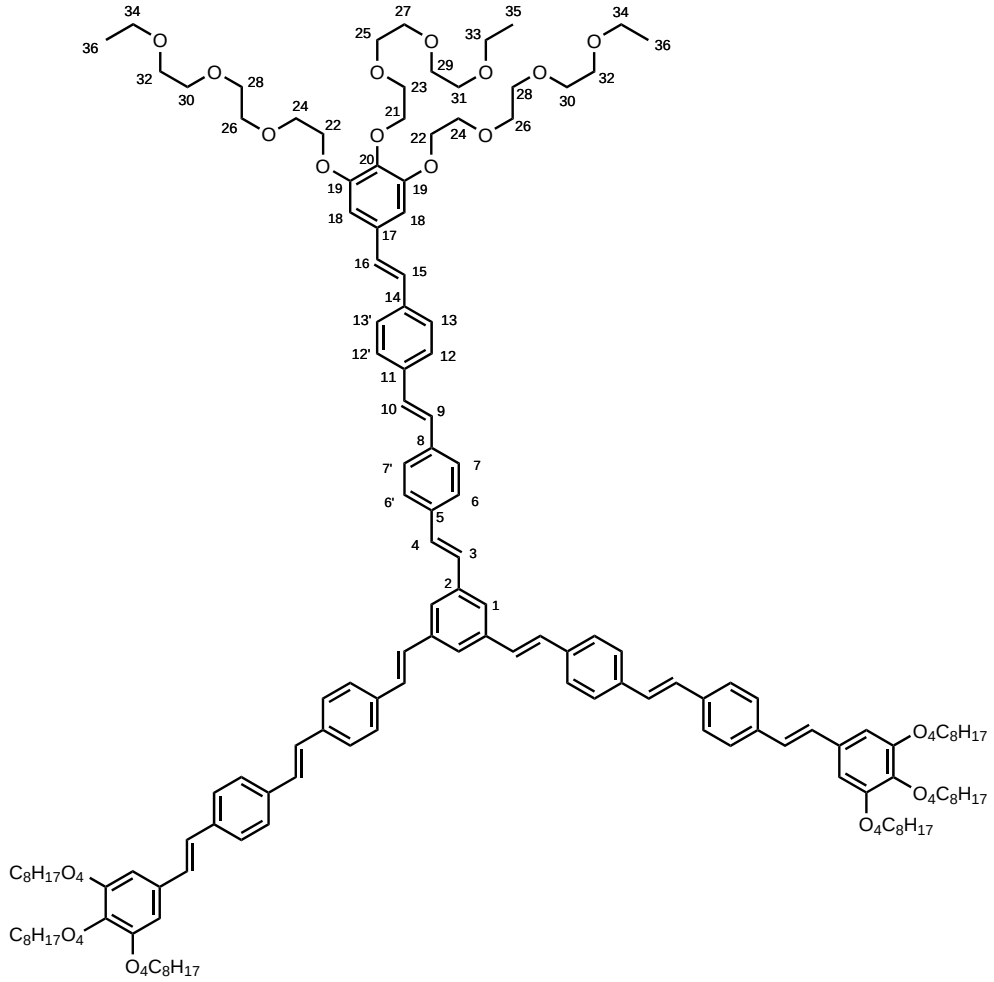

66.0 mg (588 µmol) potassium *tert*-butoxide was added in portions to a stirred solution of 59.2 mg (126 µmol) core building block **3** and 337 mg (392 µmol) arm building block **109** in 10 mL dry THF under nitrogen atmosphere. After stirring overnight, the reaction was quenched with 1N HCl and extracted with ethyl acetate. The organic solvent was dried over Na_2SO_4 and evaporated under reduced pressure. The residue was dissolved in few DCM and poured into 100 ml *n*-hexane. The mixture was stored at -35 °C for 4 days and the precipitate collected by a filter funnel (P4). The purification procedure was repeated to yield 238 mg of a yellow solid. The raw product was subjected to preparative recycling GPC to give 203 mg (78.6 µmol, 62%) of a yellow solid. ^{1}H NMR ($CDCl_3$): δ = 1.20(0) (t, ^3J = 7.00 Hz, 18 H; H-36), 1.20(1) (t, ^3J = 6.92 Hz, 9 H; H-35), 3.51(3) (q, ^3J = 6.98 Hz, 12 H; H-34), 3.51(6) (q, ^3J = 7.01 Hz, 6 H; H-33), 3.56 - 3.77 (m, 72 H; H-25 + H-26 + H-27 + H-28 + H-29 + H-30 + H-31 + H-32), 3.80 (t, ^3J = 5.12 Hz, 6 H; H-23), 3.87 (t, ^3J = 5.04 Hz, 12 H; H-24), 4.17 (t, ^3J = 5.10 Hz, 6 H; H-21), 4.21 (t, ^3J = 5.14 Hz, 12 H; H-22), 6.75 (s, 6 H; H-18),

6.95 (d, ^3J = 16.33 Hz, 3 H; H-15), 7.00 (d, ^3J = 16.33 Hz, 3 H; H-16), 7.13 (s, 6 H; H-9 + H-10), 7.14 (d, ^3J = 16.46 Hz, 3 H; H-3), 7.20 (d, ^3J = 16.46 Hz, 3 H; H-4), 7.48 (AA' of AA'BB', ^3J = 8.62 Hz, 6 H; H-13 + H-13'), 7.51 (BB' of AA'BB', ^3J = 8.62 Hz, 6 H; H-12 + H-12'), 7.54 (s, 12 H; H-6 + H-6' + H-7 + H-7'), 7.56 (s, 3 H; H-1); ^{13}C NMR ($CDCl_3$): δ = 15.3 (C_p; C-35 + C-36), 66.7 (C_s; C-33 + C-34), 68.9 (C_s; C-22), 69.8 + 69.9 + 70.5(9) + 70.6(2) + 70.7(5) + 70.7(8) + 70.9 (C_s; C-23 + C-24 + C-25 + C-26 + C-27 + C-28 + C-29 + C-30 + C-31 + C-32), 72.5 (C_s; C-21), 106.3 (C_t; C-18), 124.1 (C_t; C-1), 126.9 + 127.0 + 127.1 (C_t; C-6 + C-6' + C-7 + C-7' + C-12 + C-12' + C-13 + C-13'), 127.8 (C_t; C-15), 128.1 + 128.9 (C_t; C-3 + C-4), 128.2(9) + 128.3(1) (C_t; C-9 + C-10), 128.5 (C_t; C-16), 133.0 (C_q; C-17), 136.6 + 136.6(6) + 136.7(1) + 136.9 (C_q; C-5 + C-8 + C-11 + C-14), 138.1 (C_q; C-2), 138.5 (C_q; C-20), 152.9 (C_q; C-19); MALDI-MS: m/z (%) calcd.: 2582.42 ([M+1]$^{+\cdot}$,100), found: 2582.42 ([M+1]$^{+\cdot}$,100); ESI-HRMS: m/z calcd. for $C_{150}H_{204}O_{36}Na_2^{2+}$ ([M+2Na]$^{2+}$): 1313.6958, found: 1313.6929. Elemental analysis (%) for $C_{150}H_{204}O_{36}$ calcd.: C 69.74, H 7.96, found: C 69.52, H 7.98.

Compound 102

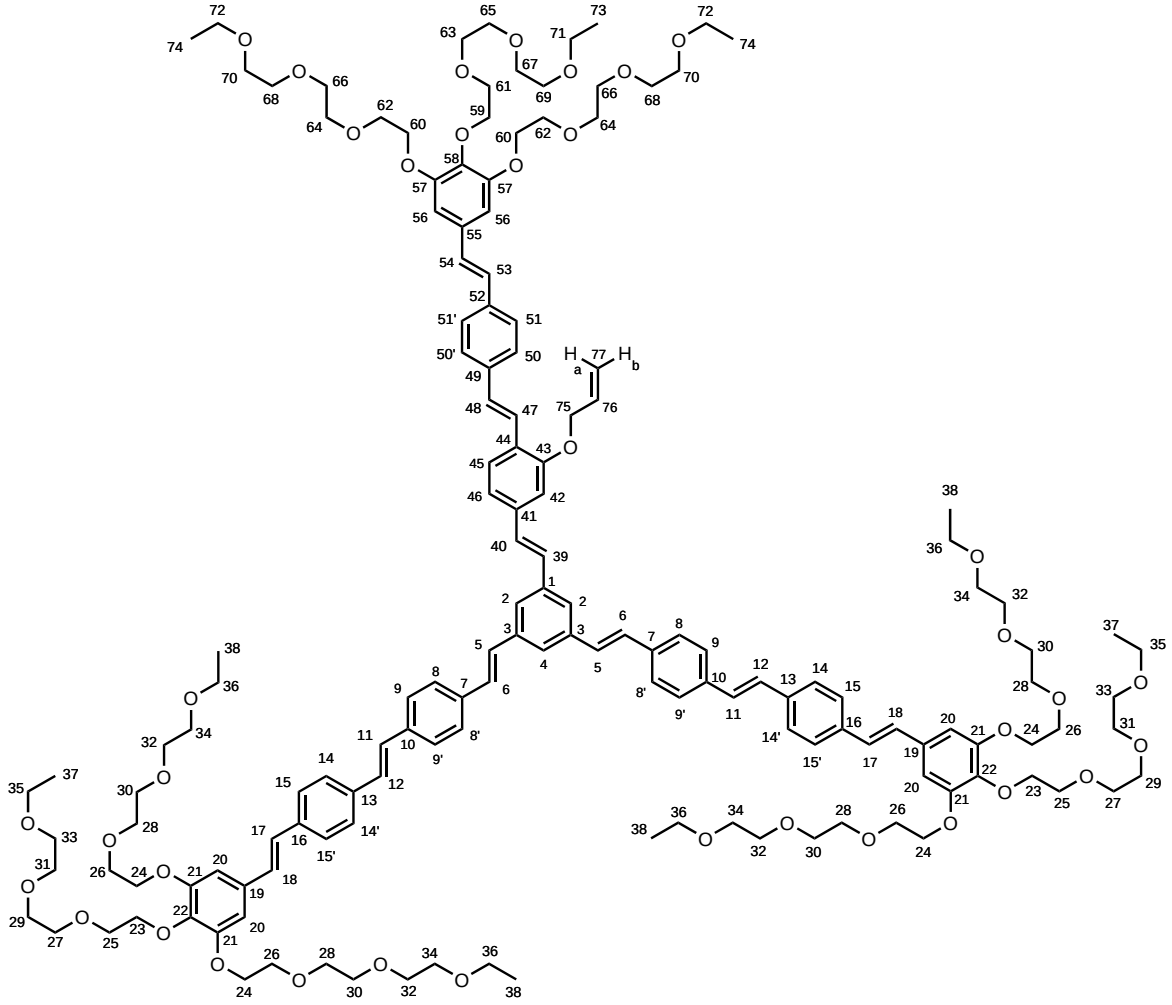

51.9 mg (463 µmol) potassium *tert*-butoxide was added in portions to a stirred solution of 259 mg (136 µmol) V-shaped building block **101** and 170 mg (190 µmol) arm building block **97** in 10 mL dry THF under nitrogen atmosphere. After stirring overnight, the reaction was quenched with 2N HCl and extracted with chloroform four times. The organic solvent was dried over Na_2SO_4 and evaporated under reduced pressure. The residue was subjected to silica gel chromatography with $CHCl_3$ / EtOH

(20 / 1) as eluent. The crude product was dissolved in few chloroform and precipitated from 100 ml *n*-hexane at -30°C twice. Further purification was achieved by preparative recycling GPC to give 208 mg (78.8 µmol, 58%) of an orange-colored, highly viscous oil. ^{1}H NMR ($CDCl_3$): δ = 1.21 (t, ^{3}J = 7.12 Hz, 27 H; H-37 + H-38 + H-73 + H-74), 3.52 (q, ^{3}J = 6.96 Hz, 18 H; H-35 + H-36 + H-71 + H-72), 3.56 - 3.77 (m, 72 H; H-27 + H-28 + H-29 + H-30 + H-31 + H-32 + H-33 + H-34 + H-63 + H-64 + H-65 + H-66 + H-67 + H-68 + H-69 + H-70), 3.81 (t, ^{3}J = 5.10 Hz, 6 H; H-25 + H-61), 3.88 (t, ^{3}J = 5.08 Hz, 12 H; H-26 + H-62), 4.17 (t, ^{3}J = 5.10 Hz, 6 H; H-23 + H-59), 4.23 (t, ^{3}J = 5.10 Hz, 12 H; H-24 + H-60), 4.73 (dt, ^{3}J = 5.04 Hz, ^{4}J = 1.42 Hz, 2 H; H-75), 5.38 (m, 1 H; H-77b), 5.54 (m, 1 H; H-77a), 6.19 (m, 1 H; H-76), 6.78 (s, 6 H; H-20 + H-56), 6.97 (d, ^{3}J = 15.88 Hz, 3 H; H-17 + H-53), 7.02 (d, ^{3}J = 16.33 Hz, 3 H; H-18 + H-54), 7.10 (m, 1 H; H-42), 7.12 - 7.25 (m, 12 H; H-5 + H-6 + H-11 + H-12 + H-39 + H-40 + H-46 + H-48), 7.45 - 7.62 (m, 24 H; H-2 + H-4 + H-8 + H-8' + H-9 + H-9' + H-14 + H-14' + H-15 + H-15' + H-47 + H-50 + H-50' + H-51 + H-51'), 7.65 (d, ^{3}J = 8.52 Hz, 1 H; H-45); ^{13}C NMR ($CDCl_3$): δ = 15.3 (C_p; C-37 + C-38 + C-73 + C-74), 66.7 (C_s; C-35 + C-36 + C-71 + C-72), 69.0 (C_s; C-24 + C-60), 69.4 (C_s; C-75), 69.8(5) + 69.9(0) + 70.6(0) + 70.6(3) + 70.7(6) + 70.7(7) + 70.7(9) + 70.9 (C_s; C-25 + C-26 + C-27 + C-28 + C-29 + C-30 + C-31 + C-32 + C-33 + C-34 + C-61 + C-62 + C- + C-63 + C-64 + C-65 + C-66 + C-67 + C-68 + C-69 + C-70), 72.5 (C_s; C-23 + C-59), 106.4 (C_t; C-20 + C-56), 110.4 (C_t; C-42), 117.5 (C_s; C-77), 119.8 (C_t; C-46), 123.0 (C_t; C-47), 124.1 (C_t; C-2 + C-4), 126.5 (C_q; C-44), 126.7 + 126.8 + 126.9 + 127.0 + 127.1 + 127.8 + 127.9 (C_t; C-8 + C-8' + C-9 + C-9' + C-14 + C-14' + C-15 + C-15' + C-17 + C-45 + C-50 + C-50' + C-51 + C-51' + C-53), 128.1 + 128.2(6) + 128.3(4) + 128.5 + 128.7 + 129.0 + 129.1 (C_t; C-5 + C-6 + C-11 + C-12 + C-18 + C-39 + C-40 + C-48 + C-54), 132.9(6) (C_q; C-19), 133.0(4) (C_q; C-55), 133.4 (C_t; C-76), 136.5 + 136.6 + 136.6(5) + 136.7(3) + 137.0 + 137.4 + 138.0 + 138.2 (C_q; C-1 + C-3 + C-7 + C-10 + C-13 + C-16 + C-49 + C-52), 137.8 (C_q; C-41), 138.4(9) (C_q; C-58), 138.5(4) (C_q; C-22), 152.9 (C_q; C-21 + C-57), 156.2 (C_q; C-43); MALDI-MS: m/z (%) calcd.: 2638.44 ($[M+1]^{+\cdot}$,100), found: 2638.44 ($[M+1]^{+\cdot}$,100).

Compound 103

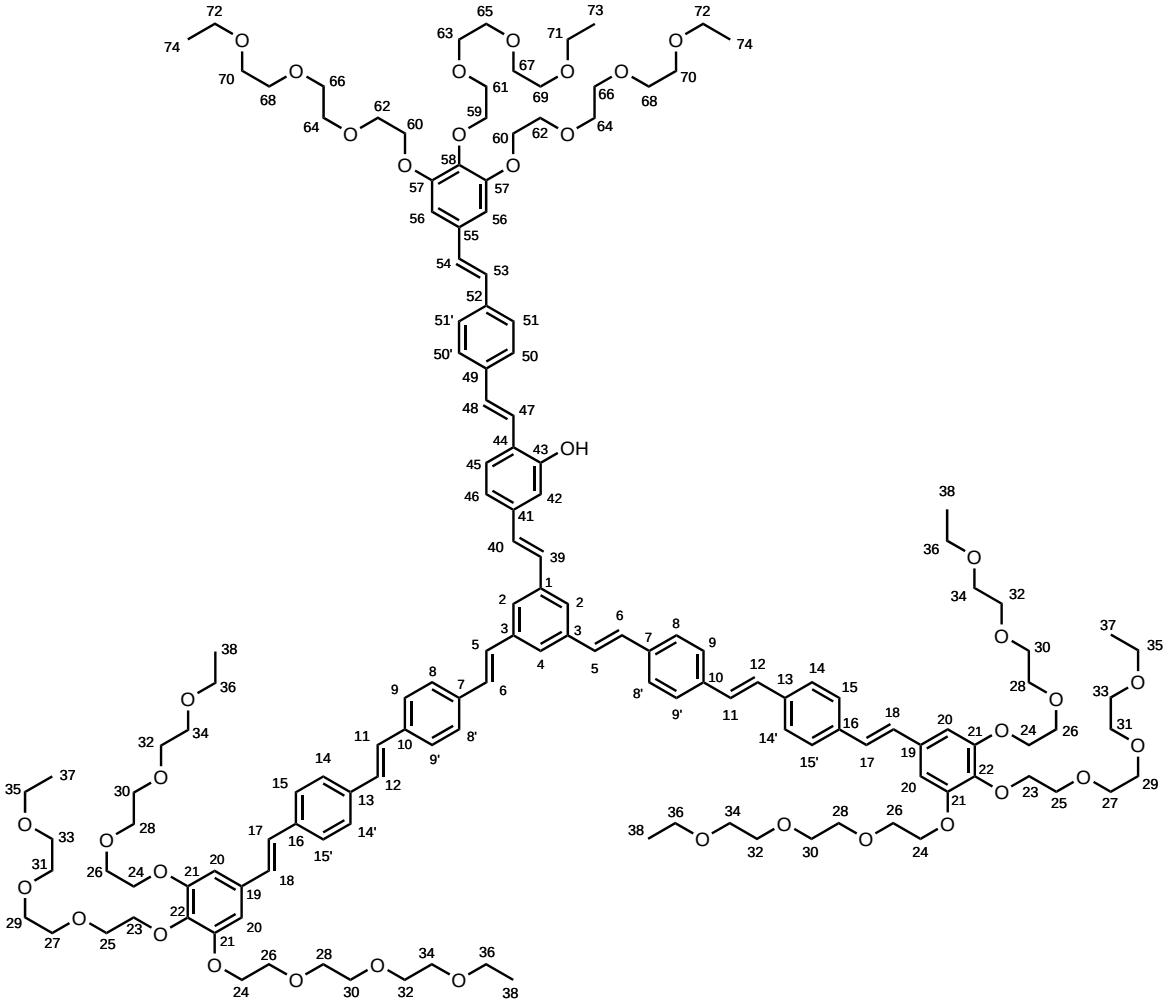

207 mg (78.4 µmol) **102** and 80.3 mg (69.5 µmol) $Pd(PPh_3)_4$ were stirred at room temperature in 5 ml degassed THF under nitrogen atmosphere. 0.1 ml (100 mg, 1.15 mmol) morpholine was then added drop by drop and the mixture was stirred for 5 days. The reaction was quenched with 1N HCl and extracted with chloroform. The organic solvent was dried over Na_2SO_4 and evaporated under reduced pressure. The residue was subjected to silica gel chromatography with $CHCl_3$ / EtOH (50 / 1 → 5 / 1) as eluent. The crude product was dissolved in 6 ml chloroform, filtered through a syringe filter (0.2 µm, PTFE) and injected into 75 ml of petroleum ether. The precipitate was washed with petroleum ether and dried to yield 143 mg (55.0 mmol, 70%) of an orange-colored oil. ^{1}H NMR ($CDCl_3$): δ = 1.20 (t, ^3J = 7.09 Hz, 9 H; H-37 + H-73), 1.21 (t, ^3J = 6.98 Hz, 18 H; H-38 + H-74), 3.52(0) (q, ^3J = 6.96 Hz, 6 H; H-35 + H-71), 3.52(4) (q, ^3J = 7.05 Hz, 12 H; H-36 + H-72), 3.56 - 3.77 (m, 72 H; H-27 + H-28 + H-29 + H-30 + H-31 + H-32 + H-33 + H-34 + H-63 + H-64 + H-65 + H-66 + H-67 + H-68 + H-69 + H-70), 3.81 (t, ^3J = 4.98 Hz, 6 H; H-25 + H-61), 3.88 (m, 12 H; H-26 + H-62), 4.19 (m, 18 H; H-23 + H-24 + H-59 + H-60), 6.74 + 6.77 (s, 6 H; H-20 + H-56), 6.92 - 7.01 (m, 6 H; H-17 + H-18 + H-53 + H-54), 7.04 (m, 1 H; H-46), 7.09 - 7.25 (m, 12 H; H-5 + H-6 + H-11 + H-12 + H-39 + H-40 + H-42 + H-48), 7.40 - 7.62 (m, 25 H; H-2 + H-4 + H-8 + H-8' + H-9 + H-9' + H-14 + H-14' + H-15 + H-15' + H-45 + H-47 + H-50 + H-50' + H-51 + H-51'); ^{13}C NMR ($CDCl_3$): δ = 15.2 (C_p; C-37 + C-38 + C-73 + C-74), 66.7 (C_s; C-35 + C-36 + C-71 + C-72), 68.8 (C_s; C-60), 68.9 (C_s; C-24), 69.8 + 69.9 + 70.5(6) + 70.6(1) + 70.7 + 70.8(5) + 70.8(7) (C_s; C-25 + C-26 + C-27 +

C-28 + C-29 + C-30 + C-31 + C-32 + C-33 + C-34 + C-61 + C-62 + C- + C-63 + C-64 + C-65 + C-66 + C-67 + C-68 + C-69 + C-70), 72.5 (C_s; C-23 + C-59), 106.1 + 106.2 (C_t; C-20 + C-56), 114.1 (C_t; C-42), 118.9 (C_t; C-46), 123.4 (C_t; C-47), 124.2 (C_t; C-2 + C-4), 124.4 (C_q; C-44), 126.8 + 126.9 + 127.0 + 127.2 (C_t; C-8 + C-8' + C-9 + C-9' + C-14 + C-14' + C-15 + C-15' + C-45 + C-50 + C-50' + C-51 + C-51'), 127.6 (C_t; C-17), 127.7 (C_t; C-53), 127.9 + 128.1 + 128.2 + 128.3 + 128.7 + 128.9 (C_t; C-5 + C-6 + C-11 + C-12 + C-18 + C-39 + C-40 + C-48 + C-54), 133.0 (C_q; C-19), 133.1 (C_q; C-55), 136.2 + 136.5(7) + 136.6(3) + 136.8 + 137.5 + 137.6 + 137.9 + 138.0 + 138.2 + 138.3 + 138.4 (C_q; C-1 + C-3 + C-7 + C-10 + C-13 + C-16 + C-22 + C-41 + C-49 + C-52 + C-58), 152. 7 + 152.8 (C_q; C-21 + C-57), 154.8 (C_q; C-43); MALDI-MS: m/z (%) calcd.: 2598.41 ($[M+1]^{+\cdot}$,100), found: 2598.40 ($[M+1]^{+\cdot}$,100); MALDI-HRMS: m/z calcd. for $C_{150}H_{204}O_{37}Na^+$ ($[M+Na]^+$): 2620.3974, found: 2620.3923.

Compound $S2_{O3}$-$F1_{C4}$

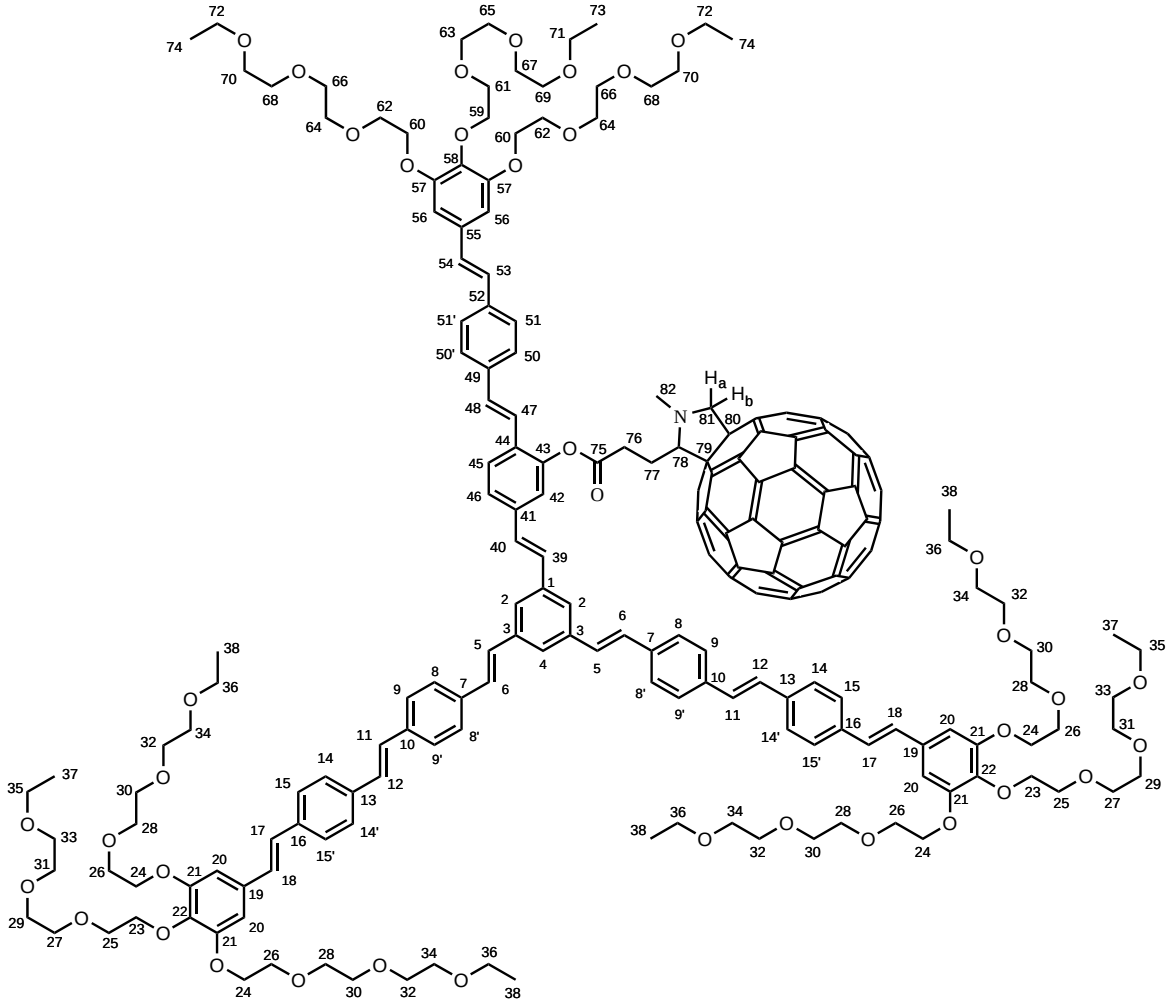

97.2 mg (37.4 µmol) **103**, 63.6 mg (74.8 µmol) carboxylic acid **23** and 29.6 mg (101 µmol) DPTS were stirred in 10 ml dry DCM at room temperature under nitrogen atmosphere for 15 minutes. 87.7 mg (425 µmol) DCC was then added and stirring was continued for 4 days. The solution was subjected to silica gel chromatography with $CHCl_3$ / EtOH (20 / 1) as eluent. The crude product was dissolved in few chloroform, filtered through a syringe filter (0.2 µm, PTFE) and injected into petroleum ether. The precipitate was collected with a filter funnel (P4) and the procedure was repeated, once with petroleum ether and twice with methanol (filter funnel (P5)) as supernatant, to yield

88.9 mg (25.9 µmol, 69%) of a brown solid. ^{1}H NMR ($CDCl_3$): δ = 1.21 (t, ^{3}J = 6.82 Hz, 27 H; H-37 + H-38 + H-73 + H-74), 2.99 + 3.37 (m, 4 H; H-76 + H-77), 3.05 (s, 3 H; H-82), 3.44 - 3.78 (m, 90 H; H-27 + H-28 + H-29 + H-30 + H-31 + H-32 + H-33 + H-34 + H-35 + H-36 + H-63 + H-64 + H-65 + H-66 + H-67 + H-68 + H-69 + H-70 + H-71 + H-72), 3.78 - 3.94 (m, 18 H; H-25 + H-26 + H-61 + H-62), 4.08 - 4.33 (m, 20 H; H-23 + H-24 + H-59 + H-60 + H-78 + H-81a), 5.87 (d, ^{2}J = 8.24 Hz, 1 H; H-81b), 6.74 + 6.78 (s, 6 H; H-20 + H-56), 6.88 - 7.25 (m, 18 H; H-5 + H-6 + H-11 + H-12 + H-17 + H-18 + H-39 + H-40 + H-47 + H-48 + H-53 + H-54), 7.31 (m, 1 H; H-42), 7.40 - 7.64 (m, 24 H; H-2 + H-4 + H-8 + H-8' + H-9 + H-9' + H-14 + H-14' + H-15 + H-15' + H-46 + H-50 + H-50' + H-51 + H-51'), 7.72 (d, ^{3}J = 8.76 Hz, 1 H; H-45); ^{13}C NMR ($CDCl_3$): δ = 15.3 (C_p; C-37 + C-38 + C-73 + C-74), 25.4 + 31.2 (C_s; C-76 + C-77), 40.2 (C_p; C-82), 66.7 (C_s; C-35 + C-36 + C-72 + C-73), 69.0 (C_s; C-24 + C-60), 69.8(6) + 69.9(1) + 70.6(1) + 70.6(3) + 70.8 + 70.9 (C_s; C-25 + C-26 + C-27 + C-28 + C-29 + C-30 + C-31 + C-32 + C-33 + C-34 + C-61 + C-62 + C-63 + C-64 + C-65 + C-66 + C-67 + C-68 + C-69 + C-70), 70.1 (C_q; C-80), 70.2 (C_s; C-81), 72.5 (C_s; C-23 + C-59), 75.9 (C_q; C-79), 76.8 (C_t; C-78), 106.2 + 106.4 (C_t; C-20 + C-56), 120.5 (C_t; C-42), 121.4 (C_t; C-47), 124.2 (C_t; C-2 + C-4), 124.9 (C_t; C-46), 126.9 + 127.0 + 127.1 (C_t; C-8 + C-8' + C-9 + C-9' + C-14 + C-14' + C-15 + C-15' + C-17 + C-45 + C-50 + C-50' + C-51 + C-51' + C-53), 127.8 + 128.1(7) + 128.2(1) + 128.4 + 128.5 + 129.3(1) + 130.4 (C_t; C-5 + C-6 + C-11 + C-12 + C-18 + C-39 + C-40 + C-48 + C-54), 129.2(9) (C_q; C-44), 132.9 + 133.0 (C_q; C-19 + C-55), 135.5 + 136.2 + 136.6 + 137.5 + 139.9 + 140.1 + 140.3 + 140.4 + 141.9 + 142.0 + 142.2 + 142.3 + 142.7 + 142.8 + 143.2 + 143.3 + 144.4 + 144.5 + 144.6 + 144.8 + 145.3 + 145.4 + 145.4(8) + 145.5(3) + 145.6 + 145.8 + 146.1 + 146.1(6) + 146.2(1) + 146.3 + 146.4 + 146.4(9) + 146.5(4) + 147.3 + 147.4 + 152.8 + 154.1 + 154.5 + 156.3 (C_q; C_{58}), 136.5 + 136.6(8) + 136.7(3) + 137.0 + 137.1 + 137.4 + 137.8 + 138.0 + 138.2 (C_q; C-1 + C-3 + C-7 + C-10 + C-13 + C-16 + C-41 + C-49 + C-52), 138.5(1) + 138.5(4) (C_q; C-22 + C-58), 148.5 (C_q; C-43), 152.9 (C_q; C-21 + C-57), 171.8 (C_q; C-75); MALDI-MS: m/z (%) calcd.: 3430.48 ([M+2]$^{\cdot\cdot}$,100), found: 3430.64 ([M+2]$^{\cdot\cdot}$,100); MALDI-HRMS: m/z calcd. for $C_{216}H_{213}NO_{38}^{\cdot\cdot}$ ([M]$^{\cdot\cdot}$): 3428.4760, found: 3428.4696; Elemental analysis (%) for $C_{216}H_{213}NO_{38}$ calcd.: C 75.61, H 6.26, N 0.41, found: C 74.46, H 6.01, N 0.63. For the discussion of elemental analysis results regarding fullerene containing materials, see page 119.

10.14 Synthesis of the porphyrin stars

In some cases, the porphyrins were isolated as a mixture of the desired compounds **Por** and the corresponding diacid salts **Por**·2HCl. This is a consequence of the large amounts of chloroform used to purify the products in terms of liquid chromatography or gel permeation chromatography, as this solvent always contains traces of hydrogen chloride.[265] The porphyrin salts can be distinguished from the desired porphyrins by the strong upshift of the β-pyrrole signal and other characteristic variances in ^{1}H NMR experiments.[266] The target compounds have been isolated by following procedure: Approx. 100 mg of the porphyrin was dissolved in 30 ml of dichloromethane and washed with an aqueous solution of sodium carbonate. The organic phase was dried over Na_2SO_4 and evaporated. The lack of salt was confirmed by NMR experiments with deuterated chloroform, which was stored over molecular sieves 5Å, in the dark and at 4 °C.

Compound Por_{C12}

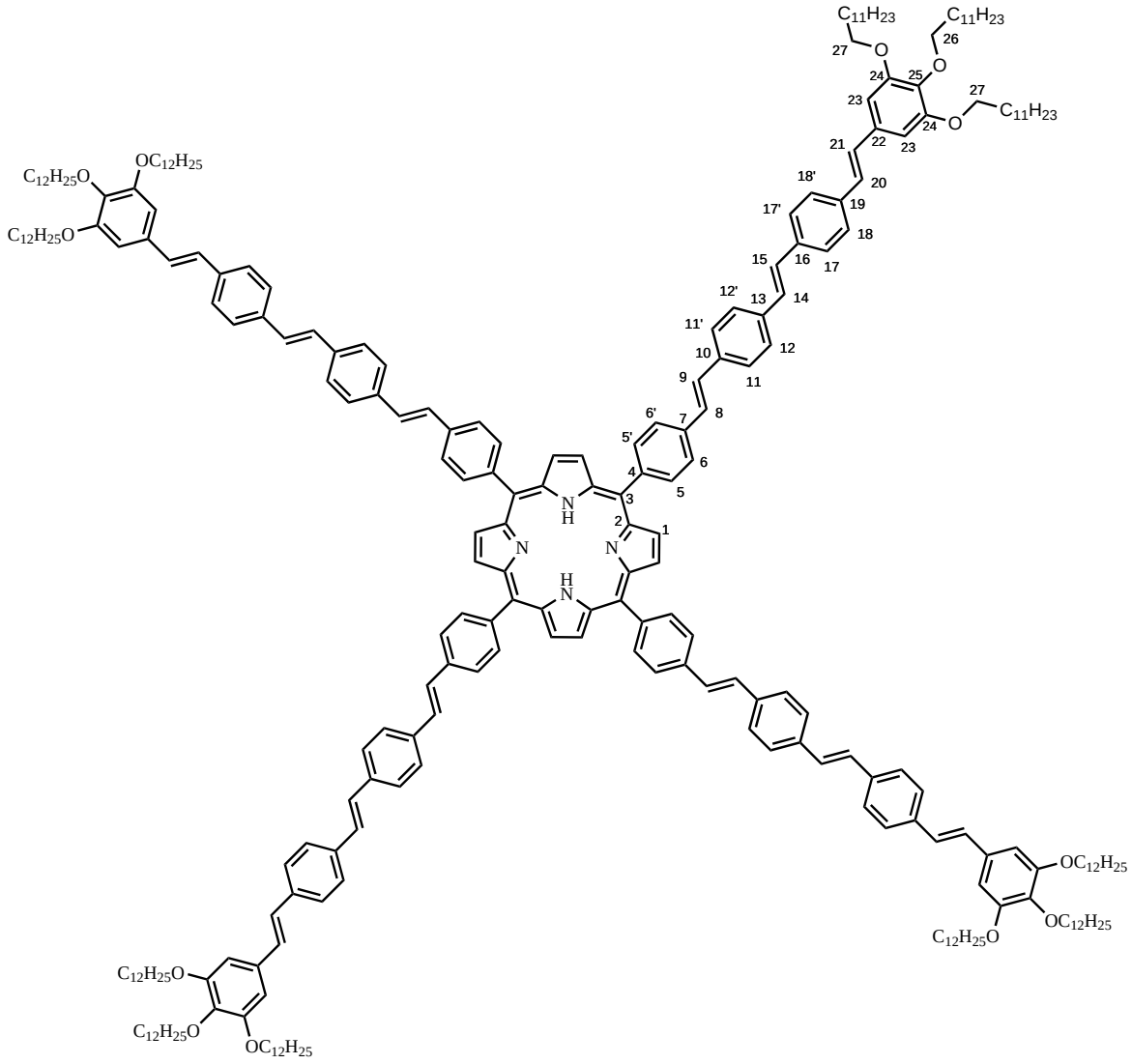

590 mg (683 µmol) arm building block **44** and 166 mg (137 µmol) core building block **12** were mixed with 10 ml THF under nitrogen atmosphere and stirred for 1 hour at room temperature. In portions, 100 mg (891 µmol) potassium *tert*-butoxide was added and stirring continued. The course of reaction was monitored by mass spectrometry and further additions of aldehyde (883 mg; 1.02 mmol) and potassium *tert*-butoxide (164 mg; 1.46 mmol) were required to complete the reaction. After 5 days of stirring, the solution was poured into 1N HCl and extracted with DCM. The organic solvent was dried over Na_2SO_4 and evaporated under reduced pressure. The crude product was subjected to silica gel chromatography with DCM as eluent. Further purification was achieved by preparative recycling GPC to give 362 mg (89.3 µmol, 65%) of a brown solid. ^{1}H NMR ($CDCl_3$): δ = -2.70 (s, 2 H; NH), 0.89 (t, ^3J = 6.88 Hz, 36 H; CH_3), 1.18 - 1.56 (m, 216 H; $(CH_2)_9$–CH_3), 1.70 - 1.90 (m, 24 H; OCH_2CH_2), 3.98 (t, ^3J = 6.55 Hz, 8 H; H-26), 4.04 (t, ^3J = 6.51 Hz, 16 H; H-27), 6.74 (s, 8 H; H-23), 6.99 (d, ^3J = 15.95 Hz, 4 H; H-20), 7.06 (d, ^3J = 15.95 Hz, 4 H; H-21), 7.18 (s, 8 H; H-14 + H-15), 7.43 + 7.48 (d, ^3J = 16.52 Hz, 8 H; H-8 + H-9), 7.51 (AA' of AA'BB', ^3J = 8.53 Hz, 8 H; H-18 + H-18'), 7.55 (BB' of AA'BB', ^3J = 8.80 Hz, 8 H; H-17 + H-17'), 7.60 (AA' of AA'BB', ^3J = 8.40 Hz, 8 H; H-12 + H-12'), 7.67 (BB' of AA'BB', ^3J = 8.93 Hz, 8 H; H-11 + H-11'), 7.92 (AA' of AA'BB', ^3J = 8.19 Hz, 8 H; H-6 + H-6'), 8.22 (BB' of AA'BB', ^3J = 7.86 Hz, 8 H; H-5 + H-5'), 8.92

(s, 8 H; H-1), ^{13}C NMR ($CDCl_3$): δ = 14.3 (C_p; CH_3), 22.9 (C_s; CH_2), 26.3 (C_s; CH_2), 29.5 - 30.0 (C_s; CH_2), 30.6 (C_s; CH_2), 32.1 (C_s; CH_2), 69.3 (C_s; C-27), 73.7 (C_s; C-26), 105.3 (C_t; C-23), 120.0 (C_q; C-3), 124.9 (C_t; C-6 + C-6'), 126.9 + 127.0 + 127.1 (C_t; C-11 + C-11' + C-12 + C-12' + C-17 + C-17' + C-18 + C-18'), 127.4 (C_t; C-20), 128.1 + 128.2 + 128.4 + 129.0 + 129.1 (C_t; C-8 + C-9 + C-14 + C-15 + C-21), 131.0* (C_t; C-1), 132.7 (C_q; C-22), 135.1 (C_t; C-5 + C-5'), 136.6 + 136.7 + 136.9 (C_q; C-7 + C-10 + C-13 + C-16 + C-19), 138.5 (C_q; C-25), 141.4 (C_q; C-4), 153.5 (C_q; C-24); † MALDI-MS: m/z (%) calcd.: 4052.01 ($[M+3]^{+\cdot}$,100), found: 4052.01 ($[M+3]^{+\cdot}$,100); MALDI-HRMS: m/z calcd. for $C_{284}H_{390}N_4O_{12}^{+\cdot}$ ($[M]^{+\cdot}$): 4049.0025, found: 4049.0137; Elemental analysis (%) for $C_{284}H_{390}N_4O_{12}$ calcd.: C 84.18, H 9.70, N 1.38, found: C 84.01, H 10.09, N 1.50. For the discussion of elemental analysis results regarding porphyrin containing materials, see page 119.

Compound Por$_{O2}$

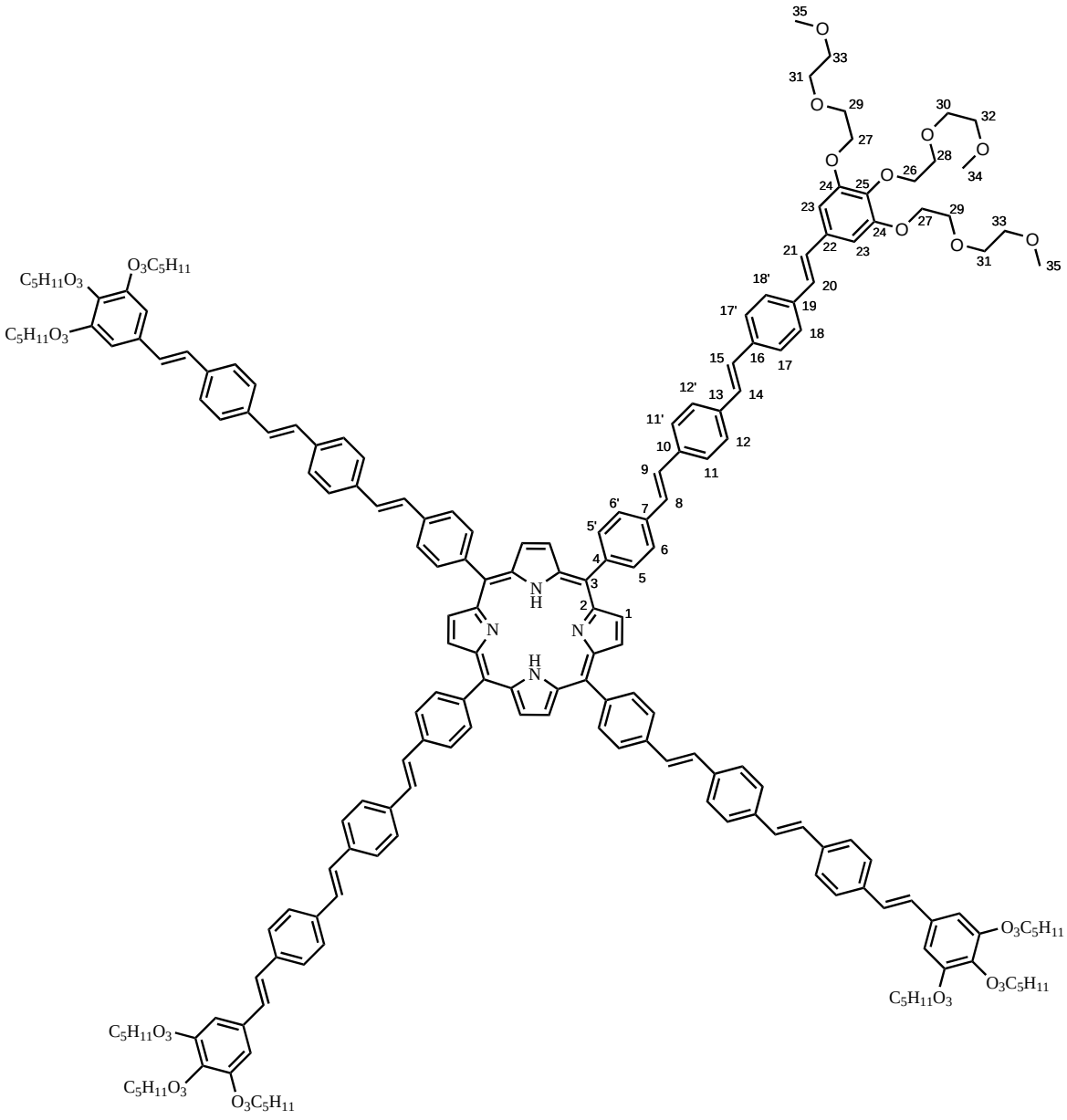

817 mg (1.23 mmol) arm building block **89** and 307 mg (253 µmol) core building block **12** were

*Observed as highly broadened peak.

†The signal for C-2 is indistinguishable from the noise, which is in accordance with published data [267]

mixed with 30 ml THF under nitrogen atmosphere and stirred for 1 hour at room temperature. In portions, 179 mg (1.60 mmol) potassium *tert*-butoxide was added and stirring continued. The course of reaction was monitored by mass spectrometry and further additions of aldehyde (387 mg; 582 µmol) and potassium *tert*-butoxide (379 mg; 3.38 mmol) were required to complete the reaction. After 9 days of stirring, the solution was poured into 100 ml 1N HCl and extracted with chloroform. The organic solvent was dried over Na_2SO_4 and evaporated under reduced pressure. The residue was dissolved in 10 ml acetone, injected into 150 ml petroleum ether and stored at -35 °C for 6 hours. The precipitate was collected with a filter funnel (P4). The purification procedure was repeated twice at room temperature with chloroform as solvent and cyclohexane as supernatant. The crude product was subjected to silica gel chromatography with $CHCl_3$ / EtOH (20 / 1 → 5 / 1) as eluent. Further purification was achieved by preparative recycling GPC to give 457 mg (140 µmol, 55%) of a brown solid. ^{1}H NMR ($CDCl_3$): δ = -2.69 (s, 2 H; NH), 3.40 (m, 12 H; H-34), 3.41 (m, 24 H; H-35), 3.58 (m, 24 H; H-32 + H-33), 3.75 (m, 24 H; H-30 + H-31), 3.83 (t, ^3J = 5.17 Hz, 8 H; H-28), 3.90 (t, ^3J = 5.10 Hz, 16 H; H-29), 4.20 (t, ^3J = 5.10 Hz, 8 H; H-26), 4.25 (t, ^3J = 5.07 Hz, 24 H; H-27), 6.79 (s, 8 H; H-23), 6.98 (d, ^3J = 16.19 Hz, 4 H; H-20), 7.03 (d, ^3J = 16.19 Hz, 4 H; H-21), 7.19 (s, 8 H; H-14 + H-15), 7.44 + 7.49 (d, ^3J = 16.19 Hz, 8 H; H-8 + H-9), 7.51 (AA' of AA'BB', ^3J = 8.56 Hz, 8 H; H-18 + H-18'), 7.56 (BB' of AA'BB', ^3J = 8.56 Hz, 8 H; H-17 + H-17'), 7.61 (AA' of AA'BB', ^3J = 8.40 Hz, 8 H; H-12 + H-12'), 7.68 (BB' of AA'BB', ^3J = 8.40 Hz, 8 H; H-11 + H-11'), 7.93 (AA' of AA'BB', ^3J = 8.13 Hz, 8 H; H-6 + H-6'), 8.24 (BB' of AA'BB', ^3J = 8.13 Hz, 8 H; H-5 + H-5'), 8.94 (s, 8 H; H-1); ^{13}C NMR ($CDCl_3$): δ = 59.1(5) (C_p; C-34), 59.1(9) (C_p; C-35), 68.9 (C_s; C-27), 69.9 (C_s; C-29), 70.5 + 70.7 (C_s; C-28 + C-32), 70.9 (C_s; C-31), 72.1 (C_s; C-33), 72.2 (C_s; C-30), 72.6 (C_s; C-26), 106.3 (C_t; C-23), 120.0 (C_q; C-3), 124.9 (C_t; C-6 + C-6'), 126.9 + 127.0 + 127.1 (C_t; C-11 + C-11' + C-12 + C-12' + C-17 + C-17' + C-18 + C-18'), 127.8 (C_t; C-20), 128.2 + 128.3 + 128.5 + 129.1 (C_t; C-8 + C-9 + C-14 + C-15 + C-21), 131.4* (C_t; C-1), 133.0 (C_q; C-22), 135.1 (C_t; C-5 + C-5'), 136.7 + 136.9 (C_q; C-7 + C-10 + C-13 + C-16 + C-19), 138.5 (C_q; C-25), 141.4 (C_q; C-4), 152.9 (C_q; C-24); † MALDI-MS: m/z (%) calcd.: 3257.57 ($[M+2]^{+\cdot}$,100), found: 3257.56 ($[M+2]^{+\cdot}$,100); ESI-HRMS: m/z calcd. for $C_{200}H_{222}N_4O_{36}Na_2^{2+}$ ($[M+2Na]^{2+}$): 1650.7724, found: 1650.7641; Elemental analysis (%) for $C_{200}H_{222}N_4O_{36}$ calcd.: C 73.73, H 6.87, N 1.72, found: C 71.82, H 6.84, N 1.63. For the discussion of elemental analysis results regarding porphyrin containing materials, see page 119.

*Observed as highly broadened peak.

†The signal for C-2 is indistinguishable from the noise, which is in accordance with published data[267]

Compound Por_{O3}

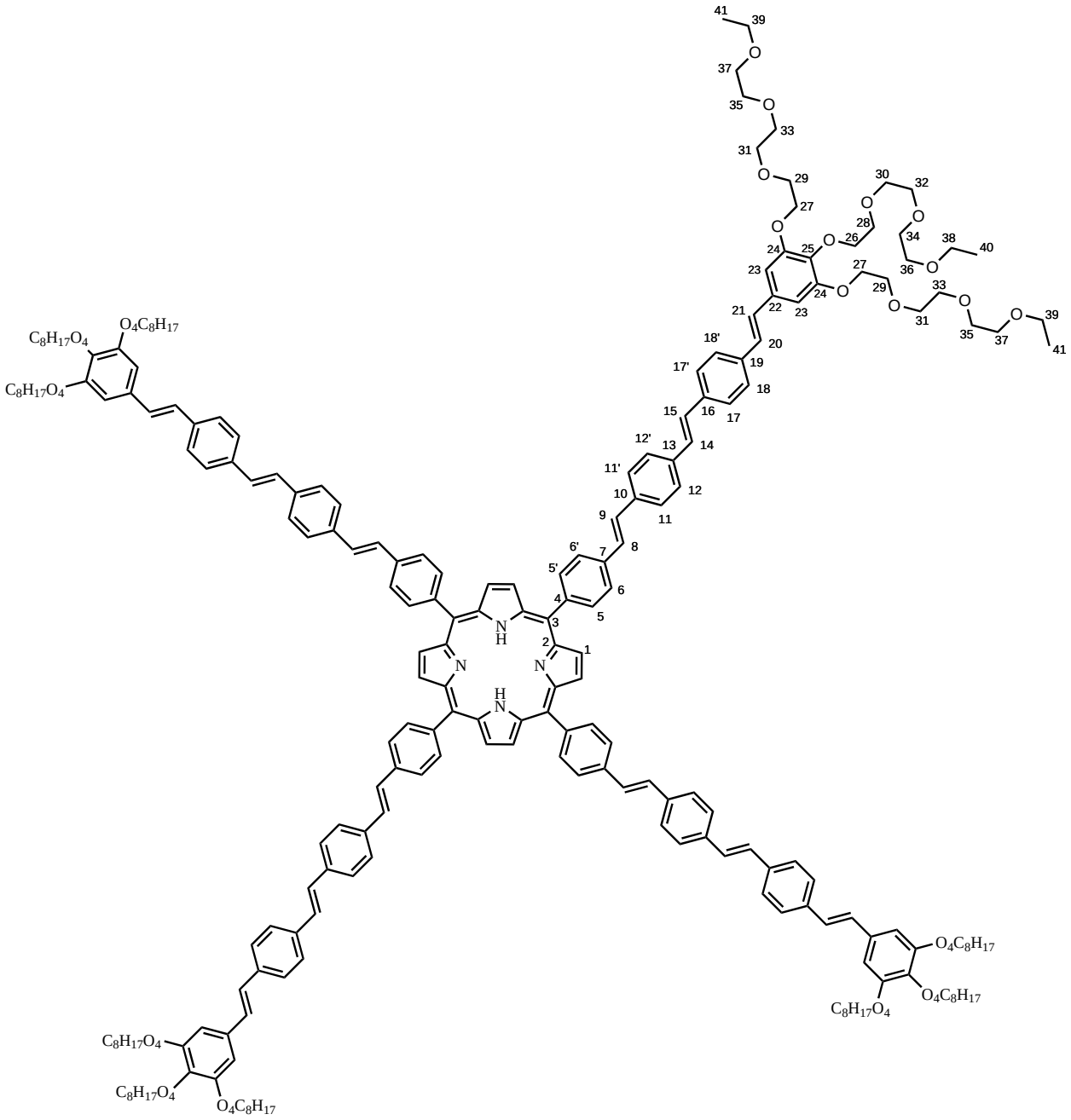

665 mg (793 µmol) arm building block **98** and 200 mg (165 µmol) core building block **12** were mixed with 20 ml THF under nitrogen atmosphere at room temperature. In portions, 133 mg (1.19 mmol) potassium *tert*-butoxide was added and stirring continued. The course of reaction was monitored by mass spectrometry and further additions of aldehyde (438 mg; 522 µmol) and potassium *tert*-butoxide (225 mg; 2.01 mmol) were required to complete the reaction. After 6 days of stirring, the solution was poured into 1N HCl and extracted with chloroform. The organic solvent was dried over Na_2SO_4 and evaporated under reduced pressure. The residue was subjected to silica gel chromatography with $CHCl_3$ / EtOH (20 / 1 $\rightarrow$ 6 / 1) as eluent. The crude product was dissolved in few $CHCl_3$, precipitated from petroleum ether at -30 °C and collected with a filter funnel (P4). Further purification was achieved by preparative recycling GPC to give 228 mg (57.6 µmol, 35%) of a brown solid. ^{1}H NMR ($CDCl_3$): δ = -2.70 (s, 2 H; NH), 1.21 (t, ^3J = 7.02 Hz, 36 H; H-40 + H-41), 3.53 (q, ^3J = 7.00 Hz, 24 H; H-38 + H-39), 3.57 - 3.78 (m, 96 H; H-30 + H-31 + H-32 + H-33 + H-34 + H-35

+ H-36 + H-37), 3.81 (t, ^3J = 5.14 Hz, 8 H; H-28), 3.89 (t, ^3J = 5.08 Hz, 16 H; H-29), 4.18 (t, ^3J = 5.26 Hz, 8 H; H-26), 4.23 (t, ^3J = 5.24 Hz, 16 H; H-27), 6.79 (s, 8 H; H-23), 6.98 (d, ^3J = 15.92 Hz, 4 H; H-20), 7.03 (d, ^3J = 15.92 Hz, 4 H; H-21), 7.19 (s, 8 H; H-14 + H-15), 7.44 + 7.49 (d, ^3J = 16.67 Hz, 8 H; H-8 + H-9), 7.51 (AA' of AA'BB', ^3J = 8.50 Hz, 8 H; H-18 + H-18'), 7.56 (BB' of AA'BB', ^3J = 8.50 Hz, 8 H; H-17 + H-17'), 7.61 (AA' of AA'BB', ^3J = 8.26 Hz, 8 H; H-12 + H-12'), 7.68 (BB' of AA'BB', ^3J = 8.26 Hz, 8 H; H-11 + H-11'), 7.93 (AA' of AA'BB', ^3J = 7.34 Hz, 8 H; H-6 + H-6'), 8.24 (BB' of AA'BB', ^3J = 7.34 Hz, 8 H; H-5 + H-5'), 8.94 (s, 8 H; H-1); ^{13}C NMR ($CDCl_3$): δ = 15.3 (C_p; C-40 + C-41), 66.8 (C_s; C-38 + C-39), 69.0 (C_s; C-27), 69.8(9) + 69.9(4) + 70.6 + 70.8(0) + 70.8(3) + 71.0 (C_s; C-28 + C-29 + C-30 + C-31 + C-32 + C-33 + C-34 + C-35 + C-36 + C-37), 72.5 (C_s; C-26), 106.4 (C_t; C-23), 120.1 (C_q; C-3), 125.0 (C_t; C-6 + C-6'), 126.9 + 127.0 + 127.1 + 127.2 (C_t; C-11 + C-11' + C-12 + C-12' + C-17 + C-17' + C-18 + C-18'), 127.8 (C_t; C-20), 128.2 + 128.3(5) + 128.3(9) + 128.5 + 129.1 (C_t; C-8 + C-9 + C-14 + C-15 + C-21), 131.3* (C_t; C-1), 133.0 (C_q; C-22), 135.2 (C_t; C-5 + C-5'), 136.8 + 137.0 (C_q; C-7 + C-10 + C-13 + C-16 + C-19), 138.6 (C_q; C-25), 141.6 (C_q; C-4), 152.3 (C_q; C-24); † MALDI-MS: m/z (%) calcd.: 3954.08 ($[M+2]^{+\cdot}$,100), found: 3953.99 ($[M+2]^{+\cdot}$,100); MALDI-HRMS: m/z calcd. for $C_{236}H_{295}N_4O_{48}^+$ ($[M+H]^+$): 3953.0760, found: 3953.0925; Elemental analysis (%) for $C_{236}H_{294}N_4O_{48}$ calcd.: C 71.67, H 7.49, N 1.42, found: C 68.63, H 7.36, N 1.23. For the discussion of elemental analysis results regarding porphyrin containing materials, see page 119.

*Observed as highly broadened peak.

†The signal for C-2 is indistinguishable from the noise, which is in accordance with published data[267]

Compound 104

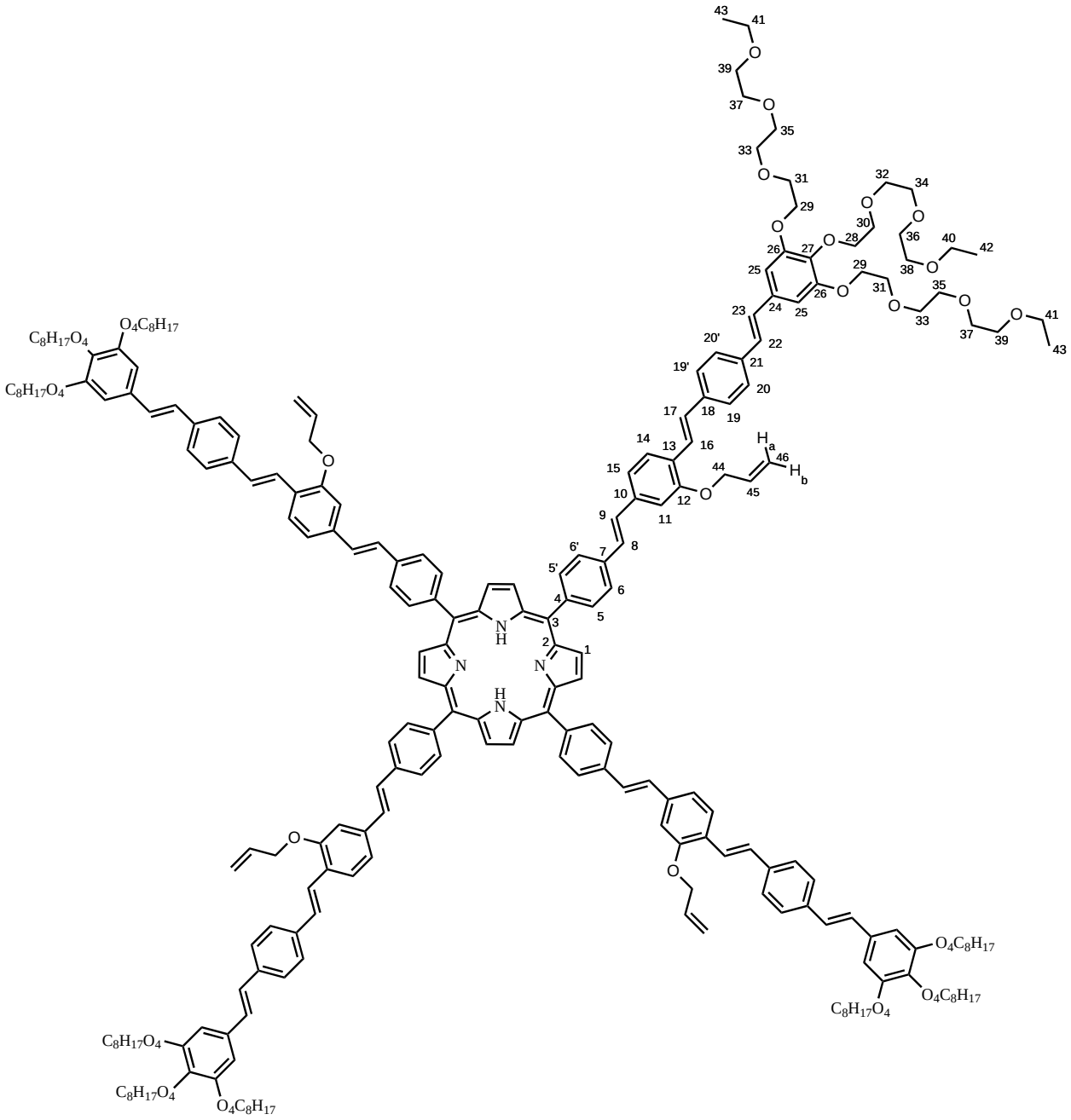

756 mg (845 µmol) arm building block **97** and 214 mg (176 µmol) **12** core building block were mixed with 22 ml THF under nitrogen atmosphere at room temperature. In portions, 142 mg (1.27 mmol) potassium *tert*-butoxide was added and stirring continued. The course of reaction was monitored by mass spectrometry and further additions of aldehyde (362 mg; 404 µmol) and potassium *tert*-butoxide (194 mg; 1.73 mmol) were required to complete the reaction. After 2 days of stirring, the solution was poured into 1N HCl and extracted with chloroform. The organic solvent was dried over Na_2SO_4 and evaporated under reduced pressure. The residue was subjected to silica gel chromatography with $CHCl_3$ / EtOH (20 / 1 → 6 / 1) as eluent. The crude product was dissolved in few $CHCl_3$, precipitated from petroleum ether at -30 °C and collected with a filter funnel (P3). Further purification was achieved by preparative recycling GPC to give 382 mg (91.4 µmol, 52%) of a brown solid. ^{1}H NMR ($CDCl_3$): δ = -2.69 (s, 2 H; NH), 1.21 (t, ^3J = 7.00 Hz, 36 H; H-42 + H-43), 3.53 (q, ^3J = 7.02 Hz, 24 H; H-40 + H-41), 3.57 - 3.78 (m, 96 H; H-32 + H-33 + H-34 + H-35 + H-36 + H-37 +

H-38 + H-39), 3.81 (t, ^3J = 5.20 Hz, 8 H; H-30), 3.89 (t, ^3J = 5.14 Hz, 16 H; H-31), 4.18 (t, ^3J = 5.10 Hz, 8 H; H-28), 4.23 (t, ^3J = 5.10 Hz, 16 H; H-29), 4.78 (dt, ^3J = 5.20 Hz, ^4J = 1.36 Hz, 4 H; H-44), 5.41 (m, 4 H; H-46b), 5.57 (m, 4 H; H-46a), 6.23 (m, 4 H; H-45), 6.79 (s, 8 H; H-25), 6.98 + 7.03 (d, ^3J = 16.35 Hz, 8 H; H-22 + H-23), 7.20 (m, 4 H; H-11), 7.22 (d, ^3J = 16.45 Hz, 4 H; H-17), 7.32 (d, ^3J = 7.76 Hz, 4 H; H-15), 7.41 + 7.46 (d, ^3J = 16.65 Hz, 8 H; H-8 + H-9), 7.51 + 7.57 (AA'BB', ^3J = 8.22 Hz, 16 H; H-19 + H-19' + H-20 + H-20'), 7.60 (d, ^3J = 16.45 Hz, 4 H; H-16), 7.70 (d, ^3J = 8.28 Hz, 4 H; H-14), 7.93 (AA' ofAA'BB', ^3J = 8.12 Hz, 8 H; H-6 + H-6'), 8.24 (BB' of AA'BB', ^3J = 8.12 Hz, 8 H; H-5 + H-5'), 8.94 (s, 8 H; H-1); ^{13}C NMR ($CDCl_3$): δ = 15.3 (C_p; C-42 + C-43), 66.7 (C_s; C-40 + C-41), 69.0 (C_s; C-29), 69.5 (C_s; C-44), 69.8(8) + 69.9(3) + 70.6 + 70.7(8) + 70.7(9) + 70.8(2) + 70.9 (C_s; C-30 + C-31 + C-32 + C-33 + C-34 + C-35 + C-36 + C-37 + C-38), 72.5 (C_s; C-28), 106.4 (C_t; C-25), 110.6 (C_t; C-11), 117.7 (C_s; C-46), 119.9 (C_t; C-15), 120.1 (C_q; C-3), 123.1 (C_t; C-16), 125.0 (C_t; C-6 + C-6'), 126.7 (C_q; C-13), 126.8 (C_t; C-14), 126.9 + 127.0 (C_t; C-19 + C-19' + C-20 + C-20'), 127.9 + 128.3 (C_t; C-22 + C-23), 128.4 + 129.5 (C_t; C-8 + C-9), 128.8 (C_t; C-17), 131.2* (C_t; C-1), 133.1 (C_q; C-24), 133.5 (C_t; C-45), 135.2 (C_t; C-5 + C-5'), 136.5 (C_q; C-21), 136.8 (C_q; C-7), 137.4 (C_q; C-18), 137.9 (C_q; C-10), 138.5 (C_q; C-27), 141.6 (C_q; C-4), 152.9 (C_q; C-28), 156.3 (C_q; C-12); † MALDI-MS: m/z (%) calcd.: 4178.18 ($[M+2]^{+\cdot}$,100), found: 4178.27 ($[M+2]^{+\cdot}$,84).

*Observed as highly broadened peak.

†The signal for C-2 is indistinguishable from the noise, which is in accordance with published data[267]

Compound 105

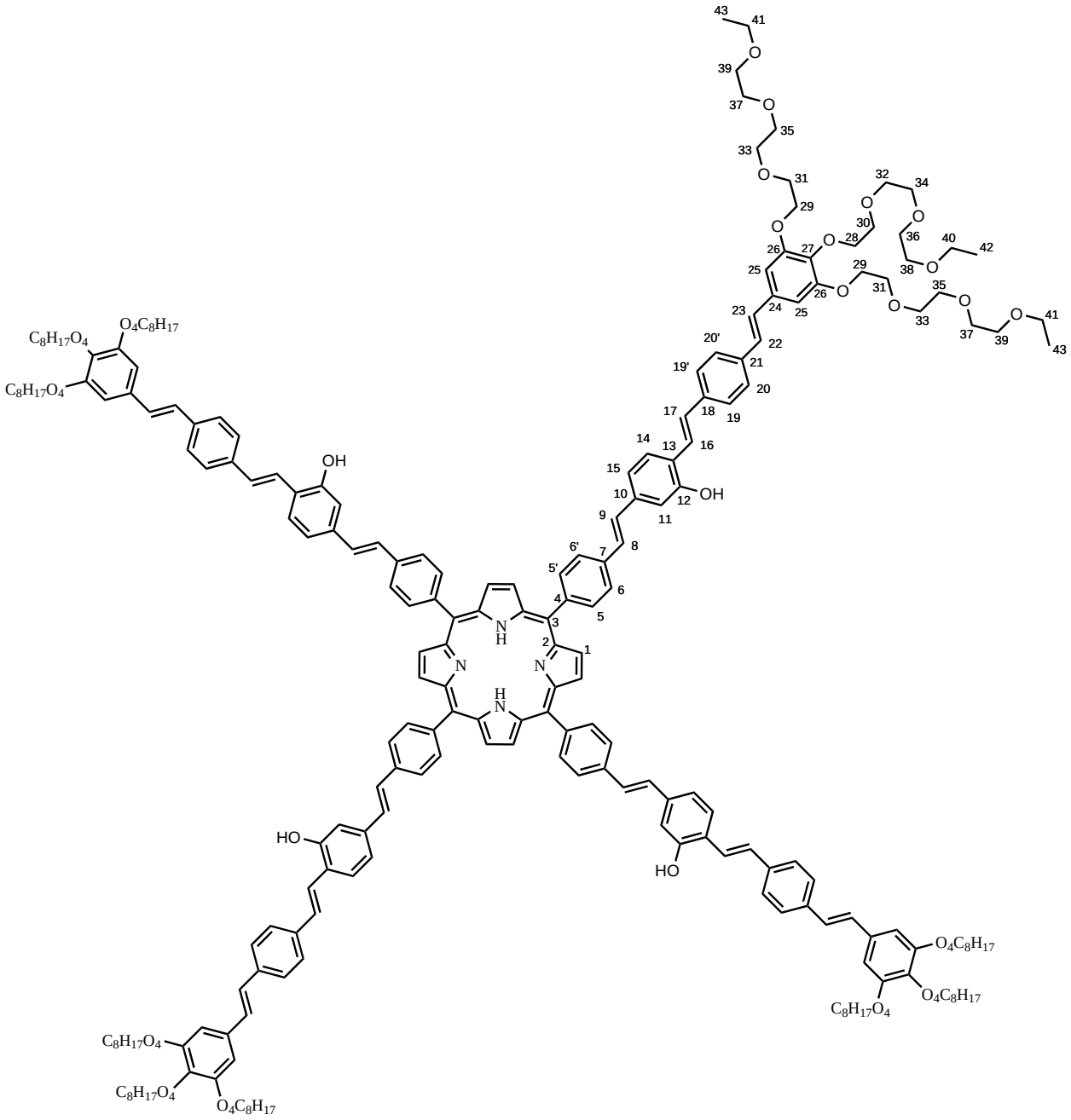

183 mg (43.8 µmol) **104** and 89.6 mg (77.5 µmol) $Pd(PPh_3)_4$ were stirred at room temperature in 8 ml degassed THF under nitrogen atmosphere. 0.2 ml (200 mg, 2.30 mmol) morpholine was then added drop by drop and the mixture was stirred for 18 days. The reaction was quenched with 1N HCl and extracted with $CHCl_3$. The organic solvent was dried over Na_2SO_4 and evaporated under reduced pressure. The residue was subjected to silica gel chromatography with $CHCl_3$ / EtOH (25 / 1 → 5 / 1) as eluent. The crude product was dissolved in few $CHCl_3$, precipitated from petroleum ether at -30 °C and collected with a filter funnel (P4) to yield 107 mg (26.6 µmol, 61%) of a brown solid. ^{1}H NMR (THF-d_8): δ = -2.62 (s, 2 H; NH), 1.12 (t, ^3J = 6.98 Hz, 36 H; H-42 + H-43), 3.44 (q, ^3J = 6.98 Hz, 24 H; H-40 + H-41), 3.42 - 3.69 (m, 96 H; H-32 + H-33 + H-34 + H-35), 3.75 (t, ^3J = 5.37 Hz, 8 H; H-30), 3.82 (t, ^3J = 4.94 Hz, 16 H; H-31), 4.12 (t, ^3J = 5.20 Hz, 8 H; H-28), 4.18 (t, ^3J = 4.97 Hz, 16 H; H-29), 6.87 (s, 8 H; H-25), 7.10 (m, 8 H; H-22 + H-23), 7.11 (m, 4 H; H-11), 7.20 - 7.30 (m, 8 H; H-15 + H-17), 7.46 (m, 8 H; H-8 + H-9), 7.51 + 7.54 (AA' and BB' of AA'BB',

^3J = 8.30 Hz, 16 H; H-19 + H-19' + H-20 + H-20'), 7.58 (d, ^3J = 16.20 Hz, 4 H; H-16), 7.64 (d, ^3J = 8.16 Hz, 4 H; H-14), 7.96 (AA' of AA'BB', ^3J = 8.12 Hz, 8 H; H-6 + H-6'), 8.19 (BB' of AA'BB', ^3J = 7.32 Hz, 8 H; H-5 + H-5'), 8.78 (s, 4 H; OH), 8.91 (s, 8 H; H-1); ^{13}C NMR (THF-d_8): δ = 15.7 (C_p; C-42 + C-43), 67.0 (C_s; C-40 + C-41), 69.9 (C_s; C-29), 70.7 + 70.9 + 71.4 + 71.5 + 71.5(5) + 71.5(8) + 71.5(9) + 71.6(3) + 71.7 (C_s; C-30 + C-31 + C-32 + C-33 + C-34 + C-35 + C-36 + C-37 + C-38 + C-39), 73.3 (C_s; C-28), 107.1 (C_t; C-25), 114.5 (C_t; C-11), 119.3 (C_t; C-15), 120.9 (C_q; C-3), 124.1 (C_t; C-16), 125.5 (C_q; C-13), 125.8 (C_t; C-6 + C-6'), 127.4 - 127.5 (C_t; C-14 + C-19 + C-19' + C-20 + C-20'), 128.2 (C_t; C-22), 128.5 (C_t; C-17), 128.7 (C_t; C-8), 129.2 (C_t; C-23), 130.4 (C_t; C-9), 133.8 (C_q; C-24), 135.8 (C_t; C-5 + C-5'), 137.6 + 138.1 + 138.5 + 138.8 (C_q; C-4 + C-7 + C-10 + C-18 + C-21), 139.8 (C_q; C-27), 142.2 (C_q; C-2), 154.0 (C_q; C-26), 156.5 (C_q; C-12); * MALDI-MS: m/z (%) calcd.: 4018.06 ($[M+2]^{+\cdot}$,100), found: 4017.97 ($[M+2]^{+\cdot}$,100); ESI-HRMS: m/z calcd. for $C_{236}H_{294}N_4O_{52}Na_2^{2+}$ ($[M+2Na]^{2+}$): 2031.0134, found: 2031.0073; Elemental analysis (%) for $C_{236}H_{294}N_4O_{52}$ calcd.: C 70.53, H 7.37, N 1.39, found: C 63.82, H 6.90, N 1.23. For the discussion of elemental analysis results regarding porphyrin containing materials, see page 119.

*A signal corresponding to the atom C-1 could not be observed.

Compound Por_{O3}-$F4_{C4}$

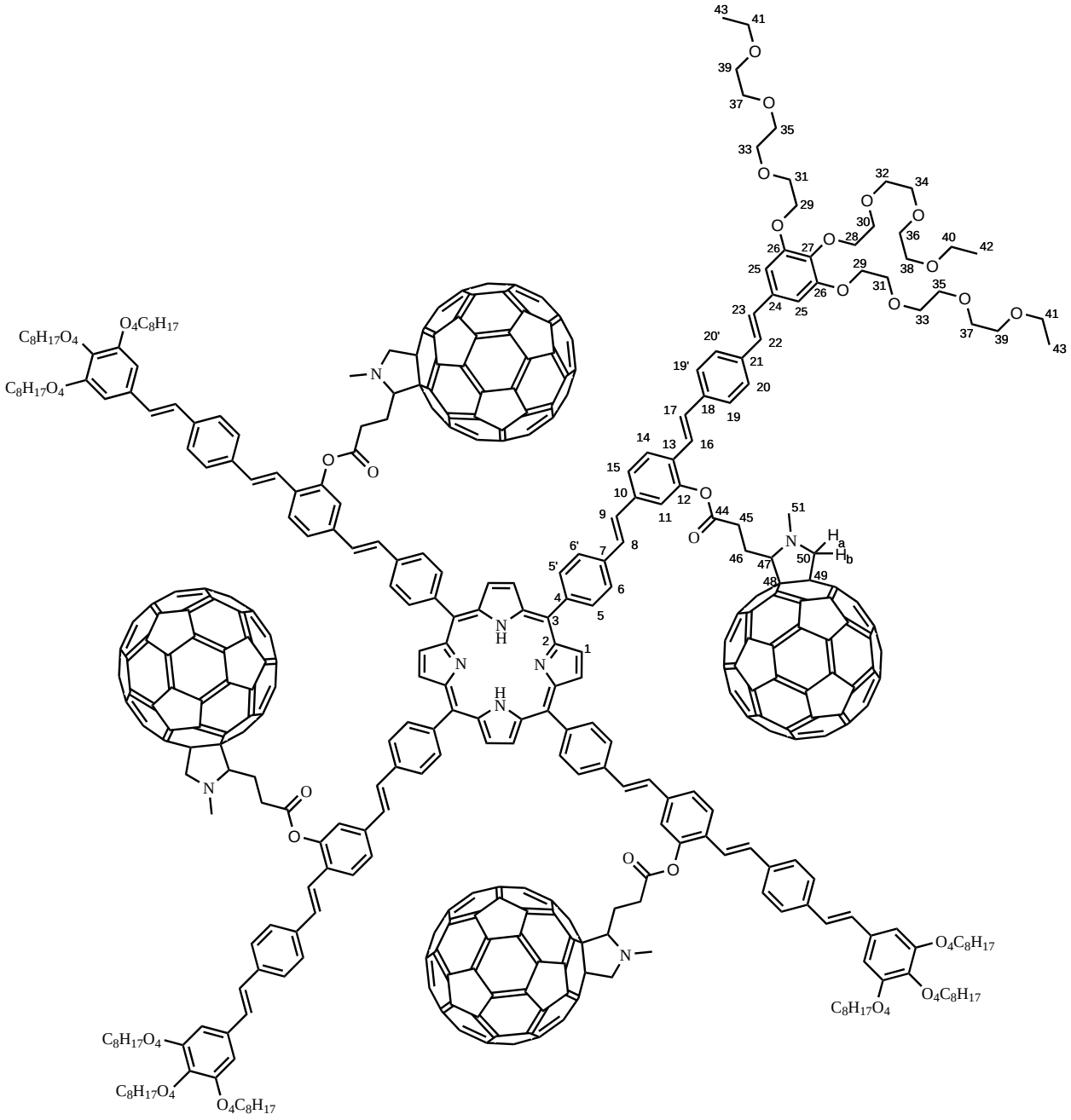

77.2 mg (19.2 µmol) **105**, 131 mg (154 µmol) carboxylic acid **23** and 67.8 mg (230 µmol) DPTS were stirred in 9 ml dry DCM at room temperature under nitrogen atmosphere. After 30 minutes, 190 mg (921 µmol) DCC was added and the mixture was stirred for 26 days. The solution was concentrated in vacuo and subjected to silica gel chromatography with $CHCl_3$ / EtOH (20 / 1 → 3 / 1) as eluent. The crude product was then precipitated from following solvents in the given order: MeOH (-30 °C); PE; $CHCl_3$ / PE = 1 / 3; $CHCl_3$ / PE = 1 / 2 (-30 °C); $CHCl_3$ / PE = 15 / 20 (-30 °C); $CHCl_3$ / MeOH = 1 / 2. Yield: 95.3 mg (13.0 µmol; 68%) of a brown solid. ^{1}H NMR ($CDCl_3$): δ = -2.77 (s, 2 H; NH), 1.20 (m, 36 H; H-42 + H-43), 2.57 - 3.41 (m, 20 H; H-45 + H-46 + H-51), 3.31 - 3.99 (m, 144 H; H-30 + H-31 + H-32 + H-33 + H-34 + H-35 + H-36 + H-37 + H-38 + H-39 + H-40 + H-41), 4.02 - 4.39 (m, 32 H; H-28 + H-29 + H-47 + H-50a), 4.82 (m, 4 H; H-50b), 6.76 (m, 8 H; H-25), 6.84 - 7.77 (m, 44 H; H-8 + H-9 + H-11 + H-14 + H-15 + H-16 + H-17 + H-19 + H-19' + H-20 + H-20' + H-22 + H-23), 7.90 (m, 8 H; H-6 + H-6'), 8.22 (m, 8 H; H-5 + H-5'), 8.93 (m, 8 H; H-1). For discussion

of NMR results, see page 63. Elemental analysis (%) for $C_{500}H_{330}N_8O_{56}$ calcd.: C 81.75, H 4.53, N 1.53, found: C 82.17, H 3.91, N 1.86. For the discussion of elemental analysis results regarding porphyrin containing materials, see page 119.

10.15 Synthesis of the compounds in the alternative routes

Compound 46

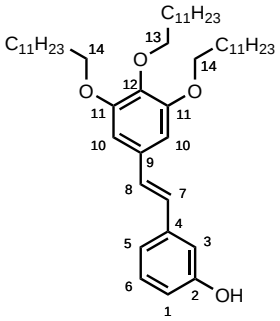

150 mg (1.23 mmol) 3-hydroxybenzaldehyde (**45**), 970 mg (1.24 mmol) phosphonate **36** and 690 mg (6.15 mmol) potassium *tert*-butoxide were mixed with 2 ml THF under argon atmosphere and refluxed for 1.5 hours. The solution was poured into 1N HCl and extracted with ethyl acetate. The organic solvent was dried over Na_2SO_4 and evaporated under reduced pressure. The residue was subjected to silica gel chromatography with cyclohexane / DCM = 1 / 1 as eluent to yield 455 mg (607 µmol, 49%) of an off-white solid. ^{1}H NMR ($CDCl_3$): δ = 0.88 (t, ^3J = 6.85 Hz, 9 H; CH_3), 1.20 - 1.90 (m, 60 H; $C_{10}H_{20}$), 3.97 (t, ^3J = 6.62 Hz, 2 H; H-13), 4.02 (t, ^3J = 6.51 Hz, 4 H; H-14), 6.70 (s, 2 H; H-10), 6.72 (ddd, ^3J = 8.04 Hz, ^4J = 2.53 Hz, ^4J = 0.89 Hz, 1 H; H-1), 6.90 + 6.98 (d, ^3J = 16.38 Hz, 2 H; H-7 + H-8), 6.96 (m, 1 H; H-3), 7.06 (m, 1 H; H-5), 7.21 (m, 1 H; H-6); ^{13}C NMR ($CDCl_3$): δ = 14.3 (C_p; CH_3), 22.8 - 32.1 (C_s; $C_{10}H_{20}$), 69.3 (C_s; C-14), 73.7 (C_s; C-13), 105.5 (C_t; C-10), 113.0 (C_t; C-3), 114.6 (C_t; C-1), 119.5 (C_t; C-5), 127.4 + 129.6 (C_t; C-7 + C-8), 130.0 (C_t; C-6), 132.5 (C_q; C-9), 138.6 (C_q; C-12), 139.4 (C_q; C-4), 153.5 (C_q; C-11), 156.0 (C_q; C-2).

Compound 48

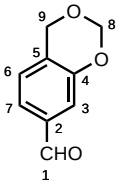

3.24 g (17.0 mmol) pTsOH·H_2O and 25.6 g (852 mmol) paraformaldehyde were stirred in 250 ml acetic acid at 135 °C. 5.05 g (41.3 mmol) 3-hydroxybenzaldehyde (**45**) was dissolved in warm 25 ml acetic acid and added drop by drop to the stirring solution. After refluxing for 4 hours, the reaction was cooled to room temperature and mixed with 300 ml of water. The formed precipitate was filtered, and washed with water. The residue was extracted with toluene four times, the solution washed with water two times and with aqueous NaOH until pH-neutral and again washed with water. The organic phase was dried over Na_2SO_4 and evaporated under reduced pressure. The residue was subjected to silica gel chromatography with cyclohexane / ethyl acetate = 5 / 1 as eluent to yield 942 mg (5.74 mmol, 14%) of a colorless solid. ^{1}H NMR ($CDCl_3$): δ = 4.96 (m, 2 H; H-9), 5.28 (s, 2 H; H-8), 7.13 (m, 1

H; H-6), 7.37 (d, ^4J = 1.56 Hz, 1 H; H-3), 7.46 (dd, ^3J = 7.80 Hz, ^4J = 1.56 Hz, 1 H; H-7), 9.93 (s, 1 H; H-1).

Compound 49

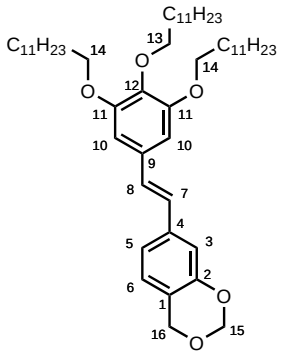

298 mg (1.82 mmol) **48** and 1.17 g (1.50 mmol) phosphonate **36** were mixed with 1 ml THF and stirred under nitrogen atmosphere. 500 mg (4.46 mmol) potassium *tert*-butoxide was added and stirring was continued for 5 minutes. 20 ml 1N HCl was added and extracted with petroleum ether. The organic solvent was dried over Na_2SO_4 and evaporated under reduced pressure. The residue was subjected to silica gel chromatography with cyclohexane / ethyl acetate = 30 / 1 as eluent to yield 551 mg (696 µmol, 46%) of an off-white solid. ^{1}H NMR ($CDCl_3$): δ = 0.88 (t, ^3J = 6.86 Hz, 9 H; CH_3), 1.20 - 1.90 (m, 60 H; $C_{10}H_{20}$), 3.97 (t, ^3J = 6.60 Hz, 2 H; H-13), 4.02 (t, ^3J = 6.52 Hz, 4 H; H-14), 4.91 (s, 2 H; H-16), 5.26 (s, 2 H; H-15), 6.69 (s, 2 H; H-10), 6.88 + 6.97 (d, ^3J = 16.25 Hz, 2 H; H-7 + H-8), 6.93 (d, ^3J = 7.92 Hz, 1 H; H-6), 7.00 (d, ^4J = 1.68 Hz, 1 H; H-3), 7.07 (dd, ^3J = 7.84 Hz, ^4J = 1.68 Hz, 1 H; H-5).

Compound 52

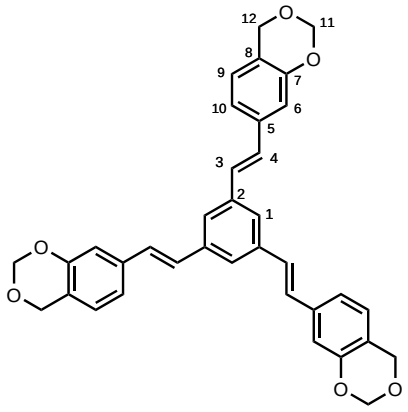

1.26 g (7.68 mmol) **48** and 1.23 g (2.33 mmol) phosphonate **1** were mixed with 10 ml THF and stirred under nitrogen atmosphere. 1.72 g (15.3 mmol) potassium *tert*-butoxide was added in portions and stirring was continued for 40 minutes. The solution was poured into water and the residue was filtered and dried in vacuo to yield 632 mg (1.13 mmol, 48%) of an off-white solid, which was used in the next step without further purification. ^{1}H NMR ($CDCl_3$): δ = 4.93 (m, 6 H; H-12), 5.28 (s, 6 H; H-11), 6.97 (d, ^3J = 7.88 Hz, 3 H; H-9), 7.07 (d, ^4J = 1.32 Hz, 3 H; H-6), 7.12 (s, 6 H; H-3 + H-4), 7.14 (dd, ^3J = 7.90 Hz, ^4J = 1.78 Hz, 3 H; H-10), 7.54 (s, 3 H; H-1).

Compound 55

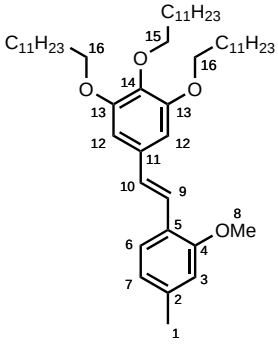

386 mg (2.57 mmol) **48** and 2.01 g (2.57 mmol) phosphonate **36** were mixed with 10 ml THF and stirred under nitrogen atmosphere. 1.16 g (10.3 mmol) potassium *tert*-butoxide was added in portions and stirring was continued for 5 minutes. The solution was poured into ice water and acidified with 1N HCl. The mixture was extracted with DCM and the organic phase was dried over Na_2SO_4 and evaporated under reduced pressure. The residue was subjected to silica gel chromatography with petroleum ether / ethyl acetate = 50 / 1 as eluent to yield 1.58 g (2.03 mmol, 79%) of an almost colorless solid, which was used in the next step without further purification. ^{1}H NMR ($CDCl_3$): δ = 0.88 (t, ^3J = 6.82 Hz, 9 H; CH_3), 1.20 - 1.90 (m, 60 H; $C_{10}H_{20}$), 2.36 (s, 3 H; H-1), 3.88 (s, 3 H; H-8), 3.96 (t, ^3J = 6.62 Hz, 2 H; H-15), 4.02 (t, ^3J = 6.50 Hz, 4 H; H-16), 6.71 (m, 3 H; H-3 + H-12), 6.77 (m, 1 H; H-7), 6.96 + 7.28 (d, ^3J = 16.41 Hz, 2 H; H-9 + H-10), 7.44 (d, ^3J = 7.80 Hz, 1 H; H-6); ^{13}C NMR ($CDCl_3$): δ = 14.3 (C_p; CH_3), 19.5 + 25.6 + 30.8 (C_s; C-16 + C-17 + C-18), 22.8 - 32.1 (C_s; $C_{10}H_{20}$), 62.3 (C_s; C-15), 68.8 (C_s; C-1), 69.4 (C_s; C-13), 73.7 (C_s; C-12), 97.9 (C_t; C-14), 105.4 (C_t; C-9), 126.5 (C_t; C-4 + C-4'), 127.6 + 129.0 (C_t; C-6 + C-7), 128.4 (C_t; C-3 + C-3'), 132.7 (C_q; C-8), 136.9 (C_q; C-5), 137.7 (C_q; C-2), 138.6 (C_q; C-11), 153.5 (C_q; C-10).

Compound 58

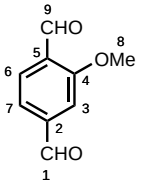

13.0 g (95.5 mmol) 2,5-dimethylanisole (**53**) and 113.7 g (719 mmol) $KMnO_4$ were refluxed in 600 ml H_2O overnight. At room temperature, the solution was filtered and the filtrate was carefully acidified with half-concentrated HCl until pH = 1. The precipitate was filtered, washed with water and dried in vacuo to obtain 5.10 g of a colorless solid.

The material was dissolved in 50 ml THF and 2.90 g (76.4 mmol) $LiAlH_4$ was added in portions at 0 °C. After refluxing overnight, the solution was carefully mixed with water and 1N HCl at 0 °C, respectively. The aqueous phase was saturated with a mixture of NaCl and Na_2SO_4 and extracted with ethyl acetate twelve times. The organic phase was dried over Na_2SO_4 and evaporated under reduced pressure. The remaining liquid was mixed with 20 ml petroleum ether and stored at 4 °C overnight.

The formed precipitate was collected and dissolved in 100 ml acetone. 37.9 g (436 mmol) activated MnO_2 was added in portions and the mixture was stirred at 50 °C for 24 hours. At room temperature, the mixture was filtered and the residue was extracted with DCM. The combined filtrates were

evaporated under reduced pressure to yield 1.61 g (9.81 mmol, 10%) of an off-white solid. ^{1}H NMR ($CDCl_3$): δ = 4.02 (s, 3 H; H-8), 7.52 (s, 1 H; H-3), 7.53 (m, 1 H; H-7), 7.99 (d, ^{3}J = 8.26 Hz, 1 H; H-6), 10.06 (s, 1 H; H-1), 10.54 (d, ^{4}J = 0.67 Hz, 1 H; H-9), ^{13}C NMR ($CDCl_3$): δ = 56.2 (C_p; C-8), 110.9 (C_t; C-3), 123.3 (C_t; C-7), 128.8 (C_q; C-5), 129.4 (C_t; C-6), 141.5 (C_q; C-2), 162.1 (C_q; C-4), 189.5 (C_t; C-9), 191.6 (C_t; C-1); Analytical data in accordance with literature.[268]

Compound 60

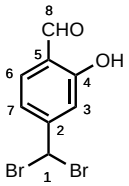

At 0 °C, 4.0 ml (10.6 g, 42.3 mmol) BBr_3 in 30 ml DCM was added in drops to a solution of 1.61 g (9.81 mmol) **58** in 30 ml DCM and the mixture was stirred overnight. 50 ml water was added and stirring was continued for 30 minutes. The aqueous phase was saturated with Na_2SO_4 and extracted with ethyl acetate four times. The organic phase was dried over Na_2SO_4 and evaporated under reduced pressure. The residue was subjected to silica gel chromatography* with petroleum ether / DCM = 1 / 1 as eluent to yield 1.45 g (4.93 mmol, 50%) of a colorless solid. ^{1}H NMR ($CDCl_3$): δ = 6.55 (s, 1 H; H-1), 7.17 (d, ^{4}J = 1.56 Hz, 1 H; H-3), 7.25 (dd, ^{3}J = 8.08 Hz, ^{4}J = 1.76 Hz, 1 H; H-7), 7.60 (d, ^{3}J = 8.12 Hz, 1 H; H-6), 9.91 (d, ^{4}J = 0.60 Hz, 1 H; H-8), 11.08 (s, 1 H; OH); ^{13}C NMR ($CDCl_3$): δ = 39.2 (C_t; C-1), 115.9 (C_t; C-3), 118.4 (C_t; C-7), 121.2 (C_q; C-5), 134.3 (C_t; C-6), 149.9 (C_q; C-2), 161.5 (C_q; C-4), 195.9 (C_t; C-8).

Compound 61

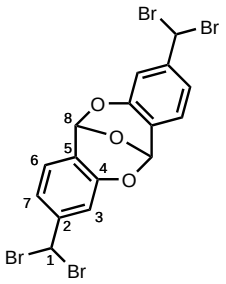

2 drops of a solution composed of 1 ml pivalic anhydride and 2 drops of H_2SO_4 conc. were added to a mixture of 718 mg (2.44 mmol) **60** and 455 mg (2.44 mmol) pivalic anhydride. The reaction was warmed for a short time to initiate the reaction and then was stirred with a spatula until the mixture completely solidified (10 minutes). The material was washed with petroleum ether and dried to yield 495 mg (869 µmol, 71%) of a pale pink solid ^{1}H NMR ($CDCl_3$): δ = 6.62 (s, 2 H; H-8), 7.09 (s, 2 H; H-1), 7.20 (d, ^{4}J = 1.88 Hz, 2 H; H-3), 7.35 (dd, ^{3}J = 7.92 Hz, ^{4}J = 2.01 Hz, 2 H; H-7), 7.53 (d, ^{3}J = 8.06 Hz, 2 H; H-6); ^{13}C NMR ($CDCl_3$): δ = 41.1 (C_t; C-1), 90.6 (C_t; C-8), 115.4 (C_t; C-3), 121.1 (C_t; C-7), 122.3 (C_q; C-5), 129.7 (C_t; C-6), 146.5 (C_q; C-2), 165.5 (C_q; C-4).

*The product appears orange-colored on silica gel.

Compound 62

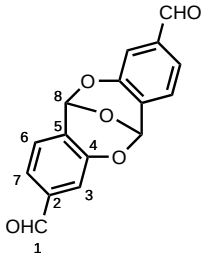

495 mg (869 µmol) **61** was stirred in 10 ml DMF at 160 °C overnight. At room temperature, 10 ml water was added. The formed precipitate was filtered, washed with water and dried to yield 165 mg (585 µmol, 67%) of an off-white solid. ^{1}H NMR (DMSO-d$_6$): δ = 6.87 (s, 2 H; H-8), 7.45 (d, ^4J = 1.40 Hz, 2 H; H-3), 7.56 (dd, ^3J = 7.84 Hz, ^4J = 1.48 Hz, 2 H; H-7), 7.67 (d, ^3J = 7.92 Hz, 2 H; H-6), 9.90 (s, 2 H; H-1).

Compound 47

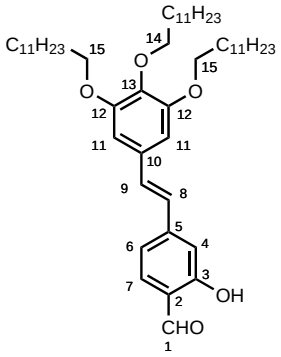

370 mg (3.30 mmol) potassium *tert*-butoxide was added in portions to a stirred solution of 155 mg (549 µmol) **62** and 858 mg (1.10 mmol) phosphonate **36** in 1 mL dry THF under argon atmosphere. After stirring for 20 minutes, the reaction was quenched with water and extracted with mixtures of THF and ethyl acetate. The organic phase was dried over Na_2SO_4 and evaporated under reduced pressure. The residue was subjected to silica gel chromatography with petroleum ether / ethyl acetate = 10 / 1 as eluent to yield 425 mg of a yellow oil.

The material was dissolved in 10 ml $CHCl_3$ and mixed with 10 ml 1N HCl. At 80 °C, 1.0 ml H_2SO_4 was added in portions and the mixture was stirred for 3 hours. At room temperature, the mixture was extracted with DCM and the organic phase was washed with water, dried over Na_2SO_4 and evaporated under reduced pressure. The residue was subjected to silica gel chromatography with petroleum ether / ethyl acetate = 50 / 1 as eluent to yield 285 mg (367 µmol, 33%) of a yellow solid. ^{1}H NMR (250 MHz, $CDCl_3$): δ = 0.88 (m, 9 H; CH_3), 1.20 - 1.90 (m, 60 H; $C_{10}H_{20}$), 3.97 (t, ^3J = 5.50 Hz, 2 H; H-14), 4.03 (t, ^3J = 5.34 Hz, 4 H; H-15), 6.73 (s, 2 H; H-11), 6.92 + 7.16 (d, ^3J = 16.18 Hz, 2 H; H-8 + H-9), 7.07 (m, 1 H; H-4), 7.14 (dd (ov), ^3J = 8.03 Hz, ^4J = 1.53 Hz, 1 H; H-6), 7.52 (d, ^3J = 8.23 Hz, 1 H; H-7), 9.84 (s, 1 H; H-1), 11.11 (s, 1 H; OH).

10.16 Density measurements

In the first step, the samples were heated to the isotropic or near-isotropic state, depending on the clearing temperature of the material, to avoid inclusion of air.[269] Since the star compounds decom-

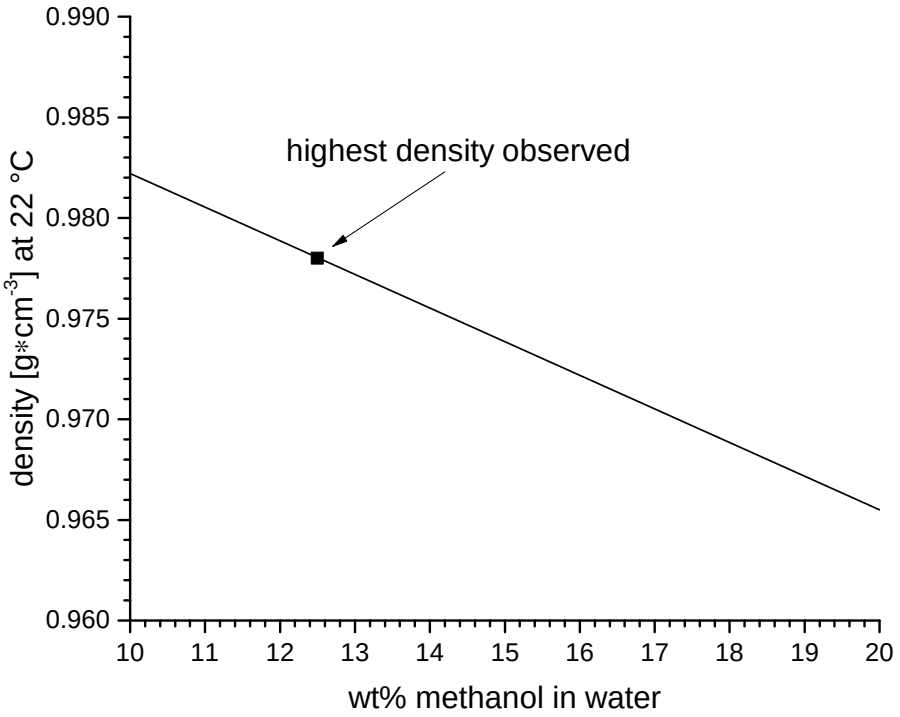

Figure 83: Determination of the density of the material $\mathbf{S2}_{C12}$ at 22 °C. The density values for 10 and 20 wt% are calculated from literature.[270]

pose at elevated temperatures, the materials could only be heated for a short period of time. Therefore, the calculated densities should be regarded as minimum values. In the next step, the samples were extruded to give thin fibers, which were then cut into smaller specimens. These samples were put in a sealed vial containing ultrasonicated methanol at 22 °C. Deionized water was added in portions until all pieces were floating. The wt% of methanol for each floating sample was then calculated. The density of the mixtures were determined according to literature[270] for the average wt% of methanol for the piece with the lowest wt% of methanol added (highest density). According to reference, a linear relationship is given for the density of methanol-water mixtures and wt% of methanol at 25 °C. Therefore, it is reasonable to assume the same for 22 °C. The highest density observed for one specimen of compound $\mathbf{S2}_{C12}$ amounts to 0.978 g·cm^{-3}. Therefore, a density of 0.98 g·cm^{-3} is specified. The fullerene specimens $\mathbf{S2}_{C12}$-$\mathbf{F1}_{C4}$ prepared by this method did not float even in neat water, thus the density must be larger than 0.9978 g·cm^{-3} (density of water at 22 °C).

11 Miscellaneous

11.1 Cell parameter determination

The experimental cell parameters for all compounds forming columnar phases have been obtained from the Bragg angles and were adjusted to minimize the deviation from the theoretical values of the planar spacings. The signals were fitted to gaussian curves. The heated samples did not reach the set temperatures T_{set} in the XRD measurements. The real values T were estimated by using a line of best fit for verified values at certain temperatures: $T = (T_{set} + 6.4751°C)/1.1468°C$. If not stated otherwise, the cell parameters were determined at a sample-detector distance of 27 cm.

S1$_{C12}$ (2D: Col_h)

T (T_{set}) [°C]	*a* [Å]	*hk*	2θ exp. [°]	d_{hk} exp. [Å]	d_{hk} theor. [Å]
25 (25)	49.7	10	2.04	43.2	43.0
		11	3.56	24.8	24.9
		20	4.11	21.5	21.5
		21	5.44	16.2	16.3
49 (50)	48.5	10	2.10	42.0	42.0
		11	3.65	24.2	24.3
		20	4.20	21.0	21.0
		21	5.58	15.9	15.9
93 (100)	46.7	10	2.18	40.5	40.4
		11	3.79	23.3	23.4
		20	4.37	20.2	20.2
		21	5.80	15.2	15.3
106 (115)	46.2	10	2.21	40.0	40.0
		11	3.83	23.1	23.1
		20	4.41	20.0	20.0
		21	5.87	15.1	15.1

S2$_{C12}$ (2D: Col$_h$)

T (T$_{set}$) [°C]	a [Å]	hk	2θ exp. [°]	d$_{hk}$ exp. [Å]	d$_{hk}$ theor. [Å]
25 (25)	61.5	10	1.65	53.4	53.3
		11	2.87	30.8	30.8
		20	3.31	26.7	26.6
		21	4.38	20.2	20.1
		30	4.98	17.8	17.8
49 (50)	61.7	10	1.65	53.7	53.4
		11	2.88	30.7	30.9
		20	3.31	26.7	26.7
		21	4.38	20.2	20.2
		30	4.95	17.8	17.8
93 (100)	60.7	10	1.68	52.6	52.6
		11	2.93	30.1	30.4
		20	3.35	26.3	26.3
		21	4.45	19.9	19.9
136 (150)	60.2	10	1.70	52.1	52.1
		11	2.95	29.9	30.1
		20	3.39	26.1	26.1
		21	4.49	19.7	19.7
180 (200)	59.5	10	1.71	51.6	51.5
		11	2.98	29.6	29.8
		20	3.43	25.8	25.8
		21	4.54	19.5	19.5

S3$_{C12}$ (2D: Col$_h$)

T (T$_{set}$) [°C]	a [Å]	hk	2θ exp. [°]	d$_{hk}$ exp. [Å]	d$_{hk}$ theor. [Å]
25 (25)	69.4	10	1.47	60.1	60.1
		11	2.55	34.7	34.7
		20	2.93	30.2	30.1
150 (136)	70.0	10	1.46	60.6	60.6
		11	2.54	34.8	35.0
		20	2.90	30.5	30.3

S1$_{C12}$**-F1**$_{C4}$ (2D: Col_h)

T (T_{set}) [°C]	*a* [Å]	*hk*	2θ exp. [°]	d_{hk} exp. [Å]	d_{hk} theor. [Å]
25 (25)	44.0	10	2.31	38.2	38.1
		11	4.03	21.9	22.0
		20	4.64	19.1	19.1
49 (50)	44.2	10	2.30	38.3	38.3
		11	4.02	22.0	22.1
		20	4.62	19.1	19.1
136 (150)	43.8	10	2.32	38.1	37.9
		11	4.04	21.9	21.9
		20	4.66	18.9	19.0

S2$_{C12}$**-F1**$_{C4}$ (2D: Col_h); sample-detector distance: 68 cm

T (T_{set}) [°C]	*a* [Å]	*hk*	2θ exp. [°]	d_{hk} exp. [Å]	d_{hk} theor. [Å]
25 (25)	56.1	10	1.83	48.4	48.6
		11	3.16	28.0	28.1
		20	3.64	24.3	24.3
136 (150)	56.7	10	1.80	49.0	49.1
		11	3.12	28.3	28.4
		20	3.59	24.6	24.6
224 (250)	55.9	10	1.83	48.3	48.4
		11	3.16	28.0	28.0
		20	3.64	24.3	24.2

S2$_{C12}$**-F1**$_{C10}$ (Col_{borh}); sample-detector distance: 107 cm

T (T_{set}) [°C]	*a* [Å]	*b* [Å]	*c* [Å]	*hkl*	2θ exp. [°]	d_{hkl} exp. [Å]	d_{hkl} theor. [Å]
30 (30)	97.1	56.4	121.5	011	1.72	51.4	51.2
				200	1.82	48.5	48.6
				310	3.15	28.1	28.1
128 (140)	96.8	55.9	129.4	011	1.72	51.3	51.3
				200	1.83	48.4	48.4
				310	3.17	27.8	27.9

S2$_{C12}$**-F1**$_{C16}$ (Col_{borh}); sample-detector distance: 107 cm

T (T_{set}) [°C]	*a* [Å]	*b* [Å]	*c* [Å]	*hkl*	2θ exp. [°]	d_{hkl} exp. [Å]	d_{hkl} theor. [Å]
30 (30)	96.7	56.1	142.5	011	1.69	52.2	52.2
				110	1.82	48.3	48.4
				310	3.17	27.9	27.9

Mix_S (2D: Col_h); sample-detector distance: 107 cm

T (T_{set}) [°C]	*a* [Å]	*hk*	2θ exp. [°]	d_{hk} exp. [Å]	d_{hk} theor. [Å]
30 (30)	55.7	10	1.83	48.4	48.2
		11	3.16	27.9	27.9
150 (165)	56.2	10	1.82	48.7	48.7
		11	3.14	28.1	28.1
197 (220)	55.7	10	1.83	48.3	48.2
		11	3.18	27.8	27.9

S2$_{O3}$ (2D: Col_h)

T (T_{set}) [°C]	*a* [Å]	*hk*	2θ exp. [°]	d_{hk} exp. [Å]	d_{hk} theor. [Å]
25 (25)	53.5	10	1.90	46.4	46.3
		11	3.31	26.7	26.8
		20	3.80	23.3	23.2
		21	5.05	17.5	17.5
49 (50)	53.4	10	1.91	46.2	46.2
		11	3.32	26.6	26.7
		20	3.80	23.2	23.1
75 (80)	53.2	10	1.92	46.0	46.1
		11	3.32	26.6	26.6
		20	3.83	23.1	23.0
97 (105)	53.0	10	1.92	45.9	45.9
		11	3.34	26.5	26.5
		20	3.84	23.0	22.9

Por$_{C12}$ (2D: Col_h)

T (T_{set}) [°C]	*a* [Å]	*hk*	2θ exp. [°]	d_{hk} exp. [Å]	d_{hk} theor. [Å]
25 (25)	62.3	10	1.64	54.0	54.0
		11	2.85	31.1	31.2
		20	3.28	27.0	27.0
		21	4.35	20.3	20.4
93 (100)	63.1	10	1.61	54.8	54.6
		11	2.81	31.5	31.6
		20	3.24	27.3	27.3
		21	4.29	20.6	20.7
136 (150)	63.8	10	1.60	55.2	55.3
		20	3.21	27.6	27.6
		21	4.25	20.8	20.9
224 (250)	63.9	10	1.60	55.4	55.3
		20	3.19	27.7	27.7
		21	4.23	20.9	20.9

11.2 Modeling and simulation

The cell parameters obtained from X-ray scattering investigations were used to build models of the corresponding structures. Initial structures were build with the BIOVIA *Materials Studio* software. The number of molecules per cell was obtained from the cell unit volumes and the densities of the materials, which were either determined experimentally or estimated as 1.0 g·cm^{-3}. The value then was fitted to obtain an integer as number of molecules per cell. Geometry optimizations were performed with the associated *Forcite* module using *COMPASS* as forcefield and atom based non-bond interactions. Annealing steps were integrated to locate low energy areas. In the final geometry optimization step, the *Ewald* summation method was used for non-bond interactions. The obtained structures were then used for the calculation of fiber diffraction patterns using the software *CLEARER*.[271] Note that this software is not purposely designed to simulate fluid phases like LC phases. Especially the peripheral chains of the mesogens do not possess periodicity in the columnar arrangements but *CLEARER* uses well-defined crystallites based on the unit cell input. Therefore, simulated reflections can be caused by the chains and can appear much more intense compared to the experimental diffraction patterns.

11.3 Software programming

X-Ray measurements were executed automatically via a script written with the programming language python 3.4. The graphical user interface requires the modul pyqt5. The software is composed of the following code:

```
from PyQt5.QtCore import *
from PyQt5.QtWidgets import *
from PyQt5.QtGui import *


class Dialog(QDialog):


    def __init__(self):
        super(Dialog, self).__init__()


        # Box for general settings
        self.buttonBox = QDialogButtonBox(QDialogButtonBox.Save)
        self.buttonBox.accepted.connect(self.save)
        self.tiltcheckbox = QCheckBox("Tilt angle:")
        self.tiltcheckbox.setChecked(False)
        self.tiltangle = QLineEdit()
        self.tiltangle.setDisabled(True)
        self.tilt = False
        def tiltswitch():
            sender = self.sender()
            if sender.isChecked():
                self.tilt = True
                self.tiltangle.setEnabled(True)
            else:
                self.tilt = False
                self.tiltangle.setDisabled(True)
        self.tiltcheckbox.toggled.connect(tiltswitch)
        self.usesample = [True,False,False]

        GeneralGroupBox = QGroupBox("General settings:")

        self.date = QLineEdit("YYYYMMDD")
        self.distance = QLineEdit("28")
        self.ramp = QLineEdit("10.0")
        self.hold = QLineEdit("300")
        self.rsw = QLineEdit("8")
        self.WMS = QComboBox()
        self.WMSitems = ("WAXS", "MAXS", "SAXS")
        self.WMS.addItems(self.WMSitems)

        generallayout = QGridLayout()
```

```
44          generallayout.addWidget(QLabel("date:"), 2, 0)
45          generallayout.addWidget(self.date, 2, 2)
46          generallayout.addWidget(QLabel("detector distance:"), 3, 0)
47          generallayout.addWidget(self.WMS, 3, 1)
48          generallayout.addWidget(self.distance, 3, 2)
49          generallayout.addWidget(self.tiltcheckbox, 3, 3)
50          generallayout.addWidget(self.tiltangle, 3, 4)
51          generallayout.addWidget(QLabel("ramp:"), 4, 0)
52          generallayout.addWidget(self.ramp, 4, 2)
53          generallayout.addWidget(QLabel("hold:"), 5, 0)
54          generallayout.addWidget(self.hold, 5, 2)
55          generallayout.addWidget(QLabel("RefSampWheel:"), 6, 0)
56          generallayout.addWidget(self.rsw, 6, 2)
57          generallayout.setColumnStretch(0, 20)
58          generallayout.setColumnStretch(1, 10)
59          generallayout.setColumnStretch(2, 20)
60          generallayout.setColumnStretch(3, 5)
61          generallayout.setColumnStretch(4, 5)
62          generallayout.setColumnStretch(5, 20)
63          GeneralGroupBox.setLayout(generallayout)
64
65
66
67          #Box for temperature stages
68          StagesGroupBox = QGroupBox("Stages:")
69          self.stageslayout = QVBoxLayout()
70          self.addrow = QPushButton("Insert row")
71          self.table = QTableWidget(10,2)
72          self.table.setSortingEnabled(False)
73          self.tableheaders = ["Temperature [Â°C]","Duration [s]"]
74          self.table.setHorizontalHeaderLabels(self.tableheaders)
75          def newrow():
76              self.table.insertRow(1)
77          self.addrow.clicked.connect(newrow)
78          self.stageslayout.addWidget(self.table)
79          self.stageslayout.addWidget(self.addrow)
80          StagesGroupBox.setLayout(self.stageslayout)
81
82
83
84          # Box for sample-boxes
85          self.sampleslayout = QVBoxLayout()
86          SamplesGroupBox = QGroupBox("Samples:")
87          self.code = []
88          self.title = []
89          self.positionx = []
90          self.positiony = []
91          self.heatcycle = []
92          for i in range(3):
93              self.addSampleBox(i)
94          SamplesGroupBox.setLayout(self.sampleslayout)
95
96
97
98          #Box for General-settings-box and samples-box
99          LowerGroupBox = QGroupBox()
100         lowerlayout = QHBoxLayout()
101         lowerlayout.addWidget(StagesGroupBox)
102         lowerlayout.addWidget(SamplesGroupBox)
103         LowerGroupBox.setLayout(lowerlayout)
104
105
106
107         #Main box
108         self.setWindowTitle("slmgui")
109         mainlayout = QVBoxLayout()
110         mainlayout.addWidget(GeneralGroupBox)
111         mainlayout.addWidget(LowerGroupBox)
112         mainlayout.addWidget(self.buttonBox)
113         self.setLayout(mainlayout)
114
115
116
117     #Create a dynamic number of sample-boxes
118     def addSampleBox(self, BoxNo):
119         lines = 6
120         if BoxNo == 0:
121             TF = True
122         else:
123             TF = False
124         code = QLineEdit()
125         title = QLineEdit("Extruded")
126         positionx = QLineEdit()
127         positiony = QLineEdit()
128         heatcycle = QLineEdit("1")
```

```
129         samplebox = QGroupBox("#%i" % (BoxNo+1))
130         samplebox.setCheckable(True)
131         samplebox.setChecked(TF)
132         sampleboxlayout = QGridLayout()
133         sampleboxlayout.addWidget(QLabel("Sample code:"), (BoxNo+1)*lines, 1)
134         sampleboxlayout.addWidget(code, (BoxNo+1)*lines, 2)
135         sampleboxlayout.addWidget(QLabel("Title:"), (BoxNo+2)*lines, 1)
136         sampleboxlayout.addWidget(title, (BoxNo+2)*lines, 2)
137         sampleboxlayout.addWidget(QLabel("Position x:"), (BoxNo+3)*lines, 1)
138         sampleboxlayout.addWidget(positionx, (BoxNo+3)*lines, 2)
139         sampleboxlayout.addWidget(QLabel("Position y:"), (BoxNo+4)*lines, 1)
140         sampleboxlayout.addWidget(positiony, (BoxNo+4)*lines, 2)
141         sampleboxlayout.addWidget(QLabel("Heatcycle:"), (BoxNo+5)*lines, 1)
142         sampleboxlayout.addWidget(heatcycle, (BoxNo+5)*lines, 2)
143         def triggered():
144             if samplebox.isChecked():
145                 self.usesample[BoxNo] = True
146             else:
147                 self.usesample[BoxNo] = False
148         samplebox.toggled.connect(triggered)
149         samplebox.setLayout(sampleboxlayout)
150         self.sampleslayout.addWidget(samplebox)
151         self.code.append(code)
152         self.title.append(title)
153         self.positionx.append(positionx)
154         self.positiony.append(positiony)
155         self.heatcycle.append(heatcycle)
156
157
158
159     #Event of save-button clicked
160     def save(self):
161         name = QFileDialog.getSaveFileName(self,"Choose file name", os.getcwd(), ".slm")
162         if name[0] == "":
163             pass
164         else:
165             if self.tilt == True:
166                 tilttext = ("_"+self.tiltangle.text()+"G")
167             else:
168                 tilttext = ""
169             if not ".slm" in name[0]:
170                 filename = name[0]+ name[1]
171             else:
172                 filename = name[0]
173             output = open(filename, "w")
174             samplehold = [int(self.hold.text()),int(self.hold.text()),int(self.hold.text())]
175             if self.usesample[0]:
176                 samplehold[1] = 5;
177                 samplehold[2] = 5;
178             if self.usesample[1]:
179                 samplehold[2] = 5;
180             self.sh = []
181             self.sh.append("0")
182             self.sa = []
183             self.sa.append("0")
184             stages = 0
185             for i in range(self.table.rowCount()+1):
186                 if self.table.item(i,0) == None:
187                     self.table.removeCellWidget(i,0)
188                     self.table.removeCellWidget(i,1)
189                 else:
190                     self.sh.append(self.table.item(i,0).text())
191                     self.sa.append(self.table.item(i,1).text())
192                     stages = stages+1
193             hc = []
194             for i in range(3):
195                 if self.usesample[i] == True:
196                     hc.append(int(self.heatcycle[i].text()))
197                 else:
198                     hc.append(0)
199             counter = 1
200             while counter <= stages:
201                if int(self.sh[counter]) >= int(self.sh[counter-1]):
202                   hk = "H"
203                if int(self.sh[counter]) < int(self.sh[counter-1]):
204                   hk = "K"
205                if int(self.sh[counter]) >= int(self.sh[counter-1]) and int(self.sh[counter-1]) < int(self.sh[counter-2]) and counter >
                       1:
206                   for i in range(3):
207                     if self.usesample[i] == True:
208                         hc[i] = hc[i] + 1
209                for i in range(3):
210                   if self.usesample[i] == True:
211                      savename = (self.code[i].text() + "_" + hk + str(hc[i]) + "_" + self.sh[counter] + "_" + str(self.WMS.currentText
                             ()) + self.distance.text() + tilttext + "_" + self.date.text())
```

```
212                     output.write("GONIOMETER␣/TEMP␣" + self.sh[counter] + ".00␣/RAMP=" + self.ramp.text() + "␣/HOLD=" + str(
                            samplehold[i]) + "␣/WAIT\n")
213                     output.write("GONIOMETER␣/GENERATOR␣50.0␣0.600\n")
214                     output.write("GONIOMETER␣/DRIVE␣" + self.positionx[i].text() + "␣" + self.positiony[i].text() + "␣" + self.rsw.
                            text() + "\n")
215                     output.write("ADD␣" + self.sa[counter] + "␣/CLEAR␣/COUNTS=1000000000␣/DISPLAY=31␣/REALTIME␣/RESET=0␣&\n")
216                     output.write("␣/SHUTTER␣/SLAM=$null␣/BARTIME=0.0␣/SLAM=$null\n")
217                     output.write("SAVE␣" + savename + ".gfrm␣/TITLE=\"" + self.title[i].text() + "\"␣/DISPLAY=0\n")
218                     output.write("SPATIAL␣/UNWARP␣" + savename + ".gfrm␣1␣" + savename + ".unw␣/NOBEAMCENTER␣/DISPLAY=16\n")
219                     output.write("\n")
220                 counter = counter + 1
221             output.write("GONIOMETER␣/TEMP␣25.00␣/RAMP=10.0␣/HOLD=300␣/WAIT\n");
222             output.write("GONIOMETER␣/GENERATOR␣20.0␣0.100");
223             output.close()
224             webbrowser.open(filename)
225
226
227
228 if __name__ == '__main__':
229
230     import sys,os,webbrowser
231     app = QApplication(sys.argv)
232     dialog = Dialog()
233     sys.exit(dialog.exec_())
```

References

[1] Mazzio, K. A.; Luscombe, C. K. *Chem. Soc. Rev.* **2015**, *44*, 78 – 90.

[2] Hayashi, H.; Nihashi, W.; Umeyama, T.; Matano, Y.; Seki, S.; Shimizu, Y.; Imahori, H. *J. Am. Chem. Soc.* **2011**, *133*, 10736 – 10739.

[3] Lehmann, M.; Kestemont, G.; Gomez Aspe, R.; Buess-Herman, C.; Koch, M. H. J.; Debije, M. G.; Piris, J.; de Haas, M. P.; Warman, J. M.; Watson, M. D.; et al., *Chem. Eur. J.* **2005**, *11*, 3349 – 3362.

[4] van de Craats, A. M.; Warman, J.; Fechtenkötter, A.; Brand, J. D.; Harbison, M.; Müllen, K. *Adv. Mater.* **1999**, *11*, 1469 – 1472.

[5] Concellón, A.; Marcos, M.; Romero, P.; Serrano, J. L.; Termine, R.; Golemme, A. *Angew. Chem. Int. Ed.* **2017**, *56*, 1259 – 1263.

[6] Wang, C.-L.; Zhang, W.-B.; Sun, H.-J.; Van Horn, R. M.; Kulkarni, R. R.; Tsai, C.-C.; Hsu, C.-S.; Lotz, B.; Gong, X.; Cheng, S. Z. D. *Adv. Energy Mater.* **2012**, *2*, 1375 – 1382.

[7] Tauchi, L.; Nakagaki, T.; Shimizu, M.; Itoh, E.; Yasutake, M.; Ohta, K. *J. Porphyrins Phthalocyanines* **2013**, *17*, 1080 – 1093.

[8] Ishikawa, A.; Ono, K.; Ohta, K.; Yasutake, M.; Ichikawa, M.; Itoh, E. *J. Porphyrins Phthalocyanines* **2014**, *18*, 366 – 379.

[9] Dong, L.; Li, W.; Li, W.-S. *Nanoscale* **2011**, *3*, 3447 – 3461.

[10] Yu, G.; Gao, J.; Hummelen, J. C.; Wudl, F.; Heeger, A. J. *Science* **1995**, *270*, 1789 – 1790.

[11] Deibel, C.; Strobel, T.; Dyakonov, V. *Phys. Rev. Lett.* **2009**, *103*, 036402.

[12] Peeters, E.; van Hal, P. A.; Knol, J.; Brabec, C. J.; Sariciftci, N. S.; Hummelen, J.; Janssen, R. A. *J. Phys. Chem. B* **2000**, *104*, 10174 – 10190.

[13] Camaioni, N.; Po, R. *J. Phys. Chem. Lett.* **2013**, *4*, 1821 – 1828.

[14] Girón, R. M.; Reboredo, S.; Marco-Martínez, J.; Filippone, S.; Martín, N. *Faraday Discuss.* **2014**,

[15] Goodby, J.; Collings, P.; Kato, T.; Tschierske, C.; Gleeson, H.; Raynes, P. *Handbook of Liquid Crystals Vol. 1*; Wiley VCH Verlag GmbH, 2014.

[16] Chandrasekhar, S.; Sadashiva, B. K.; Suresh, K. A. *Pramana-J. Phys.* **1977**, *9*, 471 – 480.

[17] Levelut, A. *J. Phys. Lett.-Paris* **1979**, *40*, 81 – 84.

[18] Goodby, J.; Collings, P.; Kato, T.; Tschierske, C.; Gleeson, H.; Raynes, P. *Handbook of Liquid Crystals Vol. 4*; Wiley VCH Verlag GmbH, 2014.

[19] Barón, M. *Pure Appl. Chem.* **2001**, *73*, 845 – 895.

[20] Laschat, S.; Baro, A.; Steinke, N.; Giesselmann, F.; Hägele, C.; Scalia, G.; Judele, R.; Kapatsina, E.; Sauer, S.; Schreivogel, A.; Torsoni, M. *Angew. Chem. Int. Ed.* **2007**, *46*, 4832 – 4887.

[21] Goodby, J.; Collings, P.; Kato, T.; Tschierske, C.; Gleeson, H.; Raynes, P. *Handbook of Liquid Crystals Vol. 5*; Wiley VCH Verlag GmbH, 2014.

[22] Letko, I.; Diele, S.; Pelzl, G.; Weissflog, W. *Liq. Cryst.* **1995**, *19*, 643 – 646.

[23] Saez, I. M.; Goodby, J. W. *J. Mater. Chem.* **2005**, *15*, 26 – 40.

[24] Detert, H.; Lehmann, M.; Meier, H. *Materials* **2010**, *3*, 3218 – 3330.

[25] Dierking, I. *Textures of Liquid Crystals*; Wiley-Blackwell, 2003.

[26] Kumar, S. *Chemistry of discotic liquid crystals: from monomers to polymers*; CRC press, 2010.

[27] Nehring, J.; Saupe, A. *J. Chem. Soc. Farad. T. 2* **1972**, *68*, 1 – 15.

[28] Scherrer, P. *Nachr. von der Ges. der Wiss. zu Göttingen, Math.-Phys. Kl.* **1918**, *1918*, 98 – 100.

[29] Langford, J. I.; Wilson, A. J. C. *J. Appl. Cryst.* **1978**, *11*, 102 – 113.

[30] Hammond, C. *The Basics of Crystallography and Diffraction*; Oxford University Press, 2009.

[31] Fredriksson, H.; Akerlind, U. *Physics of Functional Materials*; John Wiley & Sons, 2008.

[32] Zhao, H.; He, Z.; Xu, M.; Liang, C.; Kumar, S. *Phys. Chem. Chem. Phys.* **2016**, *18*, 8554 – 8560.

[33] Cisse, L.; Destruel, P.; Archambeau, S.; Seguy, I.; Jolinat, P.; Bock, H.; Grelet, E. *Chem. Phys. Lett.* **2009**, *476*, 89 – 91.

[34] Dvinskikh, S. V.; Sandström, D.; Zimmermann, H.; Maliniak, A. *Prog. Nucl. Mag. Res. Sp.* **2006**, *48*, 85 – 107.

[35] Hu, N.; Shao, R.; Shen, Y.; Chen, D.; Clark, N. A.; Walba, D. M. *Adv. Mater.* **2014**, *26*, 2066 – 2071.

[36] Yoshio, M.; Konishi, R.; Sakamoto, T.; Kato, T. *New J. Chem.* **2013**, *37*, 143 – 147.

[37] Miyajima, D.; Araoka, F.; Takezoe, H.; Kim, J.; Kato, K.; Takata, M.; Aida, T. *Angew. Chem. Int. Ed.* **2011**, *50*, 7865 – 7869.

[38] Sato, K.; Itoh, Y.; Aida, T. *J. Am. Chem. Soc.* **2011**, *133*, 13767 – 13769.

[39] Shimura, H.; Yoshio, M.; Hamasaki, A.; Mukai, T.; Ohno, H.; Kato, T. *Adv. Mater.* **2009**, *21*, 1591 – 1594.

[40] Van Winkle, D. H.; Clark, N. A. *Phys. Rev. Lett.* **1982**, *48*, 1407.

[41] Peterca, M.; Percec, V.; Imam, M. R.; Leowanawat, P.; Morimitsu, K.; Heiney, P. A. *J. Am. Chem. Soc.* **2008**, *130*, 14840 – 14852.

[42] Basova, T. V.; Hassan, A.; Durmuş, M.; Gürek, A. G.; Ahsen, V. *Synthetic Met.* **2011**, *161*, 1996 – 2000.

[43] Basova, T.; Latteyer, F.; Atilla, D.; Gürek, A. G.; Hassan, A.; Ahsen, V.; Peisert, H.; Chassè, T. *Thin Solid Films* **2010**, *518*, 5745 – 5752.

[44] Basova, T. V.; Durmuş, M.; Gürek, A. G.; Ahsen, V.; Hassan, A. *J. Phys. Chem. C* **2009**, *113*, 19251 – 19257.

[45] Grelet, E.; Bock, H. *Europhys. Lett.* **2006**, *73*, 712 – 718.

[46] Sergeyev, S.; Pisula, W.; Geerts, Y. H. *Chem. Soc. Rev.* **2007**, *36*, 1902 – 1929.

[47] Eccher, J.; Zajaczkowski, W.; Faria, G. C.; Bock, H.; von Seggern, H.; Pisula, W.; Bechtold, I. H. *ACS Appl. Mater. Interfaces* **2015**, *7*, 16374 – 16381.

[48] Gupta, R. K.; Pathak, S. K.; Pradhan, B.; Rao, D. S.; Prasad, S. K.; Achalkumar, A. S. *Soft Matter* **2015**, *11*, 3629 – 3636.

[49] Gupta, R. K.; Pradhan, B.; Pathak, S. K.; Gupta, M.; Pal, S. K.; Ammathnadu Sudhakar, A. *Langmuir* **2015**, *31*, 8092 – 8100.

[50] Yang, T.; Pu, J.; Zhang, J.; Wang, W. *J. Org. Chem.* **2013**, *78*, 4857 – 4866.

[51] Charlet, E.; Grelet, E. *Phys. Rev. E* **2008**, *78*, 041707–1 – 041707–8.

[52] Rybak, A.; Pfleger, J.; Jung, J.; Pavlik, M.; Glowacki, I.; Ulanski, J.; Tomovic, Z.; Müllen, K.; Geerts, Y. *Synthetic Met.* **2006**, *156*, 302 – 309.

[53] Sosa-Vargas, L.; Nekelson, F.; Okuda, D.; Takahashi, M.; Matsuda, Y.; Dao, Q.-D.; Hiroyuki, Y.; Fujii, A.; Ozaki, M.; Shimizu, Y. *J. Mater. Chem. C* **2015**, *3*, 1757 – 1765.

[54] Ariyoshi, M.; Sugibayashi-Kajita, M.; Suzuki-Ichihara, A.; Kato, T.; Kamei, T.; Itoh, E.; Ohta, K. *J. Porphyrins Phthalocyanines* **2012**, *16*, 1114 – 1123.

[55] Cour, I.; Pan, Z.; Lebruin, L. T.; Case, M. A.; Furis, M.; Headrick, R. L. *Org. Electron.* **2012**, *13*, 419 – 424.

[56] Schweicher, G.; Gbabode, G.; Quist, F.; Debever, O.; Dumont, N.; Sergeyev, S.; Geerts, Y. H. *Chem. Mater.* **2009**, *21*, 5867 – 5874.

[57] Nekelson, F.; Monobe, H.; Shiro, M.; Shimizu, Y. *J. Mater. Chem.* **2007**, *17*, 2607.

[58] Ohta, K.; Hatsusaka, K.; Sugibayashi, M.; Ariyoshi, M.; Ban, K.; Maeda, F.; Naito, R.; Nishizawa, K.; Van de Craats, A. M.; Warman, J. M. *Mol. Cryst. Liq. Cryst.* **2003**, *397*, 25 – 45.

[59] Kroon, J. M.; Koehorst, R. B.; van Dijk, M.; Sanders, G. M.; Sudhölter, E. J. *J. Mater. Chem.* **1997**, *7*, 615 – 624.

[60] Zhou, X.; Kang, S.-W.; Kumar, S.; Li, Q. *Liq. Cryst.* **2009**, *36*, 269 – 274.

[61] Sun, Q.; Dai, L.; Zhou, X.; Li, L.; Li, Q. *Appl. Phys. Lett.* **2007**, *91*, 253505.

[62] Eichhorn, S. H.; Bruce, D. W.; Guillon, D.; Gallani, J.-L.; Fischer, T.; Stumpe, J.; Geue, T. *J. Mater. Chem.* **2001**, *11*, 1576 – 1584.

[63] Li, Q.; Zhou, X. Light-harvesting discotic liquid crystalline porphyrins and metal complexes. 2007; WO Patent App. PCT/US2006/047,842.

[64] Umesh, C.; Marcelis, A. T.; Zuilhof, H. *Liq. Cryst.* **2014**, *41*, 1911 – 1922.

[65] Tatum, L. A.; Johnson, C. J.; Fernando, A. A. P.; Ruch, B. C.; Barakoti, K. K.; Alpuche-Aviles, M. A.; King, B. T. *Chem. Sci.* **2012**, *3*, 3261.

[66] Miyake, Y.; Fujii, A.; Ozaki, M.; Shimizu, Y. *Mol. Cryst. Liq. Cryst.* **2010**, *516*, 246 – 252.

[67] Wang, J.; He, Z.; Zhang, Y.; Zhao, H.; Zhang, C.; Kong, X.; Mu, L.; Liang, C. *Thin Solid Films* **2010**, *518*, 1973 – 1979.

[68] Terasawa, N.; Monobe, H. *Liq. Cryst.* **2007**, *34*, 447 – 455.

[69] Monobe, H.; Hori, H.; Heya, M.; Awazu, K.; Shimizu, Y. *Thin Solid Films* **2006**, *499*, 259 – 262.

[70] Schönherr, H.; Manickam, M.; Kumar, S. *Langmuir* **2002**, *18*, 7082 – 7085.

[71] Li, J.; He, Z.; Zhao, H.; Gopee, H.; Kong, X.; Xu, M.; An, X.; Jing, X.; Cammidge, A. N. *Pure Appl. Chem.* **2010**, *82*, 1993 – 2003.

[72] Zucchi, G.; Viville, P.; Donnio, B.; Vlad, A.; Melinte, S.; Mondeshki, M.; Graf, R.; Spiess, H. W.; Geerts, Y. H.; Lazzaroni, R. *J. Phys. Chem. B* **2009**, *113*, 5448 – 5457.

[73] Zhou, X.; Kang, S.-W.; Kumar, S.; Kulkarni, R. R.; Cheng, S. Z. D.; Li, Q. *Chem. Mater.* **2008**, *20*, 3551 – 3553.

[74] Pisula, W.; Kastler, M.; Wasserfallen, D.; Robertson, J. W. F.; Nolde, F.; Kohl, C.; Müllen, K. *Angew. Chem. Int. Ed.* **2006**, *45*, 819 – 823.

[75] Samorì, P.; Yin, X.; Tchebotareva, N.; Wang, Z.; Pakula, T.; Jäckel, F.; Watson, M. D.; Venturini, A.; Müllen, K.; Rabe, J. P. *J. Am. Chem. Soc.* **2004**, *126*, 3567 – 3575.

[76] Tchebotareva, N.; Yin, X.; Watson, M. D.; Samorì, P.; Rabe, J. P.; Müllen, K. *J. Am. Chem. Soc.* **2003**, *125*, 9734 – 9739.

[77] Nakagawa, K.; Yokoyama, T.; Toyota, K.; Morita, N.; Ito, S.; Tahata, S.; Ueda, M.; Kawakami, J.; Yokoyama, M.; Kanai, Y.; et al., *Tetrahedron* **2010**, *66*, 8304 – 8312.

[78] Xu, J.; Ling, T. C.; He, C. *J. Polym. Sci. Pol. Chem.* **2008**, *46*, 4691 – 4703.

[79] Meier, H.; Lehmann, M.; Holst, H. C.; Schwöppe, D. *Tetrahedron* **2004**, *60*, 6881 – 6888.

[80] Dickstein, W. H.; Lillya, C. P. *Mol. Cryst. Liq. Cryst. Inc. Nonlin. Opt.* **1988**, *157*, 69 – 78.

[81] Monobe, H.; Shimizu, Y. *Mol. Cryst. Liq. Cryst.* **2011**, *542*, 151/[673] – 157/[679].

[82] Monobe, H.; Hori, H.; Shimizu, Y.; Awazu, K. *Mol. Cryst. Liq. Cryst.* **2007**, *475*, 13 – 22.

[83] Monobe, H.; Awazu, K.; Shimizu, Y. *Adv. Mater.* **2006**, *18*, 607 – 610.

[84] Furumi, S.; Kidowaki, M.; Ogawa, M.; Nishiura, Y.; Ichimura, K. *J. Phys. Chem. B* **2005**, *109*, 9245 – 9254.

[85] Shimizu, Y.; Monobe, H.; Awazu, K. *Rev. Laser Eng.* **2003**, *31*, 811 – 817.

[86] Kajitani, T.; Suna, Y.; Kosaka, A.; Osawa, T.; Fujikawa, S.; Takata, M.; Fukushima, T.; Aida, T. *J. Am. Chem. Soc.* **2013**, *135*, 14564 – 14567.

[87] Al-Lawati, Z. H.; Bushby, R. J.; Evans, S. D. *J. Phys. Chem. C* **2013**, *117*, 7533 – 7539.

[88] Sergeyev, S.; Levin, J.; Balandier, J.-Y.; Pouzet, E.; Geerts, Y. H. *Mendeleev Commun.* **2009**, *19*, 185 – 186.

[89] Gearba, R. I.; Anokhin, D. V.; Bondar, A. I.; Bras, W.; Jahr, M.; Lehmann, M.; Ivanov, D. A. *Adv. Mater.* **2007**, *19*, 815 – 820.

[90] Archambeau, S.; Séguy, I.; Jolinat, P.; Farenc, J.; Destruel, P.; Nguyen, T.; Bock, H.; Grelet, E. *Appl. Surf. Sci.* **2006**, *253*, 2078 – 2086.

[91] Pouzet, E.; Cupere, V. D.; Heintz, C.; Andreasen, J. W.; Breiby, D. W.; Nielsen, M. M.; Viville, P.; Lazzaroni, R.; Gbabode, G.; Geerts, Y. H. *J. Phys. Chem. C* **2009**, *113*, 14398 – 14406.

[92] Grelet, E.; Dardel, S.; Bock, H.; Goldmann, M.; Lacaze, E.; Nallet, F. *Eur. Phys. J. E* **2010**, *31*, 343 – 349.

[93] Kawata, K. *Chem. Rec.* **2002**, *2*, 59 – 80.

[94] Tang, C. W. *Appl. Phys. Lett.* **1986**, *48*, 183 – 185.

[95] Heeger, A. J. *Adv. Mater.* **2014**, *26*, 10 – 28.

[96] Halls, J. J. M.; Walsh, C. A.; Greenham, N. C.; Marseglia, E. A.; Friend, R. H.; Moratti, S. C.; Holmes, A. B. *Nature* **1995**, *376*, 498 – 500.

[97] Kumar, M.; Kumar, S. *Polym. J.* **2017**, *49*, 85 – 111.

[98] Fleischmann, E.-K.; Zentel, R. *Angew. Chem. Int. Ed.* **2013**, *52*, 8810 – 8827.

[99] Bushby, R. J.; Hamley, I. W.; Liu, Q.; Lozman, O. R.; Lydon, J. E. *J. Mater. Chem.* **2005**, *15*, 4429 – 4434.

[100] Geerts, Y. H.; Debever, O.; Amato, C.; Sergeyev, S. *Beilstein J. Org. Chem.* **2009**, *5*, 49.

[101] Wang, C.-L.; Zhang, W.-B.; Horn, R. M. V.; Tu, Y.; Gong, X.; Cheng, S. Z. D.; Sun, Y.; Tong, M.; Seo, J.; Hsu, B. B. Y.; Heeger, A. J. *Adv. Mater.* **2011**, *23*, 2951 – 2956.

[102] Schmidt-Mende, L.; Fechtenkötter, A.; Müllen, K.; Moons, E.; Friend, R.; MacKenzie, J. *Science* **2001**, *293*, 1119 – 1122.

[103] Schmidt-Mende, L.; Fechtenkötter, A.; Müllen, K.; Friend, R. H.; MacKenzie, J. *Physica E* **2002**, *14*, 263 – 267.

[104] Schmidtke, J. P.; Friend, R. H.; Kastler, M.; Müllen, K. *J. Chem. Phys.* **2006**, *124*, 174704/1 – 174704/6.

[105] Al-Hussein, M.; Hesse, H.; Weickert, J.; Dössel, L.; Feng, X.; Müllen, K.; Schmidt-Mende, L. *Thin Solid Films* **2011**, *520*, 307 – 313.

[106] Jeong, S.; Kwon, Y.; Choi, B.-D.; Ade, H.; Han, Y. S. *Appl. Phys. Lett.* **2010**, *96*, 183305.

[107] Stalmach, U.; Kolshorn, H.; Brehm, I.; Meier, H. *Eur. J. Org. Chem.* **1996**, 1449 – 1456.

[108] Lagowski, J. B. *J. Mol. Struc-Theochem* **2002**, *589*, 125 – 137.

[109] Meier, H. *Angew. Chem. Int. Ed.* **1992**, *31*, 1399 – 1420.

[110] Lei, T.; Dou, J.-H.; Cao, X.-Y.; Wang, J.-Y.; Pei, J. *J. Am. Chem. Soc.* **2013**, *135*, 12168 – 12171.

[111] Likhtenshtein, G. *Stilbenes. Applications in Chemistry, Life Sciences and Materials Science.*; Wiley VCH Verlag GmbH, 2009.

[112] Boutagy, J.; Thomas, R. *Chem. Rev.* **1974**, *74*, 87 – 99.

[113] Ando, K. *J. Org. Chem.* **1999**, *64*, 6815 – 6821.

[114] Ngwendson, J. N.; Schultze, C. M.; Bollinger, J. W.; Banerjee, A. *Can. J. Chem.* **2008**, *86*, 668 – 675.

[115] Arbusow, B. A. *Pure Appl. Chem.* **1964**, *9*.

[116] Schuster, D. I.; Nuber, B.; Vail, S. A.; MacMahon, S.; Lin, C.; Wilson, S. R.; Khong, A. *Photochem. Photobiol. Sci.* **2003**, *2*, 315 – 321.

[117] Kroto, H. W.; Heath, J. R.; O'Brien, S. C.; Curl, R. F.; Smalley, R. E. *Nature* **1985**, *318*, 162 – 163.

[118] Johansson, M. P.; Jusélius, J.; Sundholm, D. *Angew. Chem. Int. Ed.* **2005**, *44*, 1843 – 1846.

[119] Liu, T.; Troisi, A. *Adv. Mater.* **2013**, *25*, 1038 – 1041.

[120] Guldi, D. M. *Chem. Soc. Rev.* **2002**, *31*, 22 – 36.

[121] Andreas Hirsch, F. W., Michael Brettreich *Fullerenes*; Wiley VCH Verlag GmbH, 2005.

[122] Maggini, M.; Scorrano, G.; Prato, M. *J. Am. Chem. Soc.* **1993**, *115*, 9798 – 9799.

[123] Prato, M.; Maggini, M. *Acc. Chem. Res.* **1998**, *31*, 519 – 526.

[124] Kesters, J.; Verstappen, P.; Kelchtermans, M.; Lutsen, L.; Vanderzande, D.; Maes, W. *Adv. Energy Mater.* **2015**, *5*, 1500218.

[125] Usol'Tseva, N.; Bykova, V.; Zharnikova, N.; Alexandrov, A.; Semeikin, A.; Kazak, A. *Mol. Cryst. Liq. Cryst.* **2010**, *525*, 184 – 193.

[126] Shimizu, Y.; Miya, M.; Nagata, A.; Ohta, K.; Yamamoto, I.; Kusabayashi, S. *Liq. Cryst.* **1993**, *14*, 795 – 805.

[127] Lindsey, J. S.; Hsu, H. C.; Schreiman, I. C. *Tetrahedron Lett.* **1986**, *27*, 4969 – 4970.

[128] Lindsey, J. S.; Schreiman, I. C.; Hsu, H. C.; Kearney, P. C.; Marguerettaz, A. M. *J. Org. Chem.* **1987**, *52*, 827 – 836.

[129] Zhou, M.; Xu, D.-P.; Liu, T.-C.; Zhang, P.; Gao, S.-Q.; Li, Z.-W.; Lu, G.-H. *J. Phys. Chem. B* **2008**, *112*, 15562 – 15568.

[130] de la Torre, G.; Giacalone, F.; Segura, J. L.; Martín, N.; Guldi, D. M. *Chem. Eur. J.* **2005**, *11*, 1267 – 1280.

[131] Wielopolski, M.; Molina-Ontoria, A.; Schubert, C.; Margraf, J. T.; Krokos, E.; Kirschner, J.; Gouloumis, A.; Clark, T.; Guldi, D. M.; Martín, N. *J. Am. Chem. Soc.* **2013**, *135*, 10372–10381.

[132] Lehmann, M. Synthesis and Structure-Property-Relationships of Stilbenoid Dendrimers and Star-shaped Compounds. Ph.D. thesis, Johannes Gutenberg University of Mainz, 1999.

[133] Lehmann, M.; Schartel, B.; Hennecke, M.; Meier, H. *Tetrahedron* **1999**, *55*, 13377 – 13394.

[134] Wolffs, M.; Hoeben, F. J. M.; Beckers, E. H. A.; Schenning, A. P. H. J.; Meijer, E. W. *J. Am. Chem. Soc.* **2005**, *127*, 13484 – 13485.

[135] Hoeben, F. J. M.; Wolffs, M.; Zhang, J.; Feyter, S. D.; Leclère, P.; Schenning, A. P. H. J.; Meijer, E. W. *J. Am. Chem. Soc.* **2007**, *129*, 9819 – 9828.

[136] Bestmann, H. J.; Hadawi, D.; Röder, T.; Moll, C. *Tetrahedron Lett.* **1994**, *35*, 9017 – 9020.

[137] Hügel, M. Diploma thesis; Sternförmige stilbenoide Hybride mit Fullerenbausteinen. Julius Maximilian University of Würzburg, 2012.

[138] Neises, B.; Steglich, W. *Angew. Chem. Int. Ed.* **1978**, *17*, 522 – 524.

[139] Tsumoto, H.; Takahashi, K.; Suzuki, T.; Nakagawa, H.; Kohda, K.; Miyata, N. *Bioorg. Med. Chem. Lett.* **2008**, *18*, 657 – 660.

[140] Reiriz, C.; Brea, R. J.; Arranz, R.; Carrascosa, J. L.; Garibotti, A.; Manning, B.; Valpuesta, J. M.; Eritja, R.; Castedo, L.; Granja, J. R. *J. Am. Chem. Soc.* **2009**, *131*, 11335 – 11337.

[141] Wei, Q.; Tajima, K.; Tong, Y.; Ye, S.; Hashimoto, K. *J. Am. Chem. Soc.* **2009**, *131*, 17597 – 17604.

[142] Guibé, F. *Tetrahedron* **1998**, *54*, 2967 – 3042.

[143] Harrowven, D. C.; Nunn, M. I.; Fenwick, D. R. *Tetrahedron Lett.* **2002**, *43*, 3189 – 3191.

[144] Mizoshita, N.; Ikai, M.; Tani, T.; Inagaki, S. *J. Am. Chem. Soc.* **2009**, *131*, 14225 – 14227.

[145] Díez-Barra, E.; García-Martínez, J. C.; Merino, S.; del Rey, R.; Rodríguez-López, J.; Sánchez-Verdú, P.; Tejeda, J. *J. Org. Chem.* **2001**, *66*, 5664 – 5670.

[146] Easson, M. W.; Fronczek, F. R.; Jensen, T. J.; Vicente, M. G. H. *Bioorgan. Med. Chem.* **2008**, *16*, 3191 – 3208.

[147] Wen, L.; Li, M.; Schlenoff, J. B. *J. Am. Chem. Soc.* **1997**, *119*, 7726 – 7733.

[148] Coluccini, C.; Sharma, A. K.; Merli, D.; Griend, D. V.; Mannucci, B.; Pasini, D. *Dalton T.* **2011**, *40*, 11719.

[149] Chatterjee, S.; Ramakrishnan, S. *ACS Macro Lett.* **2012**, *1*, 593 – 598.

[150] Drozd, J. *Chemical Derivatization in Gas Chromatography*; Elsevier Science, 1986.

[151] Kang, M. S.; Oh, J. B.; Seo, K. D.; Kim, H. K.; Park, J.; Kim, K.; Park, N.-G. *J. Porphyrins Phthalocyanines* **2009**, *13*, 798 – 804.

[152] Field, L.; Engelhardt, P. R. *J. Org. Chem.* **1970**, *35*, 3647 – 3655.

[153] Tanabe, K. K.; Allen, C. A.; Cohen, S. M. *Angew. Chem. Int. Ed.* **2010**, *49*, 9730 – 9733.

[154] Morishima, H.; Yoshizawa, J.; Ushijima, R.; Takeuchi, T.; Umezawa, H. *J. Antibiot.* **1982**, *35*, 1500 – 1506.

[155] Ajito, K.; Ikeda, D.; Komuro, K.; Nosaka, C.; Wako, N.; Kondo, S.; Takeuchi, T. *J. Antibiot.* **1989**, *42*, 1133 – 1144.

[156] Corbett, J.; Groppi, V. Treatment of diseases with combinations of alpha 7 nicotinic acetylcholine receptor agonists and other compounds. 2004; WO Patent App. PCT/IB2003/005,525.

[157] Ohashi, A.; Satake, A.; Kobuke, Y. *B. Chem. Soc. Jpn.* **2004**, *77*, 365 – 374.

[158] Brown, H. C.; Keblys, K. A. *J. Org. Chem.* **1966**, *31*, 485 – 487.

[159] Parikka, K.; Wähälä, K. *Beilstein J. Org. Chem.* **2009**, *5*.

[160] Taber, D. F.; Amedio, J. C.; Jung, K. Y. *J. Org. Chem.* **1987**, *52*, 5621 – 5622.

[161] Pantoş, G. D.; Wietor, J.-L.; Sanders, J. K. *Angew. Chem. Int. Ed.* **2007**, *46*, 2238 – 2240.

[162] Kordatos, K.; Bosi, S.; Da Ros, T.; Zambon, A.; Lucchini, V.; Prato, M. *J. Org. Chem.* **2001**, *66*, 2802 – 2808.

[163] Bottari, G.; Dammann, C.; Torres, T.; Drewello, T. *J. Am. Soc. Mass Spectrom.* **2013**, *24*, 1413 – 1419.

[164] Maroto, E.; Filippone, S.; Martín-Domenech, A.; Suárez, M.; Martín, N.; Martínez-Alvarez, R. *J. Mass Spectrom.* **2011**, *46*, 1016 – 1029.

[165] Delgado, J. L.; Osuna, S.; Bouit, P.-A.; Martinez-Alvarez, R.; Espildora, E.; Sola, M.; Martin, N. *J. Org. Chem.* **2009**, *74*, 8174–8180.

[166] Figueira-Duarte, T. M.; Gégout, A.; Olivier, J.; Cardinali, F.; Nierengarten, J.-F. *Eur. J. Org. Chem.* **2009**, *2009*, 3879 – 3884.

[167] Chen, L.; Wu, J.; Yuwen, L.; Shu, T.; Xu, M.; Zhang, M.; Yi, T. *Langmuir* **2009**, *25*, 8434 – 8438.

[168] Lejnieks, J.; Zhu, X.; Wang, J.; Mourran, A.; Keul, H.; Möller, M.; Anokhin, D. V.; Ivanov, D. A. *ChemPhysChem* **2010**, *11*, 3638 – 3644.

[169] Albrecht, M.; Baumert, M.; Winkler, H.; Schalley, C. *Synthesis* **2010**, *2010*, 953 – 958.

[170] Gutiérrez-Nava, M.; Jaeggy, M.; Nierengarten, H.; Masson, P.; Guillon, D.; Dorsselaer, A. V.; Nierengarten, J.-F. *Tetrahedron Lett.* **2003**, *44*, 3039 – 3042.

[171] Flitsch, W.; Langer, W. *Liebigs Ann. Chem.* **1988**, 391 – 395.

[172] Wagner, A.; Heitz, M.-P.; Mioskowski, C. *J. Chem. Soc. Chem. Comm.* **1989**, 1619.

[173] Armaroli, N.; Accorsi, G.; Gisselbrecht, J.-P.; Gross, M.; Krasnikov, V.; Tsamouras, D.; Hadzioannou, G.; Gómez-Escalonilla, M. J.; Langa, F.; Eckert, J.-F.; Nierengarten, J.-F. *J. Mater. Chem.* **2002**, *12*, 2077 – 2087.

[174] Wynberg, H. *Chem. Rev.* **1960**, *60*, 169 – 184.

[175] Sasson, Y.; Yonovich, M. *Tetrahedron Lett.* **1979**, *20*, 3753 – 3756.

[176] Duff, J. C. *J. Chem. Soc.* **1941**, 547 – 550.

[177] Allevi, P.; Cribiu, R.; Anastasia, M. *Tetrahedron-Asymmtr.* **2004**, *15*, 1355 – 1358.

[178] Bonner, T. G.; Lewis, D.; Rutter, K. *J. Chem. Soc. Perk. T. 1* **1981**, 1807 – 1810.

[179] Ma, D.; Zhang, T.; Wang, G.; Kozikowski, A. P.; Lewin, N. E.; Blumberg, P. M. *Bioorg. Med. Chem. Lett.* **2001**, *11*, 99 – 101.

[180] De Mendoza, J.; Nieto, P. M.; Prados, P.; Sánchez, C. *Tetrahedron* **1990**, *46*, 671 – 682.

[181] Watanabe, T.; Iwamoto, A.; Miyashita, S.; Watanabe, M. Production of dimethylolcarboxylic acid. 2002; US Patent App. 10/051,025.

[182] Yoakim, C.; Oḿeara, J.; Simoneau, B.; Ogilvie, W.; Déziel, R. Non-nucleoside reverse transcriptase inhibitors. 2004; WO Patent App. PCT/CA2003/001,410.

[183] Bacon, R.; Doggart, J. *J. Chem. Soc.* **1960**, 1332 – 1338.

[184] Hauser, F. M.; Ellenberger, S. R. *Synthesis* **1987**, *1987*, 723 – 724.

[185] Vermoortele, F.; Vandichel, M.; Van de Voorde, B.; Ameloot, R.; Waroquier, M.; Van Speybroeck, V.; De Vos, D. E. *Angew. Chem. Int. Ed.* **2012**, *51*, 4887 – 4890.

[186] Kulkarni, V.; Hosangadi, B. *Synthetic Commun.* **1986**, *16*, 191 – 193.

[187] Cao, L.; Li, X.; Wang, S.; Li, S.; Li, Y.; Yang, G. *Chem. Commun.* **2014**, *50*, 8787 – 8790.

[188] Nishizawa, R.; Nishiyama, T.; Hisaichi, K.; Hirai, K.; Habashita, H.; Takaoka, Y.; Tada, H.; Sagawa, K.; Shibayama, S.; Maeda, K. *Bioorgan. Med. Chem.* **2010**, *18*, 5208 – 5223.

[189] Lee, Y. J.; Heo, H. G.; Oh, C. H. *Tetrahedron* **2016**, *72*, 6113 – 6117.

[190] Yang, C.; Edsall, R.; Harris, H. A.; Zhang, X.; Manas, E. S.; Mewshaw, R. E. *Bioorgan. Med. Chem.* **2004**, *12*, 2553 – 2570.

[191] El-Khouly, M. E.; Shim, S. H.; Araki, Y.; Ito, O.; Kay, K.-Y. *J. Phys. Chem. B* **2008**, *112*, 3910 – 3917.

[192] Lansinger, J. M.; Ronald, R. C. *Synthetic Commun.* **1979**, *9*, 341 – 349.

[193] Ragot, J. P.; Prime, M. E.; Archibald, S. J.; Taylor, R. J. *Org. Lett.* **2000**, *2*, 1613 – 1616.

[194] Quesada, E.; Stockley, M.; Taylor, R. J. *Tetrahedron Lett.* **2004**, *45*, 4877 – 4881.

[195] Quesada, E.; Stockley, M.; Ragot, J. P.; Prime, M. E.; Whitwood, A. C.; Taylor, R. J. *Org. Biomol. Chem.* **2004**, *2*, 2483 – 2495.

[196] Bankston, D. *Synthesis* **2004**, *2004*, 283 – 289.

[197] Krivchun, M.; Khramchikhin, A. *Russ. J. Gen. Chem.* **2017**, *87*, 1527 – 1530.

[198] Beugelmans, R.; Bourdet, S.; Bigot, A.; Zhu, J. *Tetrahedron Lett.* **1994**, *35*, 4349 – 4350.

[199] Meerpoel, L.; Linders, J.; Jaroskova, L.; Viellevoye, M.; Backx, L.; Berthelot, D.; Busscher, G. Piperidine or piperazine substituted tetrahydro-naphthalene-1-carboxylic acid mtp inhibiting compounds. 2008; WO Patent App. PCT/EP2007/061,286.

[200] Meerpoel, L.; Backx, L.; Ten, H.; Busscher, G. Mtp inhibiting tetrahydro-naphthalene-1-carboxylic acid derivatives. 2008; WO Patent App. PCT/EP2007/061,289.

[201] Polaske, N. W.; Szalai, M. L.; Shanahan, C. S.; McGrath, D. V. *Org. Lett.* **2010**, *12*, 4944 – 4947.

[202] Carlson, W. W.; Cretcher, L. H. *J. Am. Chem. Soc.* **1947**, *69*, 1952 – 1956.

[203] Parrish, J. P.; Salvatore, R. N.; Jung, K. W. *Tetrahedron* **2000**, *56*, 8207 – 8237.

[204] Teeuwen, R. L. M.; van Berkel, S. S.; van Dulmen, T. H. H.; Schoffelen, S.; Meeuwissen, S. A.; Zuilhof, H.; de Wolf, F. A.; van Hest, J. C. M. *Chem. Commun.* **2009**, 4022 – 4024.

[205] Bolchi, C.; Catalano, P.; Fumagalli, L.; Gobbi, M.; Pallavicini, M.; Pedretti, A.; Villa, L.; Vistoli, G.; Valoti, E. *Bioorgan. Med. Chem.* **2004**, *12*, 4937 – 4951.

[206] Pettit, G. R.; Rhodes, M. R.; Herald, D. L.; Hamel, E.; Schmidt, J. M.; Pettit, R. K. *J. Med. Chem.* **2005**, *48*, 4087 – 4099.

[207] Liu, Y.; Turner, S. R.; Wilkes, G. *Macromolecules* **2011**, *44*, 4049 – 4056.

[208] Gudipati, V.; Curran, D. P.; Wilcox, C. S. *J. Org. Chem.* **2006**, *71*, 3599 – 3607.

[209] Li, W.; Zhang, A.; Schlüter, A. D. *Chem. Commun.* **2008**, 5523 – 5525.

[210] Bédard, A.-C.; Collins, S. K. *Chem. Eur. J.* **2012**, *19*, 2108 – 2113.

[211] Abdel-Rahman, M. A.; Al-Abd, A. M. *Eur. J. Med. Chem.* **2013**, *69*, 848 – 854.

[212] Becker, E. D.; Bradley, R. B. *J. Chem. Phys.* **1959**, *31*, 1413 – 1414.

[213] Lee, E. C.; Kim, D.; Jurecˇka, P.; Tarakeshwar, P.; Hobza, P.; Kim, K. S. *J. Phys. Chem. A* **2007**, *111*, 3446 – 3457.

[214] Lehmann, M.; Hügel, M. *Angew. Chem. Int. Ed.* **2015**, *54*, 4110 – 4114.

[215] Singh, S. *Phase Transit.* **2000**, *72*, 183 – 209.

[216] Prasad, S. K.; Rao, D. S. S.; Chandrasekhar, S.; Kumar, S. *Mol. Cryst. Liq. Cryst.* **2003**, *396*, 121 – 139.

[217] Lu, H.; Zhou, Z.; Hao, T.; Ye, X.; Ne, Y. *Macromol. Theory Simul.* **2015**, *24*, 335 – 343.

[218] Wang, J.; Zhu, X.; Lu, X.; Zhou, Z.; Wang, G. *Comput. Theor. Chem.* **2015**, *1052*, 26 – 34.

[219] Gearba, R.; Lehmann, M.; Levin, J.; Ivanov, D.; Koch, M.; Barberá, J.; Debije, M.; Piris, J.; Geerts, Y. *Adv. Mater.* **2003**, *15*, 1614 – 1618.

[220] Praefcke, K.; Bilgin, B.; Usol'tseva, N.; Heinrich, B.; Guillon, D. *J. Mater. Chem.* **1995**, *5*, 2257 – 2264.

[221] Lehmann, M.; Jahr, M. *Chem. Mater.* **2008**, *20*, 5453 – 5456.

[222] Maringa, N.; Lenoble, J.; Donnio, B.; Guillon, D.; Deschenaux, R. *J. Mater. Chem.* **2008**, *18*, 1524 – 1534.

[223] Deschenaux, R.; Donnio, B.; Guillon, D. *New J. Chem.* **2007**, *31*, 1064 – 1073.

[224] Mannhold, R.; Kubinyi, H.; Folkers, G. *Fragment-based approaches in drug discovery*; John Wiley & Sons, 2006; Vol. 34.

[225] Krishnamurthy, V. M.; Semetey, V.; Bracher, P. J.; Shen, N.; Whitesides, G. M. *J. Am. Chem. Soc.* **2007**, *129*, 1312 – 1320.

[226] Li, M.; Chen, Q. *Polymer* **2003**, *44*, 2793 – 2798.

[227] Grimm, B.; Santos, J.; Illescas, B. M.; Munoz, A.; Guldi, D. M.; Martín, N. *J. Am. Chem. Soc.* **2010**, *132*, 17387 – 17389.

[228] Ladizhansky, V.; Vega, S. *J. Am. Chem. Soc.* **2000**, *122*, 3465 – 3472.

[229] May, F.; Marcon, V.; Hansen, M. R.; Grozema, F.; Andrienko, D. *J. Mater. Chem.* **2011**, *21*, 9538 – 9545.

[230] Ji, L.; Jing, L.; Lin, S.; Deng, X.; Zhu, P.; Zhang, X. *Dyes Pigments* **2014**, *106*, 176 – 181.

[231] Kroon, J. M.; Schenkels, P. S.; Van Dijk, M.; Sudhölter, E. J. *J. Mater. Chem.* **1995**, *5*, 1309 – 1316.

[232] Cook, M. J.; McMurdo, J.; Miles, D. A.; Poynter, R. H.; Simmons, J. M.; Haslam, S. D.; Richardson, R. M.; Welford, K. *J. Mater. Chem.* **1994**, *4*, 1205 – 1213.

[233] Dechant, M. Masters thesis; Phthalocyanin-Sternmesogene und ihre Selbstorganisation in kolumnaren Mesophasen. Julius Maximilian University of Würzburg, 2016.

[234] Matsen, M.; Bates, F. S. *Macromolecules* **1996**, *29*, 1091 – 1098.

[235] Fedors, R. F. *Polym. Eng. Sci.* **1974**, *14*, 147 – 154.

[236] Kohmoto, S.; Mori, E.; Kishikawa, K. *J. Am. Chem. Soc.* **2007**, *129*, 13364 – 13365.

[237] Percec, V.; Cho, W.-D.; Ungar, G.; Yeardley, D. J. *Chem. Eur. J.* **2002**, *8*, 2011 – 2025.

[238] Datta, S.; Bhattacharya, S. *Soft Matter* **2015**, *11*, 1945 – 1953.

[239] Kleinpeter, E.; Klod, S.; Koch, A. *J. Org. Chem.* **2008**, *73*, 1498 – 1507.

[240] Prato, M.; Suzuki, T.; Wudl, F.; Lucchini, V.; Maggini, M. *J. Am. Chem. Soc.* **1993**, *115*, 7876 – 7877.

[241] Cardullo, F.; Seiler, P.; Isaacs, L.; Nierengarten, J.-F.; Haldimann, R. F.; Diederich, F.; Mordasini-Denti, T.; Thiel, W.; Boudon, C.; Gisselbrecht, J.-P.; Gross, M. *Helv. Chim. Acta* **1997**, *80*, 343 – 371.

[242] Bühl, M.; Hirsch, A. *Chem. Rev.* **2001**, *101*, 1153 – 1184.

[243] Braslavsky, S. E. *Pure Appl. Chem.* **2007**, *79*, 293 – 465.

[244] Thompson, B. C.; Fréchet, J. M. *Angew. Chem. Int. Ed.* **2008**, *47*, 58 – 77.

[245] Yang, X.; van Duren, J. K.; Janssen, R. A.; Michels, M. A.; Loos, J. *Macromolecules* **2004**, *37*, 2151–2158.

[246] Hummelen, J. C.; Knol, J.; Sanchez, L. Stability issues of conjugated polymer/fullerene solar cells from a chemical viewpoint. Org. Photovol.; P. SPIE. 2001; pp 76–85.

[247] Hashimoto, T.; Choe, Y.-K.; Nakano, H.; Hirao, K. *J. Phys. Chem. A* **1999**, *103*, 1894 – 1904.

[248] Maggini, M.; Karlsson, A.; Scorrano, G.; Sandonà, G.; Farnia, G.; Prato, M. *J. Chem. Soc. Chem. Comm.* **1994**, 589 – 590.

[249] Marrec, P.; Fabre, B.; Simonet, J. *J. Electroanal. Chem* **1997**, *437*, 245 – 253.

[250] Wu, J.; Li, J.; Kolb, U.; Müllen, K. *Chem. Commun.* **2006**, 48 – 50.

[251] Sakurai, T.; Tsutsui, Y.; Kato, K.; Takata, M.; Seki, S. *J. Mater. Chem. C* **2016**, *4*, 1490 – 1496.

[252] Kushida, T.; Shuto, A.; Yoshio, M.; Kato, T.; Yamaguchi, S. *Angew. Chem. Int. Ed.* **2015**, *54*, 6922 – 6925.

[253] Feringán, B.; Romero, P.; Serrano, J. L.; Folcia, C. L.; Etxebarria, J.; Ortega, J.; Termine, R.; Golemme, A.; Giménez, R.; Sierra, T. *J. Am. Chem. Soc.* **2016**, *138*, 12511 – 12518.

[254] Hünig, S.; Kreitmeier, P.; Märkl, G.; Sauer, J. *Arbeitsmethoden in der organischen Chemie*; LOB-Lehmanns, 2006.

[255] Fulmer, G. R.; Miller, A. J.; Sherden, N. H.; Gottlieb, H. E.; Nudelman, A.; Stoltz, B. M.; Bercaw, J. E.; Goldberg, K. I. *Organometallics* **2010**, *29*, 2176 – 2179.

[256] Brown, T.; Clipston, N. L.; Simjee, N.; Luftmann, H.; Hungerbühler, H.; Drewello, T. *Int. J. Mass Spectrom.* **2001**, *210*, 249 – 263.

[257] Wyatt, M. F.; Stein, B. K.; Brenton, A. G. *Anal. Chem.* **2006**, *78*, 199 – 206.

[258] Stinchcombe, J.; Penicaud, A.; Bhyrappa, P.; Boyd, P. D.; Reed, C. A. *J. Am. Chem. Soc.* **1993**, *115*, 5212 – 5217.

[259] Lee, J. U.; Cirpan, A.; Emrick, T.; Russell, T. P.; Jo, W. H. *J. Mater. Chem.* **2009**, *19*, 1483 – 1489.

[260] Berrada, M.; Hashimoto, Y.; Miyata, S. *Chem. Mater.* **1994**, *6*, 2023 – 2025.

[261] Davey, S. N.; Leigh, D. A.; Moody, A. E.; Tetler, L. W.; Wade, F. A. *J. Chem. Soc. Chem. Comm.* **1994**, 397 – 398.

[262] Modak, A.; Nandi, M.; Mondal, J.; Bhaumik, A. *Chem. Commun.* **2012**, *48*, 248 – 250.

[263] Brandon, E. J.; Arif, A. M.; Burkhart, B. M.; Miller, J. S. *Inorg. Chem.* **1998**, *37*, 2792 – 2798.

[264] Buathong, S.; Ung, D.; Daou, T. J.; Ulhaq-Bouillet, C.; Pourroy, G.; Guillon, D.; Ivanova, L.; Bernhardt, I.; Begin-Colin, S.; Donnio, B. *J. Phys. Chem. C* **2009**, *113*, 12201 – 12212.

[265] Clover, A. M. *J. Am. Chem. Soc.* **1923**, *45*, 3133 – 3138.

[266] Rosa, A.; Ricciardi, G.; Baerends, E. J.; Romeo, A.; Scolaro, L. M. *J. Phys. Chem. A* **2003**, *107*, 11468 – 11482.

[267] Mohajer, D.; Zakavi, S.; Rayati, S.; Zahedi, M.; Safari, N.; Khavasi, H. R.; Shahbazian, S. *New J. Chem.* **2004**, *28*, 1600 – 1607.

[268] Gajewy, J.; Szymkowiak, J.; Kwit, M. *RSC Adv.* **2016**, *6*, 53358 – 53369.

[269] Lehmann, M.; Jahr, M.; Donnio, B.; Graf, R.; Gemming, S.; Popov, I. *Chem. Eur. J.* **2008**, *14*, 3562 – 3576.

[270] Mikhail, S. Z.; Kimel, W. R. *J. Chem. Eng. Data* **1961**, *6*, 533 – 537.

[271] Sumner Makin, O.; Sikorski, P.; Serpell, L. C. *J. Appl. Cryst.* **2007**, *40*, 966 – 972.

List of Figures

List of Tables

List of schemes